MINERALOGY, PETROLOGY AND GEOCHEMISTRY OF SOME ZONED DIORITE COMPLEXES IN SCOTLAND

Layla A. Mahmood

A Thesis Submitted for the Degree of PhD
at the
University of St Andrews

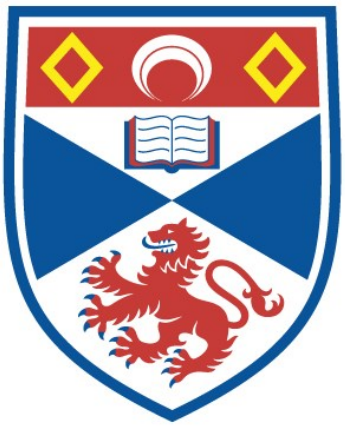

1986

MINERALOGY, PETROLOGY AND GEOCHEMISTRY

OF

SOME ZONED DIORITIC COMPLEXES

IN

SCOTLAND

Thesis presented for the degree of Doctor of Philosophy in the Faculty of Science, University of St Andrews.

by

LAYLA A MAHMOOD

1986

ProQuest LLC.
789 East Eisenhower Parkway
P.O. Box 1346
Ann Arbor, MI 48106 – 1346

This thesis is dedicated to

my husband, my daughters Likáa and

Zaháa and to my sisters.

ACKNOWLEDGEMENTS

I am gratefully indebted to my supervisor Dr W E Stephens, for suggesting the project, his kind advice, stimulating discussions and encouragement throughout my study period. His help in computing work and providing programmes is unforgetable.

I have no words to express my gratefulness to my husband, Mohammed for his help, understanding, patience and encouragement throughout this study. Not forgetting my family members at home for their constant support and encouragement during this study.

Many thanks are due to Professor E K Walton, for his constant encouragement, and to every staff member of this department for their help and co-operation.

The technical staff at the Geology Department, particularly Jim Allan, Andy Mackie, Richard Batchelor, Alistair Reid, Donald Herd, and Angus Calder are gratefully acknowledged for their efforts over the last years. Many thanks are due to Ian Franchi for his help in sample collection.

I am also very grateful to Mrs J Galloway and Mr S Bateman for their general help. Great thanks to Kit Finlay for typing the manuscript.

Many thanks to Dr P J Hill and D Russell of the Grant Institute of Geology, Edinburgh University for their help during electron microprobe analyses. Sincere thanks are due to Dr J Whitley for his help at the SURRC at East Kilbride during rare earth element analyses.

Special thanks are due to Mrs J Bowman for looking kindly after my daughters throughout this study.

I owe special thanks to the Ministry of Higher Education in Iraq for awarding me the grant to do this study.

CERTIFICATE

I LAYLA A MAHMOOD hereby certify that this thesis has been composed by myself, that it is a record of my own work, and that it has not been accepted in partial or complete fulfillment of any other degree or professional qualification.

I was admitted to the Faculty of Science of the University of St Andrews under Ordinance General No 12 on May 1980 and as a candidate for the degree of PhD on November 1981.

Signed ..... Date 29.7.1986

I hereby certify that the candidate has fulfilled the conditions of the Resolution and Regulations appropriate to the Degree of PhD.

Signed ..... Date .....

Abstract

This study is an investigation into the nature and causes of petrological zonation in calc-alkaline diorite-granite plutons from the Newer granites of the Caledonian orogeny in Scotland. Six plutons were used for the study, namely Garabal Hill-Glen Fyne in the western Highlands, Glen Tilt and Glen Doll in the eastern Highlands, Comrie in the southern Highlands, and Carsphairn and Loch Doon in the Southern Uplands. The petrological zoning is concentric in the Southern Uplands and Comrie and irregular in the other three.

The approach has been to acquire data on the petrography, mineral chemistry, and whole rock major and trace element chemistry for representative rock types of the petrological range within each pluton. Variations in mineral compositions are related to equilibrium crystallisation processes and indicate falling crystallisation temperatures with evolving magma composition. Mineral compositions have also been used in chemical models used to explain the observed wide variations in whole rock major oxide compositions. These models are then independently tested using models of trace element behaviour. The principal conclusions are that the main variations within the gabbro-diorite series (including cumulate peridotites and pyroxenites) are best explained by processes of fractional crystallisation from a parental gabbro or diorite magma, but in some cases the more evolved rocks (granites and granodiorites) have a more complex origin including possibly contamination of the parental magma or a distinctive magma source. The assemblage of fractionating minerals in the Garabal Hill, Comrie and Loch Doon plutons is dominated by the relatively anhydrous assemblage of orthopyroxene, clinopyroxene, plagioclase, and biotite whereas in Glen Doll it is a

more hydrous assemblage dominated by amphibole. Processes of magma mixing and multi-source pulses are considered appropriate in a few cases.

Regional comparisons of the within-pluton compositional variations reveal significant differences. The dominantly calc-alkaline trend shows marked differences in Fe/Mg between plutons as do trace element abundances, reflecting both differences in source region compositions and the influence of fractionating mineral phases. All plutons are I-type and high-K calc-alkaline. Parental magmas for the gabbro-diorite series have features of mantle-derived magmas though the more evolved rock types including granodiorites and granites indicate a significant contribution by crustal anatexis to the magmas.

CONTENTS

Page No

Page No

Page No

Page No

Page No

Page No

LIST OF FIGURES

Page No

Page No

Page No

List of Plates

Page No

Page No

LIST OF TABLES

Page No

CHAPTER 1

INTRODUCTION

1.1 General

The present study is concerned with six Caledonian granitoid plutons in Scotland. The plutons have in common the feature of petrological zoning from dioritic types (normally early) to late acidic types. Four of these plutons were emplaced in the southern Grampian Highlands (namely Garabal Hill-Glen Fyne to the west, Comrie to the south, Glen Doll and Glen Tilt to the east). All four intrude the Dalradian except for Glen Tilt which intrudes Moine metasediments (Fig 1.1). The other two plutons were emplaced in the Southern Uplands (namely Loch Doon and the Cairnsmore of Carsphairn) intruding Ordovician metasediments (Fig 1.1).

Throughout the Caledonian fold-belt zoned granitoid intrusive complexes are a common manifestation of late granitoid magmatism, probably post-dating the closure of the Iapetus Ocean, and with emplacement ages of 400 $\pm$ 10 Ma. These post-tectonic plutons are petrologically zoned ranging from diorites through to granodiorites and granites, though some are associated with more mafic and even ultramafic rocks occurring with the earliest intrusive phases. Hornblende rocks (the appinite suite) occur in the Garabal Hill, Glen Doll and Glen Tilt plutons, while peridotites occur in the Garabal Hill and pyroxenites occur in the Glen Doll plutons respectively.

Compositional zoning has attracted the attention of several workers, particularly with respect to the processes involved and the magma source regions. Some processes which have been suggested include:

a) closed system fractionation of basic parental magmas from mantle sources, possibly by side-wall accumulation,

b) partial melting of subducted oceanic lithosphere with or without

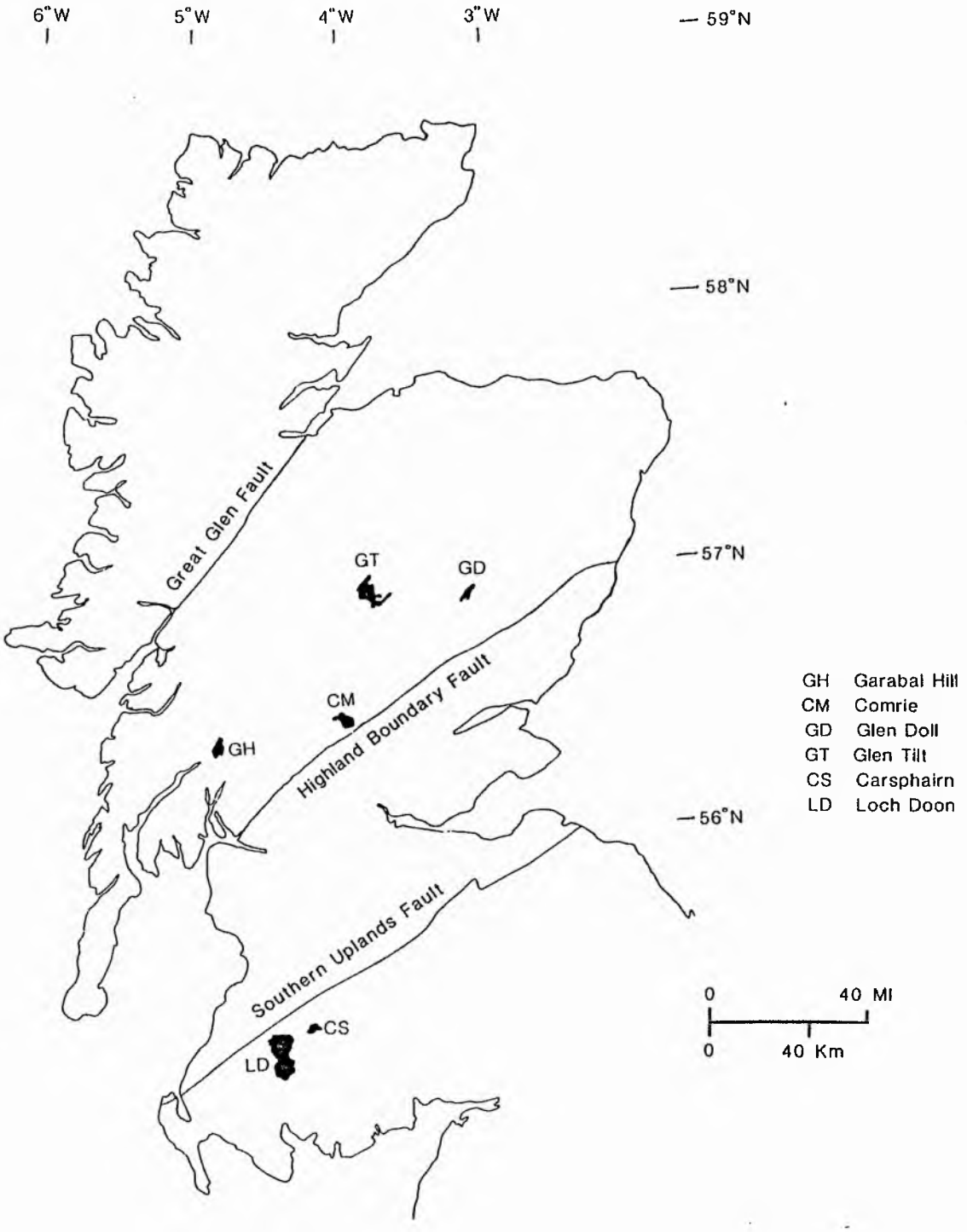

Fig 1.1 Location map of plutons studied in this thesis

intercalated sediments.

c) derivation from isotopically heterogeneous upper mantle and or lower crust.

d) high-level contamination of melts generated in the mantle or lower crust.

Chemically, although all plutons exhibit calc-alkaline trends on the AFM plot, there are significant differences between all plutons studied. Petrogenetic processes giving rise to such variations potentially include fractional crystallisation, multiple magma sources, magma mixing, and contamination through assimilation.

All six plutons studied fall into the I-type category of Chappell & White (1974) and have many features in common with those of Cordilleran granites. The granitoids were generated at the end-stages of the Caledonian orogeny, probably post-dating the closure of the Iapetus Ocean, and these factors are important when seeking modern analogues in equivalent tectonic settings.

1.2 Aims and objectives:

The principal objectives of this study are as follows:

1. To determine the petrological processes giving rise to compositional zoning in Caledonian diorite-granite complexes, often with concentric zonation arrangements.

2. To constrain potential source rocks for the parental magmas of these rock series.

3. To investigate regional variations in granitoid compositions by examining the same range in rock types (namely diorite to granite) in

several plutons over the region.

1.3 Methodology:

The techniques employed in this study are primarily petrographic and geochemical and applied to six selected zoned plutons. After studying and classifying the rocks using optical petrographic techniques including point counting, a selected group of samples were studied further using the electron microprobe for mineral analyses, XRF and wet chemical techniques for major oxides and trace elements of whole rock samples and neutron activation analysis for rare earth elements (REE) determination on whole rocks. Computer techniques were used to aid data interpretation and the plotting of mineral and whole rock analyses. Details of these techniques are given in Appendices B and C.

CHAPTER 2

GENERAL GEOLOGY
AND
PREVIOUS WORK

2.1 The Garabal Hill-Glen Fyne complex

2.1a Introduction:

The Garabal Hill-Glen Fyne igneous complex lies west of the head of Loch Lomond and stretches westward into Glen Fyne (Fig 2.1). The whole complex has an area of about 32 Km^2 covered by sheets 37, 38, 45 and 46 of the 1" Geological Survey maps of Scotland. The complex was first studied by Dakyns & Teall (1892) who delineated the boundaries of the complex and mapped most of the rock types, described them petrographically and chemically analysed some varieties.

Later a study of part of the western portion of the pluton and of the thermal metamorphism of the schists surrounding the complex was published in the Cowal Geological Survey Memoir by Gunn et al. (1897, p 96-101), and in the mid-Argyll Memoir by Hill et al. (1905, p 92-93). Subsequently a paper by Wyllie & Scott (1913) dealt mainly with the ultrabasic rocks and also described some of the intermediate rocks. The most detailed work of the petrology and petrography of the complex was published by Nockolds (1941) who also mapped the area on a scale of two inches to the mile, and studied all of the principal rock types chemically. Summerhayes (1966) determined the age of the intrusion using whole rock Rb and Sr isotope methods. Harmon & Halliday (1980) and Halliday (1984) presented new isotopic data for the medium granodiorites of this pluton.

2.1b General geology and previous work:

The Garabal Hill-Glen Fyne complex was intruded forcefully

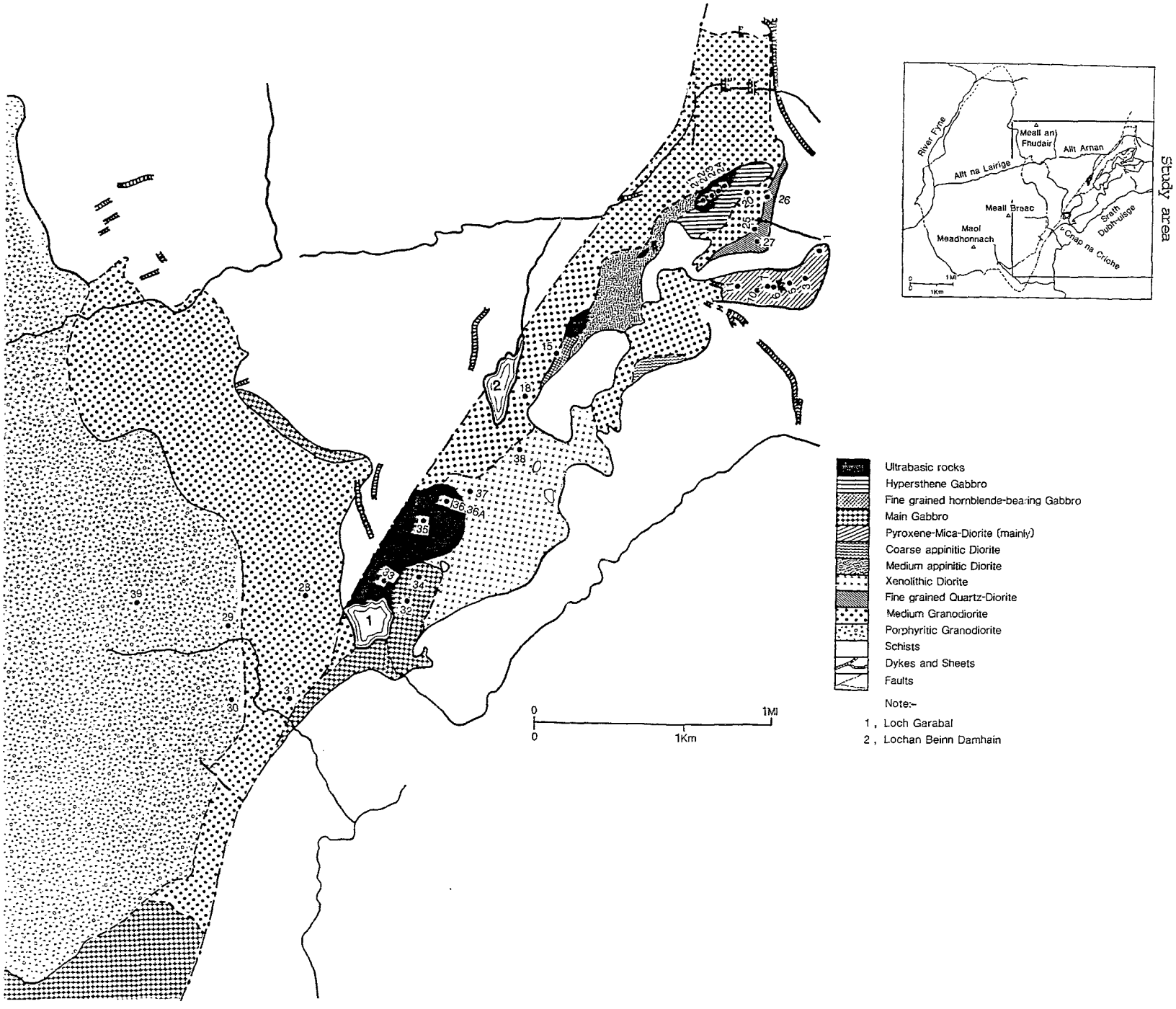

Fig 2.1 Geological sketch map of the Garabal Hill - Glen Fyne pluton (after Nockolds, 1941) showing sample locations.

into the Dalradian metasediments (late PreCambrian to Cambro-Ordovician) of the Cowal anticline at the northern tip of Loch Lomond (Read, 1961).

Nockolds (1941) proposed the age of the complex as Lower Old Red Sandstone (LORS), equivalent in age to LORS volcanics. Summerhayes (1966) found that all types of rocks of the complex were intruded within a very short time as there was no significant difference in the initial $(^{87}Sr/^{86}Sr)_0$. Values average 0.702-0.708 and determined the age of the complex as 392 $\mp$ 4 my by the Rb-Sr method and recalculated as 404 $\mp$ 4 my using a decay constant of 1.42×10^{-11} years (Steiger & Jaegar 1977).

Dakyns & Teall (1892) delineated the boundaries of the complex and mapped some of the rock types. They also determined the specific gravity of the principal rock types and briefly described their mineralogy, texture and chemical analyses. From the field evidence, they established the fact that rocks rich in ferromagnesian constituents preceded those poor in these constituents. Their microscopic examination of thin sections proved that iron ores precede olivine, olivine precedes the other ferro-magnesian constituents, and the ferro-magnesian minerals as a whole precede alkali feldspar and quartz in the individual rocks. They supposed the area to represent a vast subterranean reservoir which differentiated during the process of consolidation. The peridotites were the first rocks to form, the latest rocks to form are those rich in quartz and orthoclase, which occur in the form of veins and probably represent the residual liquid remaining after the other constituents separated out. Their conclusion was that the various rocks are the result

of differentiation of an originally homogeneous magma from a subterranean reservoir.

Wyllie & Scott (1913) concentrated on the ultrabasic and intermediate rocks. They concluded that separate origins of ultrabasic and acid magmas were responsible for the formation of the rocks in the complex. Nockolds (1941) mapped the different rock types in the area, studied the petrography in detail and analysed the chemical composition of the several rocks in the complex. He concluded that the rocks were formed by crystallisation-differentiation process of a parental magma of pyroxene-mica-diorite composition as these are the early rocks within the intrusion. He argued that contamination by earlier igneous or sedimentary rocks gave rise to certain rock types like the xenolithic diorite, the medium granodiorite, the whole of the fine grained quartz diorite, and the porphyritic granodiorite. He also concluded that there was no evidence for in situ differentation and the process operated at depth.

Nockolds & Mitchell (1946) studied the relationship between the major and trace elements of igneous rocks and their minerals for several Caledonian complexes including Garabal Hill. They concluded that the regularity in the behaviour of the trace elements in the rocks and in a given mineral species was evidence that the process of crystallisation-differentiation had been operated. The rocks belong to the calc-alkaline series but the process of differentiation cannot be observed in situ. The study by Summerhayes (1966) as well as determining the age of the complex as 392 $\mp$ 4 my and also presented $(^{87}Sr/^{86}Sr)_0$ values of a variety of rocks. The main pluton has values of about 0.705 but

marginal contaminated rocks have higher values of 0.710. He concluded that fractional crystallisation of a single homogeneous magma (Nockolds' hypothesis) or fractional melting of a low Rb/Sr source region (eg. basalt) deep within crust were suitable mechanisms for the origin of the complex. Summerhayes proposed that contamination occurred by assimilation of metasedimentary rocks to generate the quartz diorite, medium and porphyritic granodiorites. More recent studies by Harmon & Halliday (1980) and Halliday (1984) gave $(^{87}Sr/^{86}Sr)_0$ of 0.70778 and εNd values of -3.7 respectively for the medium granodiorites suggesting some crustal involvement in the petrogenesis of this rock type.

2.2 The Comrie complex

2.2a Introduction:

The Comrie complex is one of the largest diorite masses associated with the Caledonian Newer Granites of Scotland. Its outcrop extends from Glen Turret in the east to Glen Lednock in the west, its centre is about 4 Km north of Comrie in Perthshire (Fig 2.2). It is approximately oval in shape with its long dimension of 8.8 Km in the NW-SE direction and short dimension of 4 Km in the NE-SW direction. The complex is one of the forceful Newer Granite intrusions (Read, 1961) and is confined to the Ben Ledi grit zone of the Dalradian metasediments, except in the south where it has intruded the Aberfoyle slates some 1.6 Km NE of the village of Comrie.

2.2b General geology and previous work:

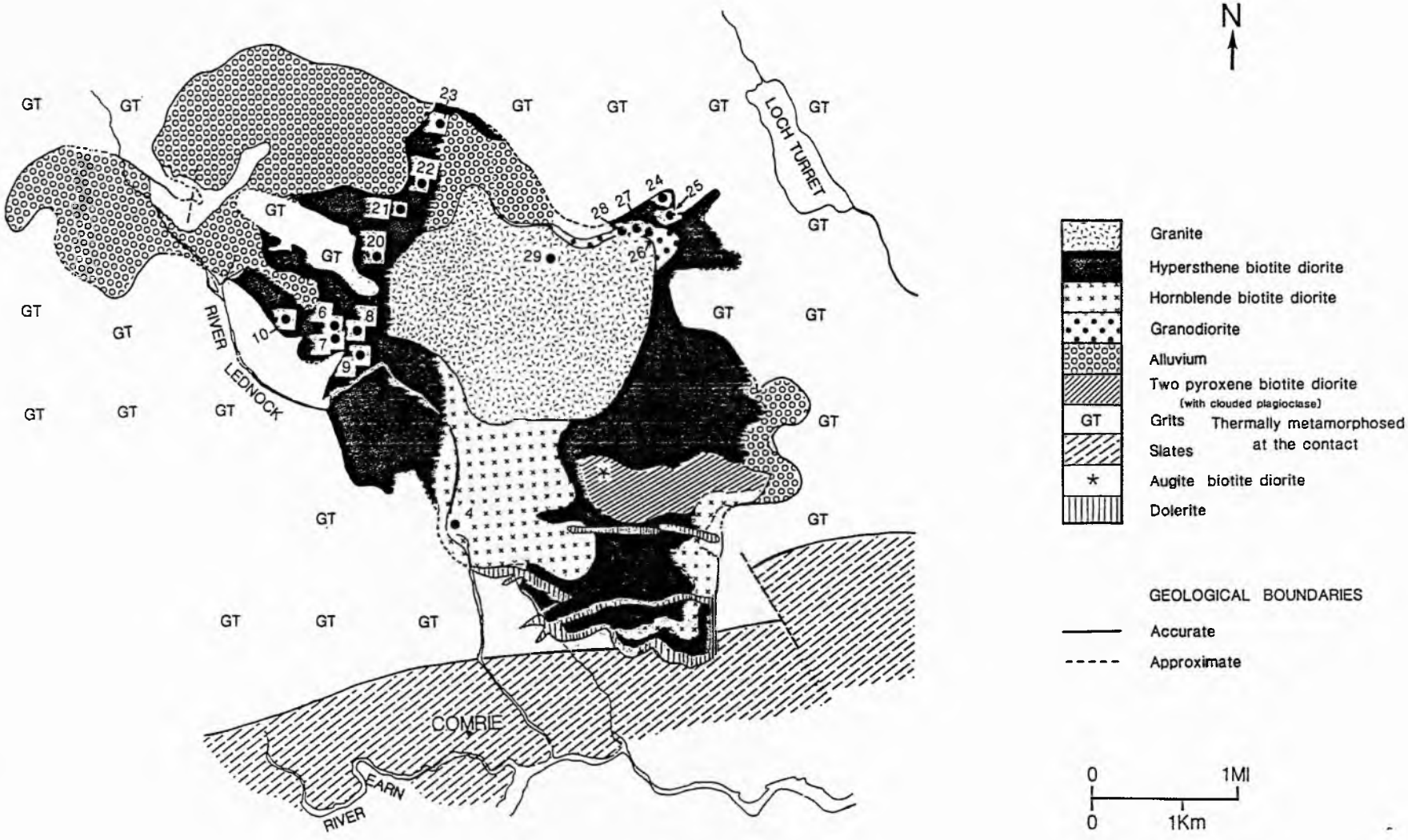

Fig 2.2 Generalised geological sketch map of the Comrie pluton showing studied sample locations after Majid, 1974).

Nicol (1863) was the first to observe the hardening of the slates in the surrounding aureole, and their recrystallisation as they approached the igneous contact. The area was mapped by the Geological Survey on the 6-inch scale, the results appeared on the 1-inch map published in 1888 but no description of the area has been written. Wyllie & Scott (1913) mentioned the plutonic rocks for the first time in their paper about the plutonic rocks of Garabal Hill (p 577). They stated that the rocks of the Glen Lednock intrusion near Comrie have the same nature as the diorite intrusion of Garabal Hill, but differing from the latter in the fact that part had undergone more rapid cooling, and formed the diorite porphyry of Comrie. Tilley (1924) studied the contact metamorphism of the aureole in a classic paper describing the various thermal metamorphic mineral assemblages in the slates and grits.

Wilde (1971) mapped and studied the metamorphic rocks around the intrusion and the different rock types within the complex. He concluded that magma mixing was responsible for the formation of the variety of Comrie rocks (with a gabbroic magma inducing melting of sedimentary material at depth forming granitic magma). Wilde thought that the pyroxene mica diorite is the parental magma of the diorite-granodiorite suite which developed by fractional crystallisation from the original gabbroic magma.

Majid (1974) studied in detail the diorites of the complex petrographically and chemically and divided them into four types (i.e. hypersthene biotite diorite, hornblende biotite diorite, two- pyroxene biotite diorite and augite biotite diorite). He

proposed that the diorites represent a period of calc-alkaline magmatism during the decline of orogenic cycle and concluded that the complex was formed by partial melting within the mantle. He suggested that the pluton belongs to a high alumina basalt magma type.

2.3 The Glen Doll complex

2.3a Introduction:

The complex lies at the head of Glen Clova, it is trisected by the two streams that unite to form the South Esk. The total area of the complex is about 11 Km^2 (Fig 2.3). The complex as a whole is markedly basic, composed of serpentinite, peridotite, basic diorite, diorite, tonalite and granodiorite.

Barrow & Craig (1912) mapped the complex for the 1" map which accompanies memoir no.65 of the Geological Survey of Scotland. Wyllie & Scott (1913) in their Garabal Hill paper mentioned that there were peridotites in the Glen Doll complex, porphyritic diorites with green hornblendes, and some acidic diorites. Mackintosh (1960) and Carroll (1960) prepared short B.Sc. theses on the complex.

2.3b General geology and previous work:

Barrow & Craig (1912) believed the complex to be a series of intrusions of decreasing basicity from serpentinite to acid pegmatite, and that magmatic differentiation took place below present exposure level. Wyllie & Scott (1913) also recognised peridotites in the complex along with porphyritic diorite bearing

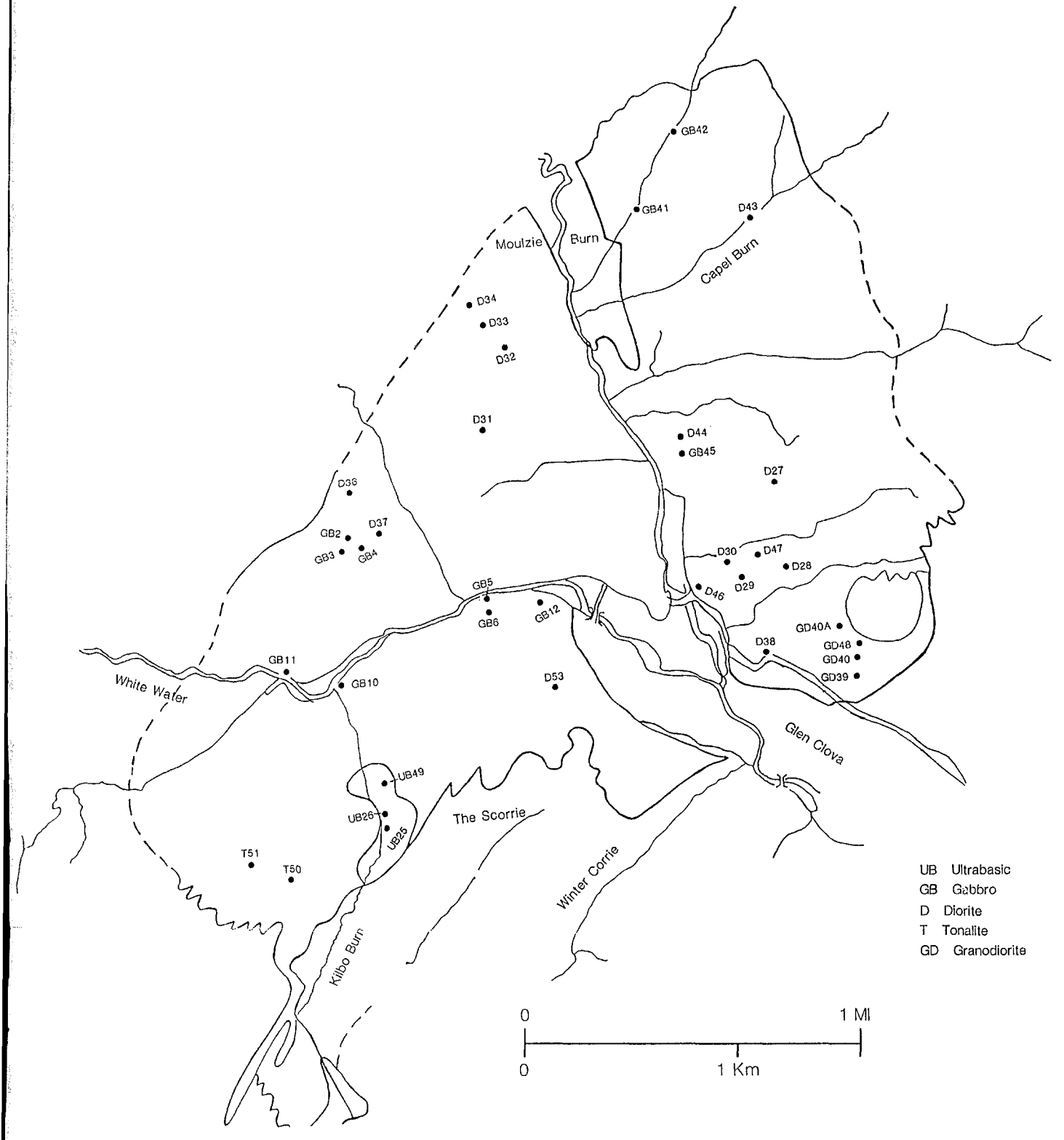

Fig 2.3 Geological map of the Glen Doll pluton taken from the one-inch geological map of Scotland (sheet no 65) showing sample locations and their nomenclature according to the present study. Though detailed petrology of map area still has not been mapped, general areas of petrographic types are clear from the samples.

green hornblende, and some acid diorites.

Mackintosh (1960) divided the southern part of the complex into two parts, the first one in Glen Doll which consists mainly of peridotite, while the second one is made up of rocks found in the Scorrie and adjoining crags (Fig. 2.3). He found that the most continuous exposure of the peridotite was in the White Water and Kilbo Burn. The Scorrie contains mainly tonalites which extend from the mouth of the Winter Corrie along the crags of the Scorrie down to the White Water at the footbridge above the Youth Hostel (Fig 2.3). He described the petrography of the rocks in his area, and found hybrid rocks in the complex, the tonalite underneath the hornblende diorite having a hybridised zone, that this zone of hybridisation extends for about 6 m down into the tonalite. The final product of hybridisation was a melanocratic rock with pink feldspars and even grain size, like the granodiorite. Aplite veins occur to the south-east of the complex. They are from 2.5 cms to 15 cms across and cut the tonalite and the hornblende diorite. Mackintosh (1960) suggested a Lower Devonian age for the complex. He considered the complex to be the plutonic equivalent of the andesite-dacite-rhyolite volcanic association. The tonalite could be a late differentiate from an unspecified parental magma while the more basic rocks are a differentiated series of an earlier fraction from that magma.

Carroll (1960) studied the petrography of diorites in the north-eastern part of the complex with the tonalites and granodiorites.

According to Carroll:

(i) The augite diorite ends in the Moulzie Burn and extends to

the south and east in the Capel Burn (Fig 2.3). There is also a passage from this into hornblende diorite downstream in the Moulzie Burn.

(ii) The tonalite can be seen in the Capel Burn and on the lower slopes of Dog Hillock above the Moulzie Burn.

(iii) The tonalite grades into hornblende diorite, which becomes visibly more leucocratic as it is followed downstream.

(iv) The granodiorite shows sharp contacts against the basic diorite, and also intrudes tonalite.

Carroll suggested that the basic magma underwent crystallisation-differentiation, forming a zone of ultrabasic rocks . The complementary intermediate rocks (the diorites) migrated to areas of lower stress, probably along the line of the Glen Doll Fault. Another acid magma then formed a tonalitic hybrid at depth by reaction with solid basic rocks and it was intruded as a uniform phase before the basic diorites had completely solidified.

2.4 The Glen Tilt complex

2.4a Introduction

The Glen Tilt complex is one of the large masses of the Newer Granites in the Central Highlands and is included in sheet no. 64 of the Geological Survey of Scotland covering an area of nearly 77 Km^2. Two thirds of the complex consists of the Beinn Dearg granite while the remainder is a series of intermediate and basic rocks to the south-east of the complex. The complex was intruded into Moine metasediments.

2.4b General geology and previous work:

A classic intrusion first described by Hutton in 1785 as an example of the intrusive nature of granite and thus its behaviour as a fluid magma. Barrow et al. (1913) wrote an explanation of sheet no. 64 of the Geological Survey of Scotland (Fig. 2.4). They described the country rocks as consisting of quartzite, limestone, dark-schist and calc-silicates which occur above the Forest Lodge in Glen Tilt. The northern half of the complex is composed of coarse-grained granite with dykes of biotite muscovite granite and the southern half is composed of varying types of diorite, but in the south-west Barrow et al. (1913) found a large mass of acid granite, forming the mountain of 'Sron a Chro' (Fig 2.4) near the Tilt valley. These authors did not separate the different types of diorite on the map and postulated that the variations of composition were formed during consolidation of magma, presumably by some process of differentiation.

Deer (1938a) described the diorites and the associated rocks of the complex and analysed some of the rocks although he did not present a map. His principal findings were as follows:

(i) The biotite granite outcrops on the high undulating peaty moorland of Aonach na Cloiche Moire.

(ii) The Sron a Chro granite is red in colour and is a medium to coarse-grained rock.

(iii) Towards the centre of the main granite intrusion, the biotite granite of Aonach na Cloiche Moire gives way to a muscovite-bearing granite, but no contacts between those two

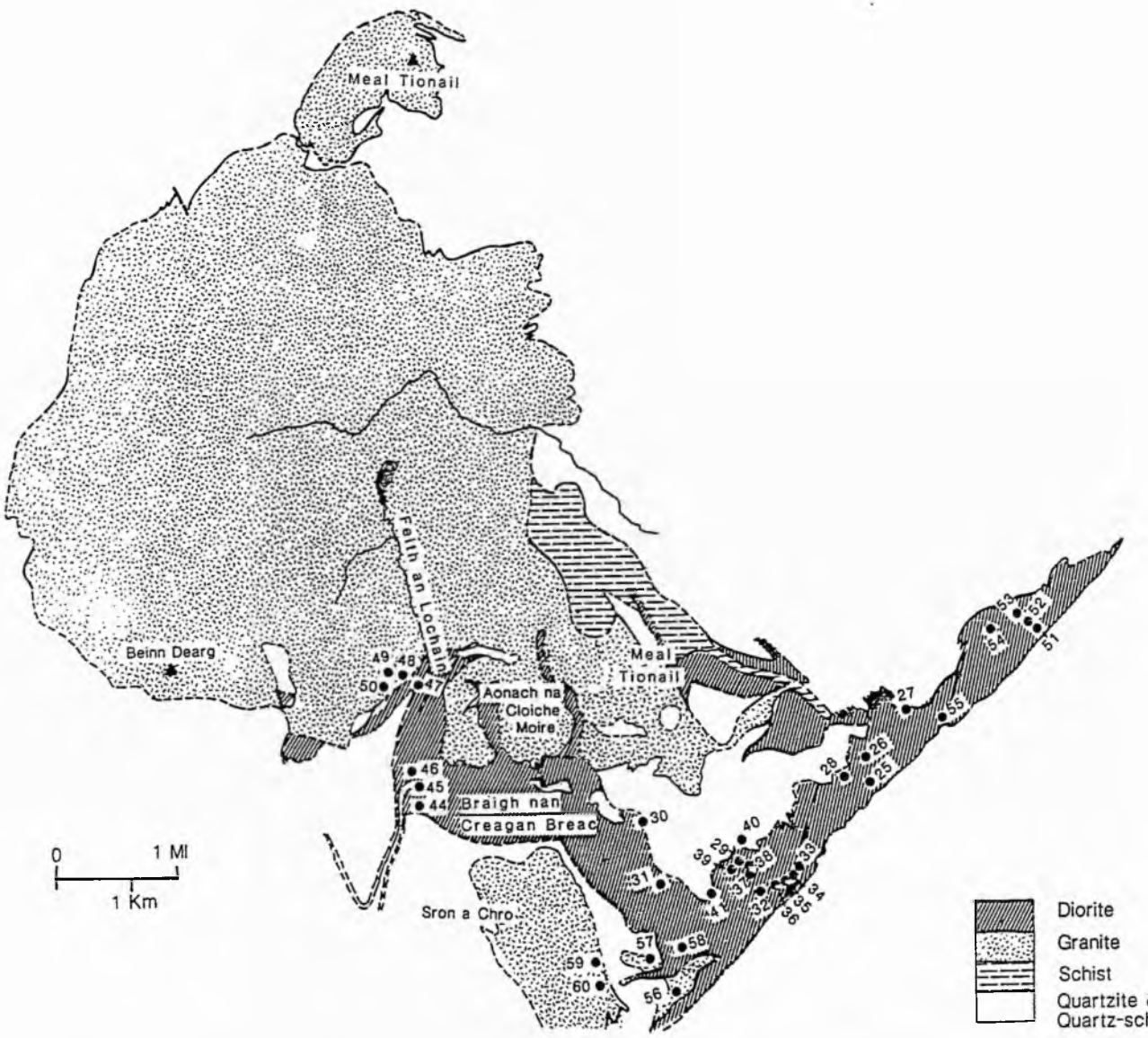

Fig 2.4 Geological Sketch map of the Glen Tilt pluton taken from the one-inch geological map of Scotland (sheet no 64) showing locations of studied samples.

granites were observed.

(iv) A series of granite- diorite hybrids developed close to the granite, along the eastern side of Feith an Lochain and the Braigh nan Creagan Breac and to the south-east of Meal Tionail.

(v) Acid hybrids occur to the east of the intermediate hybrids on the east side of Feith an Lochain.

Deer (1950) described the diorites and appinitic diorites of the complex and found them to extend for 13 kms in a northeasterly direction along the Tilt valley. The coarse and medium appinitic diorites of Garabal Hill-Glen Fyne (Nockolds, 1941) are comparable in chemical composition to the Glen Tilt diorites (Deer, 1950). There is an absence of sharp contacts, each rock passes by a more or less gradual transition from one variety to another. Deer (1953) published another paper on the hornblende-schist and hornblendite xenoliths derived from the Dalradian epidiorites of the country rocks and found in the diorites and the 'Sron a Chro' granites of the Glen Tilt complex.

The geological history of the area is as follows:

(i) Intrusion of diorite and quartz diorite magma.

(ii) Appinite intrusion before the consolidation of the intermediate rocks.

(iii) Intrusion of feldspar and amphibole-feldspar porphyries after consolidation of intermediate rocks.

(iv) Development of faults and shear zones within intermediate plutonic rocks.

(v) Intrusion of Sron a Chro granodiorite and leucocratic

granite magmas.

(vi) Movement along Clais Fhearnaig fault.

(vii) Intrusion of lamprophyres.

(viii) Intrusion of quartz porphyries.

The intrusions invaded Moinian metasediments at sillimanite grade (Winchester, 1974).

2.5 The Cairnsmore of Carsphairn complex

2.5a Introduction:

The Cairnsmore of Carsphairn plutonic complex lies in the NE part of sheet no.8 and adjacent sheets of the 1" Geological map. It is the smallest of the four large plutonic masses intruded into the Lower Palaeozoic rocks of the Southern Uplands of Scotland. The complex occupies a triangular area of nearly 18 Km^2. It intruded Ordovician sediments which are mainly , greywackes and dark shales of flysch facies.

2.5b General geology and previous work

Teall (1899) referred briefly to this complex in "The Silurian Rocks of Scotland" . Teall found the complex to be composed of granitite, hornblende granitite with sphene, quartz augite biotite diorite, and quartz biotite hyperite. Some altered rocks contain pyrrhotite which is associated with norites and hyperites. (Hyperite was a name given to gabbro with equal amounts of hypersthene and clinopyroxene and granitite as a biotite granite).

Deer (1935a) in a paper on the Cairnsmore of Carsphairn

intrusion published a map for the complex (Fig 2.5) and described it as consisting of an outer heterogeneous area of basic group (dioritic hybrids) succeeded by tonalite, then a fine-grained granite-tonalite hybrid and lastly a small central mass of granite. Deer (1935a) chemically analysed some of the rock types in the complex, and the analyses showed the linear interelement variations and the calcalkaline trend. He concluded that the complex has a laccolithic form, and was initiated by the intrusion of a gabbroic magma followed by a tonalitic magma producing the basic hybrids. The tonalite was incompletely crystallised at the time of the third (granite) intrusion, when the acid hybrid was formed. Deer considered the original basic intrusion now to be represented by dioritic lenses, the tonalite itself being a granite-gabbro hybrid formed at depth before intrusion, and the hybridisation of the tonalite was a result of interaction of tonalite with a "partial magma" only, i.e. potash feldspar, quartz, and volatiles.

Deer (1937) found the FeO/MgO ratios in the biotites of the complex increase with acidity of the rocks as the micas change from phlogopite to lepidomelane. The RO/R_2O_3 increases in the biotites of the more basic rocks, Al replaces Mg in Y group and Si in the tetrahedral sites in the more acidic rocks, and the biotites show a close chemical relationship with the host rock. He concluded that they were formed directly from a magmatic liquid though the same relationship does not hold for case of hybridisation.

2.6 The Loch Doon complex

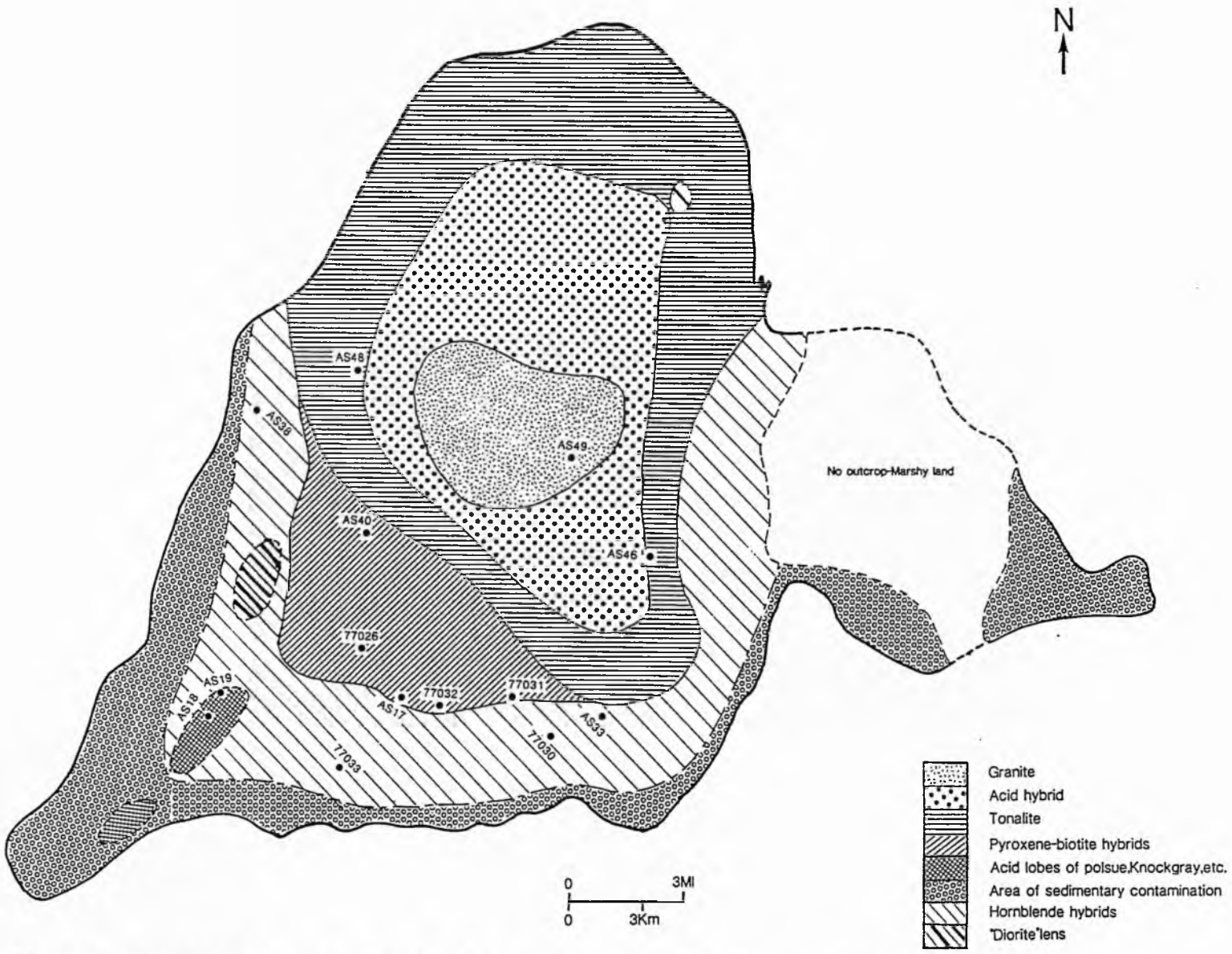

Fig 2.5 Geological sketch map of the Cairnsmore of Carsphairn pluton (after Deer, 1935) showing the locations of samples used in this study.

2.6a Introduction:

The Loch Doon complex intruded Ordovician sediments of flysch facies. It is included in sheet no. 8 of the 1" map of the Geological Survey of Scotland. The complex is hour-glass shaped, about 18.8 kms long in a north-south direction and is 9.7 kms across its widest part and 7.8 kms at its narrowest, occupying an area of about 126 Km^2 (Fig. 2.6).

2.6b General geology and previous work

Geikie (1866), remarked upon the gradual passage from feldspathic greywacke to granite and the similarity of 'nests' (xenoliths in the granite) to the metamorphosed shale of the aureole. His conclusion was that the granite had resulted from alteration (by hydrothermal action) in situ, of certain bedded deposits. Horne (1893) mapped the area for the Geological Survey, with later revision by Peach and Horne (1899). The first detailed petrographic description of the rocks was by Teall in the Memoir of Peach & Horne(1899).

Teall described five rock types: biotite granite, hornblende biotite granite, quartz diorites of the tonalite type, quartz augite diorite, and hyperite. He suggested a magmatic origin for these rocks and compared them with rocks he described in the Cairnsmore of Fleet and Criffel complexes. The differences in composition between the masses he attributed to differentiation in a deep-seated reservoir, before the emplacement of the rocks.

Gardiner & Reynolds (1932) mapped the rocks in the complex

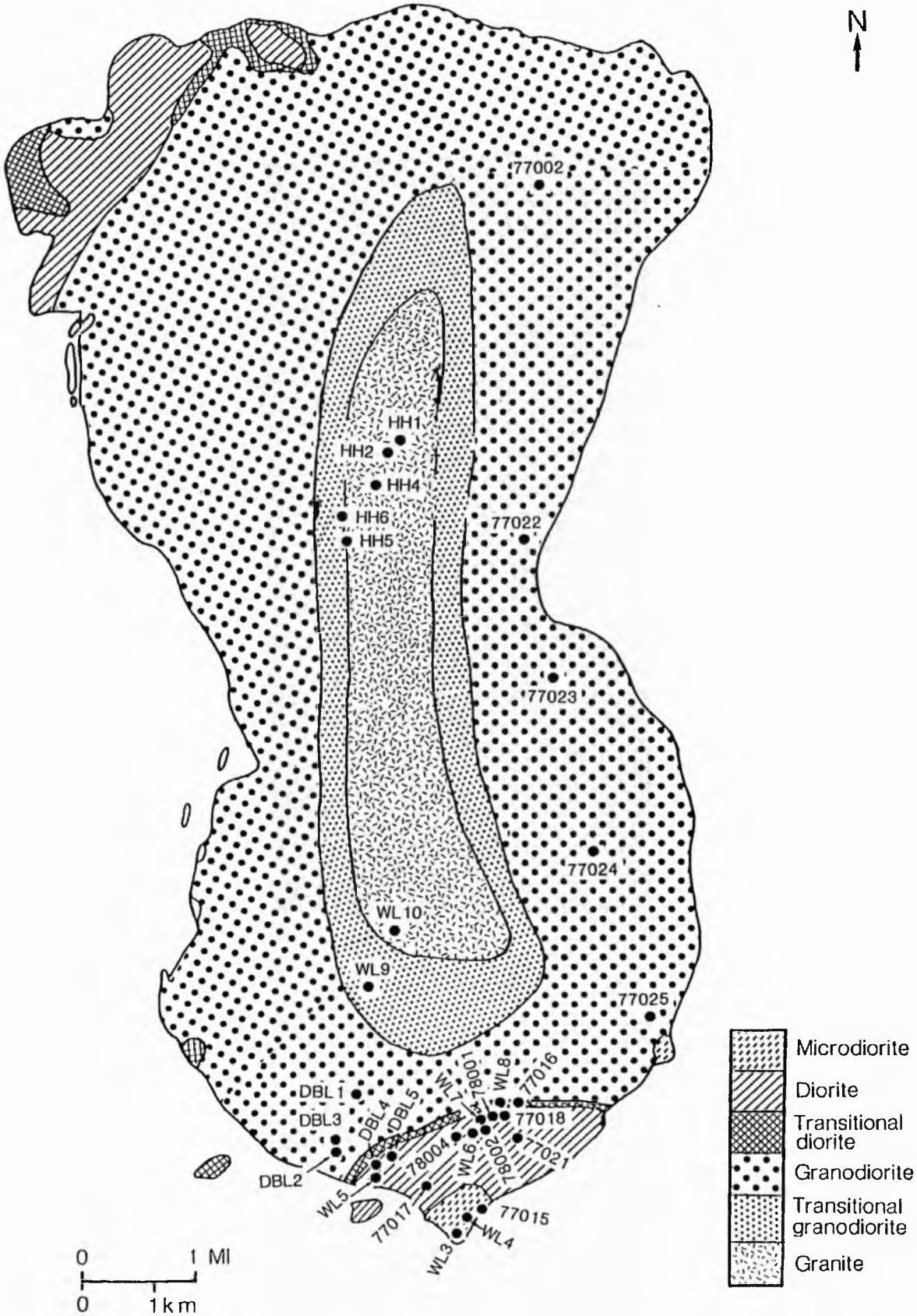

Fig 2.6 Geological sketch map of Loch Doon pluton showing sample locations (after Gardiner & Reynolds, 1932; Ruddock, 1969, and Halliday et al., 1980b).

and illustrated the zonal arrangement of the main rock types. The rocks of the central ridge were described as granites, and those in the NW and S corners were termed norites. The rocks surrounding the granite which form most of the complex were termed tonalite and transitional types for rocks between norite and tonalite, and others between tonalite and granite. These authors reported chemical analyses of each of the three main rock types. Their conclusion, which is different from Teall's conclusion, was that the three main rock types resulted from three successive intrusions in order of decreasing basicity, and hybridisation was found along the norite-tonalite and tonalite-granite boundaries. They found that the metamorphic aureole around the complex indicated subsurface extension of the plutonic rocks at no great depth and that the mass is laccolithic in shape.

McIntyre (1950) studied the NW part of the complex and suggested that the magmatic hypothesis cannot explain the fundamental features of the rocks that he examined. He thought that the granites of the area were formed by granitisation of the country rock sediments. The pyroxene bearing rocks which were thought by Gardiner and Reynolds (1932) to be intrusive norites, were considered by McIntyre to represent basic fronts. McIntyre reported chemical analyses of rocks representing different stages of feldspathisation and basification.

Rutledge (1952) studied the southern part of the complex and suggested that a basic front was present between the granodiorite and the country rocks, on the southern slopes of Buchan Hill in Glen Trool which he described in detail. Rutledge

reported chemical analyses of contact sediments and plutonic rocks, to support his views and his conclusions were similar to those of McIntyre (1950) favouring the metasomatic derivation of the rocks of the complex.

Higazy (1954) studied the behaviour of the trace elements in the plutonic rocks of the complex. He suggested that the relations between the trace elements would not support the idea of magmatic origin for the rocks of the complex, and that the surrounding rocks played an essential role in the development of the acidic rocks, and that the rocks of the complex developed metasomatically. The conclusions of McIntyre, Rutledge, and Higazy are that the granitic rocks were formed in the solid, by transformation in situ, which was brought about by the ionic diffusion of emanations rich in K and Si which arose from the centre of the complex. The pressure caused by expansion of the complex from the centre produced shear planes in the rocks.

Ruddock (1969) studied the petrology and geochemistry of the southern half of the pluton, his main aim was to obtain and interpret detailed information about the chemical variations within this intrusion based on a grid sampling scheme. His analyses were interpreted as differentiation trends from the hypersthene rocks to biotite granite indicating that the rocks all crystallised from the same parental magma (of intermediate composition). The chemical data suggested that the initial magma could have been derived from the association of crustal and mantle-derived material.

Brown et al. (1979) studied the complex using field radiometric mapping to determine the origin and subsequent

evolution of the magma and its relation to the prevailing tectonic regime. They found that the two small norite bodies of Gardiner and Reynolds are actually hypersthene diorites, on the basis of studying their mineralogy, in agreement with the nomenclature of Ruddock (1969) . The tonalite group of Gardiner and Reynolds are ascribed to quartz monzonite and quartz monzodiorite ranging to granite among the more leucocratic varieties. The rocks in the middle of the intrusion are granites with the final stage of magmatic evolution alkali feldspar granite. According to Brown et al. (1979) the gradational change from diorite to granite is the most significant petrographic feature in the complex. They proposed fractional crystallisation of a single parental magma as being responsible for the evolution of the complex. Their evidence from studying the xenoliths and autoliths favours a progressively crystallising and fractionating magma model. Brown et al. (1979) concluded that the Loch Doon parental magma was of monzodiorite composition generated from metabasaltic lower crust or crustal underplate which rose and fractionated progressive skins of diorite, quartz monzodiorite and monzonite leaving granitic residual liquids.

Halliday et al. (1980) studied the Rb-Sr and O isotopic relationships in three zoned Caledonian granitic plutons in the Southern Uplands including Loch Doon. According to these authors the age of the complex is 408 $\pm$ 2 Ma, the pluton gave the lowest $^{87}Sr/^{86}Sr$ initial ratios in the Southern Uplands. The $^{18}O/^{16}O$ ratios show gradation from 'igneous source' to ^{18}O enriched 'sediment source' values with the progression from more basic to more felsic compositions (O^{18} range of 7.87 - 10.32). With each

successive intrusive pulse there were both inter- and intra-plutonic progressions in the magma towards emplacement of a greater metasedimentary-derived and a lesser proportion of metabasite-derived component. The magmas were derived from melting of a source with $^{87}Sr/^{86}Sr$ of about 0.704 which yielded the microdiorite, overlain by source region which had $^{87}Sr/^{86}Sr$ of close to 0.705 which yielded the main diorites. Acid magmas related to the diorites by fractional crystallisation were sealed at depth, where they were probably contaminated to an extent that the $^{87}Sr/^{86}Sr$ ratio was increased to 0.70524 $\pm$ 4. The emplacement of that slightly modified differentiate was accompanied by fractional crystallisation, from the margins inwards, and minor in situ hybridisation within the diorite. Then a final pulse of magma enriched in a metasediment-derived component was emplaced in the centre of the Loch Doon pluton and hybridised with acid magmas formed by differentiation of the granodiorite.

Harmon and Halliday (1980) analysed five samples from the pluton for strontium and oxygen isotopes. They found that both ratios increase from diorite to granite (^{18}O from 7.8 to 10.3 and $^{87}Sr/^{86}Sr$ from 0.7042 to 0.7059. They have suggested magma mixing model is responsible for the origin of the pluton. One magma was derived from the mantle and the other from the Southern Uplands metasediments which could provide the evolved melt of the required Sr isotopic composition.

Tindle and Pearce (1981) studied the complex and concluded that it formed by in situ fractional crystallisation of two distinct magmas. The first one was minor and the more basic in

nature (of quartz diorite composition) followed by the second which was of granodioritic composition. They also noted that apart from a few diorites, which they interpret as almost pure cumulates, and a few granites and aplite granites (which they interpret as almost pure liquids), most of the granitic rocks have a crystal mush composition. The mechanism of the fractional crystallisation could have involved extensive filter pressing in addition to accumulation of phenocrysts.

Brown et al. (1984) used trace element abundances in subduction - related granites in an examination of the Siluro - Devonian intrusions and concluded that the Loch Doon pluton represents "normal continental arc" magmatism characterised by diorite, tonalite, monzogranite, granite and intermediate Rb, Th, and U values. Halliday (1984) gave new Nd isotopic data and found that εNd_t ranges from -1.0 in the diorite to -1.4 in the granodiorites suggesting significant crustal involvement in the genesis of this pluton.

2.7 Summary and comparison

The above plutons show regional variations, whereby the Southern Uplands plutons show good concentric zoning of petrographic types ranging from diorites in the outer margins through to granites in the centre. Plutons studied from the southern Grampian Highlands do not show this regular zoning (except for the Comrie pluton which is rather concentric) and the distribution of the outer parts of diorites with granodiorites or granites is geographically irregular.

Some of the plutons have some more basic and ultrabasic

rocks like the Garabal Hill-Glen Fyne and Glen Doll as has been mentioned in earlier sections. Appinitic rocks are present only in the Garabal Hill and Glen Tilt plutons.

CHAPTER 3

PETROGRAPHY

3. Introduction:

The petrographic descriptions of the complexes are arranged in order of apparent intrusive sequence for each rock type. The samples described were selected as being representative of their types and differences within the same general type are outlined at the end of the description of the representative sample.

Streckeisen's (1976) classification is used for petrographic nomenclature , and for the diorites in fields 10* and 10 of his felsic classification the mafic minerals have been used in this study to further classify the different types of diorites. Occasionally diorites have more than 5% quartz and the boundary between the two fields is a dashed line (Streckeisen, 1976, p 15) which allows some flexibility in assigning appropriate names. Staining was used to differentiate between orthoclase and plagioclase for samples used in modal analysis. (see Appendix A for details).

3.1 The GARABAL HILL - GLEN FYNE COMPLEX

Introduction:

The complex as a whole is formed of ultrabasic rocks mainly of peridotite (wehrlite) type; gabbros which contain some olivine; diorites with pyroxene , amphibole and biotite as the main mafic minerals, appinitic diorites and granodiorites. Modal analyses are listed in Table 3-1, and plotted on Figs 3-1a and 3-1b.

3.1.1 The Ultrabasic Rocks

Table 3-1: Modal analyses of the Garabal Hill - Glen Fyne rock types

Sample No	Olivine %	Opx %	Cpx %	Amph %	Biot %	Plag %	Alk-feld %	Qz %	Opaque %	Accessories %	Rock type
GH36 (a)	44.6	-	55.4	-	-	-	-	-	-	-	Peridotite (wehrite)
GH10	2.17	7.84	24.75	-	14.88	43.6	-	1.09	2.55	3.12	Gabbro
GH3	6.0	7.4	17.3	-	16.8	48.3	-	0.9	3.0	0.3	Two-pyroxene biotite diorite
GH5	2.9	1.2	17.3	4.8	14.3	49.8	1.6	4.2	3.3	0.6	" "
GH26	-	-	-	15.9	19.7	57.4	-	6.4	0.4	0.2	Hornblende biotite diorite
GH28	-	-	-	9.0	7.5	42.8	18.1	21.2	0.6	0.8	Medium granodiorite
GH39	-	-	-	6.3	5.3	43.3	20.3	22.2	1.2	1.4	Porphyritic granodiorite

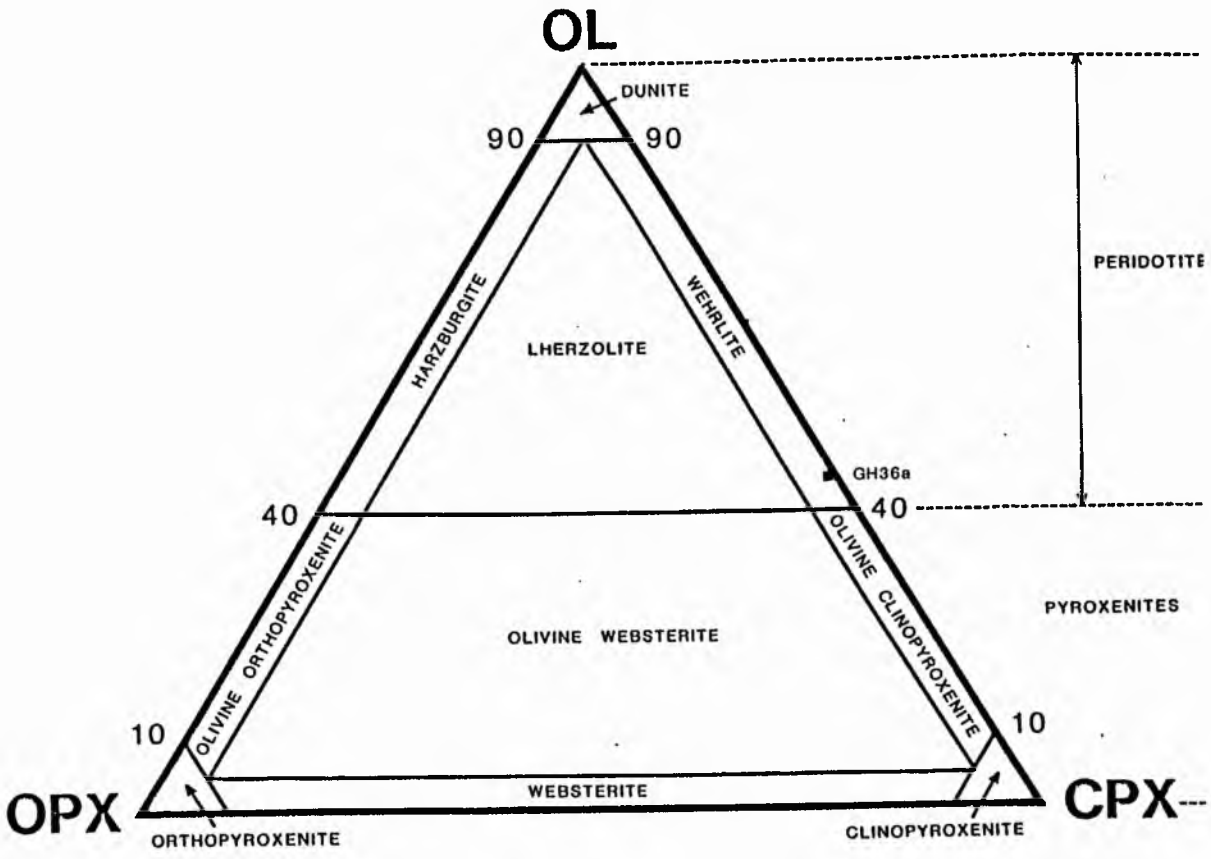

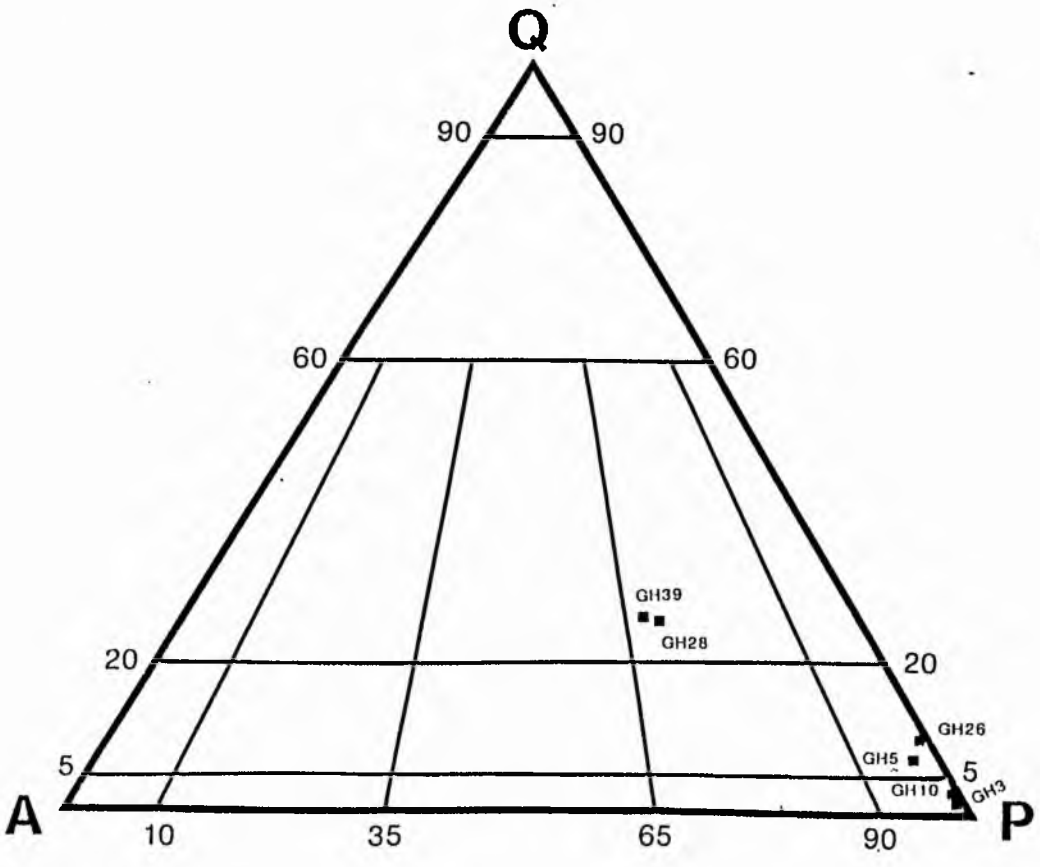

Fig 3.1a,b Modal classification and nomenclature of the Garabal Hill - Glen Fyne rock types (after Streckeisen, 1976)

Peridotite:

Representative sample: GH36A

Petrographic name: Medium-grained serpentinised wehrlite.

Plates 3-1a and 3-1b.

Description:

The hand specimen is dark grey to black, medium grained, weathers with a brown crust, and show numerous small shining crystals of pyroxene. It is serpentinised, and the colour of a fresh-broken surface is greyish-olive because of the serpentine. The mode is given in Table 3-1.

Olivine (approximately 45%) forms anhedral grains up to 3 mm, many of which are serpentinised. The olivine grains are highly fractured with iron oxides and serpentine replacing olivine along the fractures. Clinopyroxene (diopside, approximately 55%) forms anhedral grains and elongate crystals (up to 5 mm) which are light brown in colour and often show schiller structure. Most crystals contain iron oxide in the form of small rods. Hornblende (accessory) forms very small anhedral grains associated with diopside and usually brown in colour. Biotite (also accessory) forms small crystals again associated with replacement of diopside. Small primary opaque oxides occur associated mostly with diopside, abundant opaque oxides result from breakdown of the primary olivine and pyroxene to serpentine.

This is an ultramafic rock with serpentinised olivine and pyroxene grains of medium grain size probably representing a cumulate (plate 3-1) rock with the olivine preceding pyroxene both of which are early phases. It has no observable preferred orientation.

Plate 3-1a: Sample GH36a. Serpentinised peridotite (wehrlite) showing olivine (along the fractures) and clinopyroxene, some are twinned. Fractures are filled by serpentine and iron oxide.
Ppl, x 20.

Plate 3-1b: As 3-1a in cpl

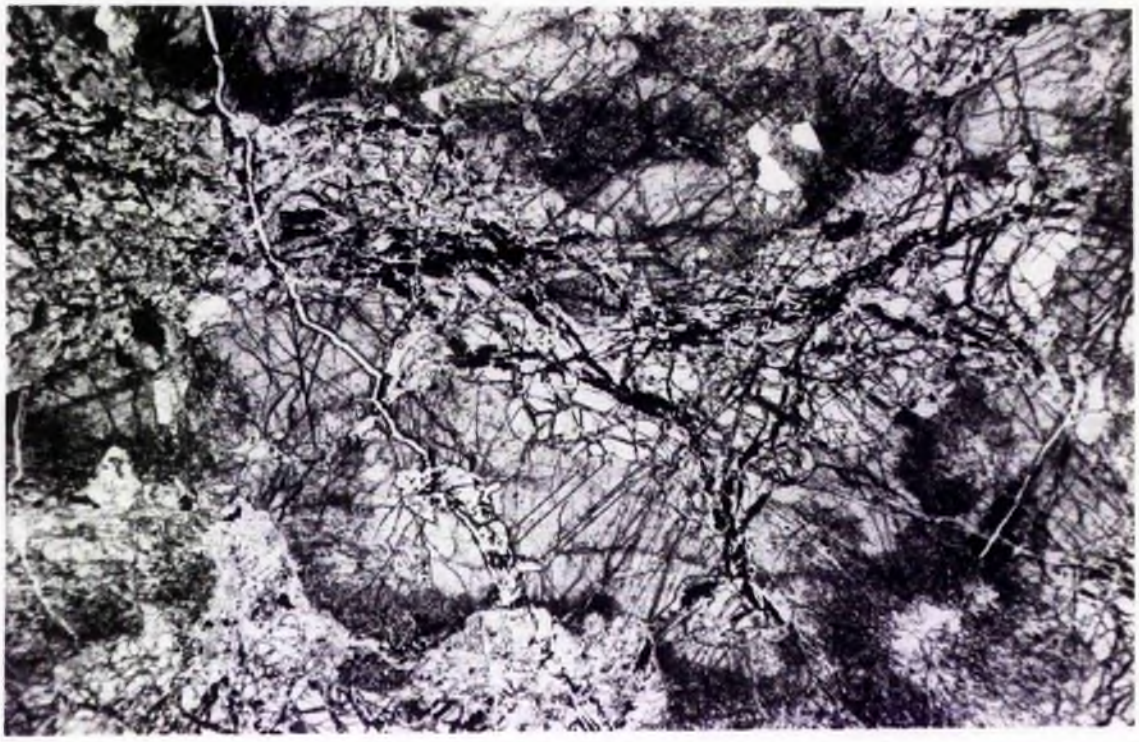

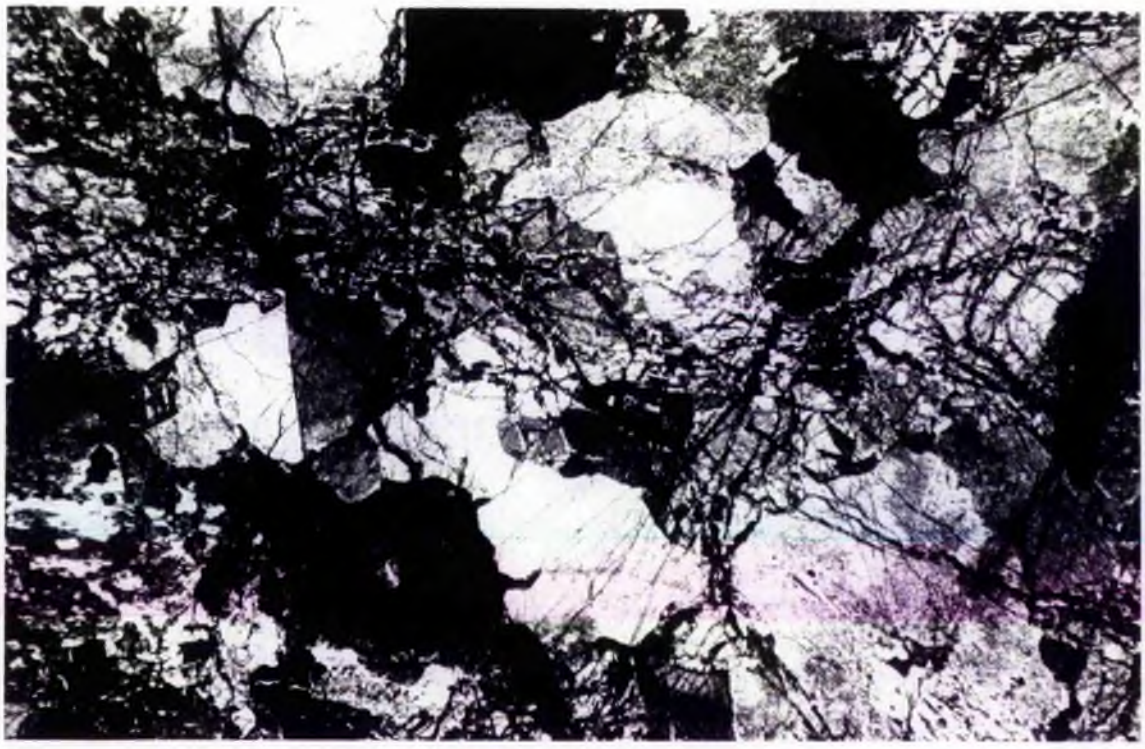

3.1.2 The Basic Rocks

Gabbro

Representative sample: GH10

Petrographic name: Medium-grained gabbro.

Plates 3-2, 3-3, 3-4a, and 3-4b

Description:

In hand specimen the rock is grey in colour, medium-grained with shining phenocrysts of pyroxene and mica.

Olivine (approx. 2% modal) forms anhedral grains (1-3 mm) which are highly fractured, altering along the fractures to secondary magnetite and the outer rims to brownish red iddingsite. Some are altered to serpentine. Orthopyroxene (about 8%) forms small elongate crystals sometimes subhedral crystals (up to 1.0 mm) and as very fine grains in the matrix (0.1 to 0.2 mm). It displays pink pleochroism and some have exsolution lamellae of diopside. Clinopyroxene (24.8% modal) forms subhedral to anhedral phenocrysts (maximum 3.0 mm) and in the matrix (<1.0 mm). It varies from pale green to pale brown in colour, some of the grains are twinned, others have lamellar texture. Biotite (about 15%) forms elongate crystals (up to 4 mm) having greenish brown to dark brown colour, some irregular grains are present having orange to dark brown colour. Plagioclase (44%) forms elongate crystals (up to 2.0 mm) and some small grains (<1.0 mm) in the matrix of labradorite composition (An 52). They are cloudy in p.p.l. due to minute inclusions of iron ores and micas, some show alteration to sericite and saussuritised. Quartz (1.0% modal) is a late-stage

Plate 3-2: Sample GH10. Medium grained porphyritic gabbro, where the clino- and orthopyroxene phenocrysts are surrounded by a matrix of plagioclase, biotite, quartz and small pyroxene grains. Plagioclase shows preferred orientation.
Cpl, x 12.

Plate 3-3: Sample GH10. Olivine phenocryst surrounded by a rim of iron ore, and altered along the fractures to serpentine and iron oxide.
Cpl, x 40.

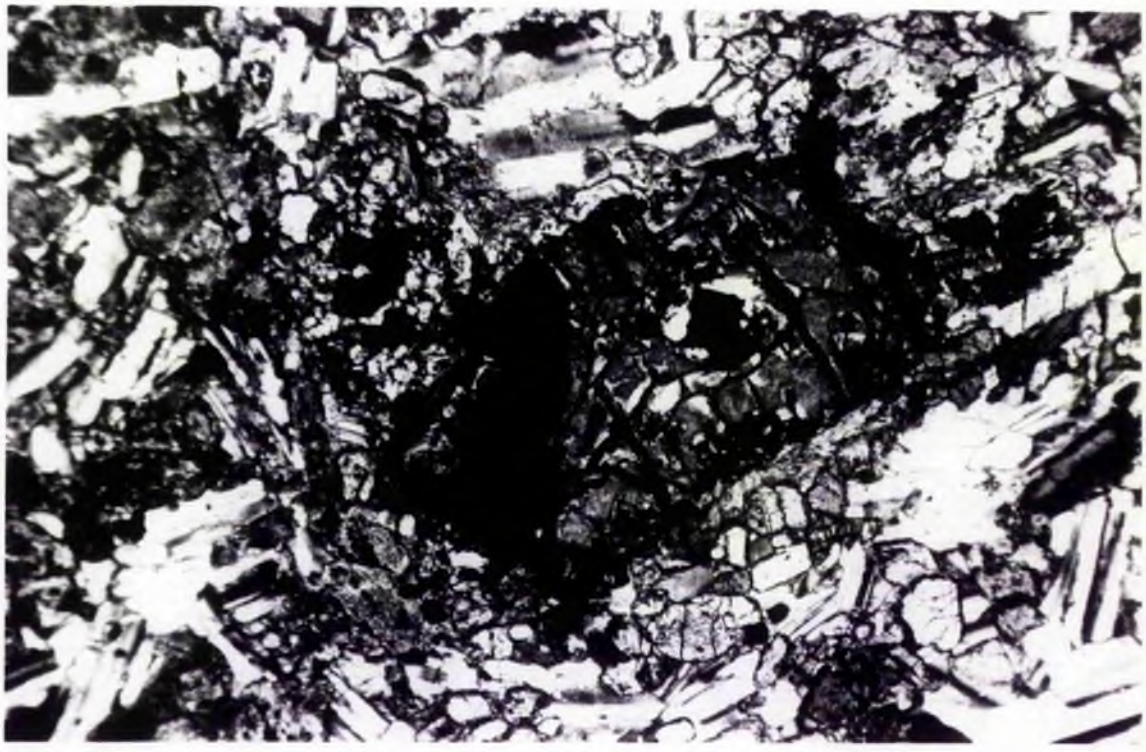

Plate 3-4a: Medium grained porphyritic gabbro Sample GH10, showing olivine overgrown by several pyroxene grains in a large phenocryst. The matrix is formed of plagioclase, ortho- and clinopyroxene, and biotite grains. Ppl, x 20.

Plate 3-4b: As 3-4a in cpl

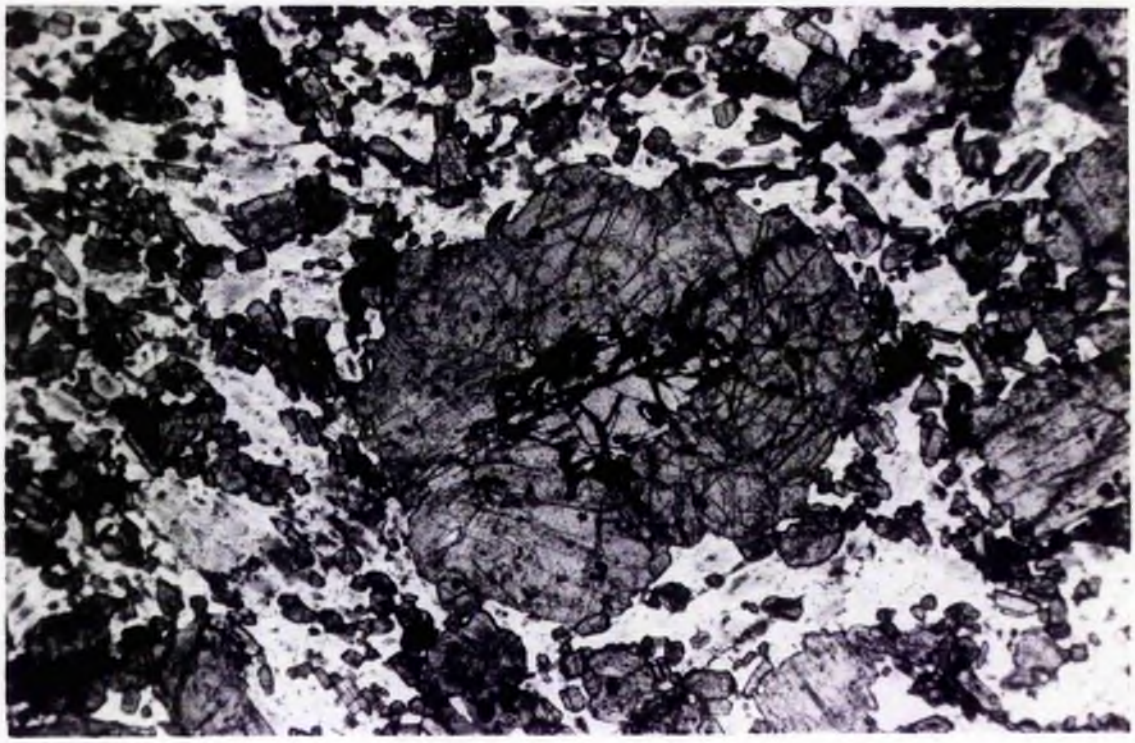

mineral forming grains interstitial to all others (<1.0 mm). Small opaque minerals, including magnetite and ilmenite form subhedral to anhedral grains (2.5% modal). Abundant opaque oxides result from alteration of the primary olivine and pyroxenes.

This is a basic rock with olivine, pyroxene and biotite of medium-grain with olivine preceding pyroxene (Plates 3-3a and b). It has a porphyritic texture with phenocrysts of olivine and pyroxene surrounded by a matrix of plagioclase, biotite, quartz and small pyroxenes. Plagioclase shows preferred orientation.

Additional samples of this type are GH22, GH23 and GH24 which are altered, with clinopyroxene altered to secondary amphibole and talc; the plagioclase is sericitised and saussuritised. Sample GH21 is a gabbro with clinopyroxene rimmed by amphiboles, few hypersthenes and brown amphibole, biotite and plagioclase. Clinopyroxene is altered to secondary amphibole, other mafics are altered to chlorite and secondary iron oxide.

3.1.3 The Intermediate Rocks

DIORITES

The dioritic rocks are medium grained with abundant plagioclase. The mafic constituents are hypersthene, augite, hornblende, biotite and some olivine. Quartz and alkali feldspar are present, quartz often more than 5% modal of the rock but it is more appropriate to name the rocks according to the principal ferromagnesian minerals. The composition of the plagioclase is andesine from An49 to An30, so that these rocks are diorites in any rock classification. Clouding of plagioclase is quite a common feature in the diorites which may be due to small inclusions of iron

ores and micas. Most of the rocks are comparatively fresh but alteration of pyroxene , amphibole and biotite to talcose material, chlorite and secondary magnetite occurs. Plagioclase is altered sometimes to sericite and saussurite.

The diorites can be classified into the following types:

1. Two-pyroxene biotite diorite.
2. Hornblende biotite diorite.

3.1.3a Two-pyroxene biotite diorite

Representative Sample: GH3

Petrographic name: Fine to medium-grained porphyritic diorite.

Plates 3-5 to 3-10

Description:

The rock is grey in hand specimen, of fine to medium grain with some crystals of pyroxene and dark phenocrysts of olivine.

Olivine (6% modal) forms small-medium phenocrysts (up to 4 mm), which are highly fractured, altered to serpentine and magnetite along the fractures and usually rimmed by clinopyroxene, though some are rimmed by opaque minerals. Orthopyroxene (hypersthene, about 7% modal) forms small elongate crystals (maximum 1.0 mm) and some subhedral grains having pink pleochroism. Some show exsolution lamellae of clinopyroxene. Clinopyroxene (17% modal) forms subhedral to euhedral phenocrysts (up to 1.5 mm) which are pale green to pale brown in colour, with another generation forming small anhedral grains (<1.0 mm) in the matrix. Biotite (16.8% modal) forms elongate crystals (maximum 2.0 mm) with some small grains (<1.0 mm) in the matrix, having yellow to dark brown pleochroism. Some irregular

Plate 3-5a: Sample GH3- Porphyritic pyroxene biotite diorite, showing twinned euhedral clinopyroxene phenocrysts in a matrix of plagioclase, biotite and small ortho and clinopyroxenes.
Ppl, x 40.

Plate 3-5b: As 3-5a in cpl

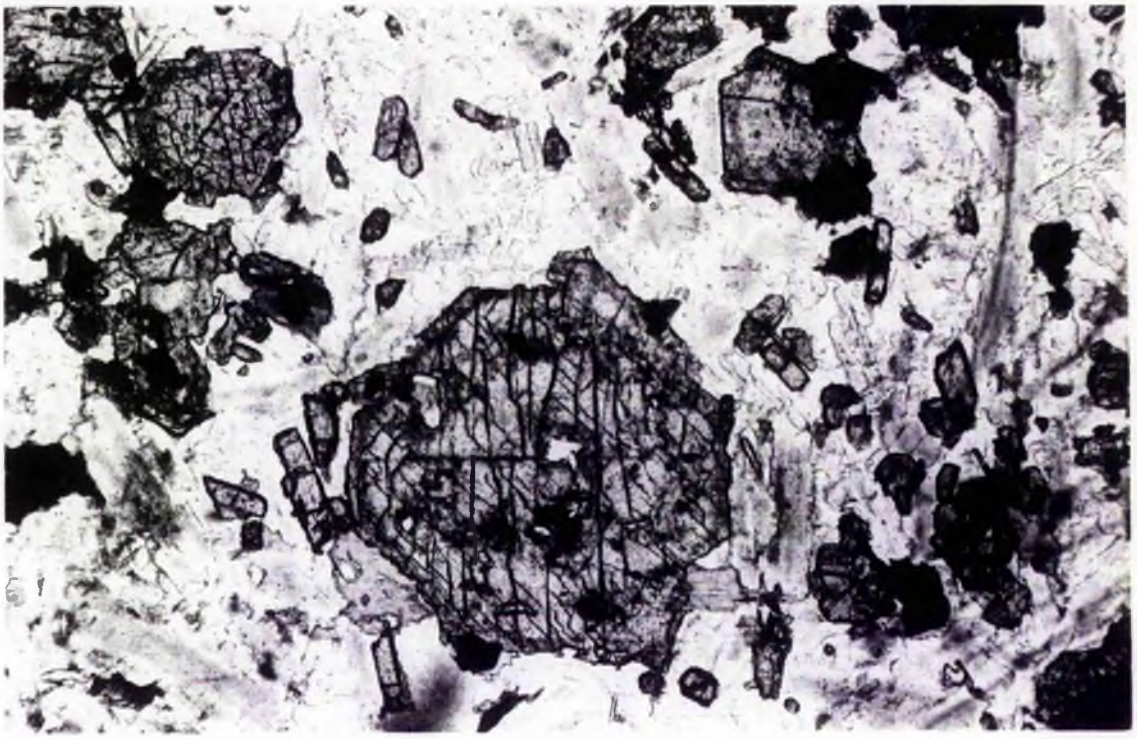

Plate 3-6: Porphyritic diorite, sample GH3, shows olivine surrounded by pyroxene grains in a large phenocryst, in a groundmass of plagioclase, biotite and small pyroxene crystals.
Ppl, x 40.

Plate 3-7: Sample GH3, showing olivine and pyroxene phenocrysts in a groundmass of plagioclase, biotite, small pyroxene grains and quartz. Plagioclase shows some preferred orientation.
Cpl, x 20.

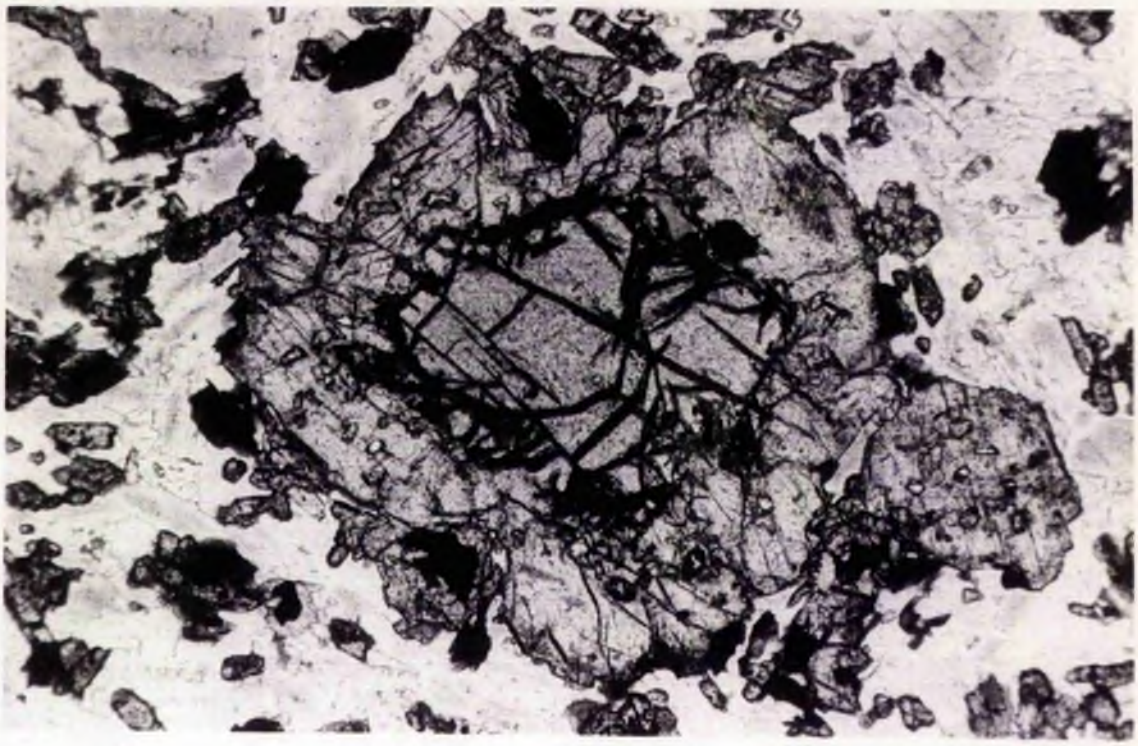

Plate 3-8: Sample GH1. Porphyritic pyroxene biotite diorite showing olivine phenocryst surrounded by magnetite rim, carbonates and talc in a matrix of plagioclase, biotite and pyroxene.
Cpl, x 12.

Plate 3-9: Sample GH5. Porphyritic diorite having corona texture where a zoned clinopyroxene phenocryst in the middle is surrounded by a rim of hornblende.
Cpl, x 40.

Plate 3-10: Sample GH7. Medium grained porphyritic pyroxene biotite diorite. The large phenocryst of clinopyroxene in the middle is surrounded by a rim of hornblende (corona texture) in a groundmass of plagioclase, biotite and small pyroxene grains.
Ppl, x 40.

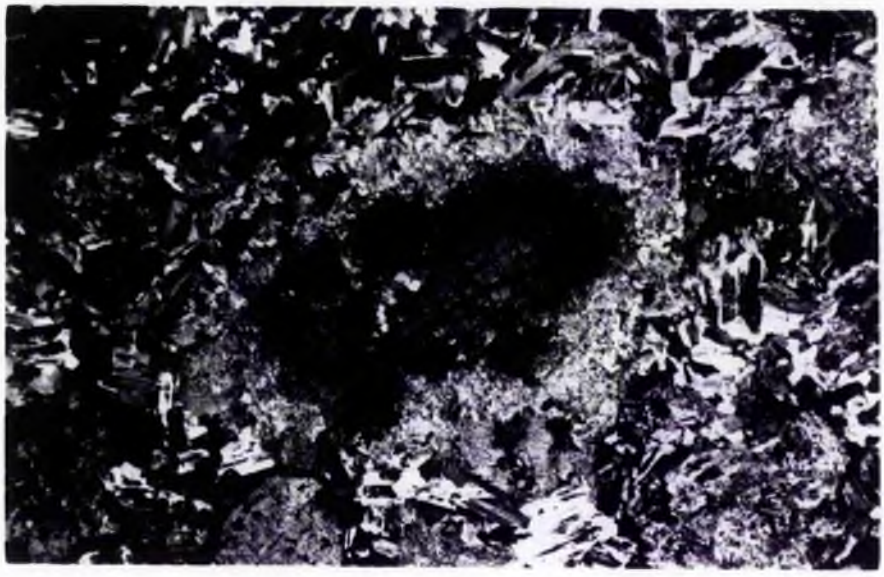

grains are present having orange to dark brown pleochroism. Plagioclase (48% modal) forms elongate crystals (up to 1.5 mm) of andesine composition (An 41.0 average) and small grains in the matrix. They have cloudy appearance in plane polarised light due to very small inclusions of iron ores and micas, some show sericitisation and the slide as a whole has preferred orientation. Quartz (accessory) is the last mineral forming anhedral interstitial grains (<1.0 mm). Apatite accessory forms fine elongate crystals (<1.0 mm) associated with biotites. Opaque minerals (accessory), mainly ilmenite and magnetite, form anhedral grains (<1.0 mm) associated mainly with biotite. Secondary iron oxides are found as alteration product of mafic minerals.

This is an intermediate rock with olivine, ortho and clinopyroxene, biotite and plagioclase of fine to medium grain size having porphyritic texture. Olivine and both pyroxenes form phenocrysts in a matrix of plagioclase, biotite and fine-grained pyroxene. Clinopyroxene is of two generations, one early medium euhedral crystals and the other fine-grains in the matrix (Plates 3-5a and b). Olivine is the first mineral to crystallise and is surrounded by pyroxenes (plate 3-6). Plagioclase shows preferred orientation (plate 3-7).

Additional samples of this type are GH5, GH1, GH6 and GH7. GH5 contains less orthopyroxene than GH3 and contains green amphibole which forms small separate crystals as well as rims for pyroxenes (corona texture, plate 3-9). In addition there are alkali feldspars which are interstitial to plagioclase. Sample GH1 is like GH3 but the mafic minerals are mostly altered to chlorite, serpentine, talc and secondary iron oxides. Some of the plagioclase crystals are altered

(especially in the cores) to sericite and saussurite. It contains green hornblende rimming the pyroxenes. Samples GH6 and GH7 are porphyritic pyroxene biotite diorite but the pyroxene phenocrysts are rimmed by hornblende forming a corona texture (plate 3-10).

3.1.3b Hornblende biotite diorite:

Petrographic name: Fine to medium grained hornblende biotite diorite.

Representative sample: GH26

Plates 3-11a, b to 3-12.

Description:

The rock is fine to medium grained in hand specimen grey in colour, with abundant dark green hornblende crystals.

Hornblende (15% modal) forms anhedral grains (up to 3.0 mm) and small grains in the matrix less than 1.0 mm, they sometimes form a rim for the clinopyroxene (accessory). Generally hornblende is largely altered to chlorite and secondary iron oxides. Biotite (19.7% modal) forms elongate crystals (up to 3.0 mm) and small grains (<1 mm) in the matrix containing inclusions of apatite, zircon, sphene and iron oxides. Local alteration to chlorite is present. Some irregular biotites associated with hornblende have greenish brown pleochroism which may have resulted from hydrothermal alteration. Plagioclase (57.4% modal) forms elongate crystals (maximum 3.0 mm) of andesine composition (An37 average) having cloudy appearance and some fine grains in the matrix. It is mostly fresh but some grains are slightly altered to sericite and saussurite. Quartz (6.4% modal) is a late-stage mineral forming interstitial anhedral grains (up to 1.5 mm). Zircon (accessory) forms small anhedral to subhedral crystals

Plate 3-11a: Sample GH26. Medium grained hornblende biotite diorite, showing strong preferred orientation. The rock is formed of hornblende, biotite, plagioclase and quartz.
Ppl, x 12.

Plate 3-11b: As 3-11a in cpl.

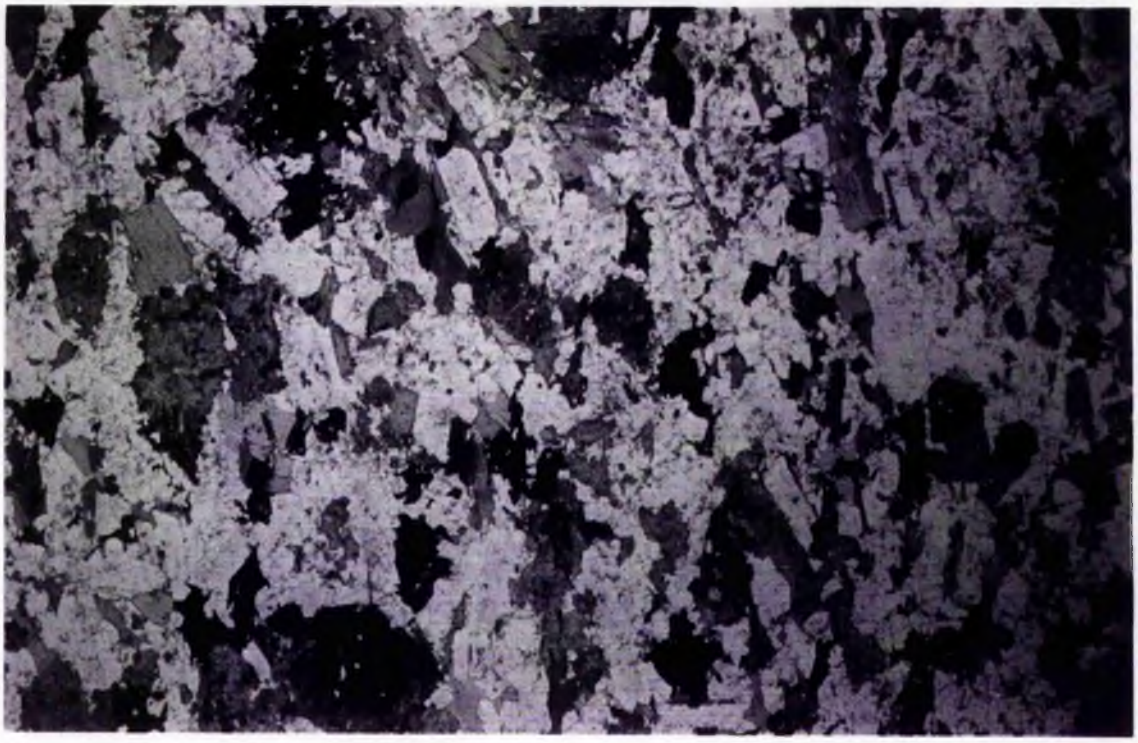

Plate 3-12: Sample GH20. Fine to medium grained hornblende biotite diorite, showing preferred orientation. The photomicrograph showing plagioclase, biotite hornblende with small clinopyroxene grains.
Cpl, x 20.

Plate 3-13: Sample GH11: Appinitic diorite showing the large grain of hornblende in the middle replaced by iron oxide.
Cpl, x 20.

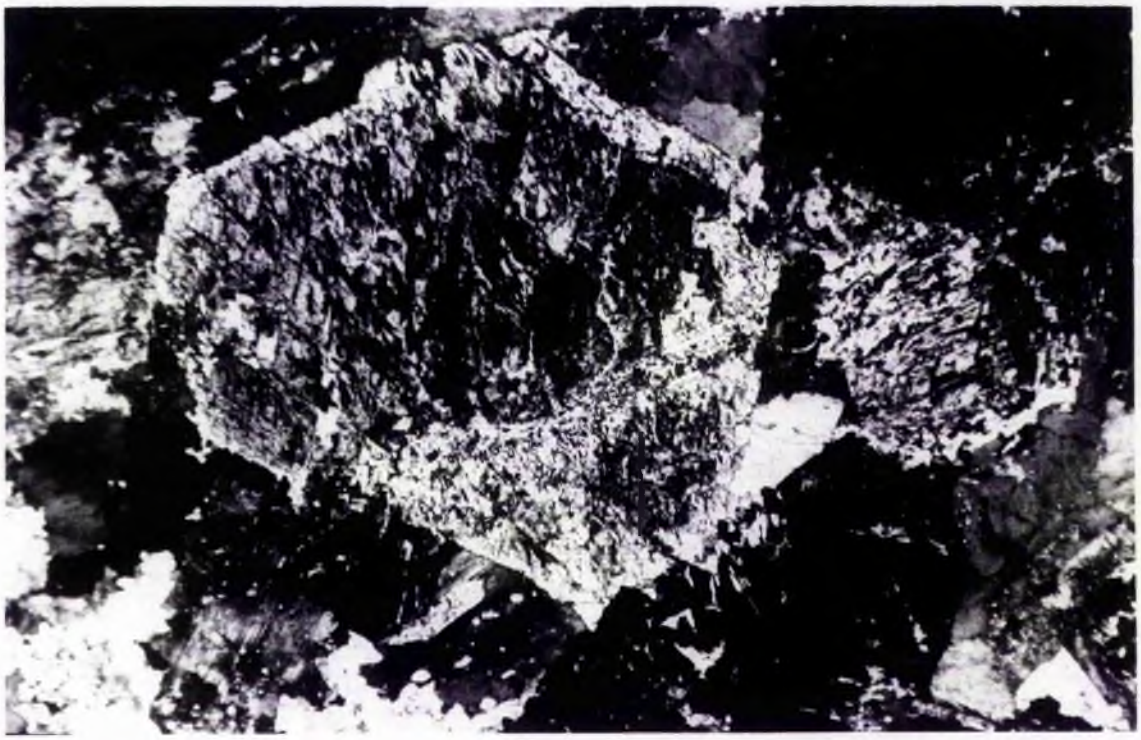

(<1.0 mm) surrounded by pleochroic haloes associated with biotite and amphibole. Apatite (accessory) forms elongate crystals and some subhedral grains (<1.0 mm) associated with biotite. Sphene (also accessory) forms anhedral small grains associated with biotite. Small primary opaque iron oxides occur as anhedral grains (<1.0 mm) associated mainly with biotite. Abundant opaque oxides result from the alteration of the primary mafic minerals.

This is an intermediate rock with hornblende, biotite, and plagioclase of medium grain size, having an observable preferred orientation (Plates 3-11a, b).

Additional samples of this type are GH20, GH25, GH27, GH32, GH34, GH37 and GH38. Sample GH20 and GH27 are somewhat altered containing pyroxene (plate 3-12). Sample GH25 contains no pyroxene. Samples GH37 and GH38 are coarse grained diorites with rather more quartz than normal, in GH37 alkali feldspars have myrmekitic margins.

3.1.4 Appinitic diorite:

Representative sample: GH11

Petrographic name: Medium grained appinitic diorite

Plate 3-13

Description:

In hand specimen, the rock is coarse grained and markedly porphyritic, with large dark greenish-black amphibole in a matrix of biotite, feldspar and quartz.

Amphibole (hornblende, approximately 62%) forms large plates (up to 7.0 mm), it generally has a pale brown colour though is sometimes green. It has poikilitic texture with biotite, and shows alteration to hematite forming tiny rods with some epidote. Biotite

(approximately 2%) forms elongate crystals (max 1.0 mm) and some anhedral grains replacing amphibole. It shows local alteration to chlorite. Plagioclase (approximately 27%) forms elongate crystals (up to 3.0 mm), sometimes forming clusters surrounding amphibole. Alteration to sericite and saussurite is quite common. Quartz (8%) is a late-stage mineral forming anhedral grains (up to 3.0 mm) with undulose extinction. Zircon (accessory) forms anhedral grains. Apatite (accessory) forms elongate crystals (<1.0 mm) associated with hornblende. Sphene (accessory) forms fine anhedral grains and some are irregular with pale reddish brown pleochroism. Some grains are associated with the opaques. Small primary opaque oxides form anhedral grains, of magnetite and ilmenite, abundant iron oxides result from the alteration of the primary hornblende.

This is a coarse grained intermediate rock with hornblende as the main mafic mineral forming almost two thirds of the rock and classified as appinitic diorite. It has a porphyritic texture.

3.1.5 Medium granodiorite

Representative sample: GH28

Petrographic name: Medium grained granodiorite.

Plates 3-14 to 3-15

Description:

In hand specimen, the rock is medium grained, light coloured, hornblende and biotite forming medium dark crystals while feldspars are pink in colour.

Amphibole (hornblende, 9% modal) forms largely prismatic crystals (max 4 mm) with some in aggregates. It has greenish brown pleochroism and some grains show replacement by biotite. Biotite

Plate 3-14: Sample GH28. Medium grained granodiorite showing a twinned phenocryst of hornblende in a matrix of plagioclase, biotite, fine grained hornblende and quartz.
Cpl, x 20.

Plate 3-15: Sample GH28. Medium grained granodiorite showing myrmekitic texture in the middle at the edge of a plagioclase crystal.
Cpl, x 100.

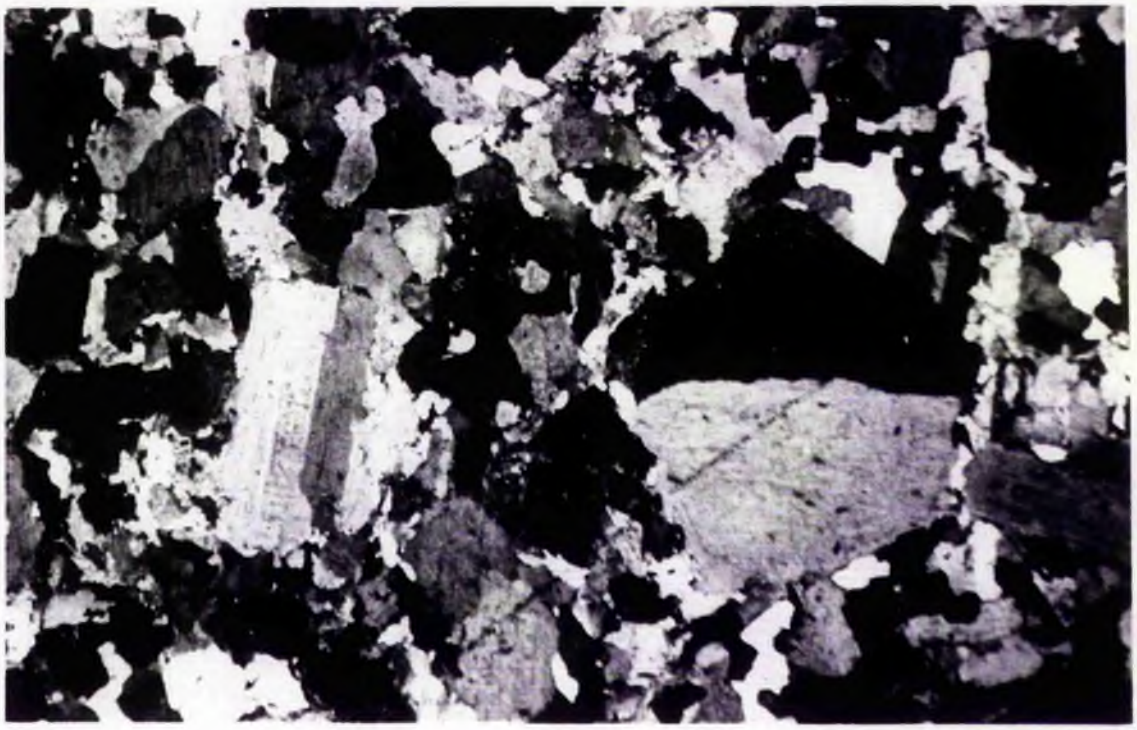

(7.5% modal) forms anhedral to elongate crystals (max 3 mm) with yellowish brown pleochroism. Some other biotites have orange to greenish brown pleochroism (up to 1 mm). Minor alteration to chlorite is present. Plagioclase (42.8 % modal) forms subhedral to elongate crystals (up to 5.0 mm), some oscillatory zoned. It shows alteration to sericite. Alkali feldspar (18.1% modal) forms anhedral grains having perthitic texture. Myrmekites are sometimes present at the edges with plagioclase, (plate 3-15). It is a late-stage mineral interstitial to other minerals. Quartz (21.2% modal) is the last mineral to form as anhedral interstitial grains with undulose extinction. Zircon (accessory) forms small euhedral to subhedral grains, associated with biotite and hornblende. Apatite (accessory) forms small subhedral and elongate crystals associated with hornblende and biotite. Sphene (accessory) forms euhedral grains with acute rhombic cross section (up to 1.5 mm), some have irregular form and grows interstitially to the felsic minerals. Small primary opaque oxides form separate euhedral to anhedral grains and also aggregates associated with hornblende, biotite, and sphene. Secondary iron oxides form as alteration products of the mafic minerals.

This is a medium grained rock of granodioritic composition, with plagioclase crystals forming a meshwork in which the rest of the minerals are interstitial phases. The rock has been strained as indicated by undulose extinction in biotite and quartz.

An additional sample of this type is GH31, which contains fewer mafic minerals than GH28.

3.1.6 Porphyritic granodiorite:

Representative sample: GH39

Petrographic name: Medium grained porphyritic granodiorites.

Plates 3-16 to 3-18.

Description:

In hand specimen the rock is medium grained, the mafic minerals are dark greenish black and the feldspars are pink with white quartz.

Amphibole (green hornblende, 6.3% modal) forms elongate to prismatic crystals (up to 4.0 mm) sometimes in aggregates and in the matrix (<1.0 mm). Biotite (5.3% modal) forms elongate crystals (up to 4 mm), and <1.0 mm in the matrix. Along with hornblende it forms aggregates of mafic knots, elsewhere it is interstitial to feldspars and quartz. It shows undulose extinction and some show alteration to chlorite. Plagioclase (43.3% modal) forms subhedral laths (maximum 6.0 mm) and <1.0 mm in the matrix. It is oligoclase in composition (An_{23} average). Some have oscillatory zoning and show alteration to sericite and saussurite. The crystals form a meshwork in which late hornblende, biotite, orthoclase and quartz are interstitial phases. Alkali feldspar (20.3% modal) forms mostly large irregular patches (up to 15.0 mm) and some small grains in the matrix (<1.0 mm). It is interstitial to the other constituents and has microperthitic texture. Myrmekites are sometimes present at the edges with plagioclase. Quartz (22.2% modal) forms anhedral interstitial grains (maximum 4.0 mm). It is a late-stage mineral, and in some areas it forms consertal texture (Plate 3-17) where quartz crystals have intergrown boundaries and undulose extinction. Fluid inclusions are common and irregular in shape. Zircon (accessory) forms euhedral to subhedral grains (<1.0 mm) associated mostly with hornblende and biotite. Sphene (1.3% modal) forms euhedral crystals with an acute rhombic cross section (up to 1.5 mm), though a few are irregular

Plate 3-16: Sample GH39. Medium grained porphyritic granodiorite showing a large crystal of orthoclase with microperthitic texture. Biotite in the middle shows alteration to chlorite.
Ppl, x 12.

Plate 3-17: Sample GH39. Quartz crystals to the right and in the middle show intergrown boundaries (consertal texture).
Cpl, x 20.

Plate 3-18: Sample GH30. Medium grained porphyritic granodiorite, showing large crystal of orthoclase to the left with microperthitic texture and interstitial quartz to the right.
Cpl, x 20.

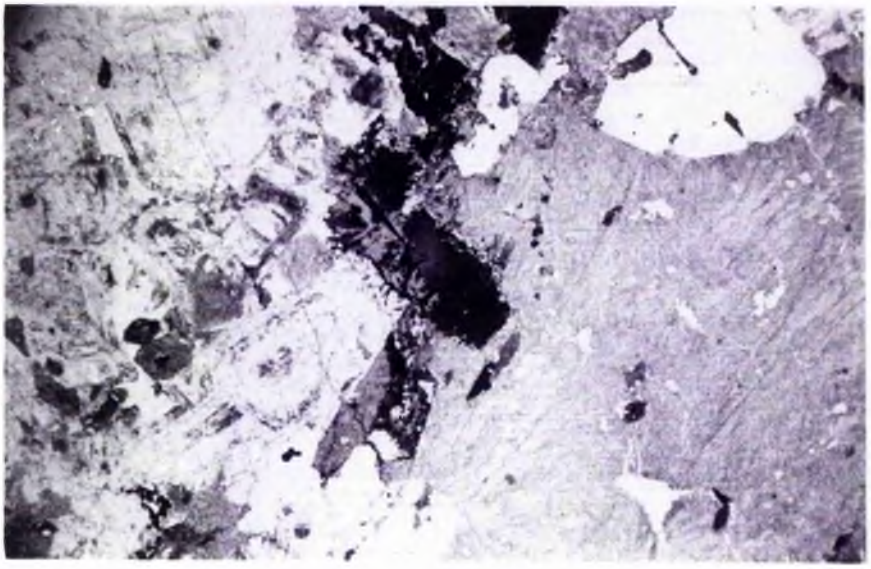

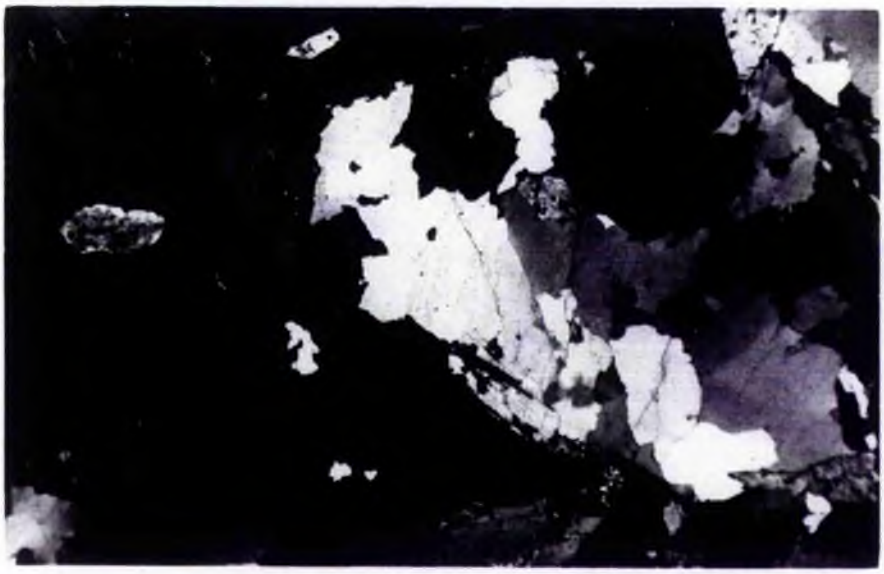

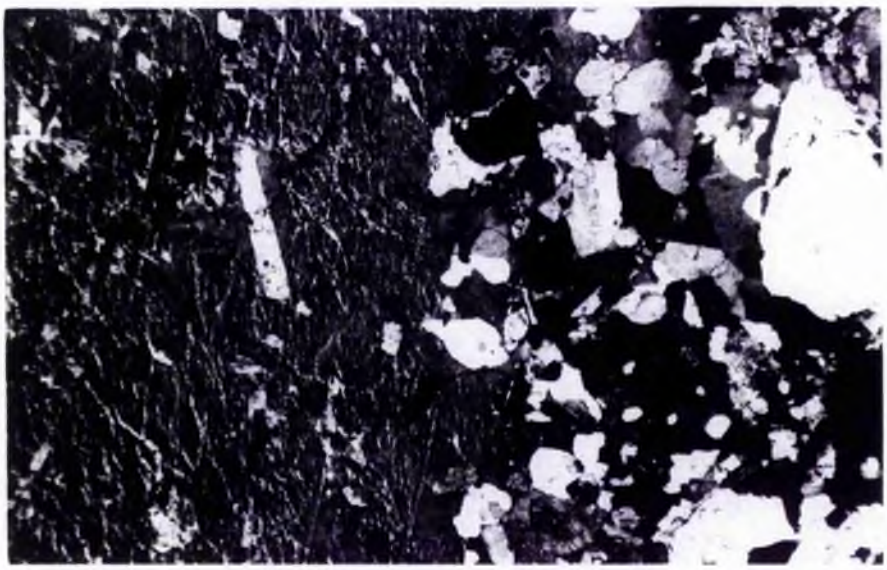

grains. It has reddish brown pleochroism and is associated with biotite and amphibole. Small primary opaque oxides form separate euhedral to anhedral grains, and also aggregates associated with the mafic minerals. Secondary opaque minerals are formed as alteration products of the mafic minerals.

This rock type is of granodiorite composition, it is coarse to very coarse grained, having porphyritic texture where orthoclase forms megacrysts in a matrix of plagioclase, mafic minerals and quartz. It shows slight evidence of strain as the biotite and quartz have undulose extinction.

Additional samples of this type are sample GH30 and GH29, they differ in containing fewer mafic minerals than GH39.

3.1.7. Summary:

No detailed petrographic studies of this complex has been published since Nockolds (1941). Using the IUGS classification of Streckeisen (1976) the rock types are ultramafic rocks of peridotite (wehrlite) type; gabbros with plagioclase of labradorite composition (An52); diorites (with plagioclase of andesine composition) of two types a) two-pyroxene biotite diorite and b) hornblende biotite diorite; appinitic diorite; and granodiorites of two types namely a) medium granodiorite and b) porphyritic granodiorite.

3.2 THE COMRIE COMPLEX

Introduction

The greater part of this complex is made up of various diorites, monzodiorite, granodiorite and granite. The diorites have been classified according to the predominant mafic minerals in the same way as those of the Garabal Hill - Glen Fyne complex. Modal analyses have been made for representative samples of each rock type, and are listed in Table 3-2 and plotted on Fig 3-2.

3.2.1 DIORITES

Rock description

The diorites in this complex are medium to coarse grained, sometimes very coarse, rather rich in plagioclase (up to 61.0% modal). The mafic constituents are hypersthene, augite, hornblende and biotite, biotite being always present. The felsic minerals are plagioclase with small amounts of alkali feldspar and quartz. The diorites can be classified into three types depending on their mafic minerals, namely:-

(a) Two-pyroxene biotite diorite

(b) Augite biotite diorite

(c) Hornblende biotite diorite

3.2.1a Two-pyroxene biotite diorite:

Representative sample: CM10

Petrographic name: Medium grained augite hypersthene biotite diorite.

Table 3-2: Modal analyses of the Comrie rock types

Sample No	Opx %	Cpx %	Amph %	Biot %	Plag %	Alk-feld %	Quartz %	Opaque %	Accessories %	Rock type
CM10	14.6	7.8	-	8.3	61.2	3.6	0.6	2.6	1.3	Two-pyroxene biotite diorite
CM4	-	-	18.0	15.3	53.4	2.1	9.4	1.4	0.4	Hornblende biotite diorite
CM21	-	8.2	0.8	11.5	59.6	4.8	13.0	1.7	0.4	Augite biotite diorite
CM25	7.3	0.8	0.4	12.0	48.1	17.6	10.5	2.8	0.5	Quartz monzodiorite
CM28	-	-	4.1	11.1	42.9	8.3	30.7	2.5	0.4	Granodiorite
CM29	-	-	-	2.4	40.5	22.9	33.2	0.8	0.2	Granite

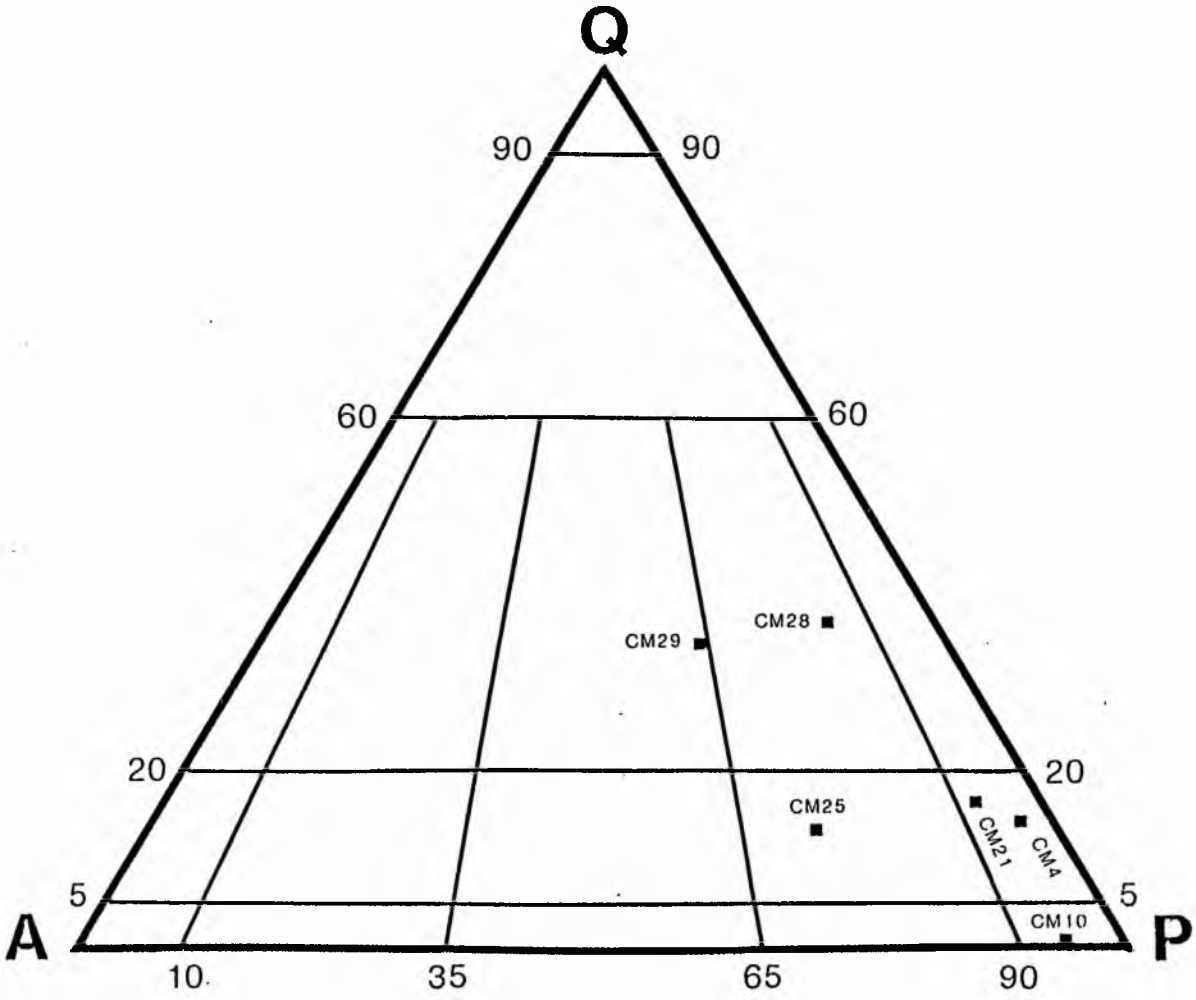

Fig 3.2 Modal classification and nomenclature of Comrie rock types (after Streckeisen, 1976).

Plates 3-19 a, b.

Description:

In hand specimen, the rock is medium grained, grey in colour with shiny pyroxene crystals.

Orthopyroxene (hypersthene, 14.6% modal) forms elongate crystals (up to 2.0 mm) with pink pleochroism. Some have exsolution lamellae of diopside. Clinopyroxene (augite, 7.8% modal) forms short prismatic crystals and anhedral grains (from 1.0 - 3.0 mm), have colourless to pale green colours. Biotite (8.3% modal) forms elongate crystals (up to 4.0 mm) having greenish brown to brown pleochroism. Some irregular grains have orange-brown pleochroism. Plagioclase (61.2% modal) forms elongate crystals (1.0 to 4.0 mm) of andesine composition (An_{40} average). Cloudy appearance is a common feature in the plagioclases of all the diorites in this complex, which is the result of very small inclusions of iron ores and mica. Alkali feldspar (3.6% modal) forms as late interstitial crystals (up to 2.0 mm). Myrmekitic texture develops at some boundaries with plagioclase. Quartz (6.6% modal) forms anhedral interstitial grains to all other minerals. Zircon (accessory) forms small anhedral crystals associated with biotite. Apatite (1.3% modal) forms euhedral and elongate crystals (up to 1.5 mm) generally associated with biotite. Small primary opaque ores (magnetites, ilmenite and some pyrite) form euhedral to anhedral grains (up to 1.0 mm) associated with biotite and some pyroxene, some secondary iron oxide is formed after pyroxene.

This is an intermediate rock with both ortho-and clinopyroxenes of medium grain size. Plagioclase crystals form a meshwork in which the mafic minerals are interstitial and quartz is the latest mineral to form, to fill the interstices.

Plate 3-19a: Sample CM10. Medium grained pyroxene biotite diorite. Plagioclase shows cloudy appearance due to very small inclusions of iron ores and micas.
The photomicrograph showing clino- and orthopyroxene grains in a matrix of plagioclase, biotite and quartz. Ppl, x 20.

Plate 3-19b: As 3-19a in cpl

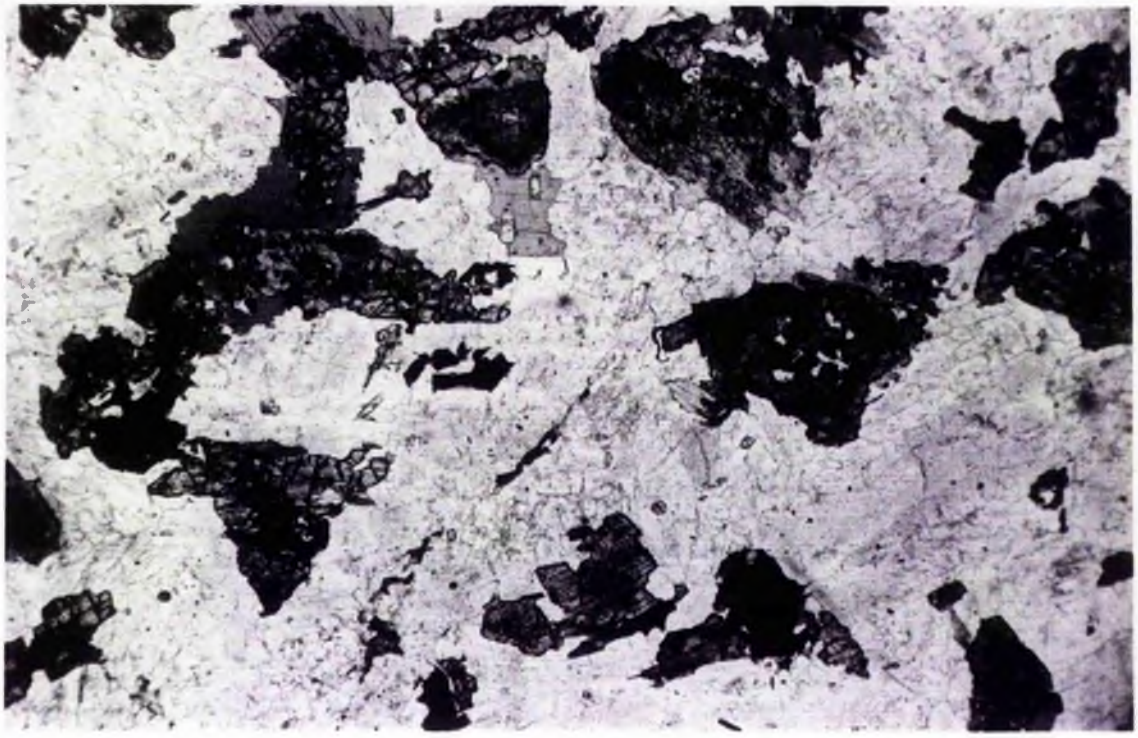

Additional samples of this type are CM22 and CM20. Sample CM22 is coarse grained pyroxene biotite diorite with some of the pyroxene replaced by hornblende. CM20 is an altered pyroxene biotite diorite where relics of hypersthene and augite are present.

3.2.1b Augite biotite diorite:

Representative sample: CM21

Petrographic name: Medium to coarse grained augite biotite diorite.

Plates 3-20, 3-21.

Description:

In hand specimen, the rock is medium to coarse grained with pale to dark greyish colour with porphyritic texture where pyroxene crystals form phenocrysts in a matrix of felsic minerals.

Clinopyroxene (augite 8.2% modal) forms irregular grains (up to 3.0 mm) which are colourless to pale green. They are sometimes replaced by amphibole and show alteration to chlorite and secondary iron oxides. Biotite (11.5% modal) forms elongate crystals (up to 5.0 mm) having greenish brown pleochroism, some occur in aggregates with pyroxene. Occasional grains are present with orange brown pleochroism. Plagioclase (59.6% modal) forms some subhedral to elongate crystals (up to 6.0 mm), andesine in composition (An_{45} average). It seems that plagioclase forms a meshwork in which other minerals are interstitial. Few show alteration to sericite. Alkali feldspar (4.8% modal) forms irregular shaped crystals (up to 3.0 mm) which are interstitial and have microperthitic texture. Quartz (13% modal) is a late-stage mineral and forms anhedral grains interstitial to other components. Zircon (accessory) forms small euhedral to

Plate 3-20: Sample CM21. Medium grained augite biotite diorite, showing augite grain in the centre surrounded by biotite and plagioclase.
Cpl, x 40.

Plate 3-21: Sample CM21 Medium grained augite biotite diorite showing late biotite grain in the centre with clinopyroxene, plagioclase and quartz.
Ppl, x 20.

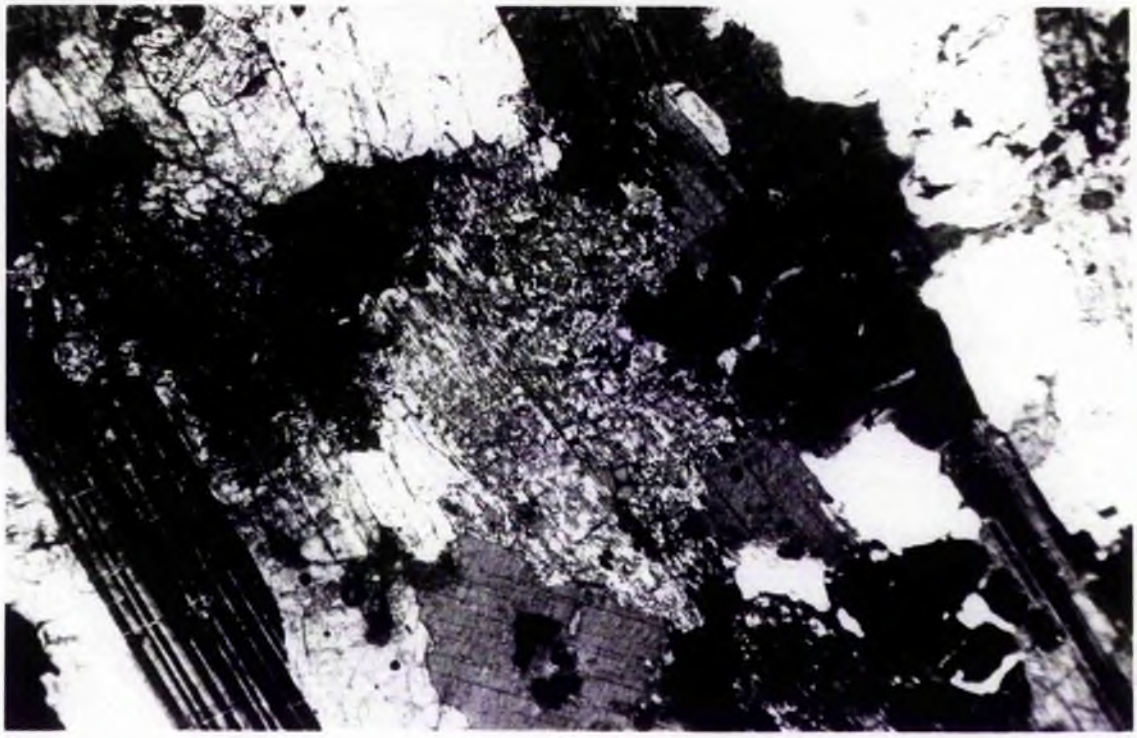

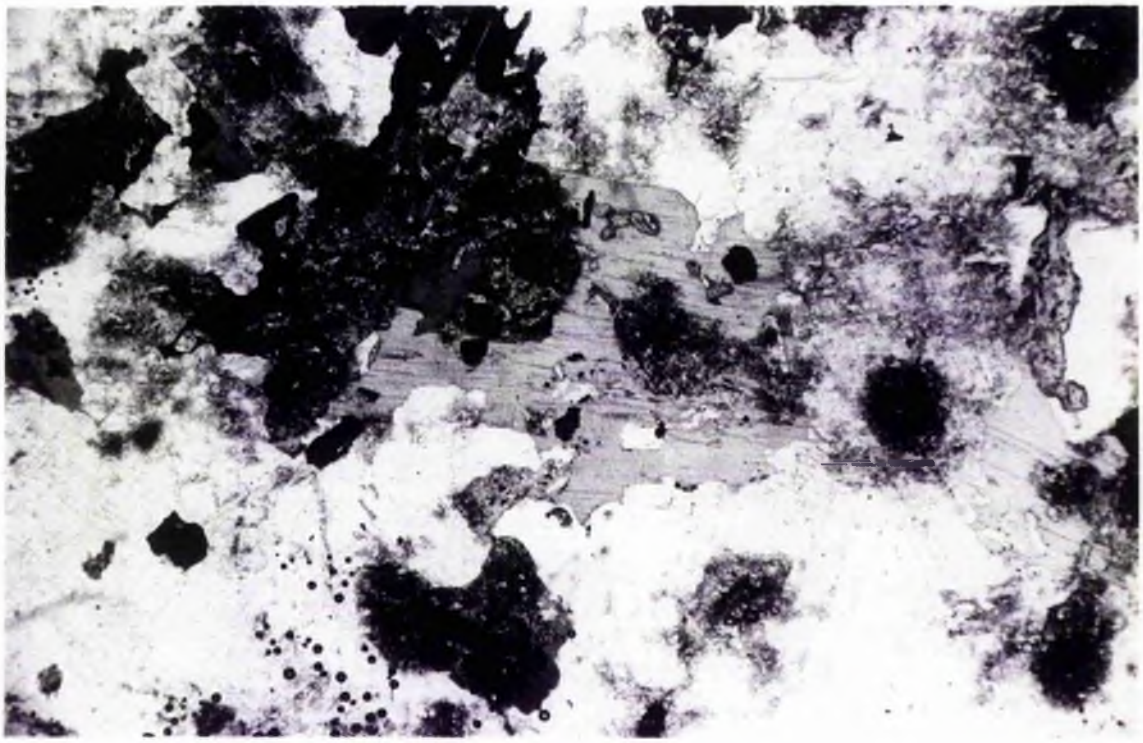

anhedral grains, surrounded by pleochroic haloes within biotite. Apatite (accessory) forms euhedral to elongate crystals associated principally with biotite. Small primary opaque minerals form mostly anhedral to subhedral grains, associated with biotite. Secondary opaques are formed as an alteration product of pyroxene.

This is an intermediate medium to coarse grained rock with clinopyroxene preceding other components, and plagioclase forming a meshwork in which other minerals are interstitial. It has no observable preferred orientation.

An additional sample of this type is CM7 which is a coarse grained rock with few hypersthenes and is somewhat more altered than CM21.

3.2.1c Hornblende biotite diorite:

Representative sample : CM4

Petrographic name: Medium to coarse grained hornblende biotite diorite.

Plates 3-22 a, b.

Description:

In hand specimen the rock is medium to coarse grained with dark greenish grey colour, hornblende forms dark prismatic crystals.

Amphibole (green hornblende, 18% modal), forms some elongate crystals (up to 3.0 mm), and some form rims to the clinopyroxene grains while the remainder replaces clinopyroxene. It has pale yellowish to green pleochroism. Alteration to chlorite, carbonate and iron ores is present. Biotite (15.3% modal) forms anhedral to elongate crystals (up to 3.0 mm) with greenish brown pleochroism, occasional grains (<1.0 mm) are present with orange-brown

Plate 3-22a: Sample CM4. Medium to coarse grained hornblende biotite diorite. Plagioclase has cloudy appearance, hornblende shows replacement by iron ores. Clinopyroxene to the upper left is forming core to the hornblende grain, in a groundmass of plagioclase, biotite, and quartz.
Ppl, x 20.

Plate 3-22b: As 3-22a in cpl.

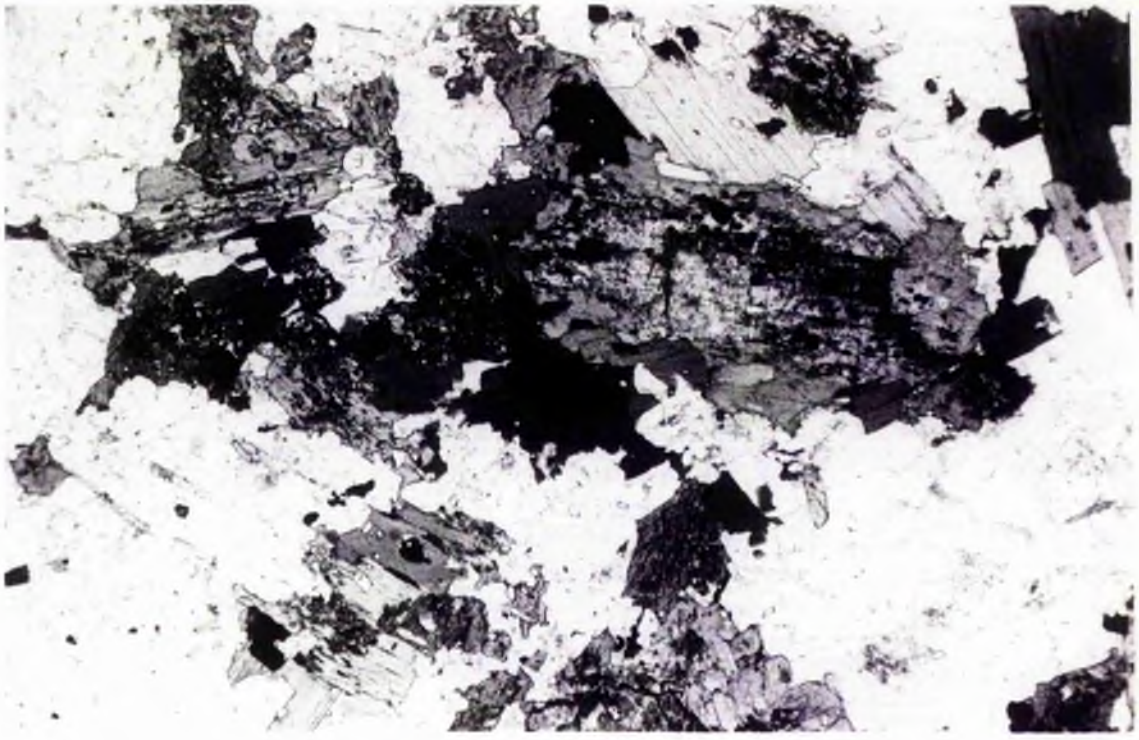

pleochroism. Plagioclase (53.4% modal) forms subhedral to elongate crystals (maximum 6.0 mm) of andesine composition (An_{37} average), with cloudy appearance. Few are zoned and some are altered to sericite and saussurite. Alkali feldspar (2.1% modal) forms anhedral interstitial grains (up to 2.0 mm). Quartz (9.4% modal) is a late-stage mineral forming interstitial grains to other minerals. Zircon (accessory) forms small euhedral to anhedral grains, associated with biotite. Apatite (accessory) forms euhedral and elongate crystals, principally associated with biotite. Sphene (also accessory) forms euhedral to subhedral grains (up to 1.0 mm). Small primary opaque minerals forms subhedral to anhedral grains (up to 1.0 mm), some being irregular, associated with biotite and hornblende. Some iron oxides are present as an alteration product of the mafic minerals.

This is an intermediate rock of medium to coarse grained size, with early clinopyroxene rimmed by hornblende. It has preferred orientation.

3.2.2 Quartz monzodiorite:

Representative sample: CM25

Petrographic name: Medium to coarse grained quartz monzodiorite.

Plates 3-23, 3-24.

Description:

In hand specimen the rock is medium to coarse grained with dark green to black crystals of pyroxene and amphibole. Feldspars are pink.

Orthopyroxene (hypersthene 6.3% modal) forms irregular shaped crystals (up to 2.0 mm) having pink pleochroism and some have exsolved

Plate 3-23: Sample CM25 Medium to coarse grained quartz monzodiorite, showing plagioclase, clinopyroxene, late biotite and quartz.
Ppl, x 40.

Plate 3-24: Sample CM25. Zoned plagioclase crystal in the centre having inclusions of pyroxene, biotite and opaque minerals.
Ppl, x 40.

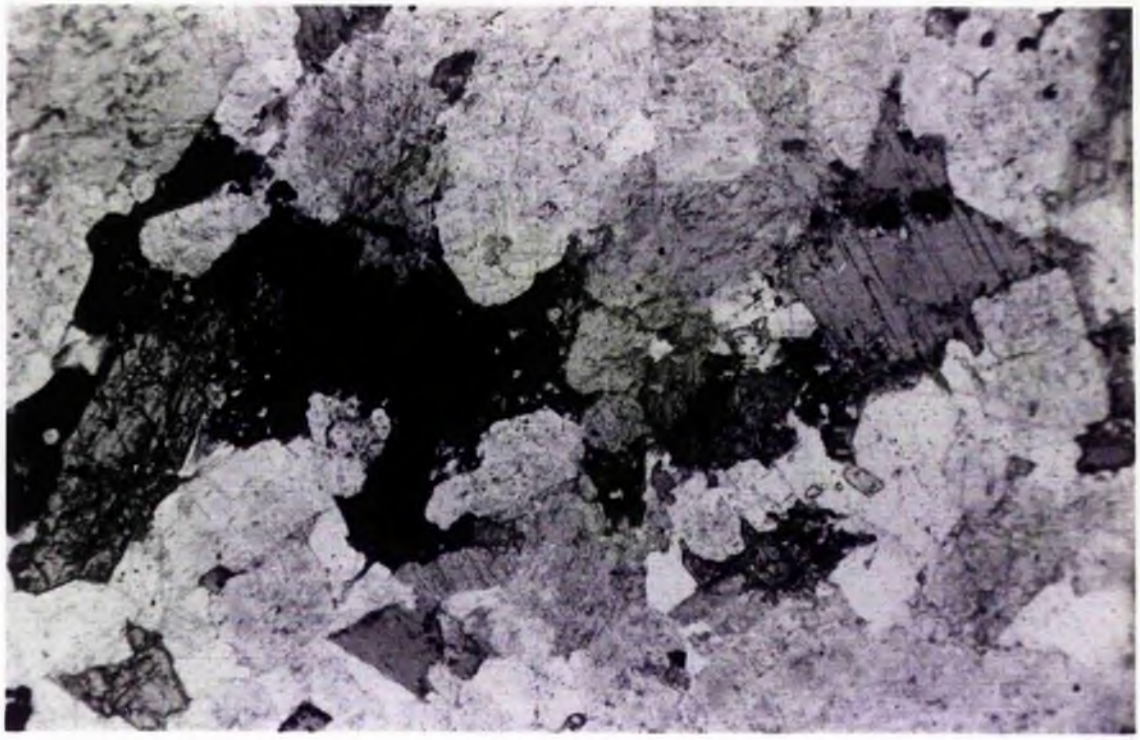

clinopyroxene. Clinopyroxene (1.8% modal) forms anhedral to irregular shaped crystals (up to 5.0 mm) colourless to pale green in colour. Anhedral small crystals (<1.0 mm) form in the matrix. Some contain exsolution lamellae of orthopyroxene, and are rendered particularly conspicuous by containing large numbers of hair-like rodlets of opaque oxides. It sometimes shows alteration to chlorite, secondary magnetite, and some are replaced by amphibole. Amphibole (green hornblende, 0.4% modal) forms small anhedral grains, having pale green pleochroism. Some show replacement of pyroxene. Biotite (12% modal) forms mostly elongate crystals (up to 5.0 mm). Plagioclase (48.1% modal) forms elongate crystals (1.0 to 8.0 mm) of An_{30} composition. Few are zoned and many are partly altered to sericite. Alkali feldspar (17.6% modal) forms late irregularly-shaped crystals (up to 5.0 mm) having microperthitic texture. Quartz (10.5% modal) is the latest mineral forming interstitital grains to the other minerals. Zircon (accessory) forms small euhedral crystals, associated with biotite. Apatite (also accessory) forms euhedral and elongate crystals (<1.0 mm) associated with biotite. Small primary opaque oxide minerals form euhedral to anhedral grains, associated with biotite, pyroxene and in the matrix.

This is an intermediate rock with both ortho- and clinopyroxene, biotite and hornblende as the mafic minerals. Orthopyroxene is earlier than the other minerals, as some are rimmed by clinopyroxene. Biotite is somewhat later than the previous minerals.

An additional sample of this type is CM24 which has more abundant clinopyroxene and hornblende than CM25.

3.2.3 GRANODIORITES

Representative sample: CM28

Petrographic name: Fine to medium grained granodiorite.

Plate 3-25

Description:

In hand specimen it is fine to medium grained with dark biotite and hornblende grains in a feldspathic matrix.

Amphibole (green hornblende, 4.1% modal) forms anhedral grains (1.0 to 2.0 mm) having green pleochroic colours. Alteration to chlorite, carbonate and iron ores is common. Biotite (11.1% modal) forms mostly subhedral to elongate crystals (up to 2.0 mm) with greenish-brown pleochroism. Alteration to chlorite is rare. Plagioclase (42.9% modal) forms elongate crystals (up to 6.0 mm), showing some alteration to sericite. Alkali feldspar (8.3% modal) forms late irregular grains (up to 4 mm) interstitial to other components. Quartz (30.7% modal) is the last mineral (up to 2.0 mm) to form, interstitial to other minerals. Zircon (accessory) forms small euhedral to anhedral crystals surrounded by pleochroic haloes associated with biotite. Apatite (also accessory) forms small euhedral to elongate crystals associated mainly with biotite. Sphene forms small anhedral grains and some irregular ones, having pale reddish-brown pleochroism associated with biotite, hornblende and some opaques. Some small primary opaque oxides form euhedral to anhedral grains. Secondary opaque minerals are present as alteration products of the mafic minerals.

This is an acidic rock with plagioclase forming a meshwork in which other minerals are interstitial. It has no preferred

Plate 3-25: Sample CM28. Fine to medium grained granodiorite, showing a phenocryst of plagioclase in a matrix of hornblende, biotite, small plagioclase grains and quartz. Cpl, x 20.

Plate 3-26: Sample CM29. Fine to medium grained granite, showing orthoclase crystal to the bottom with micro-perthitic texture with plagioclase, biotite and small quartz grains.
Cpl, x 20.

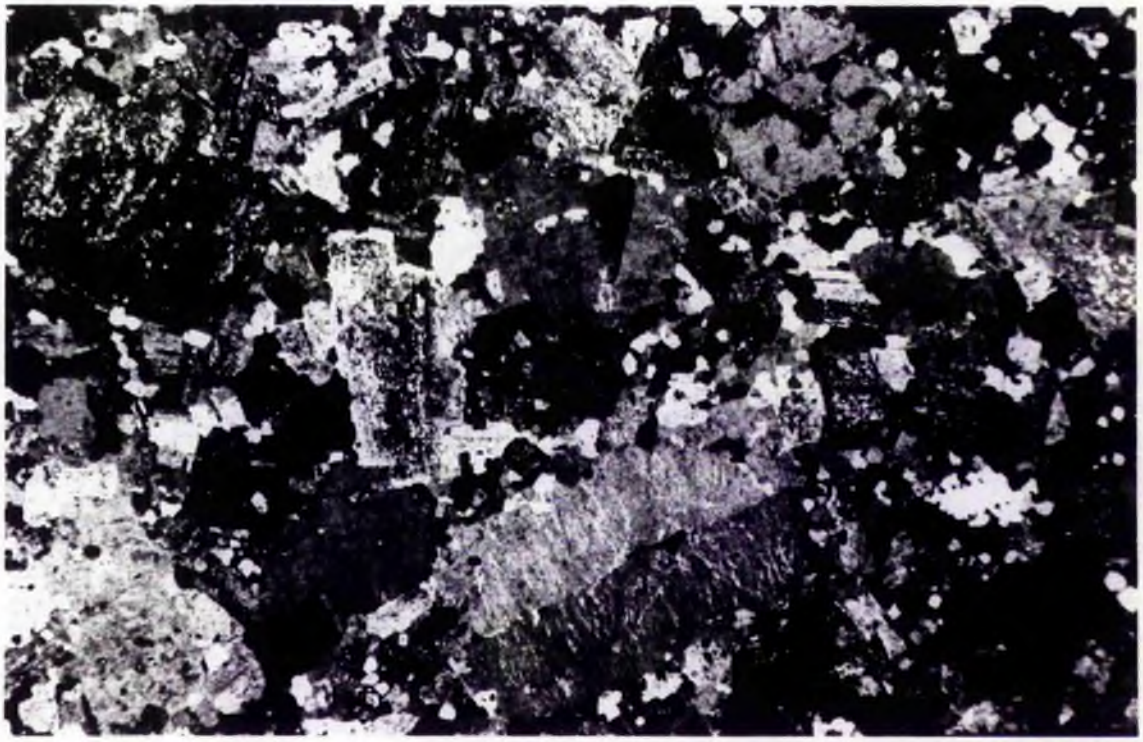

orientation.

Additional samples of this type are CM8, CM26 and CM27, but CM8 contains clinopyroxene sometimes rimmed by amphibole in addition to amphibole and biotite. CM26 contains more biotite and less amphibole, and is somewhat altered. CM27 contains more quartz.

3.2.4 GRANITE

Representative sample: CM29

Petrographic name: Fine to medium grained granite.

Plate (3-26).

Description:

In hand specimen the rock is fine to medium grained, generally pink in colour with small dark grains of biotite.

Biotite (2.4% modal) forms irregular to elongate crystals (up to 2.0 mm). It shows alteration to chlorite and opaque minerals. Plagioclase (40.5% modal) forms irregular grains (up to 4.0 mm), with little zoning and shows alteration to sericite and saussurite. Alkali feldspar (22.9% modal) is a late-stage mineral forming interstitially to other minerals (up to 3.0 mm), having microperthitic texture. Myrmekite is also present. Quartz (33.2% modal) is the last mineral to form forming interstitial anhedral grains (up to 2.0 mm). Zircon and apatite (accessories) form anhedral small crystals associated with biotite. Primary opaque oxides are present as accessories forming fine euhedral to anhedral grains of magnetite. Hematite formed as an alteration product of the biotite and feldspar.

This is an acidic rock with early plagioclase and minor biotite.

3.2.5 Summary:

No detailed petrographic studies have been published for this complex though two unpublished thesis by Wilde (1971) and Majid (1974) described the complex. According to the present study the greater part of this complex is made up of diorites, quartz monzodiorites, granodiorites and granites. The diorites are classified into three main types depending on the predominant mafic minerals a) two-pyroxene biotite diorite; b) augite biotite diorite and c) hornblende biotite diorite. They are rich in plagioclase (up to 61.0% modal) of andesine composition (An30 to An50).

3.3 THE GLEN DOLL COMPLEX

Introduction:

This complex is formed of ultrabasic rocks (olivine hornblende pyroxenite), two types of gabbro namely pyroxene hornblende gabbronorite, quartz gabbro, diorites (mainly of hornblende biotite diorite type), tonalites and granodiorites. Modal analyses are listed in Table 3-3, and plotted on Fig 3-3a, b and c.

3.3a The Ultrabasic Rocks

Olivine hornblende pyroxenite:

Representative sample: GD49

Petrographic name: Medium to coarse grained olivine hornblende pyroxenite.

Plates 3-27 to 3-30.

Description:

In hand specimen, the rock is dark coloured with large dark brown plates of amphibole and dark reflecting pyroxene crystals.

Olivine (30% modal) forms some round anhedral grains (up to 3.0 mm). It is highly fractured, altered along the fractures to serpentine, talc and iron oxides. Orthopyroxene (17.9% modal) mainly of bronzite type, forms mostly elongate crystals (max 2.0 mm) having faint pink pleochroism. Clinopyroxene (18.4% modal) forms anhedral and prismatic crystals (up to 3.0 mm) having pale brown to green pleochroism. Some are rimmed by colourless to green hornblende and biotite. Amphibole (28.9% modal) are mostly brown pleochroic plates with some colourless to pale green hornblende crystals. The brown

Table 3-3: Modal analyses of the Glen Doll rock types

Sample No	Olivine %	Opx %	Cpx %	Amph %	Biot %	Plag %	Alk-feld %	Quartz %	Opaque %	Accessories	Rock type
GD49	30.0	17.9	18.4	28.9	3.7	1.1	-	-	-	-	Olivine hornblende pyroxenite
GD41	-	6.8	8.5	27.0	1.5	53.3	-	2.1	0.8	-	Pyroxene hornblende gabbronorite
GD10	-	-	1.4	21.2	8.6	53.2	-	6.9	6.0	2.7	Quartz gabbro
GD27	-	-	-	7.7	16.3	61.0	-	10.0	3.8	1.2	Hornblende biotite diorite
GD51	-	-	-	-	28.5	44.0	2.5	19.5	2.8	2.7	Tonalite
GD40	-	-	-	1.0	6.0	48.4	17.2	24.2	2.1	1.1	Granodiorite

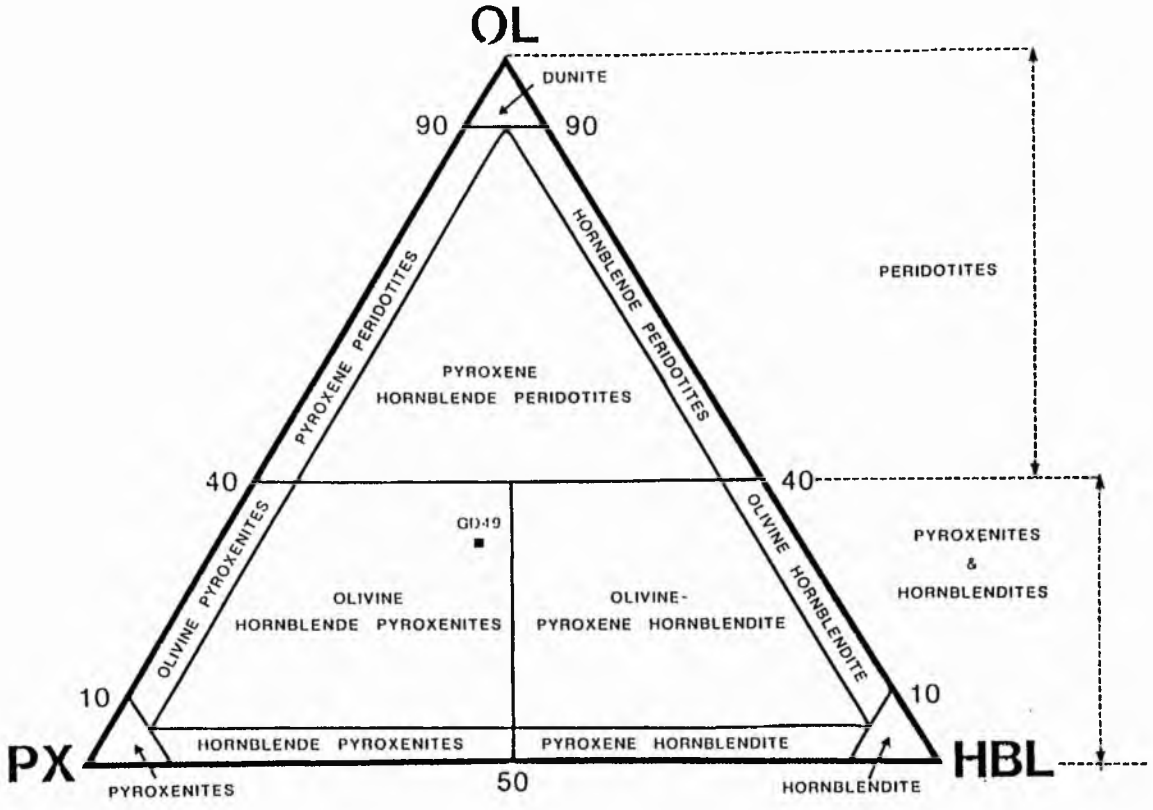

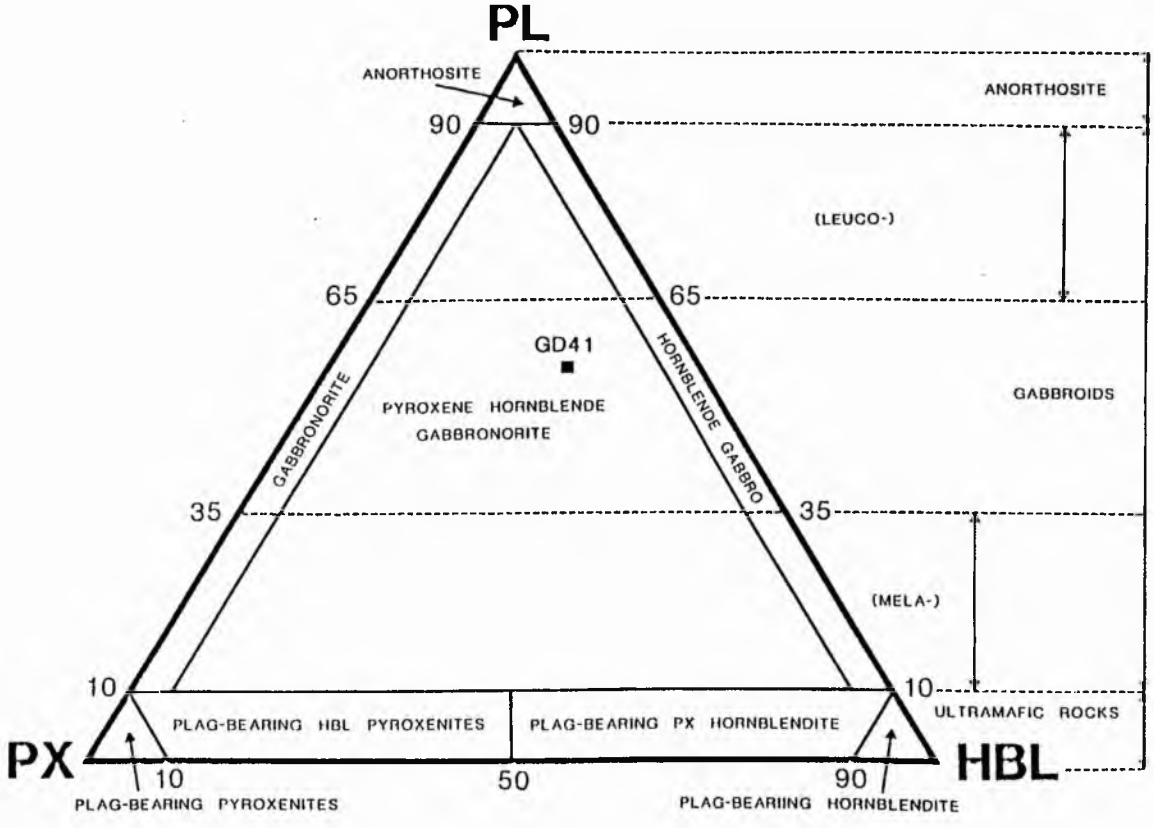

Fig 3.3a,b Modal classification and nomenclature of the Glen Doll ultrabasic and basic rock types (after Streckeisen, 1976).

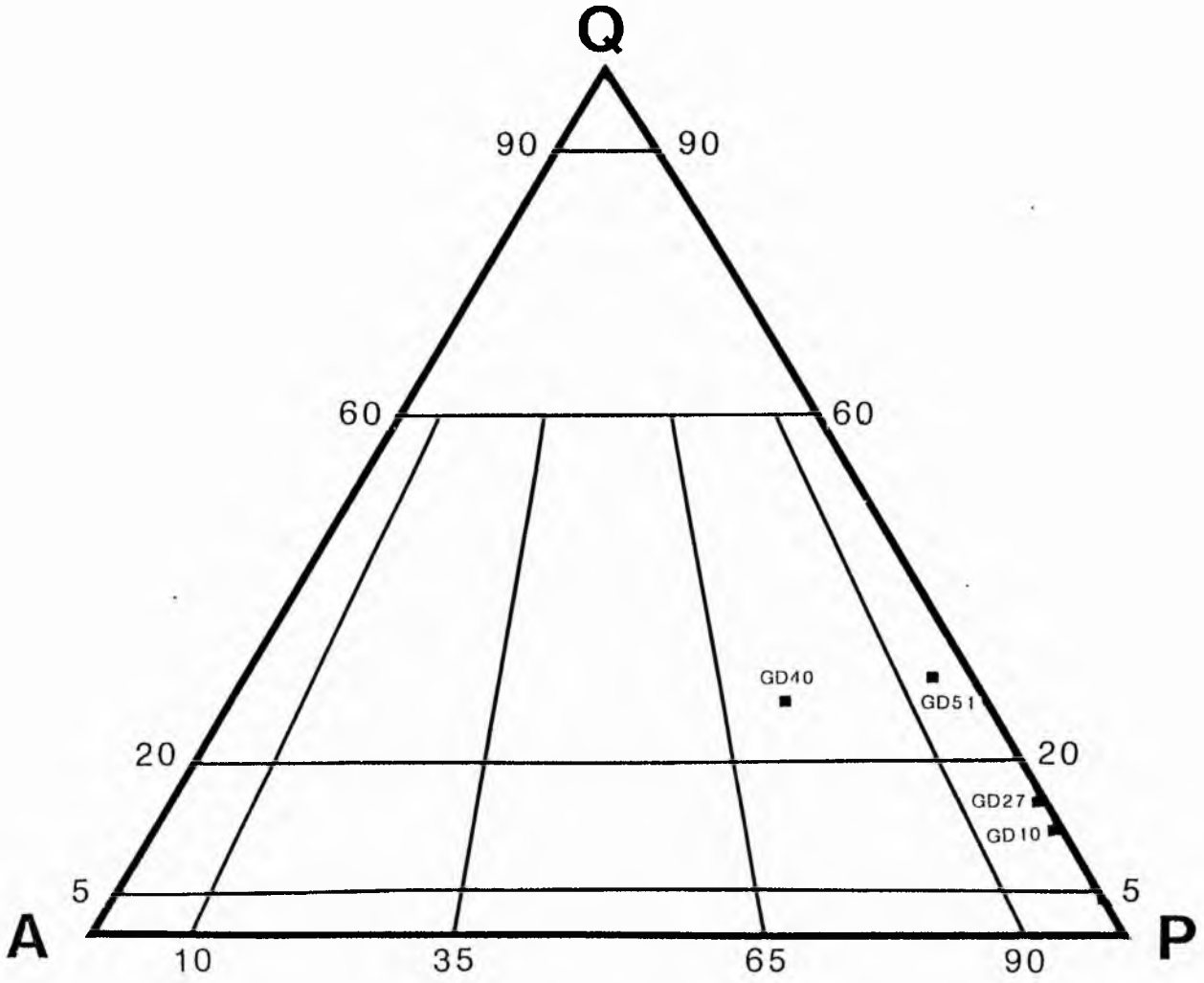

Fig 3.3c Modal classification and nomenclature of Glen Doll rock types (after Streckeisen, 1976).

Plate 3-27: Sample GD49. Medium to coarse grained olivine hornblende pyroxenite, showing a cumulate texture.
The photomicrograph showing olivine in the middle with some twinned clinopyroxene grains and brown amphibole.
Ppl, x 40.

Plate 3-28: As 3-27 in cpl.

Plate 3-29: Sample GD26. Medium to coarse grained olivine hornblende pyroxenite, showing a typical cumulate texture. The photomicrograph show olivine grains (cracked), ortho- and clinopyroxene, large brown amphibole grain to the left and some small plagioclase grains (near to the bottom).
Cpl, x 20.

Plate 3-30: Sample GD26. Large plate of brown amphibole enclosing poikilitically olivine and pyroxene grains.
Cpl, x 40.

amphiboles form medium to coarse plates (up to 8.0 mm), which are late-stage with poikilitic texture enclosing olivine, pyroxene, biotite and plagioclase. Plagioclase (1.1% modal) forms subhedral to elongate crystals (up to 2.0 mm). It is of bytownite composition (An 80 average). Biotite (3.7% modal) forms flaky crystals (up to 4.0 mm). Small primary opaque minerals (magnetite, ilmenite and pyrrhotite) are present, the abundant opaque minerals result from the breakdown of primary olivine crystals and other mafic minerals to serpentine.

This is an ultrabasic rock with early olivine crystals forming rounded grains, ortho- and clinopyroxene and brown hornblende formed comparatively late. It represents a cumulate rock, (plate 3-27).

3.3.2 The Gabbros

Rock Description:

The gabbroic rocks in this complex are medium to coarse grained with plagioclase ranging from labradorite to bytownite in composition. The mafic minerals are both ortho- and clinopyroxene, amphibole (both brown and green hornblende), some biotite, and some gabbros contain more than 5% modal quartz, and are strictly speaking quartz gabbros.

3.3.2a Pyroxene hornblende gabbronorite:

Representative sample: GD41

Petrographic name: Medium to coarse grained pyroxene hornblende gabbronorite.

Plates 3-31a, 3-31b.

Description:

Plate 3-31a: Sample GD41. Medium to coarse grained pyroxene hornblende gabbronorite, showing large brown amphibole plate enclosing poikilitically pyroxene grains with some green amphibole, and late quartz grains.
Ppl, x 40.

Plate 3-31b: As 3-31a in cpl.

In hand specimen the rock is medium to coarse grained, rather dark in colour with predominant dark greenish crystals of amphibole.

Orthopyroxene (bronzite, 6.8% modal) forms elongate crystals (up to 2.0 mm), having pink pleochroism. Some have exsolution lamellae of diopside. Clinopyroxene (augite, 8.5% modal) forms anhedral crystals (max 2.0 mm) having pale green to brown pleochroism. Some grains are rimmed by green hornblende. Amphibole (27.0% modal) is green and brown hornblende. The green hornblende forms either separate anhedral grains (max 1.5 mm) or as rims to the pyroxene. The brown hornblende which forms large plates (up to 9.0 mm) have poikilitic texture, (plate 3-31a) enclosing pyroxene, biotite and plagioclase. Biotite (1.5% modal) forms flakes (max 3.0 mm). It has an orange brown pleochroism. Local alteration to chlorite is present. Plagioclase (53.3% modal) forms subhedral to elongate crystals (up to 4.0 mm). It is of bytownite composition (An 74.0 average). Some show sericitisation. Quartz (2.1% modal) forms anhedral grains interstitial to other minerals. Zircon (accessory) forms subhedral to anhedral grains (<1.0 mm) mainly associated with biotite and hornblende . Small primary opaque oxides form separate anhedral grains and some aggregates are present.

This is a basic rock with primary pyroxenes, brown amphibole, biotite and plagioclase. The mafic minerals are interstitial to the plagioclase. Pyroxenes are formed earlier than other mafic minerals as they are frequently rimmed by amphibole. Quartz is the latest mineral filling the intersticies.

3.3.2b Quartz gabbro:

Representative sample: GD10

Petrographic name: Medium to coarse grained quartz gabbro.

Plates 3-32 and 3-33.

Description:

The rock is medium to coarse grained, medium coloured, with dark greenish-black prismatic crystals of amphibole, and white feldspars.

Clinopyroxene (augite, 1.4% modal) forms irregular grains as cores to hornblende (up to 1.5 mm), having pale brown pleochroism. Amphibole (21.2% modal) is a green to brown pleochroic mineral, forming subhedral to prismatic crystals (up to 3.0 mm). Biotite (8.6% modal) forms anhedral to elongate crystals (up to 3.0 mm), with pale to dark brown pleochroism. Plagioclase (53.2% modal) of labradorite composition (An56.0 average) forms subhedral to equidimensional crystals (up to 6.0 mm). Some crystals show alteration to sericite. Quartz (6.9% modal) is the latest mineral, forming anhedral grains interstitital to the other minerals. Zircon and apatite (accessories) form small euhedral grains, associated mainly with mafic minerals. Some of the zircon grains are very small, surrounded by pleochroic haloes associated with biotite. Primary opaque oxides form separate anhedral grains (up to 1.5 mm) and in aggregates, primarily associated with the mafic minerals.

This is a basic rock with primary clinopyroxene, amphibole, biotite and plagioclase of medium to coarse grain, with clinopyroxene preceding amphibole. Plagioclase formed early with other mafic minerals being interstitial. The rock has no preferred orientation.

3.3.3 DIORITES

Rock Description:

The diorites in this complex are hornblende biotite diorites.

Plate 3-32: Sample GD10. Medium to coarse grained quartz gabbro, showing prismatic hornblende crystals with biotite and plagioclase. Quartz is interstitial.
Ppl, x 40.

Plate 3-33: As 3-32 but rotated 45° clockwise in cpl.

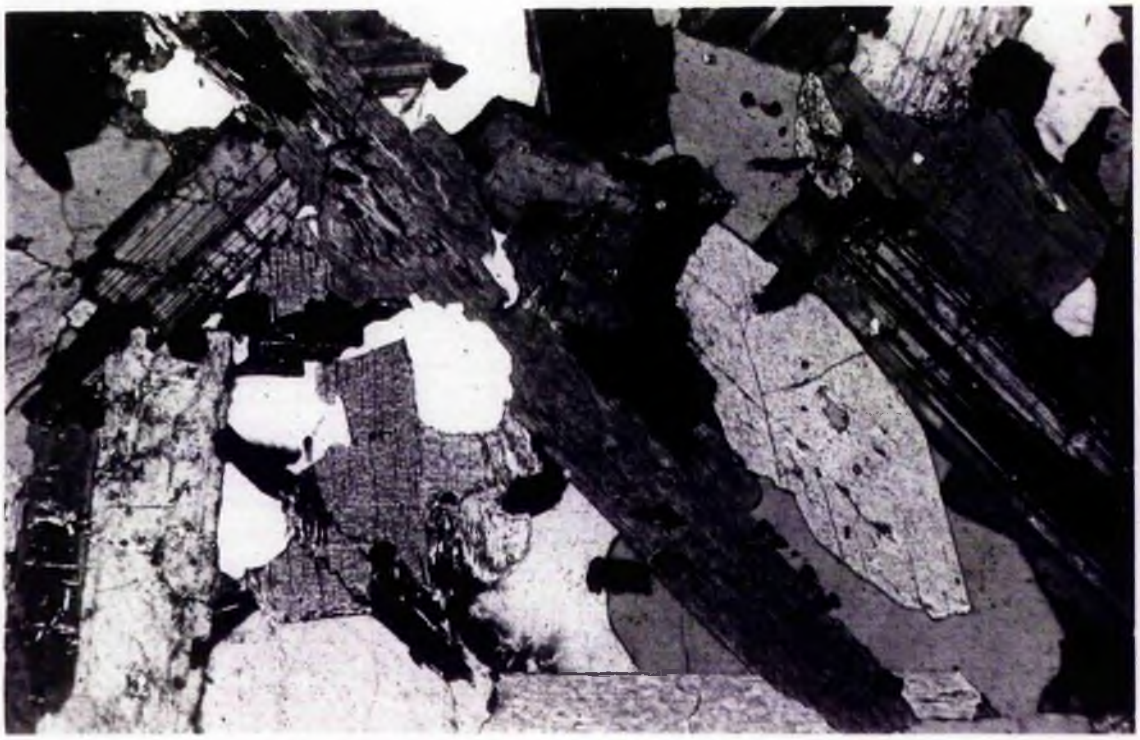

They are composed of hornblende, and biotite with rare clinopyroxene grains. Plagioclase of andesine composition forms up to 60% modal, with alkali feldspar and quartz. These diorites are medium grained.

Hornblende biotite diorite:

Representative sample: GD27

Petrographic name: Medium grained hornblende biotite diorite.

Plates 3-34a, b.

Description

In hand specimen, the rock is medium grained, medium coloured with dark to black prismatic crystals of amphibole and dark flakes of biotite.

Amphibole (hornblende, 7.7% modal) has pale green to greenish brown pleochroism, forming subhedral to anhedral prismatic crystals (up to 4.0 mm). Some form large plates poikilitically enclosing plagioclase and biotite. Biotite (16.3% modal) forms subhedral plates (up to 4 mm) which are interstitial to plagioclase. Local alteration to chlorite is present. Plagioclase (61% modal) forms euhedral to anhedral crystals (up to 4.0 mm), and (<1.0 mm) in the matrix. It is of andesine composition (An 44.0 average). Some show alteration to sericite and saussurite. Quartz (10% modal) is a late-stage mineral forming anhedral interstitial grains to the other components. Apatite (accessory) forms euhedral and prismatic crystals associated mainly with biotite. Primary opaque minerals (3.8% modal) form subhedral to anhedral grains, and aggregates (magnetite, ilmenite and pyrite).

This is an intermediate rock of hornblende biotite diorite composition with plagioclase forming a meshwork in which the mafic minerals are interstitial, while quartz is the last mineral to form.

Plate 3-34a: Sample GD27. Medium grained hornblende biotite diorite, showing intergranular texture, note the late hornblendes against the euhedral plagioclase with late biotite and quartz.
Ppl, x 20.

Plate 3-34b: As 3-34a in cpl

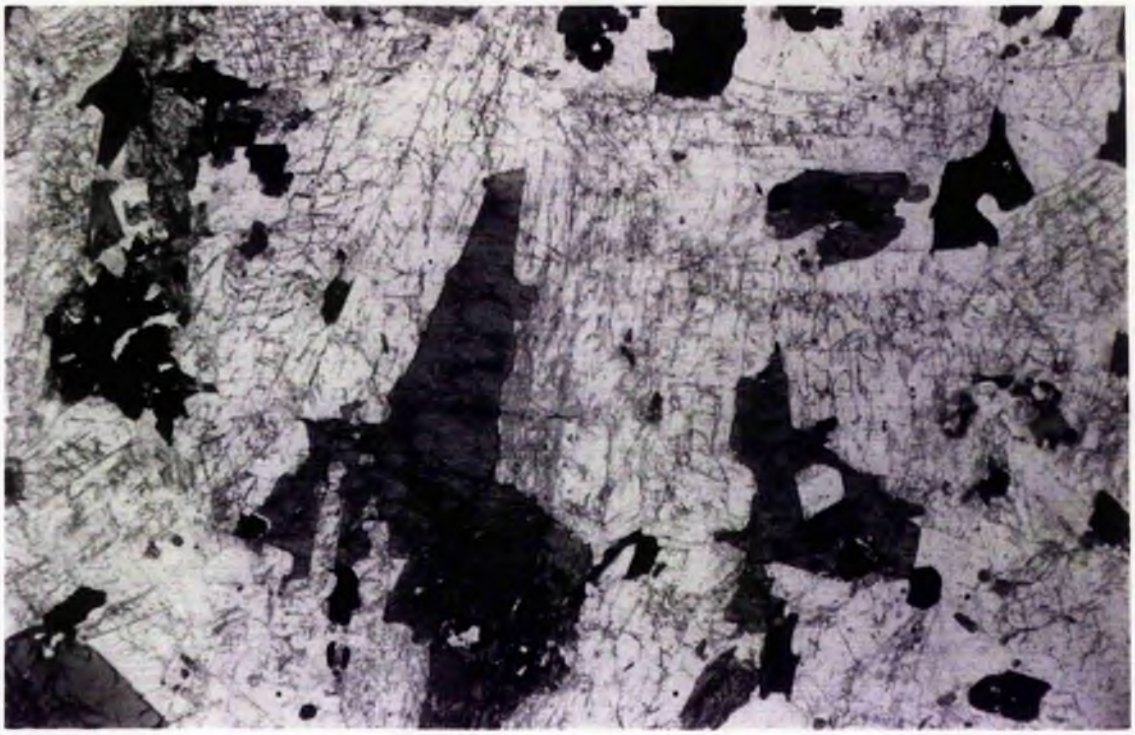

It has no observable preferred orientation.

Additional samples of this rock type are GD33, GD34, GD36, GD37, GD43, GD47 and GD53, which differ in containing few clinopyroxene grains which form either cores to hornblende or as small separate grains. Some contain alkali feldspar in addition to plagioclase and quartz.

3.3.4. TONALITES

Representative sample: GD51

Petrographic name: Medium grained tonalite.

Plates 3-35a, b.

Description:

The rock in hand specimen is medium grained, with dark flakes of biotite, also white and pink feldspars are present.

Biotite (28.5% modal) forms anhedral elongated crystals (up to 5.0 mm). Plagioclase (44% modal) forms subhedral to anhedral crystals (up to 4.0 mm) and (<1.0 mm) in the matrix, few show normal zoning. It is of andesine composition (An32.0 average). Alkali feldspar (2.5% modal) is a late-stage mineral forming anhedral interstitial grains to the plagioclase (up to 2.0 mm) having a microperthitic texture. Quartz (19.5% modal) is the latest mineral, forming anhedral grains interstitial to the other components. Zircon and apatite (accessories) form small subhedral to euhedral crystals associated mainly with biotite. Primary opaque oxides form small subhedral to anhedral crystals and also aggregates.

This is a tonalite with plagioclase preceding other minerals in which they are intersititial. It has no preferred orientation.

Additional samples of this type are GD50 which contains a few

Plate 3-35a: Sample GD51. Medium grained tonalite showing late biotite and quartz interstitial to plagioclase crystals. The biotite grains mostly surrounding iron ores, zircon and apatite grains.
Ppl, x 20.

Plate 3-35b: As 3-35a in cpl.

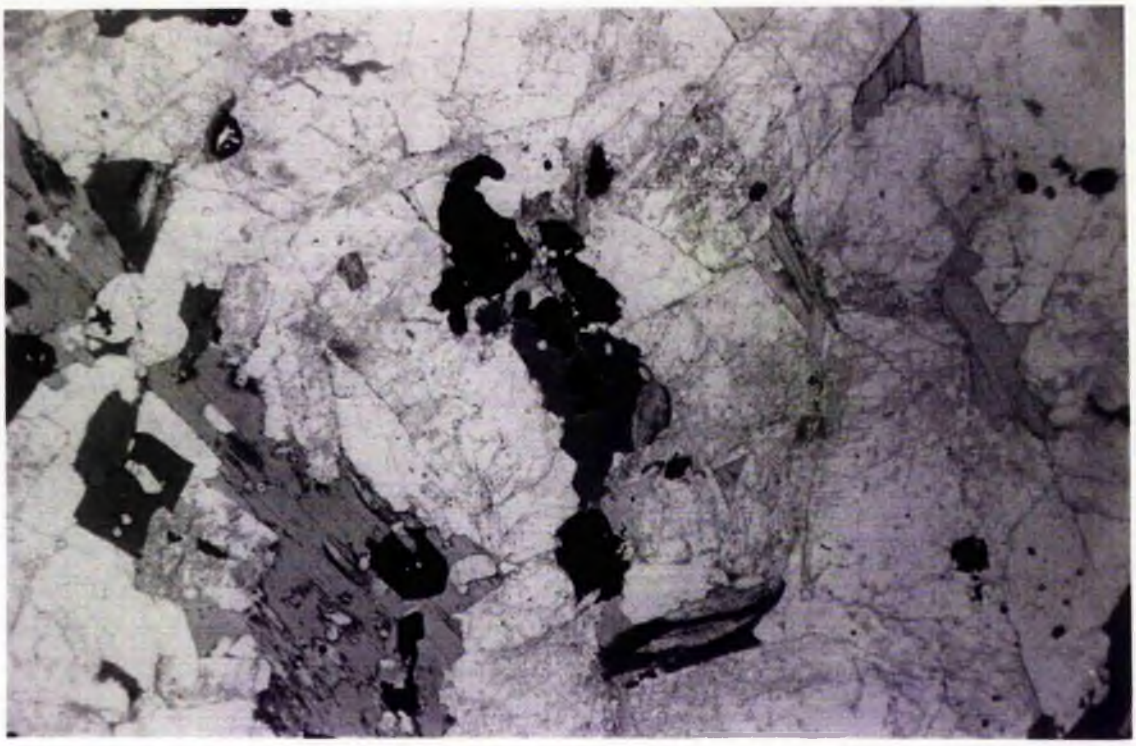

green hornblende grains with biotite, the latter show alteration to chlorite, and GD35 which contains a few clinopyroxene grains forming cores to hornblende. GD39 is an altered tonalite.

3.3.5 GRANODIORITE

Representative sample: GD40

Petrographic name: Medium grained granodiorite.

Plates 3-36a, b and 3-37.

Description:

In hand specimen the rock is medium grained light coloured with dark grains of hornblende and biotite. Feldspars are pink in colour with white quartz.

Amphibole (1.0% modal) forms anhedral crystals (up to 2.0 mm) and in aggregates with biotite. It has pale green pleochroism. Some are replaced by biotite. Biotite (6.0% modal) forms anhedral plates (up to 1.5 mm). Local alteration to chlorite is present. Plagioclase (48.4% modal) forms anhedral crystals (up to 5 mm) and small crystals in the matrix. It is of oligoclase composition ranging from An_{22} to An_{27}. Some are altered to sericite. Alkali feldspar (17.2% modal) forms anhedral intersitital grains to plagioclase. It has microperthitic texture. Quartz (24.2% modal) forms the latest anhedral interstitial grains (<2.0 mm). Zircon, apatite and sphene (accessories) form subhedral small crystals associated with biotite. Small anhedral primary opaque oxides (2.1% modal) and aggregates are present. Secondary opaques result from the breakdown of the mafic minerals.

This is an acidic rock of medium grain having a granular texture with plagioclase crystals forming a meshwork in which other

Plate 3-36a: Sample GD40. Medium grained granodiorite, showing hornblende grains and biotite with alkali feldspar and quartz interstitial to plagioclase.
Ppl, x 20.

Plate 3-36b: As 3-36a in cpl

Plate 3-37: Sample GD32. Medium grained granodiorite showing micrographic intergrowth of quartz and alkali feldspar.
Cpl, x 20.

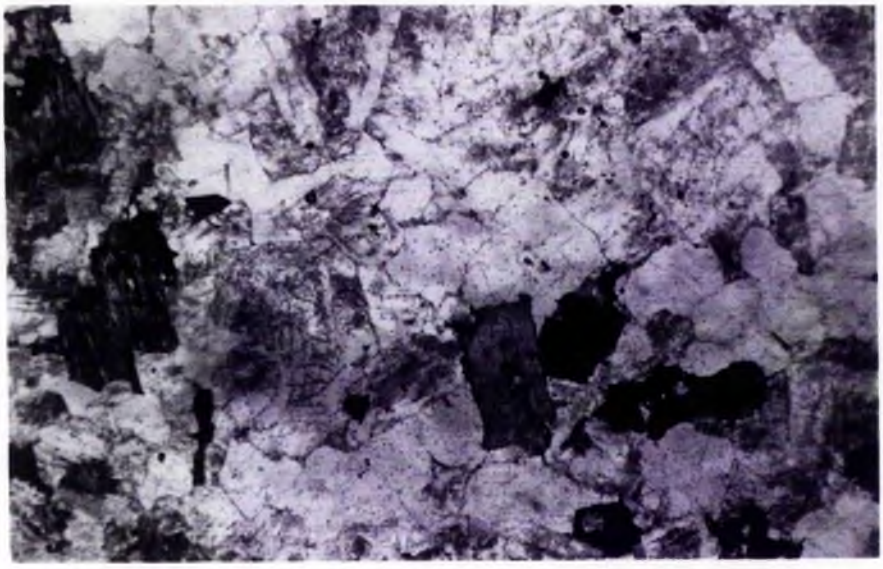

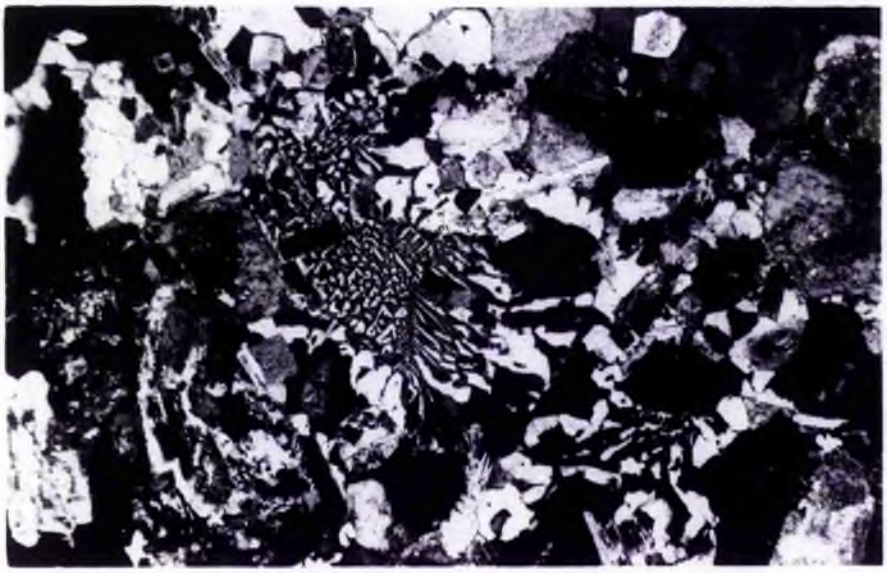

constituents are interstitial.

3.3.6 Summary:

After Barrow & Craig (1912) who mapped this complex and Wyllie & Scott (1913) who described the complex as composed of peridotite, porphyritic diorites with green hornblende and some acidic diorites, no detailed petrographic studies for this complex have been published. This study has shown the complex to be composed of olivine hornblende pyroxenite , gabbro, diorite; tonalite and granodiorite. The gabbros are of two types a) pyroxene hornblende gabbronorite and b) quartz gabbro. They contain plagioclase of labradorite to bytownite in composition. The diorites are mainly of hornblende biotite diorite type.

3.4 THE GLEN TILT COMPLEX

Introduction:

This complex is made up of hornblende biotite diorite, appinitic diorite, granodiorite and granite (biotite granite). The Sron a Chro granite described by Deer (1938a) is found to be granodiorite according to modal analysis. The Beinn Dearg granite is actually a biotite granite and muscovite is secondary as it is replacing plagioclase, thus it is not a biotite muscovite granite as originally indicated by Deer (1938a). Modal analyses are listed in Table 3-4 and plotted on Fig 3-4.

3.4.1 The Diorites:

Hornblende biotite diorite:

Representative sample: GT44

Petrographic name: Medium to coarse grained hornblende biotite diorite.

Plates 3-38a, b.

Description:

In hand specimen this rock is typically medium to coarse grained and composed of conspicuous amphibole and plagioclase.

Amphibole (21.7% modal) forms subhedral to anhedral crystals (up to 6.0 mm). This mineral contains inclusions of plagioclase, biotite and quartz. Some show alteration to carbonate, chlorite and iron oxides. Biotite (9.7% modal) forms anhedral crystals (up to 5.0 mm), have yellowish to brown pleochroism, whereas some irregular grains (up to 2.0 mm) have orange brown pleochroism with undulose extinction. Some biotite develops as flakes within the amphibole, though some

Table 3-4: Modal analyses of the Glen Tilt rock types.

Sample No	Cpx %	Amph %	Biot %	Plag %	Alk-feld %	Quartz %
GT44	-	21.7	9.7	54.4	-	7.8
GT45	-	-	20.1	63.8	1.5	11.6
GT55	0.8	38.6	-	49.3	-	7.3
GT41	-	-	12.8	46.6	13.7	26.1
GT33	-	-	9.0	37.7	15.0	37.3
GT48	-	-	2.3	36.9	22.5	37.8

Opaque %	Accessories %	Rock type
6.3	3.1	Hornblende biotite diorite
2.1	0.9	Quartz diorite
0.9	3.1	Appinite
0.6	0.2	Granodiorite
0.5	0.5	Granodiorite
0.5	-	Granite

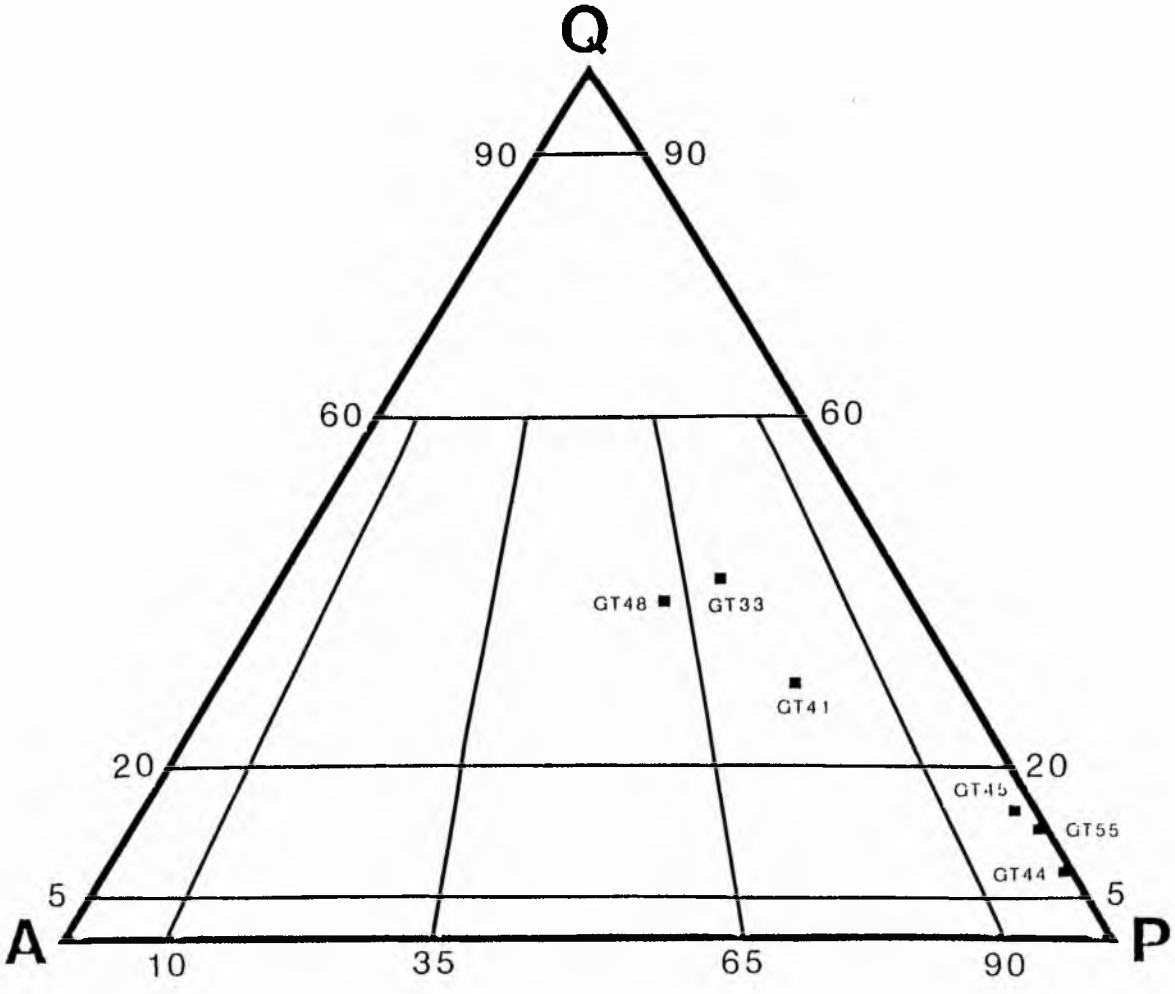

Fig 3.4 Modal classification and nomenclature of Glen Tilt rock types (after Streckeisen, 1976).

Plate 3-38a: Sample GT44. Medium to coarse grained hornblende biotite diorite. Biotite has corroded hornblende in the centre of the photomicrograph with plagioclase. Ppl, x 40.

Plate 3-38b: Sample GT44. Strained biotite showing undulose extinction. Cpl, x 20.

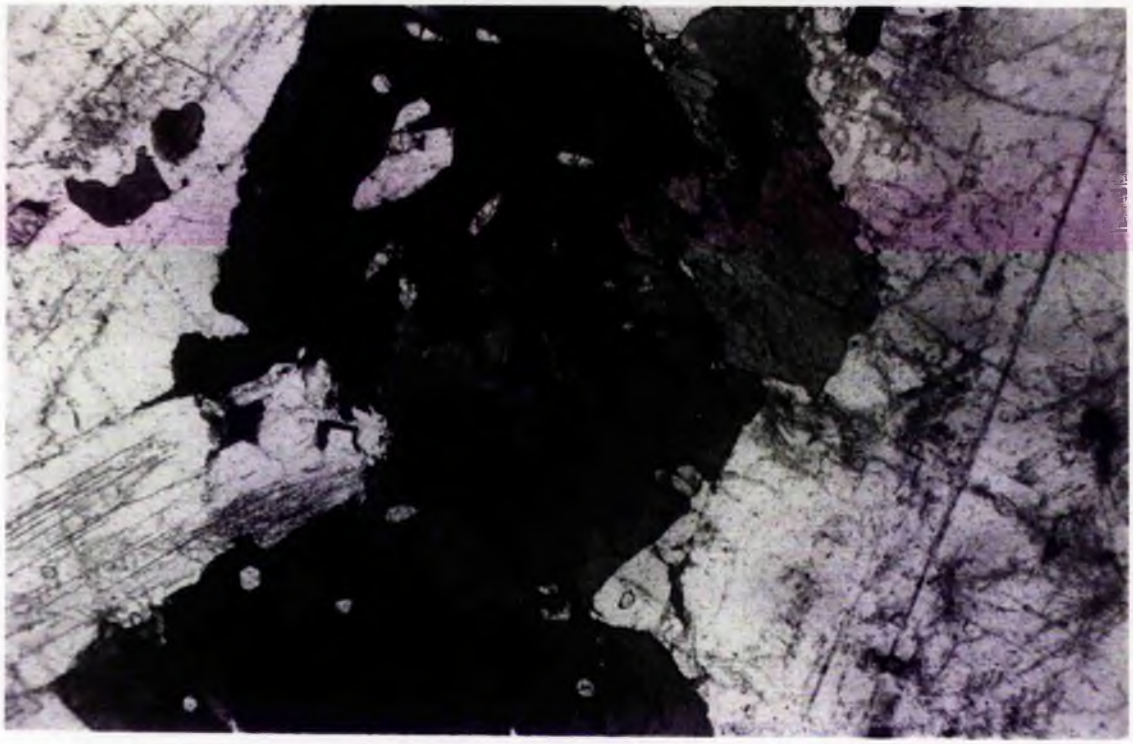

enclose the latter. They show alteration to chlorite and invariably corrode plagioclase when in contact with it. Plagioclase (54.4% modal) shows subhedral development up to 6.0 mm long. It has an andesine composition (An 42.0 average), few are zoned. Some show alteration to sericite and saussurite. Quartz (4.8% modal) forms anhedral interstitial grains (max 2.0 mm) as a late crystallising phase and exhibiting undulose extinction. Zircon and apatite (accessories) form small euhedral to anhedral grains associated mostly with biotite and hornblende. Sphene (1.7% modal) forms separate subhedral grains (up to 2.0 mm) associated with biotite, hornblende and iron oxide. Primary opaque oxides form subhedral to irregular grains (up to 1.5 mm). Alteration of primary amphibole and biotite gives rise to opaque oxides.

This is an intermediate rock having porphyritic texture where the amphibole and biotite form phenocrysts in a matrix of plagioclase mineral and small amphiboles and biotites, (plate 3-38a). Biotite crystallisation looks to have overlapped with the period of early amphibole growth. Quartz is a late crystallising phase forming interstitial anhedral grains.

Additional samples of this type are GT28 and GT29, but GT28 differs in containing a few clinopyroxene grains forming cores to hornblende, with some myrmekite. GT29 contains fewer mafic minerals than GT44 and shows alteration to chlorite.

3.4.2 Quartz diorite:

Representative sample: GT45

Petrographic name: Medium grained quartz diorite

Plates 3-39a and 3-39b.

Plate 3-39a: Sample GT45. Medium to coarse grained quartz diorite, showing intergranular texture where biotite grains are interstitial to plagioclase euhedral crystals. The rock shows crude foliation.
Ppl, x 40.

Plate 3-39b: As 3-39a in cpl.

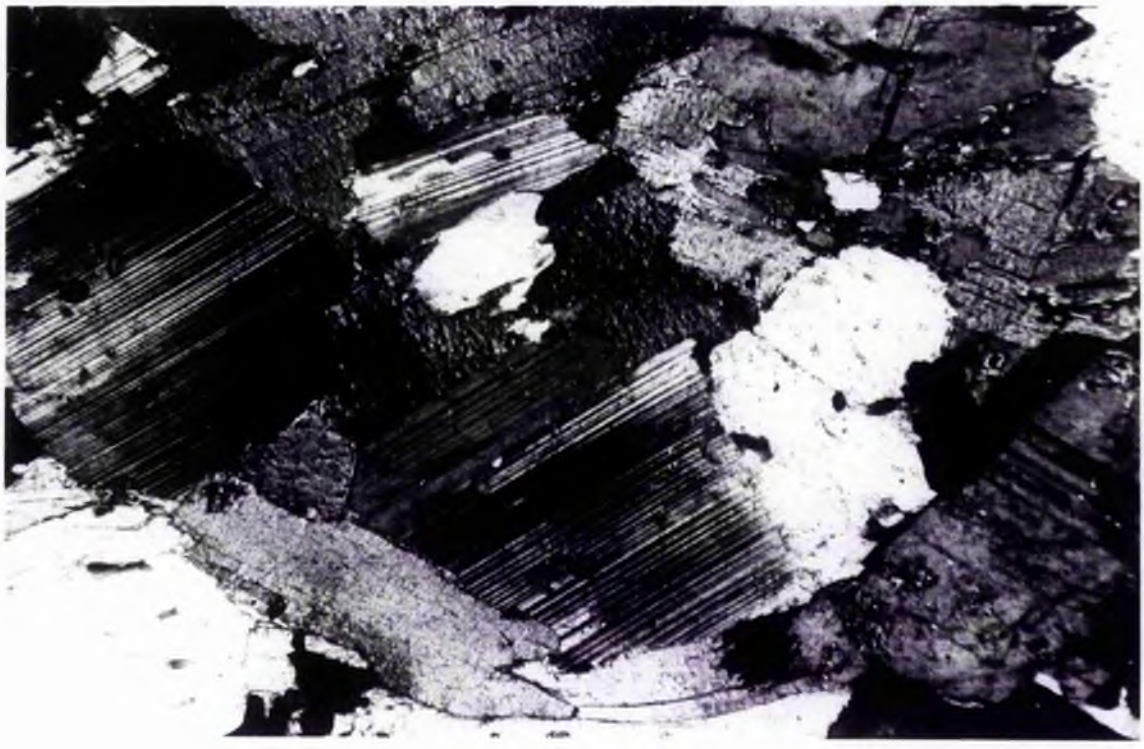

Description:

In hand specimen this rock is medium grained characterised by biotite flakes, a high quartz content, and light pink coloured feldspar.

Biotite (20.1% modal) forms anhedral to irregular crystals (up to 1.5 mm) having pale green to greenish brown pleochroism. They are highly foliated, showing undulose extinction. Plagioclase (63.8% modal) forms anhedral elongate crystals (up to 5.0 mm in length), of An36 composition, with smaller grains in the matrix. It shows alteration to sericite. Alkali feldspar forms late- stage anhedral interstitial grains (up to 2.0 mm) with microperthitic texture. Some myrmekite is present. Quartz (11.6% modal) is the latest mineral as anhedral interstitial grains. Zircon and apatite (accessories) form small subhedral crystals associated mainly with biotite. Sphene (accessory) forms irregular crystals. Some small primary opaque oxides form anhedral and irregular grains, secondary opaques result from the breakdown of biotite.

This is a quartz diorite, with biotite grains occasionally corroding the plagioclase. Quartz and alkali feldspar are both late crystallising minerals.

Additional samples of this type are GT47 and GT54 but the mafic minerals show alteration to chlorite. Sample GT42 is an altered diorite.

3.4.3 Appinitic Rocks:

Rock description:

The term 'appinite' is used for a melanocratic rock rich in large idiomorphic amphiboles, with other mafic minerals including

biotite and pyroxene. In this complex there are a number of rocks of appinitic affinity which are medium to coarse grained, some being typically coarse grained appinitic diorites.

Representative sample: GT55

Petrographic name: Medium to coarse grained appinitic diorite.

Plates 3-40a, 3-40b.

Description:

In hand specimen, this rock is medium to coarse grained consisting of abundant prismatic greenish-black crystals of hornblende in a matrix of plagioclase and quartz.

Amphibole (hornblende, 38.6% modal) forms subhedral to anhedral crystals (up to 4.0 mm), and some aggregates, having green to greenish brown pleochroism. Alteration to chlorite and iron oxide is common. A few clinopyroxene grains with pale green colour form cores to the hornblende. Plagioclase (49.3% modal) forms subhedral to anhedral crystals (up to 6.0 mm in length) and some small grains in the matrix. Amphibole and primary opaque minerals are occasionally poikilitically enclosed within plagioclase. Some of the plagioclase grains show alteration to sericite. Quartz (7.3% modal) is the last mineral to form and occurs as anhedral grains interstitial to other components. It has undulose extinction. Zircon and apatite (accessories) form small subhedral grains associated with hornblende. Sphene (accessory) forms anhedral grains (up to 1.5 mm), some associated with hornblende, a few enclose opaque minerals. Primary opaque oxides form small anhedral grains. Secondary oxides result from the breakdown of the hornblende.

Texturally the appinitic diorites are medium to coarse grained

Plate 3-40a: Sample GT55. Medium grained appinitic diorite showing hornblende with plagioclase and interstitial quartz. Note the alteration of hornblende to chlorite at the top right corner.
Ppl, x 20.

Plate 3-40b: As 3-40a in cpl.

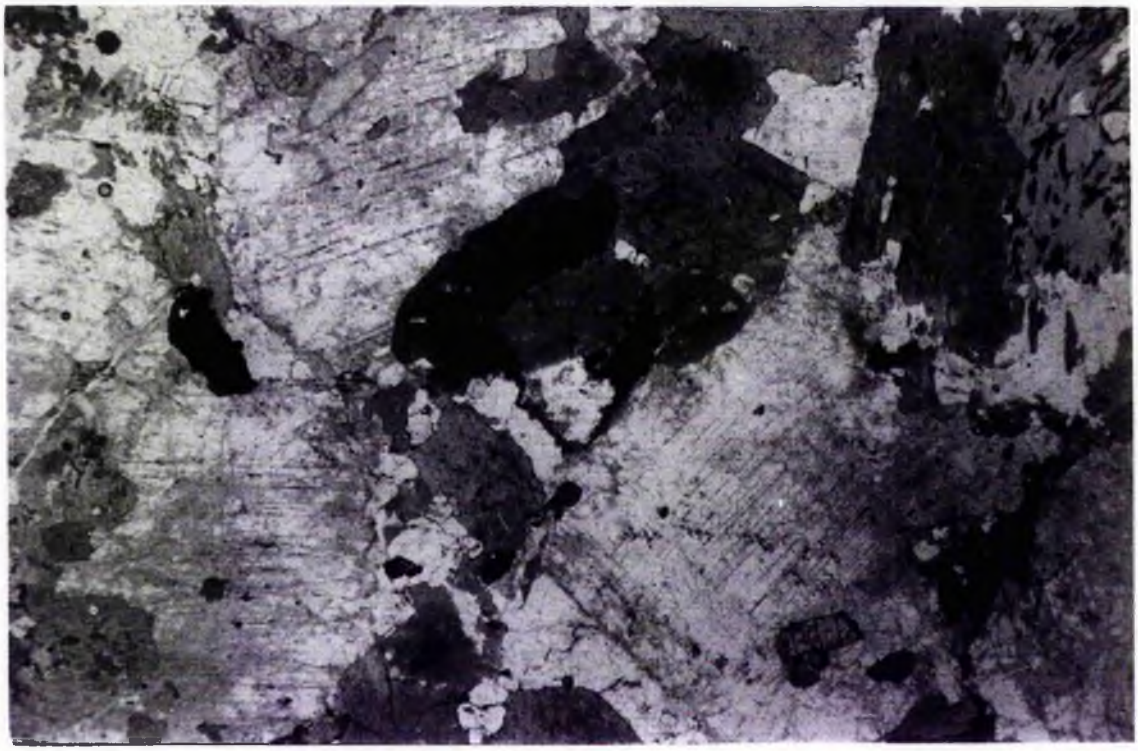

and markedly porphyritic. The presence of abundant amphibole, apatite and the alteration of plagioclase suggest that the rock has crystallised from a volatile-rich magma composition.

Additional samples of this type are GT25, GT26, GT27, GT30, GT35, GT36, GT37, GT39, GT40, GT46, GT52 and GT53. Samples GT25, GT30, GT35, GT37, GT39, GT52 and GT53 are similar to GT55 but with no pyroxene, and show a variable range of alteration. Samples GT26, GT27, GT36, GT40 and GT46 contain approximately equal amount of mafic and felsic minerals . Biotite is present in GT26, GT27 and GT46 in addition to hornblende. Sample GT31 is a coarse grained appinitic diorite containing large plates of greenish-brown amphibole rimmed by green hornblendes and separate green hornblende grains, with a few clinopyroxene grains forming cores to hornblende. Alkali feldspar (microperthite) is also present.

3.4.4 **Granodiorite**:

Representative sample: GT33

Petrographic name: Medium to coarse grained granodiorite.

Plates 3-41 to 3-44.

Description:

In hand specimen this rock is medium to coarse grained, fairly light coloured with dark flakes of biotite in a matrix of white feldspar minerals.

Biotite (9.0% modal) forms anhedral crystals (up to 3.0 mm) with pale yellowish to dark brown pleochroism and showing preferred orientation. Local alteration to chlorite is present. Plagioclase (37.7% modal) forms anhedral grains (maximum of 8.0 mm in length) of An36 composition small grains in the matrix. They show alteration to

Plate 3-41: Sample GT41. Medium grained granodiorite, showing intergranular texture. Note that the quartz grains have consertal texture.
Cpl, x 20.

Plate 3-42: Sample GT41. Medium grained granodiorite showing late biotite grains interstitial to plagioclase.
Ppl, x 20.

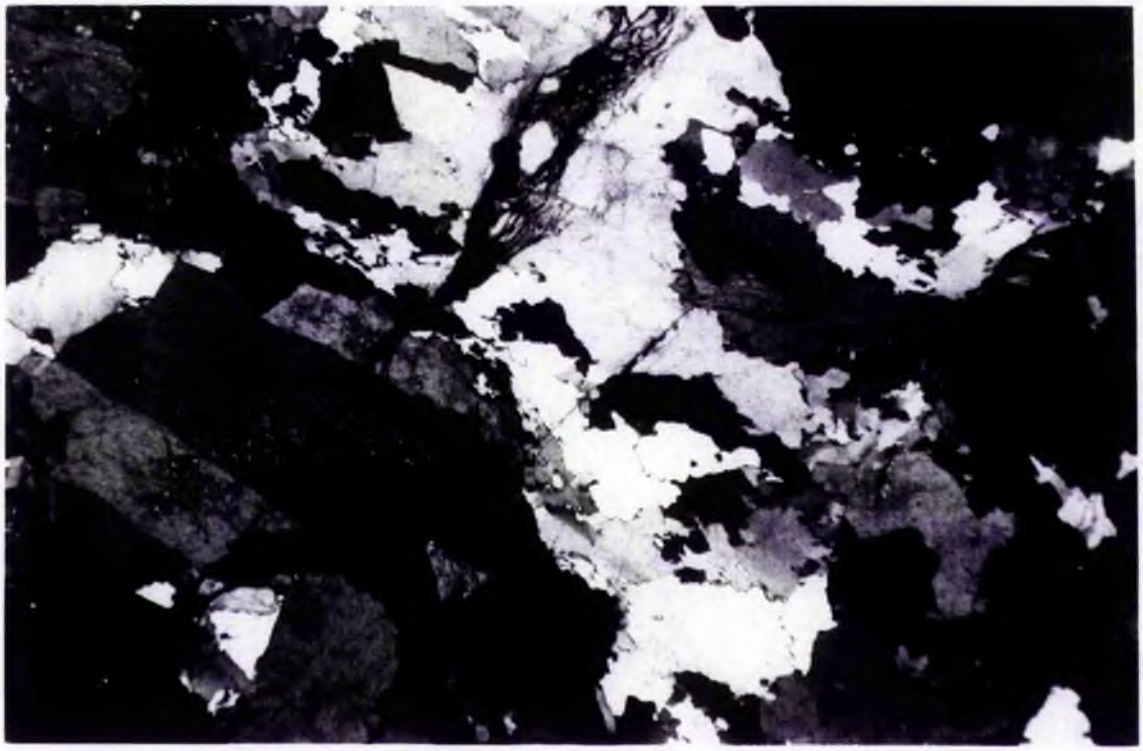

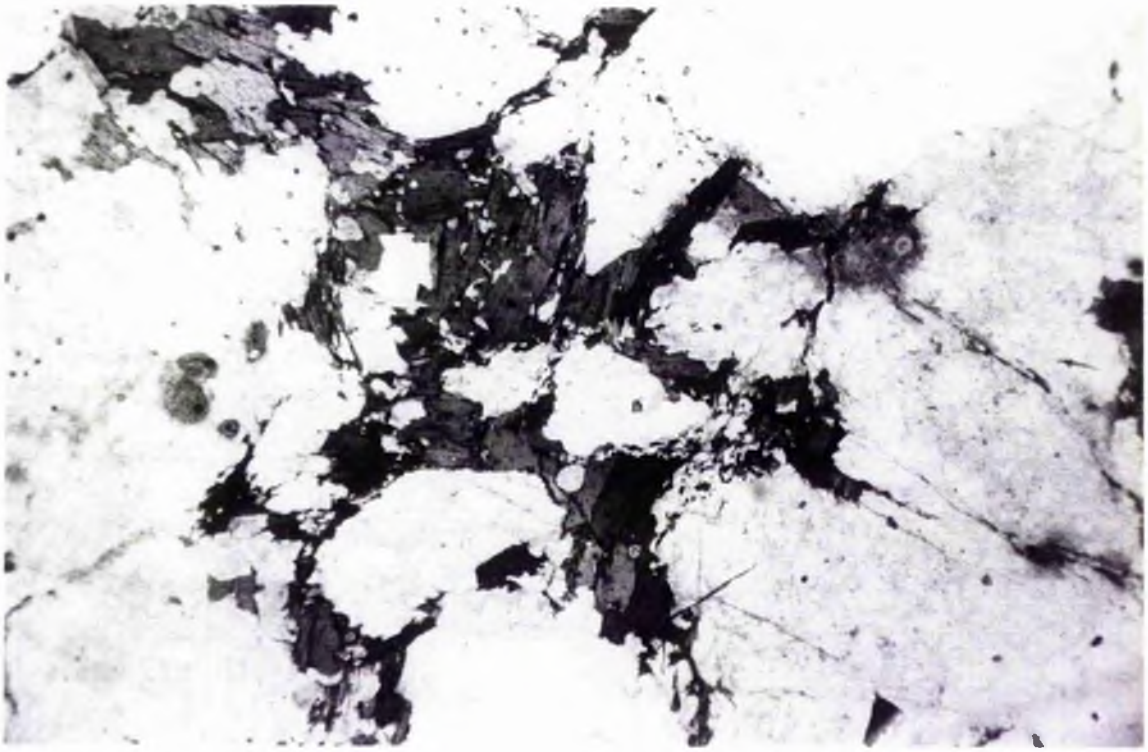

Plate 3-43: Sample GT33. Medium to coarse grained granodiorite, showing intergranular texture where biotite and quartz grains are interstitial to plagioclase. The rock is strained showing foliation with biotite and quartz having undulose extinction.
Cpl, x 40.

Plate 3-44: As 3-43 in ppl.

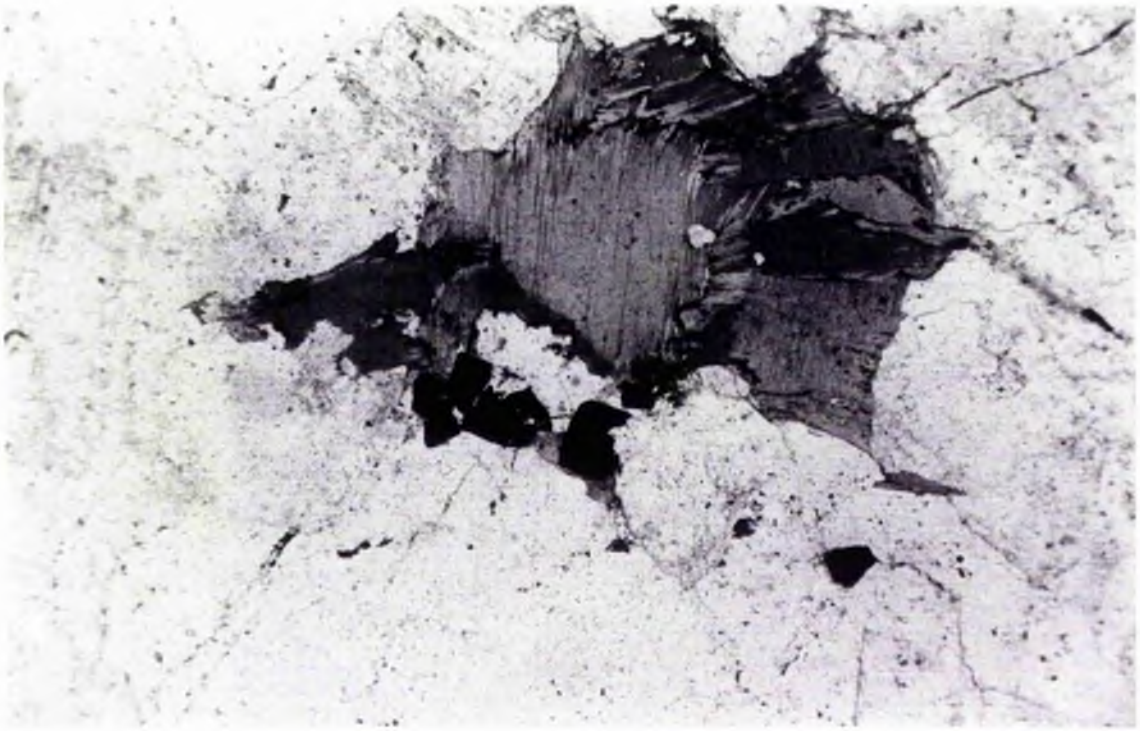

sericite. Alkali feldspar (15.0% modal) forms anhedral interstitial grains (up to 5.0 mm) having microperthitic texture. Some myrmekites are present at the edges with plagioclase. Quartz (37.3% modal) is the latest mineral forming anhedral interstitial grains. Zircon and apatite (accessories) form small euhedral crystals associated with biotite. Primary opaque oxides (mainly of magnetite) are small subhedral to anhedral grains showed alteration at the edges to hematite.

This is an acidic rock with intergranular texture. Biotite has corroded margins with plagioclase. Plagioclase seems to form a meshwork and other constituents are interstitial, alkali feldspar and quartz are late-stage minerals.

Additional samples of this type are GT32, GT34, GT41, GT57 and GT60.

3.4.5 Granite:

Representative sample: GT48

Petrographic name: Medium to coarse grained granite.

Plates 3-45 to 3-47

Description:

In hand specimen this rock is medium to coarse grained, characterised by its high quartz content and light pink colour.

Biotite (2.3% modal) forms anhedral crystals (up to 2.0 mm) showing some preferred orientation. Alteration to chlorite and iron oxide is a common feature. Plagioclase (36.9% modal) forms anhedral plates (up to 4.0 mm) with some small grains in the matrix. It shows alteration to sericite and saussurite. Some plagioclase crystals enclose abundant muscovite grains, (plate3-47). Alkali feldspar

Plate 3-45: Sample GT48. Medium to coarse grained granite, showing intergranular texture, where alkali feldspar, quartz and biotite grains are interstitial to plagioclase. Cpl, x 20.

Plate 3-46: As 3-45 in ppl.

Plate 3-47: Sample GT48. The photomicrograph shows a large sericitised plagioclase crystal replaced by muscovite grains. Cpl, x 40.

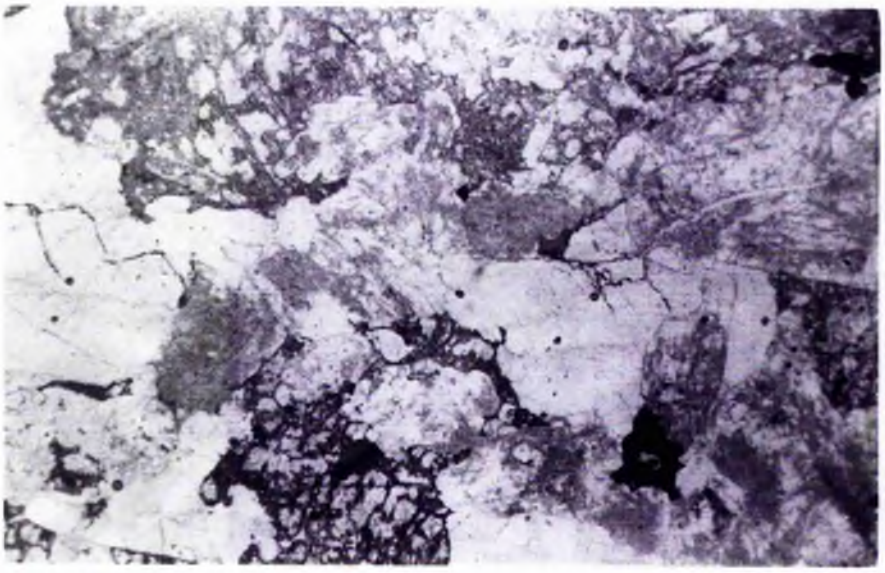

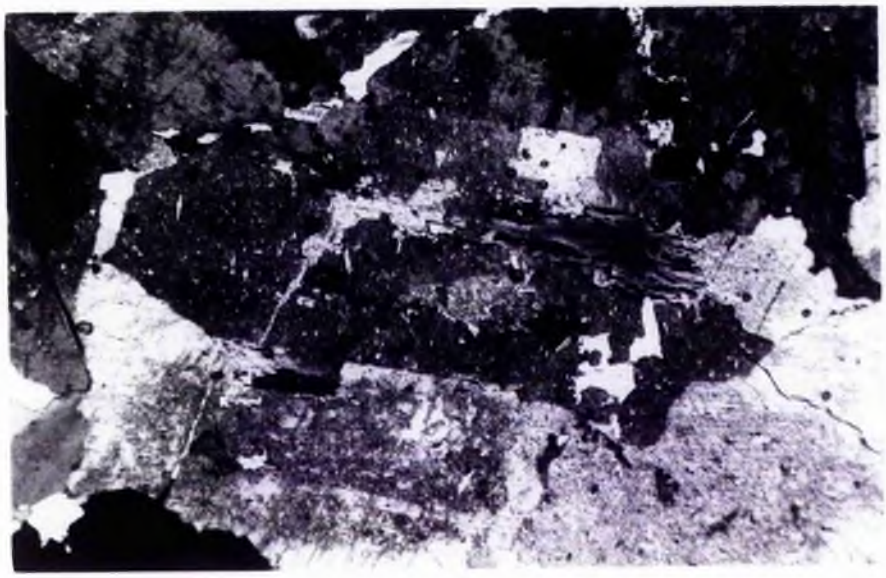

(22.5% modal) forms large patches (maximum 8.0 mm) having microperthitic texture. Myrmekites are present at the edges with plagioclase. It is a late-stage mineral as some grains poikilitically enclose plagioclase crystals. Quartz (37.8% modal) is the last mineral to form with anhedral grains interstitial to other components, and with undulose extinction. Zircon (accessory) forms small inclusions surrounded by pleochroic haloes. Small primary opaque oxides are present.

This is an acidic rock with granular foliated texture, the biotite grains have corroded the plagioclase and alkali feldspar is a late stage mineral. Quartz has a consertal texture. The rock has suffered minor strain as indicated by biotite foliation and undulose extinction in quartz.

3.4.6 Summary

After Barrow et al. (1913) who first described the complex and Deer (1938a, 1950) who described the diorites, appinitic diorites and associated granites of the complex, no detailed petrographic studies has been published. According to this study the complex is formed of diorite, mainly of hornblende biotite diorite type; quartz diorite; appinitic diorite; granodiorite and granite. The 'Sron Chro' granite described by Deer is actually of granodiorite composition, and the Beinn Dearg granite is a biotite granite. There is no muscovite biotite granite in this complex (as suggested by Deer) as muscovite is not primary.

3.5 THE CAIRNSMORE OF CARSPHAIRN COMPLEX

Introduction:

This complex is composed of microdiorite, hornblende biotite diorites, tonalite, granodiorite, and granite. Modal analyses are listed in Table 3.5 and plotted on Fig 3.5.

3.5.1 Microdiorite:

Representative sample: AS33

Petrographic name: Microdiorite.

Plates 3-48 and 3-49.

Description:

In hand specimen this rock is fine grained, grey to dark grey in colour weathering to a light brown rock. It is characterised by its dominant mafic minerals (pyroxene and biotite) with laths of plagioclase and interstitial quartz.

Orthopyroxene (hypersthene, approx. 15% modal) forms small anhedral crystals (<1.0 mm), having faint pink pleochroism. Clinopyroxene (augite, approx. 5% modal) forms small rounded crystals (<1.0 mm), irregular with colourless to pale brown colour. Biotite (approx. 15% modal) forms anhedral plates (up to 2.0 mm). Occasionally there are some interstitial irregular grains with orange to dark brown pleochroism. Plagioclase (approx. 55% modal) forms anhedral crystals (up to 1.5 mm) of andesine composition (An48). It shows cloudy appearance due to tiny inclusions of iron ores and micas. Quartz (approx. 10% modal) forms anhedral interstitial

Table 3-5: Modal analyses of the Cairnsmore of Carsphairn rock types

Sample No	Opx %	Cpx %	Amph %	Biot %	Plag %	Alk-feld %	Quartz %	Opaque %	Accessories %	Rock type
AS38	-	-	11.6	16.9	60.9	1.1	7.6	0.8	1.1	Hornblende biotite diorite
77026	5.4	4.6	0.2	11.9	53.4	-	23.4	0.7	0.4	Tonalite
AS48	-	-	8.2	17.1	42.4	8.6	22.6	0.6	0.5	Granodiorite
AS49	-	-	2.2	6.6	23.6	33.6	32.8	0.1	1.1	Granite

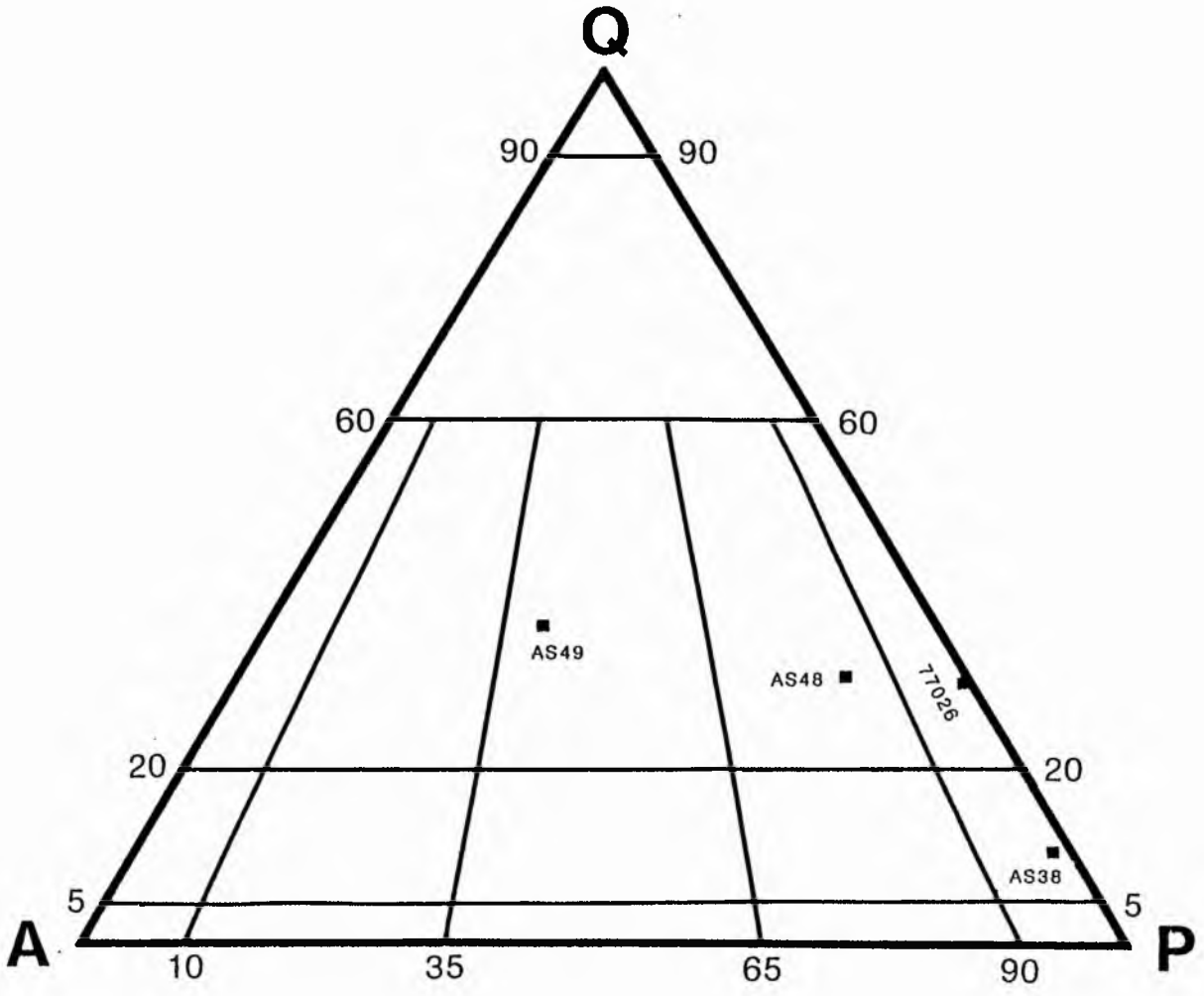

Fig 3.5 Modal classification and nomenclature of Cairnsmore of Carsphairn rock types (after Streckeisen, 1976).

Plate 3-48: Sample AS33. Microdiorite showing fine grained texture. Note the small ortho- and clinopyroxene grains and the late overgrowth of biotite.
Ppl, x 40.

Plate 3-49: As 3-48 in cpl.

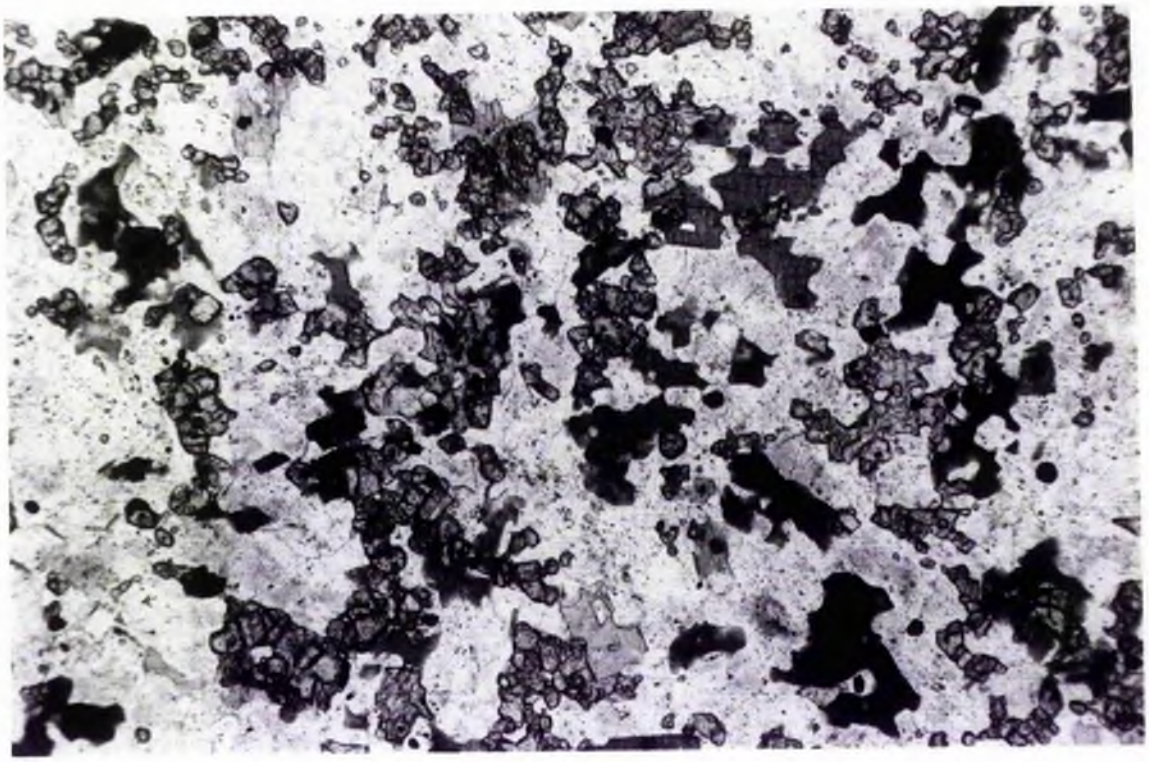

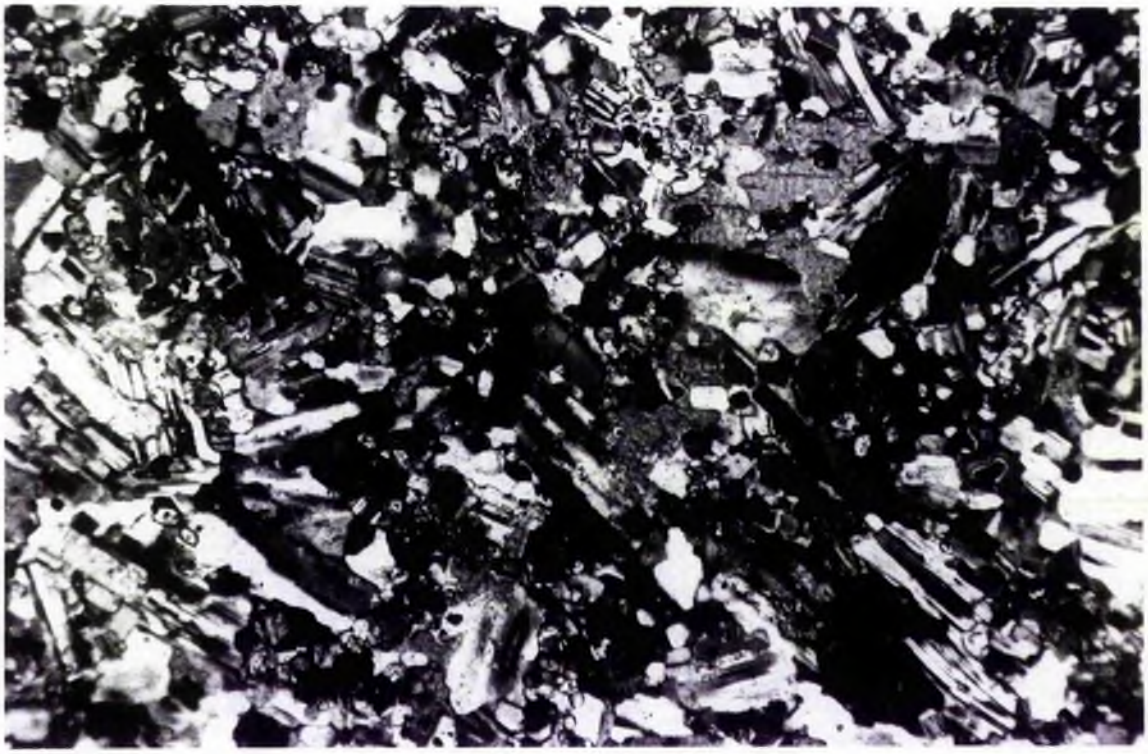

grains. Apatite (accessory) forms tiny euhedral and elongate crystals, mainly associated with biotite. Small primary anhedral opaque oxides are associated with biotite.

This is a microdiorite with early orthopyroxene. The rock has a quenched texture.

3.5.2 Hornblende biotite diorite:

Representative sample: AS38

Petrographic name: Medium grained hornblende biotite diorite.

Plates 3-50 and 3-51.

Description:

This rock is medium grained in hand specimen, grey to dark grey in colour, with dark hornblende and biotite grains enclosed in a feldspathic groundmass.

Amphibole (11.6% modal) forms anhedral crystals (up to 2.0 mm) with pale green pleochroism (green hornblende), some of them show replacement by biotite. Alteration to chlorite and iron oxide is common. Biotite (16.9% modal) forms euhedral plates. Plagioclase (60.9% modal) forms anhedral grains (maximum of 5.0 mm) of andesine composition (An44.0 average). Some show alteration to sericite. Alkali feldspar (1.1% modal) is a late-stage mineral forming anhedral intersititial grains (up to 2.0 mm). Quartz (7.6% modal) is the latest mineral to form with anhedral interstitial grains. Zircon (accessory) forms small euhedral crystals surrounded by pleochroic haloes and associated with biotite. Apatite (also accessory) forms small anhedral and elongate crystals associated with biotite. Small sphene grains with light reddish brown pleochroism are associated with mafic minerals. Small primary opaque oxides form anhedral grains associated

Plate 3-50: Sample AS38. Medium grained hornblende biotite diorite, showing hornblende, biotite and quartz grains interstitial to plagioclase.
Ppl, x 40.

Plate 3-51: Sample AS38. Medium grained hornblende biotite diorite showing late biotite and quartz grains.
Cpl, x 40.

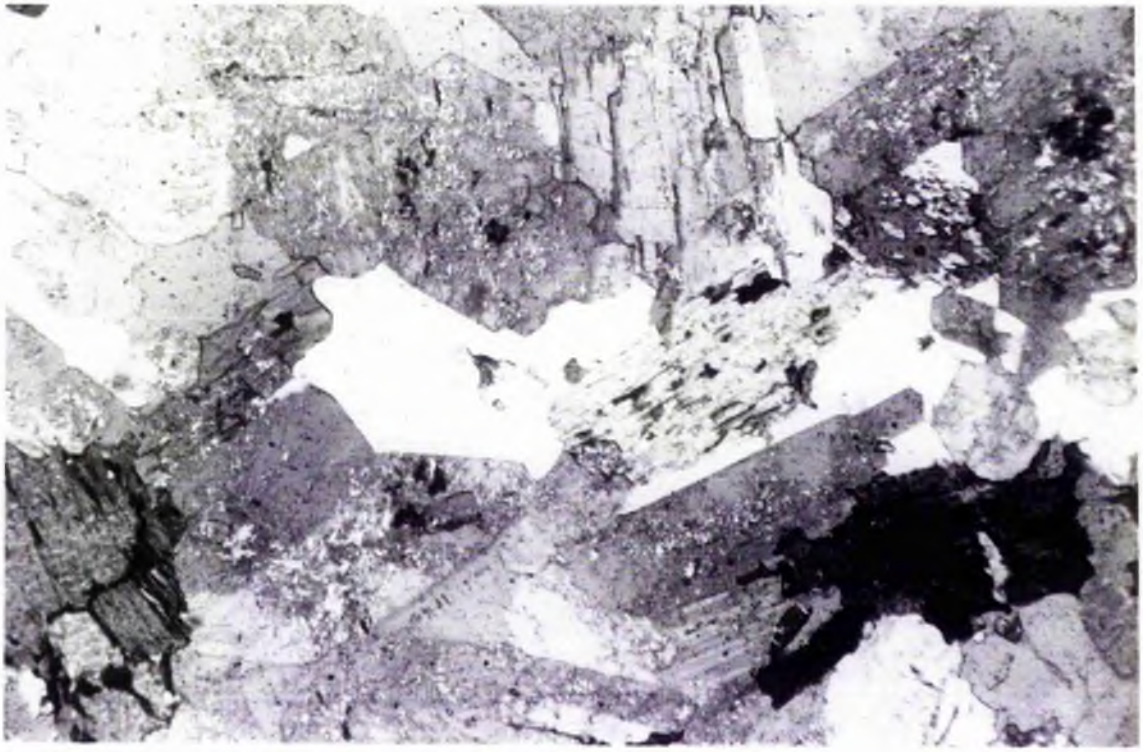

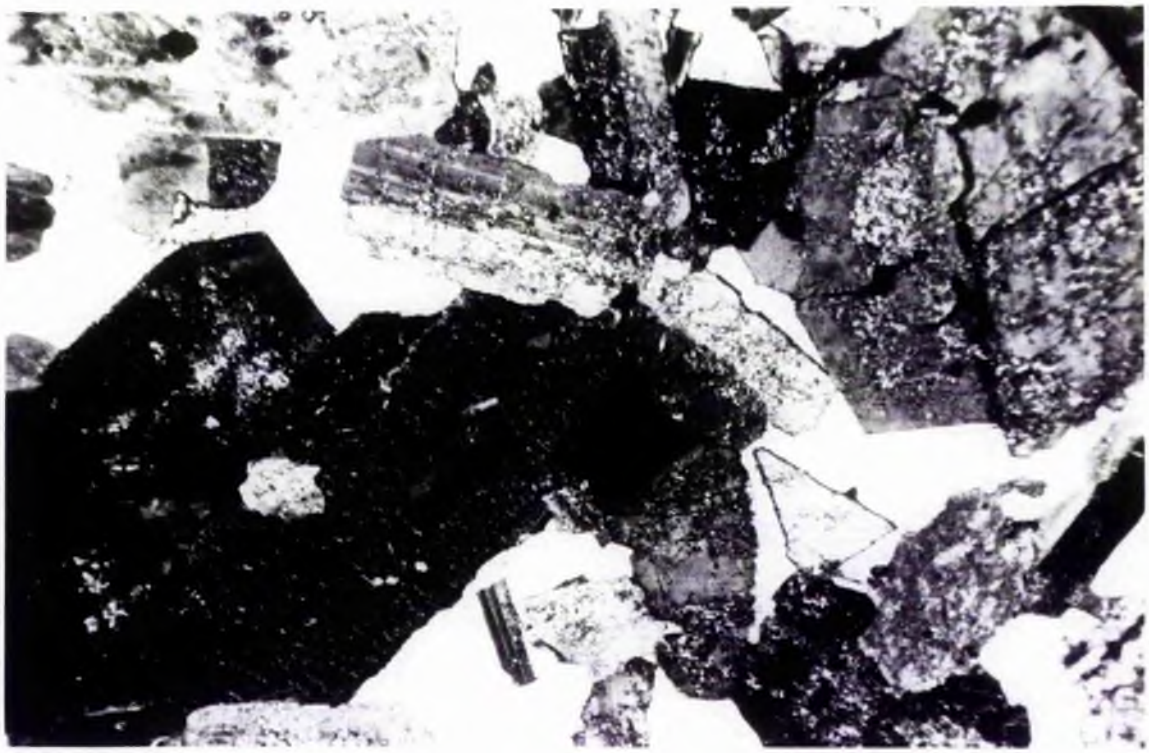

mainly with biotite. Abundant oxides result from the breakdown of mafic minerals.

This rock type is an intermediate medium grained rock with hornblende preceding biotite and the felsic minerals, having an anhedral granular texture.

3.5.3 Tonalite:

Representative sample: 77026

Petrographic name: Fine to medium grained tonalite.

Plates 3-52 to 3-54.

Description:

In hand specimen this rock is grey in colour, fine to medium grained, with laths of plagioclase and interstitial quartz.

Orthopyroxene (hypersthene, 5.4% modal) forms anhedral to prismatic crystals (maximum of 2.0 mm) showing neutral to pale pink pleochroism. Some have exsolved diopside. Others are rimmed by clinopyroxene and amphibole (corona texture). Small hypersthene crystals are scattered in the matrix. Clinopyroxene (4.6% modal) forms anhedral crystals (up to 2.0 mm) and some form rims to orthopyroxene crystals. It is colourless to pale brown. Amphibole (0.2% modal) forms small anhedral crystals associated with clinopyroxene having pale green pleochroism. Biotite (11.9% modal) forms subhedral to anhedral flakes (maximum of 3.0 mm). Alteration to chlorite is present. Plagioclase (53.4% modal) occurs mostly as tabular phenocrysts with a cloudy appearance due to fine inclusions of iron ores and pyroxene. It is of andesine composition (An36.0 average). Continuous zoning is from an inner core of An55 composition (labradorite) to an outer rim of andesine composition. Corrosion of

Plate 3-52: Sample 77026. Fine to medium grained tonalite, showing the intergranular texture. Note the early ortho- and clinopyroxene followed by plagioclase. Late biotite and quartz grains are interstitial. Cpl, x 20.

Plate 3-53: Sample 77026. The photomicrograph shows a prismatic orthopyroxene crystal rimmed by clinopyroxene (corona texture) in the centre of the field of view. Cpl, x 40.

Plate 3-54: Sample 77026. The photomicrograph shows orthopyroxene grains exsolved to diopside. Cpl, x 40.

plagioclase margins is a common feature. Some crystals show alteration to sericite. Alkali feldspar occurs interstitially forming myrmekite where it is in contact with plagioclase crystals. Quartz (23.4% modal) occurs as interstitial grains in the groundmass with undulose extinction. Zircon (accessory) forms small anhedral crystals within biotite surrounded by pleochroic haloes. Apatite (accessory) forms tabular and euhedral crystals associated with biotite and the groundmass. Primary opaque minerals form euhedral to anhedral grains associated with biotite and pyroxene. Some opaque minerals occur as breakdown products of primary mafic minerals.

This rock is a fine to medium grained granular tonalite with early orthopyroxene followed by clinopyroxene and biotite. Plagioclase has corroded textures with mafic minerals. Both alkali feldspar and quartz are late stage crystallising phases.

3.5.4 Granodiorite:

Representative sample: AS48

Petrographic name: Medium grained granodiorite.

Plates 3-55a, 3-55b and 3-56.

Description:

The hand specimen is medium grained and light grey to white in colour, with biotite and hornblende forming elongate crystals in clots within a feldspathic groundmass.

Amphibole (8.2% modal) forms anhedral grains (up to 3.0 mm) and some occur in mafic clots with biotite. It has pale green pleochroism and is frequently found with cores of relict clinopyroxene and replaced by biotite around its margins, some show alteration to chlorite. Biotite (17.1% modal) forms anhedral plates (max 4.0 mm)

Plate 3-55a: Sample AS48. Medium grained granodiorite, showing intergranular texture, biotite hornblende, alkali feldspar and quartz are interstitial to euhedral plagioclase.
Cpl, x 40.

Plate 3-55b: As 3-55a in ppl.

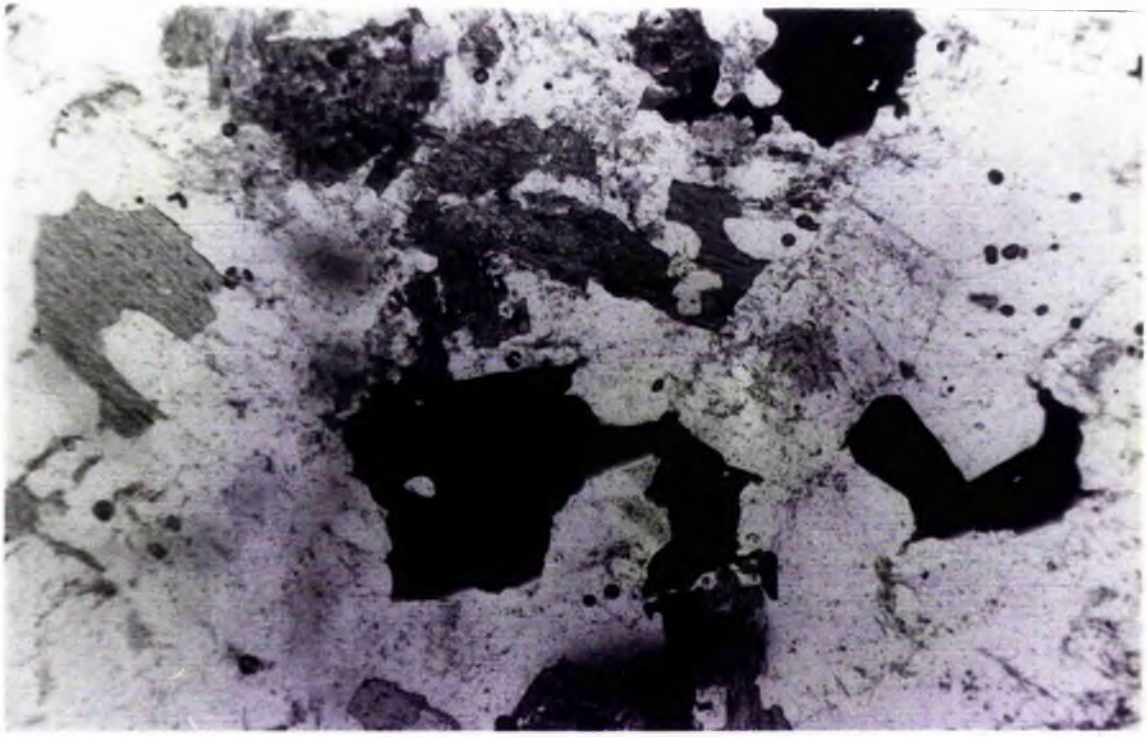

Plate 3-56: Sample AS48. The photomicrograph shows an orthoclase crystal with microperthitic texture.
Cpl, x 40.

Plate 3-57: Sample AS49. Medium to coarse grained granite.
The photomicrograph shows an orthoclase crystal with carlsbad twinning and microperthitic texture.
Cpl, x 20.

having pale to dark brown pleochroism, some form in mafic clots with hornblende. Some irregular grains with orange to dark brown pleochroism are present. Plagioclase (42.4% modal) occurs as elongate crystals (up to 4.0 mm in length). It is of andesine composition (An32.0 average). Some crystals show sericitisation. Alkali feldspar (8.6% modal) occurs as interstitial aggregates and as poikilitic plates with inclusions of hornblende, biotite and plagioclase, having microperthitic texture, (plate 3-56). The boundaries between the alkali feldspar and plagioclase are corroded and lobes of myrmekite are formed at the edges of plagioclase. Quartz (22.6% modal) forms interstitially to other minerals. Apatite is found with zircon as inclusions in the biotite. Small primary opaque minerals are present associated with biotite.

This is a granular acidic rock, hornblende biotite granodiorite, of medium grain size with clinopyroxene and plagioclase followed by hornblende and then biotite. Alkali feldspar and quartz are both late stage crystallising minerals.

3.5.5 Granite:

Representative sample: AS49

Petrographic name: Medium to coarse grained granite.

Plate 3-57.

Description:

In hand specimen, this is medium to coarse grained with light cream colour in which orthoclase is the most conspicuous mineral with subordinate quartz, plagioclase and mafic clots of biotite and hornblende.

Amphibole (2.2% modal) forms anhedral and tabular crystals (up

to 2.0 mm) having pale green pleochroism associated with biotite in mafic clots. Alteration to chlorite and iron ores is common. Biotite (6.6% modal) is found in anhedral to elongate crystals (up to 2.0 mm) with pale to dark brown pleochroism. It replaces hornblende in mafic clots. Plagioclase (23.6% modal) forms anhedral laths (up to 5.0 mm in length) of oligoclase composition (An28.0 average). Sericitisation is common. Alkali feldspar (33.6% modal) forms large anhedral plates to elongate crystals having microperthitic texture which often contain inclusions of earlier formed plagioclase and biotite. Quartz (32.8% modal) forms anhedral interstitial grains (up to 3.0 mm) with undulose extinction. Apatite and zircon are small inclusions associated with biotite. Sphene (accessory) forms anhedral grains (max 1.5 mm) with reddish brown pleochroism. Small primary opaque minerals are associated with biotite. Some opaque minerals result from the breakdown of primary hornblende.

This is an acidic rock of medium to coarse grained size with granular texture, hornblende preceding other minerals, alkali feldspar and quartz are late stage minerals.

3.5.6 Summary:

Since the work of Teall (1899) and Deer (1935a) briefly describing the petrography of this complex, no detailed study has been published. According to this study the complex is composed of microdiorite; hornblende biotite diorite; tonalite; granodiorite and granite, which are equivalent to Deer's hornblende hybrid, pyroxene biotite hybrid, tonalite, acid hybrid and granite.

3.6 THE LOCH DOON COMPLEX

Introduction:

This complex shows a petrological range from diorite through granodiorite to granite. Their distribution is approximately concentric for the granodiorites and granites, but the diorites are confined to two small bodies at either end of the pluton (Fig 2.6). Microdiorites which are present at the southern end of the complex are fined grained consisting of both ortho- and clinopyroxenes and biotite along with plagioclase, alkali feldspar and quartz. The diorites in this complex are of two types, namely two-pyroxene biotite diorite and hornblende biotite diorite, though the two-pyroxene biotite diorite is predominant. Modal analyses are listed in Table 3.6 and plotted on Fig 3.6.

3.6.1 Microdiorite:

Representative sample: 77015

Petrographic name: Fine grained diorite (microdiorite).

Plates 3-58a and 3-58b.

Description:

This rock in hand specimen is fine grained, of grey to dark grey colour, characterised by dominant mafic minerals (pyroxene and biotite) with plagioclase and interstitial quartz.

Orthopyroxene (approx. 15% modal) forms anhedral to prismatic crystals (up to 2.0 mm) and small grains in the groundmass, having faint pink pleochroism (hypersthene), some crystals have exsolved to diopside. Clinopyroxene (approx. 5% modal) forms small anhedral

Table 3.6: Modal analyses of the Loch Doon rock types

Sample No	Opx %	Cpx %	Amph %	Biot %	Plag %	Alk-Feld %
78002	10.4	6.7	0.4	6.7	59.8	1.8
WL8	-	0.8	9.8	17.3	56.1	3.7
DBL1	-	0.9	7.0	16.1	37.6	6.0
77022	-	-	6.9	15.9	38.2	7.8
77002	-	0.2	7.3	26.5	44.6	7.1
WL9	-	-	3.2	11.1	39.1	14.2
77024	-	-	8.3	12.1	41.0	13.8
HH2	-	-	-	6.6	29.8	26.6
HH4	-	-	0.8	11.1	31.4	25.6

Quartz %	Opaque %	Acces-sories	Rock Type
13.4	0.8	-	Pyroxene-biotite diorite
11.0	0.6	0.7	Hornblende-biotite diorite
31.9	-	0.5	Granodiorite
30.4	0.1	0.7	Granodiorite
24.1	-	0.2	Granodiorite
32.2	-	0.2	Granodiorite
24.8	-	-	Granodiorite
37.0	-	-	Granite
31.0	-	0.1	Granite

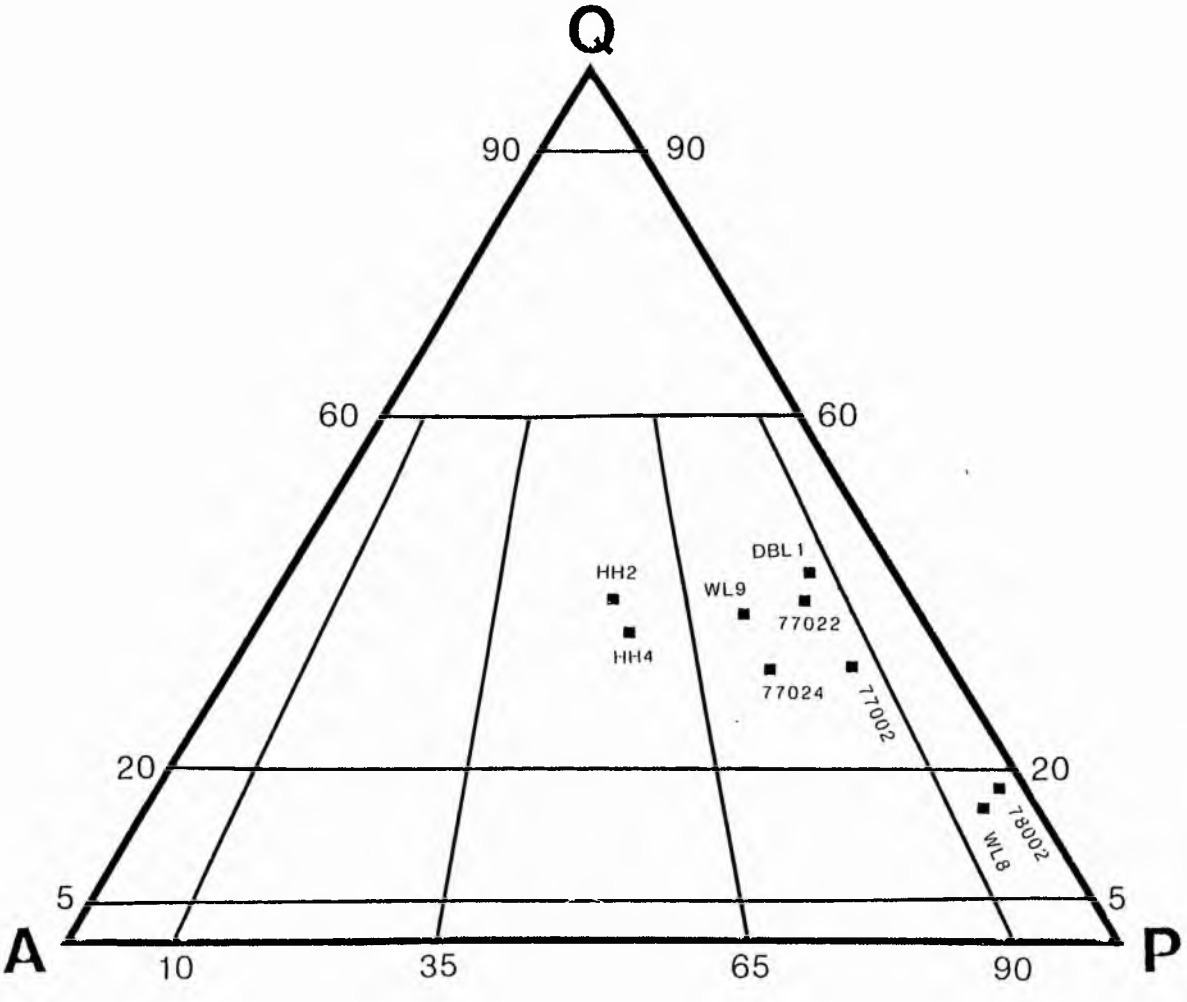

Fig 3.6 Modal classification and nomenclature of Loch Doon rock types (after Streckeisen, 1976).

Plate 3-58a: Sample 77015. Microdiorite. The photomicrograph shows early plagioclase, orthopyroxene and clinopyroxene and late biotite and quartz.
Ppl, x 40.

Plate 3-58b: As 3-58a in cpl.

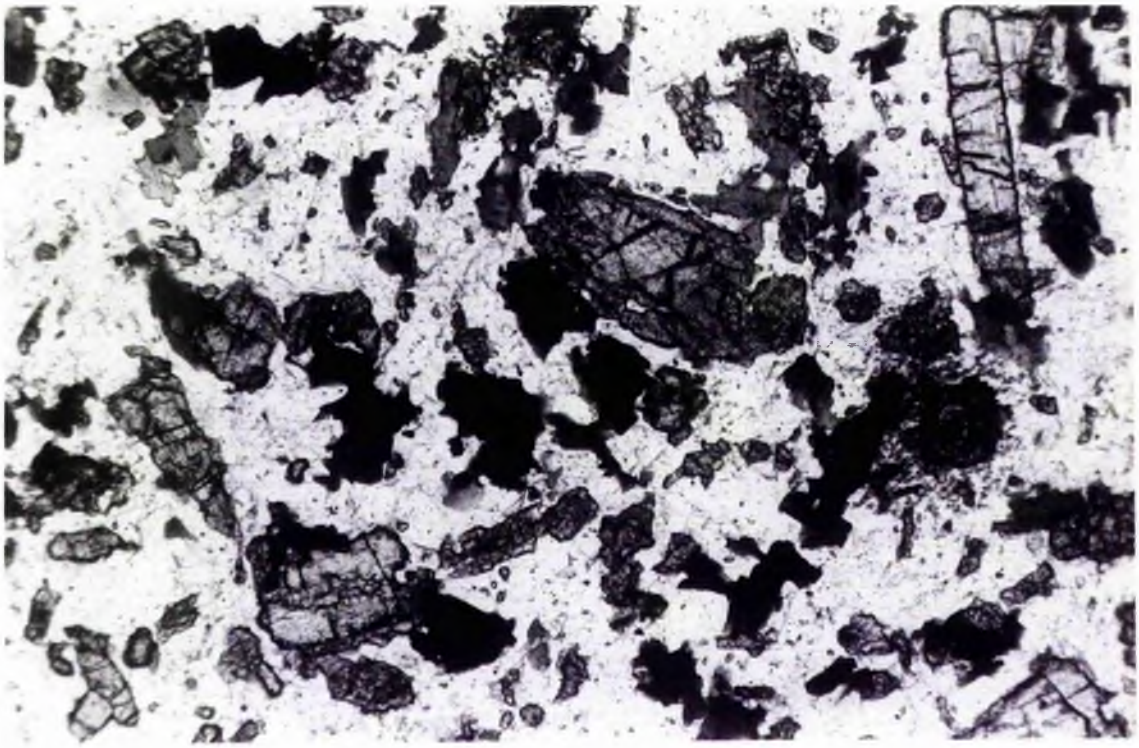

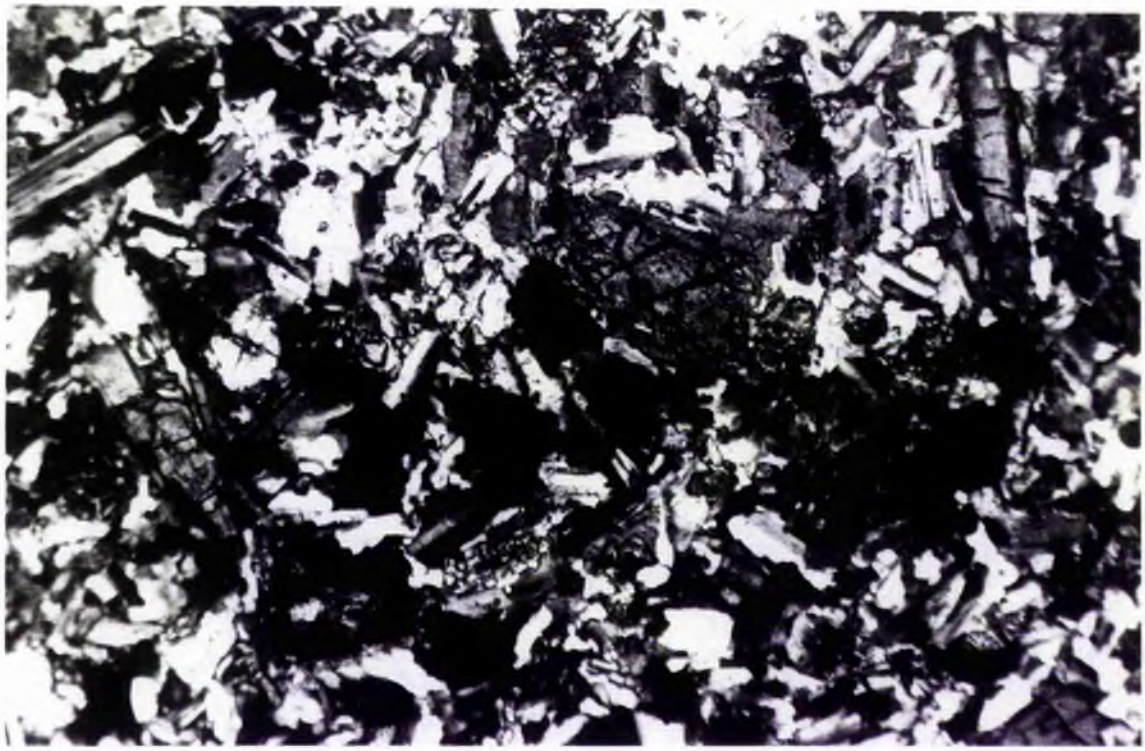

crystals, colourless to pale brown in colour (augite). Biotite (about 10% modal) forms anhedral plates replacing pyroxene in some areas with pale to dark brown pleochroism, and some irregular grains with dark reddish brown pleochroism forming interstitially. Plagioclase (about 60% modal) forms anhedral to tabular crystals (up to 3.0 mm in length) with cloudy appearance, and some as small grains in the groundmass. It is of andesine composition (An42 average). A few show normal zoning. Alkali feldspar (1-2% modal) forms small anhedral grains, interstitial to the other minerals. Quartz (about 10% modal) is the last mineral forming small anhedral grains interstitial to other components. Zircon, apatite and primary opaque minerals form small anhedral crystals, zircon is surrounded by pleochroic haloes within biotite.

This is a quartz microdiorite with porphyritic texture where medium plagioclase, ortho- and clinopyroxene and biotite phenocrysts are set in a groundmass of fine grained pyroxenes, plagioclase, biotite, alkali feldspar and quartz. Plagioclase is an early phase preceding other constituents, pyroxene started crystallising later, and then biotite. Biotite replaces pyroxene and forms individual crystals. Both alkali feldspar and quartz are late stage minerals.

Additional samples of this type are WL3 and WL4 but WL4 differs in containing more felsic minerals than 77015 and pyroxenes are generally pseudomorphed by amphibole.

3.6.2 Diorite:

The diorites in this complex are medium to coarse grained, found in the northwestern and southeastern ends of the pluton. They are classified into two types:

a) Two-pyroxene biotite diorite

b) Hornblende biotite diorite

3.6.2a Two-pyroxene biotite diorite:

Representative sample 78002

Petrographic name: Medium grained two-pyroxene biotite diorite.

Plates 3-59a and 3-59b.

Description:

In hand specimen, this rock is medium grained of grey to dark grey colour. It is characterised by its dominant pyroxene and biotite minerals with laths of plagioclase and interstitial quartz.

Orthopyroxene (hypersthene, 10.4% modal) forms anhedral and prismatic crystals (up to 2.0 mm) and small grains in the matrix. It has faint pink pleochroism, and some grains have exsolved diopside. Clinopyroxene (6.7% modal) forms anhedral and prismatic crystals (max. 3.0 mm) and small grains in the groundmass. Some crystals exhibit exsolution lamellae giving them a schiller structure. They are pale green to pale purplish brown in colour with weak pleochroism. Local alteration to chlorite and amphibole is present. Amphibole (0.7% modal) forms rims to pyroxene grains and some small separate grains at the edges of pyroxene. They have pale green pleochroism. Biotite (6.7% modal), forms anhedral flakes (up to 3.0 mm). Both biotite and hornblende show replacement of pyroxene. Plagioclase (59.8% modal) forms tabular crystals (up to 4.0 mm) with a cloudy appearance due to inclusions, and finer grained laths in the groundmass. It is of andesine composition (An38 average). Plagioclase is an early mineral with orthopyroxene forming at its

Plate 3-59a: Sample 78002. Medium grained two-pyroxene biotite diorite, showing early plagioclase crystals with laths of orthopyroxene, and some clinopyroxene crystals. Note the late biotite and quartz. Cpl, x 20.

Plate 3-59b: As 3-59a in ppl

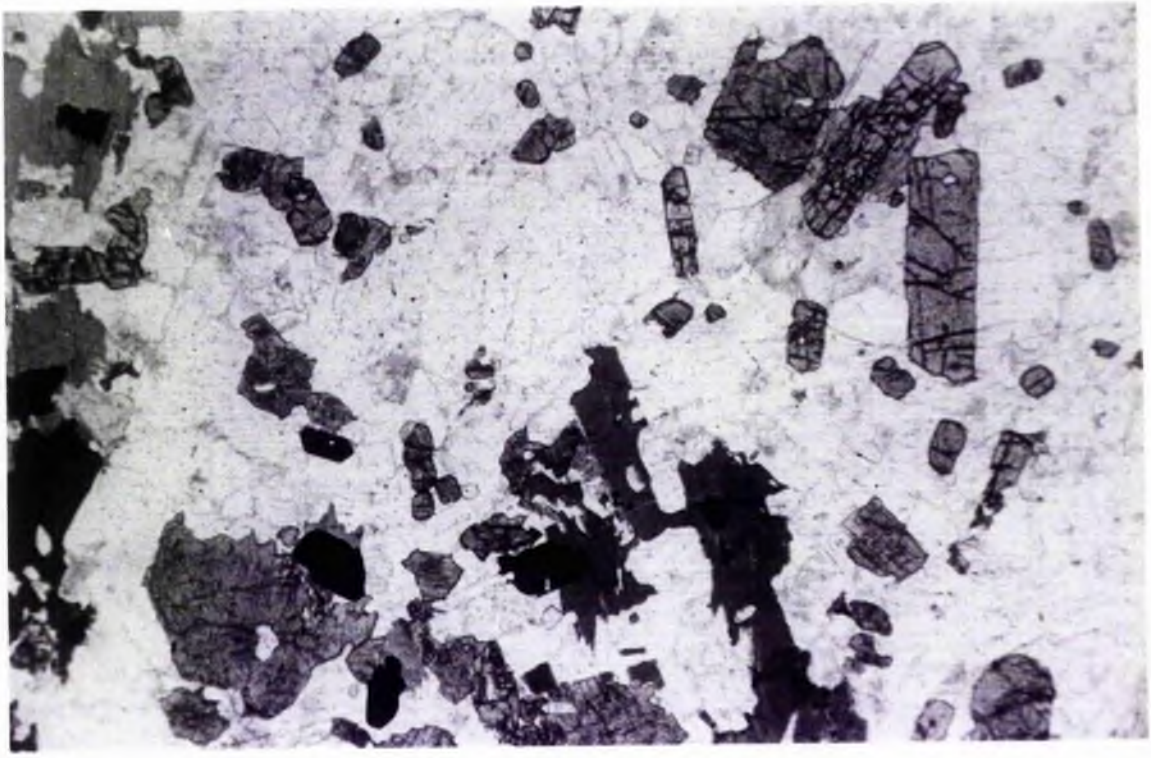

edges. Alkali feldspar (1.8% modal) forms small grains interstitial to plagioclase showing microperthitic texture. Some myrmekites are present at the edges of plagioclase. Quartz (13.4% modal) is a late stage mineral forming small anhedral grains interstitial to other minerals. Zircon, apatite and primary opaque oxides are forming small inclusions mainly in biotite.

This rock has a subhedral granular texture . Most mafic minerals are interstitial but orthopyroxene crystals are early, followed by clinopyroxene, then by amphiboles and biotite. Both alkali feldspar and quartz are late-stage phases forming interstitial grains. The rock has been slightly strained as biotite and quartz show undulose extinction.

3.6.2b Hornblende biotite diorite:

Representative sample: WL8

Petrographic name: Medium grained hornblende biotite diorite.

Plates 3-60a, 3-60b and 3-61.

Description:

In hand specimen this rock is medium grained, hornblende and biotite are dark coloured in a light coloured groundmass of felsic minerals.

Amphibole (green hornblende, 9.8% modal) forms separate anhedral grains (up to 2.0 mm) and some small grains in the groundmass. Some form rims to clinopyroxene (0.8% modal) having pale green pleochroism. Alteration to chlorite is present. Biotite (17.3% modal) forms anhedral flakes (maximum 5.0 mm), small grains in the groundmass, forming clots with hornblende. Biotite forms at the edges of plagioclase and replaces hornblende, and also forms anhedral grains

Plate 3-60a: Sample WL8. Medium grained hornblende biotite diorite, having intergranular texture where hornblende and biotite grains are interstitial to euhedral plagioclase.
Cpl, x 20.

Plate 3-60b: As 3-60a in ppl.

Plate 3-61: Sample WL8. The photomicrograph shows myrmekitic texture at the edge with plagioclase crystal.
Cpl, x 40.

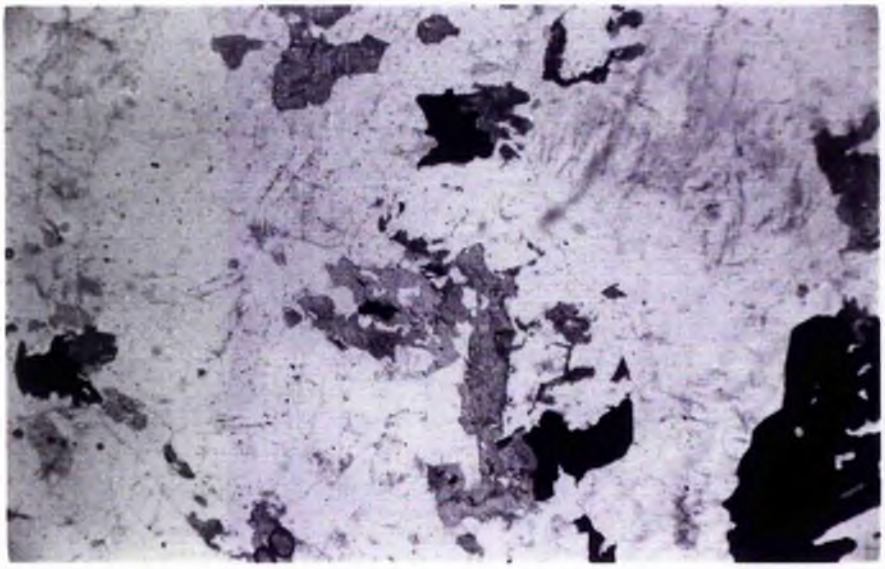

interstitial to plagioclase. Plagioclase (56.1% modal) forms subhedral to anhedral prismatic crystals (up to 7.0 mm long) and small grains in the groundmass, is of andesine composition (An42 average). Alkali feldspar (3.7% modal) forms anhedral grains (up to 3.0 mm). It is a late-stage mineral and poikilitically encloses plagioclase, hornblende and biotite, having microperthitic texture. Myrmekite develops at the edges of plagioclase crystals, (plate 3-61). Quartz (11.0% modal) is the latest mineral to form with anhedral interstitial grains growing up to 3.0 mm. Zircon, apatite and primary opaque oxides (accessories) form small euhedral to anhedral grains mainly associated with biotite, some opaque minerals result from the breakdown of primary amphibole.

This is an intermediate rock of medium grain size with primary plagioclase, early forming and also clinopyroxene, hornblende, and biotite. Both alkali feldspar and quartz are late-stage crystallising phases.

3.6.3 **Granodiorites:**

Representative sample: 77022

Petrographic name: Medium to coarse grained hornblende biotite granodiorite

Plates 3-62a to 3-63.

Description:

In hand specimen this rock is medium to coarse grained, of grey to white colour, with biotite and hornblende enclosed in a felsic groundmass in which quartz, plagioclase and occasionally interstitial pink alkali feldspar can be recognised.

Plate 3-62a: Sample DBL1. Medium grained granodiorite having intergranular texture, showing plagioclase crystals followed by hornblende and biotite. Alkali feldspar and quartz are interstitial to other minerals. Ppl, x 20.

Plate 3-62b: As 3-62a in cpl.

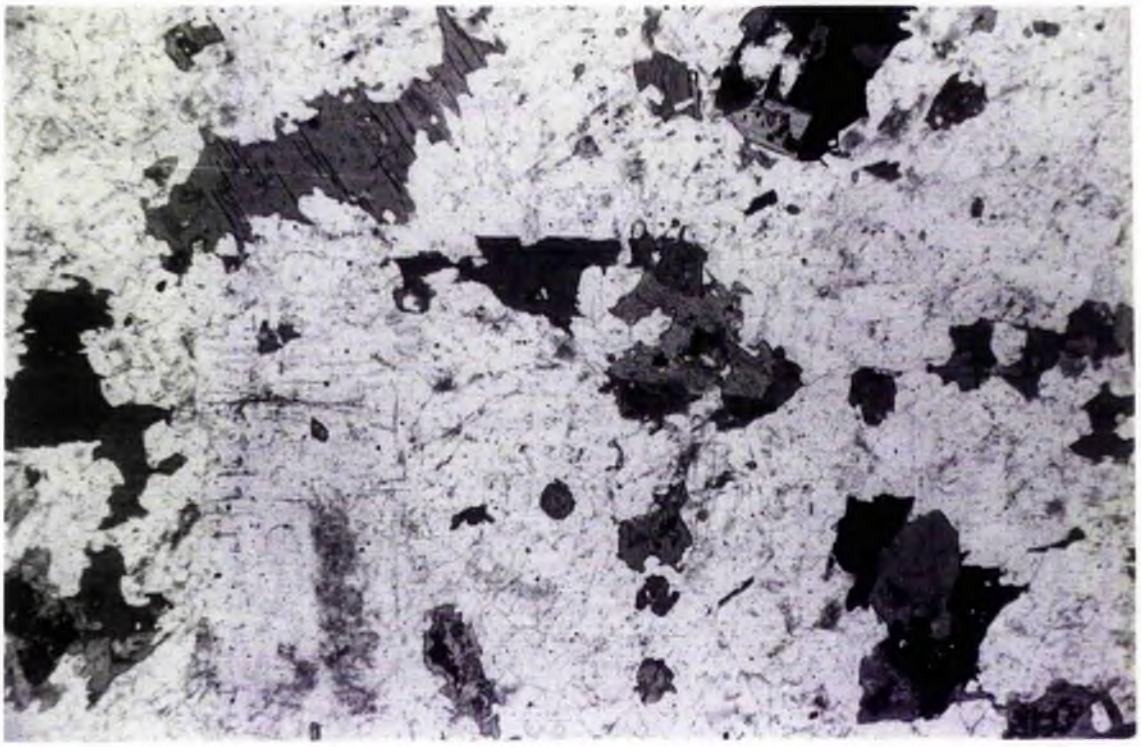

Plate 3-63a: Sample 77022. Medium grained hornblende biotite granodiorite, showing late biotite with zoned plagioclase crystal (see photomicrograph below). The rock has intergranular texture.
Ppl, x 20.

Plate 3-63b: As 3-63a in cpl.

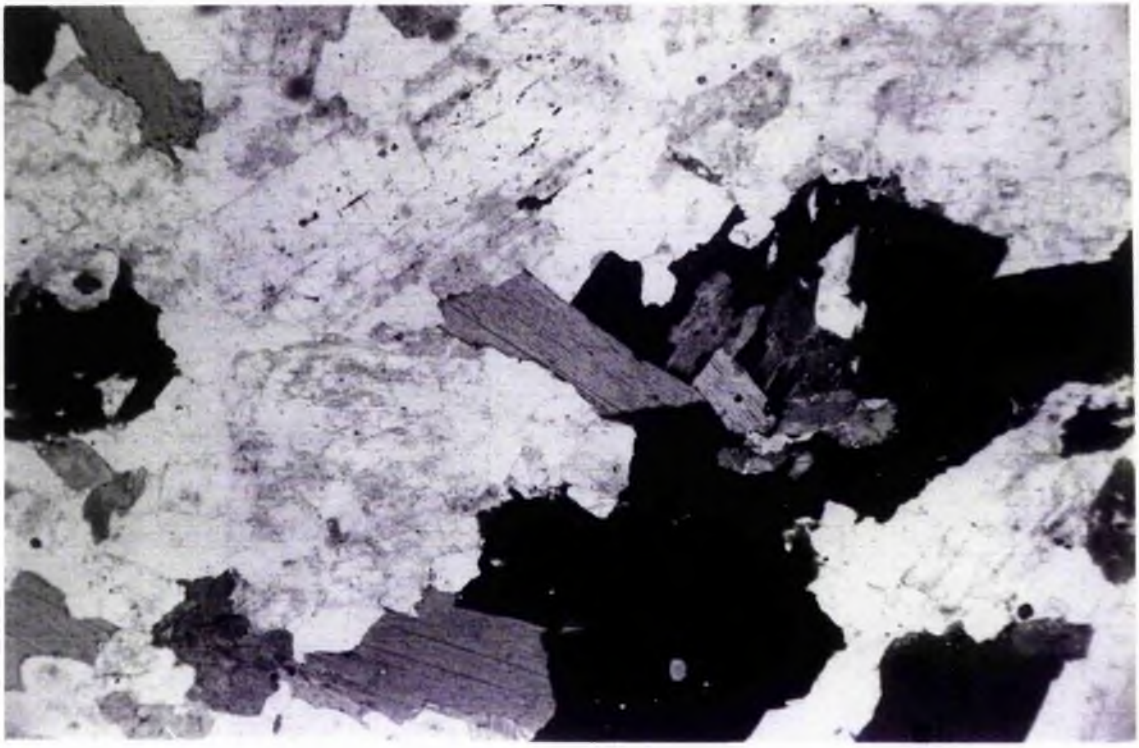

Amphibole (green hornblende 6.9% modal) forms anhedral and prismatic crystals (up to 3.0 mm) sometimes forming clots with biotite. Biotite (15.9% modal) forms anhedral flakes (up to 4.0 mm) and also replaces amphibole. Plagioclase (41.2% modal) forms subhedral tabular crystals (maximum 6.0 mm) and small grains in the groundmass. It is of andesine composition (An32.0 average). Alkali feldspar (4.8% modal) forms anhedral interstitial grains (up to 3.0 mm) with microperthitic texture. Myrmekitic texture develops at some plagioclase boundaries. Quartz (30.4% modal) is the latest mineral forming anhedral interstitial grains (up to 1.0 mm). Zircon and apatite (accessory) form euhedral small inclusions in biotite where zircon is surrounded by pleochroic haloes. Sphene (accessory) forms small euhedral to irregular crystals with pale to dark brown pleochroism forming at the edges of hornblende and corroding biotite grains. Primary opaque oxides form anhedral to elongate crystals (up to 2.0 mm), associated mainly with biotite, some oxides result from the breakdown of primary hornblende.

This is a granodioritic rock of medium to coarse grain size with subhedral granular texture. Plagioclase is an early phase followed by hornblende and biotite, both alkali feldspars and quartz are late-stage phases.

Additional samples of this type are DBL1, DBL2, DBL3, 77002, 77021, 77023, 77024 and 77025 with varying proportions of mafic and felsic minerals. WL9 is from region of the transitional granodiorite and contains less mafic minerals and more alkali feldspar (Table 3-6) relative to the main granodiorite.

3.6.4 Granite:

Representative sample: HH2

Petrographic name: Medium to coarse grained biotite granite.

Plates 3-64 and 3-65.

Description:

In hand specimen the rock is medium to coarse grained, light coloured in which orthoclase is the most conspicuous mineral present, with subordinate quartz, plagioclase and biotite.

Biotite (6.6% modal) forms anhedral and tabular crystals (up to 2.0 mm) and sometimes form in clots. It is a fairly late mineral forming at the edges of the plagioclase. Plagioclase (29.8% modal) forms anhedral to subhedral crystals (up to 5.0 mm). Alteration to sericite and saussurite is common. Alkali feldspar (26.6% modal) forms anhedral grains (maximum 6.0 mm) with microperthitic texture. Some grains show microcline twinning. It is a late-stage mineral which poikilitically encloses plagioclase and biotite grains. Quartz (37.0% modal) is the latest mineral, forming anhedral interstitial grains (up to 3.0 mm). Zircon, apatite and primary oxides form small inclusions mainly in biotite.

This is an acidic rock of medium to coarse grained size with granular texture. Plagioclase is an early phase with which other constituents are interstitial. The rock shows strain as indicated by biotite and quartz with undulose extinction.

3.6.5 Summary:

The first detailed petrographic work for this complex was published by Gardiner & Reynolds (1932) followed by Brown et al. (1979) who found this complex to comprise hypersthene diorite, quartz monzonite and quartz monzodiorite with granite in the centre. Tindle

Plate 3-64: Sample HH2. Medium to coarse grained granite showing biotite, orthoclase and quartz grains are interstitial to plagioclase crystals.
Cpl, x 12.

Plate 3-65: Sample HH2. The photomicrograph shows orthoclase and plagioclase crystals, orthoclase with carlsbad twins and microperthites.
Cpl, x 20.

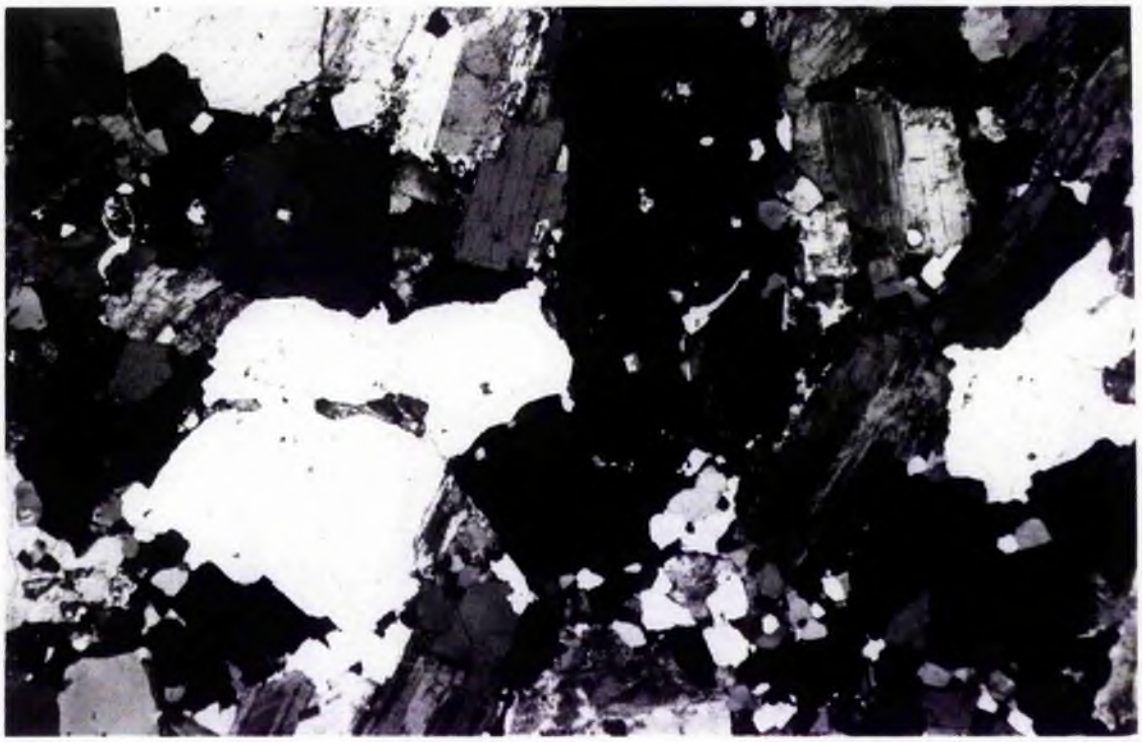

& Pearce (1981) studied this complex and described it as being formed of diorite and quartz diorite in the northwestern part and quartz diorite in the southern part followed by tonalite, granodiorite, granite and microgranite successively towards the centre. The modal analyses of the present study show this complex to consist mainly of microdiorite; diorite of two types a) two-pyroxene biotite diorite and b) hornblende biotite diorite; granodiorite and granite. Two-pyroxene biotite diorites are dominant in the dioritic zone, while the hornblende biotite diorites are found in the transitional zone between the diorites and the granodiorites.

3.7 Petrographic comparison of complexes

The new detailed petrographic studies of these complexes compares plutons in the southern Highlands (represented by the Garabal Hill-Glen Fyne and Comrie complexes), the eastern Highlands (represented by the Glen Doll and Glen Tilt complexes), and the Southern Uplands (represented by the Cairnsmore of Carsphairn and Loch Doon complexes). The data are summarised in Table 3-7. The range diorite to granite is represented in all regions and most complexes. Pyroxene diorites are not found in the eastern Highlands but are present in the other regions including hypersthene mica diorites. Gabbros are not found in the Southern Uplands and are found only in the Glen Doll and Garabal Hill -Glen Fyne complexes. These same complexes also have ultrabasic rock types including peridotites and pyroxenites. All complexes have late granodiorites. The complexes with gabbros and ultrabasic rocks (Glen Doll and Garabal Hill-Glen Fyne) do not evolve as far as true granite, whereas the other four complexes with diorites as the most basic members evolve as far as biotite granite.

Table 3-7: Comparison of petrographic types in complexes under investigation

Rock types	Garabal Hill-Glen Fyne Complex	Comrie Complex	Glen Doll Complex	Glen Tilt Complex	Cairnsmore of Casphairn Complex	Loch Doon Complex
Ultrabasic rocks	✓	x	✓	x	x	x
Pyroxene gabbro	✓	x	x	x	x	x
Hornblende gabbro	✓	x	✓	x	x	x
Quartz gabbro	x	x	✓	x	x	x
Microdiorite	x	x	x	x	✓	✓
Two-pyroxene biotite diorite	✓	✓	x	x	x	✓
Augite biotite diorite	x	✓	x	x	x	x
Hornblende biotite diorite	✓	✓	✓	✓	✓	✓
Appinitic diorite	✓	x	x	✓	x	x
Tonalite	x	x	✓	x	✓	x
Granodiorite	✓	✓	✓	✓	✓	✓
Granite	x	✓	x	✓	✓	✓

CHAPTER 4

MINERAL CHEMISTRY

4.1 INTRODUCTION

The aim of this chapter is to examine the compositions of the principal rock-forming minerals in the six complexes. Variations of single mineral species between different rock types within a single complex have been studied to provide a mineralogical basis on which to interpret the crystallisation history (including constraining temperatures) and the whole-rock geochemistry. In addition compositions of the same mineral species in similar rock types in different complexes are compared in an attempt to understand regional differences in bulk composition, crystallisation temperatures, and paths of fractional crystallisation. The minerals analysed include olivine, orthopyroxene, clinopyroxene, amphibole, biotite, and plagioclase. Alkali feldspar and quartz were not included as their variations are relatively minor.

Analysis was performed on the Cambridge Microscan V electron microprobe at Edinburgh University Geology Department using energy dispersive analysis (EDS). For details of the techniques used see Appendix C.

4.2 GARABAL HILL-GLEN FYNE

4.2.1 OLIVINE:

Olivine is present in the ultrabasic rocks (wehrlite), gabbro, and pyroxene biotite diorite of this complex and representative analyses are given in Appendix C.

It is apparent from the analyses that olivine from peridotites has a composition of Fo_{79} to Fo_{81}; Fo_{80} in gabbro, and Fo_{79} to Fo_{77} in diorites. Appendix C, Table C1 also indicates that small quantities

of Ca (less than 0.2 wt% CaO) are commonly present. Most of the analysed olivines contain Ni (0.16 - 0.55 wt%). Cr was not detected in any olivine in this study.

4.2.2a ORTHOPYROXENE:

Orthopyroxenes from representative two-pyroxene biotite diorite and gabbros have been analysed and the data are presented in Appendix C.

From these analyses it is evident that there is a compositional range from bronzite to hypersthene En_{67}-En_{74}. All of the analysed orthopyroxenes contain very low Al (less than 2.0 wt% Al_2O_3), Ca (less than 1.5 wt% CaO) and Ti (less than 0.26 wt% TiO_2), Ni is detected only in GH10. MnO is greater than 1.0 wt% only in GH10, but does not show sympathetic variation with Fe. It is apparent that there is an Fe-enrichment within the orthopyroxenes of the gabbro sample GH21.

4.2.2b CLINOPYROXENE:

Clinopyroxene has been analysed from peridotite, gabbro, and two-pyroxene biotite diorite. Representative analyses are given in Appendix C.

All analysed clinopyroxenes contain low Al, ranging from 1.36 - 3.67 wt% Al_2O_3. TiO_2 (less than 1.0 wt%), and Cr_2O_3 (less than 0.85 wt%) are consistently more abundant than in orthopyroxene. Na_2O is less than 0.5 wt%. Clinopyroxene varies in composition from augite to salite (Fig. 4.1) and with some diopside in ultrabasic rocks.

There is a very limited Fe-enrichment trend with $Mg^{\#}$ values varying commonly between 0.75 and 0.86 and are generally higher than 0.80 in the ultrabasic rocks.

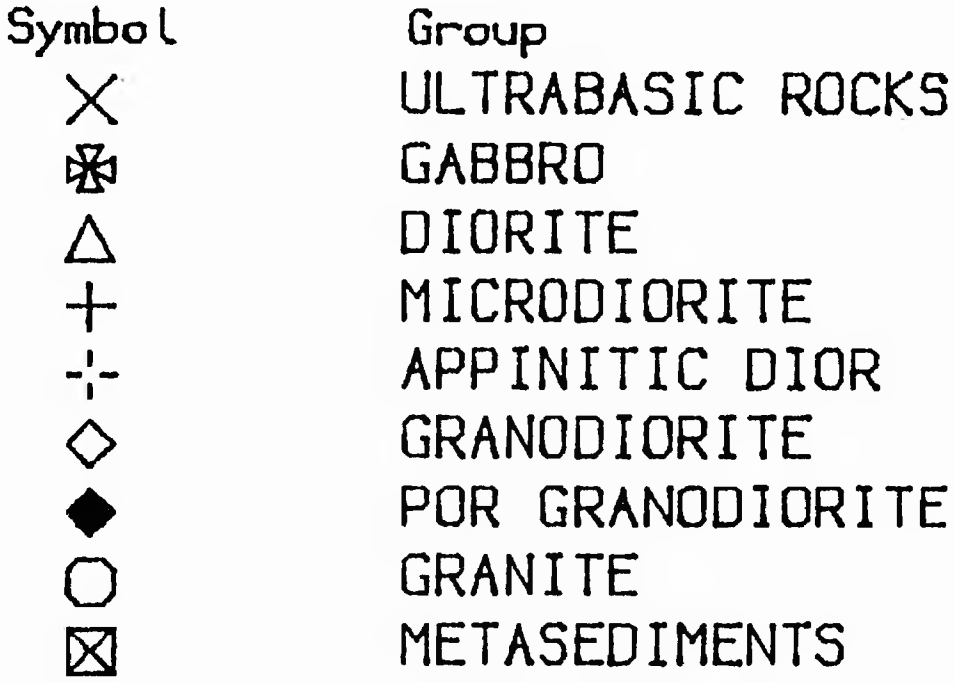

Key to symbols used in the diagrams of Chapters 4 and 5.

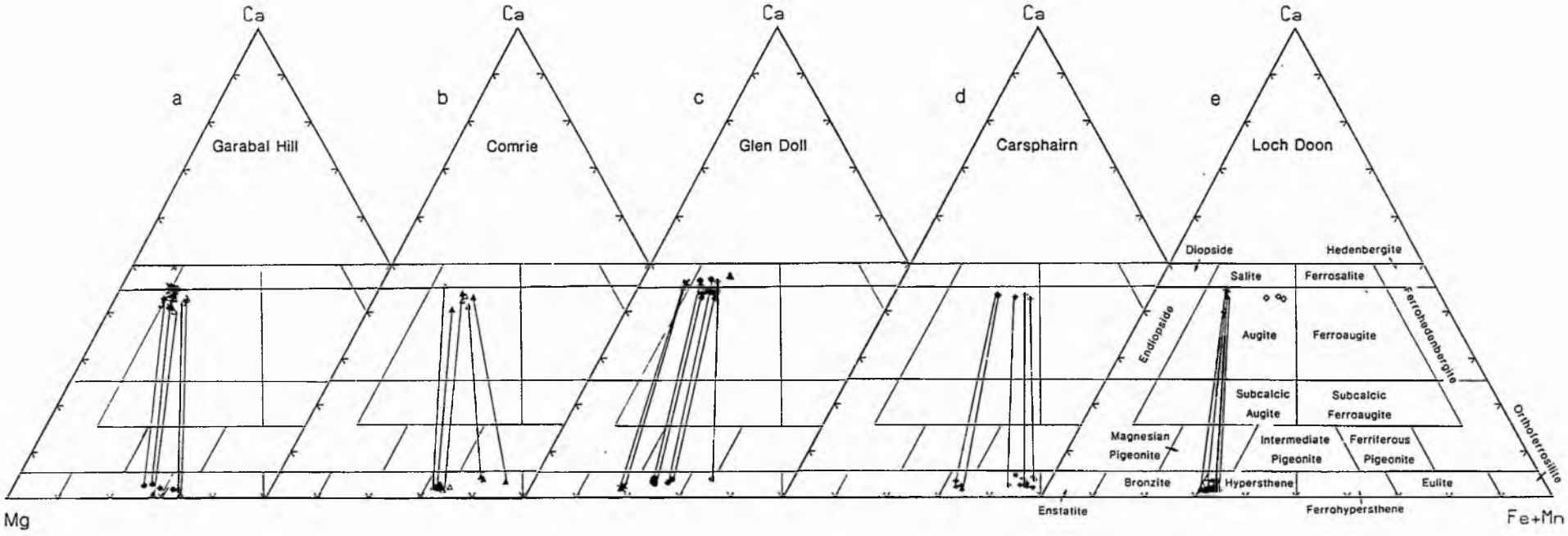

Fig 4.1 Nomenclature of ortho- and clinopyroxenes plotted in terms of Mg, Ca, ΣFe + Mn (atomic per cent) of the studied plutons (after Deer et al, 1978).

4.2.3 AMPHIBOLE:

Amphibole is present in most rocks of this complex, particularly in gabbro, diorite and granodiorite. Estimation of Fe^{3+} is important in amphibole classification schemes, the structural formula unit has been recalculated following the charge balance equation method of Papike et al. (1974). Amphibole nomenclature is based on the IMA recommendations of Leake (1978). Electron microprobe analyses of amphiboles are given in Appendix C together with their structural formulae based on 23 oxygens (H_2O-free) listed in approximate order of increasing Si content. The data are plotted as Si vs Mg values (Fig. 4.2), corresponding to the classification scheme of Leake (1978) and Al^{iv} vs (Na + K) (Fig. 4.3) after Deer et al. (1978).

Amphibole is exclusively calcic in composition (i.e. $(Ca + Na)_B$ greater than 1.34, $(Na)_B$ less than 0.67, and $(Na + K)_A$ less than 0.5). The amphiboles commonly range from magnesio-hornblende in composition with subordinate more aluminous varieties trending through tschermakitic hornblende to tschermakite. Secondary amphibole is actinolitic hornblende in composition.

SiO_2 contents vary from 41 to 52 wt%, and Al_2O_3 from 3.5 to 13 wt%, secondary amphibole being more Si-rich. MgO varies from about 13 wt% in the tschermakite to 17.5% in actinolitic hornblende. FeO varies from 9 wt% in the actinolitic hornblende to less than 16 wt% in the magnesio-hornblende. TiO_2 varies from 0.1 wt% to 3.9 wt%, the highest content being in the more aluminous amphibole (tschermakite). MnO varies from 0.1 wt% to 0.6 wt%. It is significant that the CaO content is nearly constant varying between 10 and 12 wt%. Na_2O and K_2O are more abundant in the more aluminous amphibole (tschermakite)

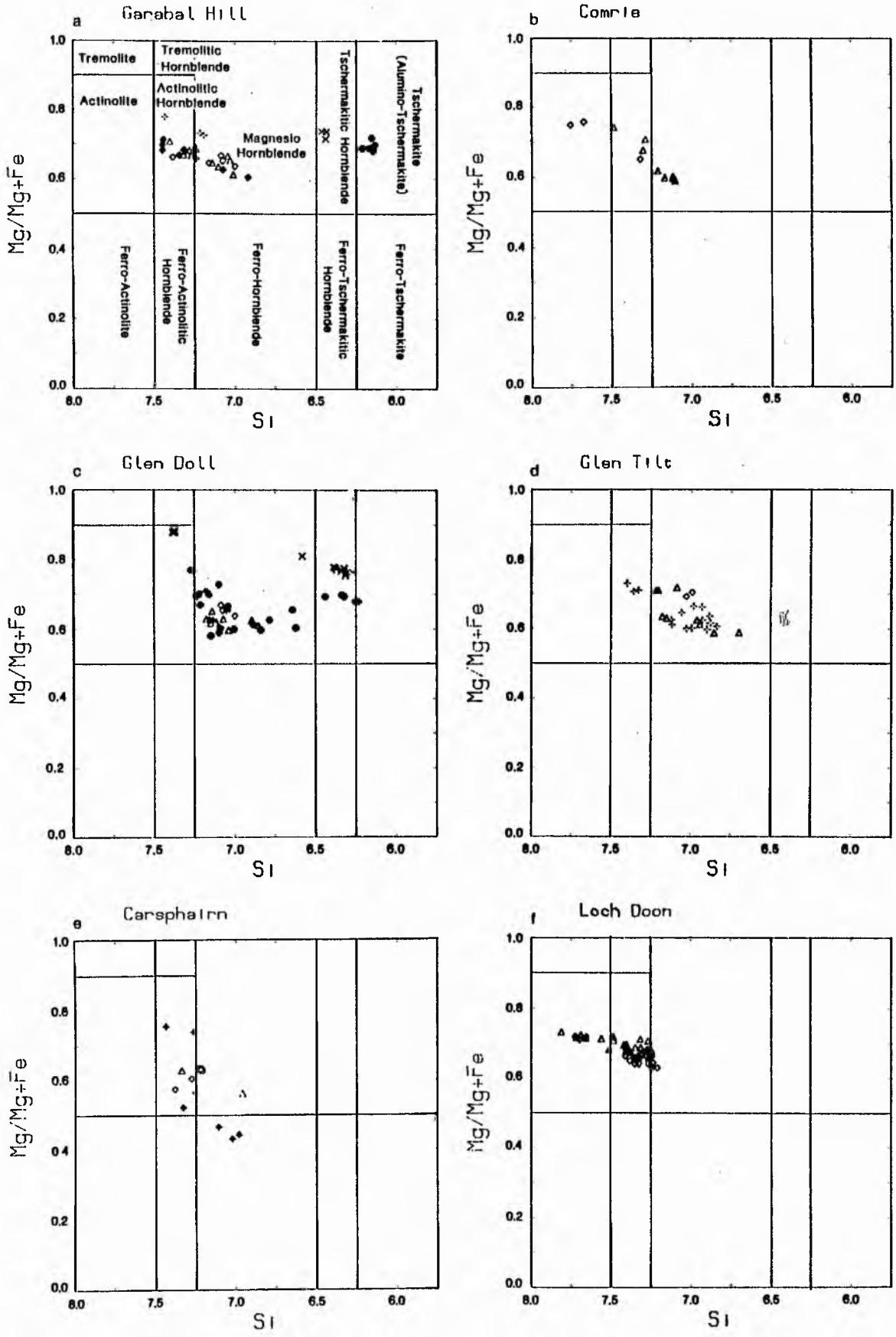

Fig 4.2 Classification and nomenclature of amphiboles from the studied plutons (after Leake, 1978).

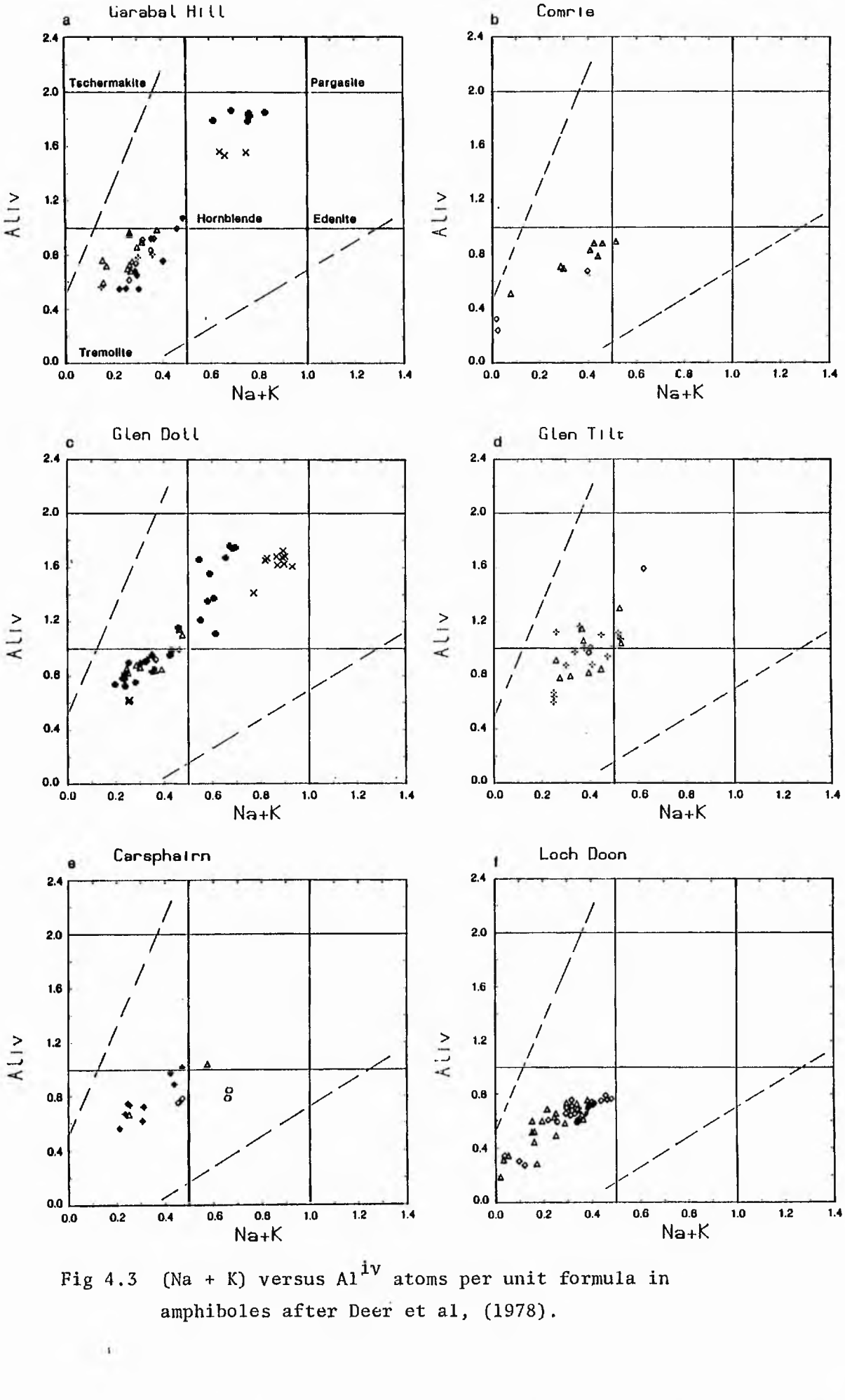

Fig 4.3 (Na + K) versus Al^{iv} atoms per unit formula in amphiboles after Deer et al, (1978).

of the gabbroic rocks. Cr is present at levels less than 0.2 wt% Cr_2O_3.

Figure 4.2 suggest that amphibole from this complex varies from tschermakite (alumino-tschermakite) in the basic and ultrabasic rocks to magnesio-hornblende in the diorites and granodiorites, with actinolitic hornblende for the altered amphiboles.

4.2.4 BIOTITE:

Biotite is found in gabbro, diorite and granodiorite in this complex and is the principal mafic mineral in the diorites and granodiorites. Representative analyses for biotites are given in Appendix C, and arranged in order of increasing whole rock acidity. SiO_2 varies from 36 to 39 wt% Al_2O_3 varies between 13 to 15 wt%. The principal variation is between Fe and Mg, which vary antipathetically; FeO from 13 to 19 wt% and MgO varies from 15 to 12 wt%. K_2O does not vary greatly ranging from 8.9 to 9.9 wt%. TiO_2 varies from 3 to 5 wt%, it plays a role in the colour of biotite and high TiO_2 contents are found in deep brown or orange biotites. MnO is present in minor amounts less than 0.5 wt%. CaO is only present in small amounts less than 0.2 wt%, and Na_2O was not detected.

Analyses from the different rock types were plotted in terms of Si per unit formula (p.u.f.) versus Fe/(Fe + Mg) (hereafter $Fe^{\#}$. Fig. 4.4 indicates that mica from appinitic diorite is phlogopite. Gabbroic, dioritic and granodioritic biotites are all true biotites, and all have Si greater than 5.7 (Fig. 4.4, after Deer et al. 1978).

All of the biotites have up to about 0.07 Mn p.u.f. and $Fe^{\#}$ of 0.3 to 0.5 (Fig. 4.5) at approximately the same $Fe^{\#}$. Mn values

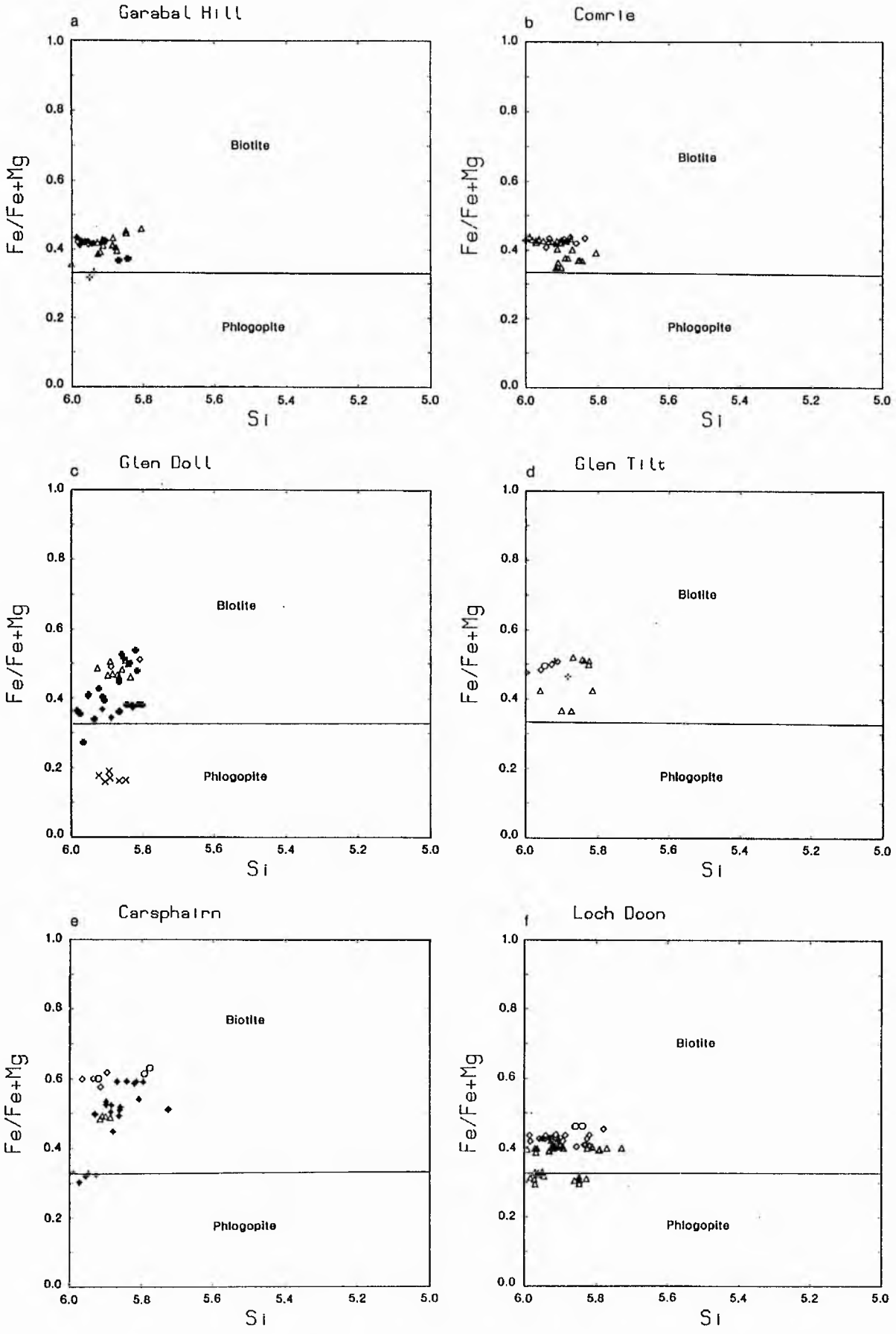

Fig 4.4 Annite-siderophyllite-eastonite-phlogopite plot after Deer et al. (1978) showing the micas analysed in the plutons of this study.

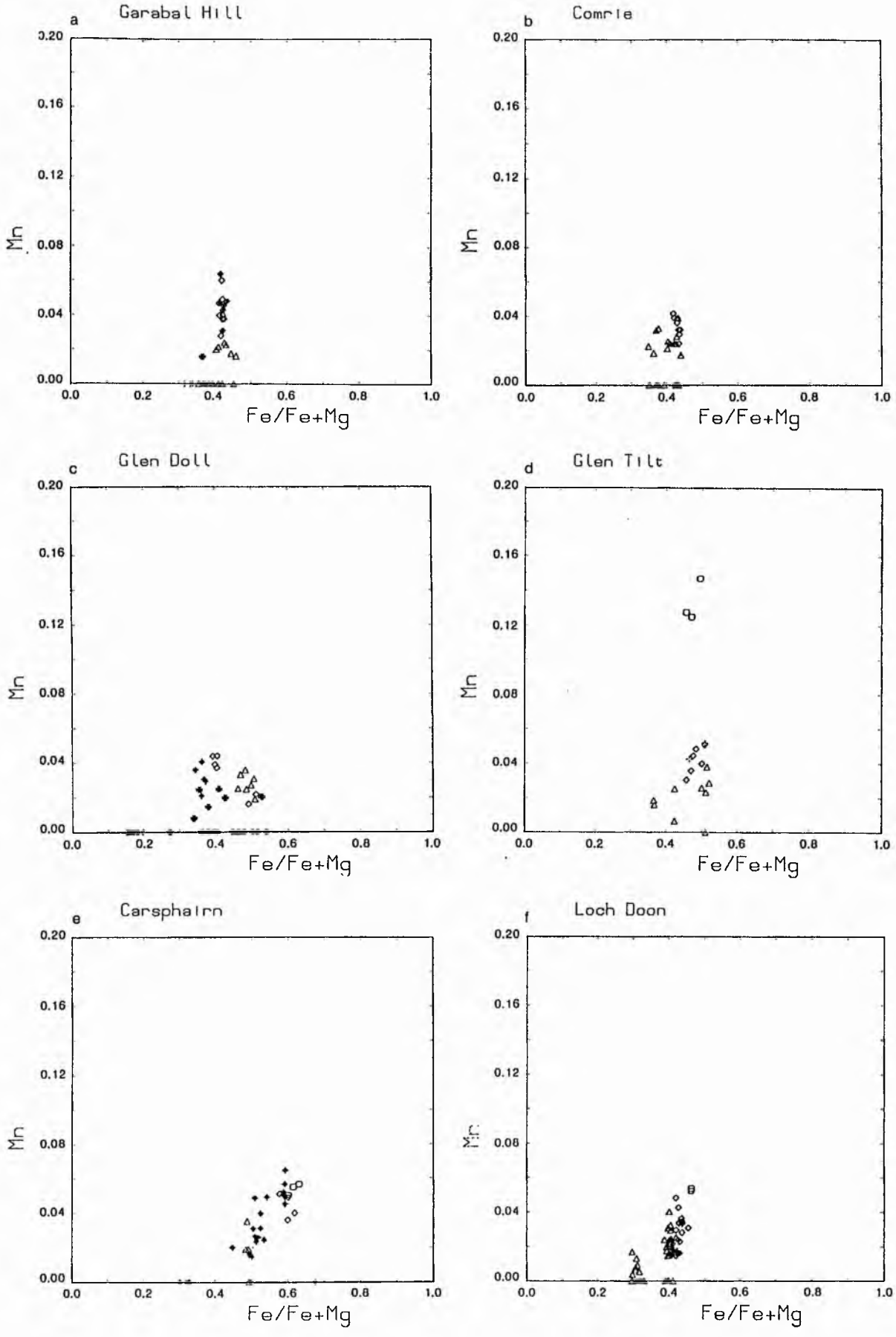

Fig 4.5 Fe/(Fe + Mg) versus Mn plots of biotites.

increase especially in the granodioritic rocks. Mn is known to increase with fractionation in biotites from acidic rocks (Mahmood, 1983).

4.2.5 PLAGIOCLASE:

Plagioclase analyses are listed in Appendix C together with their structural formulae. Plagioclase ranges in composition from An55 to An24 over the whole complex. SiO_2 varies from 55 to 63 wt%. CaO changes from 4 to ~ 11 wt%, and Na_2O from ~ 9 to ~ 5 wt%. K_2O is very minor in the more calcic plagioclase (i.e. labradorite) and is commonly up to 0.38 wt% in more sodic plagioclase. The FeO content is generally low and less than 1 wt%. Small amounts of TiO_2 have been detected in some of the plagioclase studied here but is less than 0.2 wt%.

The analyses are plotted by rock type in Fig. 4.6, from which it can be noted that:

a) Plagioclase from the gabbro is labradorite (An52 - An55).

b) Plagioclase from diorite rocks is generally andesine (An30 - An50).

c) Plagioclase from granodiorites is oligoclase (An24).

4.3 COMRIE

4.3.1 PYROXENE:

Ortho and clinopyroxene are important constituents of the two-pyroxene biotite diorites and the quartz monzodiorites.

Orthopyroxene analyses from representative two-pyroxene biotite diorites and quartz monzodiorites are given in Appendix C, and are

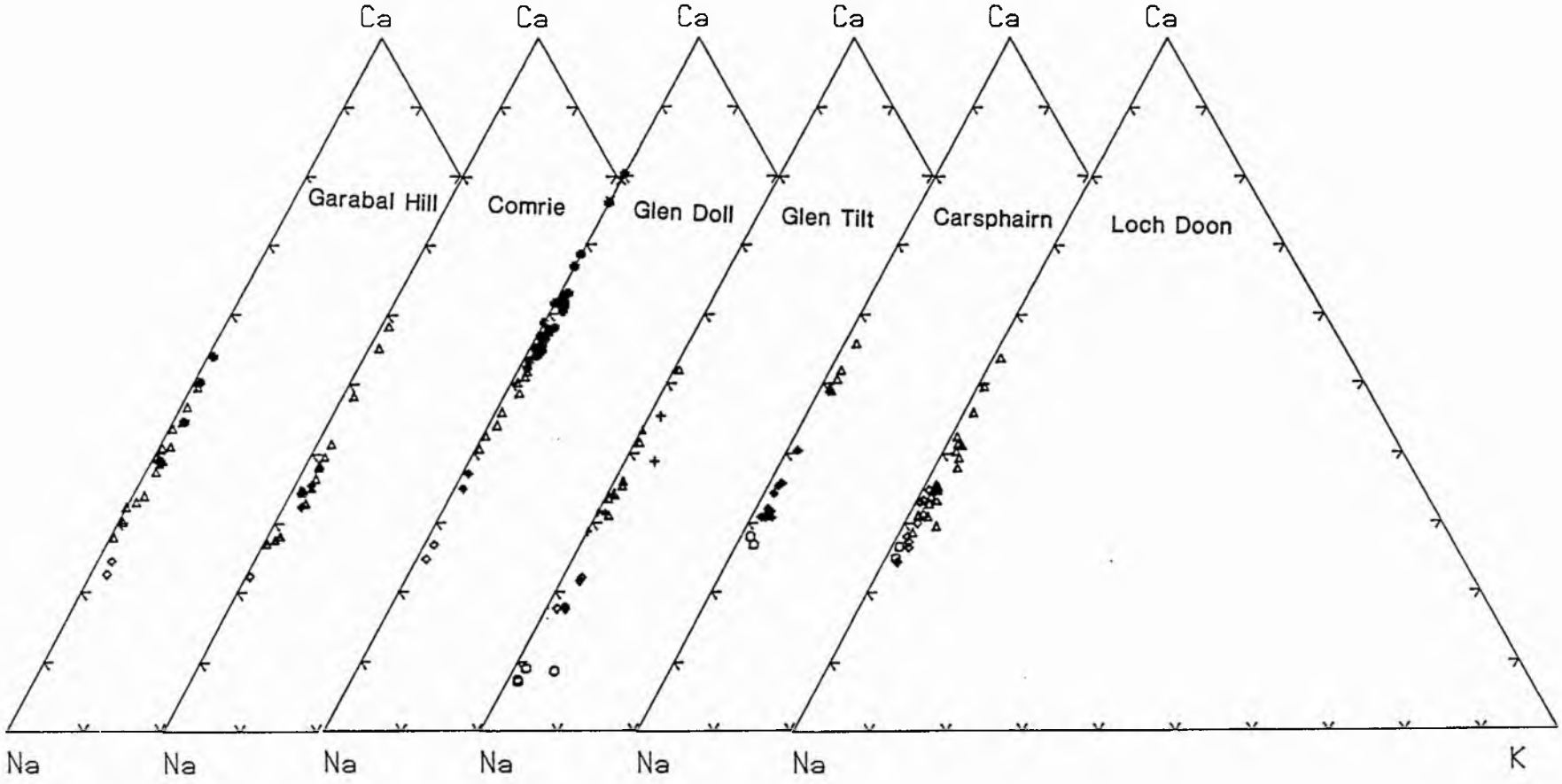

Fig 4.6 Ternary plots of feldspar compositions in the six studied plutons.

hypersthenes (Fig. 4.1, after Poldervaart & Hess, 1951). They contain low Al_2O_3 (less than 2.0 wt%), CaO (up to 2.17 wt%) and TiO_2 (less than 0.55 wt%), NiO was not detected. MnO is commonly less than 1.0 wt% and shows a sympathetic variation with FeO. It is apparent that there is an Fe enrichment from the two-pyroxene biotite diorite towards the quartz monzodiorites. The Mg ratio varies from 0.54 to 0.69.

Clinopyroxene analyses from representative two-pyroxene biotite diorite and quartz monzodiorites are given in Appendix C, and plotted on Fig. 4.1. They contain low Al_2O_3 ranging from 0.5 to 1.6 wt%. TiO_2 varies up to 2.8 wt%, and Cr_2O_3 less than 0.32 wt%, but both TiO_2 and Cr_2O_3 are more abundant than in orthopyroxene. Na_2O is less than 0.5 wt%. They vary in composition from salite to augite, with Mg ratios varying from 0.67 to 0.78.

4.3.2 AMPHIBOLE:

Analyses and structural formulae of amphiboles from this pluton are given in Appendix C. On a Si vs $Mg^{\#}$ value plot (Fig. 4.2) they are compared to the classification scheme of Leake (1978), and also plotted as Al^{iv} vs (Na + K), Fig. 4.3 after Deer et al. (1978). Amphibole is exclusively calcic in composition, commonly magnesio-hornblende. Secondary amphiboles are actinolitic hornblende and actinolite in composition (Leake, 1978).

SiO_2 contents vary from 47 to 54 wt% and Al_2O_3 from 1.8 to 5.8 wt%. Secondary amphibole is more Si-rich. MgO and FeO vary antipathetically, MgO varies from about 12.8 to 17 wt%, and the FeO varies from approximately 11 to 16 wt%. TiO_2 varies from 0.25 to 1.4 wt%, MnO varies from 0.3 to 0.6 wt%. The CaO content is fairly

constant varying between 11 to 12.5 wt% CaO. Na_2O is low in abundance.

4.3.3 BIOTITE:

Biotite is present in all of the rock types of this pluton (diorite, quartz monzodiorite, granodiorite and granite). Represenative analyses are given in Appendix C. SiO_2 varies from approximately 36.5 to 38.5 wt%. Al_2O_3 varies from 12 to 14 wt%. The principle variation is between Fe and Mg, which vary antipathetically. FeO varies from 14.5 to about 18 wt% and MgO from 12.5 to about 15.5 wt%. K_2O does not vary greatly ranging from 8.7 to 9.8 wt%. TiO_2 varies from 4 to 6 wt%. MnO is commonly minor at less than 0.3 wt%. CaO is only present occasionally and generally less than 0.2 wt%. Na was not detected in the analysed biotites.

Analyses from the different rock types were plotted in terms of Si vs Fe/(Fe + Mg) plot (Fig. 4.4) and are all true biotites (Deer et al. 1978). All of the rocks have Si greater than 5.7 p.u.f. Biotites have up to 0.045 Mn p.u.f., and Fe ratio ranges from 0.3 to 0.5 (Fig. 4.5). Mn values increase at nearly constant Fe ratio .

4.3.4 PLAGIOCLASE:

Plagioclases from different rock types of this complex are listed in Appendix C together with their structural formulae (Fig. 4.6).

The plagioclases in this pluton range in composition from labradorite (An59) to oligoclase (An23). SiO_2 varies from 54 to 62 wt% and Al_2O_3 from about 29 to 23 wt% antipathetically. CaO ranges from 4.7 to 11.9 wt% and Na_2O from 4.5 to 9.5 wt%. K_2O is very minor

ranging up to a maximum of 0.4 wt% in the more sodic plagioclase. The FeO content is generally low (less than 0.5 wt%). Very minor TiO_2 (0.15 wt%) has been detected from plagioclase in the diorites.

4.4 GLEN DOLL

4.4.1 OLIVINE:

Olivine is present only in the ultrabasic rocks of this complex. Representative analyses are given in Appendix C, and olivine has a mean composition of Fo_{78}. Only a very small amount of CaO (less than 0.1 wt%) was detected in agreement with Simkin & Smith (1970). No Al_2O_3 was detected in these olivines. Small amounts of MnO are present, up to 0.35 wt%. NiO was detected only in one olivine with 0.19 wt% NiO.

4.4.2 PYROXENE:

Representative analyses of ortho- and clinopyroxenes are plotted on Fig. 4.1. Orthopyroxene from representative pyroxenites and gabbros are given in Appendix C and plotted on (Fig. 4.1) , they are bronzites to hypersthenes in composition. All the analysed orthopyroxenes contain small amounts of Al_2O_3 (less than 0.2 wt%), and less than 2 wt% CaO, TiO_2 up to 0.6 wt%, MnO is less than 0.5 wt% and Cr_2O_3 is detected in 4 pyroxene analyses. It is apparent that there is Fe enrichment in the orthopyroxene from the gabbro. $Mg^{\#}$ varies from 0.65 to 0.82.

Representative clinopyroxene analyses are given in Appendix C, and plotted in Fig. 4.1. They contain low Al_2O_3 ranging from 0.5 to

3.5 wt%, less than 1.0 wt% TiO_2, and Cr_2O_3 is detected in most of the samples and is less than 0.9 wt%. Both TiO_2 and Cr_2O_3 are consistently more abundant than in orthopyroxene. Na_2O is only detected in the gabbro clinopyroxene at less than 0.5 wt%. Clinopyroxenes vary in composition from diopside in pyroxenites to salite-augite in the gabbroic rocks.

$Mg^{\#}$ values varies between 0.69 and 0.84, higher values generally being in the ultrabasic rocks.

4.4.3 AMPHIBOLE:

Amphibole analyses from this pluton are given in Appendix C, along with their structural formulae.

Amphibole is exclusively calcic in composition ranging from tschermakitic hornblende for the brown hornblendes in the pyroxenite and hornblende gabbro, to magnesio-hornblende in composition. Secondary amphibole is actinolitic hornblende in composition (Fig. 4.2, 4.3 after Leake, 1978; Deer et al. 1978).

SiO_2 contents vary from 42 to 52.2 wt%, and Al_2O_3 from 4.7 to 11.6 wt%. Secondary amphibole is more Si-rich. MgO vary from 12.4 to 19.9 wt% and FeO vary from 6.1 to 16.5 wt%. TiO_2 varies from 1.15 to 4.5 wt%, and MnO varies from zero to 0.4 wt%. The CaO is fairly constant varying between 11 to 12.6 wt%. Na_2O is present but commonly less than 3.0 wt%.

4.4.4 BIOTITE:

Biotite is found in all of the rock types present in this complex. Representative analyses for biotites are given in Appendix C . SiO_2 contents vary from 36 to 39 wt%, Al_2O_3 varies from 12.2 to

15.6 wt%. The principal variation is between FeO and MgO; FeO varying from 7.2 to 21.2 wt%, and MgO varying from 21.4 to 10 wt%. K_2O does not vary greatly ranging from 8.2 to 9.9 wt%. Ti varies from 1.5 to 5.4 wt%. MnO is present in small amounts less than 0.5 wt%. CaO is less than 0.2 wt%. Na_2O is present mainly in the biotites from ultrabasic rock ranging from 0.6 to 1.0 wt%.

Analyses from the different rock types were plotted in terms of Si p.u.f. vs Fe/(Fe + Mg) (Fig. 4.4) which shows that biotites from the ultrabasic rocks are entirely phlogopitic The other rock types have biotite compositions and all of the rocks have Si greater than 5.7 cations p.u.f., (Fig. 4.4, after Deer et al. 1978). All analyses show Mn values up to 0.05 Mn p.u.f. and Fe ratio ranging from 0.15 to 0.55 (Fig. 4.5). Mn values increase independently of Fe , especially in the tonalites and granodiorites, as Mn increases with fractionation in biotites from acidic rocks (Mahmood, 1983).

4.4.5 PLAGIOCLASE:

Plagioclase analyses for different rock types are listed in Appendix C along with their structural formulae. They range in composition from bytownite (An 83) to oligoclase (An25) (Fig. 4.6). SiO_2 varies from 48.9 to 62 wt% and Al_2O_3 antipathetically varies from 32.5 to 22.8 wt%. Ca varies from 16.5 to 5.5 wt%, and Na_2O from 2.3 to 9.1 wt%. K_2O is absent in the more calcic plagioclase (i.e. bytownite) and is commonly less than 0.3 wt%. The FeO content is generally low and less than 1 wt%. Minor amounts of TiO_2 have been detected in some plagioclase crystals and is less than 0.2 wt%. The analyses are plotted in Fig. 4.6 from which it can be noted that the pyroxenites have bytownite (average An_{83}), gabbros vary from

An_{54}-An_{80}, diorites from An_{40}-An_{52}, tonalites have andesines at An_{35}, and granodiorites have oligoleases from An_{25}-An_{28}.

4.5 GLEN TILT

4.5.1 AMPHIBOLE:

Amphibole is present in all of the rock types studied in this pluton except for granites and quartz diorites. Representative analyses are given in Appendix C, along with their structural formulae. They are exclusively calcic in composition and of magnesio-hornblende type. Secondary amphibole is actinolitic hornblende (classification of Leake, 1978).

SiO_2 contents vary from 44.7 to 50.7 wt%, and Al_2O_3 from 5 to 8.7 wt%. Secondary amphiboles again are the more Si-rich. MgO and FeO vary antipathetically; MgO varies from 11.5 to 16.2 wt% while FeO varies from 15.6 to 10.6 wt%. TiO_2 varies from 0.6 to 2.1 wt% and MnO from 0.1 to 0.4 wt%. The CaO is fairly constant varying between 10.9 and 12.3 wt%. Na_2O and K_2O are present in minor amounts of up to 1.4 wt% for Na_2O which is more abundant than K_2O. Figure 4.2 indicates that amphibole from this pluton is magnesio-hornblende in composition and hornblende while it is actinolitic hornblende for altered amphiboles (Leake, 1978, Fig. 4.3, after Deer et al. 1978).

4.5.2 BIOTITE:

Biotite is found in all rock types from this pluton. Representative analyses are given in Appendix C, arranged in order of increasing host rock acidity. SiO_2 varies from 36 to 38.7 wt% and

Al_2O_3 from 14.4 to 17.2 wt%. MgO and FeO again vary antipathetically; where FeO varies from 20.4 to 14.9 wt% and MgO from 9.9 to 14.5 wt%; K_2O varies from 8.7 to 9.7 wt% and TiO_2 varies from 1.6 to 4.5 wt%. MnO contents vary up to 1.1 wt% in the biotites from granites. CaO is only present in very small amounts less than 0.2 wt% and Na_2O is minor less than 0.3 wt%.

Analyses from different rock types were plotted in terms of Si p.u.f. vs Fe ratio (Fig. 4.4) which indicates that all the micas are biotites having Si greater than 5.7 cations p.u.f. (Deer et al. 1978). The Mn content of biotite p.u.f. is plotted against Fe value (Fig. 4.5). The analyses have Fe values ranging from 0.35 to nearly 0.55, and Mn contents of up to 0.15 Mn p.u.f. which is high in biotites from granitic rocks, probably reflecting fractionation processes (Mahmood, 1983).

4.5.3 PLAGIOCLASE:

Plagioclase is present in all the different rock types of this complex and ranges in composition from An 50 to An 6 (Fig. 4.6). SiO_2 varies from 54.9 to 66 wt%, and Al_2O_3 antipathetically from 29.5 to 20.6 wt%. CaO varies from 9.9 to 1.6 wt%, and Na_2O from 5 to 11.3 wt%. K_2O is generally minor less than 1.0 wt%. The FeO content is low (less than 0.3 wt%). Small amounts of TiO_2 has been detected at less than 0.1 wt%.

Generally the plagioclase from diorites and appinitic diorites are andesine in composition (An32-An50), while those from granodiorites are of oligoclase composition (An18-An24) and from granites are of albite composition (less than An10).

4.6 CAIRNSMORE OF CARSPHAIRN

4.6.1 PYROXENE:

Orthopyroxenes and clinopyroxenes are important constituents of the tonalites. Orthopyroxene analyses are given in Appendix C, and are hypersthenes in composition. They contain low Al_2O_3 less than 1.0 wt%, CaO up to 2.3 wt% and TiO_2 less than 0.5 wt%. NiO is only detected in a few grains, up to 0.2 wt%. MnO (up to 1.0 wt%), shows a sympathetic variation with FeO. Mg ratios vary from 0.48 to 0.68.

Clinopyroxenes are plotted on Fig. 4.1 and presented in Appendix C. They are principally augite in composition with Mg ratios varying from 0.55 to 0.65 containing small amounts of Al_2O_3 less than 1.0 wt% and TiO_2 less than 0.5 wt%. No Na_2O was detected in the clinopyroxenes from this complex.

4.6.2 AMPHIBOLE:

The analyses of amphibole from this pluton are given in Appendix C, along with their structural formulae based on 23 oxygens (water free). They are exclusively calcic of magnesio-hornblende and ferro-hornblende compositions (classification of Leake, 1978). Secondary amphibole is actinolitic hornblende (Fig. 4.2) and actinolite (Fig. 4.3).

SiO_2 contents vary from 45 to 52 wt% and Al_2O_3 antipathetically from 6.8 to 4.5 wt%. Secondary amphibole is more Si-rich. MgO and FeO vary antipathetically, MgO varies from 17.4 to 8.9 wt% while FeO varies from 10.4 to 20.9 wt%. TiO_2 is up to 1.5 wt% and MnO is less than 1.1 wt%. The CaO is fairly constant ranging from 10.4 to 11.5

wt%.

4.6.3 BIOTITE:

Representative analyses of biotite from different rock types are listed in Appendix C, arranged in order of increasing host rock acidity. SiO_2 contents vary from 34.5 to 39 wt% and Al_2O_3 from 12.3 to 14 wt%. FeO and MgO vary antipathetically, FeO varies from 26 to 12.5 wt% and MgO from 7 to 16 wt%. K_2O does not vary greatly ranging from 8.9 to 9.6 wt%. TiO_2 varies from 3.4 to 5.5 wt%. MnO is present in small amounts in some analyses and commonly less than 0.5 wt%.

Analyses are plotted on Fig. 4.4 in terms of Si p.u.f. vs Fe ratios indicating that micas from the different rock types are biotite in composition except for a few phlogopites from tonalites (Deer et al. 1978). The Mn content p.u.f. is plotted against Fe ratios (Fig. 4.5), and shows variations at nearly constant Fe ratio.

4.6.4 PLAGIOCLASE:

Plagioclase analyses from this pluton are listed in Appendix C, and plotted on Fig. 4.6. They range in composition from labradorite (An57) to oligoclase (An28). Analyses from the hornblende biotite diorite have both andesine and labradorite composition, but those from tonalites are exclusively andesine. Granodiorite plagioclases average An33, while those from granites average An28.

4.7 LOCH DOON

4.7.1 PYROXENE

Ortho and clinopyroxenes are important constituents of the two-pyroxene biotite diorite and a few granodiorites.

Orthopyroxene analyses from representative diorites and granodiorites are given in Appendix C. They are hypersthenes with low Al_2O_3 less than 1.0 wt%, CaO up to 2.1 wt% and TiO_2 less than 1.0 wt%, NiO has been detected in some orthopyroxene grains. The Mg ratio varies from 0.66 to 0.70.

Clinopyroxene analyses from the diorites and granodiorites are given in Appendix C. They contain low Al_2O_3 ranging from 0.4 to 2.0 wt %, TiO_2 up to 0.8 wt. % and Cr_2O_3 up to 0.32 wt%, and Na_2O less than 0.6 wt%. They vary in composition from salite to augite and the clinopyroxenes from granodiorite show minor Fe-enrichment (Fig. 4.1). Their Mg values vary from 0.56 to 0.76.

4.7.2 AMPHIBOLE:

Analyses of amphiboles from the Loch Doon pluton are given in Appendix C with their structural formulae based on 23 oxygens.

They are exclusively calcic in composition and commonly altered, but unaltered amphiboles are of magnesio-hornblende composition whereas secondary amphiboles are actinolitic hornblende and actinolite in composition (Fig. 4.2, after Leake, 1978), and hornblende (Fig. 4.3).

SiO_2 contents vary from 47.8 to 33.7 wt% and Al_2O_3 varies antipathetically from 5.4 to 1.9 wt%. Secondary amphibole is more Si-rich as in other complexes. MgO and FeO vary mostly antipathetically, MgO from 10.85 to 17.3 wt% and FeO from 14.3 to 10.9 wt%. TiO_2 varies up to 1.2 wt% and MnO less than 0.6 wt%. The CaO content ranges from 10.8 to 12.2 wt%. Na_2O has low abundances always

less than 1.3 wt%.

4.7.3 BIOTITE:

Representative analyses of biotites from this pluton are given in Appendix C along with their structural formulae. SiO_2 varies from 36 to 39 wt% and Al_2O_3 from 12.5 to 14.6 wt%. FeO and MgO vary antipathetically, FeO varies from 23.3 to 12.4 wt% and MgO from 8.7 to 16.8 wt%. K_2O does not vary greatly ranging from 9.0 to 9.6 wt%. TiO_2 varies from 3.3 to 5.2 wt%. MnO is commonly found in small amounts (less than 0.5 wt%). CaO is present in few analyses of biotites and generally less than 0.2 wt%. Na_2O is detected in few crystals and is always less than 0.2 wt%.

Analyses from representative rock types are plotted on Fig. 4.4 in terms of Si p.u.f. vs Fe ratio which indicates that most of the mica grains analysed from diorites are phlogopite while in the other rock types they are biotite. In all of these rock types they have Si greater than 5.7 p.u.f.. The biotites have up to 0.06 Mn p.u.f. and Fe ratios vary from 0.3 to 0.5 (Fig. 4.5).

4.7.4 PLAGIOCLASE

Plagioclase analyses from this pluton are presented in Appendix C, along with their structural formulae and are plotted on Fig. 4.6. They show a range in composition from labradorite (An54) to oligoclase (An25). SiO_2 varies from 54.6 to 61.5 wt%, and Al_2O_3 varies antipathetically from 29 to 23.5 wt%. CaO varies from 11 to 5.3 wt%, and Na_2O from 8.9 to 5 wt%. K_2O is very minor in the more calcic plagioclase which is present in the diorites, it is commonly less than 0.5 wt%. FeO is less than 0.5 wt% and TiO_2 is minor less than 0.15

wt%. The diorites have plagioclase of labradorite to andesine composition (An30-An54). Plagioclases from granodiorites are An28 to An35, and from granites are about An27.

4.8 VARIATIONS IN MINERAL TYPES:

4.8.1 OLIVINE

Olivines are found in peridotites, gabbros and dioritic rocks from the Garabal Hill-Glen Fyne complex and the pyroxenites from Glen Doll complex. Olivines range in composition from Fo_{81} in the peridotite to Fo_{77} in the diorites (chrysolite) from Garabal Hill with small quantities of Ca (less than 0.2 wt% CaO). Simkin & Smith (1970) studied the compositions (including minor elements) of natural igneous olivines from different environments and pointed out that Ca does not correlate with Mg but has a correlation with the crystallisation environment of the host rock. Olivines in slow-cooling plutonic rocks have lower Ca contents than that in hypabyssal rocks , a fact which fits the data above. There is also less Ca in highly magnesian olivines (Deer et al. 1982).

Small amounts of MnO are present in all samples (0.17 - 0.39 wt%) which fits the data of Simkin & Smith (1970) and Deer et al. (1982), who report significant Mn only in Fe-rich olivine.

Olivine in the Glen Doll pyroxenites is Fo_{78} composition with very low CaO (less than 0.1 wt%).

4.8.2 PYROXENE

4.8.2a Coexisting pyroxenes

Two pyroxenes are present in the gabbro, diorite and tonalite in all complexes studied here except for Glen Tilt. Tie-lines between coexisting pyroxenes are indicated on Fig. 4.1. Kretz (1961, 1963) presented data on the distribution of Mg and Fe between pyroxenes from high grade metamorphic and igneous rocks defining a distribution coefficient (K_D) as follows

$$K_D = \frac{X^O\ Mg}{1-X^O\ Mg} \cdot \frac{1-X^C\ Mg}{X^C\ Mg}$$

where X Mg = $Mg/(Mg + Fe^{2+})$

O = orthopyroxene

C = clinopyroxene

Fe^{2+} = total Fe as in microprobe analyses.

which varies from 0.51 to 0.65 in metamorphic rocks and from 0.65 to 0.86 in igneous rocks and he related the differences to equilibrium crystallisation temperatures. Samples analysed from Garabal Hill-Glen Fyne have pyroxene K_D values varying from 0.68 to 0.79. As fractionation proceeds relative Fe-enrichment and Ca depletion is reflected by lower K_D for igneous rocks. Ti is relatively enriched in the clinopyroxene and Mn in the orthopyroxene, both observations are comparable with the data of Fleet (1974b).

Many authors have attempted to use the partitioning of Mg and Fe between coexisting pyroxenes as a geothermometer notably Wood & Banno (1973), Saxena & Nehru (1975), Saxena (1976), Wells (1977), Kretz

(1982) and Lindsley (1983) using different formulations. The calculated temperature for the coexisting pyroxenes from different plutons in the present study using the formulations of Wood & Banno (1973), Wells (1977) and Kretz (1982) is given in Table (4.1) which is showing that the pyroxene biotite gabbro from Garabal Hill-Glen Fyne have the highest equilibration temperature ,followed by diorite and tonalite from the Carsphairn complex. Though the results should be treated with care because of the uncertainty of Fe^{2+}/Fe^{3+} in microprobe analyses.

Pyroxenes from the Comrie pluton (Fig. 4.1) have K_D values from 0.65 to 0.78. The Fe-enrichment and Ca-depletion trends seen here are typical of fractionation processes (Fleet, 1974a) and are similar to the pyroxene variations in the Garabal Hill pluton. Ti enrichment in clinopyroxene and Mn in orthopyroxene are comparable to those reported by Fleet (1974b). These pyroxenes are typical of calc-alkaline complexes, the limited Fe enrichment may result from co-precipitation of magnetite and/or amphibole. The build-up of P_{H_2O} may cause hornblende to become stable at the expense of pyroxene.

Coexisting pyroxenes in the ultrabasic and basic rocks from Glen Doll (Fig. 4.1) have K_D values varying between 0.81 and 0.90. The abundances of hydrous minerals (amphibole and biotite) in this pluton reflects early amphibole crystallisation as a function of relatively high water pressure (P_{H_2O}) and low crystallisation temperature.

Pyroxenes from the Carsphairn complex (Fig. 4.1) have K_D values from 0.73 to 1.56, which may reflect their Fe enrichment, but their low Na, Al and Ti contents are typical of calc-alkaline rocks. Those from Loch Doon have lower K_D values of 0.68 to 0.72 (Fig. 4.1).

Table 4.1: Temperature calculated using coexisting ortho- and clinopyroxenes and the methods of authors indicated.

Name of pluton	Rock type	Sample No	Wood & Banno (1973)	Wells 1977	Kretz (1982) using transfer reaction equations	
Garabal Hill-Glen Fyne	Gabbro Diorite	GH10 GH3	1042 984	1081 1008	1088 1026	1121 977
Comrie	Diorite Quartz monzo-diorite	CM20 CM10 Cm25	985 945 881	1042 982 938	1077 1019 956	1102 962 828
Glen Doll	Pyroxenite Gabbronorite Gabbro	GD49 GD26 GD41 GD42 GD3	990 973 971 928 960	1022 1010 976 943 971	968 946 955 902 980	853 808 826 725 896
Loch Doon	Diorite	78002 WL6	941 902	974 924	1020 955	969 827
Cairnsmore of Carsphairn	Tonalite	77026 77032	879 849	945 878	969 939	855 795

4.8.2b Discussion

Pyroxene compositional variation associated with the crystallisation of basic magmas (particularly fractional crystallisation) can be regarded as being related to two trends, tholeiitic and calc-alkaline. The major difference is that only a single Ca-rich pyroxene crystallises in the latter and fractionation trends are roughly parallel to the diopside hedenbergite join of the pyroxene quadrilateral. A considerable amount of data, both experimental and natural, is available regarding pyroxene crystallisation trends in the tholeiitic series, principally from well-studied stratiform complexes such as Skaergaard, Bushveld and Dufek (Deer et al. 1978). Two pyroxenes are common in the early stages of crystallisation, a Ca-rich clinopyroxene and a Ca-poor orthopyroxene, the latter being replaced by a monoclinic Ca-poor pigeonite when fractionation has enriched residual liquids in Fe to approximately Mg:Fe = 70:30. Further crystallisation continues with cotectic crystallisation of a progressively more Fe-rich augite and Ca-poor pigeonite, and many intrusions do not proceed beyond this point. However, with further fractionation and Fe-enrichment a single Ca-rich ferroaugite may crystallise. It is apparent that pyroxenes from the Garabal Hill-Glen Fyne complex have very restricted Fe-enrichment trends. Other chemical parameters which diverge from those normally observed in tholeiitic trends are the generally very low levels of Al, Na, and Ti, although the latter element, in addition to Cr, is more abundant in clinopyroxene.

Pyroxene compositions from calc-alkaline rocks show considerable variation, but in general tend to show less extreme compositions compared with tholeiitic trends (Deer et al. 1978). Low Na, Al, and

Ti and limited Fe-enrichment in clinopyroxene is typical of these rocks, in addition to greater abundances of hydrous minerals (such as amphibole and biotite) compared to tholeiitic rocks. The Guadalupe complex for example (Best and Mercy, 1967) shows the same limited pyroxene chemistry as that observed here. Gill (1981) described such pyroxene features as characteristic of orogenic andesites.

Although low Al, Na and Ti contents probably reflect the interaction of many factors (temperature, pressure, cooling rate, $^{a}SiO_2$ and coexisting mineral assemblage), Gill (1981) precluded pressure greater than 10 kb during pyroxene crystallisation, and the limited Fe-enrichment of clinopyroxene may be due to coprecipitation of magnetite or amphibole, or both. Best and Mercy (1967) considered that limited Fe enrichment and the relatively early amphibole crystallisation is primarily a function of high water pressure (P_{H_2O}) and low crystallisation temperature which have the effect of supressing the pyroxene solidus and thus reducing the stability field of the pyroxene. Ca-rich pyroxene which crystallises from a hydrous mafic magma will thus become unstable before significant fractionation has occurred and will be replaced by amphibole and possibly biotite.

4.8.3 AMPHIBOLE

4.8.3a Substitutional schemes

Variation in amphibole chemistry can be viewed as the result of interaction of a number of possible cation substitutions of the amphiboles. These substitutions are considered in terms of the amphibole structure (after Hawthorne, 1981).

$$A_{0-1}\ B_2\ C_5\ T_8\ O_{22}\ (OH,\ F,\ Cl)_2$$

where: A = Na, K

B = Na, Li, Ca, Mn, Fe^{2+}, Mg

c = Mg, Fe^{2+}, Mn, Al, Fe^{3+}, Ti

T = Si, Al

Within the amphibole structure substitution of Fe^{2+} for Mg commonly occurs resulting in a variation of Mg values between 0.61 to 0.78 (Garabal Hill). It is noteworthy that no ferro-hornblende has been identified from that pluton. This distribution pattern may be a function of host rock variation, but Leake (1978) pointed out that the Mg values of calcic amphibole are not a simple reflection of whole-rock composition, particularly if Fe-oxides also crystallise. Saxena and Ekstrom (1970) indicated that the Fe^{2+}-Mg substitution appears statistically to be influenced by the Al^{vi} content. Therefore this apparently simple substitution must be viewed in the context of the other but more complex coupled substitutions that can occur in the amphibole structure. These substitutions have been defined by Czamanske and Wones (1973) as:

1 Edenite

$$(Na + K)_A + Al^{iv} = ([\,]) A + Si$$

2 Tschermakite

a) $Al^{vi} + Al^{iv} = Mg + Si$

or

b) $Fe^{3+} + Al^{iv} = Mg + Si$

3 Glaucophane

a) $(Na)_B + Al^{vi} = (Ca)_B + Mg$

or

Riebeckite

b) $(Na)_B + Fe^{3+} = (Ca)_B + Mg$

4 Richterite

$(Na)_A + (Na)_B = ([]) A + (Ca)_B$

5 Ti - Tschermakite

$Ti + 2\ Al^{iv} = Mg + 2Si$

6 a) $2(Na)_B + Ti = 2Ca + Mg$

or

b) $(Na)_B + Ti = Ca + Al$

where [] is a vacancy.

Coupled substitutions of the edenite type (No. 1) are examined in Fig. 4.7, which is a plot of Al^{iv} vs $(Na + K)_A$ and in which a 1:1 slope can be expected if this is the only operative scheme. From this figure it is apparent that there is a general trend of increasing of Al^{iv} with increasing $(Na + K)_A$ with a slope of more than 2:1. Al substitutions must therefore occur in other schemes in addition to edenite. Other substitutions involving Al include Al-tschermakite (No. 2) or Ti-tschermakite (No. 5). For Al-tschermakite substitution both Al^{vi} or Fe^{3+} may be involved, by plotting Al^{iv} vs total Al (Fig. 4.8) the relative balance between Al^{vi} and Fe^{3+} may be assessed. A 1:1 slope would be expected if either Al^{vi} played only a

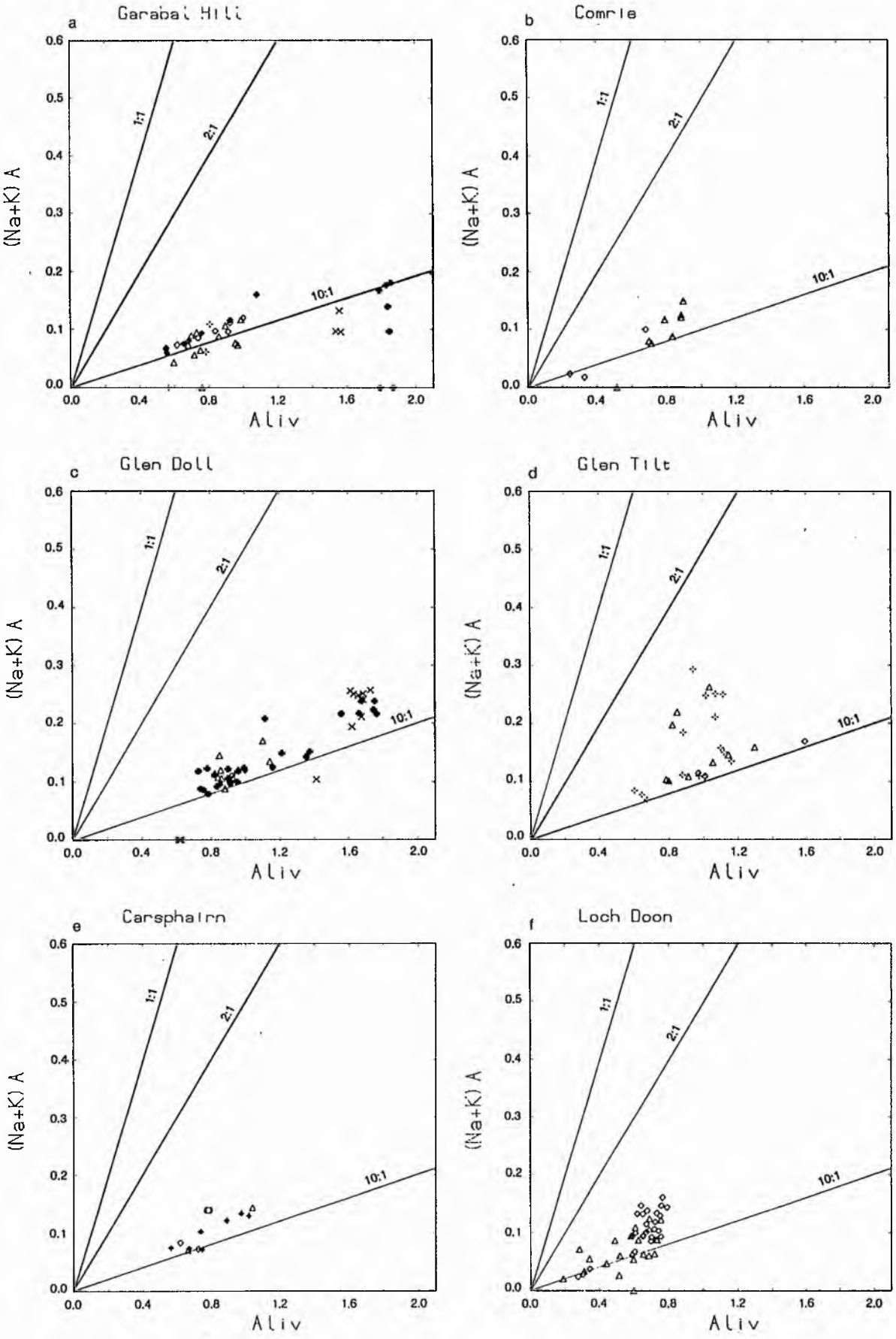

Fig 4.7 Al^{iv} versus $(Na + K)_A$ plots of amphiboles.

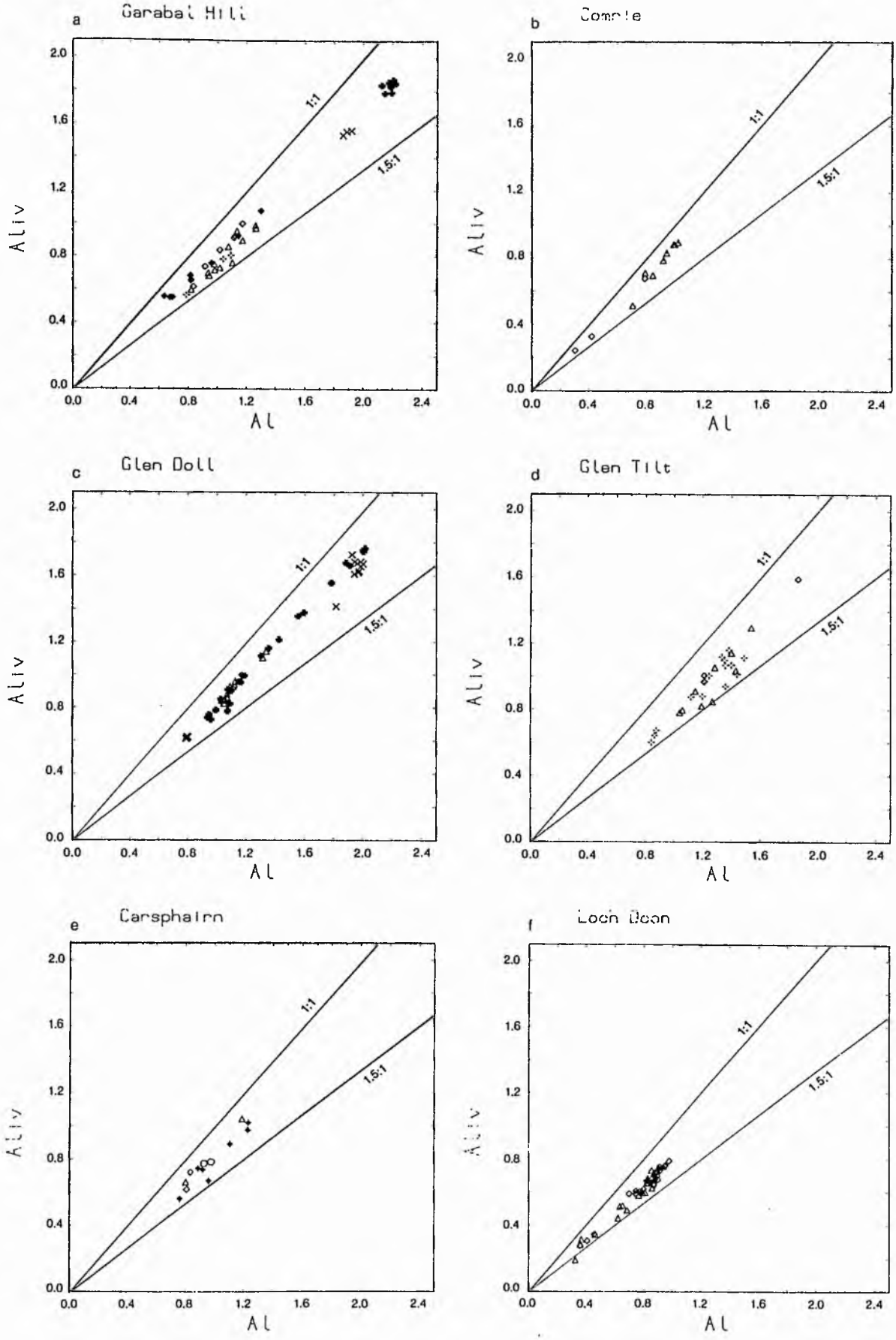

Fig 4.8 Plots of total Al versus Al^{iv} for amphiboles

minor role or if Fe^{3+} was the dominant variable trivalent cation in the C-site, thus it can be seen from Fig. 4.8 that both Al^{vi} and Fe^{3+} participate in the Al-tschermakite substitution. Figure 4.9 of Al^{vi} vs Al^{iv}, indicates that there is considerably more Al^{iv} (3:1) than required by both the edenite and Al-tschermakite substitutions.

The Ti-tschermakite substitution (No. 5) is examined in Fig. 4.10, a plot of Al^{iv} vs Ti, showing that there is a positive correlation following a slope of more than 3:1. This suggests that the Ti-tschermakite substitution is the dominant process with subsidiary edenite and Al-tschermakite schemes.

The Ti substitution schemes may be considered in terms of Ti being equivalent to two trivalent cations (Doolan et al. 1978). This means that the total increase in charge in the C-site must be equal to (Al^{vi} + Fe^{3+} + Cr + 2 Ti), and this latter quantity is a measure of both tschermakite and glaucophane substitution. Recalculation of Fe^{3+} from total Fe is unreliable from microprobe analyses preventing a true comparison with chemically analysed amphiboles of Leake (1978).

In summary all the amphiboles studied from Garabal Hill are calcic in composition and the principal variation in chemistry results from both Ti-tschermakite and edenite substitutions. Those from Comrie, Glen Doll, Glen Tilt, Loch Doon and Carsphairn show similar substitutions, and there is quite a strong similarity between amphiboles from the Garabal Hill and Glen Doll plutons as these contain both ultrabasic and gabbroic rocks (rich in amphibole). Amphibole analyses from these basic and ultrabasic rocks show low Si and high Al contents and have higher Al^{iv} relative to those from the other plutons.

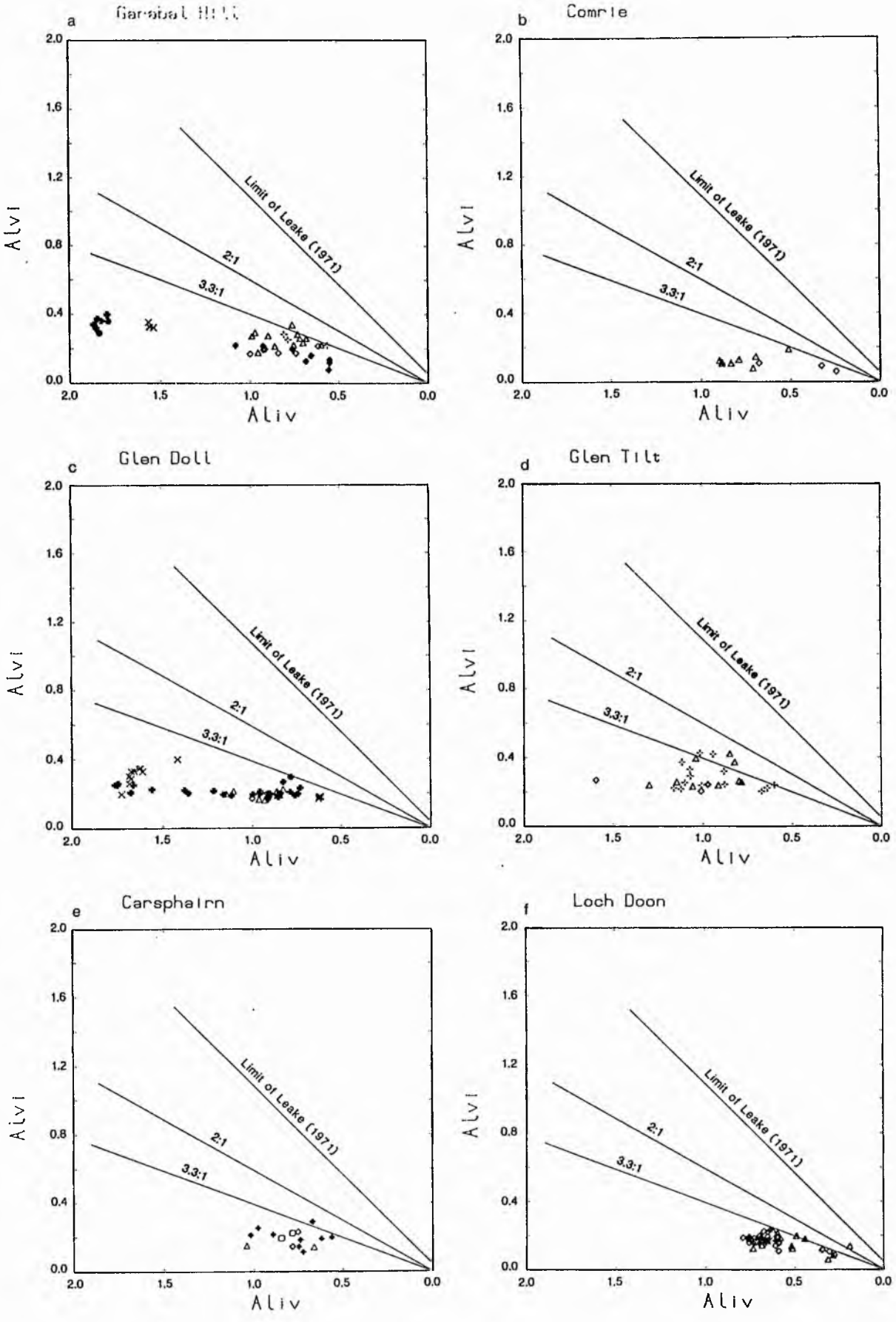

Fig 4.9 Al^{iv} versus Al^{vi} plots of amphiboles with limites of Fleet & Barnett (1978) representing line 3.3:1 and the limits of Leake (1971)

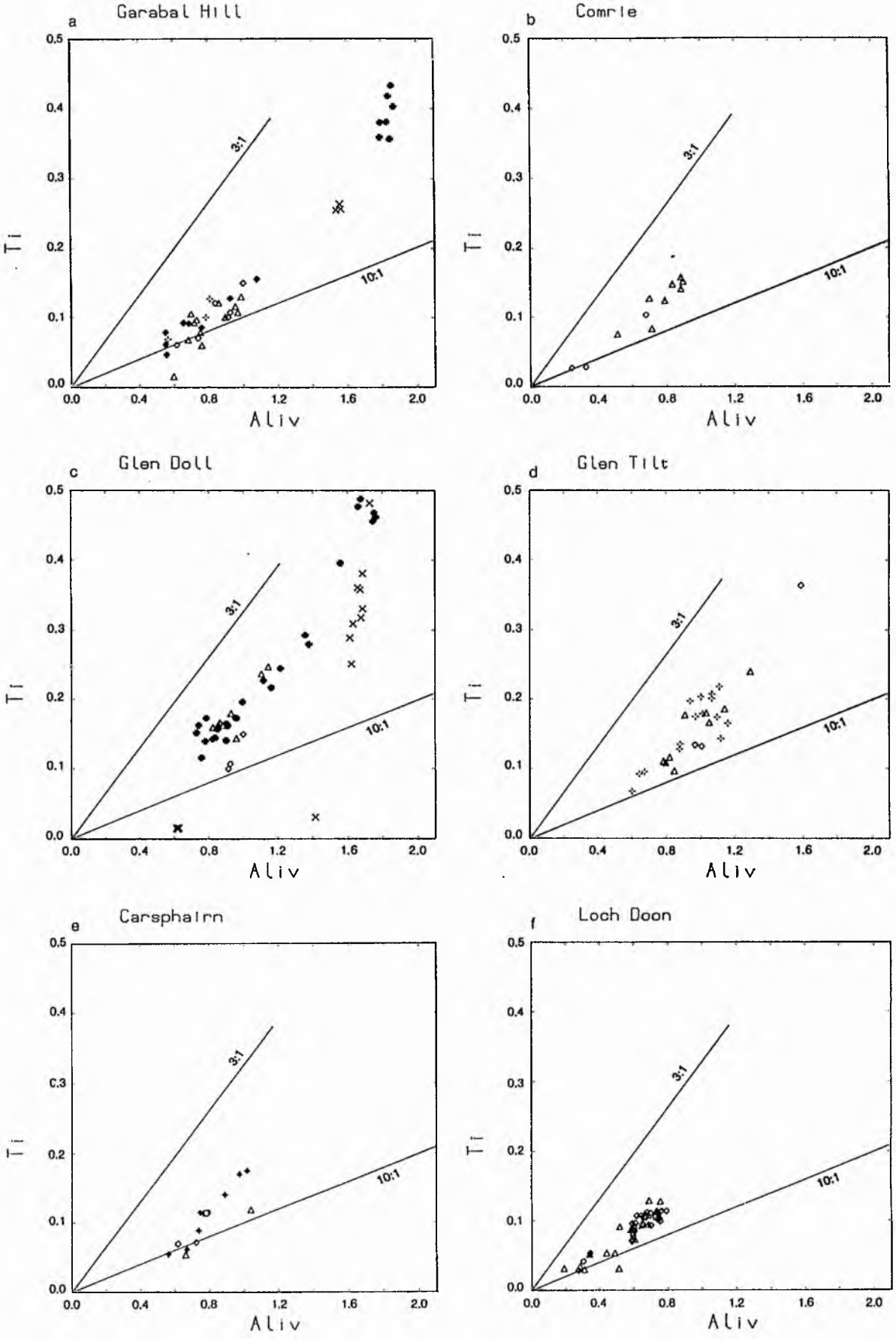

Fig 4.10 Al^{iv} versus Ti plots of amphiboles

4.8.3b Coexisting amphibole and pyroxene

Analyses from gabbro and diorite samples are plotted on the pyroxene quadrilateral in Fig. 4.11. Amphibole and orthopyroxene plot approximately parallel to the Mg-Fe baseline while clinopyroxene compositions cluster in the salite-augite area (see previous discussion).

The distribution coefficient for Mg-Fe between coexisting pyroxene-amphibole pairs is given by the following equation (after Ray & Sen, 1970):

$$K_D^{P-A} = \frac{X_p}{1-X_p} \cdot \frac{1-X_A}{X_A}$$

where $X = Mg / (Mg + Fe^{2+})$

P = pyroxene

A = amphibole

Calculated K_D values for the different plutons are plotted on Figs 4.12, 4.13, 4.14, 4.15, and 4.16, and listed in Table 4.2.

4.8.3c Discussion and summary

Amphibole compositions are dominantly magnesio-hornblende with tschermakitic types in the ultrabasic and basic rocks from Garabal Hill and Glen Doll plutons. Secondary amphibole is actinolitic hornblende and actinolite is found in several rock types. These results are similar to those published for other igneous provinces, for example the Sierra Nevada, California batholith (Dodge et al.

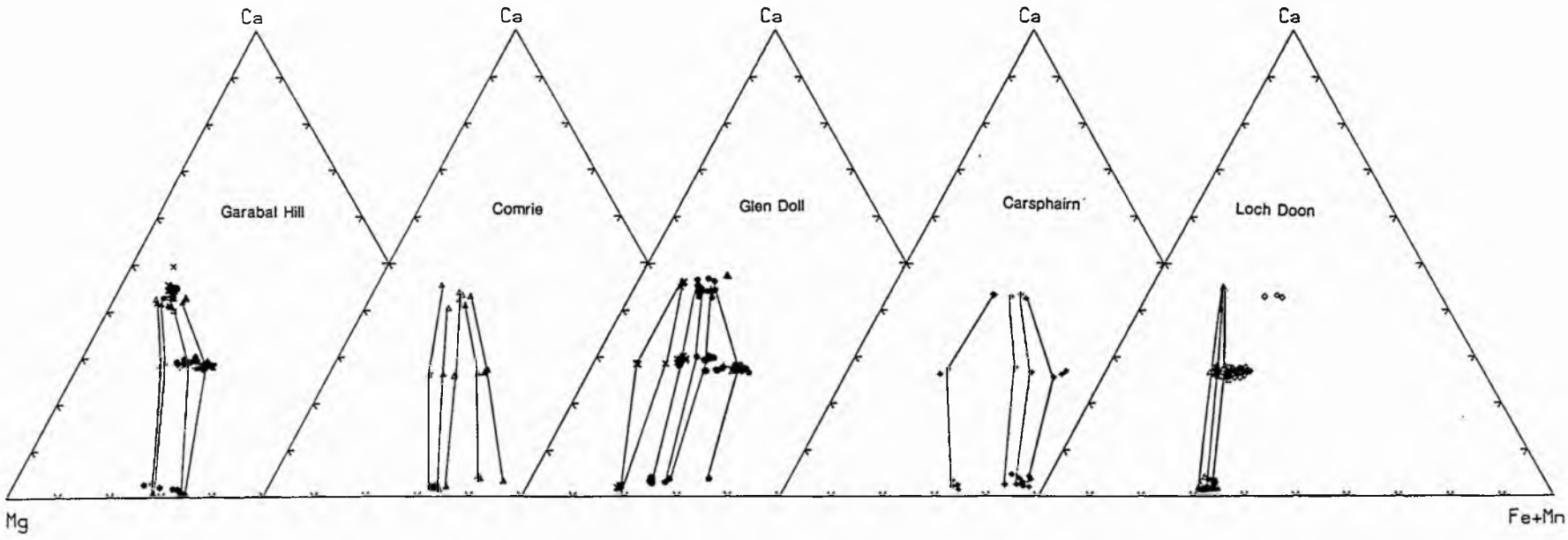

Fig 4.11 Ternary Ca-Mg-(Fe + Mn) plots with tie lines joining coexisting clinopyroxene-amphibole-orthopyroxene

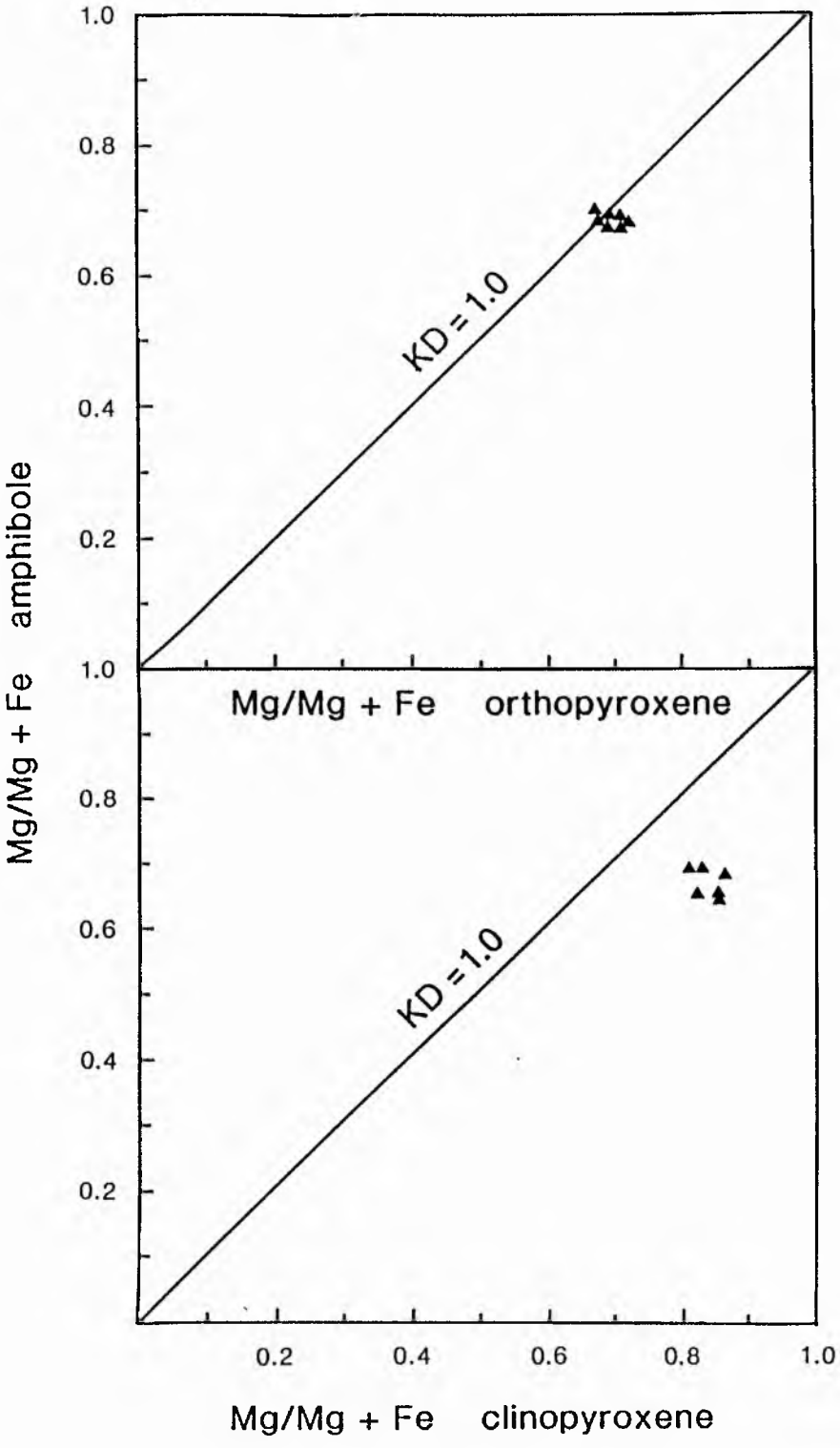

▲ Diorite

Fig 4.12 Partitioning of Mg and Fe between coexisting amphiboles and clinopyroxenes, and coexisting amphiboles and orthopyroxenes for the Garabal Hill pluton.

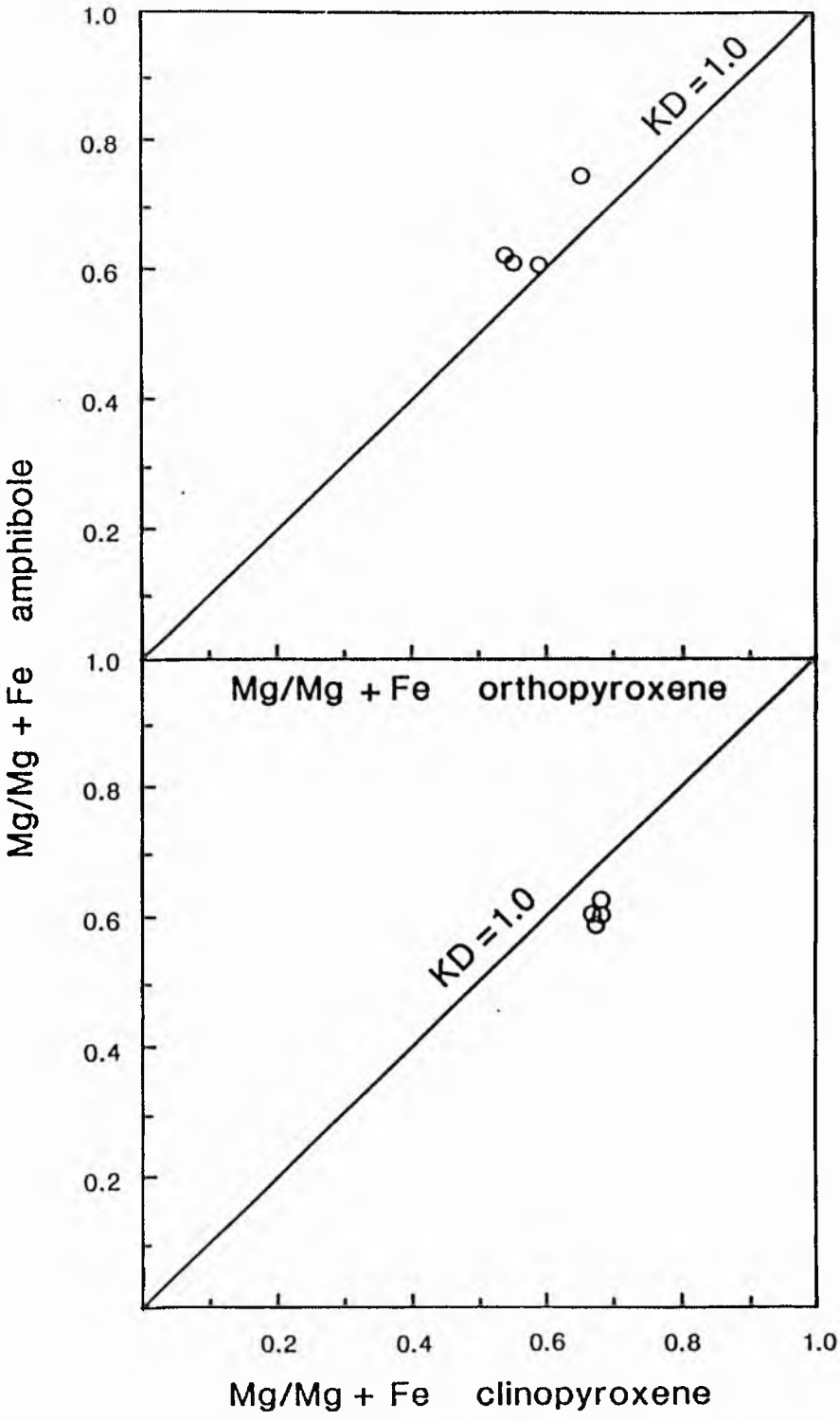

○ Quartz monzodiorite

Fig 4.13 Partitioning of Mg and Fe between coexisting amphiboles and clinopyroxenes, and coexisting amphiboles and orthopyroxenes for the Comrie pluton.

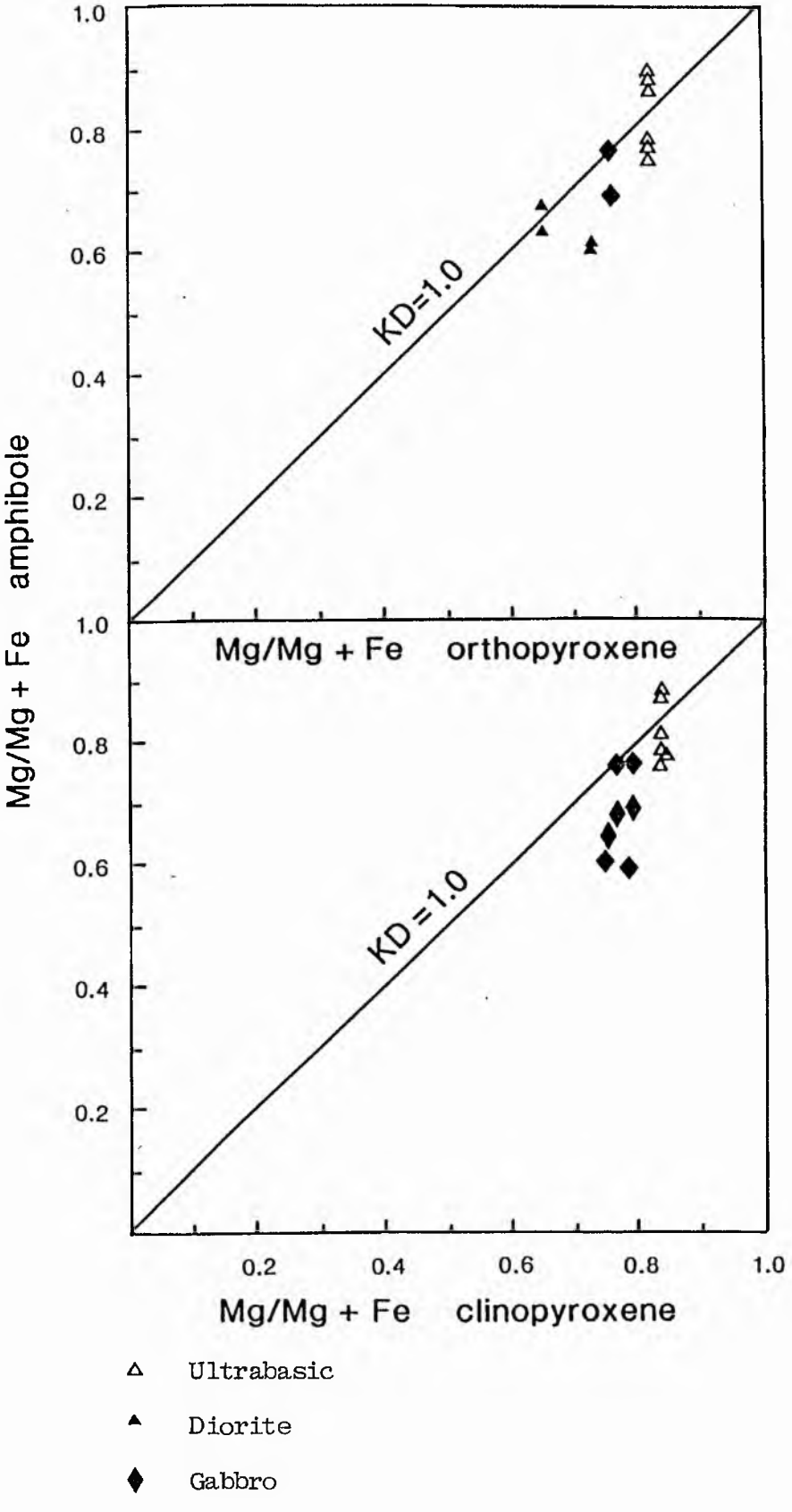

Fig 4.14 Partitioning of Mg and Fe between coexisting amphiboles and clinopyroxenes, and coexisting amphiboles and orthopyroxenes for the Glen Doll pluton.

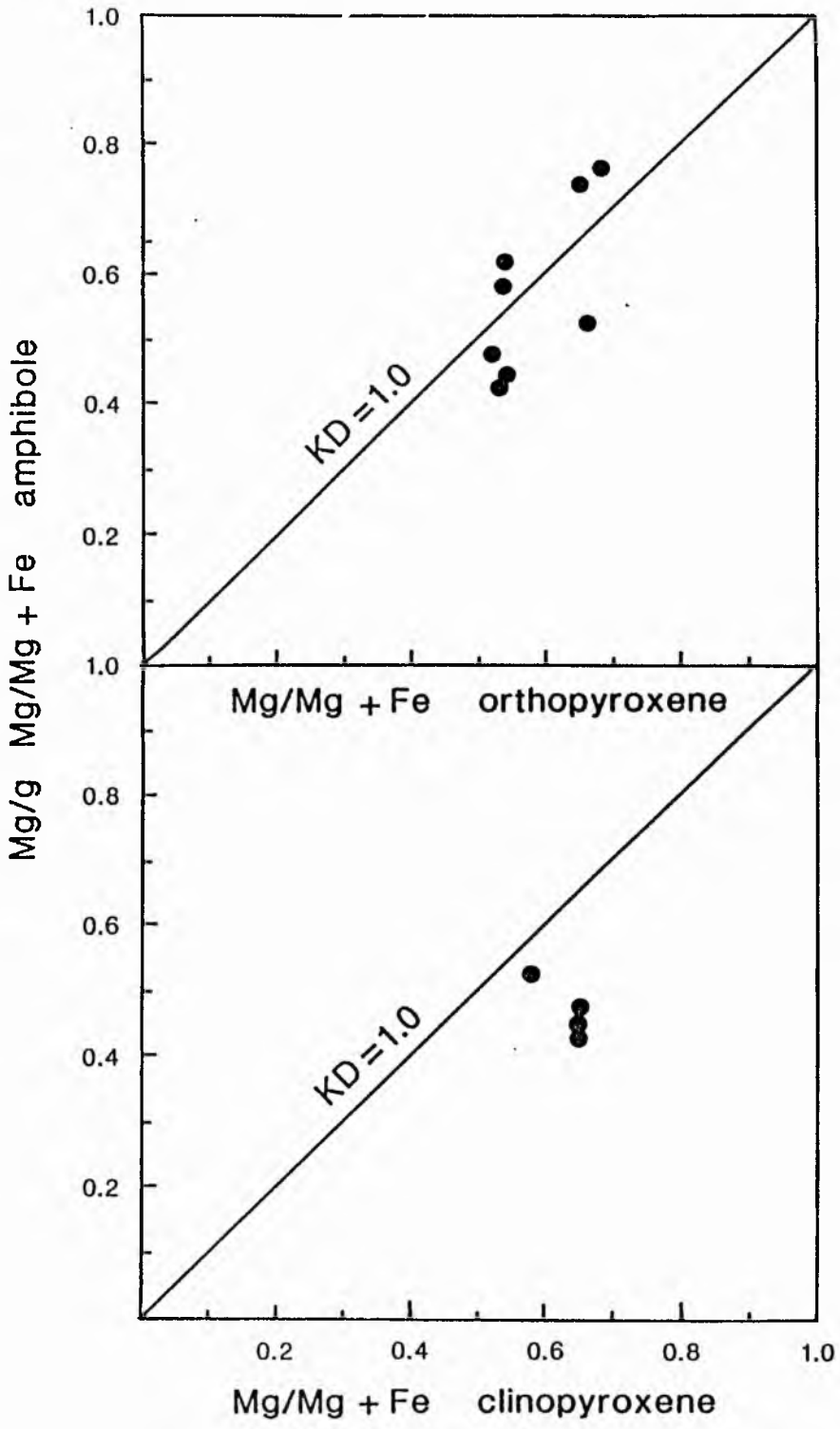

● Tonalite

Fig 4.15 Partitioning of Mg and Fe between coexisting amphiboles and clinopyroxenes, and coexisting amphiboles and orthopyroxenes for the Carsphairn pluton.

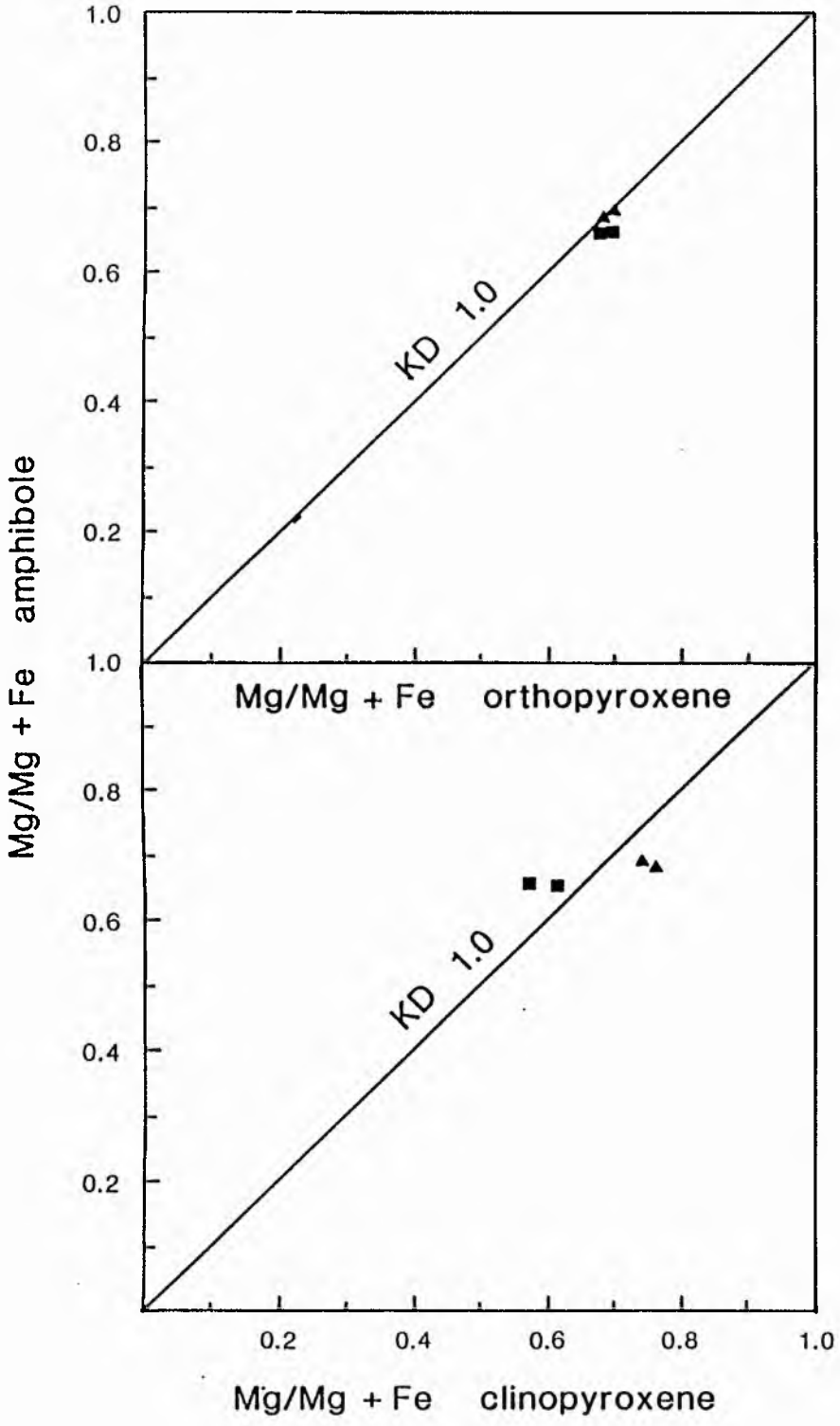

▲ Diorite

■ Granodiorite

Fig 4.16 Partitioning of Mg and Fe between coexisting amphiboles and clinopyroxenes, and coexisting amphiboles and orthopyroxenes for the Loch Doon pluton.

Table 4.2: Calculated distribution coefficients (K_D) of Mg and Fe^{2+} between coexisting pyroxenes, orthopyroxene and amphibole, clinopyroxene and amphibole, amphibole and biotite phases.

Name of pluton	Rock type	Sample No	KD_{O-C}	KD_{O-A}	KD_{C-A}	KD_{B-A}
Garabal Hill	Gabbro	GH10	0.79	-	-	-
	Pyroxene biotite diorite	GH3	0.68	-	-	-
	Hornblende biotite diorite	GH25	-	-	-	0.74
	Appinitic diorite	GH11	-	-	-	0.74
		GH28	-	-	-	0.70
	Granodiorite	GH31	-	-	-	0.68
		GH39	-	-	-	0.66
		GH29	-	-	-	0.61
Comrie	Pyroxene biotite diorite	CM20	0.78	-	-	-
		CM10	0.74			
	Hornblende biotite diorite	CM4	-	-	-	0.62
	Quartz monzodiorite	CM25	0.65	1.36	0.99	0.69
	Granodiorite	CM28	-	-	-	0.55
Glen Doll	Pyroxenite	GD26	0.90	1.43	1.61	1.50
		GD49	0.87	-	-	-
	Gabbronorite	GD41	0.85	1.40	1.64	1.01
		GD42	0.85	-	-	-
	Quartz gabbro	GD3	0.81	-	-	-
	Diorite	GD33	-	-	-	0.63
	Granodiorite	GD40A	-	-	-	0.67
Glen Tilt	Diorite	GT44	-	-	-	0.80
		GT28	-	-	-	0.70
	Appinitic diorite	GT55	-	-	-	0.59
	Granodiorite	GT41	-	-	-	0.56
Carsphairn	Tonalite	77026	0.73	1.39	1.95	0.93
		77032	1.56	1.02	0.70	0.99
	Hornblende biotite diorite	AS38	-	-	-	0.70
	Granodiorite	AS48	-	-	-	0.42
Loch Doon	Pyroxene biotite diorite	78002	0.72	-	-	0.85
		WL6	0.68	-	-	-
		DBL1	-	0.99	-	-
	Granodiorite	DBL3	-	-	1.44	0.75
		77022	-	-	-	0.68
		WL9	-	-	-	0.72

1968) and the Aleutian arc (Kay et al. 1983).

Leake (1968) published comprehensive data on calcic amphiboles from many different areas and concluded that the Ti content was temperature dependent whereas high Al^{iv} was favoured by high pressure and that overall metamorphic amphibole composition was determined principally by host rock chemistry: Leake (1965a,b, 1971) indicated that the maximum possible Al^{vi} increases with increasing Al^{iv}, that rock composition primarily controls Al^{iv} content but increasing pressure favours higher values. He suggested also that igneous amphibole has low Al^{vi} compared to metamorphic amphibole due to the higher temperature of crystallisation. Figure (4.9) and similar ones from other plutons fits these conclusions. Fleet & Barnett (1978) found that Al^{iv} increases with increasing temperature and Al^{vi} with increasing pressure, and noted that unaltered igneous amphibole generally had Al^{iv}/Al^{vi} greater than 3.3, a feature of Fig. 4.9 and the similar figures for the other plutons.

One of the effects of substitution of Al^{iv} for Si is that complimentary substitutions are required for charge balance principally involving Al^{vi}, Ti and Fe^{3+} in the C-site and Na and K in the A-site. It has already been shown that Ti substitution is important in the amphiboles from the different plutons (Fig. 4.10 and other figures). Leake (1965a) and Raase (1974) concluded that increasing temperature resulted in high Ti, whereas Cawthorn (1976a) and Hynes (1982) suggested that decreasing pressure favours increasing Ti. As the magnesio-hornblendes are commonly high in Ti components they presumably crystallised at high temperature and/or low pressure. In igneous rocks there is the probability that other crystallising phases such as biotite and ilmenite have a strong influence on the

partitioning of Ti in amphibole. Kanisawa (1972) studied the magnesio-hornblende in Kitikami granites in Japan and concluded that Mg-Fe substitution is influenced considerably by the fO_2 of the magma. At high fO_2 Fe^{2+} enters magnetite, thus the Mg ratio of the amphibole is high (i.e. magnesio-hornblende). The magnesio-hornblendes of Garabal Hill, Comrie, Glen Doll, Glen Tilt and Loch Doon may reflect high fO_2 conditions.

In Carsphairn, some amphiboles from tonalite have low Mg ratio and they are of ferro-hornblende composition (Fig. 4.2). Kanisawa (1972) found that at low fO_2 ilmenite crystallises and lowers the Mg ratios of the amphibole (i.e. ferro-hornblende). However, because of the presence of both magnesio- and ferro-hornblende and the dominance of magnetite as an opaque mineral, it is difficult to ascertain the fO_2 conditions.

4.8.4 BIOTITE

4.8.4a Discussion

Compilations of variations in biotite chemistry in different calc-alkaline series host rocks have been published by Nockolds (1947), Foster (1960), and Neilson & Hynes (1973), as well as in the Sierra Nevada batholith (Dodge et al. 1969), Japanese pluton (Kanisawa, 1972), and Hercynian plutons of N Portugal (de Albuquerque, 1973).

In general these researches indicate that:

(a) biotite from more basic rocks is Mg-rich, but phlogopite is rarely encountered,

(b) biotite from intermediate rocks has a considerable range of

compositions, trending away from Mg-rich towards Fe-rich compositions, and

(c) biotite from acidic rocks found to show the largest range of compositions often as much variation as observed in all other rock types in a calc-alkaline suite, though some contain the lowest Si, Mg and highest Fe contents.

In the Garabal Hill-Glen Fyne complex, biotites have been analysed from basic (gabbro), intermediate (diorite) and acidic (granodiorite) rock types. The biotites from the gabbros have mean Fe ratios of 0.37 which tend to increase towards the hornblende biotite diorite with mean values of 0.46, but there is a small decrease in the medium and porphyritic granodiorite (0.42) (Fig. 4.4). The compositional trend in the basic and intermediate rocks is believed to reflect a decrease in oxygen fugacity with falling temperature. The more magnesian trend in the granodiorites indicates an increase in the oxygen fugacity. This would not be the expected result if the granodiorites were fractionated from the gabbros alone, which suggests contamination of the basic magma to form the granodiorites (Walsh, 1975).

In Comrie the Fe ratio increases from pyroxene biotite diorite values of about 0.35 to granodiorite values of 0.43 which reflect a decrease in the oxygen fugacity with falling temperature.

In Glen Doll there is an increase in the Fe ratio from the pyroxene hornblende gabbro with values of about 0.33 through diorite (0.47), but a decrease in the tonalites through granodiorites which once more may reflect a contamination effect (of Garabal Hill). In Glen Tilt there is no systematic variation.

In the Carsphairn pluton the biotites from the tonalites have a

mean Fe ratio of about 0.51 which increases towards the granodiorite and granite (0.60) which correlates with the composition of the host rock. In Loch Doon, biotites show an increase in the Fe ratio from the pyroxene biotite diorite towards the granodiorites then granites which may reflect falling fO_2 conditions. (Wones & Eugster, 1965).

4.8.4b Coexisting biotite and amphibole

Biotites and amphiboles are the most common ferromagnesian silicates in the granitoid plutons under study. The distribution of Fe and Mg between coexisting amphibole and biotite has been investigated by several authors (see Speer, 1984). Although Fe^{2+} - Fe^{3+} may not be known, overall trends should remain largely unaltered.

Distribution of Fe and Mg

The apparent distribution coefficient of Fe and Mg between biotite and amphibole (hereafter K_D) is defined by (Hietanan, 1971) as:

$$K_D{}^{B-A} = \frac{X_B}{1-X_B} \cdot \frac{1-X_A}{X_A}$$

where:

X = Mg/(Mg + Fe)

A = amphibole

B = biotite

Values for K_D are given in Table 4.2 . and plotted on Figs (4.17, 4.18, 4.19, 4.20, 4.21 and 4.22) from the various plutons. They are generally less than 1.0 indicating that $Mg^{\#}$ ratio is greater in amphibole than in biotite. Leake (1968) noted a significant correlation between $Mg^{\#}$ ratios of coexisting biotite and amphibole and observed that igneous biotites have $Mg^{\#}$ ratios less than 0.65. Only the pyroxenite, pyroxene hornblende gabbros and appinitic diorites have values greater than this (up to 0.84). Kanisawa (1972) listed K_D values of 0.56 to 0.93 from a range of calc-alkaline rocks utilizing total Fe^{2+} values, and the present observed values are comparable. Variations in K_D have been ascribed to changes in pressure (Hietanan, 1971) and in temperature (de Albuquerque, 1974) with low temperature resulting in low K_D values.

More complex relationships have been suggested by other authors including relating whole rock chemistry to mineral chemistry (Gorbatschev, 1969, 1977; Kanisawa, 1972; Tanaka, 1975; and Kato et al. 1977). However Speer (1984) concluded that interpretation of the distribution coefficient will be hindered by the structural and chemical complexity of the two minerals, and it is the structure of the amphibole rather than any physical conditions which controls the distribution coefficient.

In summary amphibole-biotite K_D values from the studied plutons are always less than 1.0 (except for ultrabasic rock types in Glen Doll (Fig. 4.19) and comparable with reported values from other calc-alkaline complexes though the precise control on K_D`s are not well understood.

4.8.5 PLAGIOCLASE

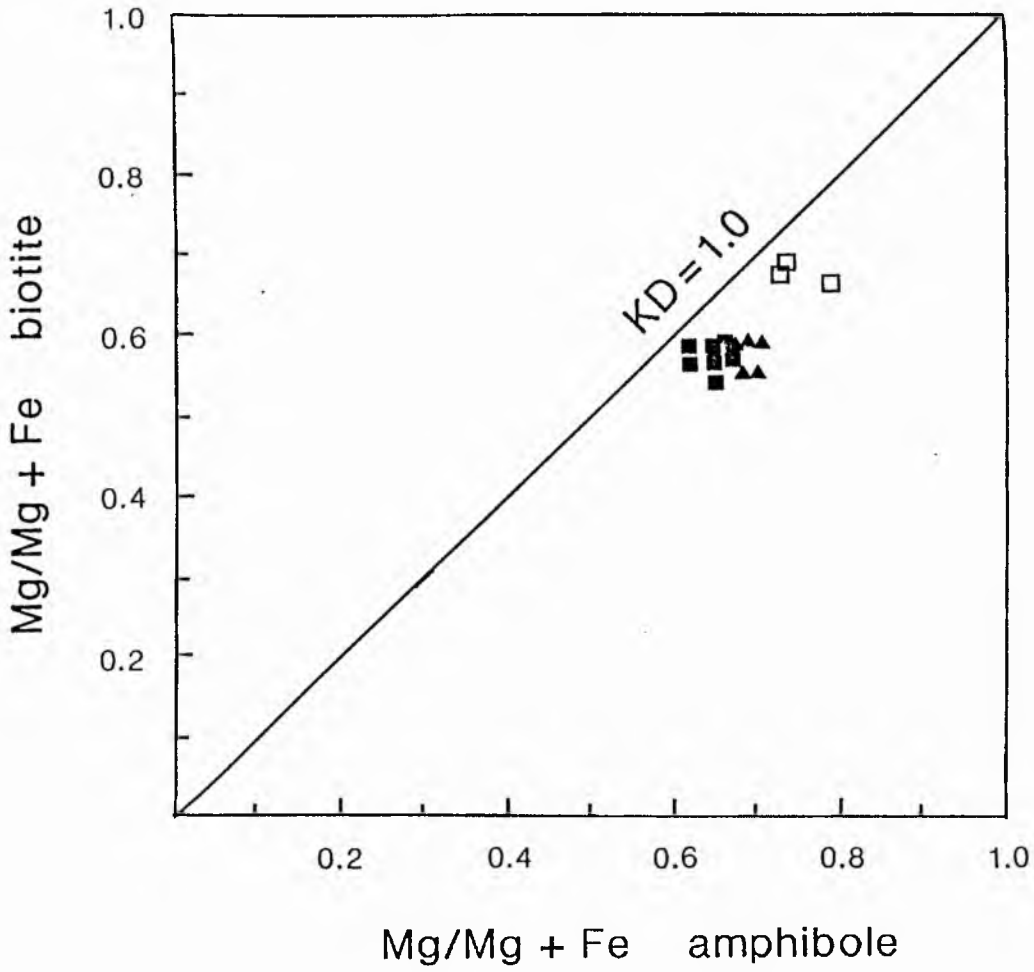

■ Granodiorite

▲ Diorite

□ Appinite

Fig 4.17 Partitioning of elements between coexisting amphiboles and biotites for the Garabal Hill pluton.

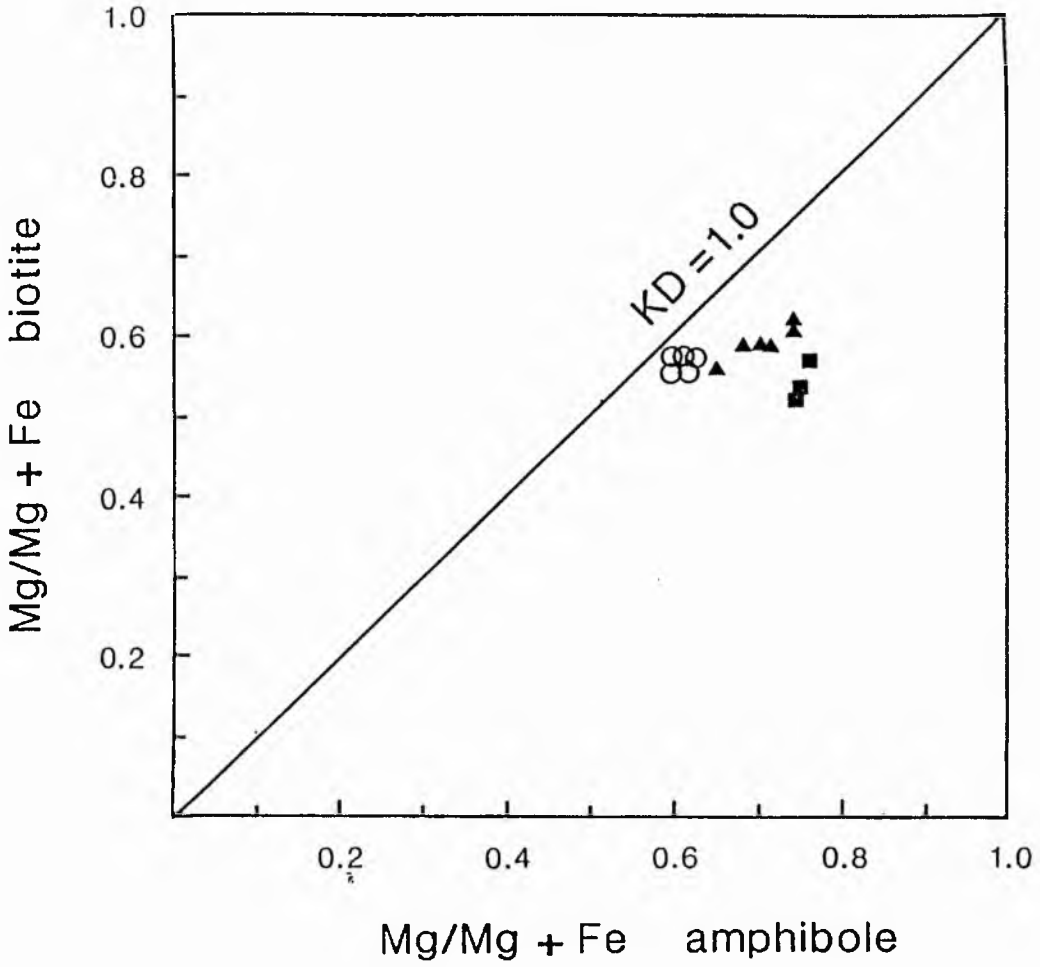

■ Granodiorite

▲ Diorite

○ Quartz monzodiorite

Fig 4.18 Partitioning of elements between coexisting amphiboles and biotites for the Comrie pluton.

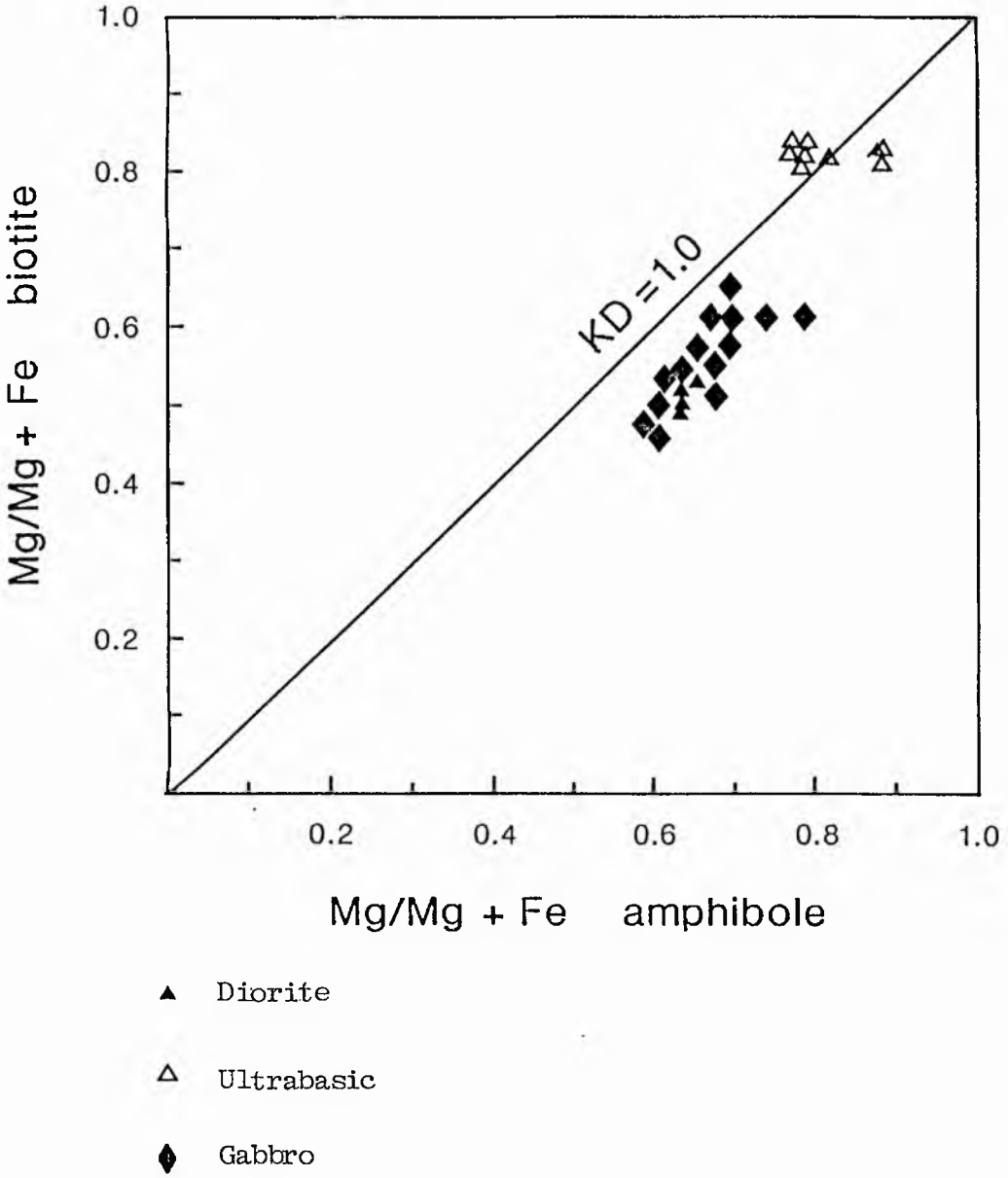

Fig 4.19 Partitioning of elements between coexisting amphiboles and biotites for the Glen Doll pluton.

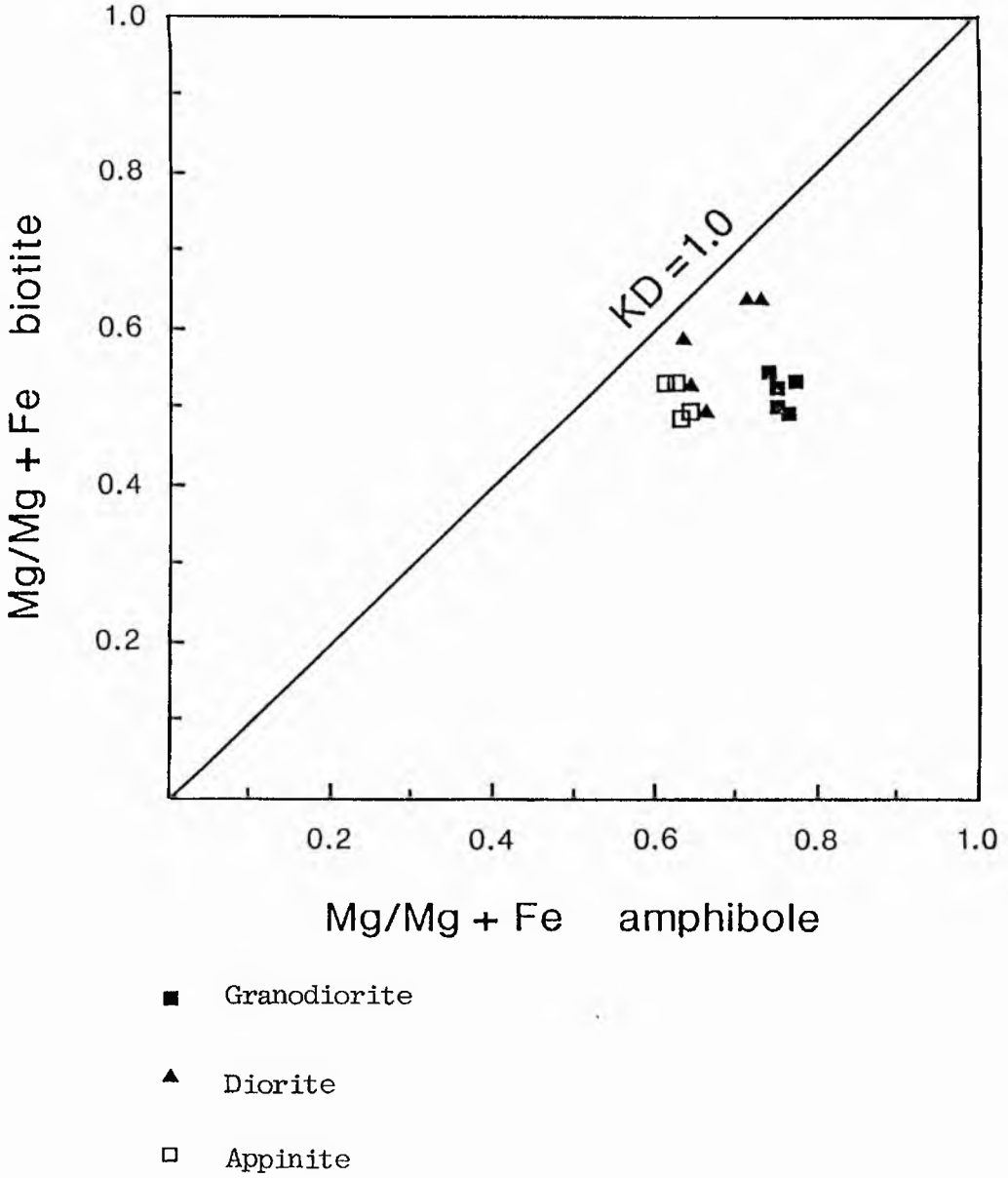

Fig 4.20 Partitioning of elements between coexisting amphiboles and biotites for the Glen Tilt pluton.

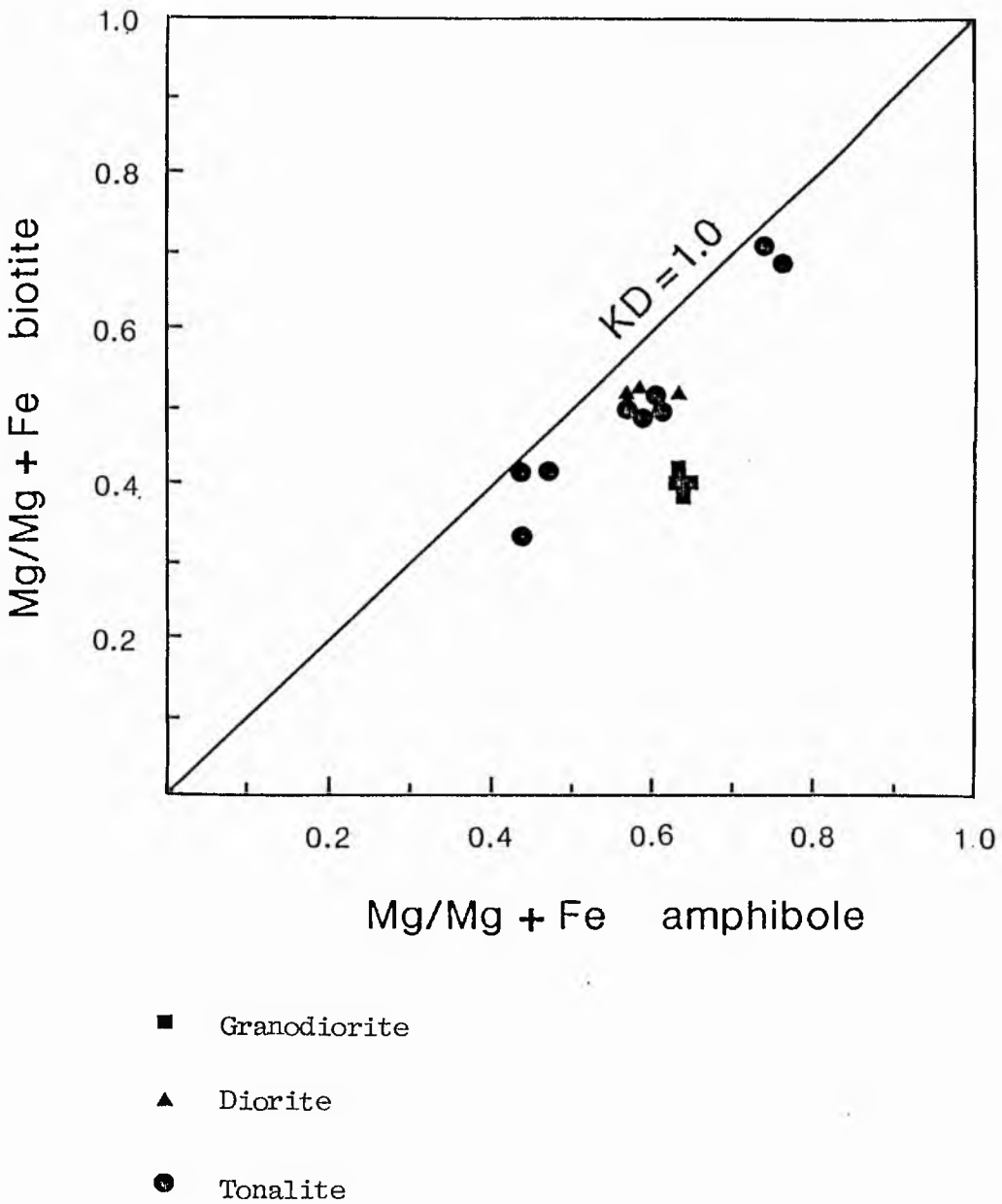

Fig 4.21 Partitioning of elements between coexisting amphiboles and biotites for the Carsphairn pluton.

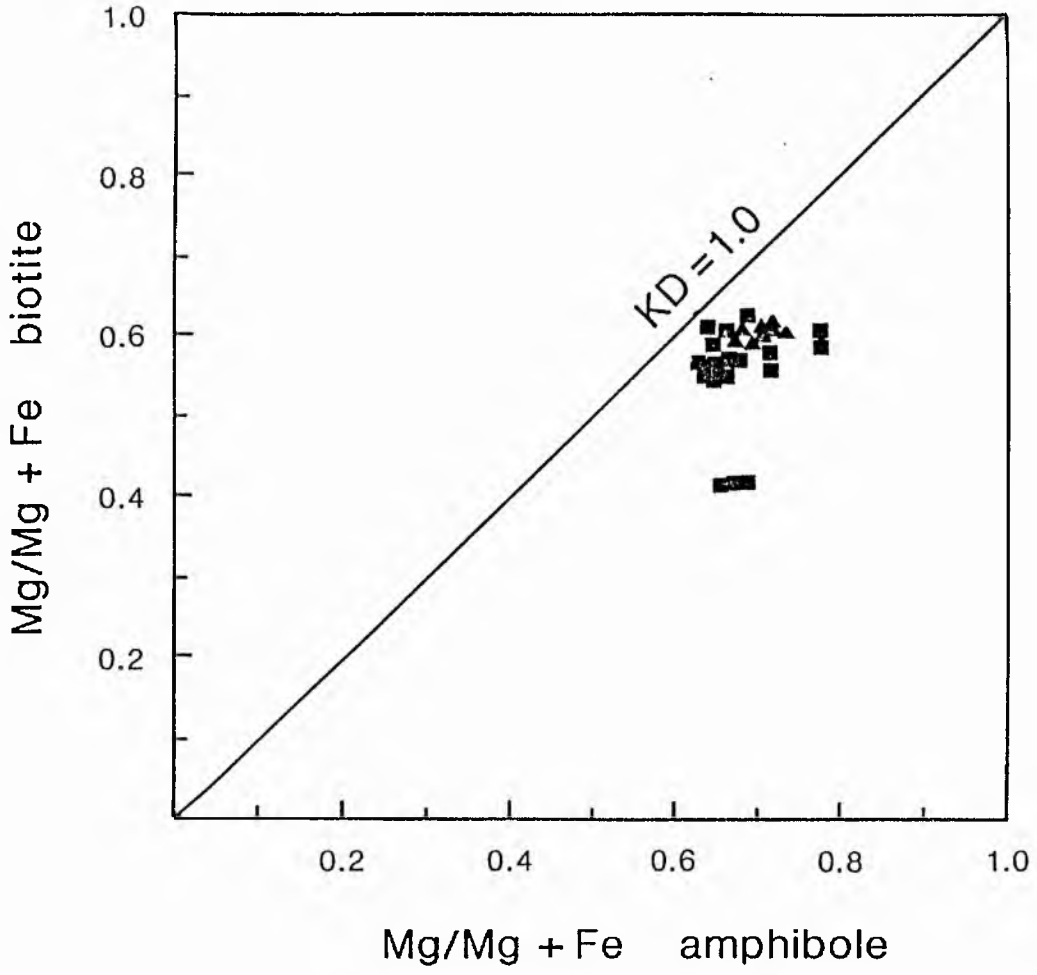

■ Granodiorite

▲ Diorite

Fig 4.22 Partitioning of elements between coexisting amphiboles and biotites for the Loch Doon pluton.

A summary of the analyses of the plagioclase from different rock types in the present study (Fig. 4.6) shows that plagioclase varies systematically being bytownite in the pyroxenite , bytownite-labradorite in gabbros, andesine in diorites and oligoclase in granodiorite and granite though the Glen Tilt granites are albite.

CHAPTER 5

MAJOR OXIDE
AND
TRACE ELEMENT GEOCHEMISTRY

5.1 Introduction:

5.1.1 Aims and objectives:

This part of the study is concerned with:

a) the use of whole rock chemistry in the understanding of the petrogenesis of some zoned dioritic complexes of the Scottish Grampian Highlands and Southern Uplands.

b) to compare variations between these complexes on a regional scale in the same way that the compositionally equivalent volcanics have been shown to vary on a similar regional scale (Thirlwall 1981, 1982), and related to plate tectonic reconstructions.

The details of the chemistry are presented in this chapter and the petrogenesis of the complexes discussed in Chapter 6.

5.1.2 Methodology:

The analyses of representative samples from all major rock types for each complex are presented in Appendix B, Tables B-1 to B-6. Major element analyses were determined on a glass bead prepared by fusion of powdered sample with a mixture of lithium tetraborate + lithium carbonate + lanthanum oxide and trace elements on pressed powder pellets, both using a Philips PW1212 X-ray fluorescence spectrometer (XRF) at the Geology Department, University of St Andrews. Ferrous iron determinations were carried out volumetrically after cold HF digestion in the presence of ammonium metavanadate (Batchelor, 1980).

Rare-earth element (REE) analyses of 11 selected samples for Garabal Hill-Glen Fyne complex rock types were carried out by

instrumental neutron activation analysis, at the East Kilbride Reactor Centre. Details of the method are presented in Appendix B, and the analyses are presented in Table 5.1.

In the following discussion, the trace elements are grouped into 'large ion lithophile' (LIL) and 'high field strength' (HFS) elements following current convention, eg. Saunders et al. (1980). LIL elements analysed include Rb, K, Sr, Ba and Th, and HFS are Ti, P, Zr, Hf and Nb, along with light rare earth elements (LREE) La and Ce which were analysed using XRF.

5.2 Garabal Hill-Glen Fyne

5.2.1. Major oxides

Major element variation is shown as a series of Harker diagrams (Fig. 5.1a-i). For the most part there is good linear correlation between the major oxides. With increasing SiO_2, the abundances of MgO, CaO, FeO (total Fe expressed as $Fe_2O_3(t)$) and MnO decrease whereas K_2O and Na_2O increase. The abundances of Al_2O_3, P_2O_5 and TiO_2 increase initially and then either remain constant (Al_2O_3) or decrease (P_2O_5 and TiO_2).

There is considerable scatter up to 60% SiO_2 especially for minor elements like Na_2O, K_2O, TiO_2, MnO and P_2O_5. This can be related to distinctive petrographic and mineralogical features discussed in Chapter 3. The ultrabasic rocks form a separate group in most of the diagrams and may be at least partly explained by cumulate effects being enriched particularly in MgO, and depleted in TiO_2 and Al_2O_3.

The variation trend is typically calc-alkaline on the AFM

Table 5.1: Rare earth element abundances (in ppm) for samples from the Garabal Hill puton. Rock types are as follows, GAB gabbro, DIO diorite, MED GD medium granodiorite and POR GD porphyritic granodiorite. See Appendix for analytical details.

Sample No	La	Ce	Nd	Sm	Eu	Tb	Yb	Lu	Rock type
GH10	11.0	29.0	22.0	3.0	0.96	0.63	1.53	0.24	GAB
GH21	6.0	26.0	26.0	4.0	1.37	1.26	2.88	0.34	GAB
GH1	18.0	38.0	24.0	4.0	1.03	1.25	2.10	0.35	DIO
GH3	18.0	42.0	26.0	5.0	1.05	1.31	2.49	0.35	DIO
GH5	22.0	49.0	28.0	5.0	1.10	1.34	2.58	0.40	DIO
GH7	20.0	44.0	29.0	5.0	1.26	1.24	2.95	0.43	DIO
GH26	20.0	43.0	25.0	4.0	1.07	0.50	1.80	0.27	DIO
GH28	29.0	56.0	38.0	4.0	1.01	0.61	1.66	0.23	MED GD
GH29	28.0	51.0	21.0	3.0	0.86	0.28	1.40	0.16	POR GD
GH30	31.0	53.0	29.0	4.0	0.87	0.31	1.45	0.20	POR GD
GH39	32.0	60.0	30.0	4.0	0.98	0.33	1.53	0.22	POR GD

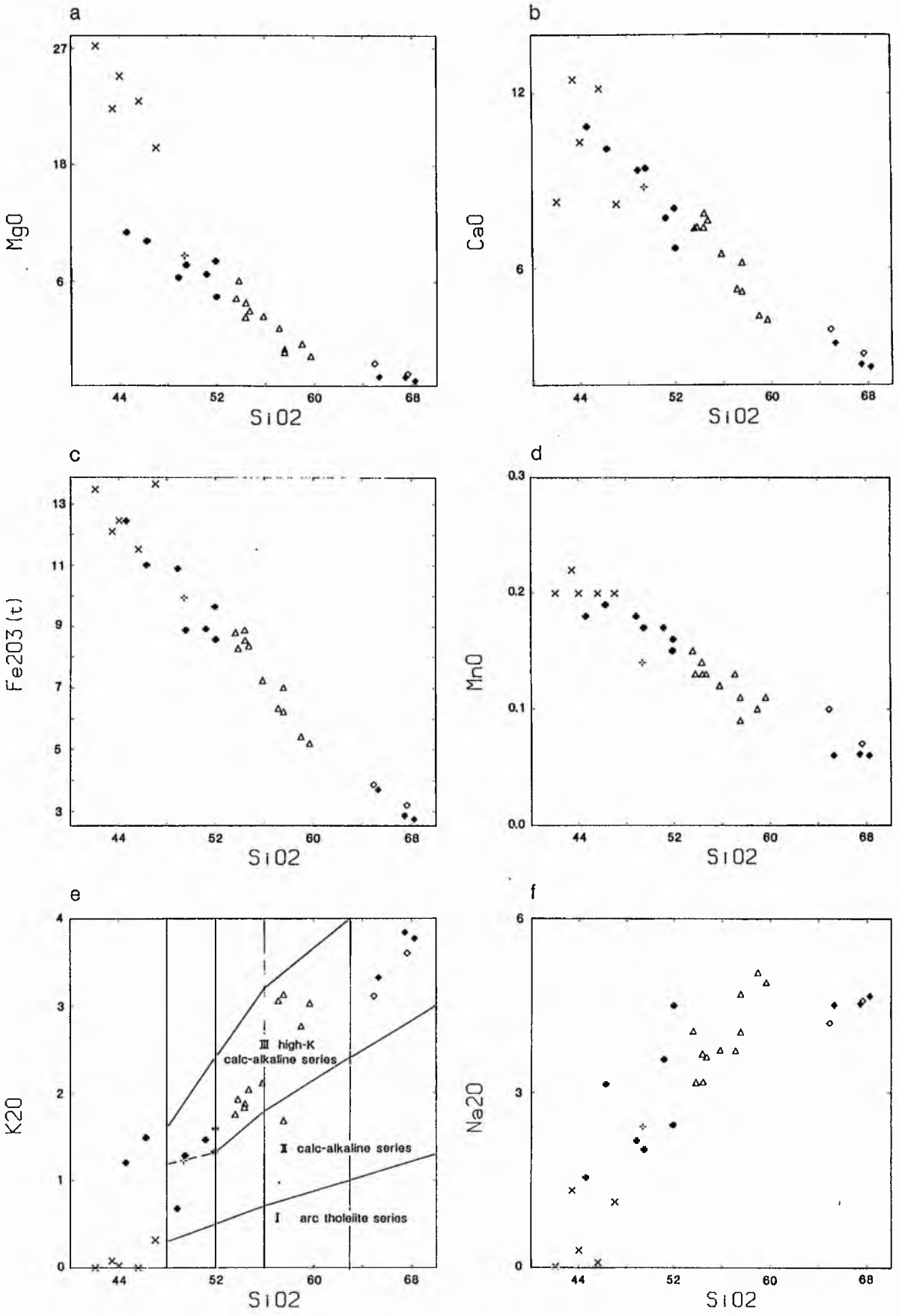

Fig 5.1$_{a-f}$ Harker variation diagrams of major oxides for the Garabal Hill pluton. Fig 5.1$_e$ shows K_2O versus SiO_2 plot with fields of Peccerillo & Taylor (1976) superimposed.

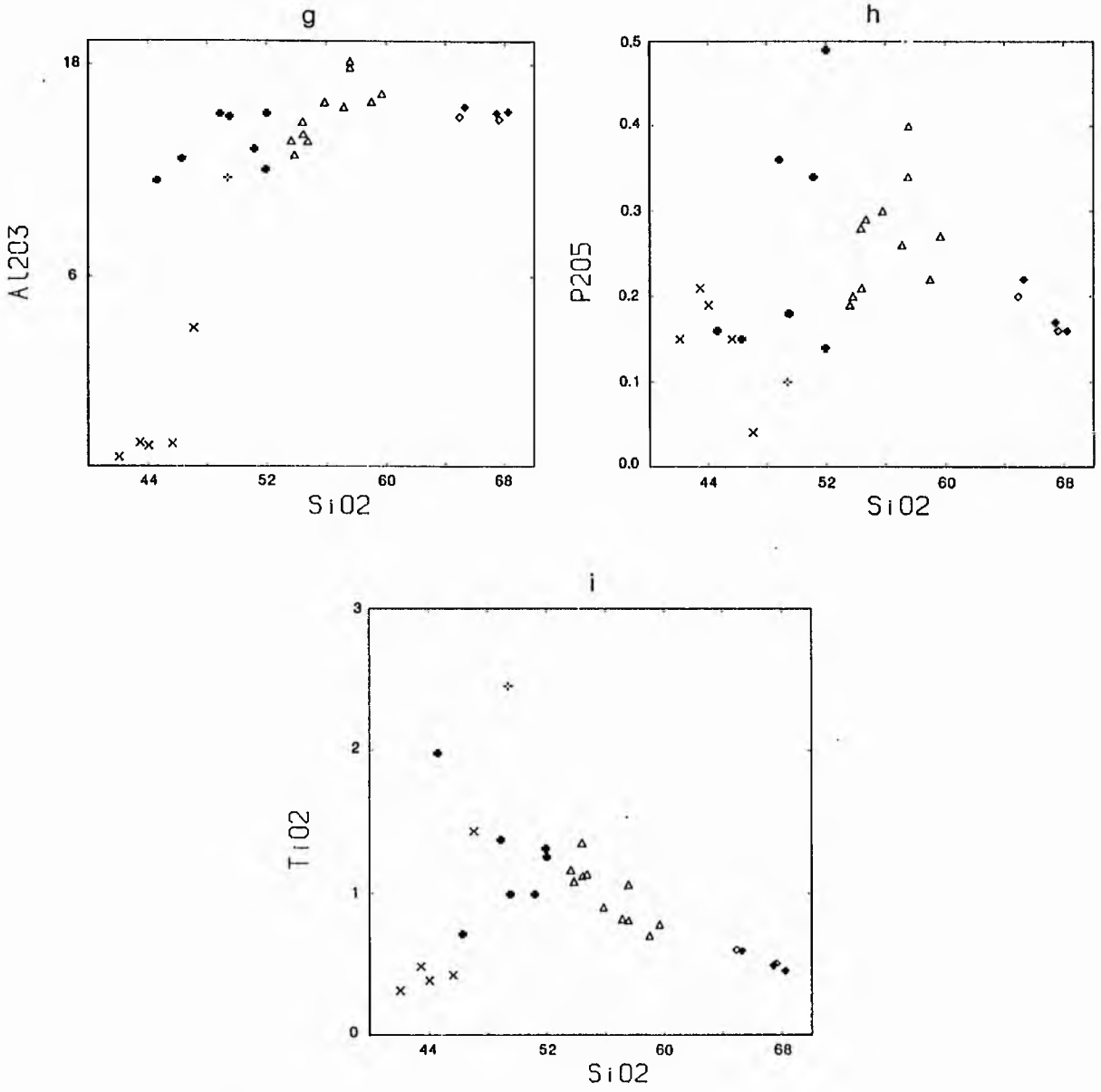

Figs 5.1$_{g-i}$ Harker variation diagrams of major oxides for the Garabal Hill Pluton.

diagram (Fig. 5-1j) and a plot of K_2O versus SiO_2 (Fig. 5.1e) indicate that this complex is calc-alkaline to high-K calc-alkaline within the scheme of Peccerillo and Taylor (1976). In general the rocks are diopside-normative or have less than 1% corundum and have typically I-type features (Chappell and White, 1974).

5.2.2 Trace elements

Plots for various trace elements versus SiO_2 (Fig. 5.1 k-z) generally shows that:

a) Cr and Ni show depletion towards the granodiorites, they are anomalously enriched in the ultrabasic rocks. High Cr greater than 1600 ppm is related to a high modal proportion of the clinopyroxene, whereas high Ni greater than 450 ppm is related to olivine accumulation. V shows a general depletion towards the granodiorites and is rather enriched in the peridotites and diorites. High V (greater than 400 ppm) is related essentially to the high proportion of magnetite, pyroxenes, amphiboles and biotites in the middle stages of fractionation and decreases towards the later stages (Wilkinson, 1959; Mason and Moore, 1982).

b) Rb increases with SiO_2 typical of its normally incompatible behaviour. The ultramafic rocks do not contain any detectable Rb. Ba shows a trend similar to Rb, both having an affinity for potassium. Sr increases towards the porphyritic granodiorite to values greater than 1000 ppm.

c) Zn in the diorites (up to 120 ppm) may be related to high modal proportions of biotite, amphibole, pyroxene and magnetite where it probably substitutes for Fe^{2+}. Cu also shows an increase towards the dioritic rocks.

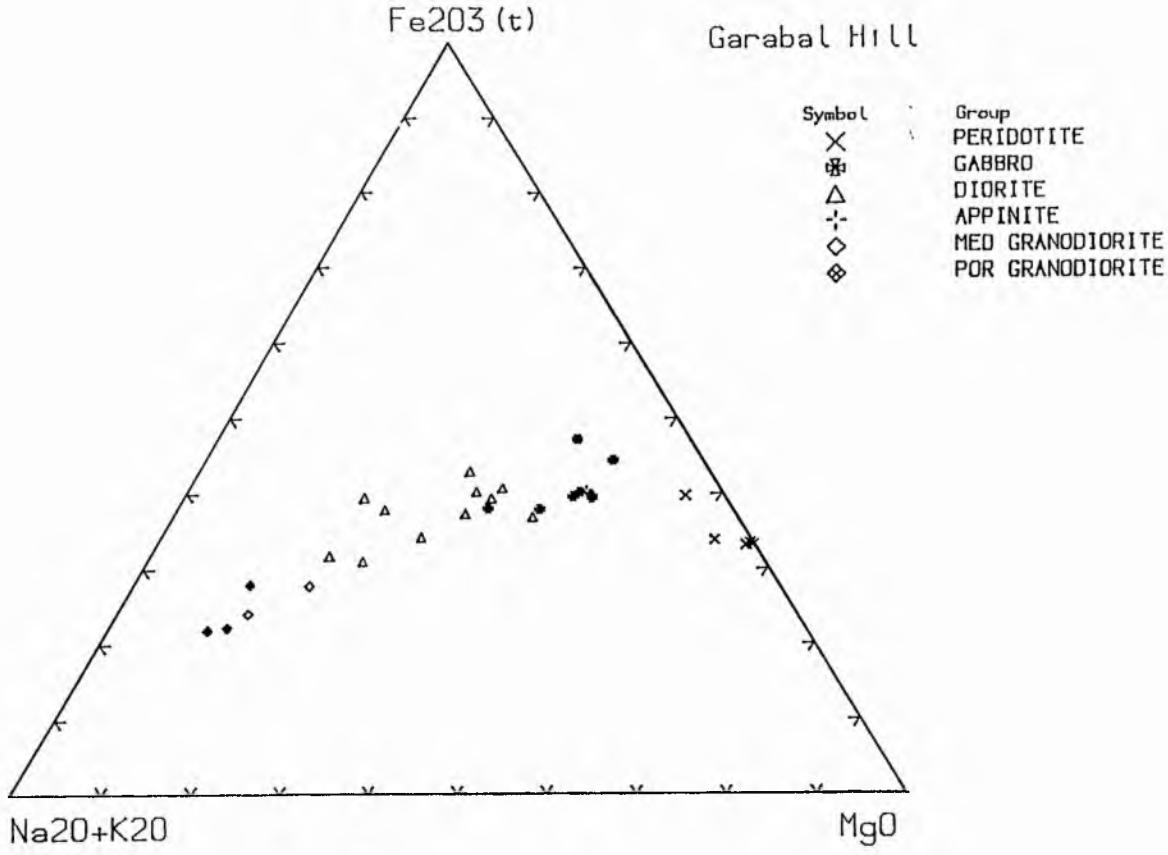

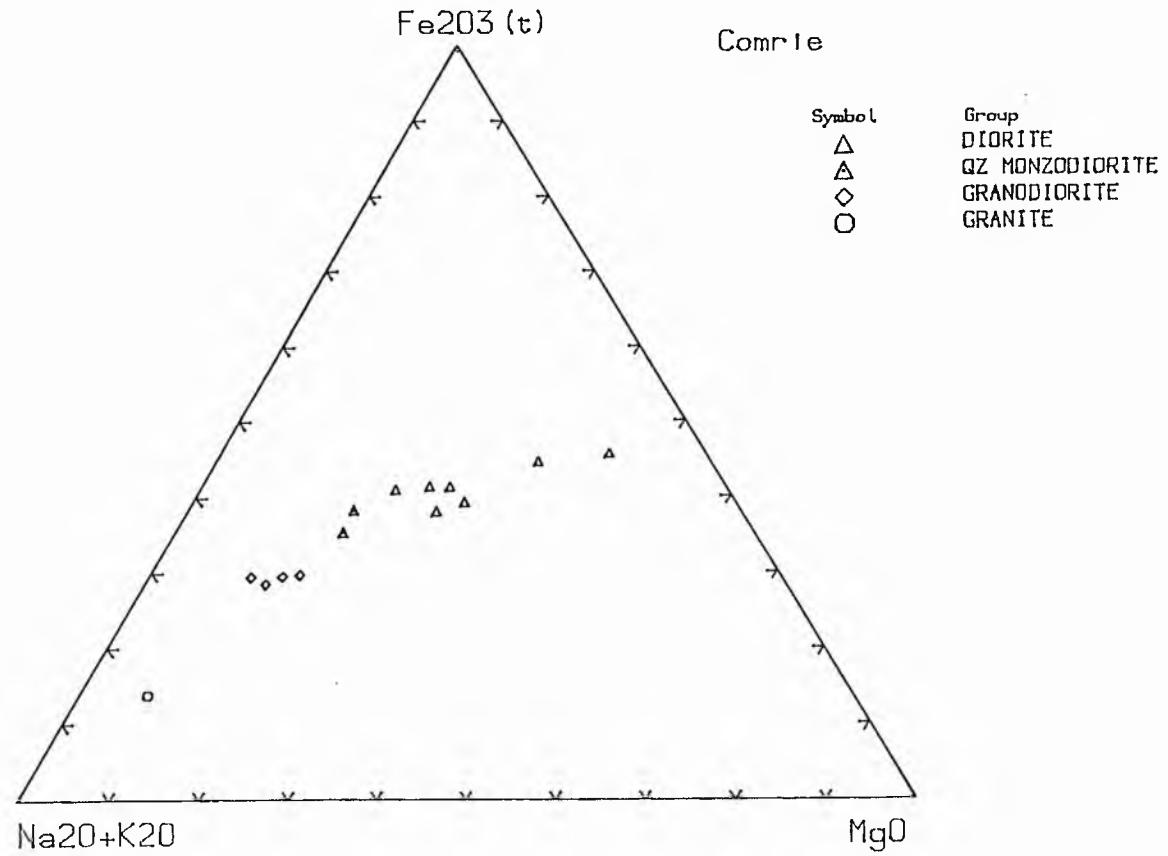

Fig 5.1_j and 5.4_j AFM plots of the Garabal Hill and Comrie plutons.

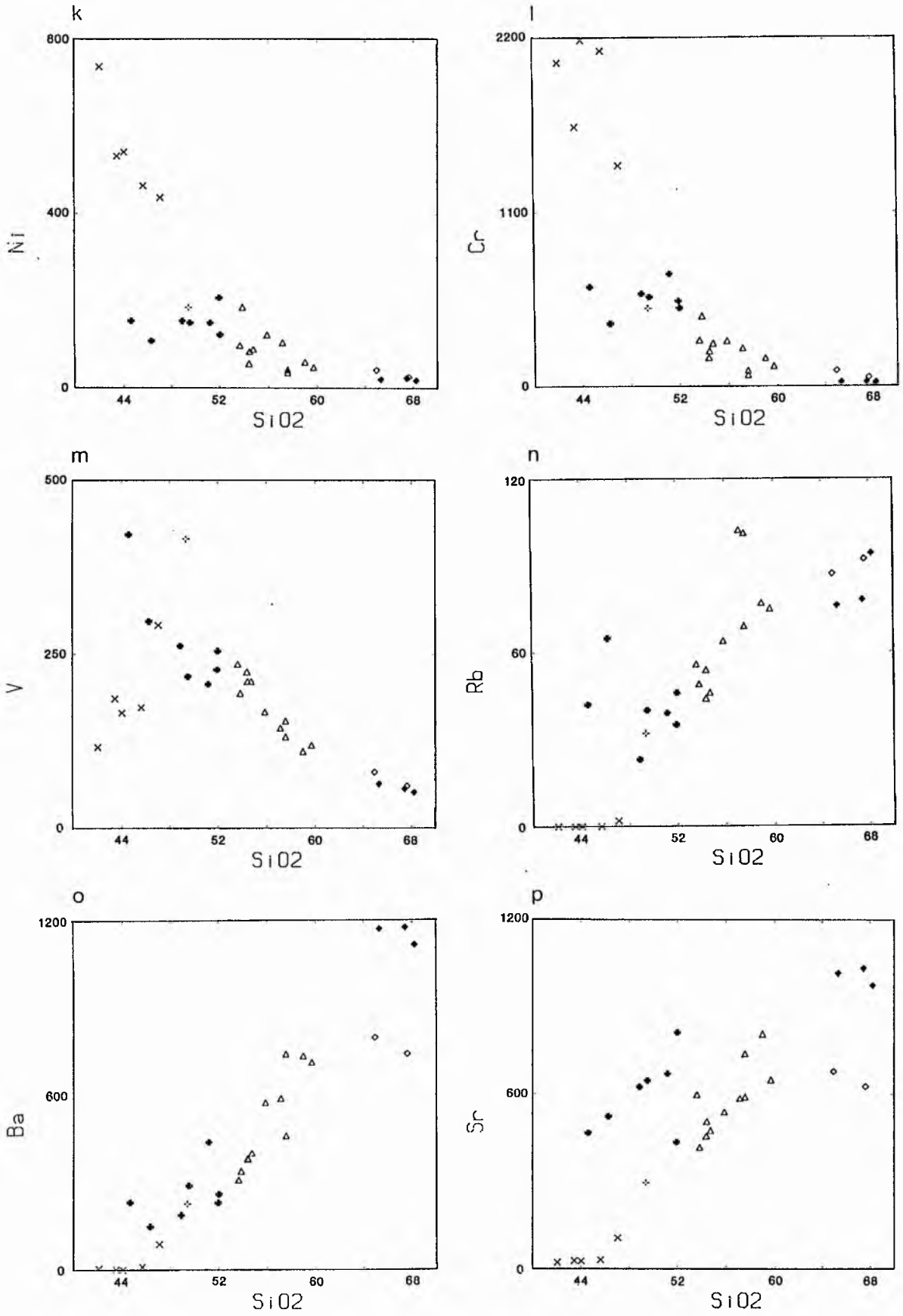

Figs 5.1$_{k-p}$ Harker variation diagrams of SiO_2 in wt % against trace elements in ppm for the Garabal Hill pluton.

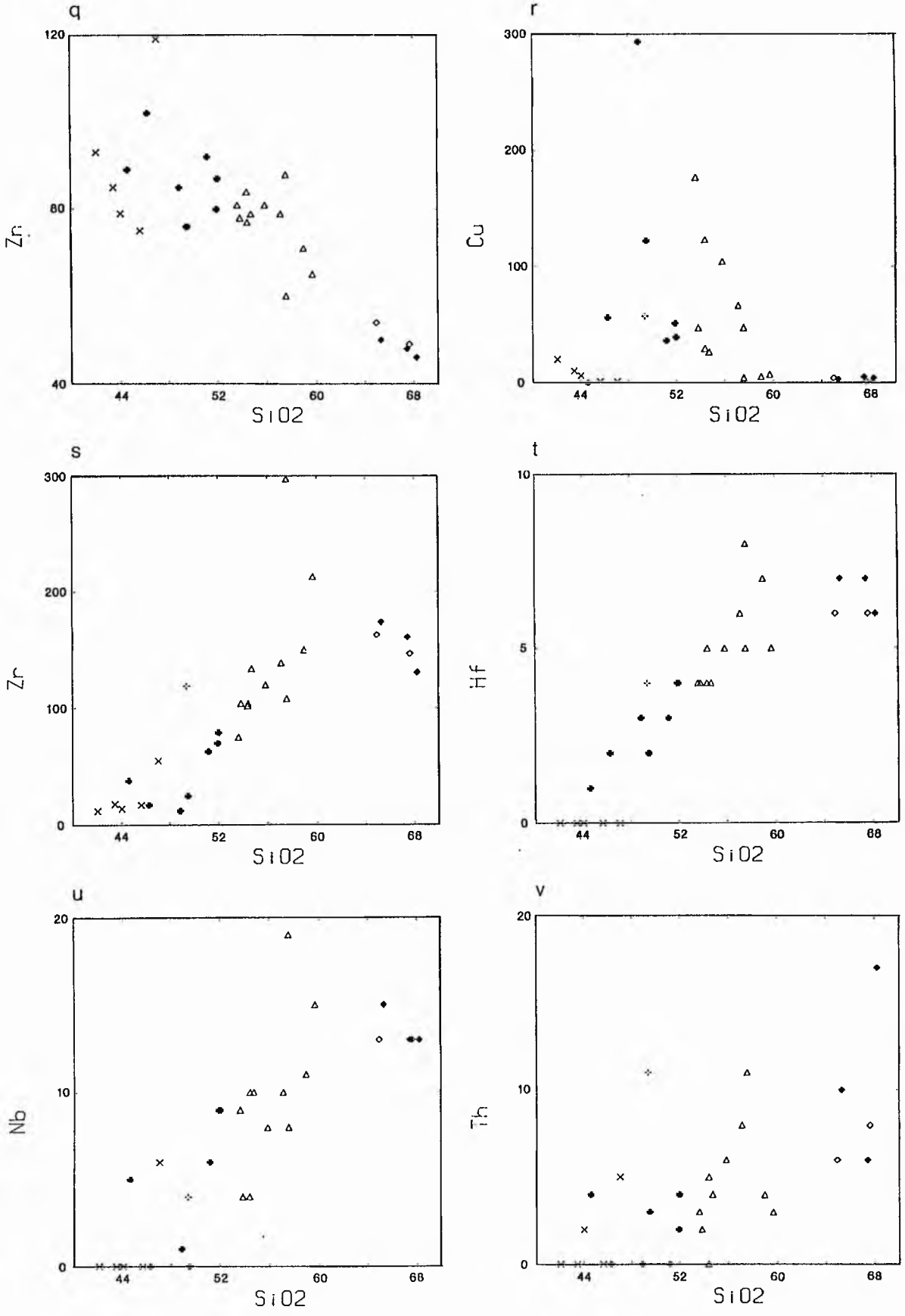

Fig 5.1$_{q-v}$ Harker variation diagrams of SiO_2 wt % against trace elements in ppm for the Garabal Hill pluton.

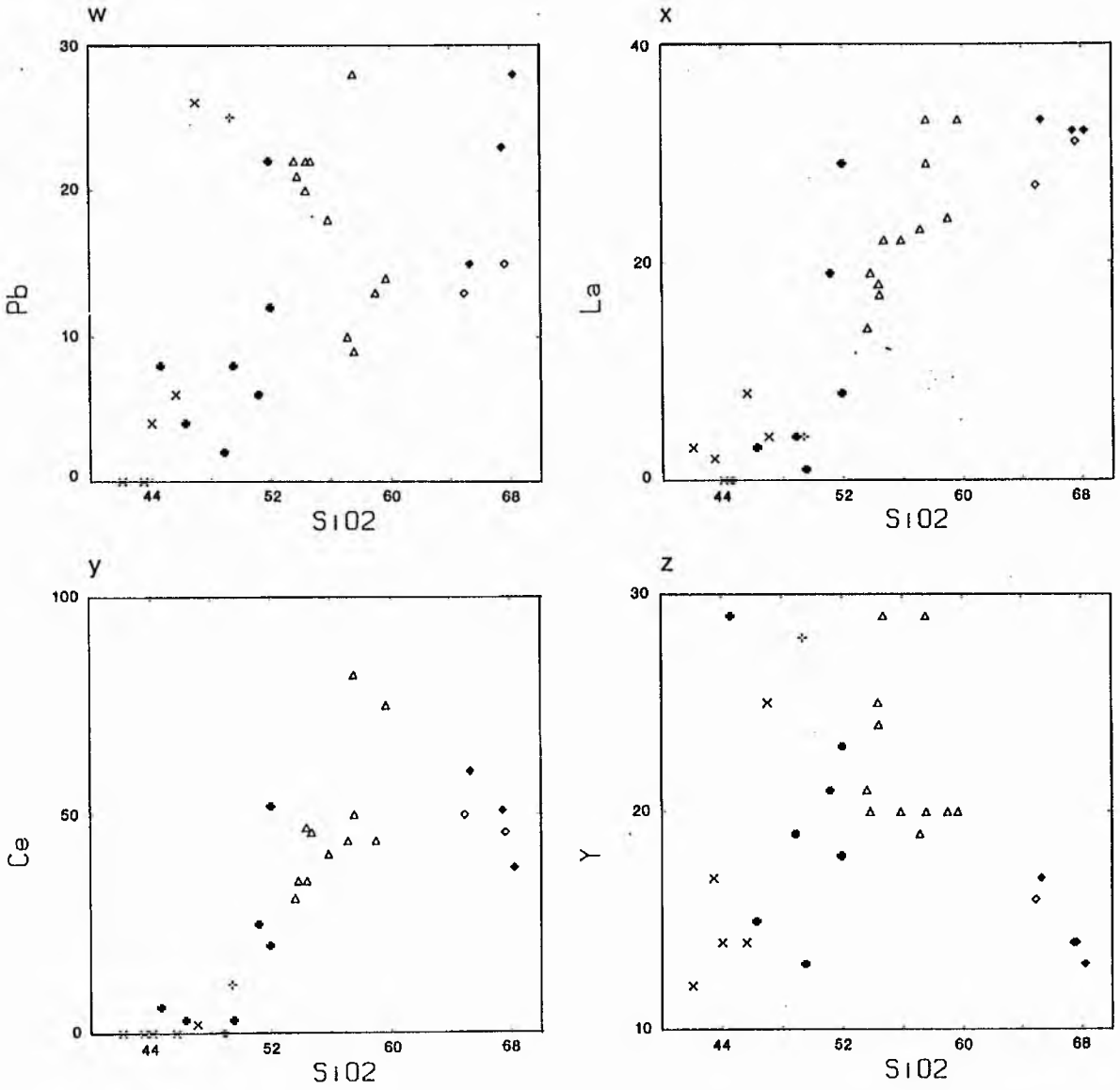

Fig 5.1$_{w-z}$ Harker variation diagrams of SiO_2 in wt % versus trace elements in ppm for the Garabal Hill pluton.

d) Zr shows an initial increase to approximately 62% SiO_2 and then decreases where it behaves as a compatible element presumably in forming zircon. It is therefore depleted in the later melts during fractionation. Hf shows a similar trend to Zr. Nb also shows a trend similar to both Zr and Hf. Shannon and Prewitt (1969) and Pearce and Norry (1979) suggested that the ionic charge of Nb^{3+} is very close to Hf^{4+} and may enter zircon mineral which itself tends to increase during fractionation. Mason and Moore (1982) suggested that Nb^{5+} will remain in solution and enriched in the residual liquid of magmatic crystallisation.

e) Th and Pb show rather scattered trends but generally increase towards the granodiorite.

f) La increases towards the granodiorite. Ce increases in the diorites and then decreases in the granodiorites probably as it replaces Ca^{2+} in apatite which is more abundant in diorites. Y increases towards the diorites and decreases rapidly in the granodiorites as it is strongly partitioned into hornblende in equilibrium with an acid melt (Arth and Barker, 1976).

Ni - Mg and Cr - Mg

There is good positive correlation between Ni, Cr and Mg as those elements will prefer to enter olivine and pyroxene respectively and are thus commonly depleted during fractionation (Fig. 5.2a, b).

Ba - K and Rb - K

Both Rb and Ba have an affinity towards K so they will tend to be enriched in late K-rich minerals (eg alkali feldspar) but removal of biotite may have an opposing effect. (Fig. 5.2c, d).

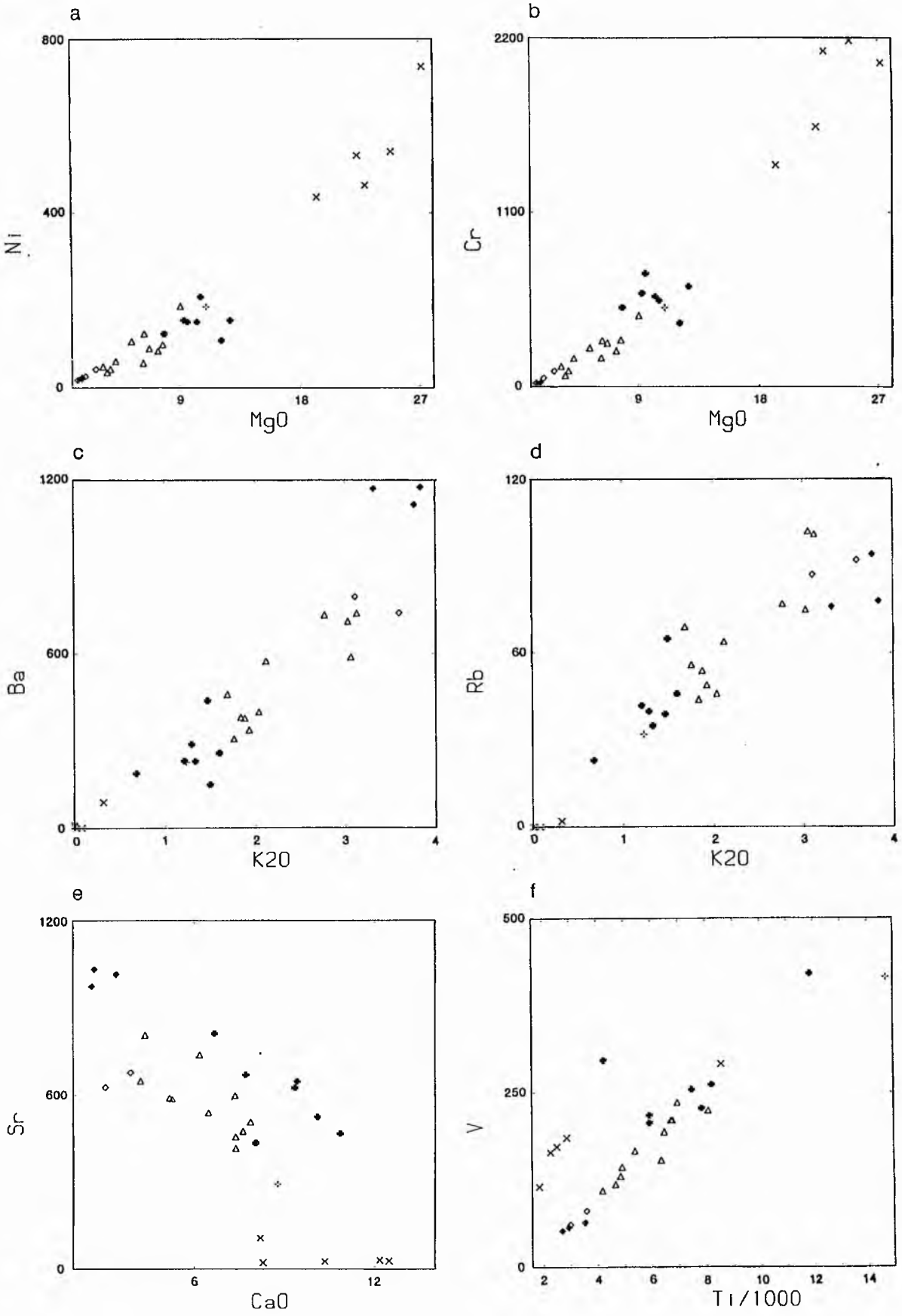

Fig 5.2$_{a-f}$ Variation diagrams for some major oxides and trace elements in the Garabal Hill pluton.

Sr -Ca

There is an inverse correlation between Sr and Ca which suggests that plagioclase fractionation alone is not controlling the trend (Fig. 5.2e).

Ti/1000 - V

This diagram (Fig. 5.2f) is particularly sensitive to variations in oxygen fugacity during both partial melting and fractional crystallisation, which influence the behaviour of ilmenite and magnetite (Shervais, 1982). At low f_{02} (10^{-11} - 10^{-12} bars) V exists primarily as V^{3+} and has similar behaviour to Fe^{3+} and Cr^{3+} substituting those cations in spinel and pyroxene. At high f_{02} ($10^{-4.5}$ bars), V exists primarily as V^{5+} and behaves like a HFS cation (K_D less than 0.1) for most common minerals. At low fO_2 values the Ti/V ratio increases rapidly with fractionation of pyroxene and magnetite. At high fO_2 V is partitioned into the melt and the Ti/V ratio falls enhanced by the crystallisation of sphene (Shervais, 1982). At Garabal Hill, the ultramafic rocks separate into a distinct field of low Ti and higher V. This is a feature of cumulates (their very low abundance of incompatible elements).

K/Rb - SiO_2

The K/Rb ratios increase with increasing SiO2 from very low in the ultrabasic rocks to 210 in the most evolved rock types (Fig. 5.2g) with a gradual increase from about 100 in basic rocks.

Rb/Sr SiO_2

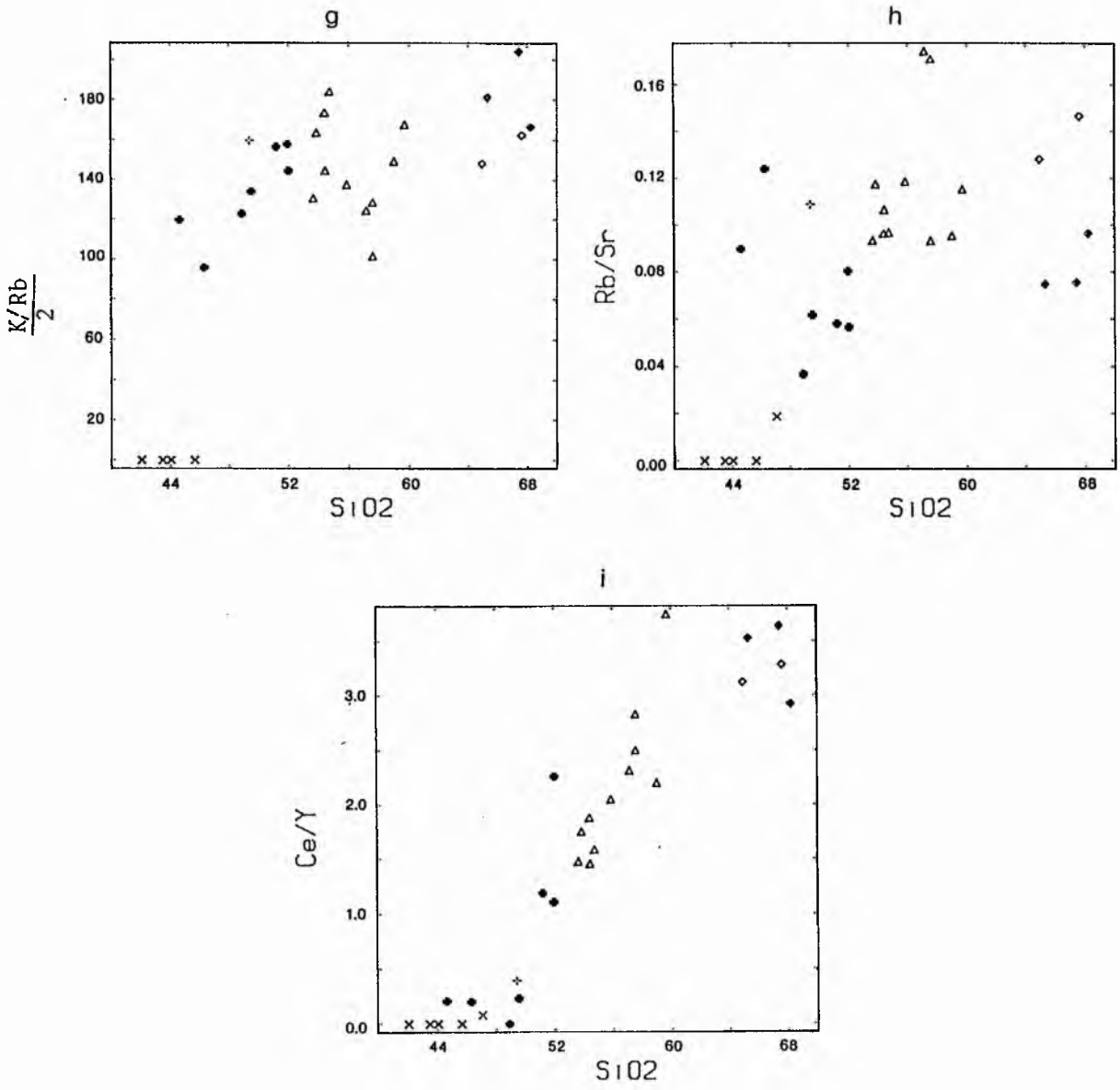

Fig 5.2$_{g-i}$ Plots of SiO_2 versus some trace element ratios for the Garabal Hill pluton.

The Rb/Sr ratios increase rapidly towards the hornblende biotite diorite (0.16) and then decrease towards the medium and porphyritic granodiorite about 0.1, (Fig. 5.2h). Values as a whole are very low.

Ce/Y - SiO_2

Ce/Y shows a good positive correlation with SiO_2 (Fig. 5.2i) as Ce replaces the Ca^{2+} in apatite and Y removed probably by hornblende, so the amphibole fractionation may be a contributory cause of this trend.

Chondrite - normalised abundance plots

The chondrite normalised trace element abundances have widely been used to display rare earth element variations, and have recently been applied more widely to other trace elements (eg Thompson et al. 1984). The sequence of elements is taken from Sun et al. (1979).

The compositions used here (Fig. 5.3a) are representative samples of each rock type discussed in Chapter 3. A number of features are highlighted in this diagram, which generally shows regular changes through the evolutionary sequence, except for the peridotites which are highly depleted in most elements and for this reason these peridotites are not represented on this plot. As a whole the rocks are generally enriched in Sr, K, Rb and Th (especially the gabbro, diorites and granodiorites). Nb has a distinct anomaly typical of calc-alkaline rocks. The medium and porphyritic granodiorites are enriched in Zr which often concentrates in the later stages of fractionation. The appinitic diorites are particularly enriched in Ti relative to other rock types which is probably due to

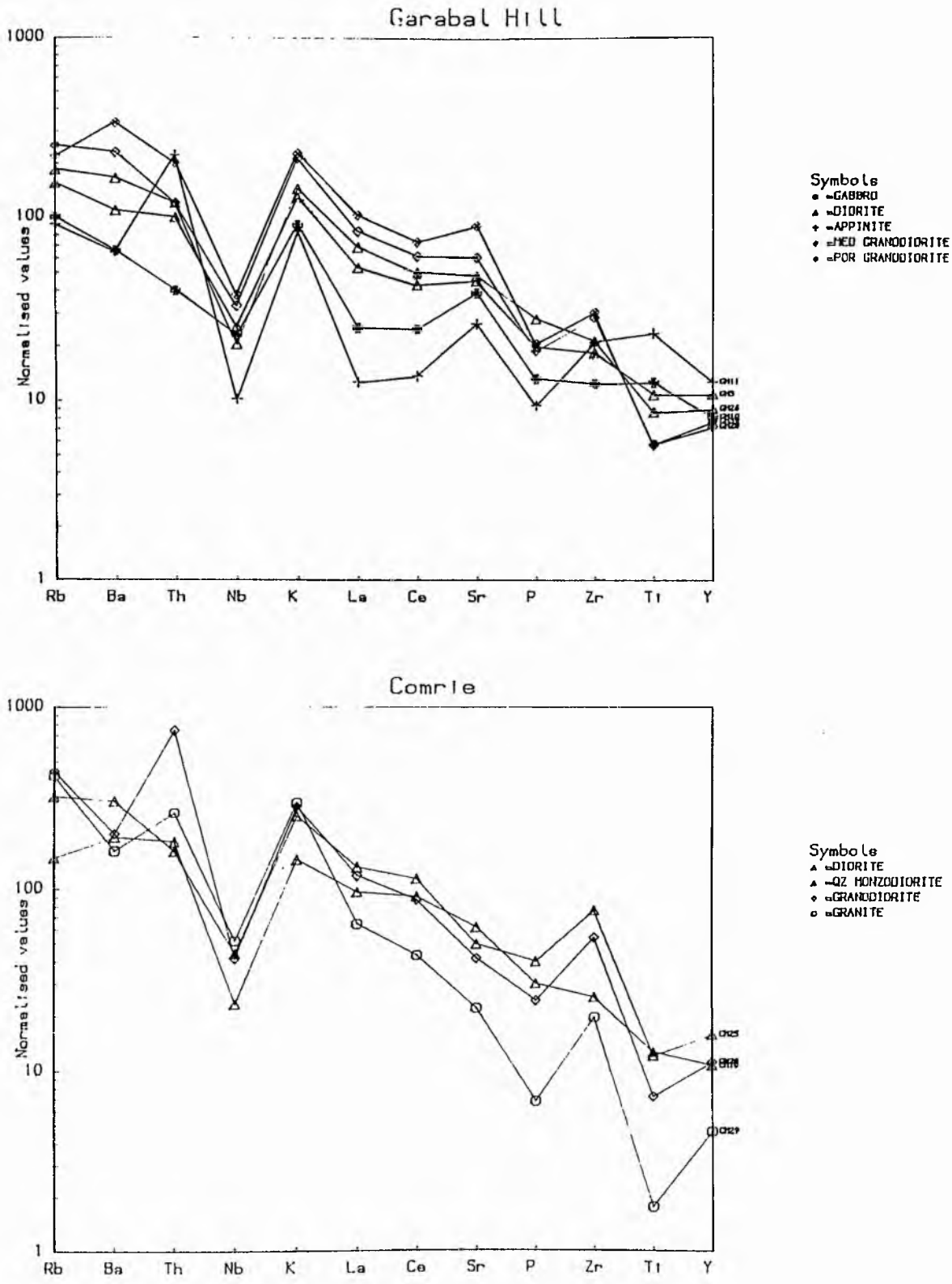

Fig 5.3a,b Chondrite - normalised plots of representative rock types in the Garabal Hill and Comrie plutons.

the presence of magnetite and ilmenite for Ti.

There is general enrichment in the incompatible elements (Sr, K, Rb and Th) which are the most readily mobilised by a fluid phase. This enrichment has been attributed to metasomatism of the mantle source region of the basalts by hydrous fluids derived from the subducted oceanic crust (Thompson et al. 1984). The relatively low abundance of the high ionic potential elements (Nb, La, Ce, P, Ti and Y) has been attributed to retaining those elements in the residuum during magma generation in a hydrous environment (Saunders et al. 1980).

Rare earth abundance

The plot of the chondrite-normalised REE abundances is shown in Fig 5.3c using the 'best unfractionated' chondrite abundances of Evensen et al. (1978). The absolute rare earth abundances for the Garabal Hill-Glen Fyne complex are presented in Table 5.1. The plot shows that concentrations of the LREE increase through the evolutionary sequence. Generally the KD's for the light rare earth elements (LREE) are less or even much less than unity for the major rock forming minerals (Hanson, 1980). Apatite and sphene have KD's much greater than unity for the LREE and may deplete the LREE in the melt during fractional crystallisation.

The La/Yb ratios vary but not systematically the highest (16) being in granodiorite and the lowest (2) being in cumulative brown amphibole gabbro.

5.2.3 Summary

Whole-rock chemical data presented in previous sections for this

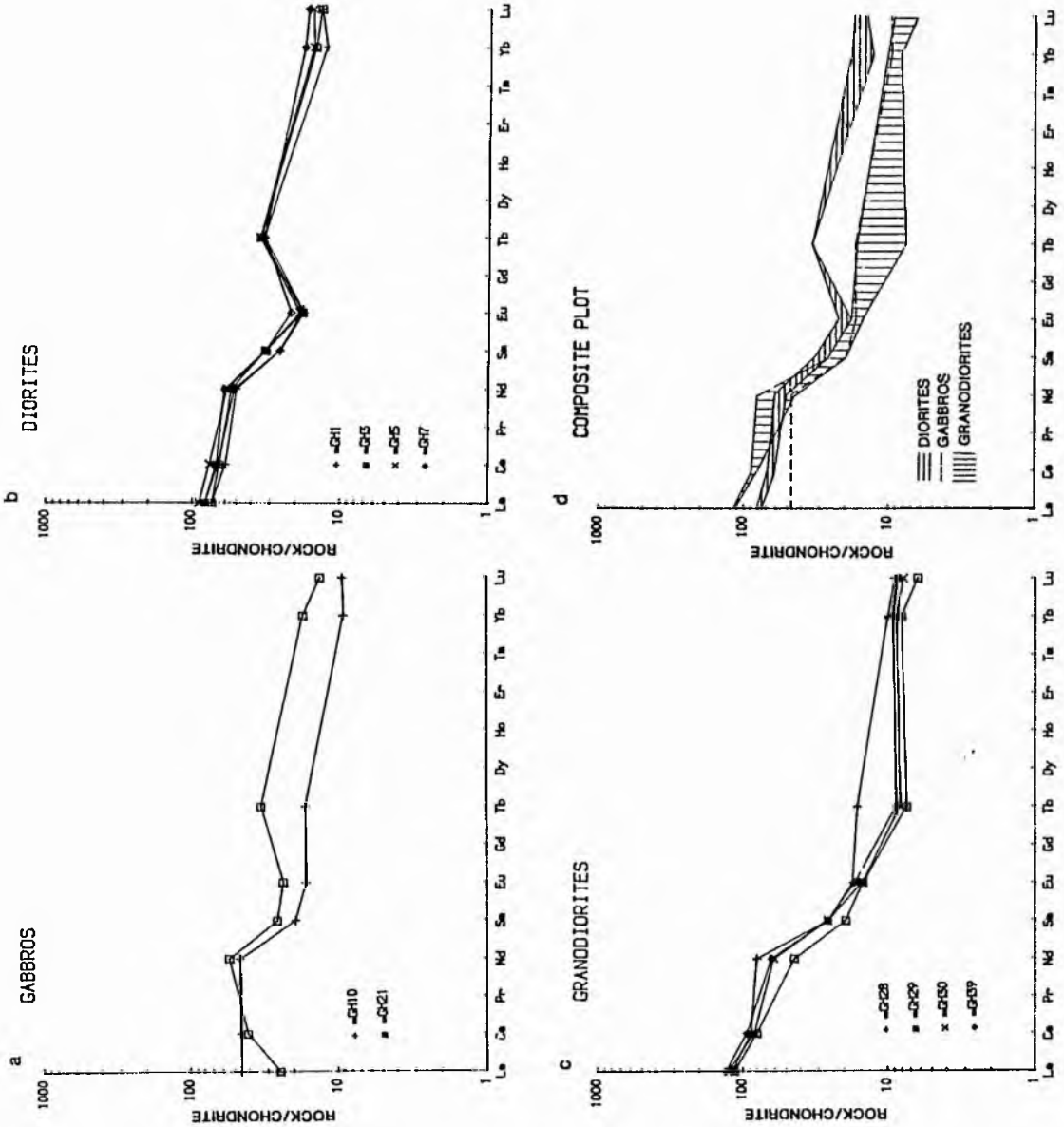

Fig 5.3c Chondrite normalised plots for 8 rare earth elements of each of the three petrological types in the Garabal Hill pluton. d Composite plot showing fields for diorites and granodiorites. Single sample of gabbro (GH10) also shown.

complex demonstrate that the majority of samples analysed here fall on smooth and regular trends on the Harker variation and AFM diagrams except for the peridotites which are more enriched in Ni, Cr relative to other rock types, best explained by a cumulative origin. Granodiorites are distinct on plots where there is a gap between 60 to 64% SiO_2 and the porphyritic granodiorites are enriched in Sr relative to the medium granodiorites falling in separate fields on Rb/Sr versus SiO_2, and Sr versus SiO_2 plots (Figs 5.2h and 5.2e).

The REE_8 increase from the basic rocks at about 68 towards the porphyritic granodiorite at about 130. The diorites and granodiorites show a smooth trend reflecting a parental magma probably of pyroxene mica diorite composition and the rock types were formed by fractional crystallisation of that magma, but some distinctive chemical features of the granodiorite suggests a probably distinctive petrogenesis. This will be modelled and discussed in Chapter 6.

5.3 Comrie

5.3.1 Major oxides

The major oxide variations are presented as a series of Harker diagrams (Fig. 5.4a-i). With increasing SiO_2, abundances of MgO, CaO, $Fe_2O_3(t)$, TiO_2, MnO and P_2O_5 decrease. K_2O increases until 64% SiO_2 then flattens off, Na_2O increases in a very scattered fashion, Al_2O_3 increases initially in the diorites and up to 58% SiO_2 then decreases towards the granites (except for sample CM22 which contains 10.12% Al_2O_3 and is a rather altered coarse grained pyroxene biotite diorite which was omitted from this plot).

The variation trend is a typically calc-alkaline trend on the

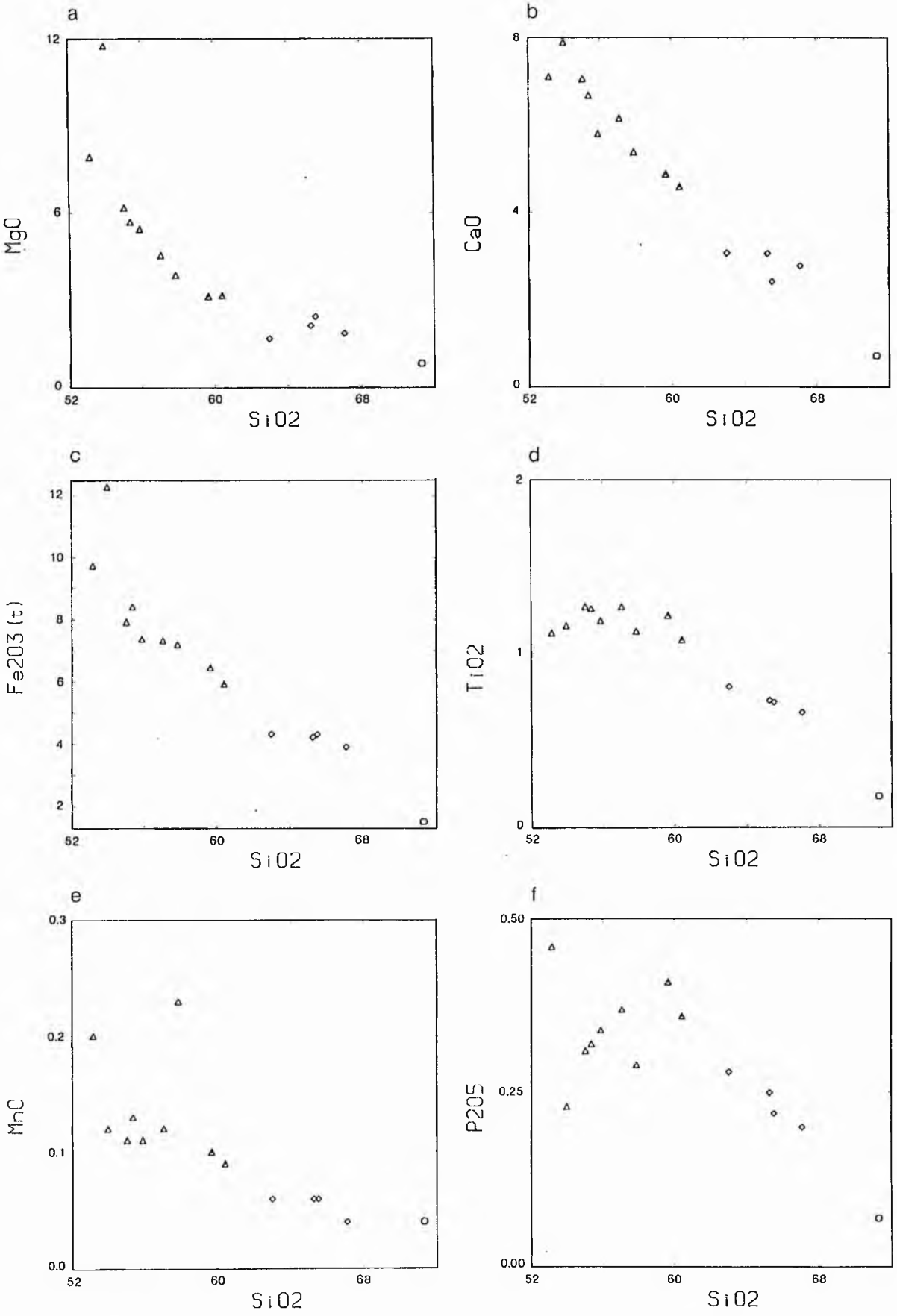

Figs 5.4$_{a-f}$ Harker variation diagrams of major oxides for the Comrie pluton.

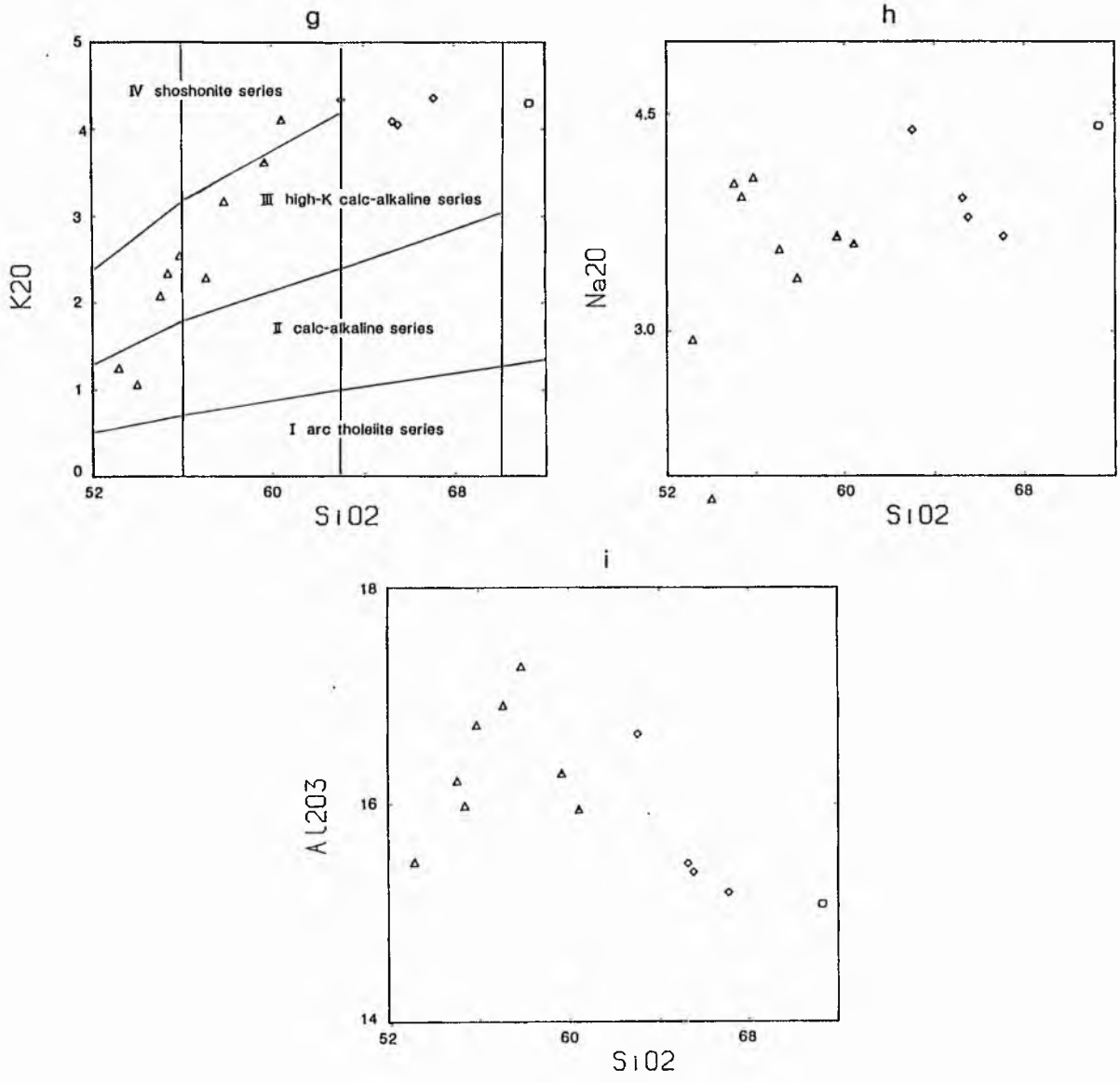

Figs 5.4$_{g-i}$ Harker variation diagrams of major oxides in the Comrie pluton. Plot 5.4$_g$ includes fields of Peccerillo & Taylor (1976).

AFM diagram (Fig. 5.4j) and a plot of K_2O versus SiO_2 indicates that this complex is calc-alkaline to high-K calc-alkaline within the scheme of Peccerillo and Taylor (1976) (Fig. 5.4g). The rocks of this complex are typically I-type in terms of classification of Chappell and White (1974).

5.3.2 Trace elements

Plots for various trace elements versus SiO_2 (Fig. 5.4 k-z) shows that:

a) Cr and Ni show depletion towards the granites except for sample CM22 which has anomalous abundances of Cr and Ni relative to other rock types. Sample CM23 contains the highest amount of Cr and this is related to its high modal proportion of clinopyroxene. V shows general depletion towards the granite. Again, sample CM23 is anomalous and contains the highest V content due to very high modal magnetite.

b) Rb increases with SiO_2 whereas Ba increases towards the granodiorites and then decreases towards the granite. Samples CM20 and CM23 contain anomalously low Ba concentrations relative to other rocks, whereas CM25 is anomalously high correlating with its high modal abundances of biotite and alkali feldspar (Table 3.2, Chapter 3). Sr shows depletion with increasing SiO_2 probably due in part to plagioclase fractionation.

c) Zn decreases with increasing SiO_2, its high concentration in the diorites (up to 115 ppm) is related principally to the high modal proportion of biotite and amphibole, substituting for Fe^{2+} in those minerals. Cu shows a very scattered trend with SiO_2.

d) Zr increases to a maximum in the quartz monzodiorites (60-62% SiO_2)

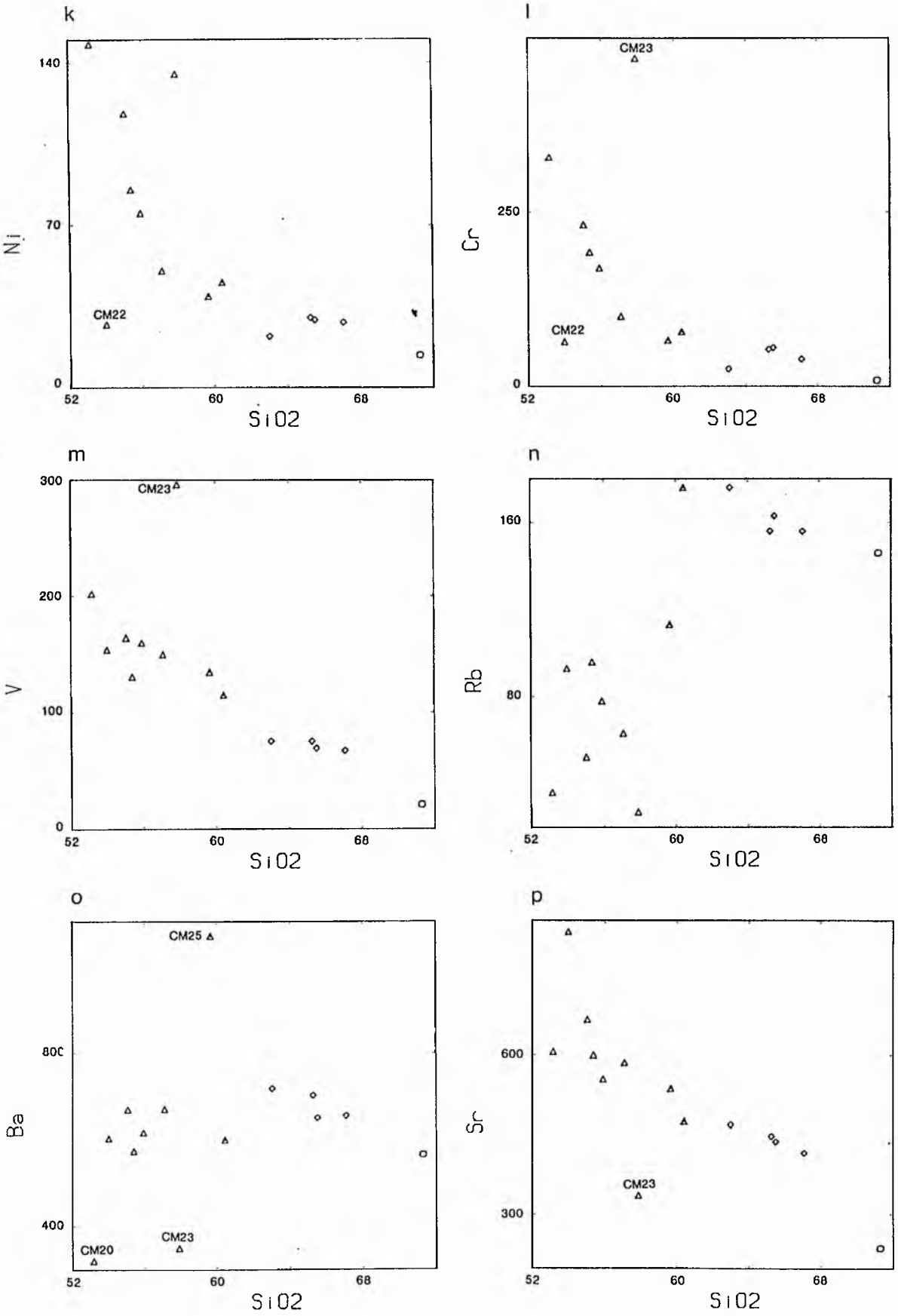

Figs 5.4$_{k-p}$ Harker variation diagrams of SiO_2 wt % versus trace elements in ppm for the Comrie pluton.

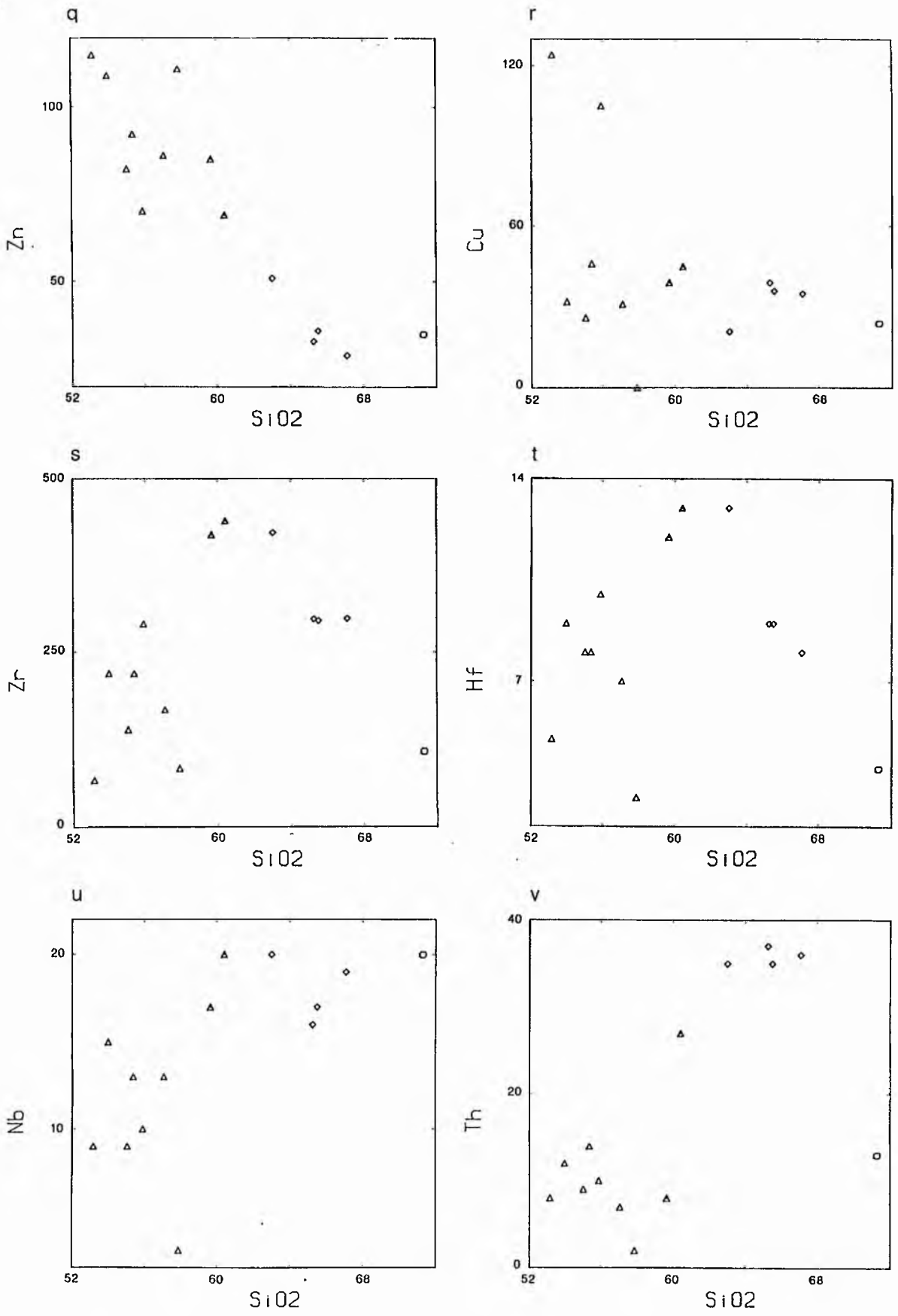

Figs 5.4$_{q-u}$ Harker plots of SiO_2 wt % versus trace elements in ppm for the Comrie pluton.

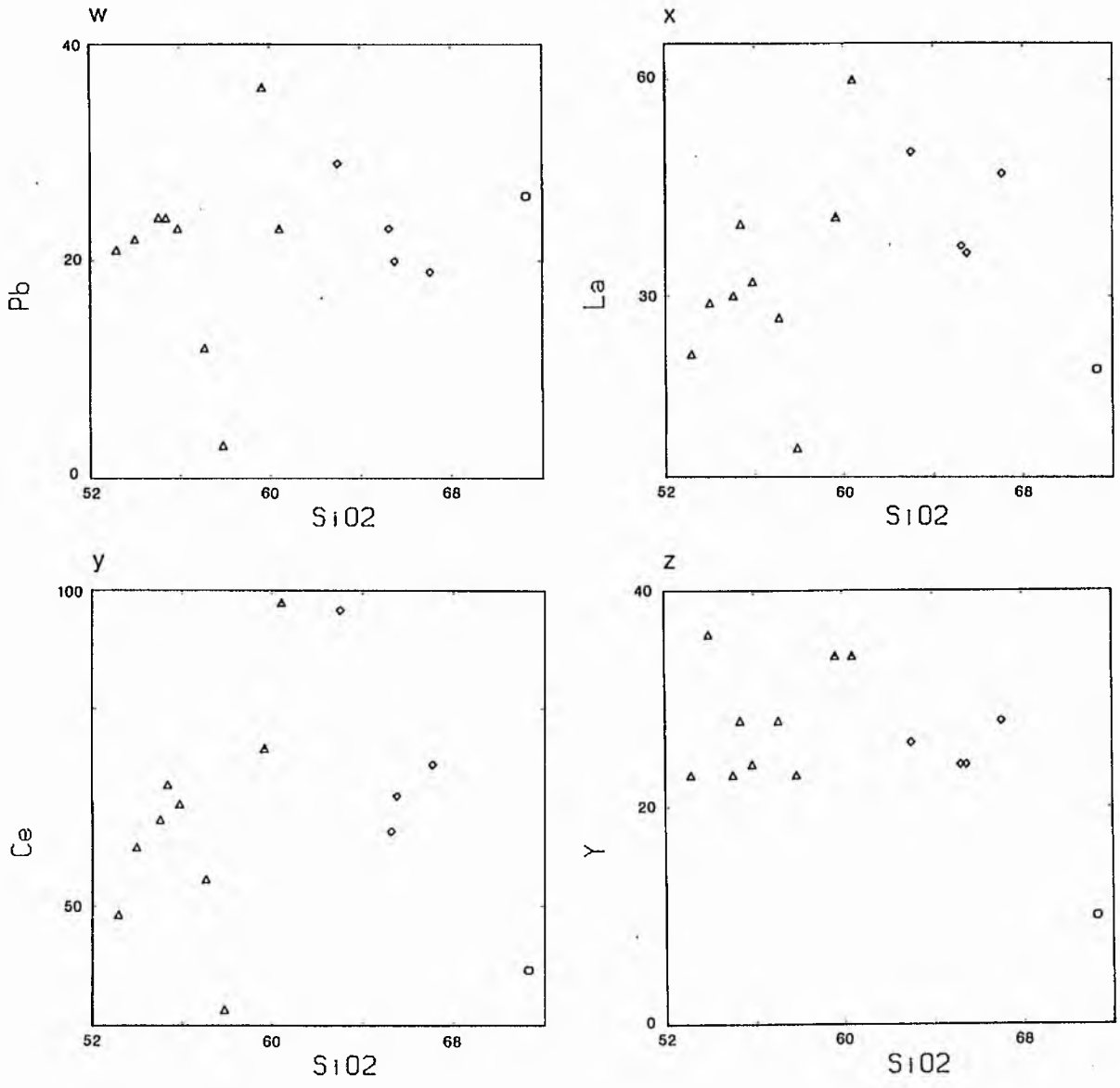

Figs 5.4$_{w-z}$ Harker variation diagrams of SiO_2 wt % versus trace elements in ppm for the Comrie pluton.

and then decreases towards the granites. This probably reflects the point at which zircon becomes a stable phase. Hf shows a very similar trend to Zr and probably reflects camouflaged behaviour in zirconium minerals (Mason and Moore, 1982). Nb increases with increasing SiO_2 in the granites which may be due to its occurrence as Nb^{5+} and consequently becomes enriched in residual liquids (Mason and Moore 1982).

e) Th increases towards the granodiorites but the one granite sample is low in Th. Pb shows a very scattered trend with SiO_2.

f) La and Ce show similar trends where they increase towards the quartz monzodiorites and then become depleted through the granodiorite and granite. Y (which resembles the behaviour of the HREE) increases towards the quartz monzodiorites and decreases towards the granodiorites and granite.

Ni - Mg and Cr - Mg

Cr and Ni show good linearity with Mg (except for anomalous samples CM22 and CM23), though Ni curves slightly towards the granite and is enriched at high Mg. These smooth trends suggest a fractional crystallisation control on the evolutionary sequence (Fig. 5.5a, b).

Rb - K

There is fairly good linearity between Rb and K except for sample CM22 which is a rather altered coarse grained diorite (Fig. 5.5c).

Ba - K

Ba content is at its highest in the quartz monzodiorite and

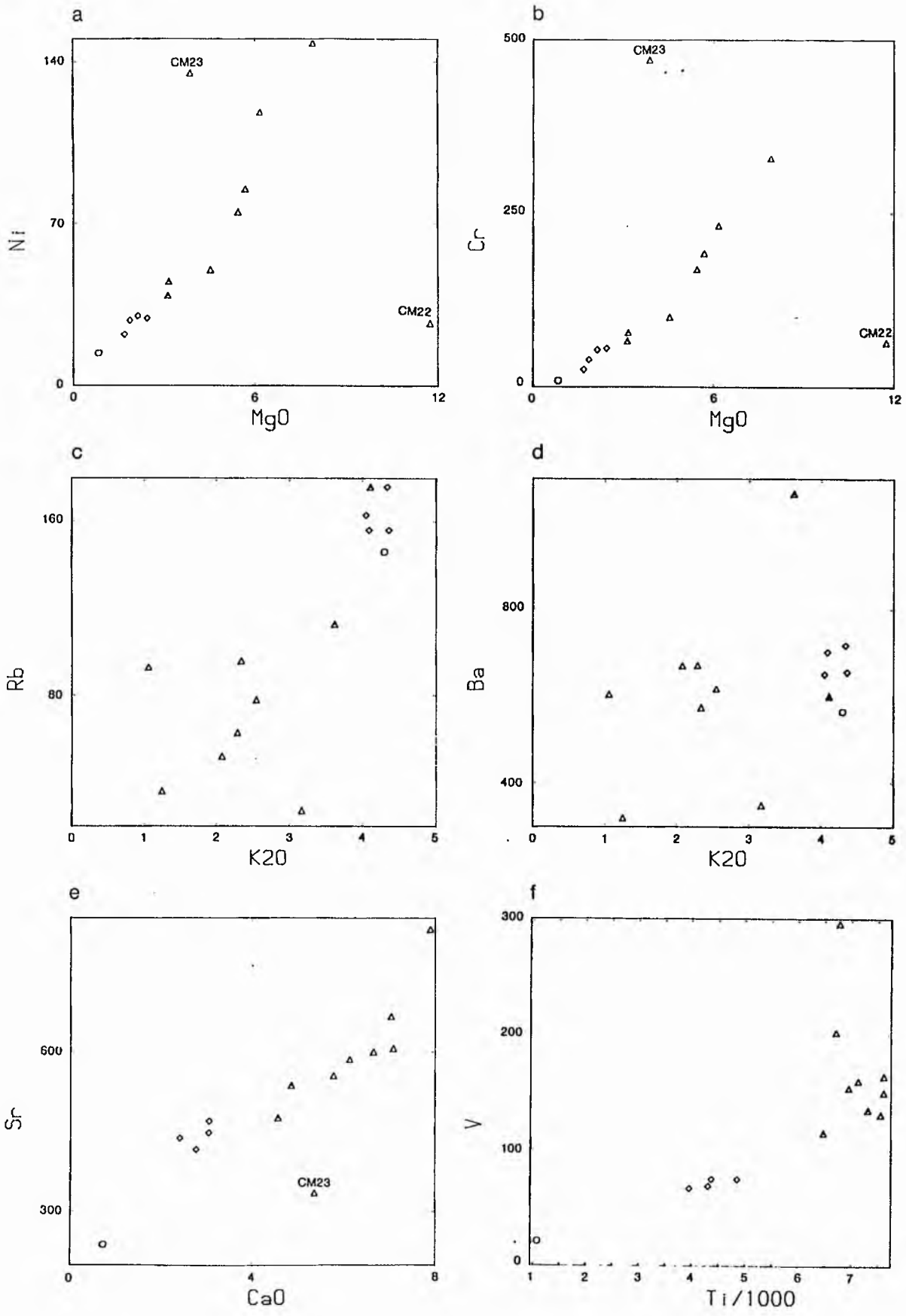

Figs 5.5$_{a-f}$ Variation diagrams relating trace elements to major oxides for the Comrie pluton

decrease towards the granodiorites and granite. This may reflect the enrichment of Ba in biotite (Fig. 5.5d).

Sr - Ca

The good linearity between Sr and Ca may reflect a plagioclase control on fractional crystallisation. One sample (CM23) has exceptionally low Sr for its Ca content because it is contaminated with small amphibolite xenoliths (Fig. 5.5e).

Ti/1000 - V plot

The fact that Ti/V ratio (Fig. 5.5f) decreases gradually with fractionation of magnetite (Shervais, 1982) except for two diorite samples (CM23 and CM20) which may be due to their pyroxene enrichment. The idea is supported by the plots of Ti and V versus SiO_2 (Figs 5.4d and 5.4m).

K/Rb - SiO_2

The K/Rb ratios decrease from 170 in the diorites to less than 90 in the granodiorites and increase to 120 in the granite (Fig. 5.5g).

Rb/Sr - SiO_2

Rb/Sr ratios increase gradually (with some scatter) from the diorite to a maximum of 0.6 in the granite (Fig. 5.5h). As a whole the Rb/Sr ratios are low even in the most evolved rocks.

Chondrite ratio plots

The trace element compositions used here are of representative

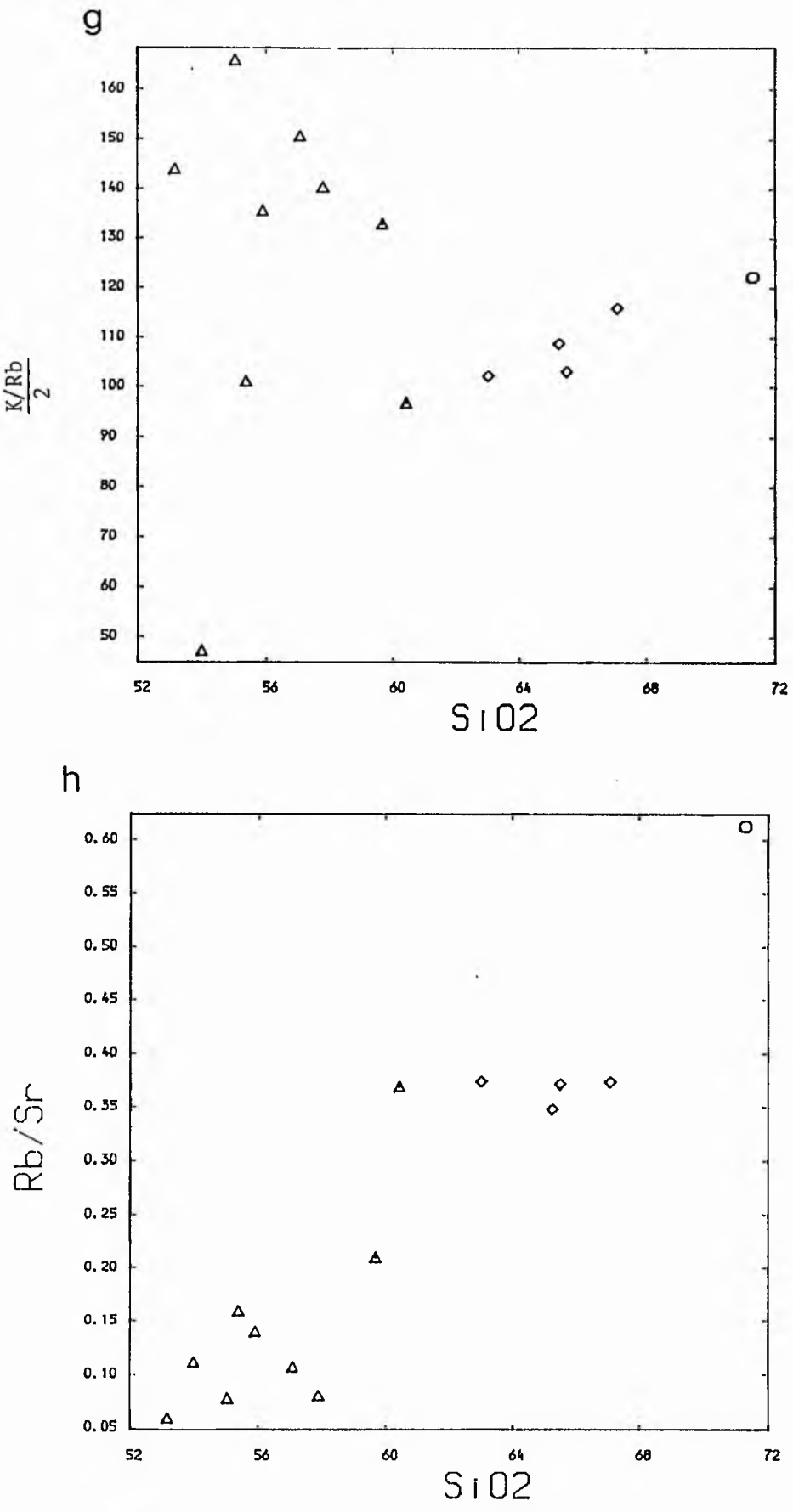

Figs 5.5_{g-h} Plots of SiO_2 versus K/Rb and Rb/Sr ratios for the Comrie pluton.

samples of each rock type discussed in Chapter 3 for the Comrie complex. This plot (Fig. 5.3b) shows coherent patterns of variation through from diorites to quartz monzodiorites. The granodiorite shows marked increase in Th and Rb and slight depletions in Sr, P and Ti. The granite is very depleted in REE, Sr, P, Zr, Ti and Y though follows a roughly parallel trend indicating that the scale of depletion is approximately constant.

5.3.3 Summary

This complex is another high-K calc-alkaline pluton. The variation diagrams indicate that a process of fractional crystallisation from a dioritic parental magma could account for the observed variations in rock type. Petrogenetic modelling of this hypothesis is presented in Chapter 6.

5.4 Glen Doll

5.4.1 Major oxides

Major oxide variation is presented here as a series of Harker diagrams (Fig. 5.6a-i). With increasing SiO_2 the abundances of MgO, CaO, $Fe_2O_3(t)$, MnO, TiO_2 and P_2O_5 decrease but with considerable scatter, whereas K_2O and Na_2O generally increase, though again with considerable scatter. Al_2O_3 remains almost constant with much scatter over the SiO_2 range, except for two very depleted pyroxenites. Scatter is most prominent at low SiO_2 which may in part be explained by cumulate effects. There is an SiO_2 gap between 60 and 65%.

On an AFM diagram (Fig. 5.6j), the variation trend is typically calc-alkaline but with rather large Fe enrichment. A plot of K_2O

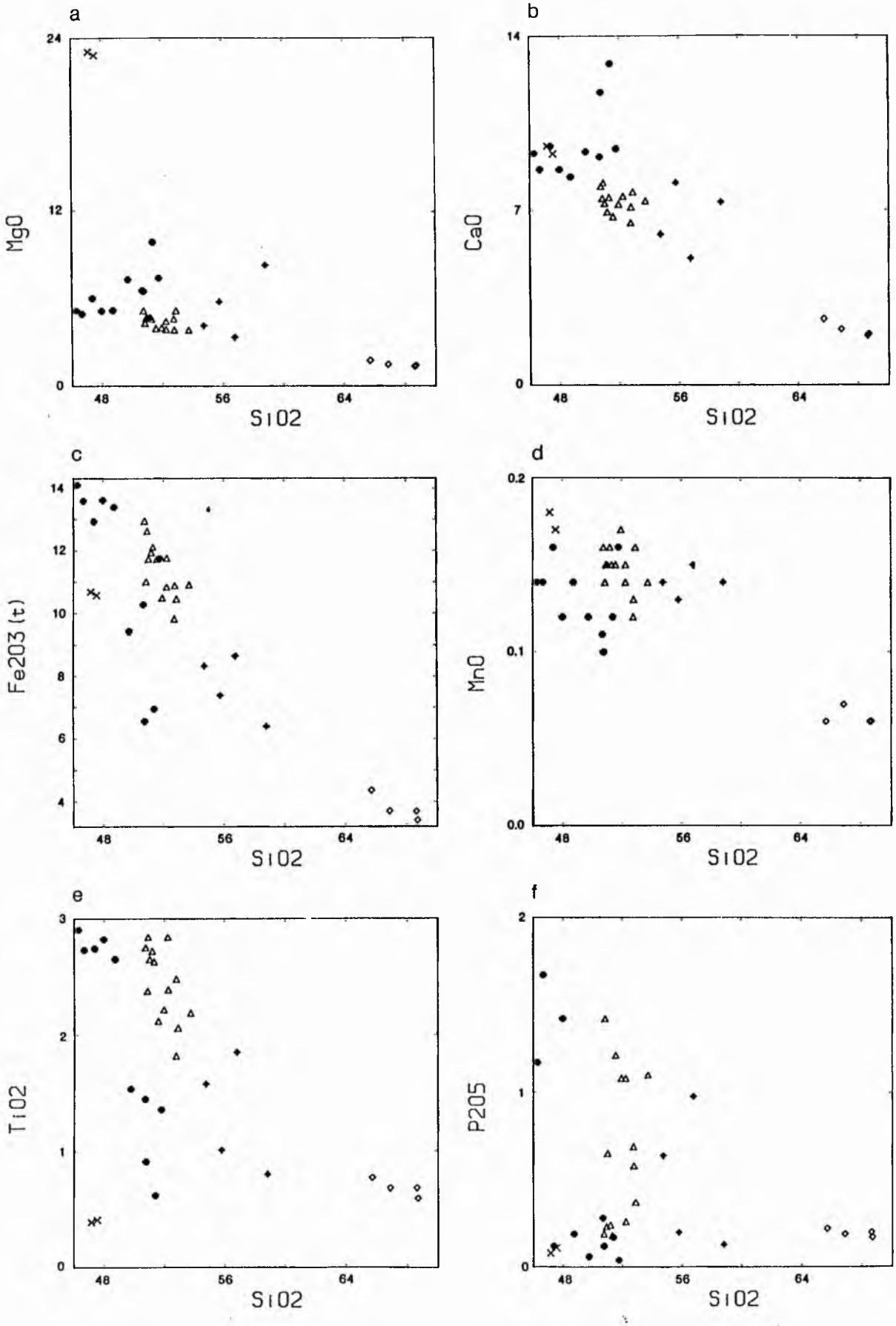

Fig 5.6$_{a-f}$ Harker variation diagrams of major oxides for the Glen Doll pluton.

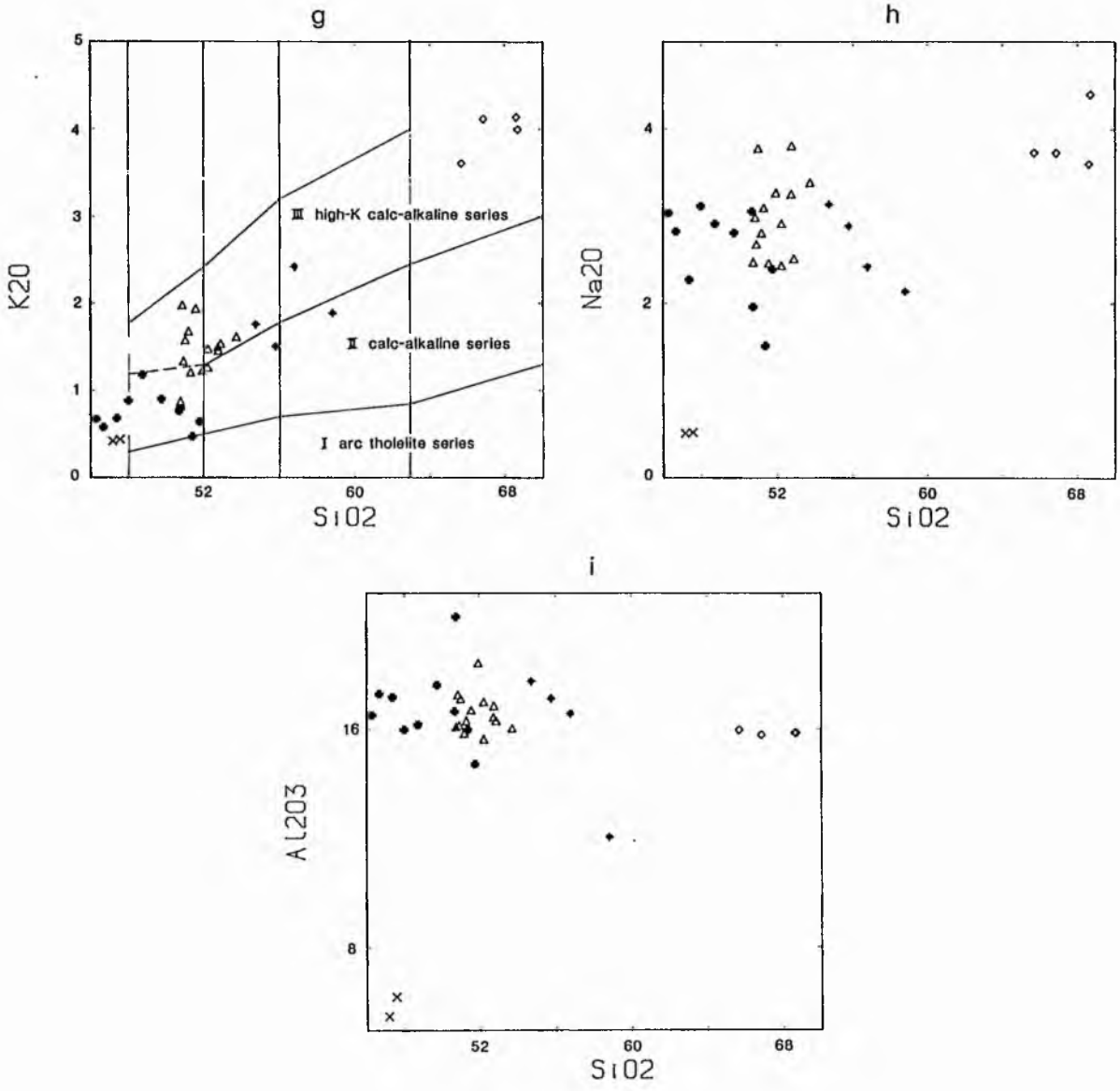

Figs 5.6$_{g-i}$ Harker variation diagrams of major oxides in the Glen Doll pluton. Plot 5.6$_g$ includes fields of Peccerillo & Taylor (1976).

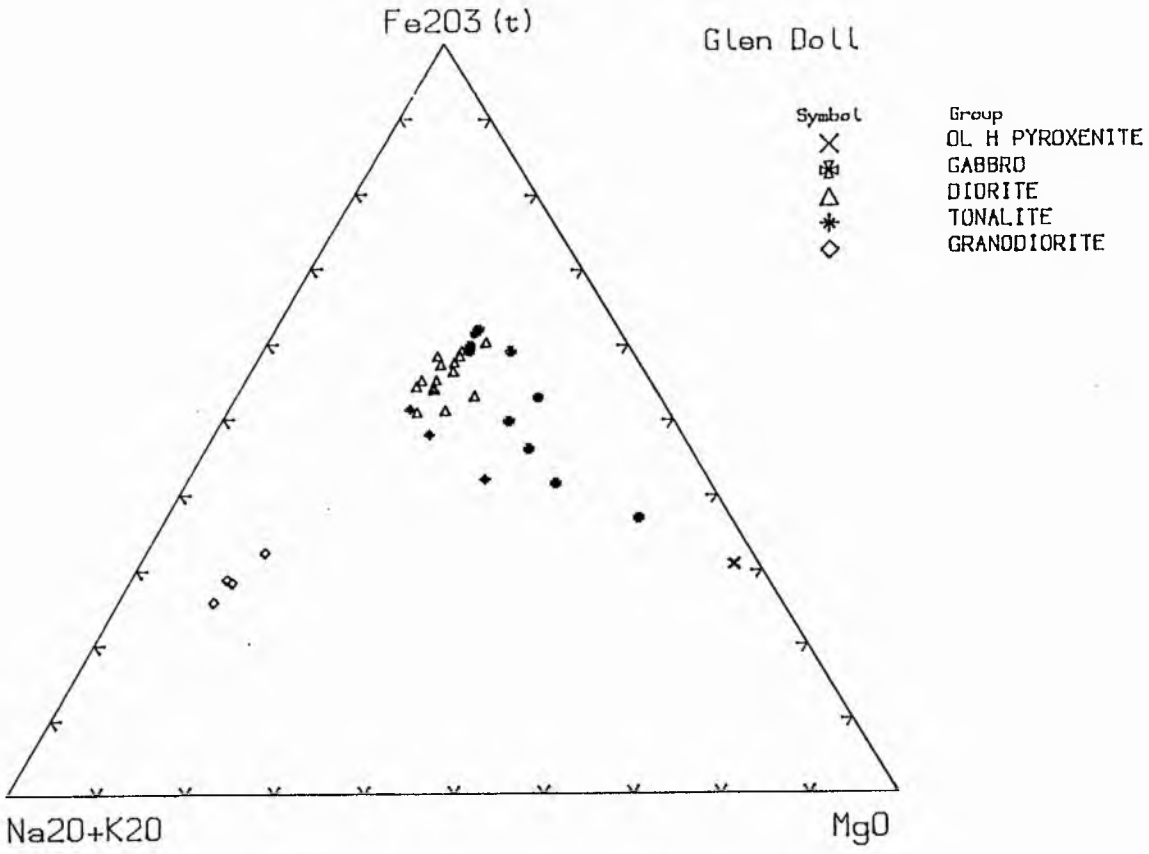

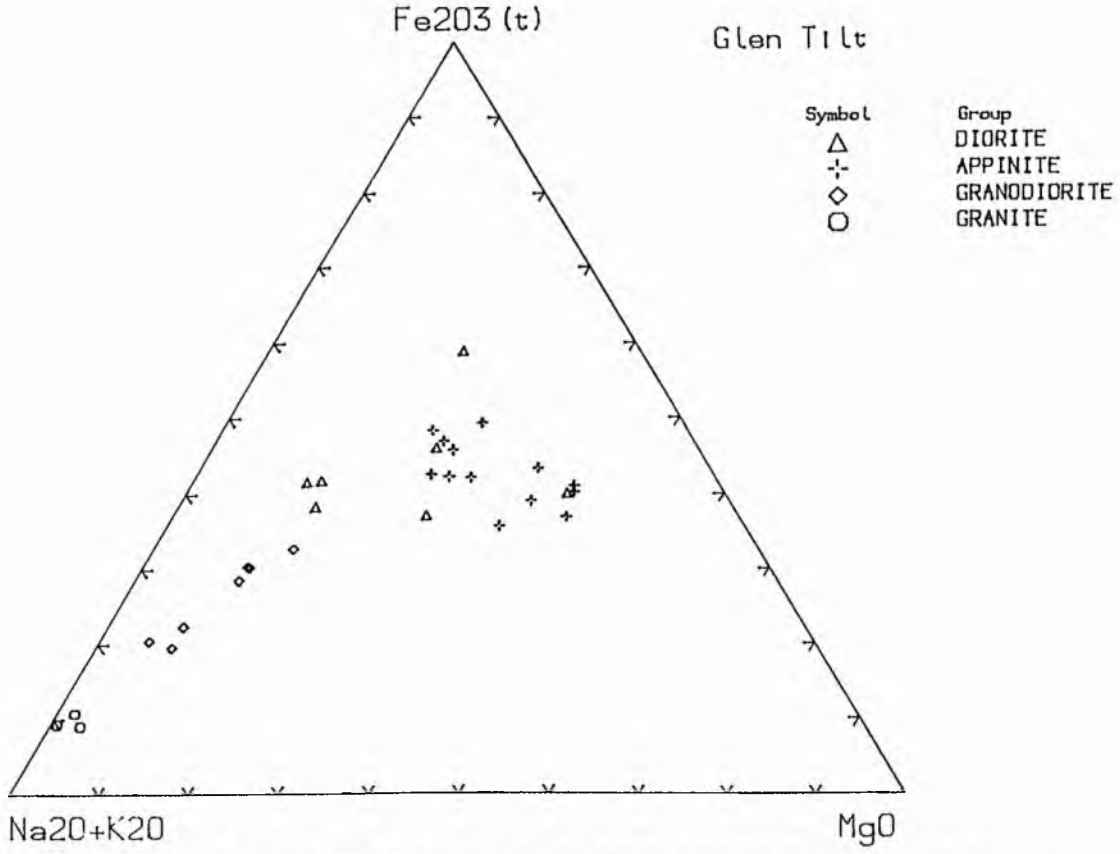

Fig 5.6$_j$ and 5.9$_j$ AFM plots of Glen Doll and Glen Tilt plutons showing Fe-enriched calc-alkaline trends particularly for Glen Doll.

versus SiO_2 (Fig. 5.6g) indicates a calc-alkaline trend for more basic rocks to high-K calc-alkaline series for the more evolved types (Peccerillo and Taylor, 1976). The rocks fit the I-type category in terms of mineralogy and geochemistry (Chappell and White, 1974).

5.4.2 Trace elements

Plots for various trace elements versus SiO_2 (Fig. 5.6 k-z) generally shows that:

a) Cr and Ni are very much enriched in the ultrabasic rocks (pyroxenites), greater than 240 ppm for Ni and about 1800 ppm for Cr reflecting their pyroxene rich composition and probable cumulate origin. The other rock types show a scattered linear trend (except for GD41 and GD39 which contain 96 and 105 ppm Ni, 549 and 393 ppm Cr respectively due to abundance of clinopyroxene). V is about 130 ppm in the ultrabasic rocks, reflecting low magnetite abundance in these rocks. V is more abundant in the diorites and becomes rapidly depleted towards the granodiorites as magnetite, pyroxene and amphiboles may efficiently remove it in intermediate stages of fractionation (Wager and Mitchell, 1951; Wilkinson, 1959; and Mason and Moore, 1982).

b) Rb and Ba increase with increasing SiO_2 though in a very scattered fashion, there surprisingly is no late-stage depletion of Ba (Fig. 5.6o). Sr is highly depleted (less than 208 ppm) in the ultrabasic rocks reflecting the small amount of plagioclase though is enriched in the gabbros and diorites followed by decrease towards the granodiorites (Fig. 5.6p).

c) Zn shows general depletion towards the granodiorites. The ultrabasic rocks contain about 35 ppm probably located in the very

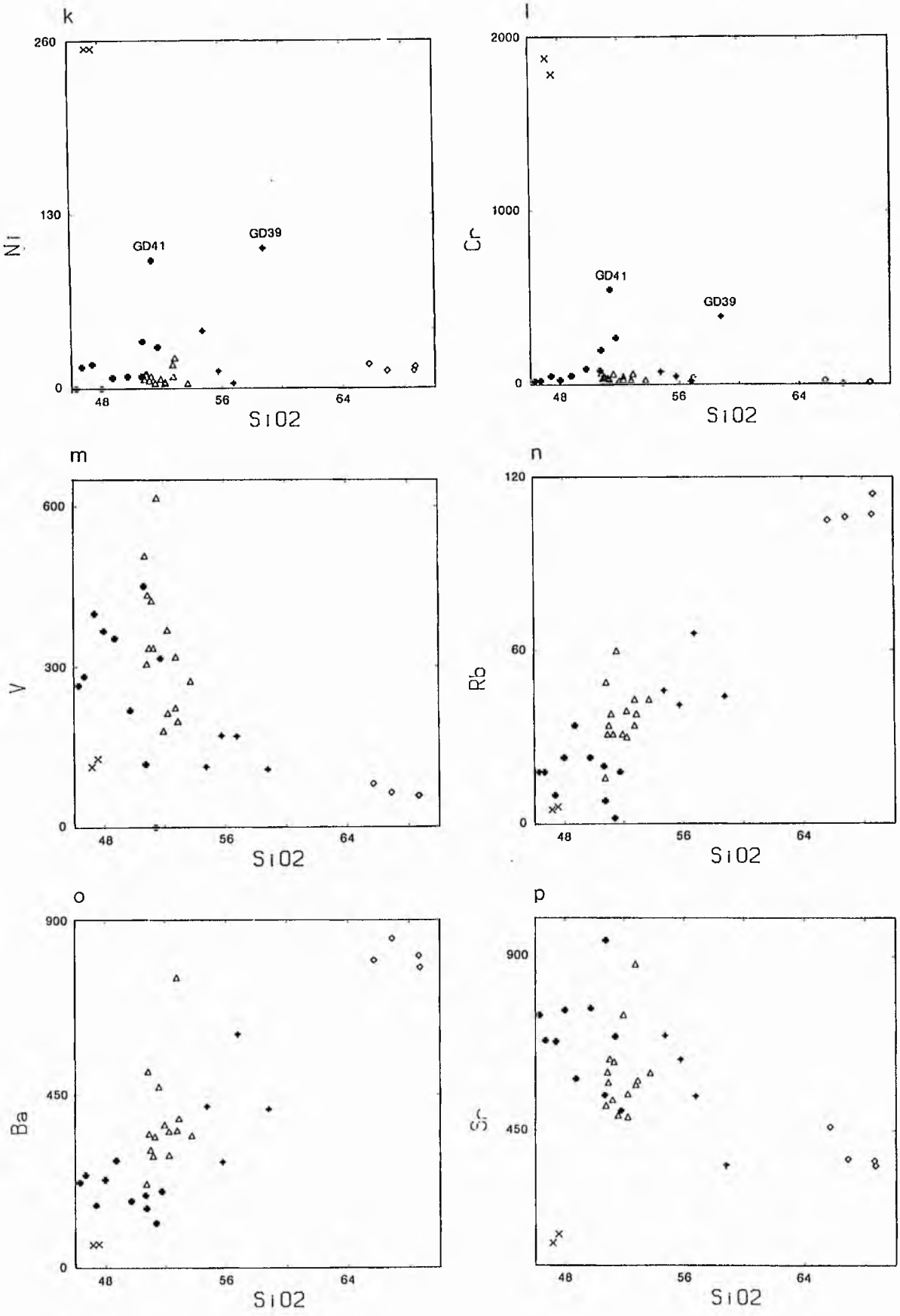

Figs 5.6$_{k-p}$ Harker variation diagrams of SiO_2 in wt % versus trace elements in ppm for the Glen Doll pluton.

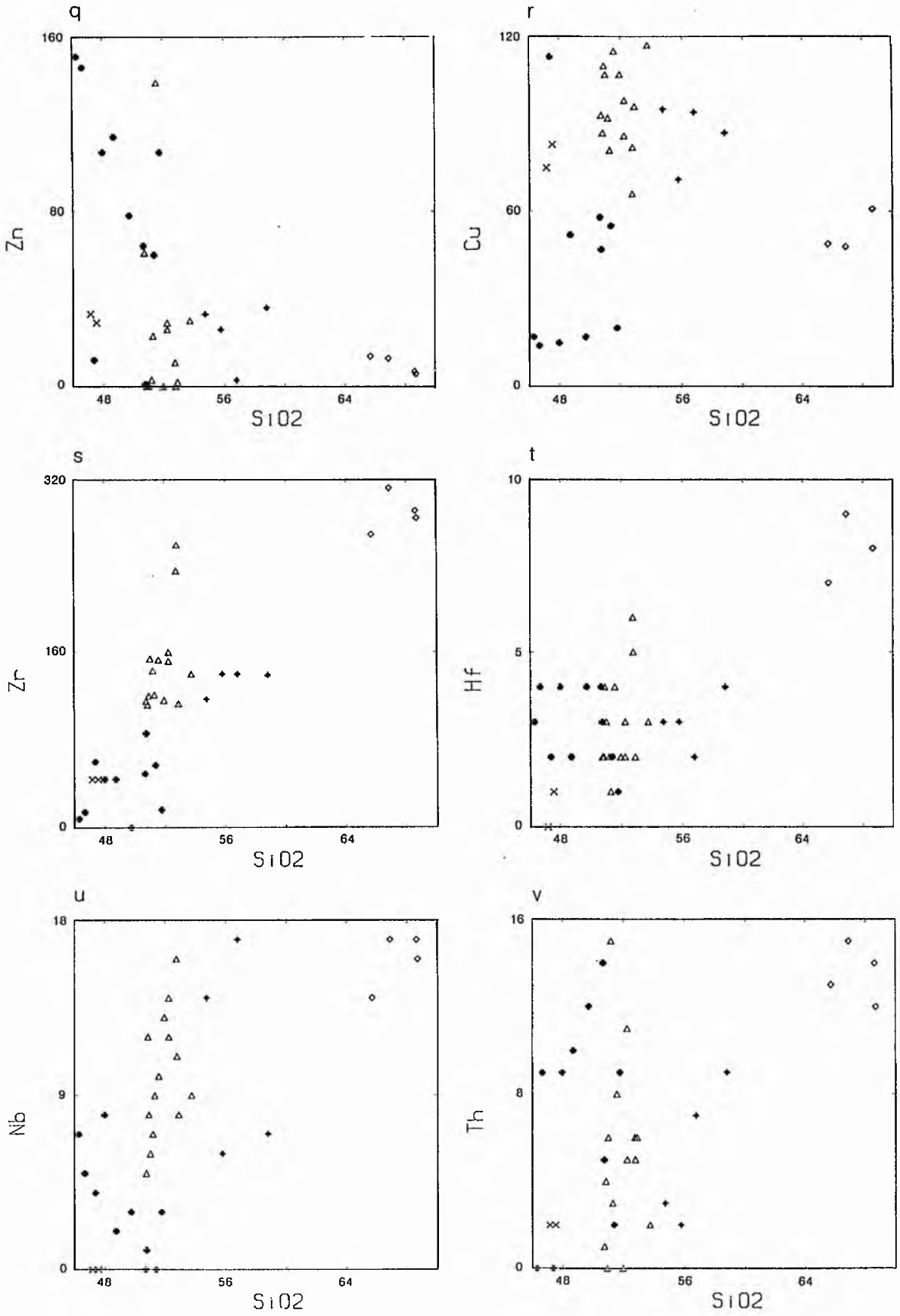

Figs 5.6$_{q-v}$ Harker variation diagrams of SiO_2 in wt % versus trace elements in ppm for the Glen Doll pluton.

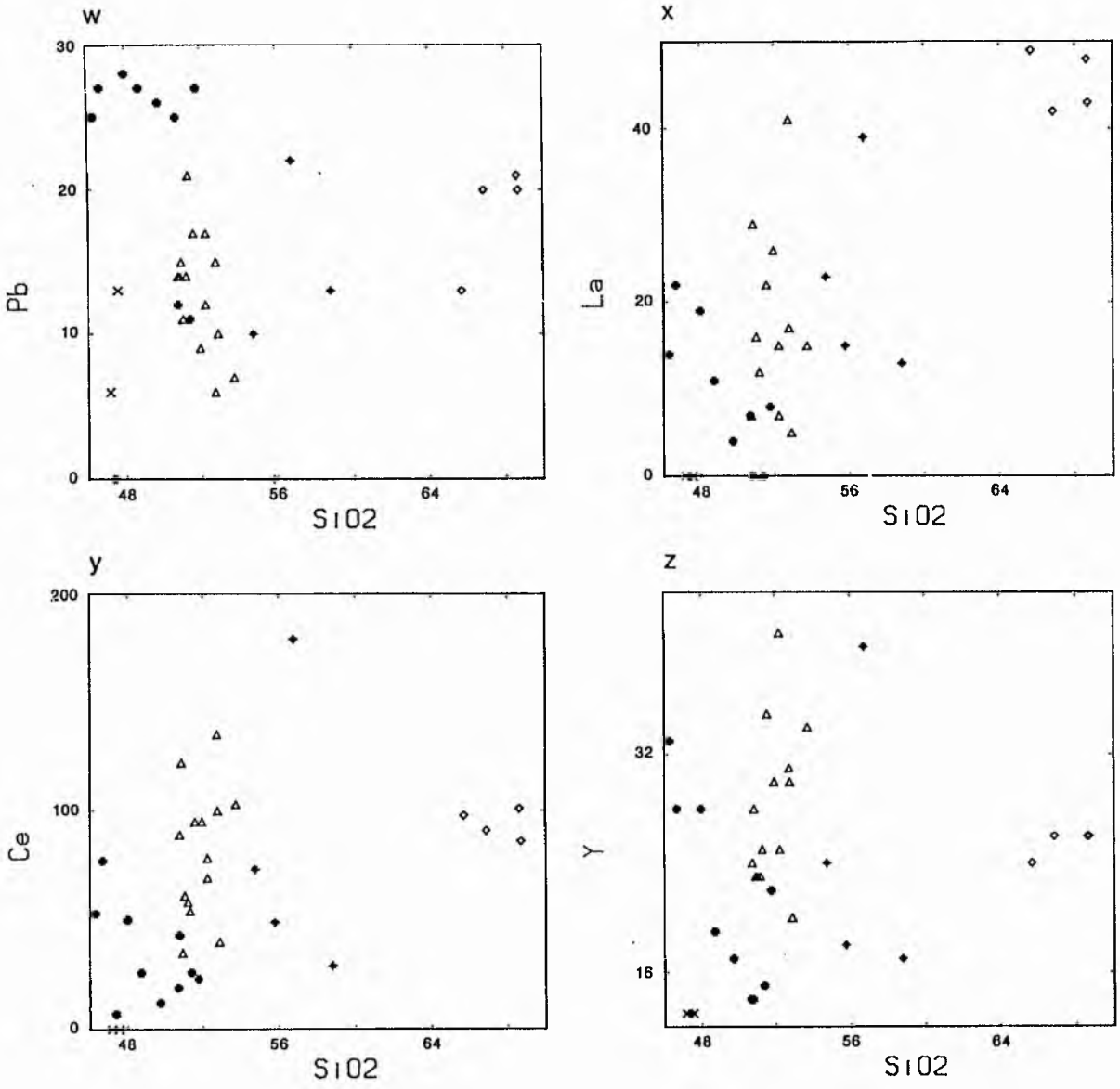

Figs 5.6$_{w-z}$ Harker variation diagrams of SiO_2 in wt % versus trace elements in ppm for the Glen Doll pluton.

small amount of primary magnetite. Cu increases up to 120 ppm in the diorites and then decrease towards the granodiorites.

b) Zr increases steadily towards the granodiorites indicating that its removal in zircon is not important in any fractionation process. Hf and Nb follow similar scattered trends.

e) Th in low silica (46 - 58% SiO_2) rocks shows no systematic variation with SiO_2, however all granodiorites (greater than 64% SiO_2) have relatively high Th (greater than 12 ppm) abundances reflecting late-stage concentration of this element. Pb shows considerable scatter.

f) La and Ce show general enrichment trends with SiO_2 though there is considerable scatter and the granodiorites are not as enriched in Ce as the earlier trend predicts suggesting a possible independent origin for the rock type. Y reflects this Ce trend towards intermediate values for the granodiorites.

Ni - Mg and Cr - Mg

Ni shows considerable scatter with Mg though with a hint of two trends, dividing tonalites and granodiorites from some other tonalites, diorites, gabbros and pyroxenites. Cr shows a trend of very rapid depletion below about 6% MgO (Fig. 5.7a, b).

Ba - K and Rb - K

Both Rb and Ba vary quite linearly with increasing K with the exception of GD43 and GD47 which contain rather more alkali feldspar than the other diorite rocks (Fig. 5.7c, d).

Sr - Ca

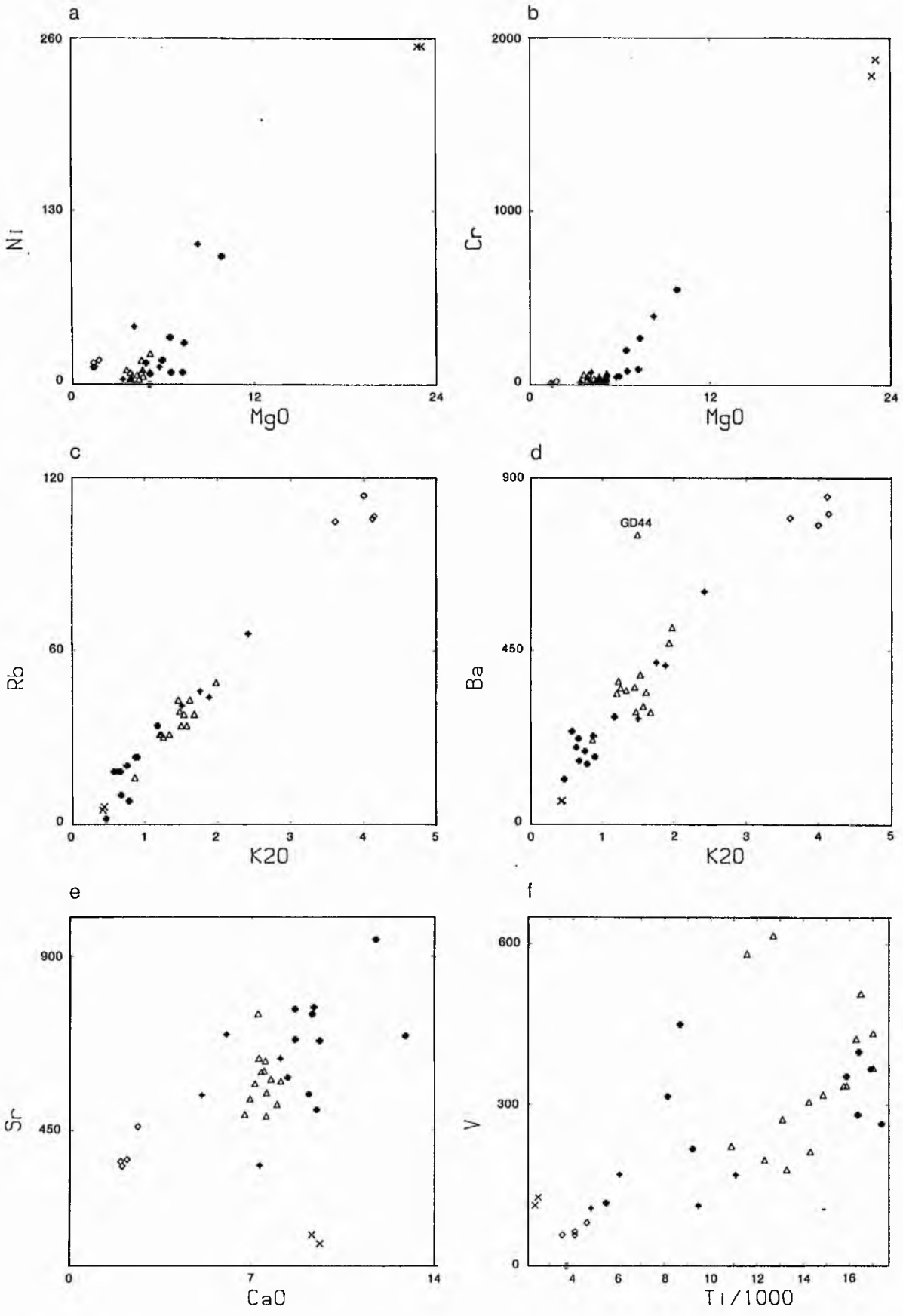

Fig 5.7$_{a-f}$ Variation diagrams for some major oxides and trace elements in the Glen Doll pluton,

This is a trend of considerably more scatter (Fig. 5.7e) than may be expected from the process of fractional crystallisation alone (cf Comrie).

Ti/1000 - V

This plot (Fig. 5.7f) suggests two main trends of evolution, namely one trend of low V values dominated by some diorites, gabbros and tonalites, and another trend reflecting a higher V group of diorites and gabbros. The two pyroxenite samples are anomalously V-rich for their TiO_2 contents. The high-V trends may reflect higher fO_2 conditions maintaining V as a less compatible element (Shervais, 1982).

K/Rb - SiO_2

K/Rb ratios are very scattered with some very high values in pyroxenites bearing phlogopite and gabbronorite.

Rb/Sr - SiO_2

Rb/Sr ratios increase generally with increasing SiO2 towards granodiorites (Fig. 5.7h) but are generally very low values.

Chondrite - normalised plots

The compositions used here (Fig. 5.8a) are of representative samples of each rock type discussed in Chapter 3 for this complex. The distribution reflects the highly scattered variation diagrams and suggests that fractional crystallisation was additionally complicated by other processes. The ultrabasic rocks and the pyroxene hornblende gabbronorites show fairly similar distributions which are depleted in

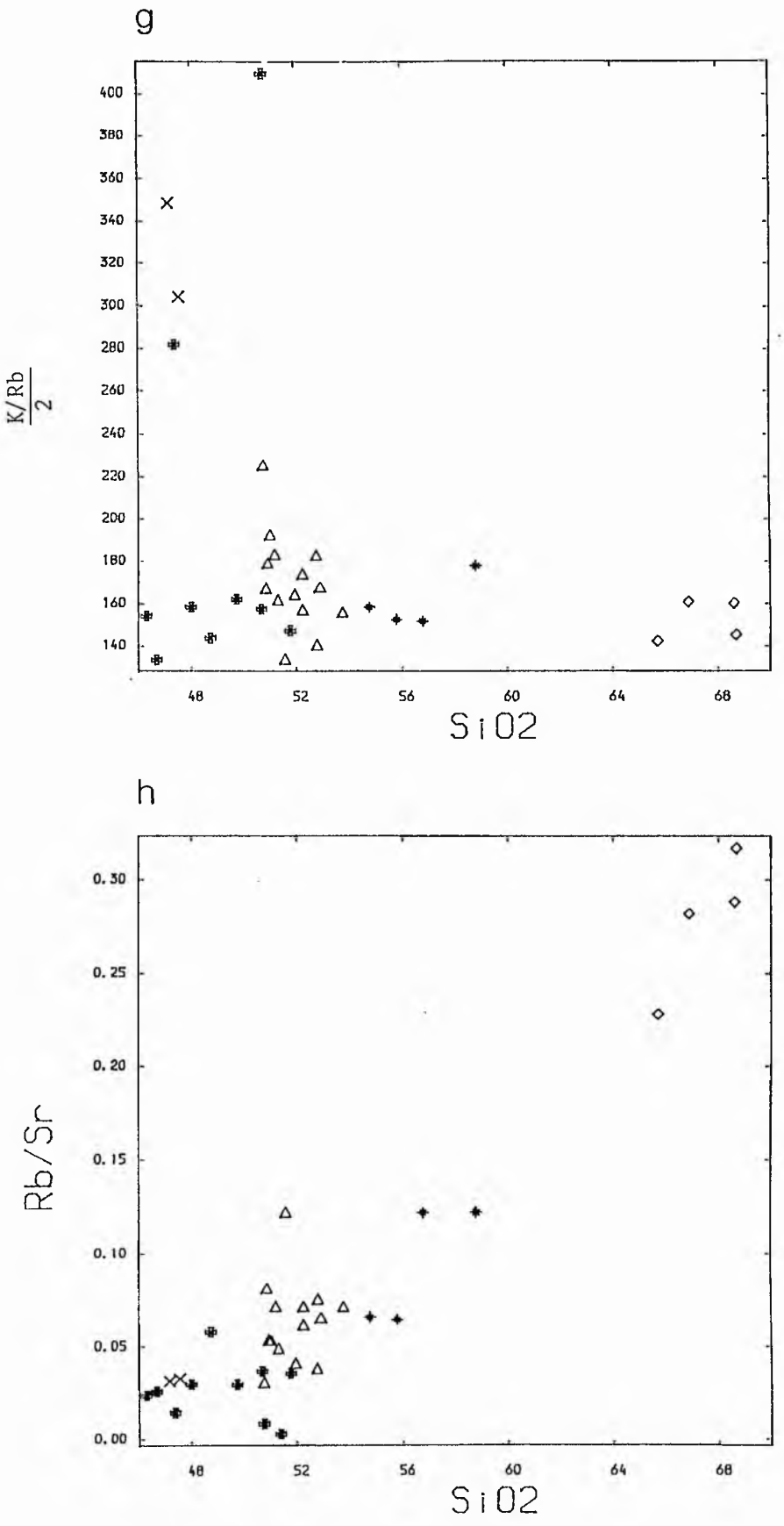

Figs 5.7 g-h Plots of SiO_2 versus K/Rb and Rb/Sr ratios for the Glen Doll pluton.

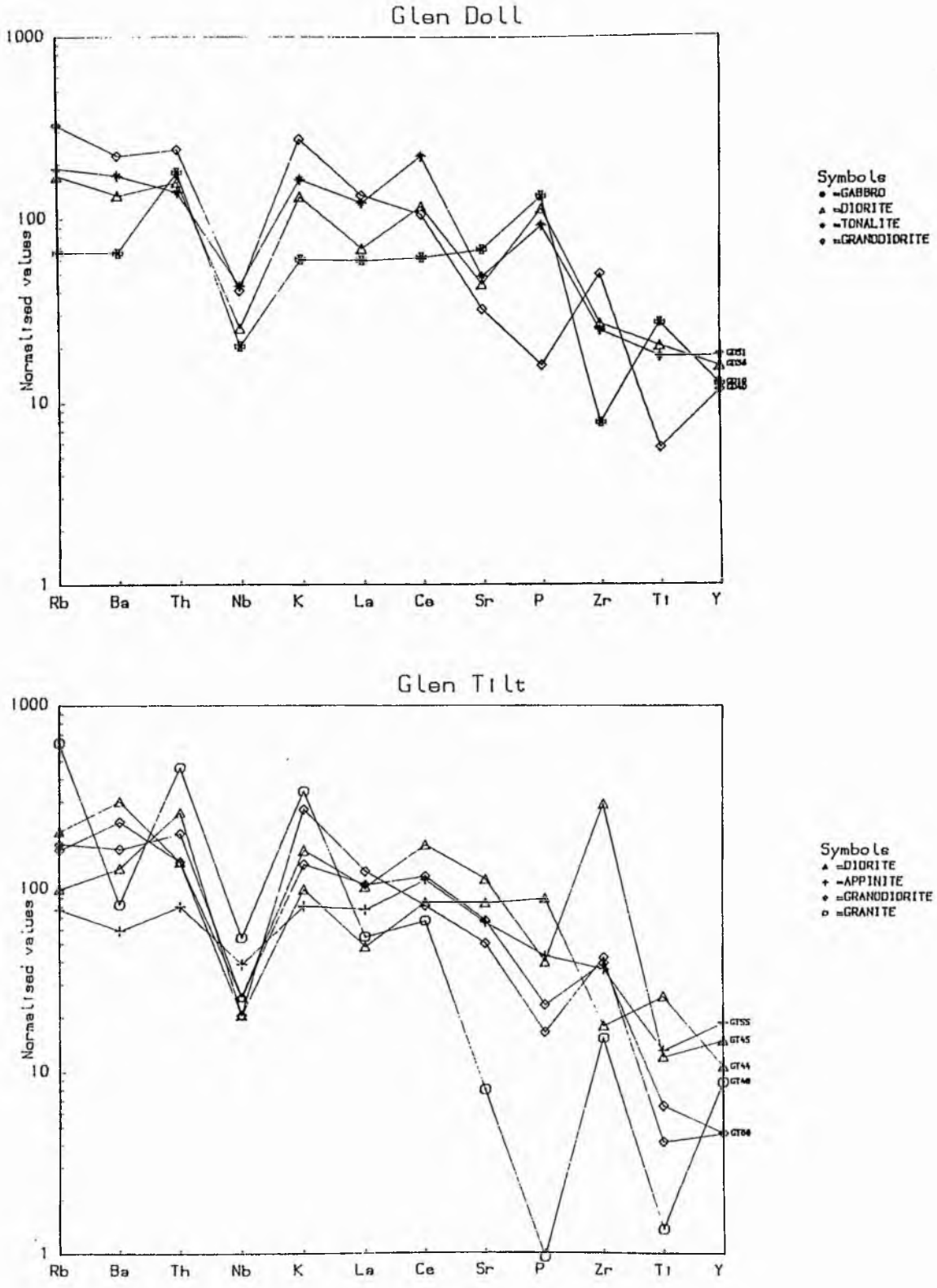

Fig 5.8a,b Chondrite - normalised plots of the representative rock types in the Glen Doll and Glen Tilt plutons.

La, Ce and Nb. The gabbros are depleted in the high field strength elements (Nb, La, Ti and Y). The positive anomaly at Ce in some types matches the same anomaly at P supporting the idea of enrichment of Ce in apatite. Tonalites and granodiorites show similar trends with depletion in La, Ce, P, Nb and Ti but enriched in Zr probably due to zircon saturation.

5.4.3 Summary

The complex belongs to the high-K calc-alkaline suite. Harker diagrams of the major and trace elements show that the ultrabasic rocks probably represent cumulates, sharing in some diagrams characteristics of the pyroxene hornblende gabbronorites. As a whole variation diagrams are very scattered.

5.5 Glen Tilt

5.5.1 Major oxides

Major oxides for this complex are presented as a series of Harker diagrams (Fig. 5.9 a-i). With increasing SiO_2 the abundances of MgO, CaO, Fe_2O_3(t), MnO, TiO_2 and P_2O_5 decrease in a fairly linear fashion though some low-SiO_2 rocks show particular enrichment of MgO, TiO_2 and P_2O_5. K_2O increases with SiO_2 whereas Na_2O and Al_2O_3 are scattered initially but tend to decrease towards the granodiorites and granites. Scatter is most prominent at low SiO_2 levels up to 65% SiO_2 and this may be related to the distinctive petrographic and mineralogic features of the diorites and appinitic diorites.

The variation trend is typically calc-alkaline with some Fe enrichment on the AFM diagram (Fig. 5.9j). A plot of K_2O versus SiO_2

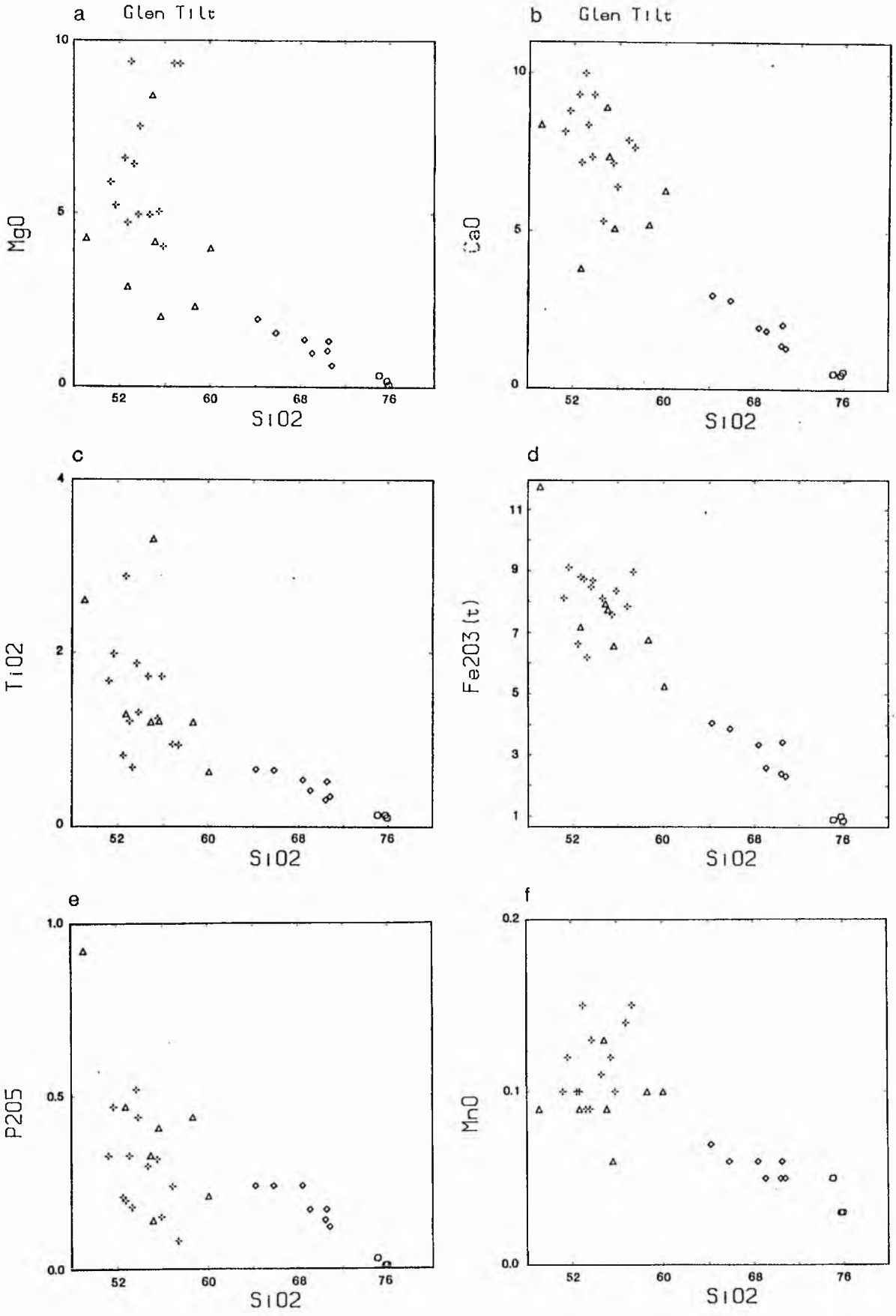

Figs 5.9$_{a-f}$ Harker variation diagrams of major oxides for the Glen Tilt pluton.

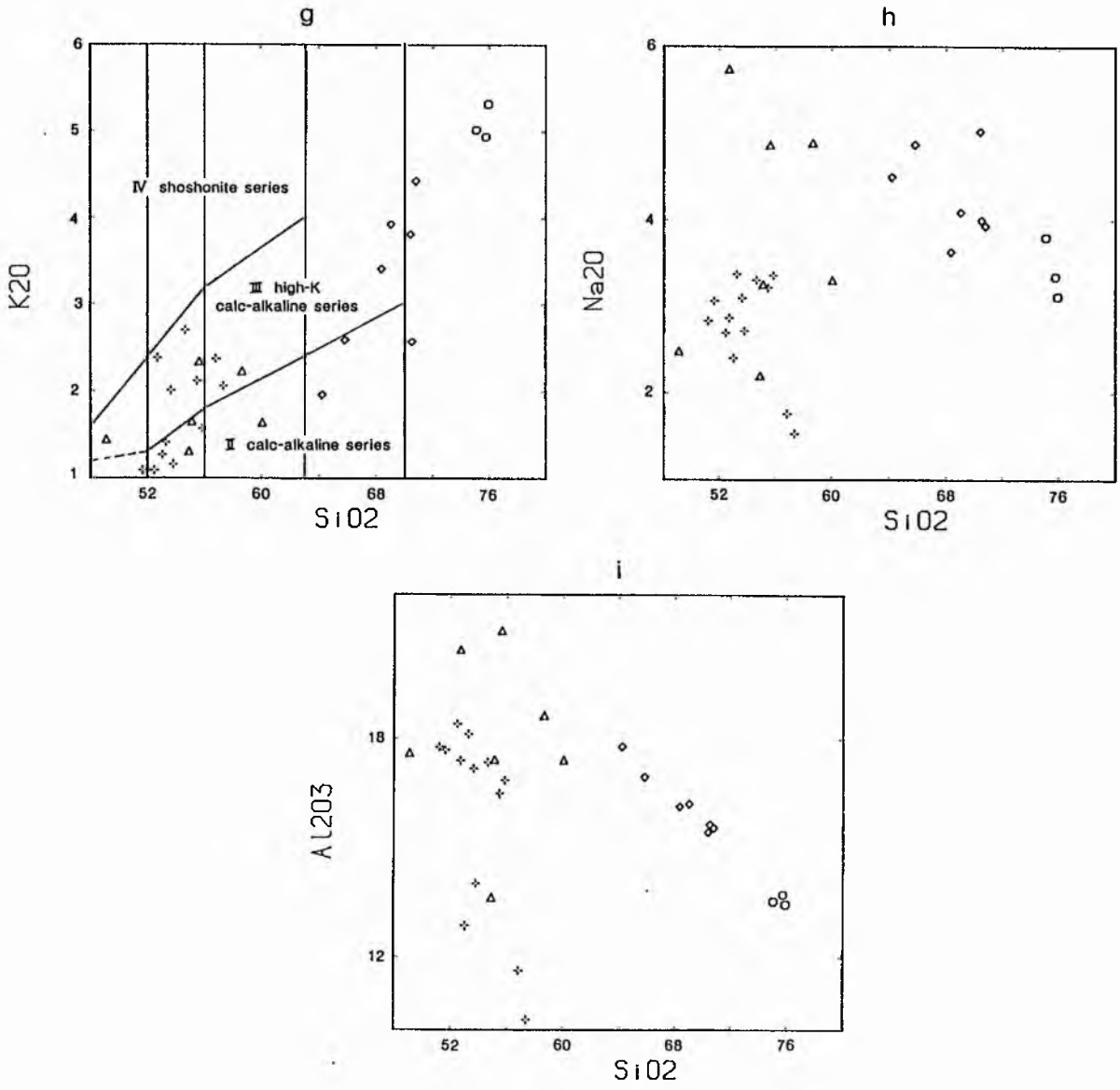

Figs 5.9$_{g-i}$ Harker variation diagrams of major oxides in the Glen Tilt pluton. Plot 5.9$_g$ includes fields of Peccerillo & Taylor (1976).

(Fig. 5.9g) shows that the complex is calc-alkaline to high-K calc-alkaline.

5.5.2 Trace elements

Plots for various trace elements versus SiO_2 (Fig. 5.9 k-z) generally show that:

a) Ni and Cr abundances are very low in the more acid varieties while below 60% SiO_2 they are very scattered. Samples GT31, GT39 and GT46 (appinitic diorites) contain the highest Cr and Ni concentrations of about 500 ppm and 180 ppm respectively reflecting clinopyroxene abundances. V decreases with increasing SiO_2 in a similar way to TiO_2 and $Fe_2O_3(t)$ trends, and probably substitutes for Ti and Fe in magnetite, clinopyroxene, amphibole and biotite.

b) Rb increases with SiO_2 and especially so in the granites. Ba is scattered initially with its highest values in the quartz diorites and then decreases towards the granodiorites and granites. Sr decreases steadily with increasing SiO_2 apart from a few depleted appinitic diorites.

c) Zn and Cu are highly scattered in low SiO_2 rocks (less than 60% SiO_2) thereafter Cu decreases steadily to a minimum of less than 35 ppm in the granites and Zn is also generally depleted in the evolved rocks.

d) Except for two anomalous samples, GT42 (1200 ppm) and GT45 (1600 ppm), Zr shows a gradual increase towards granodiorites followed by a decrease towards the granites. Hf shows a very similar trend to Zr. Nb is highly scattered with a tendency to increase towards the granites.

e) Th and Pb show irregular trends tending to increase towards the

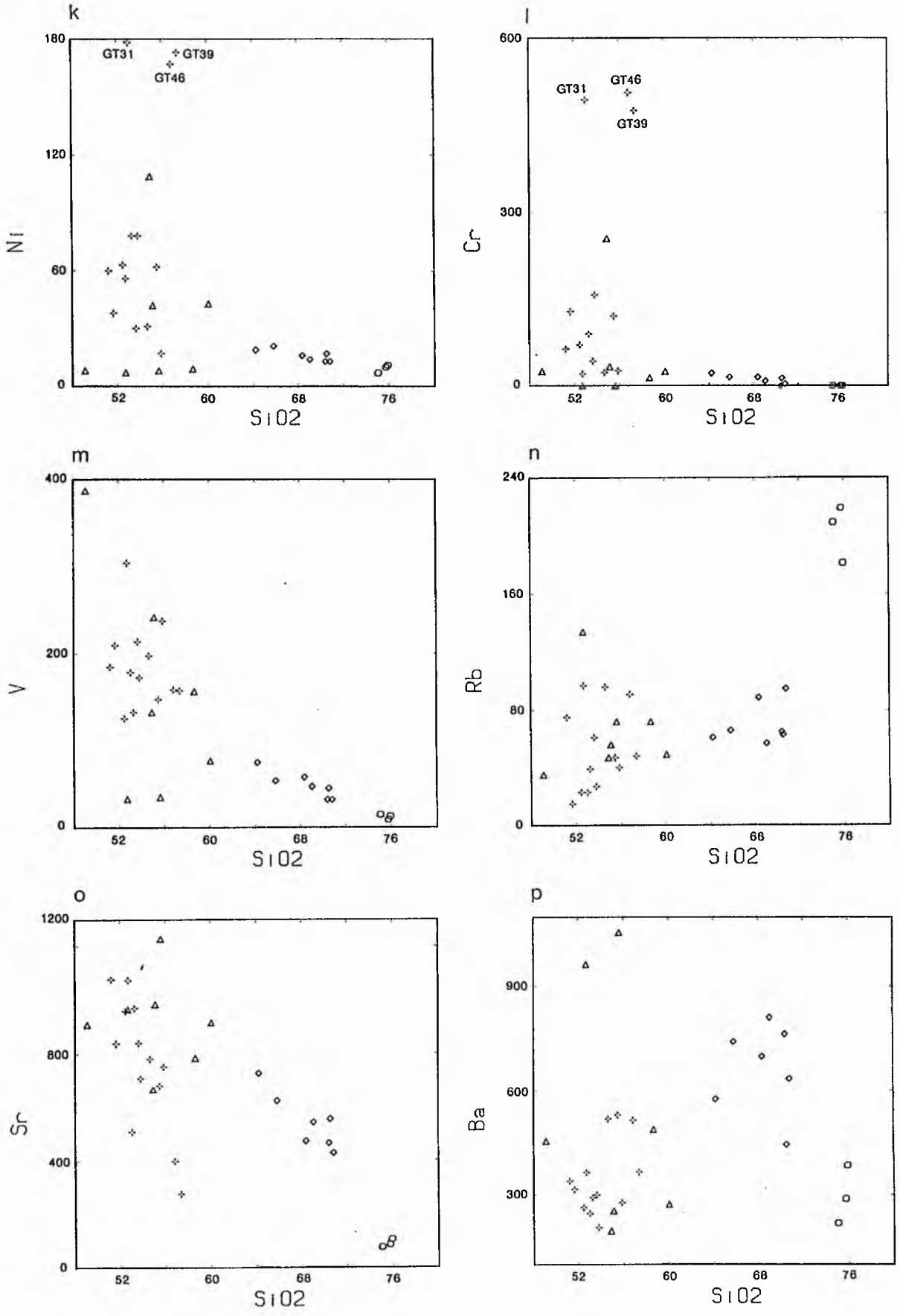

Figs 5.9$_{k-p}$ Harker variation diagrams of SiO_2 in wt % versus trace elements in ppm for the Glen Tilt pluton.

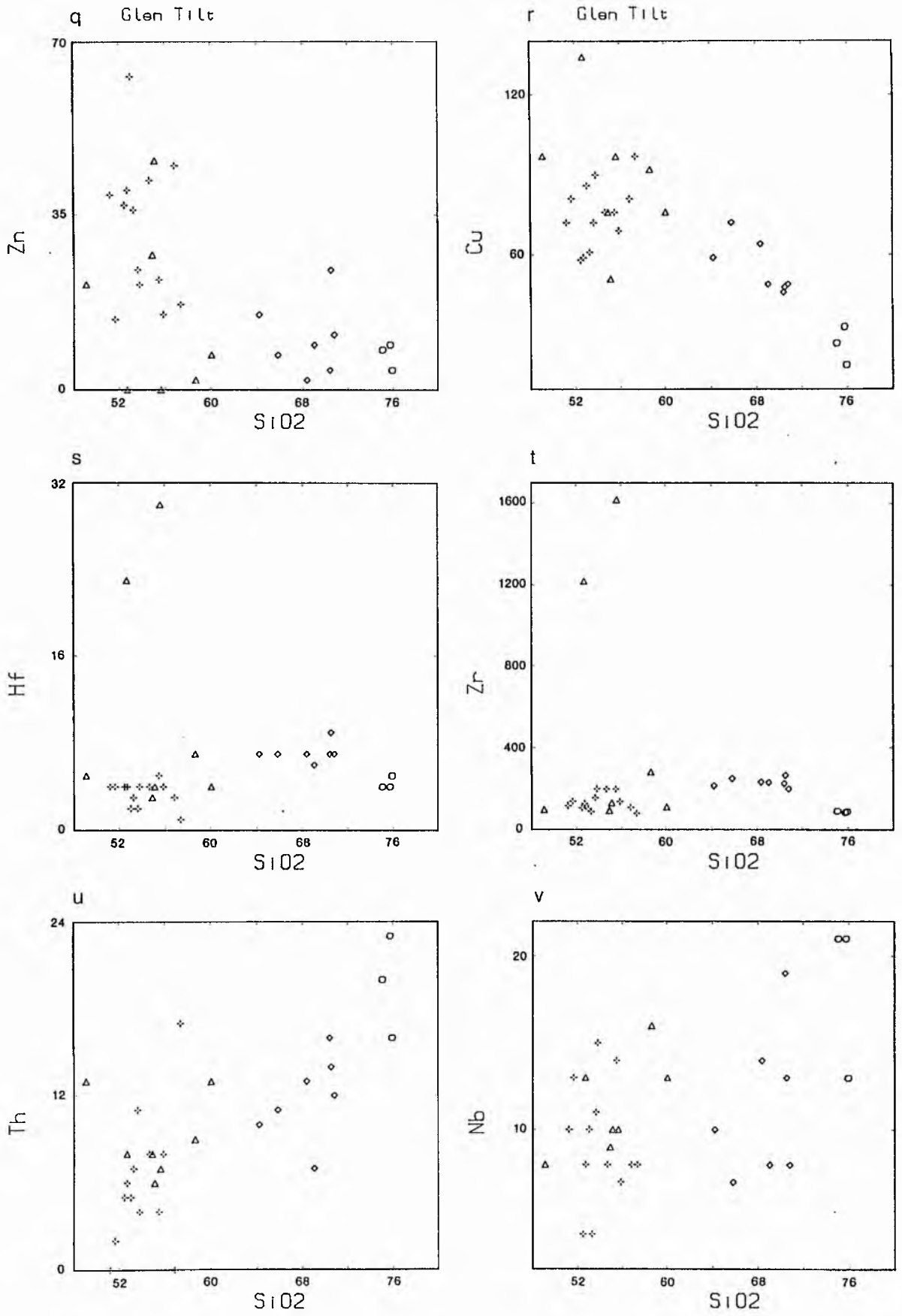

Figs 5.9$_{q-v}$ Harker variation diagrams of SiO_2 in wt % versus trace elements in ppm for the Glen Tilt pluton.

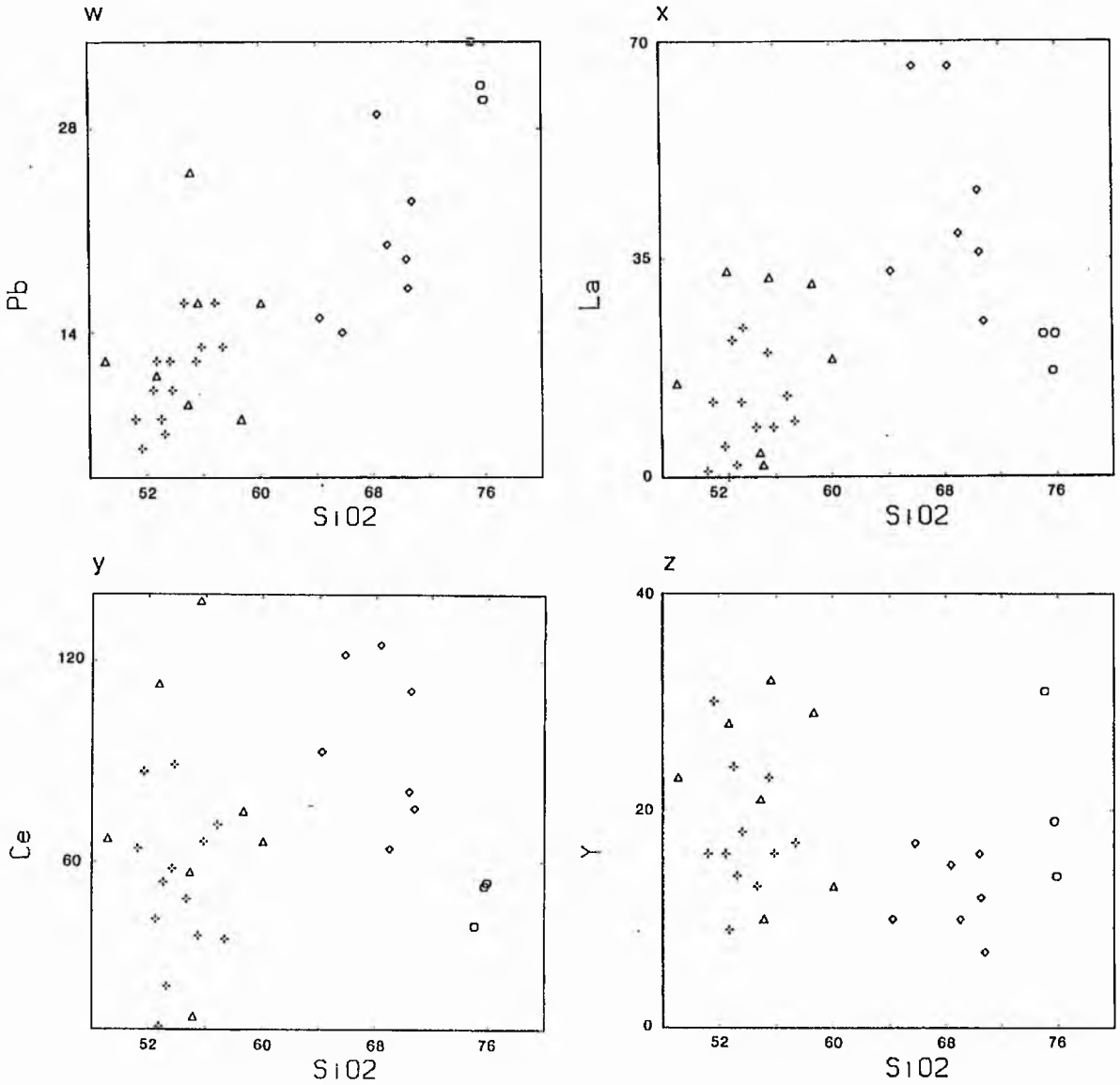

Figs 5.9$_{w-z}$ Harker variation diagrams of SiO in wt % versus trace elements in ppm for the Glen Tilt pluton 2

granites.

f) La and Ce increase in a scattered fashion initially and then decrease towards the granite. Y is highly scattered with no systematic trend.

Ni - Mg and Cr - Mg

Those two elements (Ni and Cr) decrease rapidly towards the granites, some appinitic diorites being anomalously Cr and Ni rich for their Mg abundances. (Fig. 5.10a, b).

Rb - K

There is a good linear trend between these two elements except for the granodiorites which tend to be depleted in Rb (Fig. 5.10c).

Ba - K

Ba increase with K towards the quartz diorites (greater than 1000 ppm) and then starts decreasing towards the granodiorites and granites which are very depleted probably reflecting earlier removal of biotite (Taylor, 1965), (Fig. 5.10d).

Sr - Ca

There is considerable scatter within the appinitic diorites and some diorites but very good linearity between other diorites, granodiorites and granites suggesting that these are linked through plagioclase fractionation. (Fig. 5.10e).

Ti/1000 - V

The Ti against V plot shows that there is a good positive

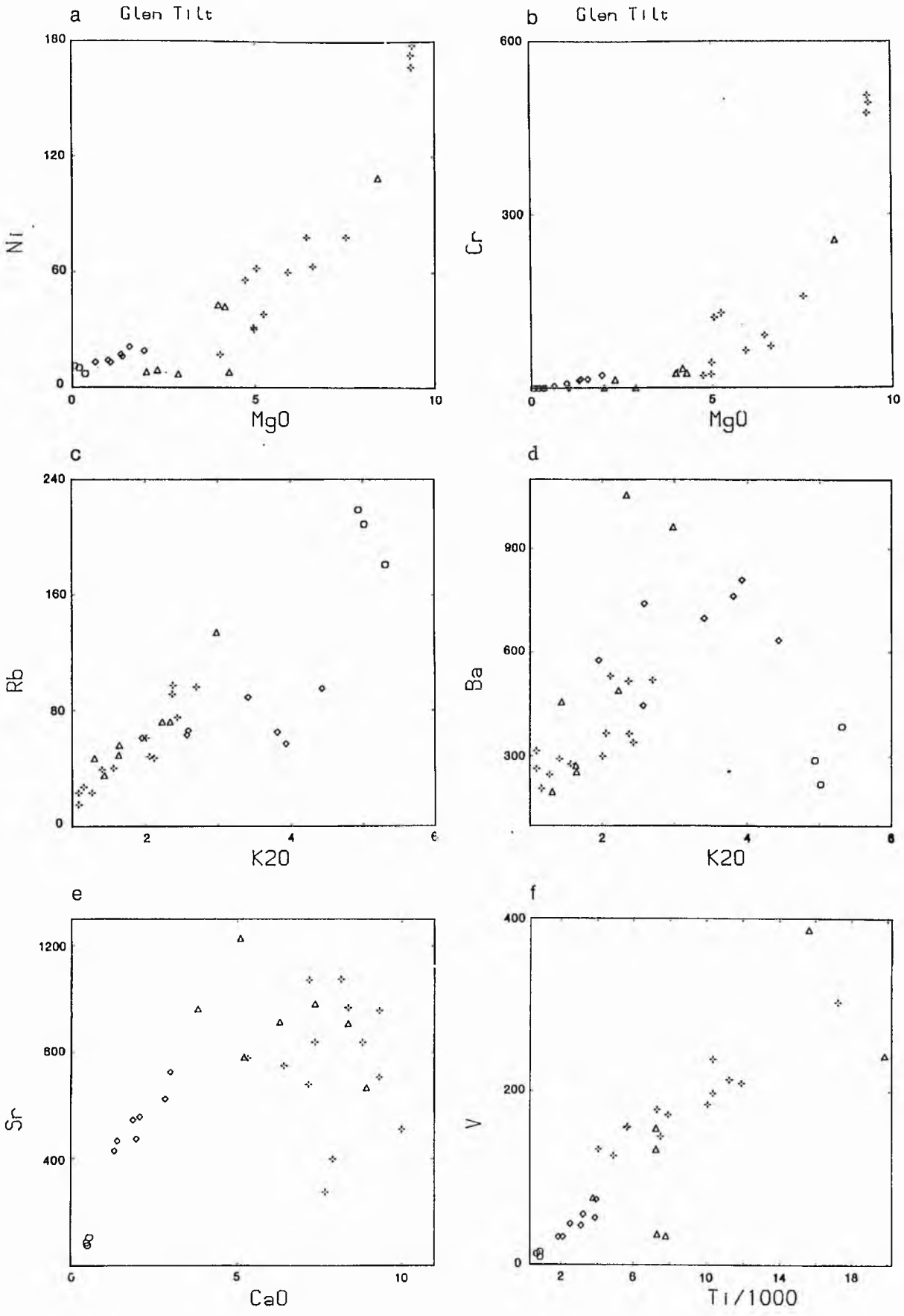

Figs 5.10$_{a-f}$ Variation diagrams for some major oxides and trace elements in the Glen Tilt pluton.

correlation between the two elements for most samples apart from a few diorites with a low-V trend. (Fig. 5.10f).

K/Rb - SiO_2

The K/Rb ratios do not show a very systematic relationship to evolutionary sequence but the granites have very low values (Fig. 5.10g).

Rb/Sr - SiO_2

The Rb/Sr ratios are very low (always less than 0.3) except for the granites which have high values (Fig. 5.10h).

Chondrite - normalised abundance plots

In this diagram (Fig. 5.8b) diorites, appinitic diorites and granodiorites show more or less parallel relationships with each other except for the quartz diorites which are relatively enriched in Ba and Zr, which is probably due to high modal biotite and zircon. The granites however are much enriched in Rb, Th, K and rather depleted in La, Ce, P, Ti and Ba compared with the more basic types.

5.5.3 Summary

Whole-rock chemical data presented in the previous sections demonstrate the majority of samples analysed here fall on smooth and regular trends on the Harker variation and AFM diagrams. Scatter within the more basic members of the suite is rather greater than other similar plutons and may in part be related to cumulate effects.

The markedly different abundance patterns on chondrite normalised plots suggest an independent origin for the granites,

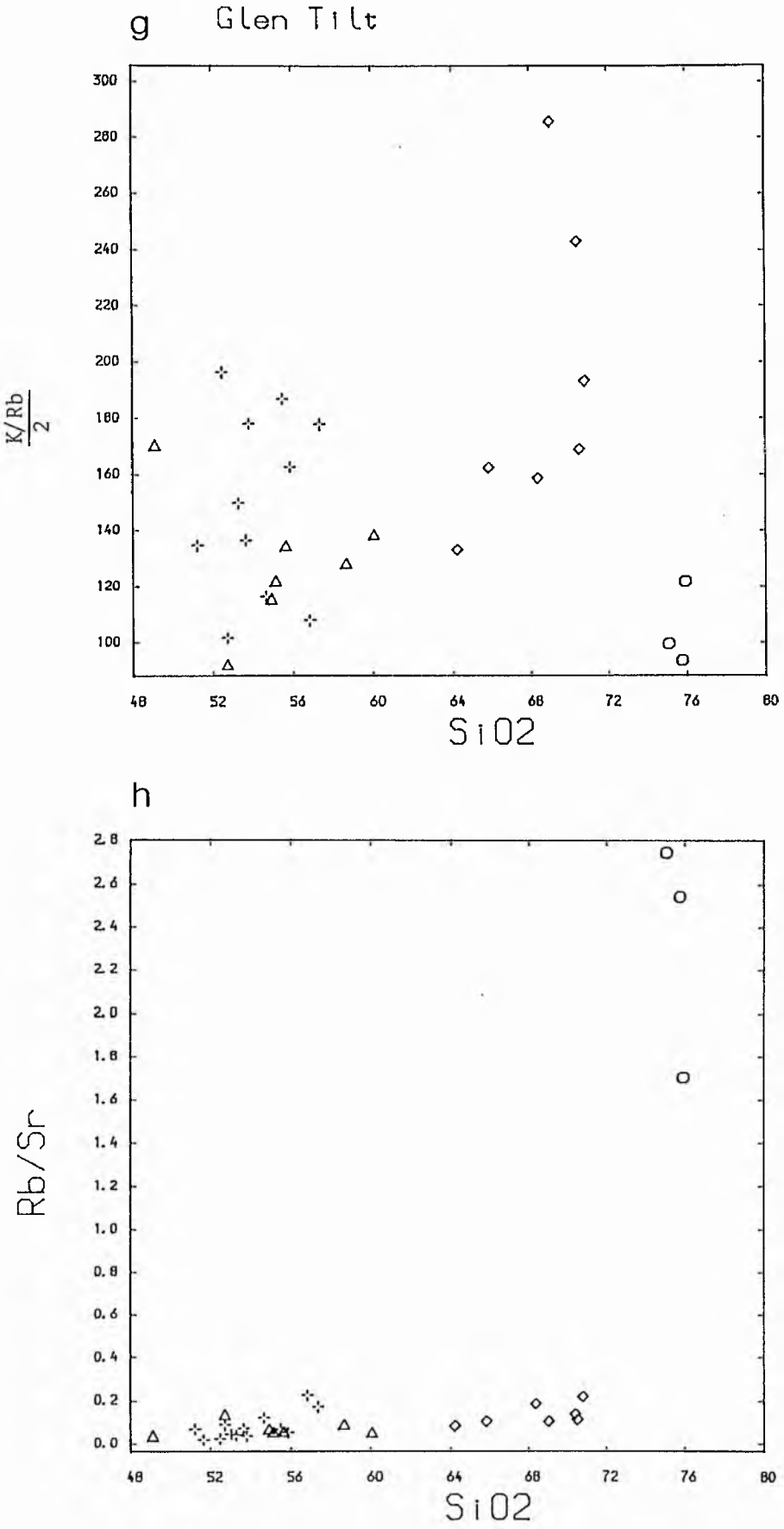

Figs 5.10$_{g-h}$ Plots of SiO_2 versus K/Rb and Rb/Sr ratios for the Glen Tilt pluton.

though the other types (except for quartz diorite) appear to be related through crystal fractionation.

5.6 Cairnsmore of Carsphairn

5.6.1 Major oxides

The major oxide plots are presented here as Harker diagrams (Fig. 5.11a-i) and show that with increasing SiO_2 the abundances of MgO, CaO, $Fe_2O_3(t)$, TiO_2, MnO and P_2O_5 decrease, whereas K_2O increases. Na_2O increases to its highest value (4.3%) in tonalite and then becomes rather depleted in the granites. A compositional gap exists between 66 and 71% SiO_2.

The whole rock analyses show a calc-alkaline trend on the AFM diagram (Fig. 5.11j). A plot of SiO_2 versus K_2O (Fig. 5.11g) shows that the rocks belong to the calc-alkaline to high-k calc-alkaline series (Peccerillo and Taylor, 1976).

5.6.2 Trace elements

The plots of various trace elements versus SiO_2 (Fig. 5.11k-z) show that:

a) Ni and Cr are enriched only in the microdiorites (about 100 ppm for Ni and 220 ppm for Cr), and are otherwise depleted in the tonalites and granites. V decreases quite linearly with increasing SiO_2.

b) Rb does not vary systematically within the diorites, tonalites and granodiorites but increases rapidly in the granites reflecting the enrichment of Rb in alkali feldspar. Ba is highly scattered but Sr decreases systematically with increasing SiO_2.

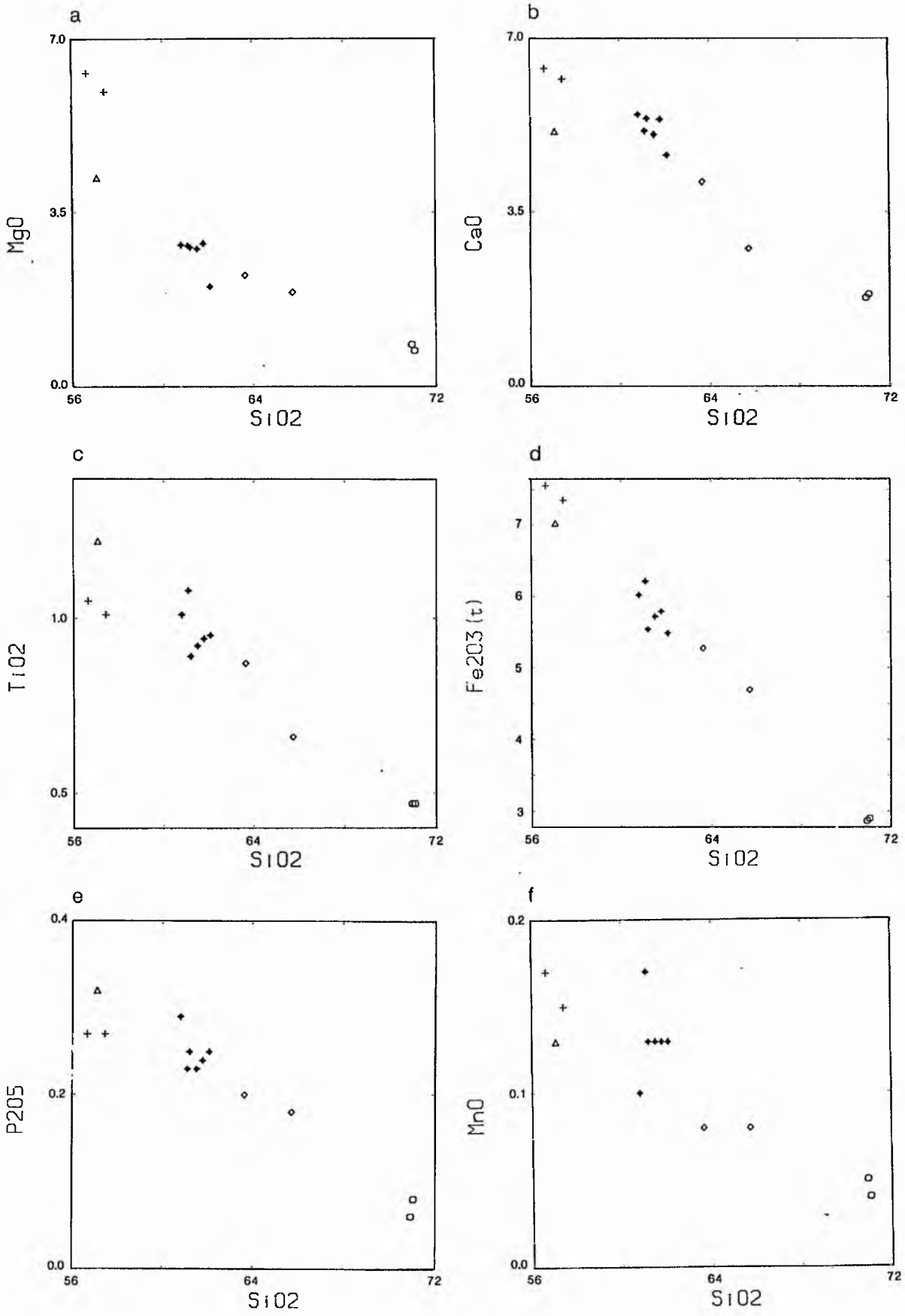

Figs 5.11$_{a-f}$ Harker variation diagrams of major oxides for the Carsphairn pluton.

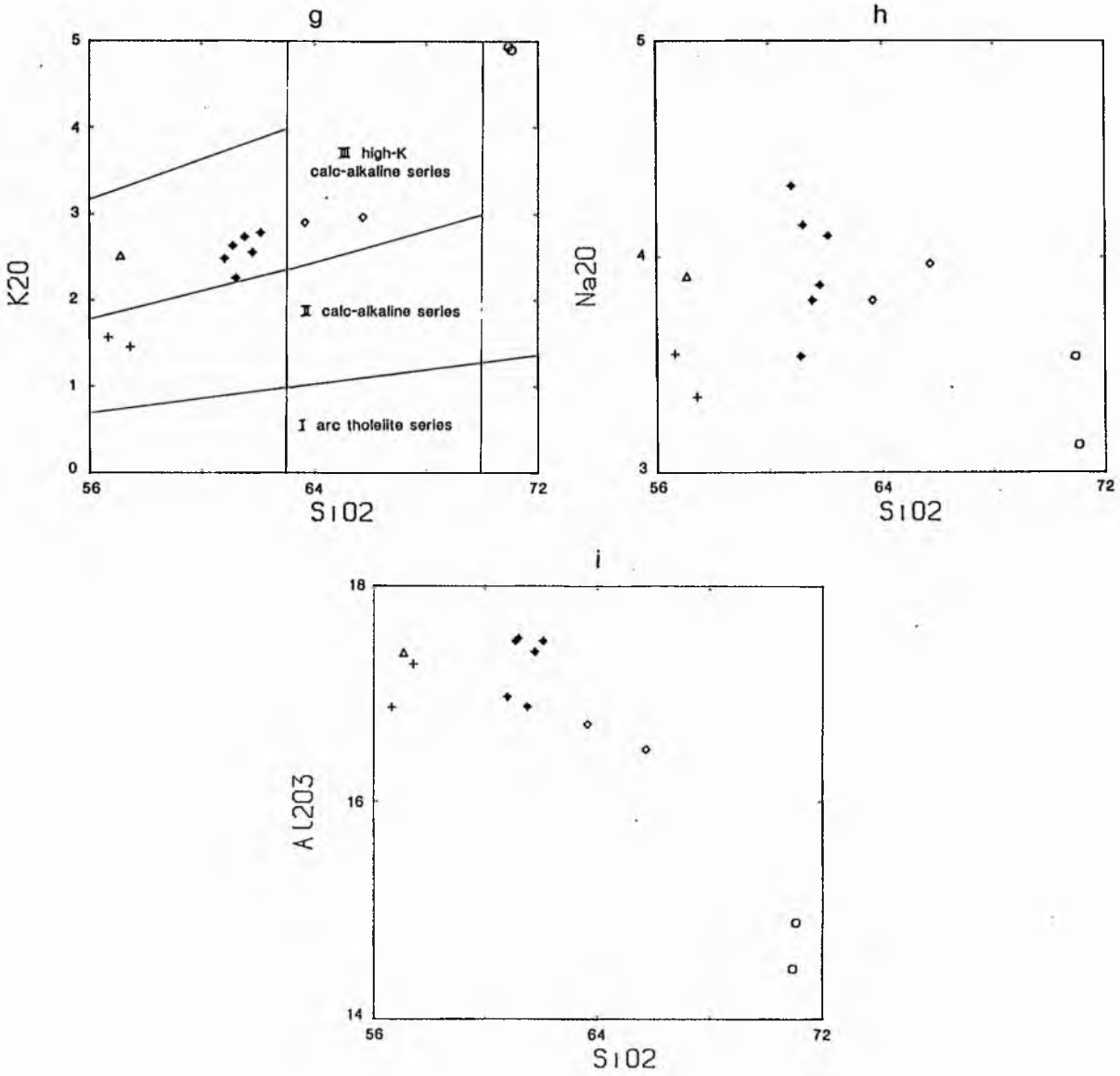

Figs 5.11$_{g-i}$ Harker variation diagrams of major oxides in the Carsphairn pluton. Plot 5.11$_g$ includes fields of Peccerillo & Taylor (1976).

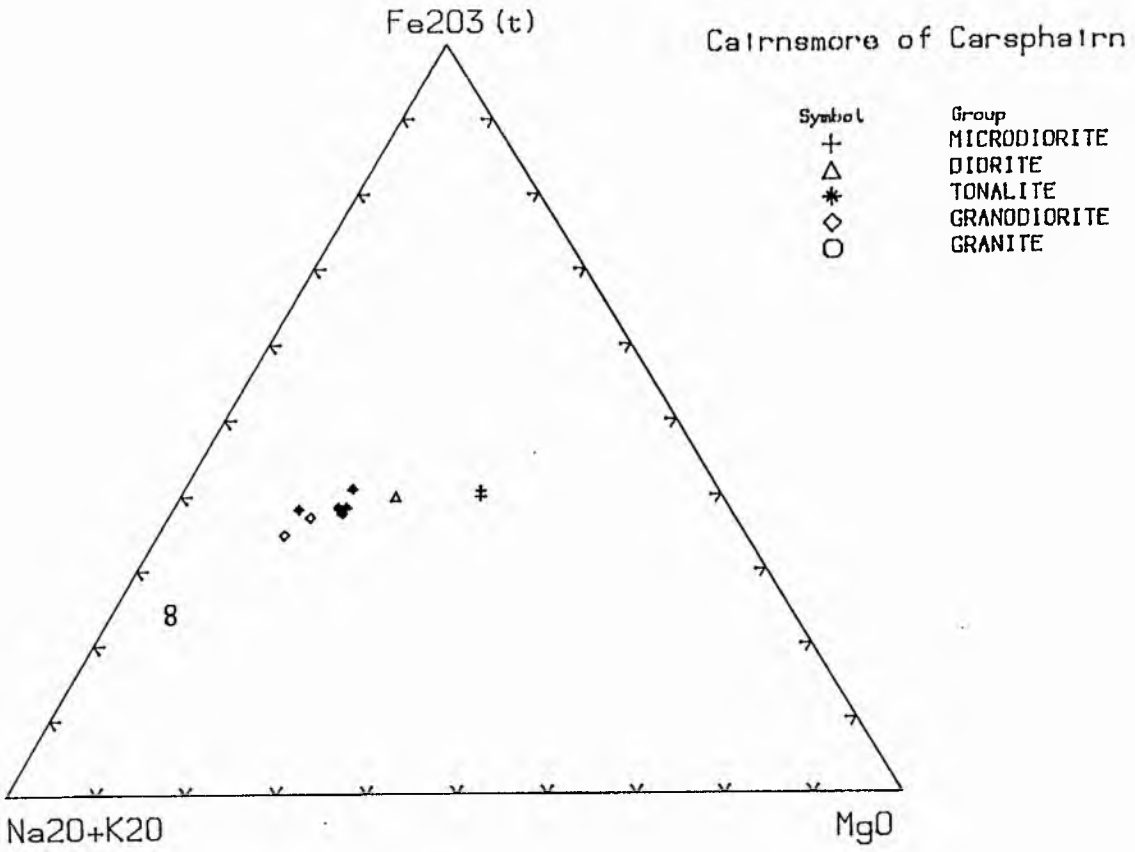

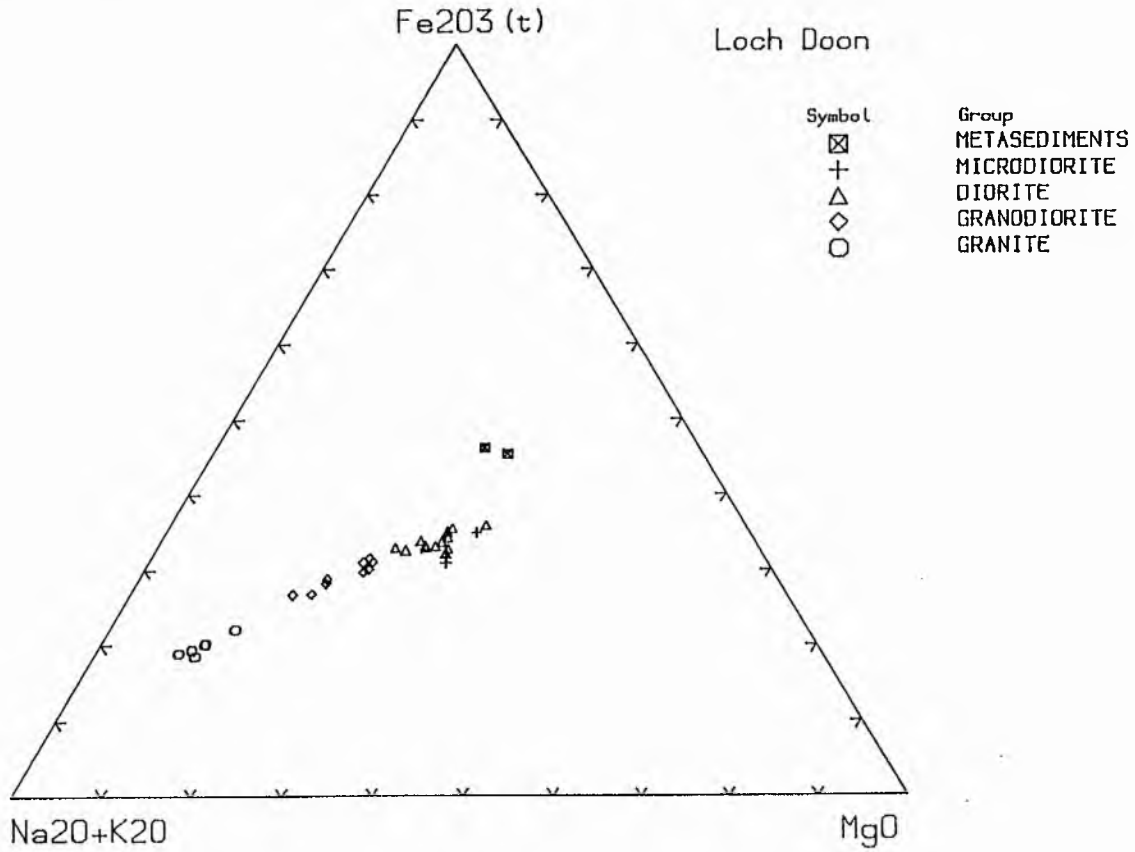

Fig 5.11$_j$ and 5.14$_j$ AFM plots of the Cairnsmore of Carsphairn and Loch Doon plutons.

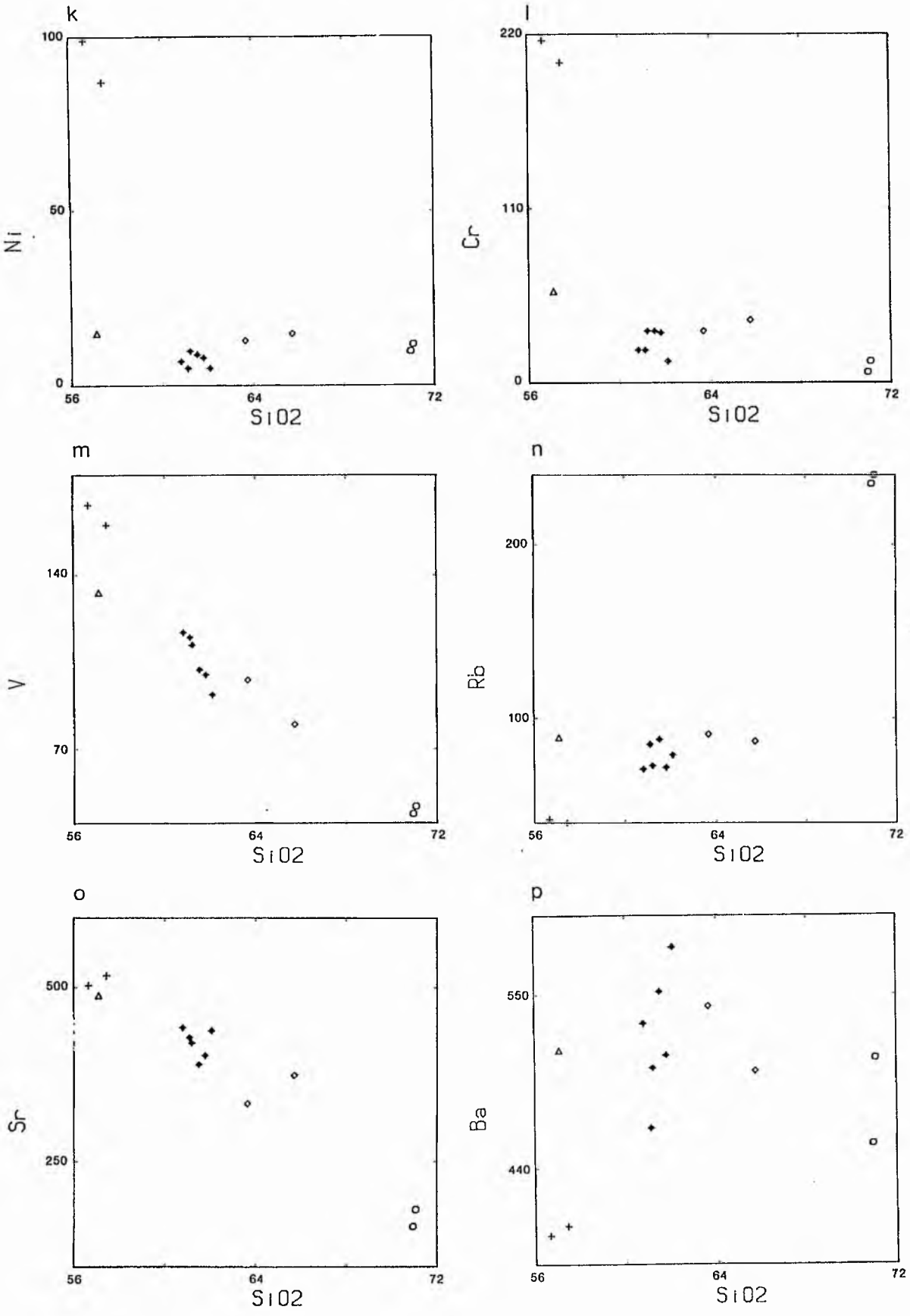

Figs 5.11$_{k-p}$ Harker variation diagrams of SiO_2 in wt % versus trace elements in ppm for the Carsphairn pluton.

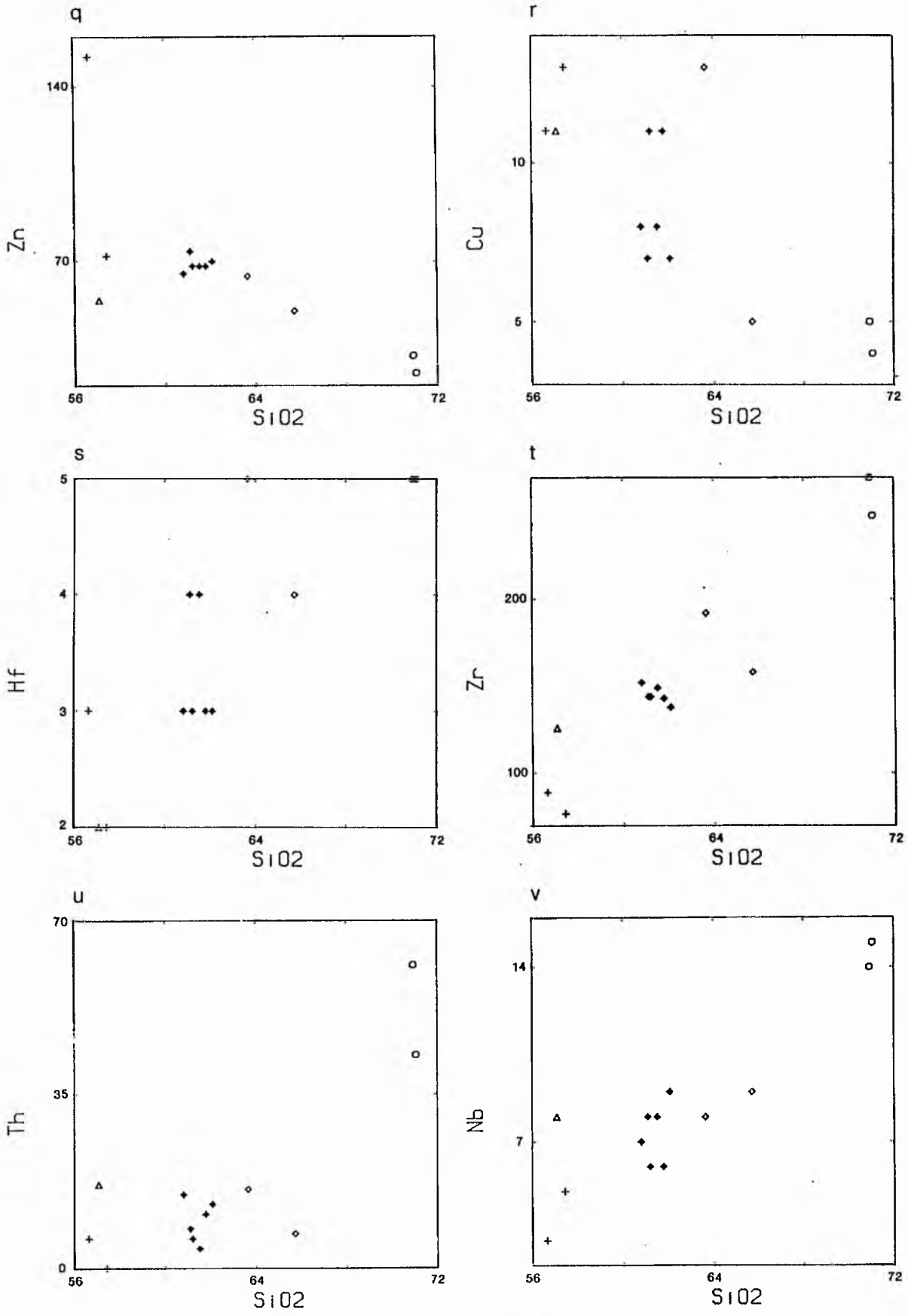

Figs 5.11$_{q-v}$ Harker variation diagrams of SiO_2 in wt % versus trace elements in ppm for the Carsphairn pluton.

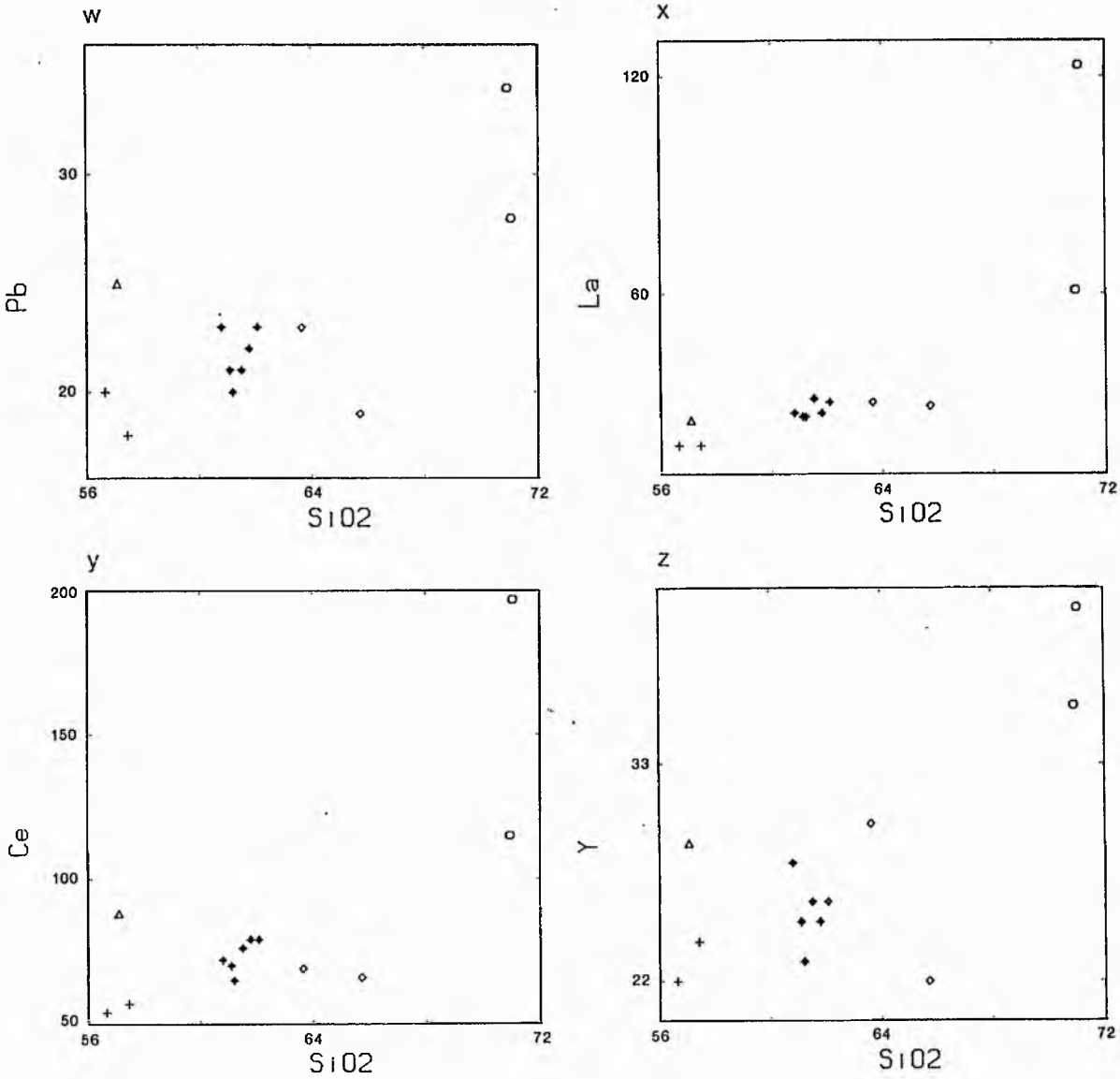

Figs 5.11$_{W-Z}$ Harker variation diagrams of SiO_2 in wt % versus trace elements in ppm for the Carsphairn pluton.

c) Zn decreases fairly linearly with increasing SiO_2 and Cu is depleted in the granites.

d) Zr increases regularly with SiO_2 indicating its concentration in the later stages of fractionation probably in the mineral zircon. Hf increases in more scattered fashion with SiO_2 whereas Nb increases quite regularly towards the granites.

e) Th and Pb have scattered trends in the diorites and granodiorites and then increase considerably in the granites.

f) La and Ce are very scattered in the diorites and granodiorites but increase rapidly in the granites probably due to incorporation in late accessory phases. Y shows a rather similar trend.

Ni - Mg and Cr - Mg

Only the microdiorites are especially enriched in Cr or Ni for their Mg content, indicating a likely mantle origin. All other rock types have low abundances of these elements (Fig. 5.12a, b).

Rb - K

There is good correlation between these two variables. (Fig. 5.12c).

Ba - K

Ba increases linearly towards a maximum in the tonalites and is then depleted in the granites (Fig. 5.12d).

Sr - Ca

There is a scattered linear positive correlation between these two variables (Fig. 5.12e).

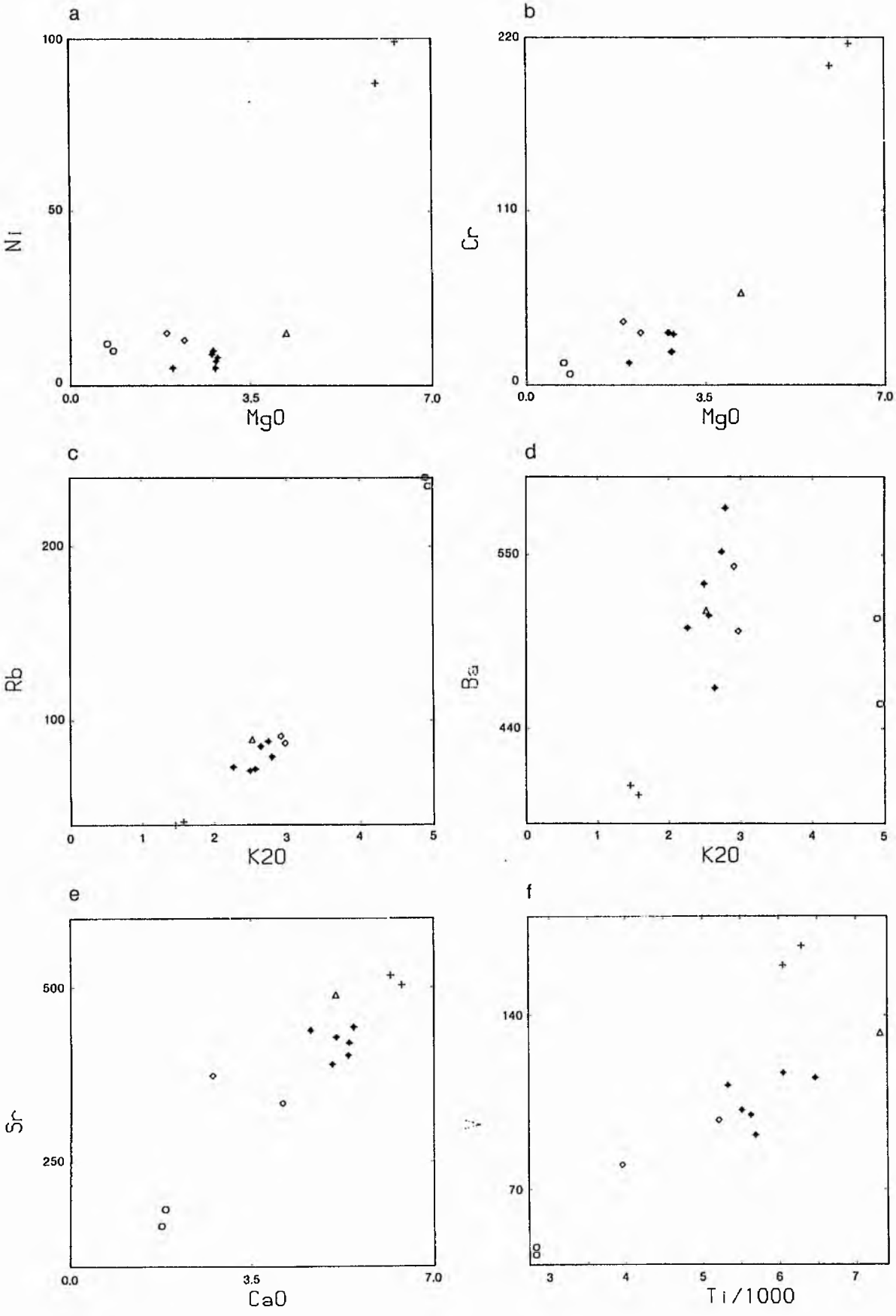

Figs 5.12$_{a-f}$ Variation diagrams for some major oxides and trace elements in the Carsphairn pluton.

Ti/1000 - V

This plot shows positive linear covariation, though the microdiorite samples contain higher V for about the same Ti in other rock types (Fig. 5.12f).

K/Rb - SiO_2

The K/Rb ratios vary from 117 to 155 in the diorites, tonalites and granodiorites but decrease very rapidly in the granites with values of about 85 (Fig. 5.12g).

Rb/Sr - SiO_2

This ratio is very low (0.1 to 0.3) in most rocks except for the granites in which the ratios vary from 1.3 to 1.5 (Fig. 5.12h).

Chondrite - normalised abundances

Generally the rocks are enriched in Rb, Th and K and depleted in Ba, Nb, La, Ce, Sr, P, Ti and Y with a marked negative Nb anomaly and enriched in Zr with positive anomaly. The granodiorites and granites become enriched in Rb, Th, K, La, Ce and Zr and depleted in Ba, Sr, P, Ti and Y (Fig. 5.13a). The subparallel trends are maintained through the various diorites, tonalites and granodiorites with a marked change in pattern in the granites.

5.6.3 Summary

Whole-rock chemical data presented in previous sections for this complex demonstrate that the majority of samples analysed here fall on relatively smooth and regular trends on the Harker variation and AFM

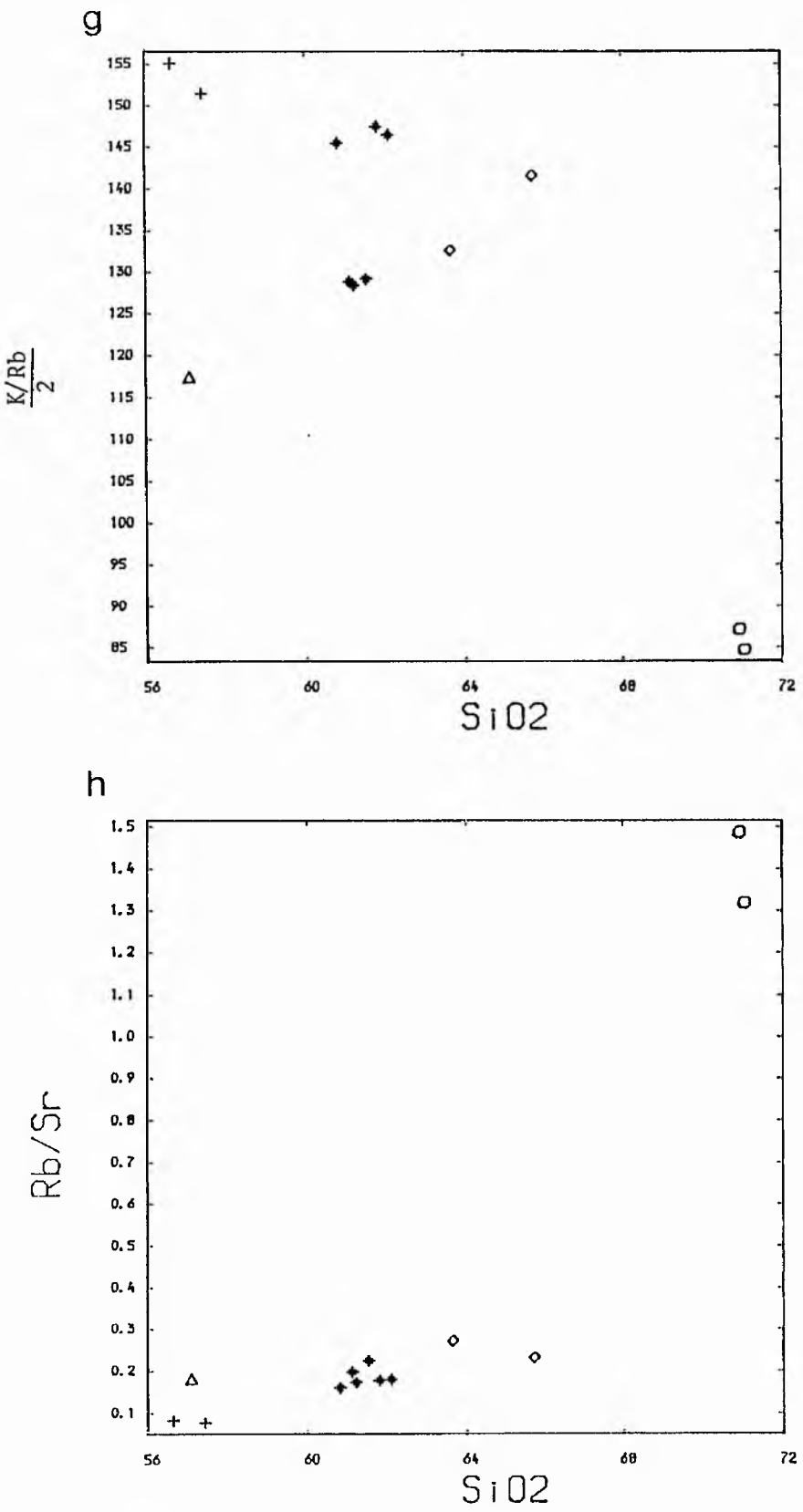

Figs 5.12_{g-h} Plots of SiO_2 versus K/Rb and Rb/Sr ratios for the Carsphairn pluton.

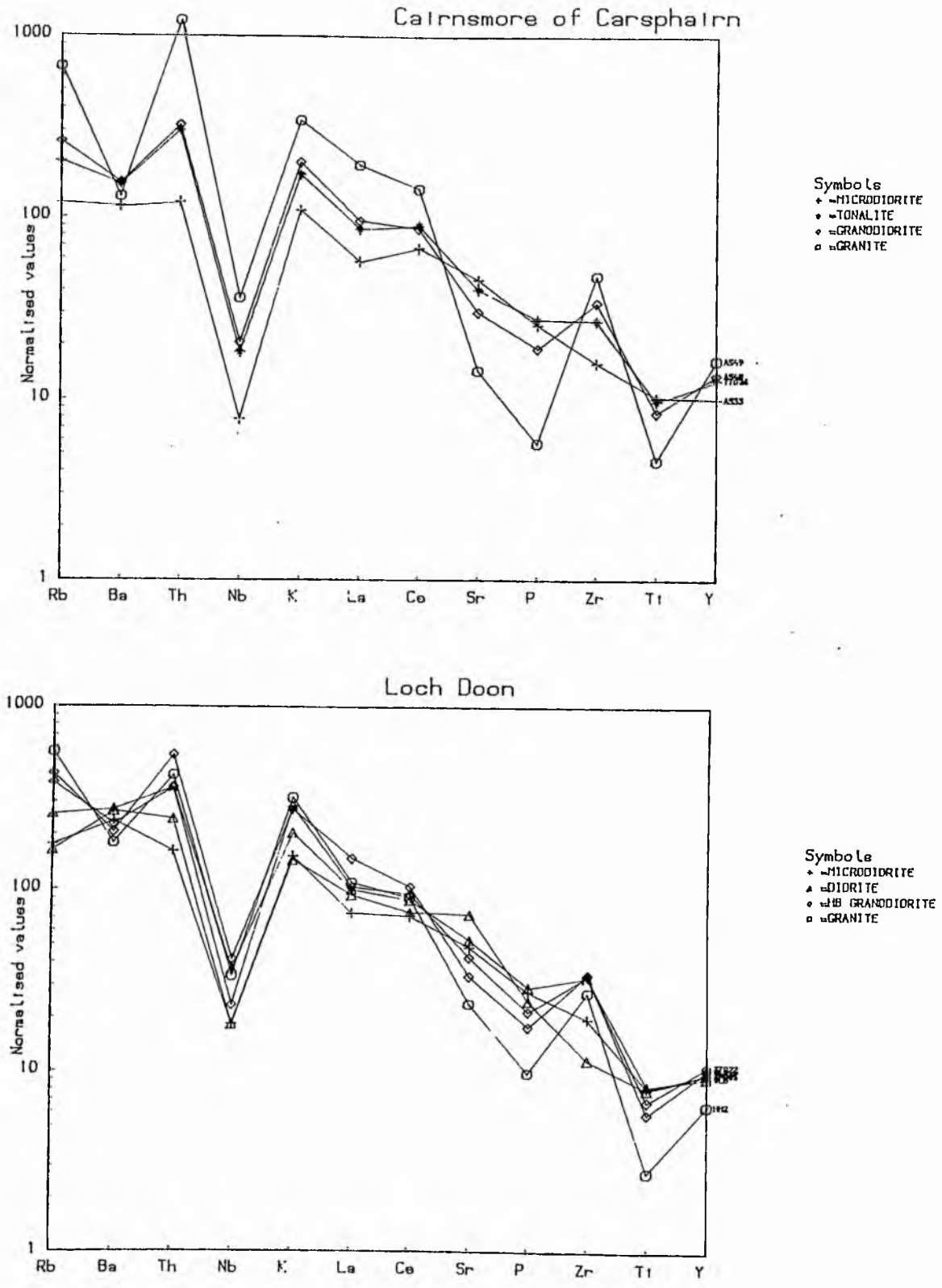

Fig 5.13$_{a,b}$ Chondrite-normalised plots of the representative rock types in the Cairnsmore of Carsphairn and Loch Doon plutons.

diagrams. The trends are essentially calc-alkaline and variation patterns are relatively coherent except for the granites suggesting a close relationship for the diorites through to granodiorites but a probable independent origin for the granite. The microdiorites have the characteristics of mantle-derived magmas.

5.7 Loch Doon

5.7.1 Major oxides

Major oxide variation is presented here as a series of Harker diagrams (Fig. 5.14a-i). With increasing SiO_2 the abundances of MgO, CaO, Fe_2O_3(t), MnO, TiO_2 and P_2O_5 fall, whereas K_2O increases; the abundances of Al_2O_3 and Na_2O are highly scattered with no covariation.

The variation trend is typically calc-alkaline on an AFM diagram (Fig. 5.14j). A plot of SiO_2 versus K_2O (Fig. 5.14g) shows that the rock types fall in the fields of high-k calc-alkaline magmas (Peccerillo and Taylor, 1976).

5.7.2 Trace elements

Plots for various trace elements versus SiO_2 (Fig. 5.14k-z) generally show that:

a) Ni and Cr show regular linear depletion towards the granites. V also show depletion towards the granites.

b) Rb increases positively with SiO_2 reflecting its affinity for K-rich minerals (biotite and alkali feldspar). Ba increases initially in the pyroxene biotite diorites and then shows a gradual decrease

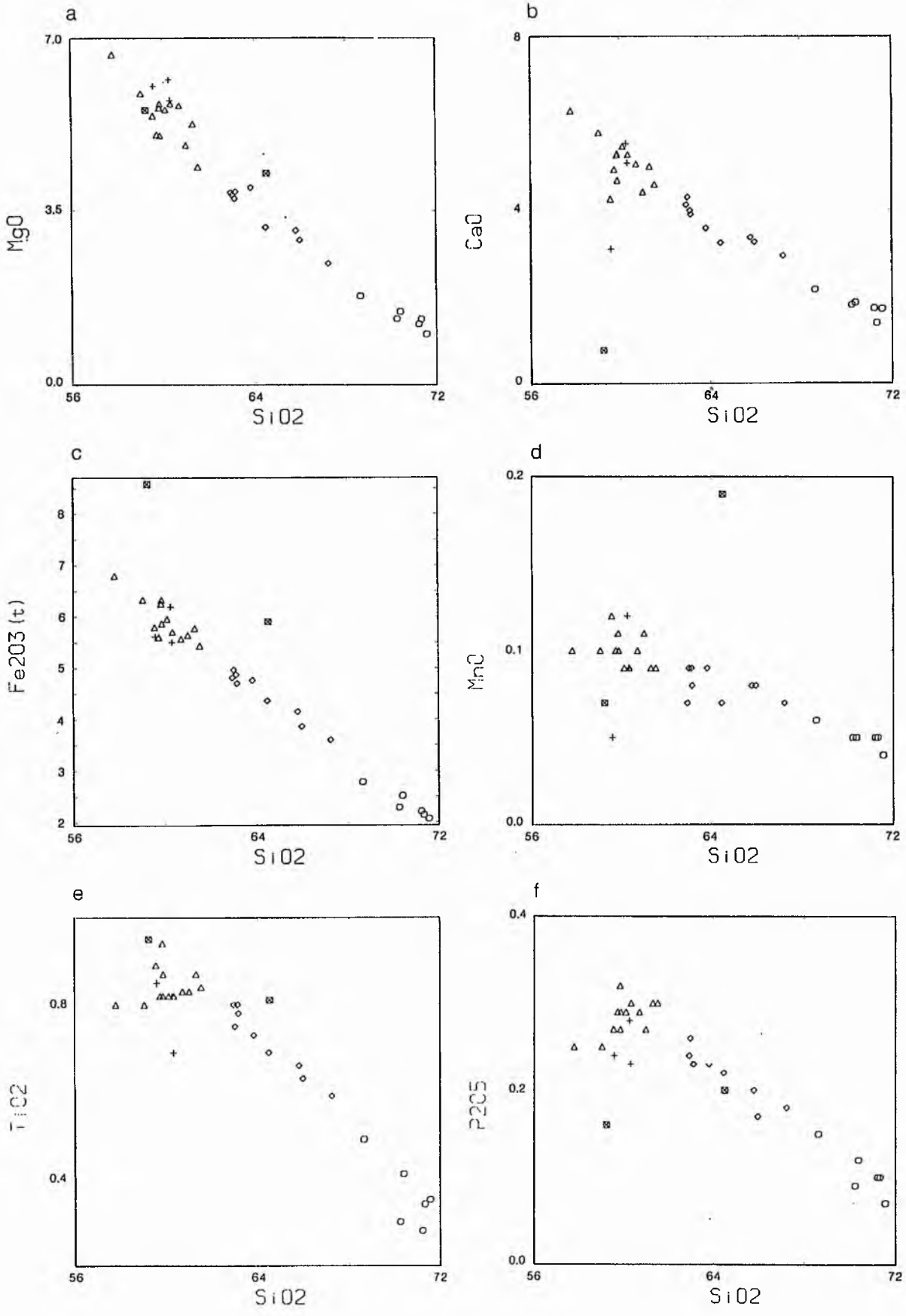

Figs 5.14$_{a-f}$ Harker variation diagrams of major oxides for the Loch Doon pluton.

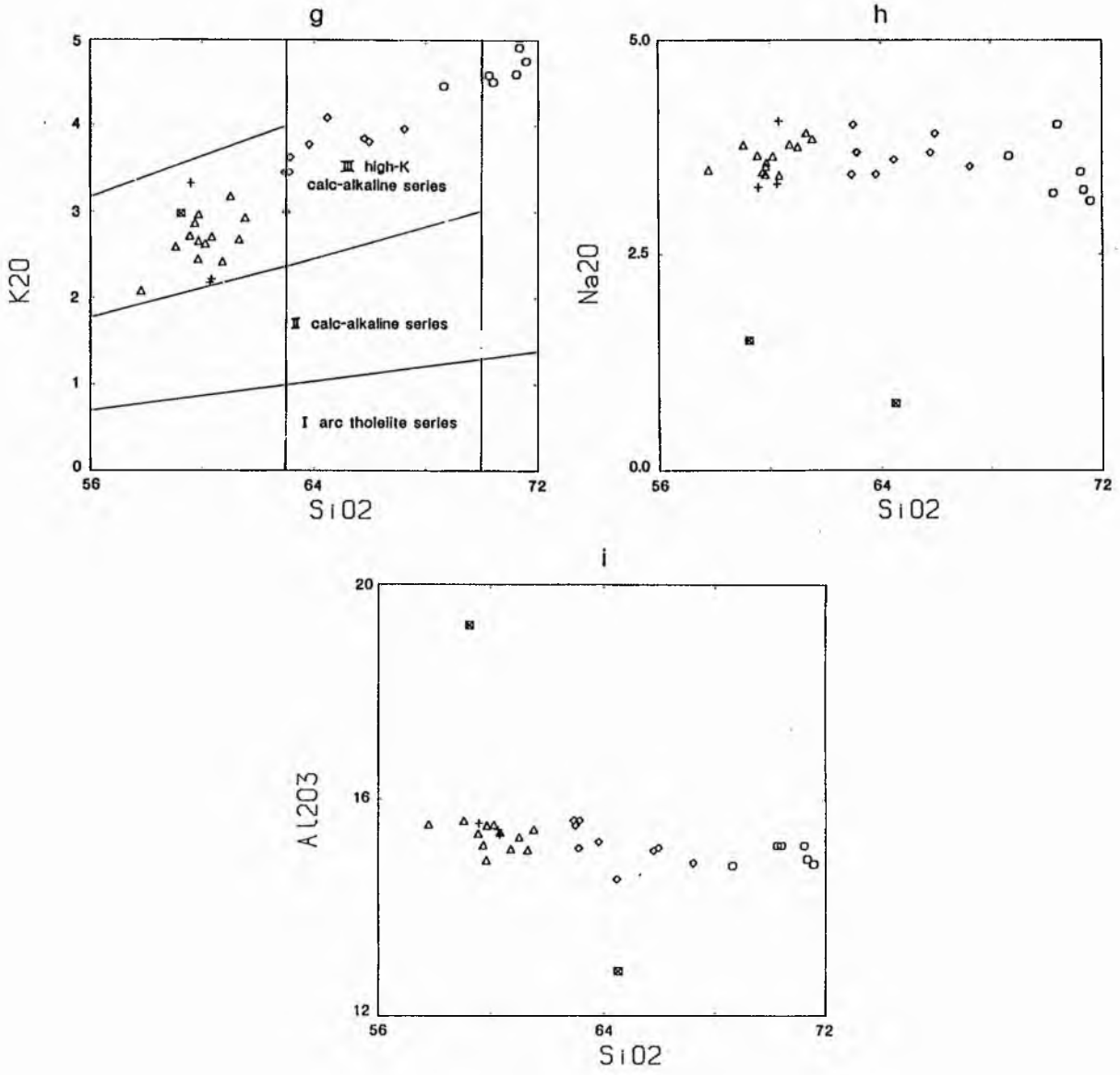

Figs 5.14$_{g-i}$ Harker variation diagrams of major oxides in the Loch Doon pluton. Plot 5.14$_{g}$ includes fields of Peccerillo & Taylor (1976).

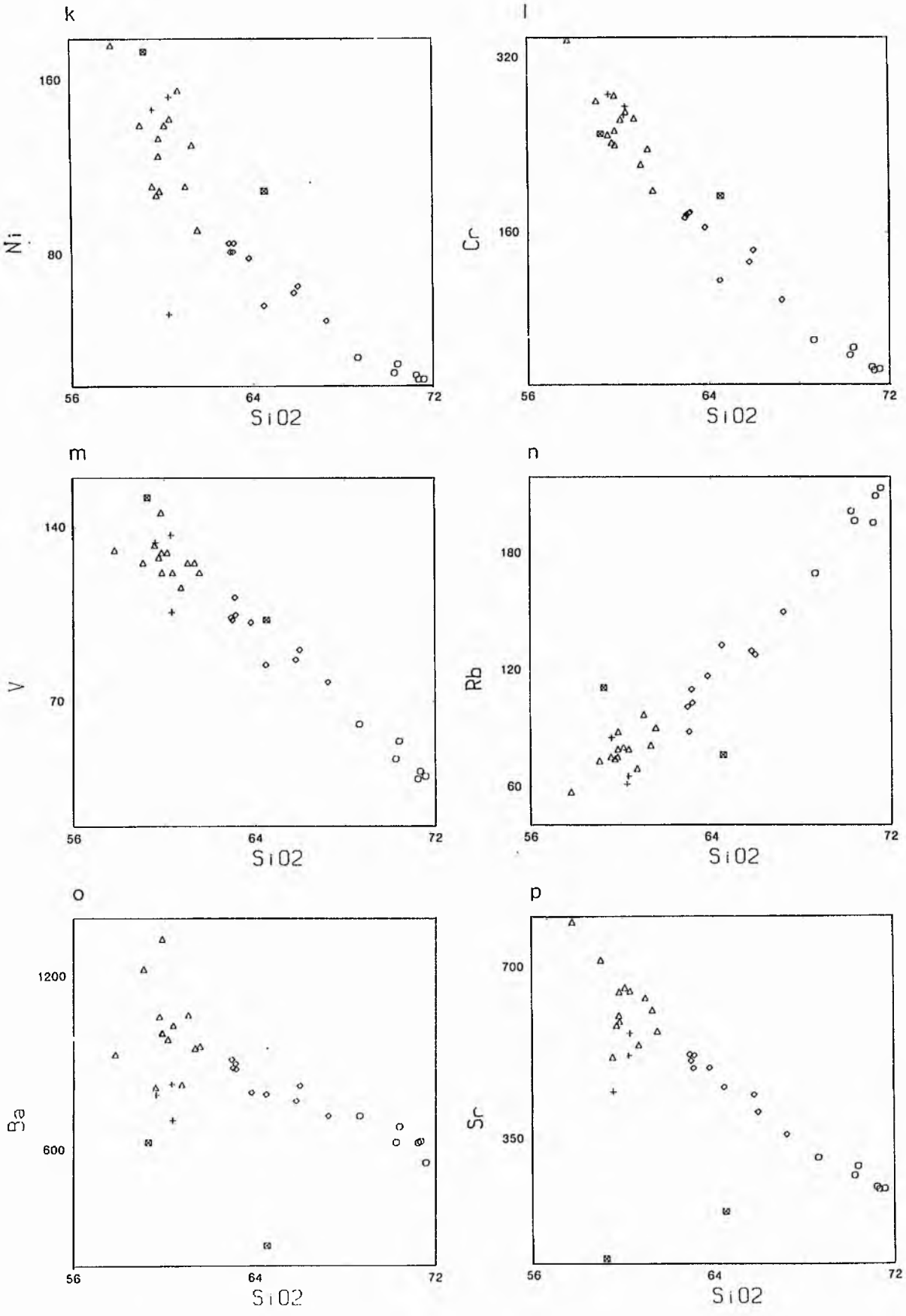

Figs 5.14$_{k-p}$ Harker variation diagrams of SiO_2 in wt % versus trace elements in ppm for the Loch Doon pluton.

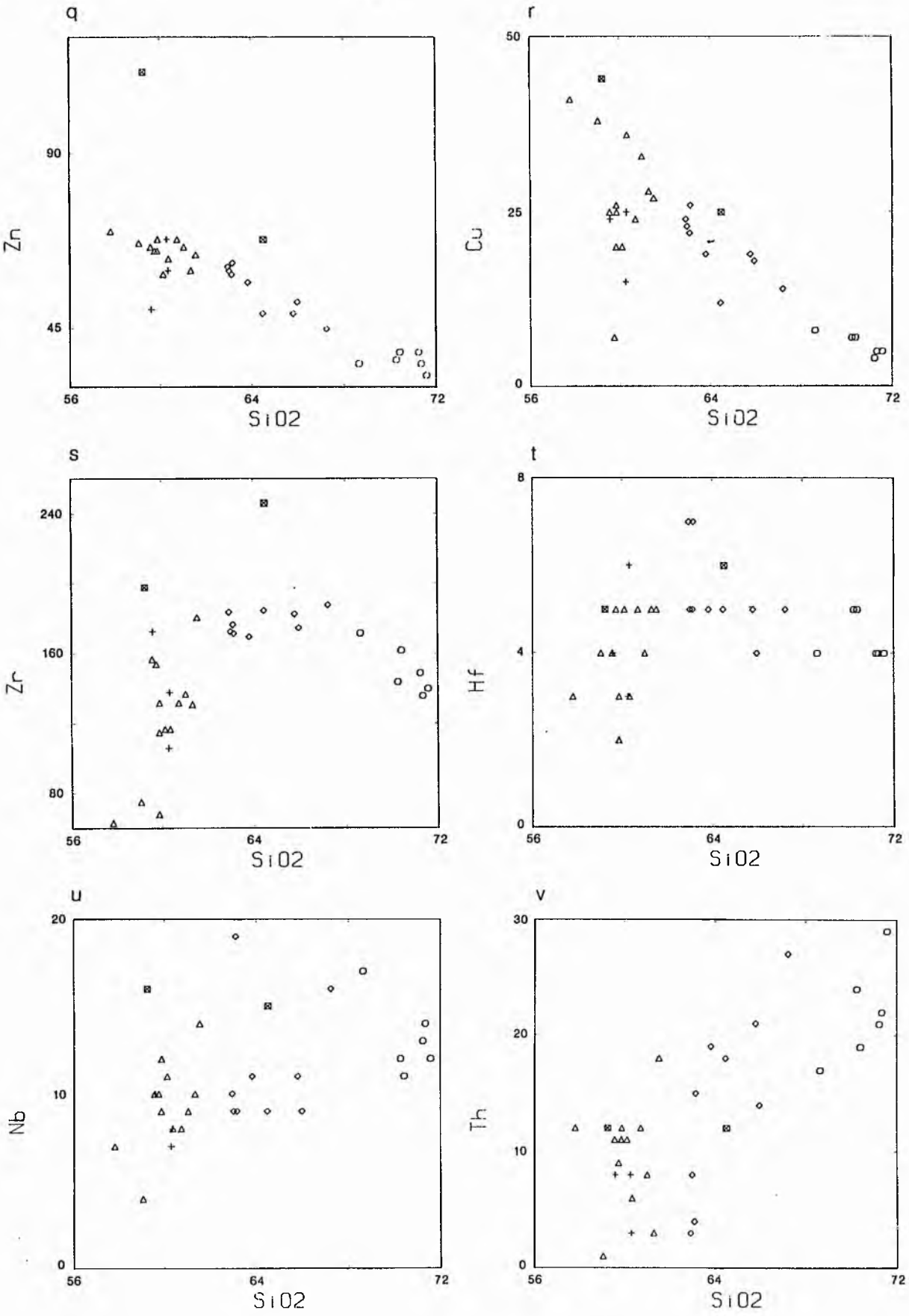

Figs 5.14$_{q-v}$ Harker variation diagrams of SiO_2 in wt % versus trace elements in the Loch Doon pluton.

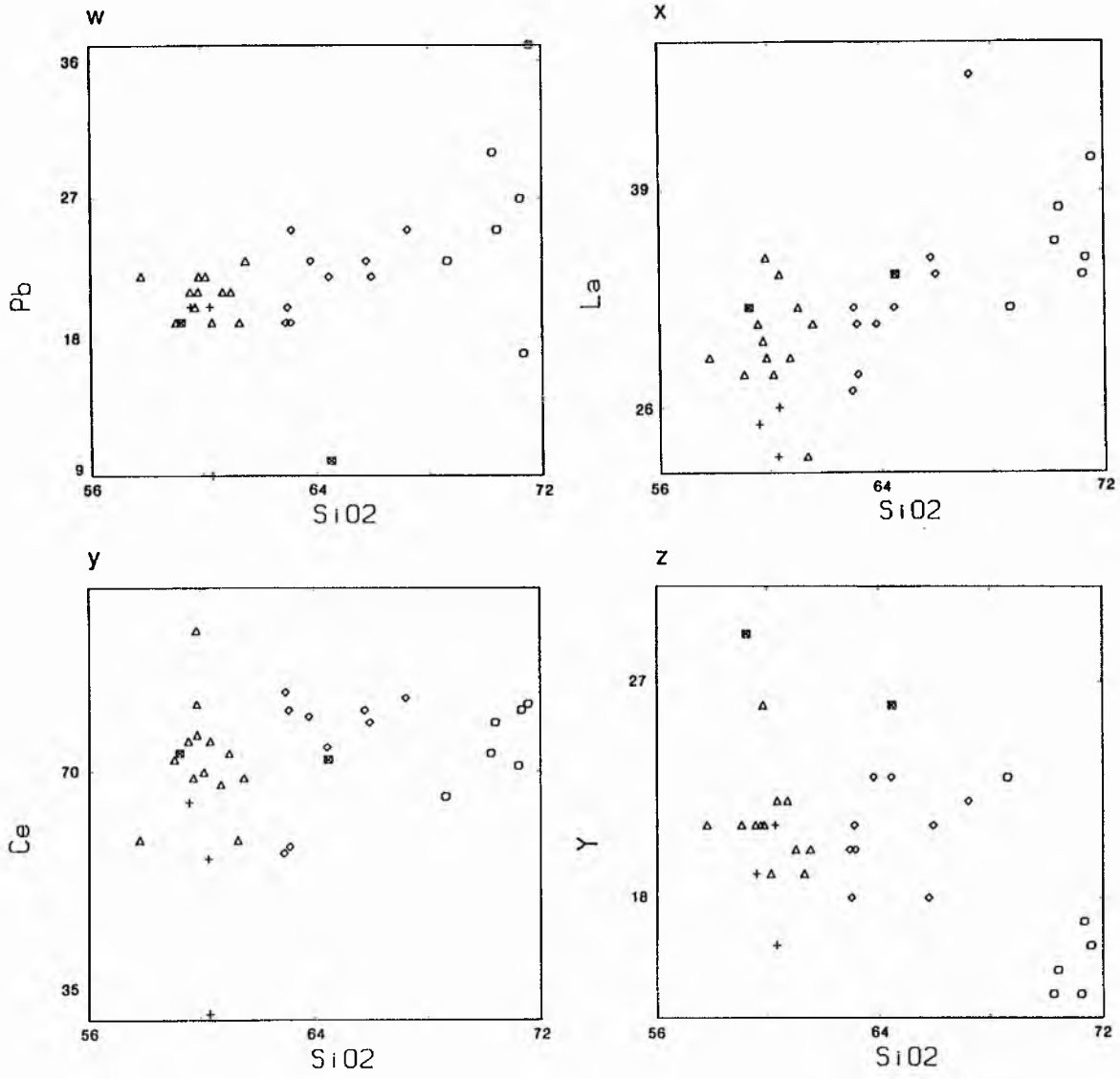

Fig 5.14$_{W-Z}$ Harker variation diagrams of SiO_2 in wt % versus trace elements in ppm for the Loch Doon pluton.

towards the granites reflecting the enrichment of Ba in early formed K-rich minerals like biotite (Taylor, 1965). Sr generally decreases with increasing SiO_2 though some diorites and microdiorites are anomalously depleted in Sr.

c) Zn decreases regularly towards the granites as does Cu which is rather more scattered.

d) Zr increases initially towards the tonalites and then decrease very slightly in the granodiorites and granites. Hf has a generally similar trend. Nb shows much scatter but generally increases with SiO_2.

e) Th generally increases with increasing SiO_2 as does Pb though less markedly.

f) La and Ce shows scattered trends slightly increasing towards the granites for La. Y also shows a scattered trend decreasing towards the granites.

Ni - Mg and Cr - Mg

Both show very good linear trends though with Ni enrichment at high (greater than 5%) MgO values (Fig. 5.15 a, b).

Rb - K

A curved relationship shows enrichment of Rb within the granites suggesting that Rb has remained incompatible within the melt (Fig. 5.15 c).

Ba - K

Ba is scattered with respect to K but shows a gradual decline above about 3% K_2O (Fig. 5.15d).

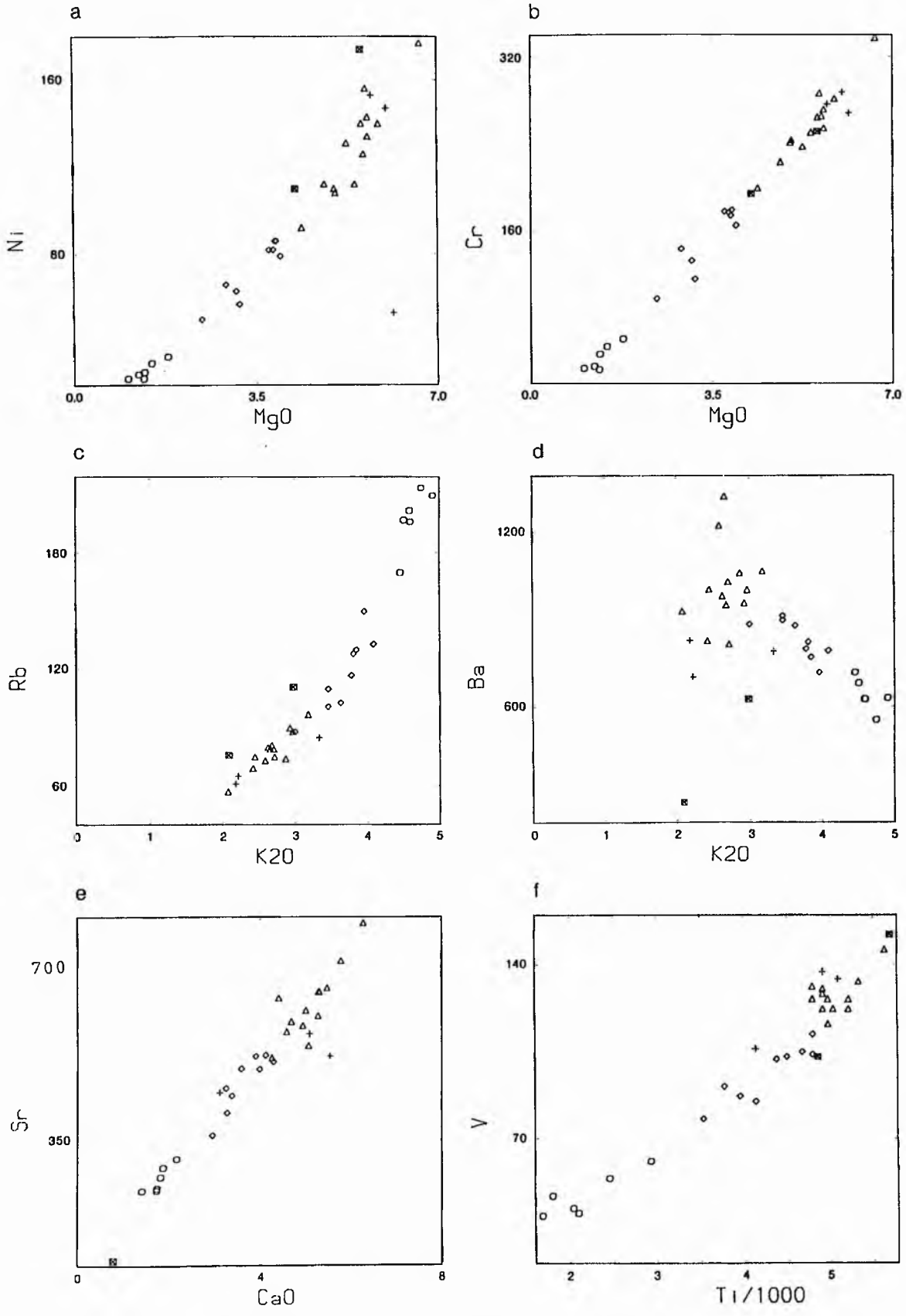

Fig 5.15$_{a-f}$ Variation diagrams for some major oxides (in wt %) and trace elements and Ti (in ppm) in the Loch Doon pluton.

Sr - Ca

The relationship is remarkably linear passing through the origin suggesting a strong plagioclase control on magma evolution (Fig. 5.15e).

Ti/1000 - V

This shows a good linear trend linking all the rock types (Fig. 5.15f).

K/Rb - SiO_2

The K/Rb ratios decrease systematically with SiO_2 from 165 in the microdiorite to 90 in the granite (Fig. 5.15g).

Rb/Sr - SiO_2

The Rb/Sr ratios vary systematically with increasing SiO_2 though slightly curved. Values exceeding 1.0 are not found even in the most evolved types (Fig. 5.15h).

Ce/Y - SiO_2

No systematic relationship is present but the ratios are high for the granites (Fig. 5.15i).

Chondrite - normalised abundances

Chondrite-normalised abundances show very similar patterns for all rock types evolving towards Rb, Th, La, Ce and K enrichment and Sr, P, Ti, Y depletion in the granites. There is marked parallelism for the most part but the granites depart from this trend suggesting a

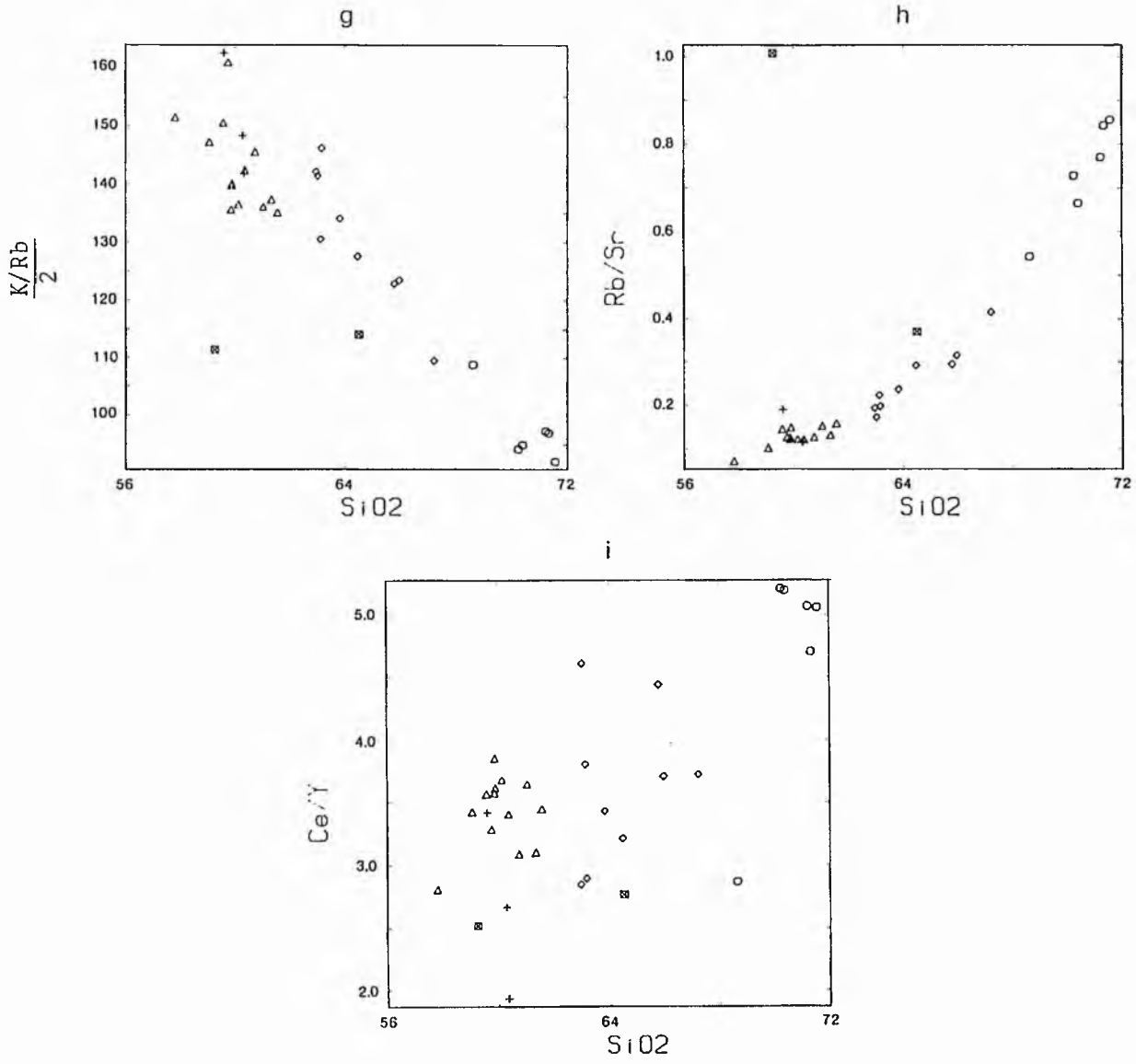

Figs 5.15 g-i Plots of SiO_2 versus some trace element ratios for the Loch Doon pluton.

potentially independent petrogenesis (Fig. 5.13b).

5.7.3 Summary

Whole-rock chemical data presented in previous sections demonstrate that the majority of samples analysed here fall on smooth and regular trends on the Harker variation and AFM diagrams.

Early scatter suggests possible cumulate effects, thereafter many trace elements show very good linear covariations even through to granite which may reflect protracted fractional crystallisation.

CHAPTER 6

PETROGENESIS OF INDIVIDUAL PLUTONS

6.1 Introduction:

6.1.1 Aims:

The aim of this chapter is to use the field, petrographic and chemical data to interpret the petrogenesis of each pluton. The whole-rock chemical data for the different plutons demonstrate that the majority of analysed samples fall on smooth and regular trends on Harker and AFM variation diagrams. Scatter within the more basic and ultrabasic members of the complexes in the region may be the result of cumulate and/or fractionation effects, and other "off-line" samples can usually be related to unusual petrographic or mineralogical features. Given that the various processes such as fractional crystallisation, multiple magma sources, magma mixing, and contamination through assimilation can give rise to similar major oxide trends, all available data are collated and used to assess the relative contributions of each potential process contributing to these evolutionary trends.

6.1.2 METHODOLOGY:

Firstly to bring together the previous information such as petrography, field relations, mineral chemistry, major and trace element geochemistry, and published work such as isotope geochemistry.

In this chapter major oxide and trace element trends have been modelled in an attempt to evaluate fractional crystallisation as a process in generating the observed variations. Major oxide modelling was used to evaluate magma mixing as well.

Fractional crystallisation modelling:

(a) Approach:

The approach taken was to examine whether model behaviour of major and trace elements approximate to observed variation by selection of parental magma, choice of fractionating minerals based on petrographic observation, of possible near-liquidus phases.

(b) Major oxide modelling:

Major oxide fractionation was modelled by "blending" proportions of observed mineral compositions with observed whole rock compositions. The method of "blending" rock analyses with mineral analyses is based on linear programming methods as described by Wright & Doherty (1970),

$$X_j = \sum_{i=1}^{n} b_i \, m_{ij}$$

where X is the whole rock major oxide composition

m are the mineral major oxide compositions.

b are the mineral proportions

i and j refer to the mineral and major oxide respectively where there are n minerals and k oxides.

The object of the method is to find values for b_i to give a composition of the blende of minerals that best fits the target whole rock major oxide composition and also conforms with a realistic fractionation model. When the sum of the squared deviations.

$$r^2 = \sum_{j=1}^{K} \left(\left(\sum_{i=1}^{n} b_i \, m_{ij} \right) - X_j \right)^2$$

is less than 1.0, the fit is deemed to be good and the model is accepted.

In each case the fractional crystallisation model was:

Parental liquid = Fractionated liquid + (fractionated x fractionated)
composition composition mineral wt mineral
proportion composition

for each oxide.

The parental magma was first selected on the basis of most-primitive but non-cumulate-textured composition and the residual liquid as a more evolved composition some 3 to 5 wt% SiO_2 along the series. The mineral analyses were actual microprobe analyses from the rock selected as the parental magma. The process was repeated by stepping through the series by successively making the parental liquid composition the residual liquid composition in 3-5 wt% SiO_2 intervals.

(c) Trace element modelling:

An independent test of the accuracy of the models described from major oxide modelling is the modelling of the consequent trace element evolution. The method used is that of equilibrium crystal fractionation, i.e. assuming equilibrium between total crystallisation solids and melt, and that the bulk distribution coefficient (D) does not change as crystallisation proceeds (Cox et al. 1979).

$$\frac{C_L}{C_0} = \frac{1}{F + D\ (1 - F)}$$

where C_L is the concentration of the trace element in the magma after fractional crystallisation, C_o is the initial concentration of the

trace element, D is the bulk distribution coefficient, and F is the fraction of melt remaining.

Bulk distribution coefficients were calculated using the equation:

$$D = \Sigma \; Wi \; KDi$$

where Wi is the weight fraction of the mineral i and KD is the partition coefficient for mineral i in the appropriate melt. Tables of partition coefficients have been compiled from the literature and values appropriate to the compositions studied here have been used and are tabulated in Appendix D.

6.1.3 Petrogenetic processes in the evolution of diorite-granite complexes:

In this chapter the petrogenesis of each pluton is discussed. It is appropriate here to describe some of the general models for petrogenesis of these types of calc-alkaline plutons, particularly with respect to compositional variation.

The close association of calc-alkaline magmas to active or recently active subduction is well known and current ideas relate to potential sources in subducted slab, the mantle wedge and the lower continental crust. Several origins have been suggested for the production of subduction-zone magmas, of which the most common are the following:

(1) Fractional crystallisation of high-Al_2O_3 tholeiite magma (Boettcher, 1973; Eggler & Burnham, 1973; Green & Ringwood, 1968).

2) Partial melting of wet ultramafic rocks in the upper mantle,

followed perhaps by fractional crystallisation (Kushiro, 1972; Nicholls & Ringwood, 1972).

3) Partial melting of upper-mantle and crustal rocks in subduction zones (Green & Ringwood, 1968; Wyllie 1973).

4) Subduction of oceanic crust with terrigenous sediments overlying mantle peridotite during final stages of closure between two continental lithospheric plates (Ringwood, 1974; McLennan & Taylor, 1980).

5) Mixing of mantle-derived basaltic magmas with sialic crustal rock or with felsic magmas (Eichelberger, 1975; Anderson, 1976; Eichelberger & Gooley, 1977).

6) Partial or complete melting of sialic crustal rocks (Wyllie, 1973, 1977, 1983; Winkler, 1976; Anderson, 1976).

Experimental phase equilibria have been determined concerning the suitability of different sources for generating parental magmas. Green and Ringwood (1968) considered many possibilities and indicated that andesite and more siliceous members of the calc-alkaline series can be produced by fractional crystallisation of high-Al_2O_3 tholeiite magma at depths of 35-100 km by removal of amphibole and clinopyroxene ($\pm$ plagioclase $\pm$ orthopyroxene) or at depths greater than 100 km by removal of garnet and clinopyroxene, and concluded that partial melting of basalt under hydrous condition was possible. Kushiro (1972) advocated direct partial melting of mantle peridotite under hydrous conditions stressing the role of water. Wyllie (1973) thought that thermal models of the crust together with experimental data indicate that felsic magmas can be produced by hydrous melting in orogenic segments of the crust at depths greater than 20 km. A contribution from both subducted oceanic crust and mantle peridotite

was postulated by Ringwood (1974). Wyllie et al. (1976) demonstrated that andesites are not primary magmas from subducted oceanic crust (requiring unrealistic water contents of 10-20 wt%), mantle peridotite or continental crust (requiring unrealistic temperatures of 1100 ^{o}C). Others have highlighted the importance of dehydration reactions in the subducted slab, resulting in either a generation of intermediate silicic magmas or a LIL - enriched fluid phase, this reacts with, or cause melting in the overlying mantle wedge (Brown, 1977; Ringwood, 1977). Sekine and Wyllie (1982a,b) concluded that even this combination will not directly produce andesite (dioritic) compositions and proposed that basaltic andesite is a more likely primary magma. This magma undergoes fractionation to produce the observed spectrum of calc-alkaline material. McLennan & Taylor (1980) stressed the role of subducted sediments in explaining some observed trace element patterns. Mixing of basic and acidic magma has been proposed by many authors (Eichelberger, 1975; Anderson, 1976; Eichelberger & Gooley, 1977) who found that evidence for mixing comes mainly from the recognition of disequilibrium (eg coexistence of olivine and quartz crystals each with pyroxene overgrowths), reverse plagioclase zoning, and incorporation of melt as glass inclusions in minerals (Gill, 1981). Eichelberger & Gooley (1977) mentioned the presence of mafic inclusions as basalt pillows in silicic magma with chilled margins as evidence of magma mixing. For plutonic rocks, the conditions are different and somewhat limited unless observation for liquid-liquid contacts can be seen, such as discrete pillows of mafic and intermediate rocks surrounded by more silicic rocks; chilling between mafic-silicic and intermediate silicic magmas such as in the net-veining complex of Ardnamurchan (Vogel, 1982).

Anderson (1976) pointed out that generating granitic magma by fractionation directly from basaltic composition is volumetrically unacceptable since only a small proportion of residual acid melt can be produced. Wyllie (1983) concluded that liquids with compositions corresponding to tonalite, diorite or andesite (including the mafic mineral components of these rocks) can be generated from crustal rock only if these are heated to temperatures at least 1100 ^{o}C or if they carry a large amount of restite in lower temperature melt, whereas batholiths composed largely of granite and granodiorite could be produced by crustal anatexis. He pointed out that in subduction zones magmas derived from subducted oceanic crust, or from mantle fluxed by fluids expelled from the crust should be considered.

Winkler (1976) argued that most granites result by anatexis of metasediments. Shales could generate up to 50% granite melt while greywacke could produced 70 or even 95%. The maximum temperature attained by anatectic melts is about 800 ^{o}C. At 2 Kb H_2O and 800 ^{o}C, a paragneiss could produced 84% melt and 16% restite including opaques, biotite and plagioclase of more anorthitic composition. The latter may disperse or remain as schlieren. A paragneiss was completely melted at 900 ^{o}C and 5 Kb PH_2O, generating a monzogranite composition. At lower temperature, 675 ^{o}C to 760 ^{o}C and 2 Kb PH_2O, the melt corresponds to alkali granite.

Wyllie (1977) found experimentally that the formation of water-undersaturated granite or granodiorite liquid can be produced from crustal rocks as a normal consequence of regional metamorphism but not diorite and tonalite. He pointed that significant contribution of heat and material from less siliceous magmas generated

in subducted oceanic crust and mantle peridotite is required for the formation of tonalite and diorite. Pitcher (1979) pointed out that neither the temperature nor the water content in the deep crust are sufficiently high to permit re-melting to occur, and found that in subduction-type mobile belts, remelting of the dehydrated, under-plated crust is unlikely to occur without the introduction of heat and water carrying magmas derived from sub-crustal sources.

A comprehensive review of andesite petrogenesis was given by Gill (1981) who concluded that orogenic andesites are generated by a variety of processes but principally by crystal fractionation of plagioclase, orthopyroxene/olivine, augite and magnetite (POAM) from a parental basaltic magma. Other factors like magma mixing, selective interaction with the crust, and vapour phase transfer are considered to be only local modifiers. It should be noted that the conclusions pertains to data from calc-alkaline volcanic rocks and the origin of granitic batholiths may be more complicated (Wyllie et al. 1976). Anderson (1982) pointed out that granodiorite and granite develop only in areas with thickened continental crust; Green (1980), suggested that tholeiitic magmatism predominates in orogenic areas until a thick crust is established, whereafter calc-alkaline suite magmatism develops. This association of tholeiitic and calc-alkaline rocks has been examined in detail by Kay et al. (1983) who concluded that crystallisation of essentially similar parental magmas under different physical conditions where the tholeiitic magma crystallises at higher temperatures, higher oxygen fugacity lower pressure and under less hydrous conditions than the calc-alkaline plutons to account for the observed chemical diversity in orogenic areas.

6.2 GARABAL HILL-GLEN FYNE

6.2.1 Introduction:

Using field, petrographic, mineral and whole rock chemical data the petrogenesis of this pluton is first considered in terms of fractional crystallisation models following the conclusions of Nockolds (1941).

6.2.2 Fractional crystallisation:

It is evident from petrography that olivine and pyroxene are early phases along with plagioclase feldspar, while biotite and amphibole are paragenetically later, with quartz and alkali feldspar last. The two pyroxene geothermometer of Wells (1977) indicated temperatures of 1080 ^{o}C for the gabbro and 1010 ^{o}C for the diorites. The $Mg^{\#}$ values for olivine decrease from 0.80 in the peridotites to 0.77 in the diorites; for orthopyroxenes from 0.74 in the gabbro to 0.72 in the diorites, while the $Mg^{\#}$ values of clinopyroxene is at its highest (0.83) in the peridotite decreasing to 0.76 in gabbros and diorites. Amphibole $Mg^{\#}$ values decrease from 0.73 in the gabbro to 0.65 in the medium granodiorite, though it increase slightly again towards the porphyritic granodiorite; while biotite have $Mg^{\#}$ values decrease from 0.63 in the gabbro to 0.54 in the quartz diorite, and then slightly increase to 0.58 in the granodiorite, which may reflect an effect of contamination or a magma of independent origin (Walsh, 1975). Generally the ferromagnesian minerals have high $Mg^{\#}$ values which is reflected in the Mg-rich trend observed on the AFM diagram (Fig 5.1j). This feature may suggest a rather high fO_2. Plagioclase ranges in composition from labradorite (An54) in the gabbro to

oligoclase (An24) in the granodiorite. These features indicate that crystal-liquid equilibria controlled the evolutionary sequence of ferro-magnesian minerals and that the various mafic-rich rock types of the pluton are related by a fractional crystallisation process from a parental magma, possibly of gabbroic composition. Peridotites, however, appear to be cumulates in petrographic and geochemical terms.

Examination of trace element variations within the pluton can also help to evaluate this hypothesis; the general depletion of Ni and Cr with Mg are attributable to removal of olivine and pyroxene. Initially increasing Sr with SiO_2 (Fig 5-1p) suggests that fractionation of mafic minerals (eg pyroxene) greatly predominated over plagioclase below 54% SiO_2. Increasing of Y towards diorites and its decreasing in the granodiorites probably reflects amphibole fractionation in the later stages (Arth and Barker, 1976). The observed Nb depletion in the normalised trace element plots (Fig 5.3a) is characteristic of subduction-related rocks (Thompson et al. 1984). REE patterns (Fig 5.3c) show that REE become more enriched with increasing SiO_2 (the REE increase from the gabbroic rocks at 68 to 130 in the porphyritic granodiorites). Fractionation of clinopyroxene which has a KD of less than one for all REE could in combination with plagioclase enrich all REE except Eu in the residual liquid (Whalen, 1985) while accessory apatite and sphene have KD's much greater than one for the REE and will deplete them in the melt if they are removed during fractional crystallisation (Hanson, 1980).

Fractionation of accessory mineral phases can have a major effect on magma composition, especially certain minor and trace elements. P_2O_5 increases initially towards 58% SiO_2 and decreases

towards the granodiorite (Fig 5-1h) indicating that P has been concentrated in the quartz diorites (hornblende biotite diorites) followed by the fractionation of apatite, a phase which tends to concentrate the middle REE (Whalen, 1985; MREE Sm-Ho). Fractionation of zircon, a HREE and Th enriched mineral, may explain the depletion of these elements along with Zr in the granodiorite, while the fractionation of Fe-Ti oxides could be responsible for decreasing V.

6.2.3 Composition modelling:

6.2.3a Major oxide modelling

The initial starting magma composition for the Garabal Hill-Glen Fyne was taken as equivalent to sample GH10, a gabbro with primary igneous texture interpreted as a crystallised melt texture.

The results of modelling are given in Table 6.1a and indicate that:

(a) Gabbro is a suitable parental magma composition with low residuals Σr^2 being less than 1.0

(b) Orthopyroxene is required to be removed in decreasing amounts as far as 57% SiO_2.

(c) Clinopyroxene is removed in increasing amounts as far as 57% SiO_2

(d) Plagioclase fractionation is dominant and changes to more albitic compositions with fractionation.

(e) Magnetite is removed in increasing amounts as far as 57% SiO_2, while ilmenite is removed in decreasing amounts.

(f) Apatite is removed in increasing amounts as far as the medium granodiorite (GH28).

(g) Fractionation of amphibole of magnesio-hornblende composition

is required to form the medium granodiorite.

(h) Biotite is removed in increasing amounts in fractionation.

In the absence of isotopic information, the data presented here is consistent with in situ fractional crystallisation of a magma approximating to pyroxene biotite gabbro. This was the dominant process for most of the series except for the porphyritic granodiorite (Table 6.1a) where the fractionation scheme was unable to produce a suitable fit. The genesis of the granodiorite will be discussed in the last section of this chapter.

The high Mg and Ni contents of the pyroxene gabbros and diorites appear to be products of a mantle-derived parental magma (Halliday & Stephens, 1984). These rocks have uniform $^{87}Sr/^{86}Sr$ initial ratios with an average of 0.705 (Summerhayes, 1966) though precision of this technique was not high.

The ultrabasic (peridotite) and brown amphibole gabbroic rocks may have originated by crystal accumulation from the same parental magma, either by crystal settling or side wall accumulation. Field evidence is required.

6.2.3b Trace element modelling:

Trace element modelling has been attempted using the proportion of minerals removed in the major oxide modelling, as a test of the fractionation model proposed in the above section. The method used was outlined in section 6.1.2c and the results are presented in Table 6.1b. The following conclusions are taken from this table.

a) The agreement between observed and modelled trace element

Table 6.1a: Summary of major oxide modelling of fractionation of bulk rock compositions of Garabal Hill-Glen Fyne pluton using the method of Wright & Doherty (1970).

	Biotite pyroxene gabbro		Biotite pyroxene diorite		Hornblende biotite diorite		Medium granodiorite	
	GH10	(GH10)	GH3	(GH3)	GH27	(GH27)	GH28	(GH28)
SiO_2	51.93	51.93	54.43	54.43	57.15	57.15	64.95	64.95
TiO_2	1.31	1.31	1.12	1.12	0.91	0.82	0.60	0.60
Al_2O_3	13.52	13.52	15.03	15.03	16.20	16.20	15.79	15.79
FeO*	8.70	8.70	7.71	7.71	6.22	5.72	3.49	3.49
MnO	0.24	0.15	0.16	0.13	0.12	0.13	0.09	0.10
MgO	10.59	10.59	7.38	7.38	5.42	5.42	2.75	2.75
CaO	8.06	8.06	7.89	7.89	5.28	5.28	3.90	3.90
Na_2O	2.50	2.46	3.69	3.19	4.11	3.73	4.59	4.21
K_2O	1.33	1.33	1.88	1.88	2.86	3.06	3.11	3.11
P_2O_5	0.14	0.14	0.21	0.21	0.26	0.26	0.26	0.26
Total	98.32	98.19	99.60	98.97	98.53	97.77	99.53	99.16
r^2		0.008		0.25		0.44		
residual liquid	(GH3)	29.67	(GH27)	36.89	(GH28)	42.48	(GH29)	no successful model
orthopyroxene		19.02		6.88		-		
clinopyroxene		13.87		17.01		-		
amphibole		-		-		15.56		
biotite		7.71		7.03		15.64		
plagioclase		27.42		30.38		26.32		
magnetite		0.28		1.58		-		
ilmenite		1.03		0.79		-		
apatite		0.19		0.27		0.42		
alkali feldspar		-		-		-		
quartz		-		-		-		
cumulate total		69.52		63.94		57.94		
cumulate composition		Gabbro		Pyroxene biotite diorite		Hornblende biotite diorite		

Table 6.1b: Summary of results of fractional crystallisation modelling of trace elements in the Garabal Hill pluton.

Sample No	GH10	GH3 modelled	GH3 actual	GH27 modelled	GH27 actual	GH28 modelled	GH28 actual
Rb	35	56	54	104	102	127*	87
Ba	230	260*	380	542	590	468*	798
Sr	435	510	507	588	586	660	679
Nb	9	10	10	13*	10	7*	13
Zr	70	134	104	222*	139	224*	163
Y	18	21	24	19	19	13	16
La	8	18	17	24	23	48	27
Ce	20	41	35	41	44	63	50
Cr	543	79*	224	26*	243	40*	99
Ni	208	75	84	32	105	41	42

% of minerals removed	70%	65%	58%
olivine	0	0	0
orthopyroxene	19	7	0
clinopyroxene	14	17	0
amphibole	0	0	15
biotite	8	7	16
plagioclase	28	31	27
spinel	1	2	0
apatite	0.2	0.3	0.4
zircon	0	0	0

* Indicates values from modelled compositions which reflect either trends opposite to those actually observed, or estimates which differ very greatly from those observed.

concentrations is generally good except for Cr and occasionally Zr, Nb, Ba and Rb.

b) The inability to model Cr probably reflects the modelling of pyroxenes and amphiboles. Modelled compositions are always much more depleted in Cr than the observed compositions. This suggests that KD values for Cr are too high for this pluton. Values of 30 for clinopyroxene, 13 for orthopyroxene and 30 for amphibole were used, in all cases lower KD values have been quoted in the literature and would have improved these results.

c) Modelling of Ba was somewhat unsuccessful, modelled compositions always being much lower than observed. This may be ascribed to the KD of 6.4 in biotite, values as low as 3 have been quoted in the literature.

d) Modelling of Zr and Nb is at least partly affected by accessory phases which were not all allowed for in this major oxide-based model.

e) For the most part agreement between the major oxide modelling and trace element modelling (both undertaken independently) was sufficiently close to support the main conclusion of the major oxide model, namely that a gabbroic parental magma fractionated orthopyroxene, clinopyroxene, plagioclase and biotite to give a series of diorites. The hornblende biotite diorite then fractionated plagioclase, amphibole and biotite to give a granodiorite. This last conclusion is tenuous in view of the Sr and Nd isotope evidence for the granodiorite (Halliday 1984) indicating that it has also suffered crustal contamination.

6.3 COMRIE

6.3.1 Introduction

Ortho- and clinopyroxene with plagioclase are early phases, while biotite and amphibole tend to be rather late. The calculated crystallisation temperature for two pyroxenes in the two-pyroxene diorite is 980 °C (sample CM10) using the geothermometer of Wells (1977), while the quartz monzodiorites equilibrated at lower temperature of about 940 °C. The $Mg^{\#}$ values for orthopyroxene decrease from the diorites (0.65 to 0.69) through quartz monzodiorites (0.57), while for clinopyroxene they range from 0.70 to 0.78 in the diorites down to 0.67 in the quartz monzodiorites. Amphibole $Mg^{\#}$ values decrease from 0.70 in the diorite to 0.62 in the quartz monzodiorite though increase in the granodiorites (0.65). For biotites, the $Mg^{\#}$ values decrease from 0.65 in the two-pyroxene biotite diorite to 0.57 in the granodiorite. Plagioclase ranges from An_{50} in diorite to An_{24} in granite. These data suggest an evolving magma system with falling temperature and increasing Fe/Mg, compositional variation probably being controlled by fractional crystallisation.

Trace element abundances within this pluton indicate a general depletion of Ni and Cr with Mg (Fig 5.5a,b) reflecting the removal of pyroxene. The linear relationship between Sr and Ca (Fig 5.5e) reflects plagioclase removal particularly from the diorites and quartz monzodiorites. The behaviour of Rb and Ba suggests the involvement of biotite in the later stages of fractionation (Fig 5.4n,o). Increasing of Y (Fig 5.4z) towards quartz monzodiorite and its decreasing towards the granodiorites and granites probably reflects amphibole fractionation in the latter stages (Arth and Barker, 1976). The

observed Nb depletion (Fig 5.3b) is characteristic of subduction-related rocks (Thompson et al. 1984). The relationship between P_2O_5 and SiO_2 (Fig 5.4f) and modelling results indicate that P has been concentrated though not systematically in the early stages, reflecting fractionation of apatite. Fe-Ti oxides fractionation may be responsible for decreasing the V contents of the more evolved rocks (Fig 5.4m).

6.3.2 Composition modelling:

Taking the initial starting liquid composition as two-pyroxene biotite diorite sample CM10, major and trace element modelling was attempted.

6.3.2a Major oxide modelling:

Results obtained from modelling sample CM10 are given in Table 6.2a. Two-pyroxene biotite diorite is a suitable parental magma composition for the generation of most of the rock types of this pluton giving a good fit, with the Σr^2 residuals less than 1.0. The following conclusions are drawn:

a) Orthopyroxene is removed only at low SiO_2, as far as diorite.

b) Clinopyroxene is removed in decreasing amounts up to 64% SiO_2.

c) Plagioclase fractionation is dominant, decreasing in amount but becoming more albitic with increasing SiO_2.

d) Magnetite and ilmenite are required as fractionating phases as far as granodiorite.

e) Apatite must be removed as far as granodiorite.

f) Amphibole does not appear to be important in this model. Biotite

Table 6.2a: Summary of major oxide modelling of fractionation of Comrie

	Pyroxene biotite diorite		Quartz monzodiorite		
	CM10	(CM10)	CM25	(CM25)	(CM28)
SiO_2	55.05	55.05	59.66	59.66	65.26
TiO_2	1.27	1.27	1.22	1.22	0.73
Al_2O_3	16.22	16.22	16.29	16.29	15.46
FeO*	7.14	7.14	5.82	5.82	3.81
MnO	0.17	0.11	0.07	0.10	0.06
MgO	6.18	6.18	3.14	3.14	2.14
CaO	7.05	7.05	4.88	4.88	3.06
Na_2O	3.86	4.02	4.26	3.66	3.92
K_2O	2.08	2.08	3.62	3.62	4.09
P_2O_5	0.31	0.31	0.41	0.31	0.25
Total	99.33	99.43	99.95	98.7	98.78
Σr^2		0.03		0.82	
residual liquid	(CM25)	27.64	(CM28)	63.73	
orthopyroxene		8.96		-	
clinopyroxene		10.89		2.97	
amphibole		-		-	
biotite		9.96		10.34	
plagioclase		40.61		20.75	
magnetite		1.03		1.06	
ilmenite		0.85		0.42	
apatite		0.47		1.98	
alkali		-		-	
feldspar		-		-	
quartz		-		-	
cumulate total		72.77		37.52	
cumulate composition		Pyroxene biotite diorite		Biotite diorite	

removal is required as far as granodiorite.

The proposed initial magma gave a good fit to produce compositions as far as granodiorite. Modelling was limited to the granodiorite as granitic samples were not considered to be sufficiently pristine to reflect original major oxide compositions.

6.3.2b Trace element modelling

Results of modelling are presented in Table 6.2b. The following are concluded from these results.

a) The agreement between observed and modelled trace element concentrations is generally good except for Cr, La, Ce and occasionally Ba and Y.

b) The inability to model Cr probably reflects the modelling of pyroxenes and amphiboles. Modelled compositions were always more depleted in Cr than the observed compositions. This suggests that KD values for Cr are too high for this pluton. KD values are the same as used for modelling each pluton in the present study (cf Garabal Hill) and may be too high for these compositions.

c) Modelling of La and Ce probably reflects the behaviour of accessory phases and biotites. Modelled compositions were much higher than observed compositions. This suggests that the bulk distribution coefficients for La, and Ce are too low for this pluton and reflects further involvement of accessory phases. In all cases higher KD values have been quoted in the literature.

d) Modelling of Y from the quartz monzodiorite to granodiorite yields higher than observed values which may in part be due to the KD value of 30 used for apatite, values up to 40 have been quoted in the literature and would have improved these results.

Table 6.2b: Summary of results of fractionation modelling of trace elements in the Comrie pluton.

Sample No	CM10	CM25	CM25	CM28	CM28
	actual	modelled	actual	modelled	actual
Rb	52	115	113	133	156
Ba	670	1069	1066	886*	702
Sr	666	592	537	477	448
Nb	9	15	17	15	20
Zr	139	363	420	291	298
Y	23	30	34	48*	24
La	30	49*	41	68*	37
Ce	72	127*	90	98*	69
Cr	232	45*	66	37*	53
Ni	118	59	39	37	30

% of minerals removed	72%	37%
orthopyroxene	9	0
clinopyroxene	11	3
amphibole	0	0
biotite	10	10
plagioclase	40	21
spinel	2	2
apatite	0.5	1
zircon	0	0

* Indicates values from modelled compositions which reflect either trends opposite to those actually observed, or estimates which differ very greatly from those observed.

e) Modelling of Ba from the quartz monzodiorite to granodiorite is higher than observed. This may be due to the KD of 6.4 in biotite, values up to 36 have been quoted in the literature and may again have improved the modelled results.

f) For the most part agreement between the major oxide modelling and trace element modelling was sufficiently close to support the main conclusion of the major oxide model, namely that a pyroxene biotite diorite parental magma fractionated orthopyroxene, clinopyroxene, plagioclase and biotite to give rise to quartz monzodiorite. The quartz monzodiorite then fractionated clinopyroxene, plagioclase and biotite to give a granodiorite.

6.4 GLEN DOLL

6.4.1 Introduction

This pluton lies in the eastern Grampian Highlands and differs petrographically from the Garabal Hill-Glen Fyne and Comrie plutons in containing essential amphiboles in the ultrabasic, basic and intermediate rocks. Olivine, pyroxene, green amphibole and plagioclase are early minerals. Brown amphibole is late in the rock found poikilitically enclosing olivine and pyroxene. Phlogopite is present in the ultrabasic rocks. Biotites are commonly interstitial.

From the mineral chemistry the calculated equilibration temperature for two pyroxenes in the pyroxenite is 980 ^{o}C, for gabbronorite is 970 ^{o}C, and in quartz gabbro 960 ^{o}C using the equation of Wells (1977). The Mg$^{\#}$ value for olivine is 0.78, for clinopyroxene it ranges from 0.84 in the pyroxenite to 0.69 in the granodiorite, for orthopyroxene it ranges from 0.82 in the pyroxenite

to 0.73 in the quartz gabbro. $Mg^{\#}$ values of amphibole range from 0.88 for the green amphibole in the pyroxenite to 0.60 in the granodiorite, $Mg^{\#}$ in mica varies from 0.84 for the phlogopite in the pyroxenite to 0.64 in biotite from the granodiorite. Plagioclase ranges in composition from bytownite (An82) in pyroxenite to oligoclase (An24) in granodiorite.

Whole-rock chemical data indicate rather scattered variation trends and high Fe-enrichment on the AFM diagram (Fig 5.6j) relative to other calc-alkaline trends.

6.4.2 Fractional crystallisation modelling:

Major and trace element compositions were modelled to evaluate fractional crystallisation as a process in generating the observed variations. The hornblende gabbro was taken as the parental magma composition (sample GD11).

6.4.2a Major oxides modelling

Fractional crystallisation modelling of hornblende gabbro fits quite well. Results are given in Table 6.3a and indicate the following:

a) Amphibole of magnesio-hornblende composition is needed to be removed in decreasing amounts to form the series as far as tonalite.

b) Plagioclase is an important fractionating phase and tends to decrease in amount and becomes more albitic with increasing SiO_2.

c) Magnetite is removed in increasing amounts, while ilmenite is also required to be removed to form tonalite.

d) Apatite is needed to be removed from about 54% SiO_2.

e) Biotite is required to be removed at low SiO_2 levels as far as

Table 6.3a: Summary of results of major oxide modelling of fractionation of Glen Doll.

	Hornblende gabbro		Hornblende biotite diorite		Tonalite	
	GD11	(GD11)	GD37	(GD37)	GD51	(GD51)
SiO_2	50.69	50.69	53.75	53.75	56.79	56.79
TiO_2	1.45	1.45	2.19	2.19	1.85	1.85
Al_2O_3	16.65	16.65	16.04	16.04	16.57	16.57
FeO*	9.26	9.26	9.83	9.83	7.80	7.80
MnO	0.12	0.11	0.16	0.14	0.08	0.15
MgO	6.54	6.54	4.32	3.84	3.36	3.36
CaO	9.81	9.17	7.38	7.38	5.09	5.09
Na_2O	2.60	3.06	2.97	3.39	3.55	2.42
K_2O	1.21	0.76	1.55	1.62	3.72	2.42
P_2O_5	0.36	0.28	1.10	1.10	1.77	0.98
Total	98.69	97.98	99.30	99.28	100.58	97.43
Σr^2		0.82		0.42		no successful model
Residual liquid		(GD37)32.50		(GD51)58.83		(GD40)
amphibole		32.78		17.26		
biotite		5.10		0.00		
plagioclase		28.94		20.32		
magnetite		0.65		1.80		
ilmenite		-		1.85		
apatite		-		1.25		
alkali feldspar		-		-		
quartz		-		-		
cumulate total		67.47		42.48		
cumulate composition		Hornblende gabbro		Hornblende diorite		

hornblende biotite diorite.

Fractional crystallisation modelling of gabbro (GD11 taken as an alternative parental magma) also gave a good fit to form the series as far as tonalite but failed to form the granodiorite.

Meighan and Neeson (1979) studied the Newry complex in Northern Ireland which contains ultramafic rocks including olivine biotite pyroxenite. They described melting experiments which indicate that this rock type has a high liquidus temperature at 1 Kb (about 1310 ^{o}C), falling to 1200 ^{o}C at 3 Kb under water - saturated conditions. They concluded that these were not magmatic compositions but formed by crystal accumulation from intermediate magmas. In Glen Doll, the pyroxenites contain olivine, two pyroxenes, amphibole and small amount of phlogopite, so the liquidus temperature is likely to be of the same order as that of the Newry pyroxenite and the conclusion of Meighan and Neeson (1979) for the Newry complex is also applicable to the pyroxenites of Glen Doll. These pyroxenites may have formed by side wall accumulation.

6.4.2b Trace element modelling

Results of modelling are presented in Table 6.3b and the following are concluded from these results.

a) The agreement between observed and modelled trace element concentrations is generally good except for Cr, Nb, Y and Ce and occasionally Ba and Zr.

b) Modelled abundances of Cr are always lower than observed compositions, and may reflect amphibole modelling. This suggests that KD values of Cr are too high for this pluton. Values of 30 for amphibole was used, though values down to 12 have been quoted in the

Table 6.3b: Summary of results of fractional crystallisation modelling of trace elements in the Glen Doll pluton.

	GD11	GD37 modelled	GD37 actual	GD51 modelled	GD51 actual
Rb	20	44	43	67	66
Ba	189	300	343	505*	606
Sr	543	570	601	551	541
Nb	2	2*	9	12*	17
Zr	49	108	140	212*	140
Y	14	8*	34	27*	40
La	7	18	15	23	39
Ce	19	46*	103	120*	179
Cr	80	7*	26	6*	19
Ni	9	3	4	2	4

% of minerals removed	68%	41%
olivine	0	0
orthopyroxene	0	0
clinopyroxene	0	0
amphibole	32	17
biotite	5	0
plagioclase	30	20
spinel	1	3
apatite	0	1
zircon	0	0

* Indicates values from modelled compositions which reflect either trends opposite to those actually observed, or estimates which differ very greatly from those observed.

literature and would have improved the results.

c) Modelling of Ce and Y is affected by accessory phases like apatite for both elements and sphene for Ce which were not allowed for in this major oxide-based model and which describe only the behaviour of the principal minerals.

d) Modelling of Nb gave lower values than those observed. This may be due to a KD value of 6.0 for biotite, values down to 3 have been quoted in the literature.

e) Modelling of Ba from the hornblende biotite diorite to tonalite gives lower abundances than those observed which may be due to the KD of 6.4 in biotite, values down to 3 have been quoted in the literature.

f) The agreement between major oxide and trace element modelling was otherwise sufficiently close to support the main conclusions of the major oxide model, namely that a gabbroic parental magma fractionated amphibole, plagioclase and biotite giving rise to hornblende biotite diorite. The hornblende biotite diorite fractionated amphibole and plagioclase to give tonalite.

6.4.3 Discussion:

In fractional crystallisation terms, amphibole plays a dominant role in the, basic to intermediate series. The trend on the AFM diagram (Fig 5.6j) shows greater Fe-enrichment than the other calc-alkaline plutons. In the calc-alkaline series the chemical evolution trend is strongly influenced by fO_2 (Osborn, 1959). When fO_2 is constant or high during crystallisation magnetite crystallises from basic magmas along with olivine and subsequently with pyroxene depleting the residual liquid in Fe and enriching it in Si.

Experimental data discussed by Gill (1981) indicates that H_2O contents of greater than 3 wt% in the melt are necessary for amphibole to precipitate (Gill, 1981). Thus moderate H_2O contents are necessary for calc-alkaline suites bearing early amphibole, which in turn has an effect on the fO_2 of the magma during crystallisation.

In high-Fe calc-alkaline series crystallisation of iron oxides may have been delayed and/or the mafic silicate minerals are relatively magnesian enriching Fe in the residual liquids (Kuno, 1968). According to Osborn (1962, 1969, 1976, 1979), who argued from experimental determinations of phase equilibria, crystallisation of basalt or andesite leads to absolute iron-enrichment in the liquid until (and sometimes even after) magnetite saturation occurs. Less relative iron enrichment occurs after magnetite saturation.

6.5 GLEN TILT

6.5.1 Introduction

This pluton in the eastern Grampian Highlands intrudes Moinian metasedimentary rocks. It is composed petrographically of diorites (hornblende biotite diorite), appinitic diorites, quartz diorites (with biotite the main mafic mineral), granodiorites and biotite granites. From the petrography it is evident that plagioclase was an early crystallising phase, as was clinopyroxene. Biotite, alkali feldspar and quartz are late stage interstitial phases. $Mg^{\#}$ values of amphibole decrease from 0.71 in the diorite (GT28) to 0.65 in some appinitic diorites, while $Mg^{\#}$ values of biotite decrease from 0.63 in the diorite to 0.50 in the granite. Amphibole is exclusively calcic of magnesio-hornblende composition. Plagioclase ranges from (An50) in

the diorite down to albite (An6) in the biotite granite.

The rocks are chemically calc-alkaline to high-K calc-alkaline (Fig 5.9g). The diorites are high in Ni and Cr (about 110 ppm and 260 ppm respectively) reflecting a probable mantle-derived magma. Some appinitic diorites contain the highest Cr and Ni concentrations (about 500 ppm and 180 ppm respectively) reflecting probably original clinopyroxene abundances. The appinite bodies accordingly are thought to be genetically related to the mafic diorite (Groome and Hall 1974). The quartz diorites, granodiorites and biotite granites show trends of enrichment in Th, Zr, K and Rb and depletion in Nb, P, Ti and La (Fig 5.8b)

6.5.2 Composition modelling:

6.5.2a Major oxide modelling

Sample GT28 was taken as the parental composition liquid, but it failed to yield a close fit to the target of quartz diorite composition. The diorites and quartz diorites may therefore have independent origins.

Major oxide modelling succeeded in generating granodiorite from quartz diorite by removal of biotite and plagioclase in decreasing amounts along with Fe-Ti oxides and apatite. Results are given in Table 6.4a, however no successful model was obtained to form the biotite granite (sample GT48) from the assumed parental quartz diorite.

6.5.2b Trace element modelling

Results of modelling are presented in Table 6.4b, the following points are concluded from these results:

Table 6.4a: Summary of major oxide modelling of fractionation of bulk rock compositions of Glen Tilt.

	Hornblende biotite diorite		Quartz diorite		Granodiorite		Granodiorite	
	GT28	(GT28)	GT47	(GT47)	GT41	(GT41)	GT33	(GT33)
SiO_2	54.91	54.91	58.65	58.65	54.84	65.84	70.53	70.53
TiO_2	1.36	1.21	1.21	1.21	0.65	0.65	0.52	0.52
Al_2O_3	13.64	13.64	18.65	18.65	16.97	16.97	15.66	15.66
FeO*	8.29	7.15	6.09	6.09	3.50	3.50	3.10	3.10
MnO	0.24	0.13	0.08	0.10	0.06	0.06	0.06	0.06
MgO	8.41	8.41	2.11	2.32	1.70	1.56	1.33	1.33
CaO	8.92	8.92	5.21	5.21	2.82	2.82	2.06	2.06
Na_2O	3.00	2.20	4.89	4.89	4.87	4.87	4.01	4.00
K_2O	1.37	1.31	2.62	2.23	2.51	2.59	4.79	2.57
P_2O_5	0.25	0.33	1.15	0.33	0.54	0.33	0.84	0.33
total	100.39	98.21	100.66	99.68	99.46	99.19	102.87	100.16
r^2		no successful model		0.87		0.07		no successful model
residual liquid	(GT47)		(GT41)	54.91	(GT33)	70.07	(GT48)	
amphibole				-		-		
biotite				11.73		6.68		
plagioclase				30.44		21.88		
magnetite				1.43		0.06		
ilmenite				0.87		0.08		
apatite				2.43		1.00		
alkali feldspar				-		-		
quartz				-		-		
cumulate total				46.90		29.70		
cumulate composition				Biotite diorite		Biotite diorite		

Table 6.4b: Summary of results of fractional crystallisation modelling of trace elements in the Glen Tilt pluton.

Sample No	GT47 actual	GT41 modelled	GT41 actual	GT33 modelled	GT33 actual
Rb	72	120*	66	68	63
Ba	489	738	742	590*	446
Sr	784	675	624	578	556
Nb	16	22*	7	6*	13
Zr	282	467*	250	317*	266
Y	29	23	17	16	12
La	31	51	66	90*	36
Ce	75	85*	122	128*	111
Cr	14	4*	15	10	13
Ni	9	6*	21	19	17

% of minerals removed	46%	30%
olivine	0	0
orthopyroxene	0	0
clinopyroxene	0	0
amphibole	0	0
biotite	12	71
plagioclase	31	22
spinel	2	0
apatite	1	1
zircon	0	0

* Indicates values from modelled compositions which reflect either trends opposite to those actually observed, or estimates which differ very greatly from those observed.

a) Generally speaking there is a good agreement between observed and modelled trace element concentrations except for Rb, Nb, Zr and Ce; and occasionally Ba, Cr and Ni.

b) Modelled compositions of Rb are higher than observed compositions which may reflect the modelling of biotite. This suggests that KD values of 3.0 for biotite are low for this pluton, values up to 4.0 have been quoted in the literature.

c) The inability of modelling to fit Nb and Zr abundances to observed compositions probably reflecting the modelling of biotite and zircon. Zircon was not included in this major oxide-based model.

d) Modelling of Ce gave much lower compositions than the observed ones indicating perhaps that KD of 30 for apatite in this pluton is a little high.

e) Cr and Ni modelling gives depletions relative to the observed compositions, probably reflecting overestimated KD values of 30 for amphibole.

f) Generally speaking the agreement between major oxide modelling and trace element modelling was sufficiently close to support the main conclusion of the major oxide model, namely that a quartz diorite parental magma fractionated biotite and plagioclase to give rise to granodiorites.

6.5.3 Discussion

Petrochemical modelling suggested that quartz diorites and granodiorites can be linked through crystal fractionation. In situ fractionation of a single intrusive pulse of magma would be expected to yield smooth gradations of rock types and gradual changes in bulk-rock and mineral chemistry. From the data presented in earlier

chapters, together with attempted modelling, such a simple model does not seem appropriate and there are abrupt changes between granodiorites and granites (Fig 5.9) so the granites may represent a separate pulse of magma.

6.5.4 Multiple intrusion model

An alternative model of multiple intrusion of magma pulses from different sources with subsequent differentiation could account for the abrupt changes in the trace element ratios (eg K/Rb, and Rb/Sr, Figs 5.10g,h).

In this pluton the diorites are forming small amount relative to the granodiorites and granites and with no evidence of concentric zoning, so there is a good evidence that the rock types represent discrete pulses of magma. Though petrochemical modelling succeeded to fractionate granodiorites from a quartz diorite parental magma.

6.6 CAIRNSMORE OF CARSPHAIRN

6.6.1 Introduction

This small pluton intrudes Lower Palaeozoic sediments of the Southern Uplands. The complex is composed of early microdiorite, tonalite, granodiorite and granite in generally concentric arrangements. The tonalites are medium grained, composed of early orthopyroxene, clinopyroxene, plagioclase and biotite with late alkali feldspar and quartz. Granodiorite on the other hand is composed essentially of amphibole, biotite, plagioclase with late orthoclase and quartz. The central granite contains only minor amphibole and biotite in addition to the felsic minerals.

The equilibrium temperature for the crystallisation of two coexisting pyroxenes in the tonalite is 910 ^{o}C using the method of Wells (1977). $Mg^{\#}$ values for orthopyroxene in tonalites range from 0.67 to 0.48 and for clinopyroxene from 0.65 to 0.57. $Mg^{\#}$ values of amphibole vary from 0.76 to 0.43. Biotite $Mg^{\#}$ values range from 0.70 to 0.41. In granodiorite and granite the $Mg^{\#}$ values range from 0.42 to 0.37 for biotites and are averaged 0.63 for the amphibole. The wide variations in mineral chemistry of the tonalites supports a possible hybrid origin between tonalite and dioritic magma as originally suggested by Deer (1935).

The whole-rock chemical pattern of the different rock types described in Chapter 5 describe relatively smooth and regular trends on Harker and AFM variation diagrams. The gap between 66% and 71% SiO_2 may be a real petrological gap suggesting an independent origin for the granites. A feature also noticed on the chondrite-normalised plot (Fig 5.13a) is the enrichment in Rb, Th, K, La, Ce and Zr and depletion in Ba, Sr, P, Ti and Y in the granite relative to other rock types though much of this may be accounted for by fractional crystallisation. The microdiorites, which are the earliest magmas, show characteristics typical of mantle-derived magmas (i.e. high Ni and Cr abundances) although they are located in the southern part of the hornblende hybrid zone (Deer, 1935) and sample AS38 which was described petrographically as a hornblende biotite diorite is located to the NW of this zone.

6.6.2 Composition modelling:

6.6.2a Major oxide modelling

The marginal rocks of this pluton as represented by the hornblende hybrid zone (Deer, 1935), and microdiorites were not used as parental magmas as these samples (AS33, 77030) are petrographically contaminated (glass inclusions and quartz grains are surrounded by biotite). Modelling tonalite (77026) from them failed to produce a satisfactory model. Tonalite was chosen as a starting point for modelling represented by sample 77026 as it has a good igneous granular texture and contain essential high temperature phases like two pyroxenes with plagioclase.

Results of modelling are given in Table 6.5a, and indicate the following:

1) Clinopyroxene is essential in the fractionation process as far as 64% SiO_2 with removal of lesser amounts of orthopyroxene.
2) Plagioclase is removed as is a small amount of biotite.
3) Ilmenite and magnetite are removed in small amounts.
4) Apatite is also required to be removed in small amounts.

The assumed tonalitic parental magma (77026) for the granodiorite failed to produce the granites which occur in the centre.

6.6.2b Trace element modelling

Results are presented in Table 6.5b and indicate the following:

a) The agreement between observed and modelled trace element concentrations is acceptable apart from Sr, Ce, Cr and Ni elements.
b) Cr and Ni modelled abundances fall while they unusually increase in the observed values, and it is difficult to reconcile this with the major oxide modelling.
c) Sr modelling fails to reduce this element as much as the observed

Table 6.5a: Summary of major oxide fractionation modelling of Carsphairn

	Tonalite		Granodiorite	
	77026	(77026)	AS48	(AS48)
SiO_2	60.81	60.81	63.66	63.66
TiO_2	1.01	1.01	0.87	0.67
Al_2O_3	16.97	16.97	16.72	16.72
FeO*	5.43	5.43	4.75	4.75
MnO	0.09	0.10	0.09	0.08
MgO	2.85	2.85	2.24	2.24
CaO	5.47	5.47	4.11	4.11
Na_2O	3.99	4.33	4.15	3.80
K_2O	2.49	2.49	2.91	2.91
P_2O_5	0.27	0.27	0.27	0.27
Total	99.38	99.73	99.77	99.21
Σr^2		0.12		
residual liquid	(AS48)73.02		(AS49)no successful model	
orthopyroxene		0.94		
clinopyroxene		5.09		
amphibole		-		
biotite		3.53		
plagioclase		16.67		
ilmenite		0.49		
magnetite		0.06		
apatite		0.30		
alkali feldspar		-		
quartz		-		
cumulate total		27.08		
cumulate composition		Pyroxene biotite diorite		

Table 6.5b: Summary of results of fractional crystallisation modelling of trace elements in the Carsphairn pluton.

Sample No	77026	AS48 modelled	AS48 actual
Rb	71	86	91
Ba	532	542	543
Sr	443	418*	334
Nb	7	8	8
Zr	152	201	192
Y	28	29	30
La	27	37	30
Ce	72	85*	69
Cr	21	8*	33
Ni	7	6*	13

% of minerals removed	30%
orthopyroxene	1
clinopyroxene	5
amphibole	0
biotite	4
plagioclase	20
spinel	1
apatite	0.3
zircon	0

* Indicates values from modelled compositions which reflect either trends opposite to those actually observed, or estimates which differ very greatly from those observed.

composition, reflecting plagioclase modelling. The KD value for plagioclase used here was 1.8 though values up to 10.5 have been quoted in the literature.

d) Modelled Ce compositions are higher than observed probably reflecting that only apatite was modelled in fractionation. Other accessories may also have fractionated Ce.

e) The agreement between major oxide and trace element modelling is sufficiently close to support the main conclusion of the major oxide model, where a tonalitic parental magma fractionated orthopyroxene, clinopyroxene, plagioclase and biotite and accessories to give rise to granodiorite.

6.6.3 Magma mixing

As this pluton show signs of hybridisation between the outer zones (Deer, 1935) magma mixing modelling was attempted using the method of Wright and Doherty (1970). End members of tonalite and granite composition were selected in an attempt to model the granodiorites. It was found possible to model the major oxide composition by mixing 75% of the tonalite with 25% of the granite to form the hybrid granodiorite with Σr^2 less than 1.0. Results are given in Table 6.5c.

6.6.4 Discussion

Tonalite has been shown to be a successful parental magma for major oxide fractionation modelling and as an end-member in mixing modelling with granite to form granodiorite. It can not be proved that this is the true parental magma or just an intermediate stage in the evolution of the magma chamber.

Table 6.5c: Summary of mixing modelling using two-end members of Carsphairn Complex

	Tonalite 77026	Granite AS49	Mixing of 77026 with AS49	Granodiorite AS48
SiO_2	60.81	70.95	63.66	63.66
TiO_2	1.01	0.47	0.88	0.87
Al_2O_3	16.97	14.46	16.44	16.72
FeO*	5.43	2.58	4.75	4.75
MnO	0.10	0.05	0.09	0.08
MgO	2.85	0.85	2.37	2.24
CaO	5.47	1.78	4.58	4.11
Na_2O	4.33	3.54	4.19	3.80
K_2O	2.49	4.94	3.11	2.91
P_2O_5	0.29	0.06	0.24	0.29
Total	99.75	99.68	100.31	99.43

$\Sigma r^2 = 0.49$

75% 77026

25% AS49

Whether the central granite is a late fractionate or a discrete pulse is not clear. An SiO_2 gap of 65-71 wt% and the distinctive trace element abundances suggests an independent origin but may also indicate metasedimentary contamination of the evolving magma (assimilation-fractional crystallisation).

6.7 LOCH DOON

6 7.1 Introduction:

This pluton (about 130 km^2) intruded Ordovician metasediments in the Southern Uplands. Only the southern part was studied where it comprises marginal microdiorites, two-pyroxene biotite diorite, hornblende biotite diorite, granodiorite and granite in a generally concentric arrangement. The microdiorites are porphyritic with orthopyroxenes, clinopyroxenes and plagioclase. The two-pyroxene biotite diorite is similar but medium grained. The main granodiorites contain essential hornblende, plagioclase, biotite alkali feldspar and quartz. The granites contain only biotite, plagioclase, alkali feldspar and quartz. Zircon, apatite and Fe-Ti oxides are important accessory phases in all these rock types.

The calculated two-pyroxene equilibration temperatures of the diorites gave values of 975 ^{o}C for sample 78002 and 925 ^{o}C for sample WL6, using the method of Wells (1977). The orthopyroxenes have $Mg^{\#}$ values from 0.70 to 0.67 and clinopyroxenes have values of 0.76 (diorites). The amphibole $Mg^{\#}$ values range from 0.73 in the diorites to 0.63 in the transitional granodiorite. $Mg^{\#}$ values for biotite range from 0.70 in the diorites to 0.40 in the granite.

Whole-rock chemical data indicate that the rocks of this complex

follow rather smooth trends on Harker and AFM variation diagrams. Interelement diagrams, eg Rb-K_2O, Ba-K_2O, Ni-MgO and Cr-MgO (Fig 5.15a-d) indicate a small gap between granodiorites and granites, though whether this is real or due to sample coverage is not clear. Ti and P decrease with SiO_2 throughout the whole sequence reflecting ilmenite (and/or biotite) and apatite fractionation. Zr follows an early enrichment trend and reaches a maximum of 190 ppm Zr between 61 and 67% SiO_2, followed by a decrease with SiO_2 (Fig 5.14s). This is probably due to zircon becoming a fractionating phase at that point in the evolutionary sequence.

The chondrite-normalised plot (Fig 5.13b) shows similar patterns for all principal rock types except for the granites which show marked enrichment in Rb, Th, La, Ce and K and depletion in Sr, P, Ti and Y.

The evidence given above suggests that fractional crystallisation has been important in the evolution of this pluton, particularly in the early dioritic stages.

6.7.2 Composition modelling

A two-pyroxene biotite diorite (78001) was taken as an initial parental magma composition in an attempt to model the fractional crystallisation process.

6.7.2a Major oxides

Results of modelling of the major oxides are given in Table 6.6a and indicate the following:

a) Orthopyroxene and clinopyroxene removals are required in decreasing quantities as far as 63% SiO_2.

b) Plagioclase fractionation is dominant in decreasing amounts and

Table 6.6a: Summary of major oxide fractionation modelling of Loch Doon pluton.

	Hornblende biotite diorite		Granodiorite		Granodiorite		Granodiorite	
	78001	(78001)	DBL3	(DBL3)	77023	(77023)	WL9	(WL9)
SiO_2	57.81	57.81	63.13	63.13	65.97	65.97	67.23	67.23
TiO_2	0.74	0.80	0.76	0.80	0.63	0.63	0.59	0.59
Al_2O_3	15.54	15.54	15.10	15.10	15.11	15.11	14.83	14.83
FeO*	6.22	6.13	4.39	4.39	3.49	3.49	3.24	3.24
MnO	0.14	0.10	0.10	0.09	0.07	0.08	0.08	0.07
MgO	6.67	6.67	3.75	3.75	2.67	2.92	2.31	2.45
CaO	6.28	6.28	3.98	3.98	3.26	3.26	2.94	2.94
Na_2O	4.03	3.48	3.87	3.69	3.63	3.90	3.53	3.52
K_2O	2.08	2.08	3.46	3.46	3.81	3.81	3.96	3.96
P_2O_5	0.25	0.25	0.25	0.25	0.25	0.25	0.25	0.25
Total	99.76	99.14	98.79	98.64	98.89	99.42	98.96	99.08
Lr^2		0.32		0.04		0.01		
residual liquid	(DBL3)	38.67	(77023)	82.28	(WL9)	90.27	(HH2)	
orthopyroxene		12.56		2.80		-		no successful model
clinopyroxene		9.18		2.32		-		
amphibole		-		-		1.13		
biotite		6.72		3.12		2.25		
plagioclase		33.11		8.56		5.54		
ilmenite		-		0.15		0.02		
magnetite		-		0.00		-		
apatite		0.38		0.26		0.21		
alkali feldspar		-		-		-		
quartz		-		-		-		
cumulate total		61.95		17.21		9.15		
cumulate composition		pyroxene biotite diorite		pyroxene biotite diorite		Hornblende biotite diorite		

becomes more albitic towards 67% SiO_2.

c) Ilmenite removal is required in small amount.

d) Apatite fractionation occurs through the whole sequence.

e) Amphibole (of magnesio-hornblende composition) removal is required to form the transitional granodiorite from the normal granodiorite.

f) Biotite removal is required throughout the series.

Fractional crystallisation modelling of pyroxene biotite diorite (78001) gave good fits to form up to the transitional granodiorite but not the granites.

6.7.2b Trace element modelling

Results of modelling are presented in Table 6.6b and the following points are concluded from this table:

a) There is an agreement between observed and modelled trace element concentration except for Sr and Nb and occasionally La, Zr, Ce and Cr.

b) Modelled Sr compositions are always higher than the observed compositions presumably indicating that the K_D value used for plagioclase (1.8) is low for this pluton. It is noteworthy that up to 10.5 have been quoted in the literature.

c) The inability to model Zr and Nb can be at least partly explained by not including accessory phases, in the models.

d) Modelling of Cr in the series from two pyroxene biotite diorite to granodiorite gave greater depletions than observed which probably reflects the modelling of pyroxenes. The K_D values for Cr are too high probably for this part of the model and lower values than those used have been quoted in the literature.

e) Modelling La from pyroxene biotite diorite to granodiorite gave

Table 6.6b: Summary of results of fractional crystallisation modelling of trace elements in the Loch Doon pluton.

Sample No	78001	DBL3	DBL3	77023	77023	WL9	WL9
	actual	modelled	actual	modelled	actual	modelled	actual
Rb	57	90	110	117	128	135	150
Ba	929	851	898	845	822	719	717
Sr	788	749*	493	456*	405	399*	360
Nb	7	7*	19	18*	9	8*	16
Zr	63	124*	177	204*	175	188	188
Y	21	22	21	22	21	23	22
La	29	65*	31	36	34	43	46
Ce	59	102*	80	91*	78	79	82
Cr	337	81*	178	135	144	100	98
Ni	177	95	82	76	66	60	50

% of minerals removed	62%	17%	9 %
orthopyroxene	12	3	0
clinopyroxene	9	2	0
amphibole	0	0	1
biotite	7	3	2
plagioclase	33	9	6
spinel	0	0	0
apatite	0.4	0.3	0.2
zircon	0	0	0

* Indicates values from modelled compositions which reflect either trends opposite to those actually observed, or estimates which differ very greatly from those observed.

much higher modelled composition than observed. Again bulk distribution coefficients could have been greater with the inclusion of accessory phases. The same is the case for Ce.

f) There is sufficient agreement between observed and modelled trace element concentrations to support the main conclusions of the major oxide model, that is parental pyroxene biotite diorite magma giving rise to granodiorite by fractionating orthopyroxene, clinopyroxene, plagioclase and biotite.

6.7.3 Magma mixing

The proposed hybridisation between diorites and granodiorite, and granodiorite and granite (Gardiner and Reynolds, 1932) is supported by the isotopic data of Halliday et al. (1980). Halliday et al. (1980) studied the Sr and O isotope variations within this pluton including some of the samples used in this study and also studied the Rb-Sr isotopes for the Southern Uplands sediments. An age of 408 + 2 Ma was derived for the pluton and the $^{87}Sr/^{86}Sr$ initial ratio ranges from 0.7041 for the microdiorite (sample WL3) from the southern tip of the pluton, to 0.7059 for the granite (sample HH3) from Hoodens Hill in the centre. The $\delta^{18}O$ varies between 7.83-10.32. The metasediments range from 0.70450 to 0.7109 in terms of $^{87}Sr/^{86}Sr$ at 408 ma and gives $\delta^{18}O$ °/oo value of 10.82 for one sample. Halliday et al. (1980) concluded that the Loch Doon magmas were chiefly derived from successive melting of a (largely) basic source with an initial $^{87}Sr/^{86}Sr$ ratio of 0.704 which yielded the microdiorite, overlain by an older source region or more probably richer in metasediments, with a higher initial $^{87}Sr/^{86}Sr$. In isotopic terms much of the variation may be considered in terms of mixing of

these two end members though whether this took place in the source region or during high level crystallisation is difficult to constrain. Either way fractional crystallisation is not precluded but the isotopic data require that this was not the sole process.

Accordingly an attempt has been made here to check the idea of magma mixing, using the Wright and Doherty (1970) blending method of two assumed end members represented by pyroxene biotite diorite (sample 78001) and granite (sample HH2), with results given in Table 6.6c. Mixing calculations of these two end members gave a good fit where Σr^2 is less than 1.0 with increasing proportions of the granite towards the more evolved granodiorites.

6.7.4 Discussion

If fractional crystallisation alone is considered as the dominant process responsible for the formation of the different rock types from a parental mantle-derived magma, as has been discussed earlier then the experimental results of Anderson (1976) must be considered. He concluded that generation of granitic magma by fractionation directly from a basic magma is volumetrically unacceptable since only a small proportion of residual acid melt can be produced. In Loch Doon the granodiorites form the greatest part of the pluton and granite is relatively minor in area and presumably volume (Fig 2.6). It is suggested that the processes should be coupled, (i.e. mixing and fractional crystallisation) may have operated in this pluton to give rise to observed major and trace element variations as well as isotopic variations.

Tindle and Pearce (1981) studied the same pluton and suggested two distinct evolved magmas, the first being volumetrically small and

Table 6.6c: Summary of mixing modelling using two end members of Loch Doon pluton

	Diorite 78001	Granite HH2	Mixing of 78001 with HH2	Hornblende biotite diorite (WL8)	Mixing of 78001 with HH2	Granodiorite (DBL3)
SiO_2	57.81	71.23	61.55	61.55	63.13	63.13
TiO_2	0.80	0.28	0.60	0.84	0.54	0.80
Al_2O_3	15.54	15.15	15.14	15.44	15.06	15.10
FeO*	6.34	1.99	4.57	4.90	4.03	4.39
MnO	0.10	0.05	0.08	0.08	0.07	0.09
MgO	6.67	1.23	4.65	4.38	3.94	3.75
CaO	6.28	1.73	4.58	4.58	3.98	3.98
Na_2O	3.48	3.46	3.42	3.84	3.40	3.69
K_2O	2.08	4.60	2.93	2.93	3.25	3.46
P_2O_5	0.25	0.10	0.19	0.30	0.17	0.23
Total	99.35	99.82	97.71	98.84	97.57	98.62
			$\Sigma r^2 = 0.51$		$\Sigma r^2 = 0.37$	
			64% 78001		51% 78001	
			36% HH2		44% HH2	

			Mixing of 78001 with HH2	Granodiorite (77023)	Mixing of 78001 with HH2	Transitional granodiorite (WL9)
SiO_2			65.97	65.97	67.23	67.23
TiO_2			0.45	0.63	0.42	0.59
Al_2O_3			15.13	15.11	15.17	14.83
FeO*			3.38	3.49	3.09	3.24
MnO			0.07	0.08	0.06	0.07
MgO			3.07	2.92	2.68	2.45
CaO			3.26	3.26	2.94	2.94
Na_2O			3.43	3.90	3.45	3.52
K_2O			3.70	3.81	3.90	3.96
P_2O_5			0.15	0.23	0.14	0.30
Total			98.61	99.4	99.08	99.13
			$\Sigma r^2 = 0.30$		$\Sigma r^2 = 0.26$	
			35% 78001		27% 78001	
			65% HH2		73% HH2	

of quartz diorite composition while the second was of granodiorite composition, both of them undergoing in situ fractional crystallisation of plagioclase-opx-cpx-biotite phases with minor apatite based on trace element modelling.

The two-end members proposed by Halliday et al. (1980) reflect mantle ($^{87}Sr/^{86}Sr$ initial = 0.703, $\delta^{18}O = 6$), or young basaltic crustal melts and a melt with isotopic characteristics similar to Southern Uplands metasediments ($^{87}Sr/^{86}Sr = 0.708$, $\delta^{18}O = 12\text{-}13$). The involvement of the Lower Palaeozoic sediments in the Southern Uplands plutons generation was supported by the results of Halliday (1984) using $^{143}Nd/^{144}Nd$ isotopic ratios in combination with the U-Pb, Rb-Sr and O isotopic relationships. Values for one diorite (77061) and one granodiorite (DBL3) samples for Loch Doon gave εNd of -1.0 and -1.4 respectively. This was interpreted as an indication that if the magma was contaminated it must have been with young continental crust.

6.8 General conclusions about processes:

The plutons studied in the Grampian Highlands (i.e. Garabal Hill, Comrie and Glen Doll) were formed by fractional crystallisation of a parental magma of gabbro or pyroxene biotite diorite composition except for the more evolved rocks (porphyritic granodiorite and the granodiorite) in Garabal Hill and Glen Doll plutons respectively. For the Glen Tilt complex it was concluded that it is generated by multiple intrusion of magma pulses from different sources with subsequent differentiation. The diorites and appinitic diorites are related to a parental magma of mantle origin while the quartz diorites and granodiorites are linked by fractionation of a magma which may

have been derived by melting of continental crust.

The Southern Uplands plutons (i.e. Loch Doon and Carsphairn) were formed by fractional crystallisation of mantle derived magma with some crustal contamination contributing to the more evolved rocks.

6.9 Discussion of the genesis of granodiorites and granites

Total melting of crustal material is not a likely mechanism in generating granitic magma because liquidus temperatures are too high for regional metamorphism (Fourcade and Allegre, 1981). However mafic magmas can bring extra heat to assist melting (Harmon et al. 1984). Moreover, if a significant proportion of a source rock is melted to give a granitic melt, it is conceivable that residual refractory material are carried upward with the anatectic liquid as a crystal mush (Piwinskii 1968; Presnall and Bateman 1973; Wyllie 1977; White and Chappell, 1977).

The porphyritic granodiorite of Garabal Hill which is intruded to the west of the pluton and forms areally about two thirds of the pluton (Nockolds, 1941) could not be modelled from the same parental magma. The unusual enrichment of Sr along with Ba in this rock type and the inverse correlation between Sr - CaO which can not apparently reflect removal of plagioclase fractionation, however major oxide petrochemical modelling requires plagioclase as a dominant fractionating phase. This apparent contradiction may partly be explained by the granodiorite being derived from a different high Sr source. However there is also the requirement for the bulk partition coefficient for Sr to be less than unity for early members of the series even while fractionating plagioclase.

The granodiorites have $^{87}Sr/^{86}Sr$ initial ratios from 0.705-0.712 (Summerhayes, 1966) the higher values being marginally contaminated samples. The high $\delta^{18}O$ °/oo of 10.4 °/oo and $(^{87}Sr/^{86}Sr)_{400}$ of 0.70778, and low εNd of -3.7 calculated for one medium granodiorite sample (GH18) by Harmon and Halliday (1980) and Halliday (1984) support the idea of substantial crustal involvement in the medium granodiorites.

The granodiorites of the Glen Doll complex show sharp contacts in the field against other rock types and some form of pulsing must have taken place. The gap between 59-65% SiO_2 may also reflect a real petrological gap. Also the failure to model the evolved compositions from a gabbro parental magma all support the contention of a separate pulse from a distinct source.

The genesis of quartz diorite, granodiorites and granites intermingled with mafic diorite in Glen Tilt is not very clear. The quartz diorites and granodiorite can be linked by a fractionation scheme. The biotite granites, which represent areally about two-thirds of the pluton (cf Fig 2.4), are enriched in Th, Rb, and K and there is a gap between 70 and 75% SiO_2, their biotite compositions show enrichment in Mn (Fig 4.5). As petrochemical modelling failed to generate any similar composition it is again that a separate intrusion which may have formed by crustal melting.

The Cairnsmore of Carsphairn and Loch Doon plutons are neighbouring plutons intruding the Lower Palaeozoic metasediments of the Southern Uplands. Granite in both plutons forms the core in true concentric zonation. Distinctive trace element patterns along with the inability of fractional crystallisation modelling to generate granitic compositions support the isotopic contention for Loch Doon

that a separate magma source is involved in the petrogenesis of the granite in both plutons. However, whether this is a truly separate pulse from a distinct source or a strongly contaminated parental magma (or fractionate thereof) is not clear from this study.

CHAPTER 7

PROCESSES IN THE FORMATION OF ZONED GRANITOID PLUTONS

7.1 Introduction:

The study so far has revealed that all the plutons show petrological variations consistent with formation through a large temperature interval. The plutons of Loch Doon, Carsphairn and Comrie show this variation in a concentric form with the highest temperature mineral assemblages at the margins and the lowest temperature assemblages in the core. The other plutons (Garabal Hill, Glen Doll and Glen Tilt) show much less regular distributions but always with the highest temperature mineral assemblages near the outer margins. This study is based on mineralogical and geochemical features of these plutons with an attempt to understand the processes that operated through the fitting of chemical model systems to the observed variations. It is clear that crystal-liquid fractionation and cumulate formation may account for much of the observed variation but that in the more evolved rocks more complex processes involving possible magma contamination and/or multiple intrusion are necessary. At this stage it is important to review the physical processes that are believed to give rise to the types of variations observed in these plutons.

7.2 Nature and motion of granitoid magma:

Magma is normally a silicate melt that generally contains suspended crystals and dissolved gaseous constituents or volatiles. The structure of the melt is that of a polymerised Si-O network modified by cations such as Ca, Mg, Na, K and Fe. The network structure gives the magma high viscosity whereas the network modifying elements effectively reduce the viscosity.

Viscosity is a measure of the resistance to flow of a liquid; more viscous liquids are less mobile. More polymerized silicic melts are more viscous and dissolved water also depolymerizes a melt making it less viscous. The viscosity is usually expressed in terms of the coefficient of viscosity , which is the ratio of the applied shear stress to the rate of shear strain. If the coefficient is constant regardless of the magnitude of the shear stress and strain, the viscosity is said to be Newtonian. Newtonian viscosity can be considered to apply for magmas above the liquidus temperatures, particularly more basic magmas. As silicate melts crystallise or vesiculate, the magma departs from Newtonian behaviour, though it may still hold true for the melt fraction or for melts supercooled metastably below their freezing temperature. Most granitoid magmas are believed to exhibit non-Newtonian plastic behaviour at least through their crystallisation range.

The physical properties of simple melts of andesitic composition were established by Kushiro (1978) who confirmed the expected reduction of viscosity with increasing water content. However, work on the properties of rock melts in general, and particularly those of silicic composition (Shaw 1965, 1969, 1972; Shaw et al. 1968) indicates that crystal-bearing magmas have much less easily definable properties and may not behave as Newtonian fluids but as Bingham bodies (i.e. pseudo-plastics having much higher apparent viscosities and well-defined yield strengths). The distinction is important in controlling internal processes within granitoid plutons, including flow, heat transfer and the settling of crystals and/or xenoliths.

Newtonian viscosity is an important parameter in determining whether convective overturning of magma takes place under a thermal

gradient (Rayleigh Law), and the zoning of plutons has been explained by thus separating melt from crystals (Pitcher, 1979). Under Bingham body conditions the process of natural convection is less easy to predict though it certainly occurs under Newtonian conditions.

It is possible to document the late stages of the evolution of granitoid plutons by determining the variety and compositions of phenocrysts in the eruptive sequence (Pitcher 1979). Hildreth (1977) has shown that systematic changes in composition in subvolcanic magma chambers cannot easily be modelled by either crystal settling, assimilation or liquid contamination, and only by involving thermal diffusion (Shaw et al. 1976) can the highly systematic and parallel changes in composition be explained. The difficulty in such explanations seems to be in the sluggishness of diffusion and this has led Hildreth (1977) to infer a convection-driven chemical diffusion. Chemical diffusion between core and periphery of a large pluton could be much more effective if its rate were increased by the convective transfer of heat (Shaw 1974).

7.3 Crystal-liquid segregation:

In partly crystallised magmas separation of crystals from melt is a powerful means of magmatic differentiation because of the normally contrasting chemical composition between crystals and melt. The evidence is most clearly found in chemical variation diagrams that show a regular pattern of compositional variation in a suite of magmatic rocks closely related in space and time such as within a single pluton.

Mechanisms commonly proposed to account for crystal-liquid fractionation include (i) flow differentiation; (ii) filter pressing

and (iii) crystal accumulation. The latter process is made possible by any of the above mechanisms or by incomplete chemical reaction between crystals and melt where these two phases are not mechanically isolated from one another. Incomplete reaction between non-segregated crystals and melt results in compositionally zoned crystals.

Crystal-liquid fractionation in flowing magma, or flowage differentiation has been documented in sills and dykes and confirmed as an applicable mechanism in theoretical and experimental studies. Greater concentrations of larger sized euhedral crystals commonly occur in the centres of dykes and sills by fluid dynamic forces causing dispersion of grains away from the walls. Barriere (1976) has shown that this process is not likely to be effective in conduits greater than 100 m in diameter, thus its role in the generation of zoned granitoid plutons is very likely to be minimal.

It is theoretically possible for the melt in mushlike, crystal-rich magma to separate from the crystals, either by draining or by being pressed out (i.e. filter pressing). It might occur on the floor of mafic intrusions where the mass of accumulating crystals presses some of the intercumulate melt out of the underlying crystal mush. Filter pressing may be important in the generation of zoned plutons, its role in the early stages of separating accumulated crystals from evolved melt compared with convective processes has not yet been clarified. It is rather more likely to play an important role at the end stages of pluton consolidation when the body becomes rather more rigid.

Crystal accumulation in plutons may be of two types:
(1) Crystal settling by the gravitational force, depending mainly upon the difference in densities between crystal and melt, and

(2) Marginal accretion in which crystals are accreted to the sidewalls of a magma chamber where they may be expected to first crystallise in the region of greatest heat loss. This has been suggested by many authors including Bateman and Chappell (1979) and Atherton (1981), based on observations from zoned granitic plutons in which mafic cumulate-like rocks are found to occur at the margins of many such plutons. Crystal-liquid fractionation has been invoked in such cases of side-wall crystallisation, with also the possibility of crystal settling, though in silicic igneous rocks convincing evidence for crystal settling as evidenced by layered structures is uncommon (Bateman and Chappell 1979).

7.4 Crystal-liquid chemical interactions:

Magmatic differentiation is the formation of a variety of rocks from an initial parental magma.

The formation of cumulates, whether by gravitative settling or by marginal accumulation, provides a means of isolating higher temperature more refractory mineral assemblages. In calc-alkaline magma systems this normally means the fractionation of a potentially wide variety of minerals including olivine, clinopyroxene, orthopyroxene, amphibole, mica, calcic plagioclase, spinels to give rise to observed bulk chemical variations (Gill, 1981). Most of these minerals have properties of higher density than their coexisting melt and may be early liquidus phases. Many authors have suggested that accumulation of these plutons either by gravitative settling or marginal accretion would give rise to variations of the type observed in zoned plutons. It is important to note that the melt from which such crystal accumulation arises will be more silicic and therefore of

lower density than the parental magma, thus providing a convective mechanism of separating the melt from the crystals and thus promoting crystal-liquid fractionation.

In slowly ascending viscous bodies such as granitoid plutons a number of open system possibilities arise such as wall-rock reaction or assimilation which will cause bulk contamination. When a magma begins to migrate towards the surface under the influence of gravity it may come into contact with wall rocks which are substantially different in composition and with which it is not in chemical equilibrium. If sufficient time is available heat transfer and chemical reactions between the magma and the enclosing host rocks will take place, potentially modifying the compositions of both. In the simplest case host wall rocks will be heated still further by loss of heat from the magma aided by exothermic crystallisation within the magma, possibly causing partial melting of the country rock. This process might be expected in many cases to produce minimum melt compositions of generally granitic composition. Blending of such compositions with basic-intermediate calc-alkaline magmas will give rise to chemical trends very similar to those observed in zoned plutons. The difficulty is to explain the normal zoning by this process which might be expected to produce reverse zoning when the outer portions are more contaminated than the inner. Such processes are best revealed by isotopic studies.

DePaolo (1981) proposed such an <u>assimilation fractional crystallisation</u> (AFC) mechanism for the Sierra Nevada and Peninsular Ranges batholiths in California on the basis of Nd and Sr isotopic variations. He argued for the assimilation of crustal rocks by magmas rising from the mantle and undergoing fractional crystallisation while

at the same time being contaminated by the mixing of anatectic crustal-derived magmas. The assimilation of relatively alkali-enriched material concurrent with fractional crystallisation could account for the variations in these calc-alkaline plutons.

Multiple source models have been proposed in recent years after detailed isotopic study of zoned plutons (eg Halliday et al. 1980). In this model an early magma of crustal or mantle source is progressively intruded by a slightly later magma from a more evolved crustal source. This model and the AFC model may be considered as end members in a range of processes that begins with AFC contamination of the more primitive magma within the evolved source area and finishes with a magma dominantly from that evolved source area, as proposed by Stephens et al. (1985).

Another justification for open systems is the observation from geophysics that magma chambers supplying volcanic eruptions are periodically tapped and then replenished. Given that such magmas may have fractionated before eruption and subsequent replenishment, the possibilities for different kinds of magma mixing are very great and difficult to predict in terms of bulk composition.

Finally it should be pointed out that in the time scale of an evolving pluton (probably a few 10^5-10^6 years) it is quite likely that a combination of the above processes may be operating. The ultimate objective is to identify these processes and to quantify their contributions. Even with the aid of several isotope systems a unique solution to this problem may not be possible, however major and trace elements as well as isotopes can be systematically interpreted to give general guides. Without the benefit of isotopes for five out of six plutons in this study interpretation is guided by analogy with plutons

for which isotopes are available.

7.5 Physical processes in magma chambers:

Crystal-liquid differentiation

The processes that occur within magma chambers cannot be observed directly and our understanding of these processes is based largely on observation of mineralogical variations in relation to known phase relationships, composition variations in relation to model behaviour of elements and isotopes in crystal-liquid equilibria; field evidence of structures, etc; and laboratory scale models of physical phenomena. From these lines of evidence various models of magma chambers processes are derived. A few processes are frequently involved to explain zonation in granitoid plutons and these are outlined below.

Fractional crystallisation implies separation of solid from residual liquid. Crystal settling provides a good mechanism to segregate crystals forming high temperature mineral assemblages as cumulate layers. The most widely quoted evidence for crystal settling comes from layered intrusions (Fig 7.1a).

In silicate igneous rocks such convincing evidence for crystal settling is less apparent (Sparks et al. 1984). In plutonic rocks the best evidence for compositional zonation comes from the horizontal zoning from mafic margins to felsic interiors found in many granitic plutons implying crystallisation from the walls inwards. The process of sidewall accumulation of early mineral assemblages has the effect of generating a less dense evolved melt fraction which will buoyantly migrate upwards from the site of crystallisation (Fig 7.1b). The upwards and inwards concentration of evolved melt has the important

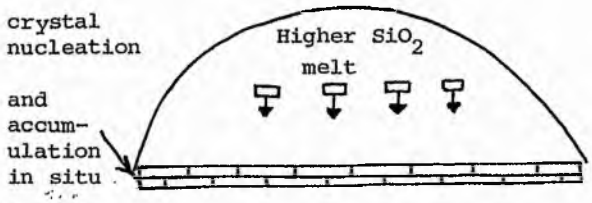

(a) Cumulate layering by crystal settling.

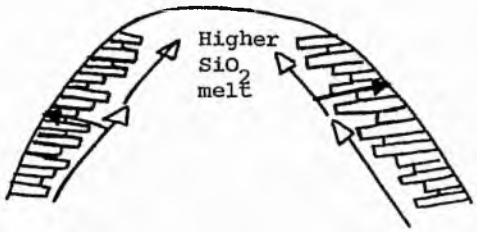

(b) Sidewall accumulation by sidewall nucleation, convective separation of boundary-layer melt.

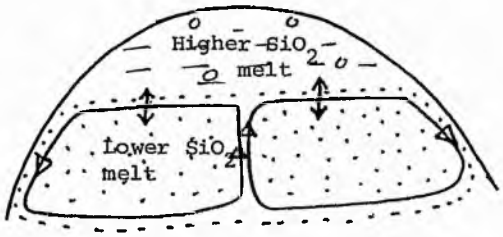

(c) Double-diffusive convection system (Liquid-state differentiation)

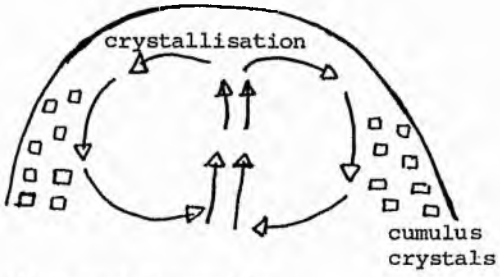

(d) Normal convection

Crystal accumulation direction

Convecting melt direction

Volatiles

Crystals

Double-diffusive transfer of heat and matter.

Fig 7.1 Schematic diagrams showing different end-member magma chamber processes leading to the formation of zoned plutons.

feature of explaining the concentric arrangement often observed in normally zoned plutons (Fig 7.1b). In addition the physical process of sidewall accumulation and convective fractionation (Sparks et al. 1984) has been observed in laboratory simulation experiments using aqueous solutions of Na_2CO_3, KNO_3, $CuSO_4$ and other salts in a tank cooled from the margins and above (Sparks et al. 1984). The formation of crystals at the wall with their subsequent accretion into a growing layer is a convincing laboratory analogy for the expected behaviour in cooling magma chambers.

Hildreth (1979) studied the Bishop Tuff, a batholith-scale acid tuff eruption in the western U.S.A. which show vertical zonation from an acidic base to a more basic top. He argued that crystal settling cannot account for the observed geochemical gradients and suggested that the phenocrysts grew essentially in situ and that the compositional gradient existed in the liquid state of the magma before the phenocrysts formed. Hildreth relates the increasing crystal content with depth in silicic magma chambers to the suppression of the liquidus temperature thus inhibiting crystallisation at the top of the chamber by the roofward concentration of volatiles (Fig 7.1c).

Natural convection may occur in a high level pluton which loses heat through its roof and walls. Crystals formed in these cooler zones may be carried onto the sides or form as cumulates in the deeper parts of the pluton while the melt is free to convect and thus effectively separate melt from crystals (Fig 7.1d). Sparks et al. (1984) proposed the term convection fractionation for a wide variety of convective phenomena caused by crystallisation with resulting separation of crystals and liquid leading to crystal-liquid fractionation.

Multiple intrusion

Whenever a pluton is chemically bimodal the possibility of multiple intrusion should be considered. If a simple layered source region became both more mafic with depth and lower in H_2O content, the degree of partial melting would probably decrease with depth and in the direction of the heat source. Under certain circumstances such melting could produce an initial layered diapir with the more acid partial melts below the more basic higher degree partial melts. Thus during final emplacement the more evolved magma could intrude the mafic cap to form the acidic core of an intrusion. It would be expected that the acid magma from the more mafic source would have lower Sr isotope initial ratios than the melt from the more evolved source. Normally the reverse is the case making this model rather unlikely. It seems more likely that the source region is stratified with earlier magmas from the deeper source followed by later, more acidic magmas from the higher-level, more evolved source.

7.6 Chemical models in relation to magma chamber processes:

Interpretation of the history of a pluton involves constraining the nature of the parental magma source region, its melting history, subsequent ascent, and magma chamber processes on emplacement. Studies of the chemistry are important in determining several of these but there are some difficulties in translating chemical variations to magma chamber processes. Field and petrographic information are often helpful.

In constraining parental magma source regions and whether subsequent contamination has occurred usually requires isotopic

information, particularly useful being the radiogenic isotopes of Sr, Nd and Pb and the stable isotopes of oxygen. In the plutons of this study detailed Sr isotopes are available only for Loch Doon, some imprecise values for Garabal Hill also being available. Nd isotope values exist for few plutons, namely Garabal Hill, Comrie and Loch Doon but not in sufficient numbers to investigate the petrogenesis of the whole zoned sequence in each case.

In the absence of detailed isotopic data this study attempts to consider possible high level processes based on other data, primarily whole rock and mineral chemistry, petrography and field relations. The first consideration is whether the pluton consolidated from a single parental magma in a closed or open system. Trace element variation diagrams showing the evolution of the magma sequence in the pluton were examined to see whether they revealed patterns that deviated from those expected by removal of appropriate mineral phases. Additionally contamination of a parental magma by mixing with a new magma may be revealed by an abrupt change in compositions of such minerals as biotites and amphiboles. Petrographic features may also reveal such processes, e.g. early formed minerals showing reaction features at their margins. Where such features are detected and indicate the magma at this stage was behaving as an open system it is possible that the earlier products of crystallisation in the pluton resulted from closed system processes.

In the closed system situation the driving force for differentiation is most likely to be crystal-liquid fractionation or liquid-state fractionation, though most researchers believe the latter to be unlikely except in high SiO_2 magma systems. In the typically diorite-granite variations described in this study the process of

differentiation is most likely to be of crystal-liquid fractionation though it is not clear whether it is possible to distinguish on chemical grounds between cumulate layer formation and side-wall cumulate formation. To distinguish between these, other data from petrography and field relations are required. The chemical modelling approach has been used to show that cumulate formation processes are important for most of the plutons studied, but it can not distinguish between the various cumulate formation processes. It has been possible to constrain the temperature of some of these closed system processes using two pyroxene geothermometers, and to show the general thermal control on the zonation processes.

Taking the plutons of this study it is clear that layering on an outcrop scale is a very uncommon feature, similarly any layering structures (as opposed to foliations) are uncommon in thin section. Considered with the fact that more basic rocks are almost exclusively found at or near the pluton margins, it is suggested that sidewall accumulation processes may have been very important in the petrogenesis of these plutons, at least in the early stages which was probably a closed-system.

Open-system processes are more difficult to interpret. Chemical variation diagrams may reveal the disturbance of closed system processes but it may be less easy (especially with isotopic data) to determine whether this is due to the influx of a new batch of magma or to magma contamination during ascent, or even due to in situ wall-rock contamination of the parental magma. One of the few studies in this area is that of Tindle and Pearce (1983) who used model calculations of the distribution of trace elements between metasedimentary (greywacke) xenoliths and their host granitoids. They showed that

these xenoliths have yielded between 66 and 88% of partial melt of trondhjemitic composition. The extent to which this process might occur to produce zoned plutons is not clear. Such a process is likely to be most effective deeper in the crust where country rocks are already hot and partial melting requires limited additional heat from the magma. In plutons such as Loch Doon which intrude country rocks at prehnite-pumpelleyite facies the assimilation of country rocks in situ is not likely to be substantial, but may have occurred at greater depths prior to intrusion.

Geometrical forms of compositional zoning

The normal arrangement of concentric zoning (more basic margin to more acid core) would be produced by the sidewall accumulation process. However, there are other processes that may also lead to the same kind of geometrical arrangement. Differentiation of a magma at depth followed by repeated release of the evolving magmas up the same conduit would give the normal concentric arrangement. Progressive contamination of parental magma as the contaminating zone heats up with passage of the magma again would lead to the normal concentric arrangement. Intrusion of a pulse from a deeper more primitive source, followed by a pulse from a higher level more evolved crustal source could also give normal concentric zonation. Whole rock major and trace elements along with isotopes may be used to distinguish between some of these processes, at least to resolve open systems from closed systems.

Generally the zoned plutons studied here have some foliation near the outer margins, usually dipping outwards. This may be a primary feature of convective flow, alternatively it may reflect a

foliation imposed by stresses on emplacement of the interior of the pluton and flattening due to inflation of the pluton during emplacement (Holder, 1979). Comrie, Loch Doon and Carsphairn are all of this type.

Reverse zoning is much less common, where the more basic rocks are found in the core of the pluton. A mechanism of the generation of of this type of pluton was described by Fridrich and Mahood (1984) who interpreted it as the result of the rearrangement of a vertically zoned magma chamber during emplacement. Progressively more mafic magma from successively deeper levels in the chamber rose into the core of the intrusions, displacing more silicic magma towards the margins. Another explanation of reverse zoning is the progressive formation of higher temperature partial melts in the source during a thermal event, first magmas being more acid than later. No examples of reverse zoning are investigated in this study.

Lateral zoning, where variations occur from one margin of the pluton to the other, is also quite common. Glen Tilt, Glen Doll (Lochnagar) and Garabal Hill all have features of lateral zoning though rather irregularly developed. In all three cases there are large granitic bodies intruded close to the highly variable intermediate to basic intrusions which form relatively small areas at the margins of these plutons. In such cases one may consider several of the processes discussed above which may not have preserved regular concentric forms due to some disruption, such as the subsequent intrusion of a very large granitic mass obliterating a previously regular geometry. Alternatively cumulates and magmas from a deeper magma chamber may have been carried into place by an ascending granite diapir, or along some structural line of weakness.

7.7 Suggested models for the formation of the studied plutons:

The laterally zoned Garabal Hill pluton comprises a wide range of rock types (ultramafic peridotite to porphyritic granodiorite). The ultramafic rocks probably formed by side-wall accumulation because of their presence near the top of the pluton and their apparent lack of layering features. Crystal settling is not precluded for these rocks and they could have been brought up to their present position by a later intrusion or by faulting, though there is no evidence for the latter. Chemically they may be explained as cumulates. Appinite pipes cut across the diorites of the complex. Other rock types probably formed by crystal-liquid fractionation processes from a gabbroic parental magma, where the rock series indicate falling crystallisation temperature towards the pyroxene biotite diorites. Geochemical modelling succeeded in generating most rock types as far as the "medium" granodiorites. However indications of contamination are reflected in the mineral chemistry, supported by marked changes in the published Sr and Nd isotope data. The porphyritic granodiorites form a large mass to the west of the pluton and it is suggested that they represent a separate pulse of magma from a different source as indicated by their unusual enrichment in Sr and Ba. The process is schematically illustrated in Fig 7.2.

The Glen Doll pluton has a similar range of rock types to Garabal Hill with ultramafic pyroxenites at the margins of the pluton. These may also have formed by side-wall accumulation from the proposed gabbroic parental magma or again (but less likely) by gravitative crystal settling. The gabbroic magma was probably also parental to most of the other rock types formed by crystal-liquid

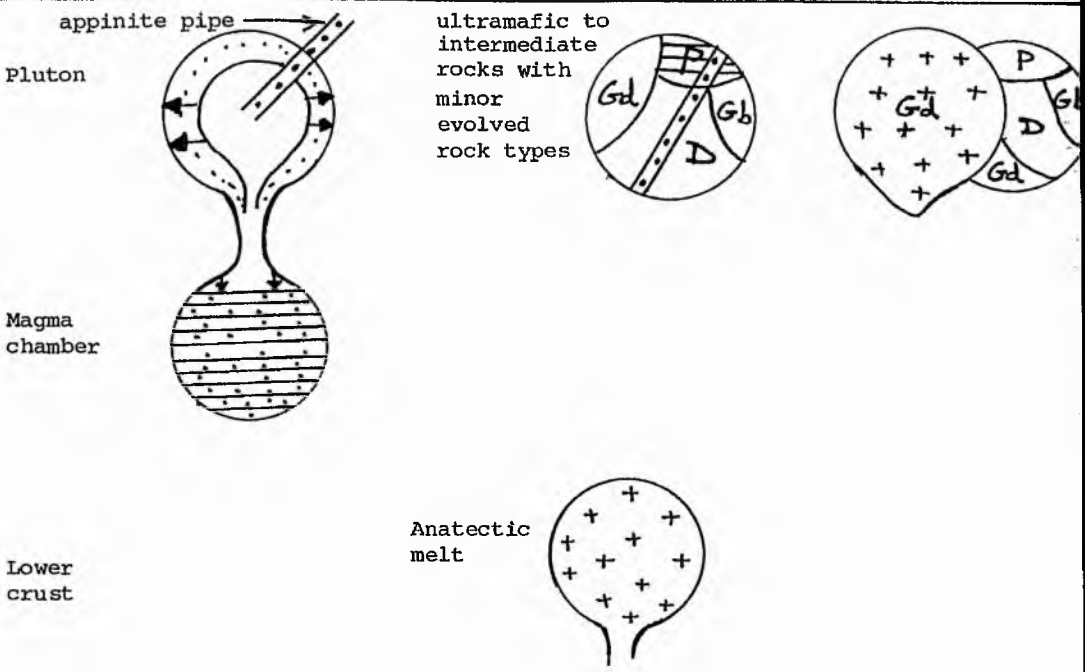

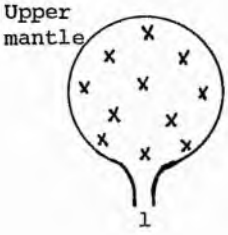

Melting to form gabbroic parental magma

2

High level magma chamber fractionating and possibly forming layered cumulates feeding pluton or forming side-wall cumulates + intrusion of appinite pipes

3

Melting of lower crust to form granodioritic magma

4

Intrusion of porphyritic granodiorite to the west leaving remnants of early basic intermediate complex

Note:

In each case of the parental magma indicated as forming in the upper mantle this should also be taken to include the potential subduction related source materials including the subducted slab.

Key to diagrams:

P = Peridotite; Gb = Gabbro; D = Diorite; T = Tonalite; Gd = Granodiorite; G = Granite

Fig 7.2 Schematic diagram for the formation of the Garabal Hill pluton.

fractionation processes. The granodiorite on the other hand probably represent a separate pulse of magma showing sharp contacts in the field against other rock types and follow a large SiO_2 gap (59-65%). The processes are schematically illustrated on Fig 7.3.

The Glen Tilt pluton has a range of rocks from diorites, appinitic diorites, quartz diorites and granodiorites to granites. The petrogenesis of all of these rock types is not clear from the available data. Geochemical modelling succeeded in producing the granodiorites from a quartz diorite parental magma, but failed to form the granites. The gaps on the variation diagrams and field characteristics support the idea of multiple pulsed intrusions possibly from different source regions or from a deeper magma chamber. The processes are illustrated schematically on Fig 7.4.

The three concentrically zoned plutons (ie Comrie, Loch Doon and Carsphairn) show normal zoning with a range from pyroxene biotite diorites at the margin through to granite in the core. Modelling of the concentrically zoned plutons using the major oxide method described in Chapter 6 gives rise to some problems in understanding the formation of progressive liquids and cumulates. The assumed parental magma gives rise to a cumulate mineral assemblage and an evolved liquid which may match the composition of observed rocks in the complex. In all cases (Comrie, Carsphairn and Loch Doon) the most basic cumulate assemblage is a diorite, a rock type common in each case of these plutons. However, diorites with frozen liquid textures are used as the bulk composition of the parental magma, the starting point for modelling. The problem arises as to which are cumulate diorites and which are magmatic compositions. Textures are sometimes ambiguous especially in the coarse grained types, and it is a problem

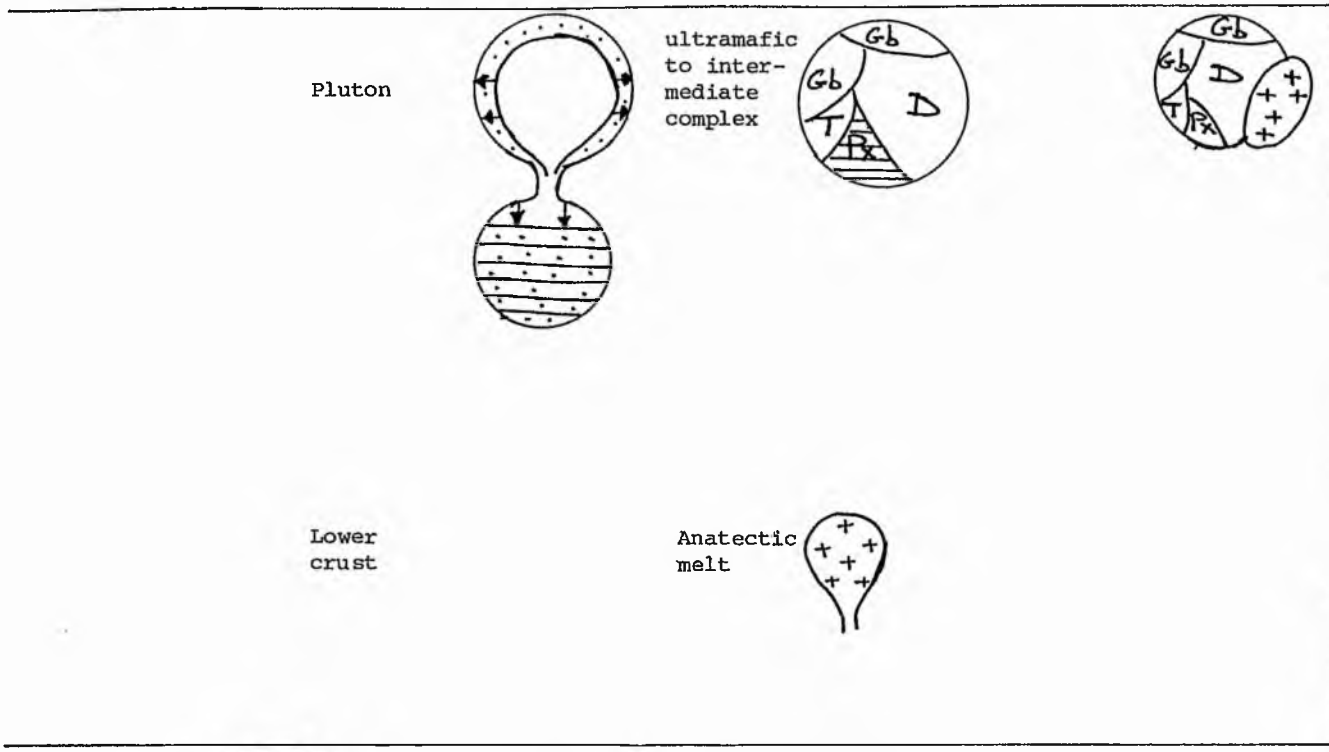

Fig 7.3 Schematic diagram for the formation of the Glen Doll pluton.

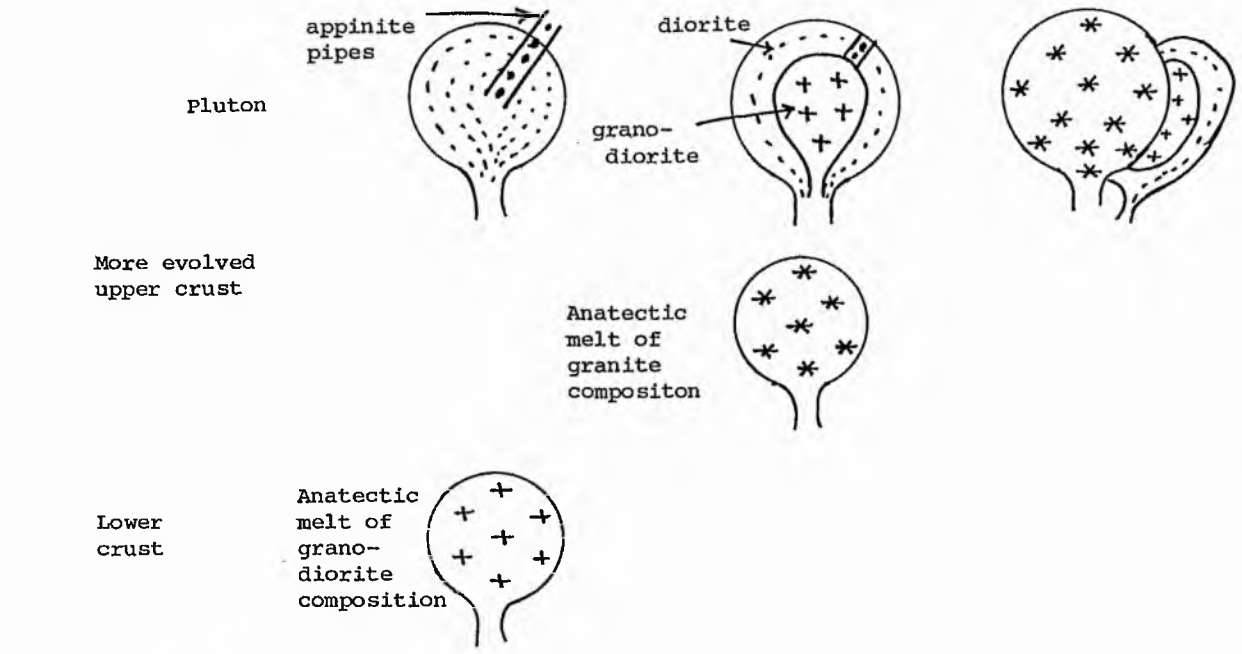

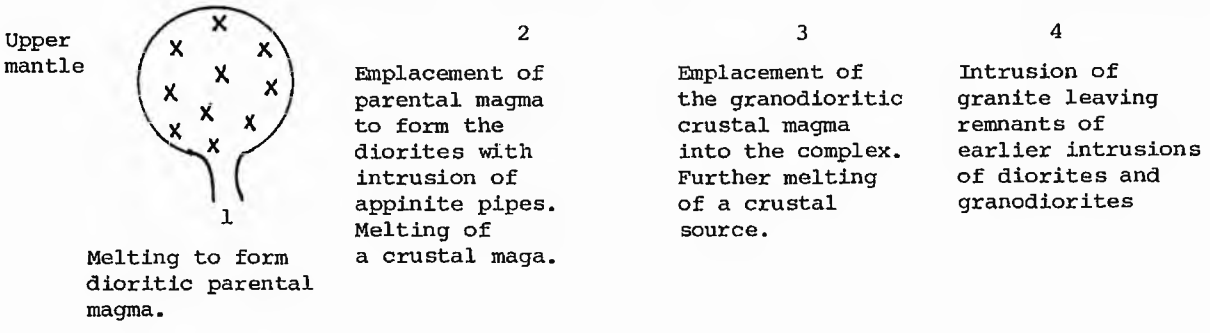

Fig 7.4 Schematic diagram for the formation of the Glen Tilt pluton.

difficult to resolve.

In the Comrie pluton the proposed parental magma of biotite pyroxene diorite composition was probably mantle-derived. It has been used as a successful parental composition for the modelling of quartz monzodiorites and granodiorites by crystal-liquid fractionation. The origin of the central granite is unclear as the nature of the samples obtained was such that they were unsuitable for analysis. The relative area of the granite and the rest of the complex suggest that it may have formed by crystal-liquid fractionation processes. The process is schematically illustrated on Fig 7.5.

In the Carsphairn pluton early microdiorites have textures suggesting that they are frozen magmas. These early magmas have high Ni and Cr abundances suggesting mantle-related origin. The petrogenesis of this pluton is complex and difficult to model, especially in the absence of isotopic data. The tonalite magma appears to be crustal in origin and may be parental to the granodiorites. Finally the granite pulse in the core of the pluton may also be from a separate source but it also has some features of evolved liquids that may be due to fractional crystallisation accompanied by contamination. The processes are schematically illustrated on Fig 7.6.

In the main part of the Loch Doon pluton the most basic rocks, the microdiorites, also appear to have the textures of frozen magma and are also the most primitive in terms of Sr isotope ratios (Halliday, et al. 1980). Isotopic studies suggest either the interaction of magmas from different source or the progressive contamination of the early magma by an evolved source. Geochemical modelling also favours crystal-liquid fractionation as a major process

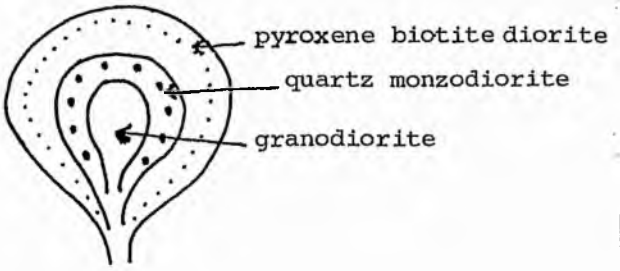

Pluton

Crust

Upper mantle

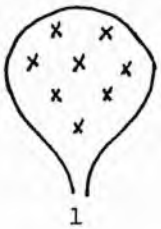

1

Melting to form dioritic parental magma

2

High level magma chamber fractionating pyroxene diorites, quartz monzodiorites and granodiorites.

Fig 7.5 Schematic diagram for the formation of the Comrie pluton.

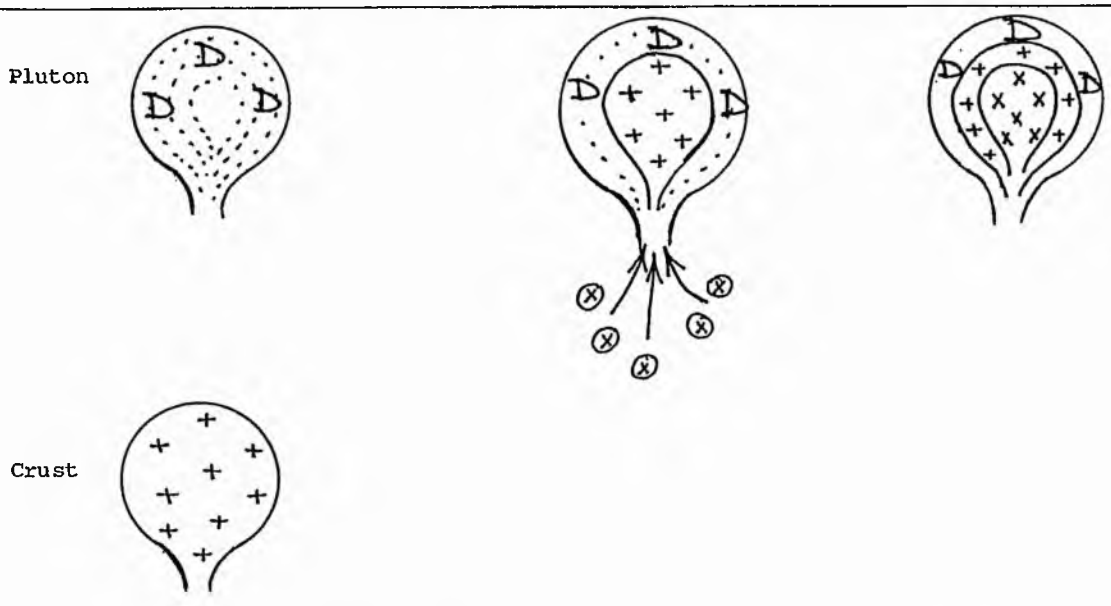

Fig 7.6 Schematic diagram for the formation of the Carsphairn pluton

contributing to compositional variation. It is difficult to quantify the effects of each process on the composition and it is likely that some or all operated at various times in the crystallisation history of this pluton. The very regular variation diagrams suggest continuity of the process through to the evolved stages of the pluton evolution. The processes are schematically illustrated on Fig 7.7.

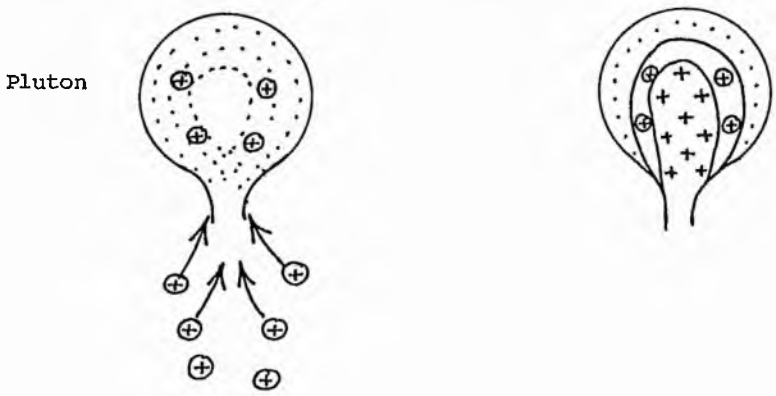

Fig 7.7 Schematic diagram for the formation of the Loch Doon pluton.

CHAPTER 8

REGIONAL ASPECTS OF PETROGENESIS

8.1 Introduction

The Caledonian granitoids of the British Isles were emplaced during the Ordovician, Silurian and early Devonian are a chemically and isotopically diverse group. The present study has been concerned mainly with plutons emplaced in the southern Grampian Highlands (namely Garabal Hill-Glen Fyne, Comrie, Glen Doll and Glen Tilt) and in the Southern Uplands (namely Cairnsmore of Carsphairn and Loch Doon) and in this chapter regional aspects of their petrogenesis are discussed.

8.2 Current models for the origin of the Scottish Caledonian granites:

The plutons of this study belong to the South of Scotland suite of Stephens and Halliday (1984) who classified the Caledonian intrusions of Scotland of the Grampian Highlands, the Midland Valley and the Southern Uplands into three suites (i.e. the S of Scotland, Cairngorm, and Argyll suites) according to their petrology and geochemistry. The South of Scotland suite is characterised by pyroxene diorites, granodiorites with some appinites in the north, showing a calc-alkaline affinity with low La, Ce, Ba and Sr relative to the Argyll and Cairngorm suites which show an abrupt change in petrography and geochemistry coinciding geographically with a similar rapid change in Nd values found by Halliday (1984) who proposed the term 'mid-Grampian line' for the boundary. Stephens and Halliday (1984) concluded that there is a change in the continental crustal basement corresponding the change in the chemistry of the underlying mantle and both mantle and crust underlying Scotland are geographically zoned from S to N, where the mantle to the N is old mantle attached to the base of the old crust and has been enriched in

elements such as K, Ba and Sr by metasomatic processes in the past.

Brown (1979) concluded from geophysical and geochemical data that Caledonian granite magma genesis was associated with ocean closure across southern Scotland during Lower Palaeozoic times with compressional tectonics during Ordovician times resulting in metamorphism, overthrusting and crustal melting on the northern Iapetus margin. Brown suggested that the break in geological continuity across the British Caledonides may occur near the Southern Uplands fault in agreement with the seismic cross-section of Bamford and Prodehl (1977) and the structural subdivison into orthotectonic and paratectonic provinces (Kelling, 1978).

Johnstone et al. (1979) studied the Caledonian granites in northern Scotland in relation to regional stream sediment geochemistry. These granites intrude Moine and Dalradian metasediments overlying a pre-Caledonian basement of Lewisian gneisses and granulites. Their geophysical and geochemical data on the Caledonian granites suggested that much of their source was sub-crustal which supplied volatiles and incompatible elements not widely available in the refractory lower crust. Johnstone et al. thought that in lower Devonian times the compressive orogenic regime was followed by the development of major faults cutting both cover and basement and by the rise of granitic magmas, and these magmas formed at subcrustal levels and their compositions varied with distance from the Iapetus suture.

Little published isotopic data is available for plutons of the Grampian Highlands studied in this thesis except for an early paper by Summerhayes (1966) on Garabal Hill, though the precision of the Rb-Sr method at that time was rather poor. Although a mean $(^{87}Sr/^{86}Sr)_0$

value for the different igneous rock types of 0.705 was presented, values for the granodiorite varied up to 0.7122. Summerhayes precluded refusion of Dalradian, Moine or Lewisian material as a source for the granodiorites and added that fractional melting of a low Rb/Sr source region deep within the crust below the "sialic" basement was probable. Table 8.1 is a summary of the isotopic data for the plutons studied, compiled from published work.

The first thorough isotopic investigation performed on these granites was the U-Pb zircon study of Pidgeon and Aftalion (1978) though it included none of the plutons of this study. This work showed a geographical control on the Pb isotopic memory in zircons, granites in the north yielding concordia upper intercept ages averaging c1600 Ma, whereas those to the south have no old inherited zircons. The implications of this are that at least some granites have a significant crustal component and that the age of the lower crust was older north of the Highland Boundary Fault correlating with Lewisian metamorphic ages. Halliday et al. (1979) showed that the local metasediments to the north (Moine and Dalradian) and to the south (Lower Palaeozoic greywacke - shale sequence) reflect this difference in degree of U-Pb zircon memory. They argued that the presence or absence of zircon memory could be explained in terms of melting and/or assimilation of differing crustal rock types regardless of the ultimate source of magma. Zircons must be derived from the continental crust since zircon is not common in the mantle and zircons from the mantle that have been analysed are very poor in U (Davis 1978). Blaxland et al. (1979) showed that common Pb isotopic composition in K-feldspars from the Caledonian granitoids became more radiogenic southwards suggesting the involvement of old U-depleted

Table 8.1: Summary of isotopic data for the studied late Caledonian granitoids south of the Great Glen Fault

Locality	Lithology	t (Ma)	$\left(\frac{^{87}Sr}{^{86}Sr}\right)$	εt_{Sr}	$\left(\frac{^{143}Nd}{^{144}Nd}\right)t$	εt_{Nd}	$\left(\frac{^{206}Pb}{^{204}Pb}\right)t$	$\left(\frac{^{207}Pb}{^{204}Pb}\right)t$	$\delta^{18}O$ (°/oo SMOW)
Garabal Hill	granodiorite	406	0.7078	(+54)	0.51192	(-3.7)			10.4
Comrie		400			0.51207	(-1.1)			
Loch Doon	diorite	408	0.7041-0.7054	(+1) -(+20)	0.51206	(-1.0)			7.8-8.3
	granodiorite	408	0.7052-0.7053	(+17)-(+18)	0.51205	(-1.4)			8.3
	granite	408	0.7052-0.7059	(+17)-(+27)			18.15	15.522	10.2-10.3

Explanation of Table 7.1: t = best estimate of emplacement age; numbers in brackets are the least certain; ε values are calculated relative to bulk earth parameters; $^{143}Nd/^{144}Nd = 0.512636$; $^{147}Sm/^{144}Nd = 0.1966$; $^{87}Sr/^{86}Sr = 0.7045$; $^{87}Rb/^{86}Sr = 0.0839$; data from Halliday et al (1979, 1980); Blaxland et al (1979); Harmon and Halliday (1980); and Halliday (1984).

(typical of granulites including Lewisian) crust in the north.

Simpson et al. (1979) studied the uranium mineralisation and granite magmatism in the British Isles and suggested that uranium enriched magmas of the Caledonian province are derived from subcontinental lithosphere underplated onto pre-existing Precambrian basement, and release of this magma was favoured by the tensional regime following the end of subduction at destructive margins. The source of the underplated magmas was said to be subducted oceanic lithosphere controlled by phlogopite dehydration.

Harmon and Halliday (1980) presented $\delta^{18}O$ values of the late Caledonian granites. The data show no systematic regional variations but display approximately linear variations of $\delta^{18}O$ with the initial $^{87}Sr/^{86}Sr$ ratios suggesting mixing between two end members. One end-member has primitive mantle-like values ($\delta^{18}O$ ~ 6 per mil, $^{87}Sr/^{86}Sr_i$ ~ 0.7030) and from this it was argued that a mantle-like component was important in the magma source. The second end-member was evolved crustal material. Both oxygen and strontium isotope data generally indicate that the parental magmas were hybrids derived from partial fusion of mantle-like material and varying proportions of a crustal component. Halliday et al. (1980) suggested hybrid origins for the Southern Upland plutons with individual plutons (eg Loch Doon) representing a mixture of mantle-derived magma and/or 'new' basic lower crust with metasedimentary rocks. The isotopic variations of Rb-Sr and O show incomplete hybridisation between magmas derived from the differing sources.

Halliday (1984) studied the initial Nd isotopic compositions of some plutons from the Caledonian of Scotland and showed that they become more radiogenic southwards, a trend closely related to the U-Pb

(zircon) systematics. He interpreted this as reflecting dominantly the age of major components of pre-existing continental crust. The Nd data in terms of model ages support the view that the age of the basement increases to the NW across the Grampian Highlands, and the basement in the Grampians south of his proposed mid-Grampian line appears to be isotopically similar to that of the Midland Valley and Southern Uplands with no evidence for old Lewisian-like continental basement (Halliday, 1984). The mid-Grampian line refers to the southerly limit of initial Nd values of less than -6 which approximately corresponds to the boundary between the presence and absence of inherited zircons. All plutons of this study lie south of the mid-Grampian line on the model of Halliday (1984) and should show little evidence of interaction with old Lewisian basement, though this does not preclude involvement of young crust. The techniques used in this study do not permit the thorough testing of this model using isotopes.

Brown et al. (1981) argued from geochemical and isotopic data of Caledonian plutons that a major contribution came from subducted ocean crust or more likely within subducted ocean crust wedge. Brown et al. (1984) used trace elements in subduction-related granites in an examination of the Siluro-Devonian intrusions of north and central Britain described by Brown et al. (1981) and concluded that the Loch Doon intrusion represents their "normal continental arcs" characterised by diorite-tonalite-monzogranite-granite and intermediate Rb, Th, U values, as opposed to mature continental arcs represented by some of the plutons of the northeastern Highlands especially Ballater and Cairngorm, (Brown et al. 1984), with two mica granites having high Rb, Th and U values representing crustal

contamination. These are thought largely to be the product of within-plate sources from which high levels of Nb, Ta, Hf and Y were derived. Accordingly they suggested that the difference between the northern and southern suites is due to separate mantle source regions, one subduction-enriched for the southern intrusions and another source with greater within plate component.

The results from the Lithospheric Seismic Profile in Britain (LISPB) study (Bamford et al. 1977) show a 'Lewisian-like' basement extending from northern Scotland and the central Highlands at a depth of 6-15 km as far south as the Midland Valley, where it rises to a depth of c.6 km. This basement was interpreted by Smith and Bott (1975) as being composed of granulites like the late Archean granulite facies rocks of the Kylesku group of NW Scotland while Hall et al. (1984) indicated that mafic basic rocks may in part form a significant component. Recent seismic experiments together with re-evaluation of some of the LISPB data indicate a further extension of this crystalline basement beneath the Southern Uplands at an even shallower depth of 1-5 km (Hall et al. 1983). Aftalion et al. (1984) found by investigation of inclusions in volcanic rocks that the basement beneath the Midland Valley is at least partly of granulite composition.

Harmon et al. (1984) studied the chemical and isotopic relationships of these granitoids and found that they exhibited systematic variations which were attributed to derivation from both mantle and crustal sources. They concluded that mantle-derived magmas with high Mg and Ni were involved in the generation of the more primitive 'younger' granitoids though they were affected by varying degrees of crustal contamination before emplacement and

crystallisation. The younger granitoids to the north of the Highland Boundary Fault in the Scottish Highlands were from both subcontinental mantle ($\delta^{18}O$ ~ 6 to 6.5 °/oo, initial $^{87}Sr/^{86}Sr$ ~ 0.7035 - 0.7040, $^{206}Pb/^{204}Pb$ ~ 17.9 - 18.1) and mafic to intermediate granulitic lower crust of the craton ($\delta^{18}O$ ~ 8 to 10 °/oo, initial $^{87}Sr/^{86}Sr$ ~ 0.705 - 0.707, $^{206}Pb/^{204}Pb$ ~ 16.5 - 17.0). The latter end-member is strongly enriched in Sr and Ba across the region. To the south in the Midland Valley and Southern Uplands the 'younger' granitoids were largely derived from the upper mantle or subducted oceanic lithosphere ($\delta^{18}O$ ~ 5.7 to 7.0 °/oo, $^{87}Sr/^{86}Sr$ ~ 0.7035 - 0.7040, $^{206}Pb/^{204}Pb$ ~ 17.9 - 18.1) and geosynclinal sediments ($\delta^{18}O$ ~ 11 to 14 °/oo, $^{87}Sr/^{86}Sr$ ~ 0.705 - 0.711, $^{206}Pb/^{204}Pb$ > 18.4).

Thirlwall (1981) demonstrated the existence of a systematic NW variation in element abundances in the ORS lavas north of the Southern Uplands Fault, and observed that the chemistry of all ORS lavas north of this fault was consistent with a subduction-related origin. He proposed a subduction zone that changed in strike from ENE in Ireland to NNE in the North Sea and that the Ni-rich lavas represent primary mantle-derived magmas. Northwestward increase in Sr, Ba, K, P and LREE, associated with northwest subduction of Iapetus ocean crust are not accompanied by changes in Rb, Th or Ti-group elements, and these relationships were explained as not simply the result of change in the degree of partial melting with depth. The Nd-Sr isotopic variations show Nd to decrease to the NW, and it is considered that it is not related to crustal contamination with a crustal source. Thirlwall (1982) preferred a model of two different mantle sources with Midland Valley lavas derived from a long-term LREE depleted mantle source modified by interaction with subducted oceanic

lithosphere. Those two mantle magmas were explained by vertical layering, with deeper more LREE-enriched layers accessible only to magmas formed at great depth in a subduction zone.

8.3 Regional petrogenesis of the six dioritic complexes

8.3a Tectonic implications

The emplacement of the granitoid plutons during the Caledonian orogeny and its collision phase with the destruction of the Iapetus Ocean has been considered by Thirlwall (1981, 1982); Brown (1979, 1984); Brown et al. (1981); Johnstone et al. (1979); Simpson et al. (1979) and Harmon et al. (1984). Others, eg Halliday et al. (1979, 1980); Halliday (1984) and Stephens and Halliday (1984) consider the relationship to subduction to be less direct.

In general there is agreement that mantle-derived magmas were responsible for the formation of the gabbros and diorites of the plutons studied. Some authors also consider a contribution from lower crustal sources by contamination or mixed processes is required for the more evolved rocks, and/or crustal anatexis, though the relative importance of this latter source is not agreed.

8.3b Regional variation in the plutons

The plutons investigated show regional differences in petrography, whole rock and mineral chemistry (Table 8.2) and the object of this section is to compare these with the other features such as published isotopic data.

The Southern Uplands plutons tend to show good concentric zoning of composition usually ranging from diorite at the outer margins, to granodiorite, ultimately to granite in the centre. Plutons studied

Table 8.2: Summary of regional petrographical, mineral and whole rock chemical variations for the studied plutons.

	Grampian Highlands				Southern Uplands	
	W	S	E	E		
Name of pluton	Garabal Hill	Comrie	Glen Doll	Glen Tilt	Loch Doon	Carsphairn
SiO_2 range	42-68	53-71	46-69	49-76	57-72	56-71
Petrographic types	peridotite, gabbro, diorite appinite and granodiorite	diorite, quartz monzodiorite, granodiorite and granite	pyroxenite, gabbro, diorite and granodiorite	diorite, appinite, quartz diorite, granodiorite and granite	diorite, granodiorite, and granite	diorite, tonalite granodiorite and granite
AFM plot	"normal" calc-alkaline	Moderate Fe calc-alkaline	Very high Fe calc-alkaline	High Fe calc-alkaline	"normal" calc-alkaline	Moderate Fe calc-alkaline
2 pyroxene temperature	1081-1008	982-938	981-960	-	974-924	911
$Mg^{\#}$ cpx	0.83-0.76	0.78-0.67	0.82-0.73	-	0.76-0.74	0.65-0.57
$Mg^{\#}$ opx	0.74-0.72	0.69-0.57	0.84-0.69	-	0.70-0.67	0.67-0.48
$Mg^{\#}$ amph	0.73-0.65	0.70-0.62	0.88-0.60	0.71-0.65	0.73-0.63	0.76-0.43
$Mg^{\#}$ biot	0.63-0.54	0.65-0.57	0.84-0.64	0.63-0.50	0.70-0.40	0.70-0.37
Average Ni at 5% MgO	>100 ppm	up to 100 ppm	up to 50 ppm	up to 50 ppm	up to 100 ppm	up to 70 ppm
Average Cr at 5% MgO	>250 ppm	up to 200 ppm	up to 170 ppm	up to 50 ppm	up to 250 ppm	up to 200 ppm

from the Grampian Highlands tend to show irregular zoning (except for Comrie which is also concentric) and the distribution of the outer diorites with granite tends to be geometrically more irregular.

Ultrabasic and basic rocks are represented only in the Grampian Highlands with peridotites (wehrlite) at Garabal Hill and pyroxenite (with brown hornblende) at Glen Doll. Gabbros are also found in these two complexes. Diorites are mainly of two types, namely pyroxene biotite diorite (in the Garabal Hill, Comrie, Carsphairn and Loch Doon plutons) and hornblende biotite diorite (in all plutons).

In major oxide terms all plutons generally follow the calc-alkaline to high-k calc-alkaline trend of Peccerillo and Taylor (1976), along with nigh Na abundances. The AFM plots summarised in Fig 8.1 generally show calc-alkaline trends but with variations. In the Southern Uplands the Carsphairn pluton shows a more Fe rich trend than its very close neighbour Loch Doon. In the Grampian Highlands the Comrie pluton shows greater Fe enrichment than Garabal Hill, while Glen Doll and Glen Tilt in the E Grampians show very strong Fe enrichment. These features follow through to the ferromagnesian mineral chemistry as by the Mg/Mg + Fe values of the ferromagnesian minerals (pyroxenes, amphibole and biotite Fig, 8.3).

The Garabal Hill, Comrie and Loch Doon plutons show the highest levels of Ni in the more basic rock types probably reflecting a substantial contribution of mantle-derived material and additionally, in the case of Garabal Hill, cumulate processes (Fig 8.2a). Cr is also enriched in Garabal Hill with lesser enrichments in Glen Doll (Fig 8.2b). High Ni values are accompanied by high Ba and Sr for the diorites and microdiorites reflecting their probable mantle-derivation (Halliday et al. in press). Plots of Sr-CaO, Ba-K_2O, and Rb-K_2O (Fig

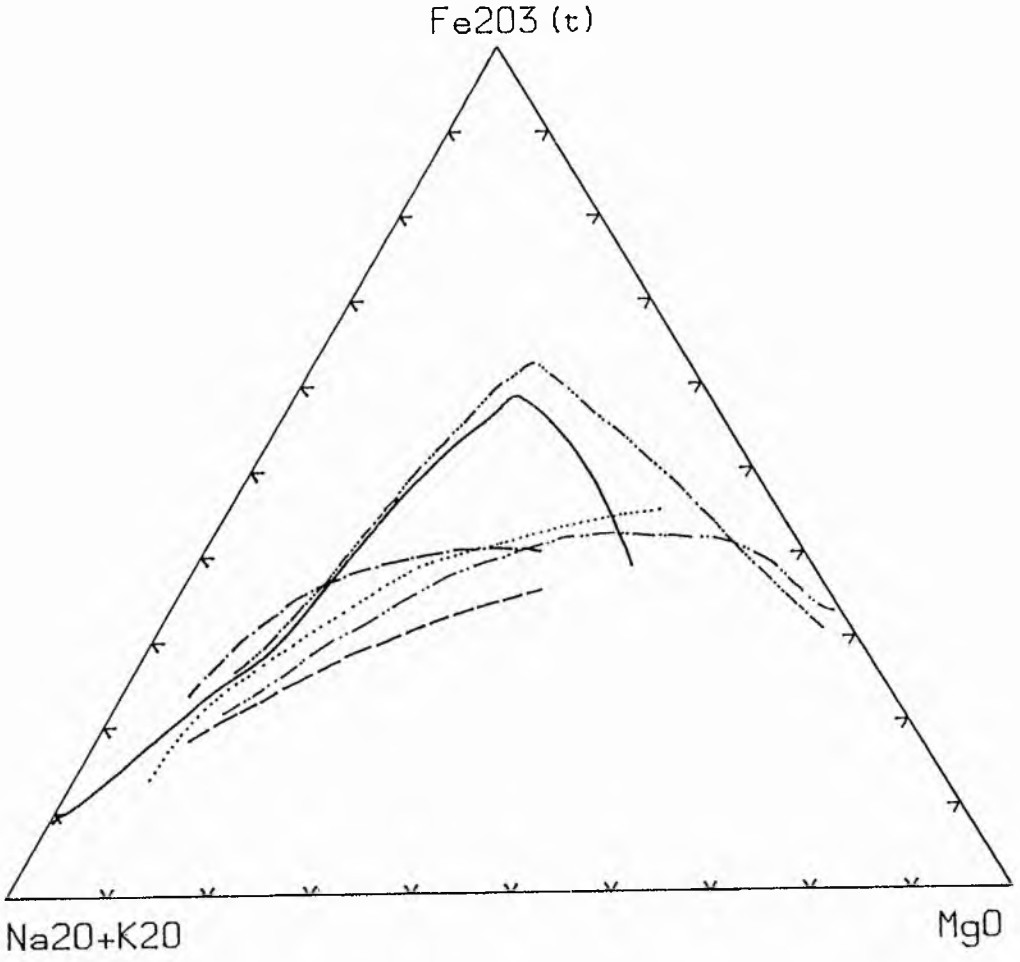

Fig 8.1 AFM plot with the average trends of the different plutons. Symbols are as in Fig 7.2.

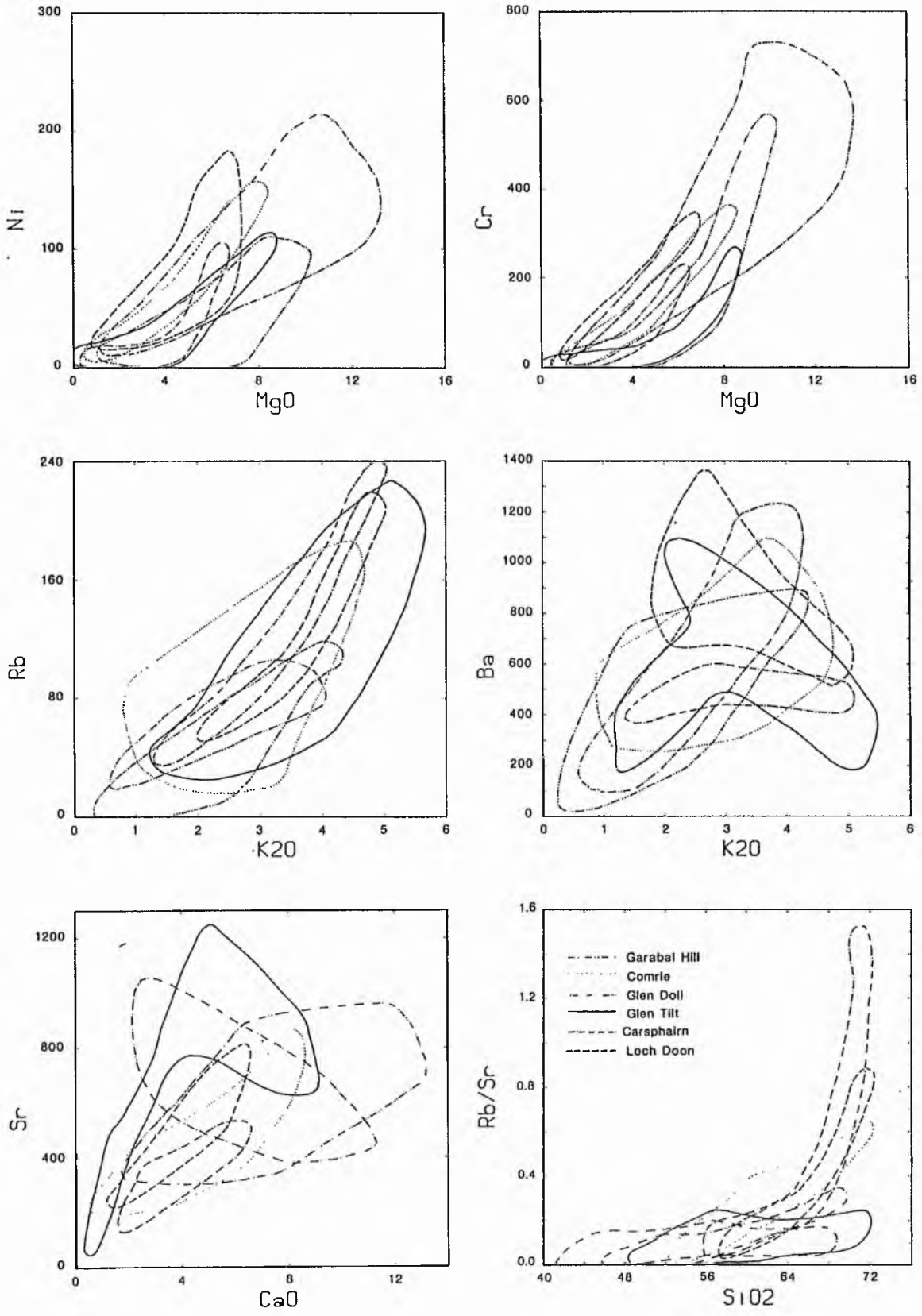

Fig 8.2 Variation diagrams for some major oxides and trace elements showing fields for each pluton.

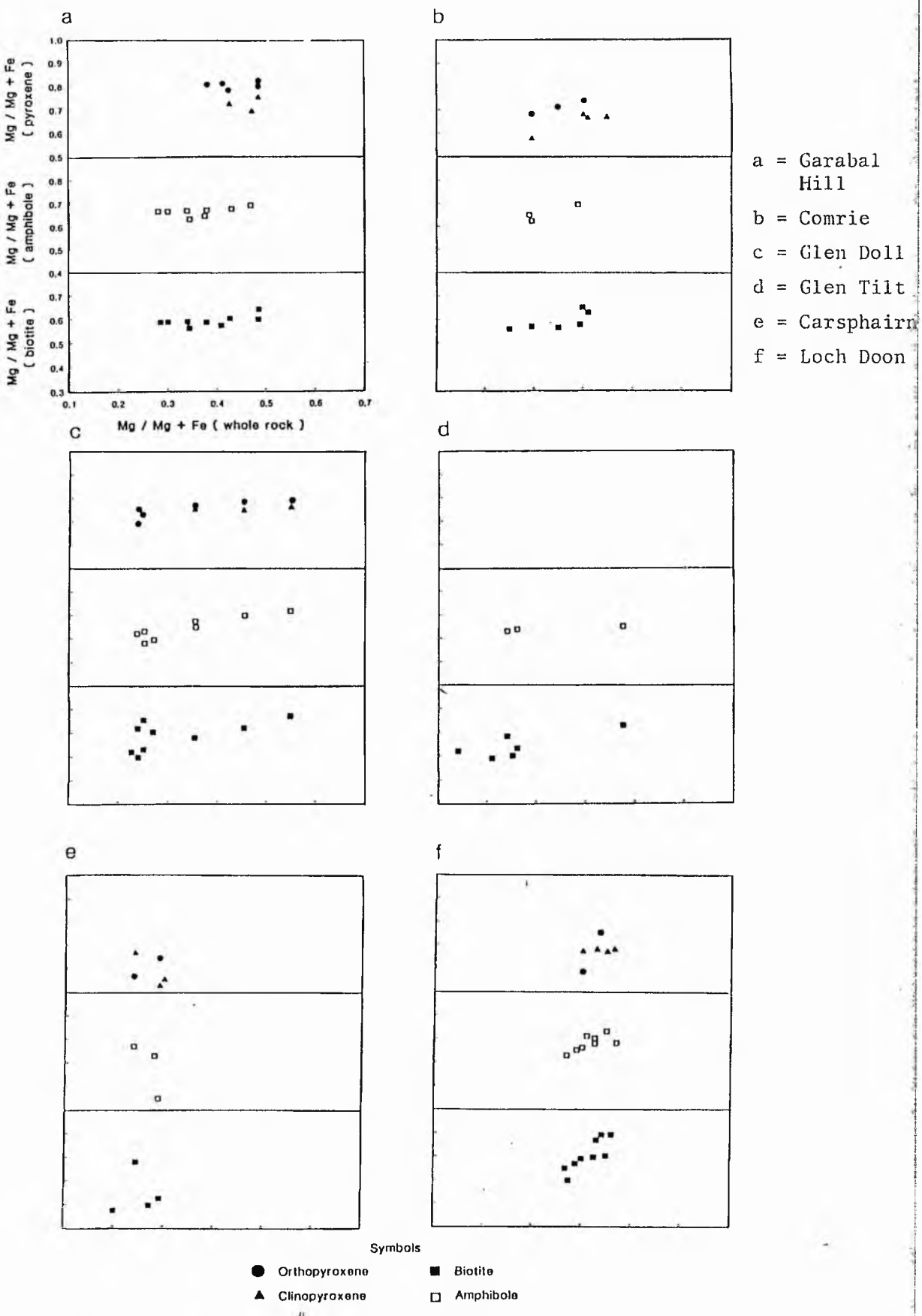

Fig 8.3 Plots of $Mg^{\#}$ values of whole rock samples versus $Mg^{\#}$ values of orthopyroxene, clinopyroxene, amphibole and biotite. All diagrams on same scale.

8.2_{c-e}) show wide variations for these plutons indicating that parental magma compositions perhaps reflect heterogeneous source regions, different degrees of partial melting as well as differences in subsequent fractional crystallisation processes.

The compositional diversity is dominated by fractionation processes of mantle-derived parental magmas mostly of pyroxene-biotite diorite or gabbroic composition. For the Garabal Hill, Comrie and Loch Doon plutons this magma fractionated mainly orthopyroxene, clinopyroxene, plagioclase and biotite, and for Carsphairn pluton a tonalitic parental magma fractionated the above minerals to form the granodiorites. Accessory phases also fractionated controlling some of the minor element abundances.

The plutons to the east of the Grampian Highlands especially Glen Doll was petrogenetically modelled from a gabbroic parental magma rich in amphibole which is rich in Mg (Fig 8.4) reflected on the AFM plots of the whole rocks and amphiboles.

The chondrite normalised plots (Fig 8.5c) for the granodiorites show great similarities except for the Garabal Hill pluton granodiorites which show large differences and were not plotted on the same figure (but see Fig 5.3a for comparison). The eastern Grampian Highland plutons are depleted in La, Rb, Ba, K and Zr relative to the other plutons and enriched in Th, Ce, Sr, P and Ti. Garabal Hill differs in having higher Sr and Ba. Lack of Th and other incompatible element depletions in these plots supports the idea that there is no Lewisian-type crust involved in the petrogenesis of even the granites in these plutons.

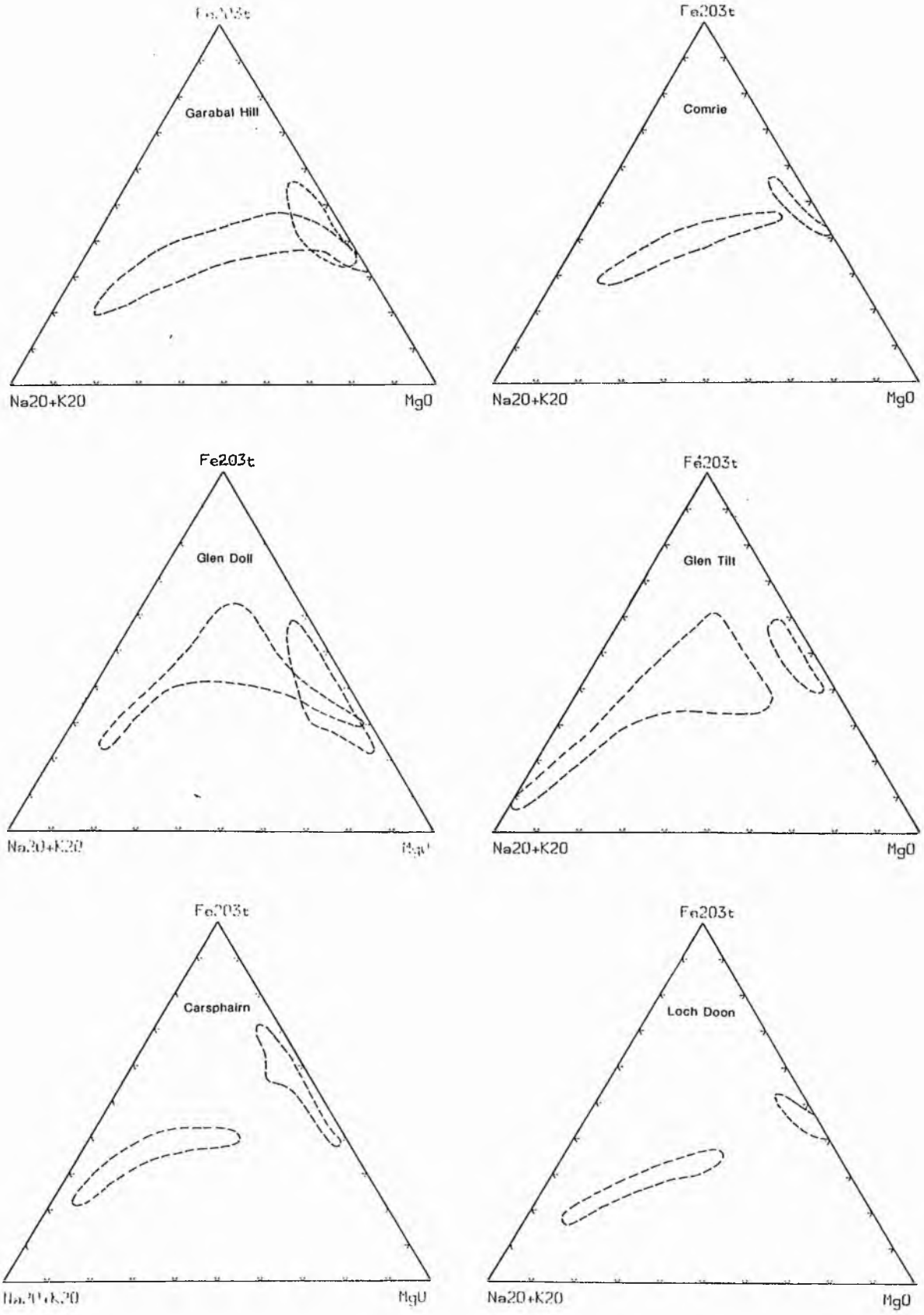

Fig 8.4 AFM plots showing the fields of the analysed amphiboles (near to Fe_2O_3t - MgO join) and the fields for their host rocks.

In key to symbols

GH = Garabal Hill

CM = Comrie

GD = Glen Doll

GT = Glen Tilt

CS = Carsphairn

LD Loch Doon

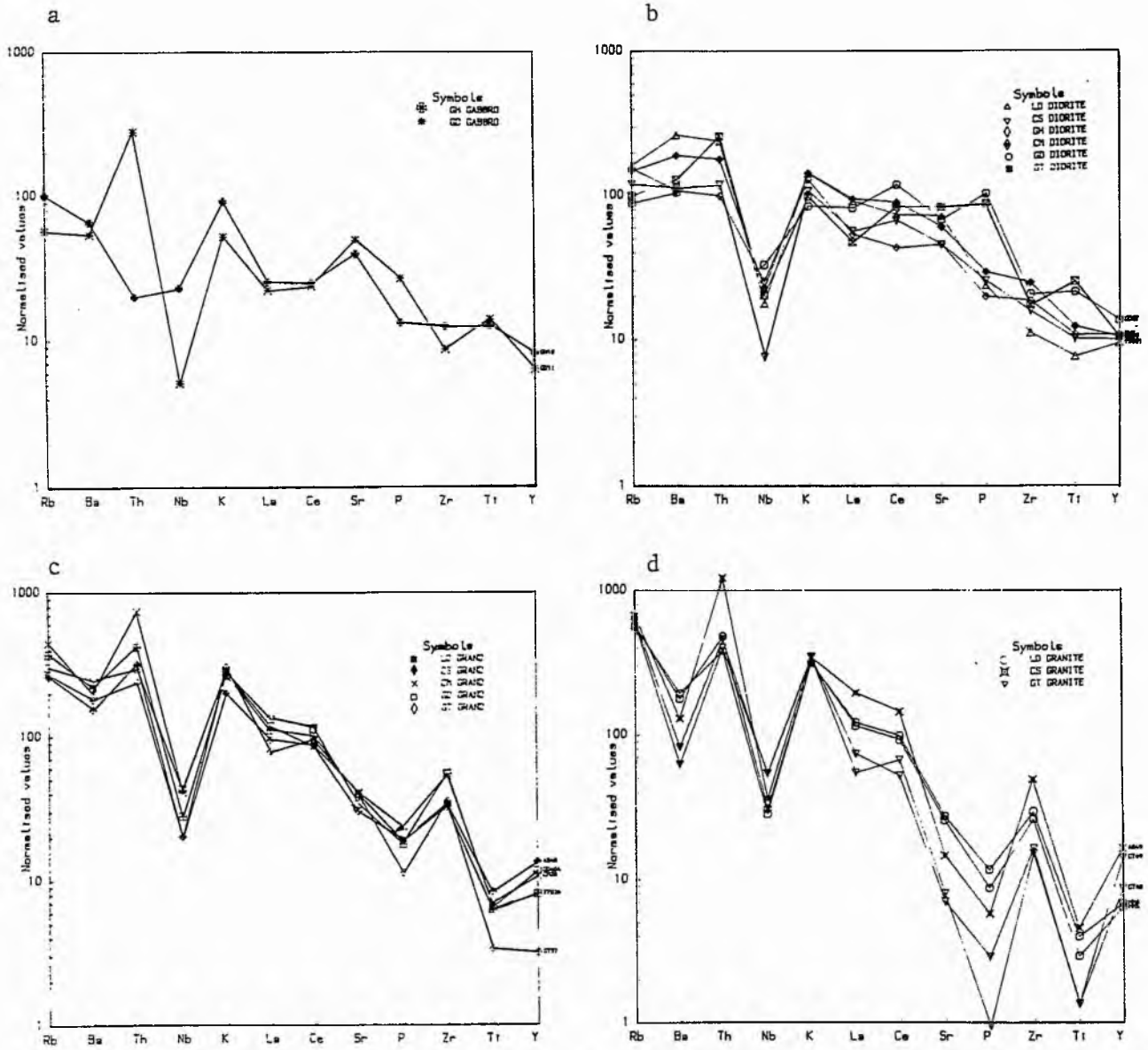

Fig 8.5 Chondrite - normalised plots of representative gabbros, diorites, granodiorites and granites from the studied plutons.

CHAPTER 9

CONCLUSION

The study has principally been aimed at using mineralogical and geochemical techniques to understand better the origins of petrological zoning in diorite - granite plutons in the Caledonian of Scotland, and at regional variations in bulk composition in plutons of this type.

The principal conclusions of this study are:

1) The petrological range in composition is wide, varying from peridotite through to granite. The plutons from the Grampian Highlands contain some ultramafic rock types of peridotite (wehrlite) and pyroxenite compositions in the Garabal Hill and Glen Doll plutons respectively, along with hornblende gabbros. Pyroxene biotite gabbros and quartz gabbros with hornblende are also present in these plutons. Diorites of two types are present in all of the studied plutons, the types being:

i) two-pyroxene biotite diorite, and

ii) hornblende biotite diorite

Appinitic diorites are present only in the Garabal Hill and the Glen Tilt plutons. Tonalites are present in the Glen Doll and Carsphairn plutons, though those from Carsphairn contain the two pyroxene minerals with biotite unlike those from Glen Doll which have biotite as the only mafic mineral. Granodiorites are common rock types in all six plutons and they vary texturally. Granites are present in four of the plutons being absent in Garabal Hill and Glen Doll.

2) From the mineral chemical data, it is concluded that:

a) Analysed olivines from the peridotites, pyroxene biotite gabbros

and diorites of Garabal Hill and from pyroxenites of the Glen Doll plutons have very small amounts of CaO and MnO, ranged from Fo_{81} to Fo_{77}.

b) Clinopyroxenes are of salite to augite in composition except for those from the ultrabasic peridotites and pyroxenites which are diopside. Clinopyroxenes from the tonalite of the Carsphairn pluton are typically of augite composition (Fig 4.1).

c) Orthopyroxenes analysed from the Comrie, Carsphairn, and Loch Doon plutons are mainly of hypersthene composition while those from the Garabal Hill and Glen Doll plutons are of bronzite and hypersthene compositions (Fig 4.1).

d) Using two-coexisting pyroxenes for calculating the equilibration temperature, decreasing temperatures are indicated from the pyroxene gabbro in Garabal Hill - Glen Fyne (1080 ^{o}C) through diorites (1010 - 925 ^{o}C) from Garabal Hill, Comrie and Loch Doon to tonalite (850 ^{o}C) from the Carsphairn pluton. Pyroxenite temperatures are the highest (1020 ^{o}C) followed by gabbros (975 - 960 ^{o}C) from Glen Doll pluton. The diorites from the Grampian Highland plutons have higher equilibration temperatures than diorites from the Loch Doon pluton in the Southern Uplands. KD values for the partitioning of Mg and Fe^{2+} between different pyroxenes gave typically igneous values (Kretz, 1961, 1963) suggested for igneous rocks varying from 0.65 to 0.86 except for higher KD's from the Carsphairn pluton related to the greater Fe abundance of this pluton.

e) Amphiboles are mainly calcic of magnesio-hornblende compositions with tschermakitic types in the ultrabasic and basic rocks from Garabal Hill and Glen Doll plutons. Secondary amphiboles are of

actinolitic hornblende to actinolite in composition in terms of Leake classification (1978). In the Carsphairn pluton some amphiboles are of ferro-hornblende composition (Fig 4.2) in addition to magnesio-hornblende again reflecting its Fe enrichement. The principal variation in the amphibole chemistry results from both Ti-tschermakite and edenite substitutions.

f) Mica analyses have shown that they are principally biotites, though with some minor phlogopite in Garabal Hill appinites, Glen Doll pyroxenites, Loch Doon and Carsphairn. Garabal Hill and Glen Doll granodiorites show signs of contamination according to the Fe values which show reversals of the normal igneous fractionation trend.

g) Plagioclases from ultrabasic and gabbronoritic rocks from the Glen Doll pluton are bytownite and labradorite, while plagioclases from pyroxene biotite gabbros and quartz gabbros are labradorites. Plagioclases from diorites are commonly of andesine composition, whereas plagioclases from granodiorites and tonalites are of high Ca oligoclase to low Ca andesine. Those from granites vary from oligoclase to albite in composition.

3) From the whole rock chemical data it is concluded that:

a) All plutons follow calc-alkaline trends on the AFM diagrams though with regional variations in Fe/Mg. Glen Doll and Glen Tilt show high Fe enrichment (see Chapter 5) whereas Loch Doon and Garabal Hill are "normal". Carsphairn and Comrie being intermediate. In terms of the Peccerillo and Taylor classification they are normal calc-alkaline to high-K calc-alkaline series, except for Loch Doon which is entirely high-K calc-alkaline. All are I-types in terms

of Chappell and White classification.

b) In terms of trace elements, Garabal Hill, Comrie, Carsphairn and Loch Doon contain high Ni and Cr concentrations in intermediate rock types with greater than 100 ppm Ni in diorites. Cu and Zn are enriched in the plutons of the Grampian Highlands (up to 300 ppm Cu and 160 ppm Zn), Glen Doll being the richest in both elements. The Southern Uplands plutons have less than 50 ppm Cu and less than 70 ppm Zn abundances. Zr is very much concentrated in the quartz diorites of Glen Tilt (up to 1600 ppm). Very high Sr and Ba values (>1000 ppm) are observed in the porphyritic granodiorites of Garabal Hill.

4) The petrogenesis of the plutons was studied individually using modelling techniques. A mantle derivation for magmas of pyroxene biotite gabbroic composition or two pyroxene biotite diorite composition is apparent. Fractionation of parental magmas was responsible for the genesis of most of the intermediate rock types in the Garabal Hill, Comrie and Loch Doon plutons. The main fractionating phases were orthopyroxene, clinopyroxene, plagioclase and biotite, along with accessory apatite and opaque phases.

The Glen Doll pluton rock types as far as tonalites were formed by fractionation of a parental gabbroic magma rich in hornblende and fractionating amphibole, plagioclase and biotite. For the Glen Tilt pluton a multi-intrusion model was proposed, though quartz diorite parental magma formed granodiorites by fractionating plagioclase and biotite. The granite was apparently a separate pulse of magma. For the Cairnsmore of Carspharin rock types a tonalitic parental magma is proposed and formed

granodiorites by fractionation of orthopyroxene, clinopyroxene, plagioclase and biotite.

Mixing modelling also succeeded for the Southern Uplands plutons by taking two end-members representing a two pyroxene biotite diorite with granitic end member for the Loch Doon pluton, and a tonalitic end member with granite for the Cairnsmore of Carsphairn pluton.

Contamination of a parental magma is also considered probable in generating some of the more acid evolved compositions but the techniques used in this study were not able to resolve the contributions of each process.

REFERENCES

Aftalion, M., van Breemen, O. and Bowes, D.R. (1984). Age constraints on basement of the Midland Valley of Scotland. Trans. R. Soc. Edinburgh, Earth Sci., 75, 53-64.

Anderson, A.T. (1976). Magma mixing: petrological processes and volcanological tool. J. Volcanol Geotherm. Res. 1, 3-33.

Anderson, A.T. (1982). Parental basalts in subduction zones: implication for continental evolution. J. Geophys. Res. 87: 7047-7060.

de Albuquerque, C.A.R. (1973). Geochemistry of biotites from granitic rocks, Northern Portugal. Geochim. Cosmochim. Acta, 37, 1779-1802.

de Albuquerque, C.A.R. (1974). Geochemistry of actinolitic hornblendes from tonalitic rocks, Northern Portugal. Geochim. Cosmochim. Acta, 38, 789-883.

Arth, J.G. (1976). Behaviour of trace elements during magmatic processes - a summary of theoretical models and their applications. Res. J. U.S. Geol. Surv. 4, 41-47.

Arth, J.G. and Barker, F. (1976). Rare-earth partitioning between hornblende and dacitic liquid and implications for the genesis trondhjemitic-tonalitic magma. Geology, 4, 534-536.

Atherton, M.P. (1981). Horizontal and vertical zoning in the Peruvian Coastal Batholith. J. Geol. Soc. London., 138, 343-350.

Bamford, D., and Prodehl, C. (1977). Explosion seismology and the continental crust-mantle boundary. J. Geol. Soc. London. 134, 139-151.

Bamford, D., Nunn, K., Prodehl, C. and Jacob, B. (1977). LISPB-III Upper crustal structure of northern Britain. J. Geol. Soc. London, 133, 481-488.

Barriere, M. (1976). Flowage differentiation: Limitation of the "Bagnold Effect" to the narrow intrusions. Contrib. Mineral. Petrol. 55, 139-145.

Barrow, G., and Craig, E.H.C., (1912). The geology of the districts of Braemar, Ballater and Glen Clova. (Explanation of sheet 65). Memoirs of the Geological Survey, Scotland.

Barrow, G., Craig, E.H.C., and Kynaston, H. (1913). The geology of Upper Strathspey, Gaick and the forest of Atholl. (Explanation of sheet 64). Memoirs of the Geological Survey, Scotland.

Batchelor, R.A. (1980). Analysis of major, minor and selected trace elements in silicate rocks and minerals. Internal Publication No 80/1, Univ. of St Andrews.

Bateman, P.C. and Chappell, B.W. (1979). Crystallisation, fractionation, and solidification of the Tuolumne Intrusive Series, Yosemite National Park. Geol. Soc. Am. Bull. 90, 465-482.

Best, M.G. and Mercy, E.L.P. (1967). Composition and crystallisation of mafic minerals in the Guadalupe igneous complex. California Amer. Mineral. 52, 436-474

Blaxland, A.B., Aftalion, M. and van Breemen, O. (1979). Pb isotopic composition of feldspars from Scottish Caledonian granites, and the nature of the underlying crust. Scott. J. Geol. 15, 139-151.

Boettcher, A.L. (1973). Volcanism and orogenic belts - the origin of andesites. Tectonophys., 17, 223-240.

Brown, G.C. (1977). Mantle origin of Cordilleran granites. Nature, London, 265, 21-24.

Brown, G.C. (1979). Geochemical and geophysical constraints on the origin and evolution of Caledonian granites. In: Harris, C.H. and Leake, B.E. (eds.). The Caledonides of the British Isles. Reviewed. 717-722. The Geological Society, London.

Brown, G.C., Cassidy, J., Tindle, A.G., and Hughes, D.J. (1979). The Loch Doon granite: an example of granite petrogenesis in the British Caledonides. J. Geol. Soc. London, 136, 745-753.

Brown, G.C., Plant, J.A. and Simpson, P.R. (1981). Caledonian plutonism in Britain: a summary. J. Geophys. Res., 86 B11, 10502-10514.

Brown, G.C., Thorpe, R.S. and Webb, P.C. (1984). The geochemical characteristics of granitoids in contrasting arcs and comments on magma sources. J. Geol. Soc. London,, 141, 413-426.

Carmichael, I., Turner, F. and Verhoogen, J. (1974). Igneous Petrology: McGraw-Hill, New York

Carroll, D.M (1960). The Forfarshire Diorites. I The N.E. Part of the Glen Doll complex. II The Hornblende-Granodiorite of Bachnagairn. Honour thesis, Univ. of St Andrews.

Cawthorn, R.G. (1976a). Some chemical controls on igneous amphibole composition. Geochim. Cosmochim. Acta, 40, 1319-1328.

Cawthorn, R.G. (1976b). Calcium-poor pyroxene reaction relations in calc-alkaline magmas. Amer. Mineral. 61, 907-912

Cawthorn, R.G. and O'Hara, M.J. (1976). Amphibole fractionation in calc-alkaline magma genesis. Amer. J. Sci. 276, 309-329.

Cawthorn, R.G., Strong, D.F. and Brown, P.A. (1976c). Origin of corundum-normative intrusive and extrusive magmas, Nature. London, 259, 102-104.

Chappell, B.W. (1984). Source rocks of I- and S-type granites in the Lachlan Fold Belt, southeastern Australia. Phil. Trans. R. Soc. London, A310, 693-707.

Chappell, B.W. and White, A.J.R. (1974). Two contrasting granite types. Pacific Geol., 8, 173-174.

Cox, K.G., Bell, J.D. and Pankhurst, R.J. (1979). The interpretation of igneous rocks. George, Allen and Unwin. London. 450 p.

Czamanske, G.K. and Wones, D.R. (1973). Oxidation during magmatic differentiation, Finnmarka complex, Oslo area, Norway: Part II, The mafic silicates. J. Petrol, 14, 349-380.

Dakyns, J.R. and Teall, J.J.H., (1892). On the plutonic rocks of Garabal Hill and Meall Breac. Q.J. Geol. Soc. London. 48, 104-

Davis, G.L. (1978). Zircons from the upper mantle. Carnegie Inst. Washington, YEARB, 77, 895-897.

Deer, W.A. (1935a). The Cairnsmore of Carsphairn igneous complex. Q. J. Geol. Soc. London, 91, 47-76.

Deer, W.A. (1937). The composition and paragenesis of the biotites of the Carsphairn igneous complex. Mineral. Mag., 24, 495-502.

Deer, W.A. (1938). The diorites and associated rocks of the Glen Tilt complex, Perthshire. I. The granites and intermediate hybrid rocks. Geol. Mag., 75, 174-184.

Deer, W.A. (1950). The diorites and associated rocks of the Glen Tilt complex, Perthshire. II. Diorites and appinites. Geol. Mag.

87, 181-194.

Deer, W.A. (1953). The diorites and associated rocks of the Glen Tilt complex, Perthshire. III. Hornblende schist and hornblendite xenoliths in the granite and diorite. Geol. Mag. 90, 27-33.

Deer, W.A., Howie, R.A. and Zussman, J. (1966). An introduction to the rock-forming minerals. Longman Group Ltd., London 528 p.

Deer, W.A., Howie, R.A. and Zussman, J. (1978). Rock-forming Minerals Vol. 2A, Single-Chain Silicates. London: Longman.

Deer, W.A., Howie, R.A. and Zussman, J. (1982). Rock-Forming Minerals, Vol 1A, Orthosilicates. Longman Group Limited, London.

Depaolo, D.J. (1981b). A neodymium and strontium isotopic study of the Mesozoic calc-alkaline granitic batholiths of the Sierra Nevada and Peninsular Ranges, California. J. geophys. Res. 86, 10470-10488.

Dodge, F.C.W., Papike, J.J. and Mays, R.E. (1968). Hornblendes from Granitic Rocks of the Central Sierra Nevada Batholith, California. J. Petrol., 9, 378-410.

Dodge, F., Smith, V. and Mays, R. (1969). Biotites from granitic rocks of the Central Sierra Nevada batholith, California. J. Petrol., 10 250-271.

Dodge, F.C.W. and Ross, D.C. (1971). Co-existing hornblendes and biotites from granitic rocks near the San Andreas fault, California. J. Geol. 79, 158-172.

Doolan, B.L., Zen, E.-an, and Bence, A.E. (1978). Highly aluminous hornblendes: compositions and occurrences from southwestern Massachusetts. Amer. Mineral. 63, 1088-1099.

Eggler, D.H., and Burnham, C.W. (1973). Crystallisation and fractionation trends in the system andesite -H_2O-CO_2-O_2 at pressures to 10 kb. Geol. Soc. Amer. Bull., 84, 2517-2532.

Eichelberger, J.C. (1975). Origin of andesite and dacite: Evidence of mixing at Glas Mountain in California and at other Circum-Pacific volcanoes. Geol. Soc. Amer. Bull.,86, 1381-1391.

Eichelberger, J.C. and Gooley, R. (1977). Evolution of silicic magma chambers and their relationship to basaltic volcanism. Geophys. Monogr. Amer. Geophys. Union, 20, 57-77.

Evensen, N.M., Hamilton, P.J. and O'Nions, R.K. (1978). Rare-earth abundances in chondritic meteorites. Geochim. Cosmochim. Acta, 42, 1199-1212.

Fleet, M.E. (1974a). Partition of Mg and Fe^{2+} in coexisting Pyroxenes. Contrib. Mineral. Petrol. 44, 251-257.

Fleet, M.E. (1974b). Partition of major and minor elements and equilibration in coexisting pyroxenes. Contrib. Mineral. Petrol. 44, 259-274.

Fleet, M.E. and Barnett, R.L. (1978). Al^{IV}/Al^{VI} partitioning in calciferous amphibole from the Flood Mine, Sudbury, Ontario, Canadian Mineral. 16, 527-532.

Foster, M.D. (1960). Interpretation of the composition of trioctahedral micas. U.S. Geol. Surv. Prof. Paper, 354-B, 1-49.

Fourcade, S., and Allegre, C.J. (1981). Trace elements behaviour in granite genesis: a case study. The calc-alkaline plutonic association from the Querigut complex (Pyrenees, France). Contrib. Mineral. Petrol. 76, 177-195.

Fridrich, C.J., and Mahood, G.A. (1984). Reverse zoning in the resurgent intrusions of the Grizzly Peak cauldron, Sawatch Range, Colorado. Bull. Geol. Soc. America. 95, 779-787.

Gardiner, C.I. and Reynolds, S.H. (1932). The Loch Doon "granite" area. Galloway, Q.J. Geol. Soc. London, 83, 1-34.

Geikie, J., (1866). On the metamorphic origin of certain granitoid rocks and granites in the Southern Uplands of Scotland. Geol. Mag. 3, 529.

Gill, J.B. (1978). Role of trace element partition coefficients in

models of andesite genesis. Geochim. Cosmochim. Acta, 42, 709-724.

Gill, J.B. (1981). Orogenic andesites and plate tectonics. Springer Verlag, Berlin-Heidelberg-New York.

Gorbatschev, R. (1969). Element distribution between biotite and Ca-amphibole in some igneous or pseudoigneous plutonic rocks. Neues Jahrb. Mineral. Abb. 111, 314-342.

Gorbatschev, R. (1970). Distribution of tetrahedral Al and Si in co-existing biotite and Ca-amphibole. Contrib. Mineral. Petrol. 28, 251-258.

Green, T.H. (1980). Island arc and continent-building magmatism a review of petrogenetic models based on experimental petrology and geochemistry. Tectonophys., 63, 367-385.

Green, T.H., and Ringwood, A.E. (1968). Genesis of the calc-alkaline igneous suite. Contrib. Mineral. Petrol., 18, 105-162.

Groome, D.R. and Hall, A. (1974). The geochemistry of the Devonian lavas of the Northern Lorne Plateau, Scotland. Mineral. Mag. 39, 621-640.

Gunn, W., Clough, C.T., and Hill, J.B. (1897). The Geology of Cowal. Mem. Geol. Surv. Scotland.

Hall. J., Powell, D.W., Warner, M.R., El_Isa, Z.M.H., Adesanya, O. and

Bluck, B.J. (1983). Seismological evidence for shallow crystalline basement in the Southern Uplands of Scotland. Nature, 305, 418-420.

Hall, J., Brewer, J.A., Matthews, D.H. and Warner, M.R. (1984). Crustal structure across the Caledonides from the 'WINCH' seismic reflection profile: influences on the evolution of the Midland Valley of Scotland. Trans. R. Soc. Edinburgh Earth Sci. 75, 97-109.

Halliday, A.N. (1984). Coupled Sm-Nd and U-Pb (zircon) systematics in the late Caledonian granites and the nature of the basement under northern Britain. Nature, 307, 229-233.

Halliday, A.N., Aftalion, M., van Breemen, O. and Jocelyn, J. (1979). Petrogenetic significance of Rb-Sr and U-Pb isotopic systems in the 400 Ma old British Isles granitoids and their hosts. In: Harris, A.L., Holland, C.H. and Leake, B.E. (eds.). The Caledonides of the British Isles. Reviewed. 653-661. The Geological Society, London.

Halliday, A.N. and Stephens, W.E. (1984). Crustal controls on the genesis of the 400 Ma old Caledonian granites. Phys. Earth Planet. Inter. 35, 89-104.

Halliday, A.N., Stephens, W.E. and Harmon, R.S. (1980). Rb, Sr, and O Isotopic relations in three zoned Caledonian granitoids from Southern Uplands, Scotland: Evidence for magma mixing. J. Geol. Soc. London, 137, 329-348.

Halliday, A.N., Stephens, W.E. Hunter, R.H., Menzies, M.A., Dickin, A.P., and Hamilton, P.J. (in press). Isotopic and chemical constraints on the building of the deep Scottish lithosphere.

Hanson, G.N. (1978). The application of trace elements to the petrogenesis of igneous rocks of granitic composition. Earth Planet Sci. Lett. 38, 16-43.

Hanson, G.N. (1980). Rare earth elements in petrogenetic studies of igneous systems. Ann. Rev. Earth Planet Sci. Lett.. 68, 371-406.

Harker, A. (1909). The Natural History of Igneous Rocks. MacMillan, New York.

Harmon, R.S. and Halliday, A.N. (1980). Oxygen and strontium isotope relationships in the British late Caledonian granites. Nature London, 283, 21-25.

Harmon, R.S., Halliday, A.N., Clayburn, J.A.P., and Stephens, W.E., (1984). Chemical and isotopic systems of the Caledonian intrusions of Scotland and Northern England: a guide to magma source region and magma-crust interaction. Phil. Trans. R. Soc. London, A310, 709-742.

Harvey, P.K., Taylor, D.M., Hendry, R.D. and Bancroff, F., (1973). An accurate fusion method for the analysis of rocks and chemically related minerals by X-ray fluorescence spectrometry X-ray Spectro., 5, 33-44.

Hawthorne, F.C. (1981). The quantitative characterization of cation ordering in minerals. A review. Amer. Mineral., 66.

Hietanan, A. (1971). Distribution of elements in biotite-hornblende pairs, and in an orthopyroxene-clinopyroxene pair from zoned plutons, northern Sierra Nevada, California. Contrib. Mineral. Petrol. 30, 161-176.

Higazy, R.A. (1954). The trace element of the plutonic complex of Loch Doon (Southern Scotland) and their petrogenetic significance. J. Geol., 62, 172-181.

Hildreth, E.W. (1977). A zoned pluton at the eruptive stage: the Long Valley magma chamber (California) as evidenced by eruption of the Bishop Tuff. In: Nozawa, T. and Yamada, N. (eds). Plutonism in relation to volcanism and metamorphism. Toyama, Japan, 38-48.

Hildreth, W. (1979). The Bishop Tuff: Evidence for the origin of compositional zonation in silicic magma chambers, in Chapin, C.E., and Elston, W.E., eds., Ash-flow tuffs: Geological Society of America Special Paper 180, 43-75.

Hildreth, W. (1981). Gradients in silicic magma chambers: Implications for lithospheric magmatism. Jour. Geophys. Res., 86, 10153-10192.

Hill, J.B., and others. (1905). The Geology of Mid-Argyll.

Mem. Geol. Surv. Scotland.

Holder, M.T. (1979). An emplacement mechanism for post-tectonic granites and its implications for their geochemical features. In: Atherton, M.P. and Tarney, J. (eds.). Origin of granite batholiths geochemical evidence. 116-133. Shiva Publishing Limited.

Horne, J. (1893). In: The Silurian rocks of Great Britain 1, Scotland Mem. Geol. Surv. U.K.

Hutton, J. (1785). Theory of the earth; or an investigation of the laws observable in the composition of Land upon the Globe Trans. Roy. Soc. Edinburgh, Vol i, p 209.

Hynes, A. (1982). A comparison of amphiboles from Medium- and Low-Pressure Metabasites. Contrib. Mineral. Petrol. 81, 119-125.

Jakes, P. and Smith, I.E. (1970). High potassium calc-alkaline rocks from Cape Nelson, eastern Papua: Contrib. Mineral. Petrol. 28, 259-271.

Jakes, P. and White, A.J.R. (1970). K/Rb ratios of rocks from island arcs: Geochim. Cosmochim. Acta, 34, 849-856

Jakes, P. and White, A.J.R. (1972). Major and trace element abundances in volcanic rocks of orogenic areas. Geol. Soc. Amer. Bull. 83, 29-40.

Jenkins, R. and De Vries, J.L. (1972). Practical X-ray spectrophotometry. 2nd ed. The MacMillan Press Ltd.

Johnstone, M.R.W., Sanderson, D.J. and Soper, N.J. (1979). Deformation in the Caledonides of England, Ireland and Scotland. Geol. Soc. London, Spec. Pub. 8, Eds. Harris et al.

Kanisawa, S. (1972). Co-existing biotites and hornblendes from some granitic rocks in southern Kitakami Mountains, Japan. J. Japan Assoc. Mineral., Petrol., Econ. Geol. 67, 332-344.

Kato, Y., Onuki, H. and Tanaka, H. (1977). Compositional dependence of the Mg/Fe^{2+} distribution coefficient between biotite-hornblende pairs from calc-alkaline rocks. J. Japan Assoc. Mineral., Petrol., Econ., Geol., 72, 252-258.

Kay, S.M. and Kay, R.W. (1982). Mafic mineralogy in Calc-Alkaline Aleutian volcanic rocks: evidence for primitive magmas and magma mixing. (abst.) Geol. Soc. Amer. Abstr. 14, 526.

Kay, S.M., Kay, R.W., Brueckner, H.K. and Rubenstone, J.L. (1983). Tholeiitic Aleutian arc plutonism: the Finger Bay pluton, Auak, Alaska. Contrib. Mineral. Petrol. 82. 99-116.

Kretz, R. (1961). Some applications of thermodynamics to co-existing minerals of variable compositions. Examples: orthopyroxene-clinopyroxene and orthopyroxene-garnet. J. Geol. 69, 361-387.

Kretz, R. (1963). Distribution of magnesium and iron between orthopyroxene and calcic pyroxene in natural mineral assemblages. J. Geol. 71, 773-785.

Kretz, R. (1982). Transfer and exchange equilibria in a portion of the pyroxene quadrilateral as deduced from natural and experimental data. Geochim. Cosmochim. Acta, 46, 411-422.

Kretz, R. and Jen, L.S. (1978). Effect of temperature on the distribution of Mg and Fe^{2+} between calcic pyroxene and hornblende. Canadian Mineral. 16, 533-537.

Kuno, H. (1968). Differentiation of basalt magmas, in Basalts: The Poldervaart Treatise on Rocks of Basaltic Composition, (Eds) H.H. Hess and A. Poldervaart, Interscience, John Wiley and Sons, New York, 623-688.

Kushiro, I. (1972). Effect of water on the composition of magmas formed at high pressure. Jour. Petrol., 13, 311-334.

Kushiro, I. (1978). Density and viscosity of hydrous calc-alkalic andesite magma at high pressures. Annu. Rep. Dir. geophys. Lab. Carnegie Inst. 77, 1977-1978.

Leake, B.E. (1965a). The relationship between composition of calciferous amphibole and grade of metamorphism. In Controls of metamorphism (ed W.S. Pitcher and G.W. Flinn), pp 299-318. Oliver and Boyd, Edinburgh and London.

Leake, B.E. (1965b). The relationship between tetrahedral aluminium and the maximum possible octahedral aluminium in natural calciferous and subcalciferous amphiboles. Amer. Mineral. 50, 843-851.

Leake, B.E. (1968a). A catalogue of analyzed calciferous and subcalciferous amphiboles together with their nomenclature and associated minerals. Geol. Soc. Amer. Spec. Paper 98, 210 p.

Leake, B.E. (1971). On aluminous and edenitic hornblendes. Mineral. Mag. 38, 389-407.

Leake, B.E. (1978). Nomenclature of amphiboles. Mineral. Mag. 42, 533-563.

Leake, B.E., Hendry, G.L., Kemp, A., Plant, A.G., Harvey, P.K., Wilson, J.R., Coats, J.S., Aucott, J.W., Lunel, T., and Howarth, R.J. (1969). The chemical analysis of rock powders by automatic X-ray fluorescence. Chem. Geol., 5, 7-86.

Lindsley, D.H (1983). Pyroxene thermometry. Amer. Mineral. 68, 477-493.

Mackintosh, D.M. (1960). The Geology of the Southern Part of the Glen Doll Igneous complex. Honours thesis, Univ. of St Andrews.

Mahmood, A. (1983). Chemistry of biotites from a zoned granitic pluton in Morocco. Mineral. Mag. 47, 365-369.

Majid, M. (1974). Mineralogy and petrology of the Comrie diorite Unpub. Ph.D. Thesis. Univ. of Manchester.

Mason, B., and Moore, C.B. (1982). Principles of geochemistry. John Wiley & Sons, New York.

McIntyre, D.B. (1950). The petrogenesis of the North West part of the Loch Doon plutonic complex, Galloway. Abstr. Proc. Geol. Soc. London. 1457, 31-38.

McLennan, S.M., and Taylor, S.R. (1980). Th and U in sedimentary rocks: Crustal evolution and sedimentary recycling. Nature, 285, 621-624.

Meighan, I.G. and Neeson, J.C. (1979). The Newry igneous complex, County Down. In: Harris, A.L., Holland, C.H. and Leake, B.E. (eds.). The Caledonides of the British Isles. Reviewed. 717-722. The Geological Society, London .

Neilson, M.J. and Haynes, S.J. (1973). Biotites in calc-alkaline intrusive rocks. Mineral. Mag. 39, 251-253.

Nicholls, I.A., and Ringwood, A.E. (1972). Production of silica-saturated tholeiitic magmas in island arcs. Earth Planet. Sci. Lett. 17, 243-246.

Nicol, J. (1863). On the geological structure of the Southern

Grampians. Q.J. Geol. Soc., 19, 180.

Nisbet, E.G. and Pearce, J.A. (1977). Clinopyroxene composition in mafic lavas from different tectonic settings. Contrib. Mineral. Petrol. 63, 149-160.

Nockolds, S.R. (1941). The Garabal Hill - Glen Fyne igneous complex. Q. J. Geol. Soc. London, 96, 451-511.

Nockolds, S.R. (1947). The relation between chemical composition and paragenesis in the biotite micas of igneous rocks. Amer. J. Sci., 245, 401-420.

Nockolds, S.R. and Mitchell, R.L. (1948). The geochemistry of some Caledonian plutonic rocks: a study in the relationship between the major and trace elements of igneous rocks and their minerals. Trans. R. Soc. Edinburgh, 61, 533-575.

Norrish, K. and Chappell, B.W. (1977). Pages 201-272 in Physical methods in determinative mineralogy. (ed.) Zussman, J., Academic Press.

Osborn, E.F. (1959). Role of oxygen pressure in the crystallisation and differentiation of basaltic magma. Amer. J. Sci. 257, 609-647.

Osborn, E.F. (1962). Reaction series for subalkaline igneous rocks based on different oxygen pressure conditions. Amer. Mineral. 47, 211-226.

Osborn, E.F. (1969). Genetic significance of V and Ni content of andesites: comments on a paper by Taylor, Kay, White, Duncan and Ewart, Geochim. Cosmochim. Acta, 33, 1553-1554.

Osborn, E.F. (1976). Origin of calc-alkali magma series of Santorini volcano type in the light of recent experimental phase equilibrium studies, Proceedings of the International Congress on Thermal Waters, Geothermal Energy and Volcanism of the Mediteranean Area, Athens, Greece, 3, 154-167.

Osborn, E.F. (1979). The reaction principle. In: The evolution of the igneous rocks (Ed) Yoder, Jr., H.S., New Jersey. 133-169.

Pankhurst, R.J. (1979). Isotopic and trace element evidence for the origin and evolution of Caledonian granites in the Scottish Highlands. In: Origin of granite batholiths - Geochemical Evidence (Ed. M.P. Atherton and J. Tarney). Shiva Publishing Ltd 18-33.

Papike, J.J., Cameron, K.I., and Baldwin, K. (1974): Amphibole and pyroxenes - characterisation of other than quadrilateral components as estimated of ferric iron from microprobe data. Abstr. Prog. Geol. Soc. Am. 6, 1053-4.

Peach, B.N. and Horne, J. (1899). The Silurian rocks of Great Britain 1, Scotland. Mem. Geol. Surv. U.K.

Pearce, J.A. and Norry, M.J. (1979). Petrogenetic implications of

Ti, Zr, Y and Nb variations in volcanic rocks. Contrib. Mineral. Petrol. 69, 33-47.

Peccerillo, A. and Taylor, S.R. (1976). Geochemistry of Eocene calc-alkaline volcanic rocks from the Kastamonu Area, Northern Turkey. Contrib. Mineral. Petrol., 58, 63-81

Pidgeon, R.T. and Aftalion, M. (1978). Cogenetic and inherited zircon U-Pb in granites: Palaeozoic granites of Scotland and England. In: Crustal evolution in northwestern Britain and adjacent regions. (Eds. Bowes, D.R. and Leake, B.E.). Geol. J. Spec. Iss. No 10, 183-248.

Pitcher, W.S. (1979a). Comments on the geological environments of granites. In: Origin of granite batholiths-geochemical evidence. (Eds. M.P. Atherton and J. Tarney). Shiva Publishing Ltd. 1-8.

Pitcher, W.S. (1979b). The nature, ascent and emplacement of granitic magmas. J. Geol. Soc. London. 136, 627-662.

Pitcher, W.S. (1983). Granite type and tectonic environment. In: Hsu, K.J. (Ed.) Mountain Building Process. London: Academic Press, 19-40.

Piwinskii, A.J. (1968). Experimental studies of igneous rock series, Central Sierra Nevada batholith, California. J. Geol. 76, 548-570.

Poldervaart, A. and Hess, H.H. (1951). Pyroxenes in the crystallisation

of basaltic magma. J. Geol., 59, 472-489.

Presnall, D.C. and Bateman, P.C. (1973). Fusion relations in the system $NaAlSi_3O_8$-$CaAl_2Si_2O_8$-$KAlSi_3O_8$-SiO_2-H_2O and generation of granitic magmas in the Sierra Nevada batholith. Geol. Am. Bull., 84, 3181-3202.

Raase, P. (1974). Al and Ti contents of hornblende, indicators of pressure and temperature of regional metamorphism. Contrib. Mineral. Petrol., 45, 231-236.

Ray, S. and Sen, S.K. (1970). Partitioning of major exchangeable cations among orthopyroxene, calcic pyroxene and hornblende in basic granulites from Madras. Neues Jahrb. Mineral. Abb. 114. 61-88.

Read, H.H. (1961). Aspects of the Caledonian magmatism in Britain. Proc. Liverpool, Manchester Geol. Soc. 2, 653-683.

Ringwood, A.E. (1974). The petrological evolution of island arc systems. J. Geol. Soc. London, 130, 183-204.

Ringwood, A.E. (1977). Petrogenesis in island arc systems. In: Island Arcs, Deep Sea Trenches and Black-arc Basins (Eds. M. Talwani and W.C. Pitman). Maurice Ewing Series, 1, 311-324; American Geophysical Union, Washington.

Robert, J.L. (1976). Titanium solubility in synthetic phlogopite solid

solutions. Chem. Geol. 17, 213-227.

Ruddock, I. (1969). The geochemistry of the southern half of the Loch Dee - Loch Doon pluton, South West Scotland. Unpub. Ph.D. Thesis. Univ. of Newcastle.

Rutledge, H. (1952). Contact phenomena of the southern part of the Loch Doon plutonic complex. Abstr. Proc. Geol. Soc. London, 1484, 60-66.

Saunders, A.D., Tarney, J. and Weaver, S.D. (1980). Transverse geochemical variations across the Antarctic Peninsula: implications for the genesis of calc-alkaline magmas. Earth Planet. Sci. Lett., 46, 344-360.

Saxena, S.K. (1971). Mg^{2+}-Fe^{2+} order-disorder in orthopyroxene and the Mg^{2+}-Fe^{2+} distribution between co-existing minerals. Lithos, 4, 375-354.

Saxena, S.K. (1976). Two-pyroxene geothermometer: a model with an approximate solution. Amer. Mineral., 61, 643-652.

Saxena, S.K., and Ekstrom, T.K. (1970). Statistical chemistry of calcic amphiboles. Contrib. Mineral. Petrol. 26, 276-284.

Saxena, S.K. and Nehru, C.E. (1975). Enstatite-diopside solvus and geothermometry. Contrib. Mineral. Petrol. 49, 259-267.

Sekine, T. and Wyllie, P.J. (1982a). Phase relationships in the system $KAlSiO_4$-Mg_2SiO_4-SiO_2-H_2O as a model for hybridisation between hydrous siliceous melts and peridotite. Contrib. Mineral. Petrol. 79. 368-374.

Sekine, T. and Wyllie, P.T. (1982b). Synthetic systems for modelling hybridisation between hydrous siliceous magmas and peridotite in subduction zones. J. Geol. 90, 734-741.

Sen, S.K. (1973). Compositional relations among hornblende and pyroxenes in basic granulites and an application to the origin of garnets. Contrib. Mineral. Petrol. 38, 299-306.

Shannon, R.D., and Prewitt, C.T. (1969). Effective ionic radii in oxides and fluorides. Acta Crystallog. Sect., B25, 925-946.

Shaw, H.R. (1965). Comments on viscosity, crystal settling and convection in granitic magmas. Am. J. Sci. 263, 120-152.

Shaw, H.R. (1969). Rheology of basalt in the melting range. J. Petrol. 10, 510-535.

Shaw, H.R. (1972). Viscosities of magmatic silicate liquids: an empirical method of prediction. Am. J. Sci. 272, 870-893.

Shaw, H.R. (1974). Diffusion of H_2O in granitic liquids: Part I. Experimental data: Part II. Mass transfer in magma chambers. In: Hofmann, A.W. (ed.). Geochemical transport and Kinetics. Pub.

Carnegie Inst. Wash. No. 635, 139-172.

Shaw, H.R., Smith, R.L. and Hildreth, W. (1976). Thermogravitation mechanisms for chemical variations in zoned magma chamber. Abst. Prog. geol. Soc. Am. 8-6, 1102.

Shaw. H.R., Wright, T.L., Peck, D.E. and Okamura, R. (1968). The viscosity of basaltic magma: On analysis of field measurements in Makaopuhi lava lake, Hawaii. Am. J. Sci. 266, 225-264.

Shervais, J.W. (1982). Ti-V plots and the petrogenesis of modern and ophiolitic lavas. Earth Planet. Sci. Lett. 59, 101-118.

Shimizu, N. and Kushiro, I. (1975). The partitioning of rare earth elements between garnet and liquid at high pressures: preliminary experiments, Geophys. Ress. Lett. 2, 413-416.

Simkin, T. and Smith, J.V. (1970). Minor element distribution in olivine. J. Geol. 78 304-325.

Simpson, P.R., Brown, G.C., Plant, J. and Ostle, D. (1979). Uranium mineralisation and granite magmatism in the British Isles. Phil. Trans. R. Soc. Lond. A291, 385-412.

Smith, J.V. (1974). Feldspar minerals. Vols. 1 and 2. Springer-Verlag, Berlin. 627 p. and 690 p.

Smith, P.J. and Bott, M.H.P. (1975). Structure of the crust

beneath the Caledonian Foreland and Caledonian Belt of the North Scottish Shelf Region. Geophys. J.R. Astron Soc., 40, 187-205.

Sparks, R.S.J., Huppert, H.E., and Turner, J.S. (1984). The fluid dynamics of evolving magma chambers. Phil. Trans. R. Soc. London, A310, 511-534.

Speer, J.A. (1984). Micas in igneous rocks. In: Bailey, S.W. (ed). Reviews in Mineralogy, 13, 299-356.

Steiger, R.H., and Jaeger, E. (1977). Subcommission on geochronology. Convention on the use of decay constants in geo- and cosmochronology: Earth Planet. Sci. Lett., 36, 359-362.

Stephens, W.E. and Halliday, A.N. (1984). Geochemical contrasts between late Caledonian granitoid plutons of northern, central and southern Scotland. Trans. R. Soc. Edinburgh, Earth Sci. 75, 259-273.

Stephens, W.E., Whitley, J.E., Thirlwall, M.F. and Halliday, A.N. (1985). The Criffell zoned pluton: correlated behaviour of rare earth element abundances with isotopic systems. Contrib. Mineral. Petrol. 89, 226-238.

Streckeisen, A. (1976). To each plutonic rock its proper name. Earth Sci. Rev., 12, 1-33.

Summerhayes, C.P. (1966). A geochronological and strontium isotope

study of the Garabal Hill - Glen Fyne igneous complex, Scotland, Geol. Mag. 103, 155-165.

Sun, S.S., Nesbitt, R.W. and Sharaskin, A.Y. (1979). Geochemical characteristics of mid-ocean ridge basalts. Earth Planet. Sci. Lett., 44, 119-138.

Sweatman, T.R., and Long, J.V.P. (1969). Quantitative electron-probe microanalysis of rock-forming minerals. J. Petrol., 10, 332-379 .

Tagiri, M. (1977). Fe-Mg partition and miscibility gab between coexisting amphiboles from the Southern Abukuma Plateau, Japan. Contrib. Mineral. Petrol. 62, 227-281.

Tanaka, H. (1975). Magnesium-iron distribution in coexisting biotite and hornblende from granitic rocks. J. Japan. Assoc. Mineral., Petrol., Econ. Geol. 70, 118-124.

Taylor, S.R. (1965). The application of trace element data to problems in petrology. Phys. Chem. Earth, 6, 133-212.

Teall, J.J.H. (1899). In 'The Silurian rocks of Britain. Vol. 1. Scotland'. Mem. Geol. Surv. U.K.

Thirlwall, M.F. (1981). Implications for Caledonian plate tectonics models of chemical data from volcanic rocks of the British Old Red Sandstone. J. Geol. Soc. London, 138,

123-138.

Thirlwall, M.F. (1982). Systematic variation in chemistry and Nd-Sr isotopes across a Caledonian calc-alkaline volcanic arc: implications for source materials. Earth Planet. Sci. Lett., 58, 27-50.

Thompson, R.N. (1982). Magmatism of The British Tertiary Volcanic Province. Scott. J. Geol. 18, 49-107

Thompson, R.N., Morrison, M.A., Hendry, G.L. and Parry, S.J. (1984). An assessment of the relative roles of crust and mantle in magma genesis: an elemental approach. Phil. Trans. R. Soc. London, A310, 549-590.

Tilley, C.E. (1924). Contact-metamorphism in the Comrie area of the Perthshire Highlands. Q. J. Geol. Soc. London, 80, 21-71.

Tindle, A.G., and Pearce, J.A. (1981). Petrogenetic modelling of in situ fractional crystallisation in the zoned Loch Doon Pluton, Scotland. Contrib. Mineral. Petrol. 78, 196-207.

Trindle, A.G. and Pearce, J.A. (1983). Assimilation and partial melting of continental crust: evidence from the mineralogy and geochemistry of autoliths and xenoliths. Lithos, 16, 185-202.

Vogel, T.A. (1982). Magma mixing in the acidic-basic complex of

Ardnamurchan: Implications on the evolution of shallow magma chambers. Contrib. Mineral. Petrol. 79, 411-423.

Wager, L.R. and Mitchell, R.L. (1951). The distribution of trace elements during strong fractionation of basic magma. Geochim. Cosmochim. Acta 1, 129-208.

Walsh, J.N. (1975). Clinopyroxene and biotites from the Centre III igneous complex, Ardnamurchan, Argyllshire. Mineral. Mag. 40, 335-345.

Wells, P.R.A. (1977). Pyroxene thermometry in simple and complex systems. Contrib. Mineral. Petrol. 62, 129-139.

Whalen, J.B. (1985). Geochemistry of an Island-Arc Plutonic Suite: the Uasilau-Yau Yau Intrusive Complex, New Britain, P.N.G., J. Petrol., 26, 603-632.

White, A.J.R. and Chappell, B.W. (1977). Ultrametamorphism and granitoid genesis. Tectonophysics, 43, 7-22.

Wilde, S.A. (1971). The Glen Lednock complex, Comrie, Perthshire. Unpub. Ph.D. Thesis, Univ. of Exeter.

Wilkinson, J.F.G. (1959). The geochemistry of a differentiated teschenite sill near Gunnedah, New South Wales.

Wilson, A.D., (1955). A new method for the determination of ferrous

iron in rocks and minerals. Gr. Britain Geol. Surv. Bull. 9, 56-58.

Winchester, J.A. (1974). The zonal pattern of regional metamorphism in the Scottish Caledonides. J. Geol. Soc. London, 130, 509-524.

Winkler, H.G.F. (1976). Petrogenesis of metamorphic rocks. Springer-Verlag, 278-324.

Wones, D.R. and Eugster, H.P. (1965). Stability of biotite: experiment, theory and applications. Am. Mineral. 50, 1228-1272.

Wood, B.J. and Banno, S. (1973). Garnet-orthopyroxene and orthopyroxene-clinopyroxene relationships in simple and complex systems. Contrib. Mineral. Petrol., 42, 109-124.

Wright, A.E. and Bowes, D.R. (1979). Geochemistry of the appinite suite. In Harris, A.L., Holland, C.H. and Leake, B.E. (eds.). The Caledonides of the British Isles - Reviewed. 699-703. Spec. Pub. Geol. Soc. London, 8.

Wright, T.L., and Doherty, P.C. (1970). A linear programming and least squares computer method for solving petrologic mixing problems. Geol. Soc. Amer. Bull., 81, 1995-2008.

Wyllie, B.K.N. and Scott, A. (1913). Intrusive rocks of Glen Lednock. Geol. Mag. 10, 544.

Wyllie, P.J. (1973). Experimental petrology and global tectonics-preview.

Tectonophys., 17, 189-209.

Wyllie, P.J. (1977). Crustal anatexis: an experimental review. Tectonophysics, 43, 41-71.

Wyllie, P.J. (1983). Experimental studies on biotite- and muscovite-granites and some crustal magmatic sources. In: Migmatites, Melting and Metamorphism. (Eds. M.P. Atherton and C.D. Gribble). Shiva 12-26.

Wyllie, P.J., Huang, W.L., Stern, C.R., and Maaloe, S. (1976). Granitic magmas: Possible and impossible sources, water contents and crystallisation sequences. Canadian, J. Earth, Sci. 13, 1007-1019.

Appendix A

Staining techniques

Thin sections used for modal classification were stained for identification of feldspars by first cleaning the uncovered thin section with acetone, then etching the surface over a bath of fresh hydrofluoric acid for approximately 30 seconds or slightly longer, followed by a light rinse then immersing the thin section in sodium cobaltinitrite solution for one minute and a light rinse getting a result of alkali feldspar stained in yellow colour so it can be differentiated from plagioclase. (Technique used in the Department of Geology, St Andrews University after Batchelor).

Modal analyses

Modal analyses techniques were performed using point counting for representative samples of each rock types of 1000-2000 points per thin section. Classification followed the scheme of Streckeisen (1976).

Table A1: Garabal Hill sample types and locations

Sample number	Rock type	Grid reference (Area NN)
GH33	Peridotite	283 161
GH35	"	285 163
GH36	"	287 164
GH36A	"	287 165
GH15	Hornblendite	295 173
GH21	Hornblende gabbro	306 182
GH22	" "	306 182
GH23	" "	306 183
GH24	" "	308 183
GH32	" "	284 159
GH34	" "	285 161
GH10	Pyroxene biotite gabbro	308 176
GH1	Pyroxene biotite diorite	312 179
GH3	" " "	311 176
GH5	" " "	309 177
GH6	" " "	309 177
GH7	" " "	309 176
GH25	Hornblende biotite diorite	307 183
GH26	" " "	308 184
GH27	" " "	309 180
GH20	Diorite	309 182
GH37	Xenolithic diorite	288 165
GH38	" "	291 169
GH11	Appinitic diorite	308 175
GH28	Medium granodiorite	277 161
GH31	" "	276 154
GH29	Porphyritic granodiorite	272 159
GH30	" "	272 155
GH39	" "	265 161

Table A2: Comrie sample types and locations

Sample number	Rock type	Grid reference (Area NN)
CM10	Two pyroxene biotite diorite	736 277
CM22	"	763 278
CM20	"	758 271
CM4	Hornblende biotite diorite	763 243
CM23	"	770 286
CM21	Augite biotite diorite	760 274
CM7	"	751 266
CM25	Quartz monzodiorite	791 277
CM24	" "	791 278
CM8	Granodiorite	754 266
CM28	"	783 272
CM26	"	785 273
CM27	"	783 273
CM29	Granite	776 273

Table A3: Glen Doll sample types and locations

Sample number	Rock type	Grid reference (Area NN)
GD49	Pyroxenite	271 753
GD26	"	270 752
GD41	Pyroxene hornblende gabbronorite	285 770
GD42	"	286 783
GD45	Quartz gabbro	286 767
GD5	" "	275 762
GD6	" "	275 761
GD10	" "	268 758
GD12	" "	277 761
GD4	" "	270 764
GD2	" "	269 764
GD11	" "	265 759
GD27	Hornblende biotite diorite	290 766
GD33	"	275 773
GD34	"	274 774
GD37	"	271 765
GD43	"	290 779
GD46	"	285 761
GD53	"	278 756
GD28	"	290 762
GD29	"	287 761
GD30	"	286 762
GD31	"	276 769
GD36	"	269 769
GD38	"	288 757
GD44	"	286 768
GD47	"	288 762
GD51	Tonalite	264 748
GD50	"	263 749
GD35	"	272 769
GD39	Granodiorite	293 756
GD40	"	293 757
GD40A	"	293 758
GD32	"	277 772
GD48	"	294 757

Table A4: Glen Tilt sample types and locations

Sample number	Rock type	Grid reference (Area NN)
GT44	Hornblende biotite diorite	889 756
GT28	"	944 759
GT29	"	932 748
GT45	Quartz diorite	889 756
GT47	" "	889 772
GT42	Diorite	928 744
GT54	Quartz diorite	964 777
GT55	Appinitic diorite	958 766
GT30	" "	917 754
GT35	" "	937 745
GT37	" "	933 747
GT39	" "	932 748
GT52	" "	970 778
GT53	" "	968 779
GT26	" "	948 761
GT27	" "	953 767
GT36	" "	936 745
GT40	" "	931 751
GT46	" "	890 761
GT31	" "	920 747
GT41	Granodiorite	928 745
GT32	"	935 744
GT33	"	938 746
GT34	"	937 746
GT57	"	919 737
GT59	"	912 735
GT60	"	911 732
GT48	Biotite granite	888 773
GT49	" "	887 774
GT50	" "	886 773

Table A5: Cairnsmore of Carsphairn sample types and locations

Sample number	Rock type	Grid reference (Area NX)
AS33	Microdiorite	593 972
77030	"	593 970
AS38	Hornblende biotite diorite	577 984
77026	Tonalite	583 975
77031	"	589 970
77032	"	586 969
AS40	"	582 979
AS17	"	584 971
AS18	Tonalite	575 969
AS48	Granodiorite	582 986
AS19	Acidic rock	575 970
AS46	"	594 979
AS49	Granite	592 984

Table A6: Loch Doon sample types and locations

Sample number	Rock type	Grid reference (Area NX)
WL1	Metasediments	475 772
WL2	"	472 771
77015	Microdiorite	473 779
WL3	"	486 772
WL4	"	469 775
78002	Two pyroxene biotite diorite	472 787
78004	"	466 785
78001	"	473 788
77017	"	465 778
77018	"	472 778
77016	Hornblende biotite diorite	469 792
77021	Two pyroxene biotite diorite	475 785
WL5	"	454 781
WL6	"	470 785
WL7	"	471 790
WL8	Hornblende biotite diorite	473 790
DBL4	"	454 785
DBL5	"	452 783
DBL1	Granodiorite	448 793
DBL2	"	448 786
DBL3	"	448 787
77022	"	478 891
77023	"	479 860
77024	"	479 828
77025	"	492 798
77002	"	477 940
WL9	"	455 809
HH1	Granite	459 895
HH2	"	457 891
HH4	"	455 887
HH5	"	451 885
HH6	"	449 882
WL10	"	459 819

Appendix B

B.1 Sample collection and whole rock geochemical analysis

Rock specimens for geochemical analyses were the freshest possible samples. Due care was noted when sampling coarse-grained types so as to obtain representative specimens.

Rock samples were cleaned by removing any weathered surfaces and joint planes then hydraulically split and passed through a rifle splitter. One split was retained and catalogued, the other powdered in a 'TEMA' Tungsten Carbide mill and passed through a 200 sieve.

B.2 XRF analysis:

X-ray fluorescence spectrometry (XRF) analysis was conducted on a Philips PW1212 automatic spectrometer linked to an Apple IIe computer in an on-line system. Software for the system and later data handling - CIPW normative mineralogy calculation, molar proportions of oxide and probe data and plotting of variation diagrams was provided by Dr W E Stephens.

Major oxides analysed were -SiO_2, Al_2O_3, TiO_2, Fe_2O_3 (t), MnO, MgO, CaO, Na_2O, K_2O and P_2O_5, following the conditions of Norrish and Chappell (1977). Analyses were performed on fused beads of 0.5 gram sample powder prepared after the method of Harvey et al. (1973) and adapted for use at St Andrews by R A Batchelor (Int Pub 1980). All beads were checked optically for quench crystals and re-fused if any found present.

FeO Determination

Determined volumetrically (redox titration) with potassium dichromate after cold HF attack on 0.1 - 0.2 gm sample in the presence of ammonium metavandate following the procedures of Batchelor (1980) adapted from Wilson (1955). To ensure accuracy, USGS standards were also analysed.

H_2O Determination

Total H_2O was determined by loss-on-ignition (T> 800 ^{o}C) during fused bead preparation (Batchelor 1980).

B.3 Trace element XRF analysis:

Trace elements Nb, Zr, Y, Sr, Rb, Th, Pb, Zn, Cu, Ni, Cr, V, Ba, Hf, Ce and La were analysed separately following the conditions of Norrish and Chappell (1977). Analysis was performed on pressed powder pellets, the powder for which had been homogenised in a 'TEMA' ball mill. This was to finely crush flakes of mica which tended to orientate themselves parallel to, and on the analysis surface of the pellet.

B.4 Rare earth element analysis

The rare earth element analyses were obtained by neutron activation analysis following the procedure used at the SURRC at East Kilbride. Duplicate samples of 0.2 gm were irradiated for 6 hours in a flux of 3.6×10^{12} cm^{-2} sec^{-1}. Gamma emitters with energies below 150 Kev were counted with a 0.5 cm planar Ge (Li) detector with a resolution of 623 ev at 122 Kev and gamma emitters with energies above 150 Kev were counted with an 80 cm coaxial Ge (Li) detector with a

resolution of 2.2 Kev at 1.33 Mev. Both detectors were controlled by an EGG-ORTEC Data Acquisition and Analysis System which processed the resulting spectra to provide net photopeak areas for the elements of interest. Results were calculated by comparing the induced activities with those induced in samples of BCR-1 which were irradiated together with the samples of the Garabal Hill pluton.

Table B1: Whole rock analyses in wt % and trace elements in ppm of the Garabal Hill pluton.

Sample	GH33	GH35	GH36	GH36A	GH15	GH21	GH22	GH23
SiO2	42.06	43.45	45.64	44.05	47.05	44.63	46.30	48.88
TiO2	0.31	0.48	0.42	0.38	1.43	1.98	0.71	1.37
Al2O3	1.39	2.00	1.97	1.87	6.85	13.04	13.97	15.90
Fe2O3	7.75	5.51	5.25	5.80	5.86	4.58	3.10	3.12
FeO	5.16	5.94	5.65	6.00	7.02	7.09	7.13	7.01
MnO	0.20	0.22	0.20	0.20	0.20	0.18	0.19	0.18
MgO	27.20	22.33	22.93	24.86	19.30	12.80	12.12	9.31
CaO	8.28	12.47	12.16	10.33	8.20	10.87	10.11	9.37
Na2O	0.02	1.33	0.09	0.30	1.13	1.55	3.15	2.19
K2O	0.00	0.08	0.00	0.02	0.32	1.21	1.50	0.68
P2O5	0.15	0.21	0.15	0.19	0.04	0.16	0.15	0.36
Loss	7.00	5.80	5.40	5.80	2.52	2.20	1.80	1.40
TOTAL	99.83	100.07	100.15	100.10	100.18	100.50	100.40	100.00
Nb	0	0	0	0	6	5	0	1
Zr	12	18	17	14	55	38	17	12
Y	12	17	14	14	25	29	15	19
Sr	22	28	30	26	106	467	524	625
Rb	0	0	0	0	2	42	65	23
Th	0	0	0	2	5	4	0	0
Pb	0	0	6	4	26	8	4	2
Zn	93	85	75	79	119	89	102	85
Cu	20	10	1	6	1	0	56	293
Ni	736	532	464	541	437	154	108	154
Cr	2041	1637	2115	2180	1397	633	400	588
V	116	186	173	165	292	421	297	262
Ba	5	2	11	0	89	232	149	188
Hf	0	0	0	0	0	1	2	3
Ce	0	0	0	0	2	6	3	0
La	3	2	8	0	4	0	3	4

Sample	GH24	GH11	GH32	GH34	GH10	GH1	GH3	GH5
SiO2	49.51	49.38	51.99	51.19	51.93	53.84	54.43	54.73
TiO2	0.99	2.45	1.25	0.99	1.31	1.08	1.12	1.13
Al2O3	15.79	13.17	15.92	14.39	13.52	14.13	15.03	14.73
Fe2O3	2.77	2.90	2.11	2.12	2.54	1.15	1.94	2.49
FeO	5.51	6.35	5.83	6.13	6.41	6.43	5.96	5.30
MnO	0.17	0.14	0.16	0.17	0.15	0.13	0.13	0.13
MgO	10.29	11.00	7.84	9.58	10.59	9.08	7.38	6.74
CaO	9.44	8.79	6.69	7.73	8.06	7.41	7.89	7.64
Na2O	2.04	2.43	4.51	3.58	2.46	3.18	3.19	3.62
K2O	1.29	1.23	1.60	1.47	1.33	1.93	1.88	2.04
P2O5	0.18	0.10	0.49	0.34	0.14	0.20	0.21	0.29
Loss	1.60	1.74	2.00	2.40	1.18	0.98	0.96	1.02
TOTAL	99.80	99.88	100.62	100.34	99.82	99.74	100.31	100.05
Nb	0	4	9	6	9	4	10	10
Zr	25	119	79	63	70	104	104	134
Y	13	28	23	21	18	20	24	29
Sr	647	294	812	670	435	417	507	475
Rb	40	32	46	39	35	49	54	46
Th	3	11	4	0	0	2	5	4
Pb	8	25	12	6	22	21	22	22
Zn	76	76	87	92	80	78	77	79
Cu	122	57	39	36	51	47	123	26
Ni	150	185	123	150	208	186	84	89
Cr	568	497	498	714	543	446	224	273
V	218	415	255	207	228	194	211	211
Ba	289	227	259	440	230	339	380	401
Hf	2	4	4	3	4	4	5	4
Ce	3	11	52	25	20	35	35	46
La	1	0	29	19	8	19	17	22

Table B1: Continued

Sample	GH6	GH7	GH26	GH27	GH25	GH20	GH37	GH38
SiO2	53.63	54.39	55.86	57.15	57.57	57.57	59.70	59.01
TiO2	1.16	1.35	0.90	0.82	0.81	1.06	0.78	0.70
Al2O3	14.75	15.56	16.41	16.20	18.14	17.87	16.77	16.43
Fe2O3	2.34	2.33	2.07	1.85	1.87	2.31	1.96	2.05
FeO	5.83	5.91	4.67	4.05	3.94	4.25	2.92	3.04
MnO	0.15	0.14	0.12	0.13	0.09	0.11	0.11	0.10
MgO	7.73	6.27	6.35	5.42	3.83	3.59	3.29	4.22
CaO	7.38	7.40	6.49	5.28	6.19	5.19	4.23	4.38
Na2O	4.07	3.67	3.74	3.73	4.70	4.05	4.90	5.07
K2O	1.76	1.84	2.12	3.06	1.69	3.13	3.03	2.77
P2O5	0.19	0.28	0.30	0.26	0.34	0.40	0.27	0.22
Loss	0.72	1.16	1.20	2.20	0.40	0.50	1.60	1.60
TOTAL	99.91	100.47	100.45	100.37	99.76	100.36	99.78	99.82
Nb	9	4	8	10	8	19	15	11
Zr	75	102	120	139	108	297	213	150
Y	21	25	20	19	20	29	20	20
Sr	599	456	539	586	739	591	650	807
Rb	56	44	64	102	69	101	75	77
Th	3	0	6	8	11	11	3	4
Pb	22	20	18	10	9	28	14	13
Zn	81	84	81	79	60	88	65	71
Cu	177	29	104	66	47	4	7	5
Ni	98	56	123	105	42	35	48	60
Cr	293	180	288	243	99	71	128	179
V	236	225	167	144	131	154	119	110
Ba	308	383	575	590	461	741	713	735
Hf	4	4	5	6	5	8	5	7
Ce	31	47	41	44	50	82	75	44
La	14	18	22	23	29	33	33	24

Sample	GH28	GH31	GH39	GH30	GH29
SiO2	64.95	67.64	65.32	67.45	68.22
TiO2	0.60	0.50	0.59	0.49	0.45
Al2O3	15.79	15.67	16.21	15.94	16.01
Fe2O3	1.22	1.15	1.66	0.94	1.15
FeO	2.39	1.86	1.85	1.75	1.45
MnO	0.10	0.07	0.06	0.06	0.06
MgO	2.75	1.96	1.72	1.71	1.40
CaO	3.90	3.07	3.43	2.71	2.62
Na2O	4.21	4.59	4.52	4.54	4.67
K2O	3.11	3.60	3.32	3.84	3.77
P2O5	0.20	0.16	0.22	0.17	0.16
Loss	0.40	0.20	0.60	0.40	0.20
TOTAL	99.83	100.66	99.78	100.28	100.42
Nb	13	13	15	13	13
Zr	163	147	174	161	131
Y	16	14	17	14	13
Sr	679	628	1016	1033	974
Rb	87	92	76	78	94
Th	6	8	10	6	17
Pb	13	15	15	23	28
Zn	54	49	50	48	46
Cu	4	1	3	5	4
Ni	42	26	21	24	18
Cr	99	56	28	28	26
V	81	61	64	57	52
Ba	798	742	1170	1175	1115
Hf	6	6	7	7	6
Ce	50	46	60	51	38
La	27	31	33	32	32

Table B2: Whole rock analyses in wt % and trace element in ppm of the Comrie pluton.

Sample	CM10	CM22	CM20	CM4	CM23	CM21	CM7	CM25
SiO2	55.05	53.98	53.17	55.91	57.89	57.08	55.38	59.66
TiO2	1.27	1.16	1.12	1.19	1.13	1.27	1.26	1.22
Al2O3	16.22	10.12	15.47	16.73	17.27	16.91	15.99	16.29
Fe2O3	2.61	2.57	1.96	2.72	2.44	2.12	3.14	1.52
FeO	4.79	8.74	7.00	4.20	4.30	4.70	4.75	4.45
MnO	0.11	0.12	0.20	0.11	0.23	0.12	0.13	0.10
MgO	6.18	11.75	7.91	5.45	3.87	4.55	5.69	3.14
CaO	7.05	7.90	7.10	5.80	5.38	6.15	6.67	4.88
Na2O	4.02	1.84	2.94	4.06	3.37	3.57	3.93	3.66
K2O	2.08	1.06	1.25	2.55	3.17	2.29	2.34	3.62
P2O5	0.31	0.23	0.46	0.34	0.29	0.37	0.32	0.41
Loss	0.66	0.80	1.40	0.94	0.40	0.60	0.40	0.60
TOTAL	100.58	100.50	100.19	100.23	99.93	99.94	100.22	99.82
Nb	9	15	9	10	3	13	13	17
Zr	139	220	67	291	84	168	220	420
Y	23	36	23	24	23	28	28	34
Sr	666	829	606	555	335	586	600	537
Rb	52	93	36	78	27	63	96	113
Th	9	12	8	10	2	7	14	8
Pb	24	22	21	23	3	12	24	36
Zn	82	109	115	70	111	86	92	85
Cu	26	32	124	105	0	31	46	39
Ni	118	27	148	75	135	50	85	39
Cr	. 232	64	329	169	471	100	192	66
V	164	154	202	160	296	150	131	135
Ba	670	604	320	617	349	671	574	1066
Hf	8	9	5	10	3	7	8	12
Ce	72	65	48	76	24	57	81	90
La	30	29	22	32	9	27	40	41

Sample	CM24	CM8	CM28	CM26	CM27	CM29
SiO2	60.42	63.02	65.26	65.51	67.08	71.30
TiO2	1.08	0.81	0.73	0.72	0.66	0.18
Al2O3	15.96	16.65	15.46	15.38	15.19	15.08
Fe2O3	1.75	1.70	1.69	1.86	1.78	1.02
FeO	3.77	2.37	2.29	2.22	1.93	0.45
MnO	0.09	0.06	0.06	0.06	0.04	0.04
MgO	3.17	1.69	2.14	2.45	1.87	0.84
CaO	4.59	3.07	3.06	2.42	2.78	0.72
Na2O	3.61	4.39	3.92	3.79	3.66	4.42
K2O	4.11	4.34	4.09	4.05	4.36	4.30
P2O5	0.36	0.28	0.25	0.22	0.20	0.07
Loss	0.60	1.29	1.40	1.00	0.60	1.40
TOTAL	99.74	99.90	100.55	99.88	100.35	99.95
Nb	20	20	16	17	19	20
Zr	440	423	298	296	299	108
Y	34	26	24	24	28	10
Sr	476	470	448	438	417	238
Rb	176	176	156	163	156	146
Th	27	35	37	35	36	13
Pb	23	29	23	20	19	26
Zn	69	51	33	36	29	35
Cu	45	21	39	36	35	24
Ni	45	22	30	29	28	14
Cr	78	25	53	55	39	9
V	115	75	75	69	67	21
Ba	600	718	702	651	656	565
Hf	13	13	9	9	8	4
Ce	127	125	69	78	86	34
La	60	50	37	36	47	20

Table B3: Whole rock analyses in wt % and trace element in ppm of the Glen Doll pluton.

Sample	GD49	GD26	GD41	GD42	GD45	GD5	GD6	GD10
SiO2	47.17	47.56	51.40	50.77	47.39	46.30	46.68	48.00
TiO2	0.39	0.41	0.62	0.91	2.74	2.90	2.73	2.82
Al2O3	5.52	6.22	15.98	20.13	17.16	16.51	17.28	15.99
Fe2O3	1.11	0.99	0.95	2.20	3.75	5.49	5.09	5.82
FeO	8.63	8.64	5.41	3.93	8.27	7.76	7.66	7.02
MnO	0.18	0.17	0.12	0.10	0.16	0.14	0.14	0.12
MgO	23.05	22.80	9.87	6.46	5.96	5.11	4.90	5.11
CaO	9.60	9.29	12.88	11.74	9.59	9.31	8.67	8.66
Na2O	0.51	0.52	1.52	1.96	2.27	3.04	2.83	3.12
K2O	0.42	0.44	0.47	0.79	0.68	0.67	0.58	0.88
P2O5	0.08	0.11	0.17	0.12	0.12	1.17	1.67	1.42
Loss	2.80	2.00	0.00	0.80	1.80	1.52	1.30	1.10
TOTAL	99.72	99.41	99.56	100.08	100.04	100.08	99.69	100.23
Nb	0	0	0	1	4	7	5	8
Zr	44	44	57	86	60	8	14	44
Y	13	13	15	14	13	33	28	28
Sr	158	181	695	942	682	750	685	763
Rb	5	6	2	8	10	18	18	23
Th	2	2	2	5	0	0	9	9
Pb	6	13	11	12	0	25	27	28
Zn	33	29	60	1	12	151	146	107
Cu	75	83	55	47	113	17	14	15
Ni	254	254	96	35	18	0	16	0
Cr	1877	1784	549	199	50	20	23	26
V	113	128	0	118	400	265	282	368
Ba	59	61	116	155	163	222	241	229
Hf	0	1	2	3	2	3	4	4
Ce	0	0	26	43	7	53	77	50
La	0	0	0	0	0	14	22	19

Sample	GD12	GD4	GD2	GD11	GD27	GD33	GD34	GD37
SiO2	49.75	48.74	51.77	50.69	51.95	50.94	50.77	53.75
TiO2	1.54	2.65	1.36	1.45	2.22	2.84	2.75	2.19
Al2O3	17.60	16.17	14.73	16.65	18.42	16.14	16.09	16.04
Fe2O3	3.10	4.29	3.46	0.93	3.62	3.05	3.44	4.22
FeO	5.70	8.20	7.48	8.42	6.19	8.63	8.57	6.03
MnO	0.12	0.14	0.16	0.11	0.17	0.15	0.16	0.14
MgO	7.29	5.15	7.41	6.54	3.99	4.65	5.15	3.84
CaO	9.37	8.37	9.48	9.17	7.26	8.12	7.98	7.38
Na2O	2.81	2.92	2.39	3.06	3.27	2.68	2.47	3.39
K2O	0.90	1.18	0.64	0.76	1.23	1.34	0.87	1.62
P2O5	0.06	0.19	0.04	0.28	1.08	0.23	0.19	1.10
Loss	1.28	1.66	0.94	1.46	0.80	0.40	1.00	0.60
TOTAL	99.67	99.82	100.02	99.67	100.38	99.35	99.61	100.47
Nb	3	2	3	2	13	8	5	9
Zr	0	44	16	49	116	120	115	140
Y	17	19	22	14	30	23	24	34
Sr	768	586	502	543	751	576	516	601
Rb	23	34	18	20	31	31	16	43
Th	12	10	9	14	0	0	1	2
Pb	26	27	27	25	9	15	14	7
Zn	78	114	107	64	0	1	61	30
Cu	17	52	20	58	107	110	93	117
Ni	9	8	31	9	7	11	9	4
Cr	91	52	268	80	22	46	68	26
V	218	354	316	451	180	435	508	273
Ba	174	279	199	189	371	348	218	343
Hf	4	2	1	4	2	4	2	3
Ce	12	26	23	19	95	35	89	103
La	4	11	8	7	26	0	7	15

Table B3: Continued

Sample	GD43	GD46	GD53	GD28	GD29	GD30	GD31	GD36
SiO2	57.01	51.02	52.25	52.79	52.24	51.32	52.90	51.59
TiO2	1.93	2.65	2.84	2.48	2.39	2.63	2.06	2.12
Al2O3	16.67	17.11	15.65	16.85	16.99	16.31	16.32	16.70
Fe2O3	0.38	4.39	4.70	4.33	4.97	4.75	3.11	2.75
FeO	7.55	6.63	6.37	5.91	5.29	6.64	6.62	8.10
MnO	0.15	0.15	0.14	0.13	0.15	0.15	0.16	0.15
MgO	3.61	4.66	4.43	3.84	3.87	4.58	5.17	3.93
CaO	5.03	7.29	7.58	7.14	7.57	7.53	7.75	6.75
Na2O	2.43	3.78	2.43	3.81	2.92	3.10	2.51	2.46
K2O	2.40	1.58	1.48	1.46	1.26	1.21	1.54	1.94
P2O5	1.01	0.65	0.26	0.58	1.08	0.18	0.37	1.21
Loss	1.60	0.40	1.60	1.20	1.60	1.40	1.20	1.80
TOTAL	99.94	100.49	99.90	100.70	100.49	99.97	99.87	99.73
Nb	7	6	14	11	12	9	8	10
Zr	80	154	152	259	160	121	113	153
Y	15	23	25	30	41	25	20	35
Sr	442	637	546	570	486	630	581	490
Rb	17	34	39	43	30	31	38	60
Th	0	6	11	5	5	3	6	8
Pb	5	11	12	15	17	21	10	17
Zn	25	0	29	0	26	23	2	139
Cu	91	107	98	82	86	81	96	115
Ni	11	11	4	9	5	9	23	4
Cr	61	42	29	25	47	32	62	61
V	582	336	370	319	213	336	198	616
Ba	259	306	292	356	354	340	388	471
Hf	1	3	2	5	3	1	2	4
Ce	63	61	69	100	78	54	40	95
La	0	16	7	17	15	0	5	22

Sample	GD38	GD44	GD47	GD51	GD50	GD35	GD39	GD40	GD40A	GD32	GD48
SiO2	51.21	52.76	50.86	56.79	54.75	55.79	58.82	68.70	66.88	65.70	68.62
TiO2	2.72	1.82	2.38	1.85	1.58	1.01	0.80	0.59	0.68	0.77	0.68
Al2O3	15.86	16.44	17.26	16.57	17.74	17.12	12.04	15.87	15.80	15.98	15.88
Fe2O3	3.18	3.13	2.77	6.91	1.02	1.58	0.90	0.70	1.07	1.87	1.78
FeO	7.90	6.03	7.43	1.57	6.59	5.24	4.96	2.44	2.37	2.25	1.72
MnO	0.16	0.12	0.14	0.15	0.14	0.13	0.14	0.06	0.07	0.06	0.06
MgO	4.71	4.60	4.29	3.36	4.13	5.77	8.31	1.42	1.50	1.78	1.37
CaO	6.95	6.51	7.49	5.09	6.05	8.11	7.32	2.04	2.23	2.64	1.97
Na2O	2.81	3.26	2.99	2.42	3.14	2.89	2.14	4.40	3.73	3.73	3.60
K2O	1.68	1.50	1.98	2.42	1.76	1.51	1.89	4.00	4.12	3.61	4.14
P2O5	0.24	0.69	1.42	0.98	0.64	0.20	0.13	0.17	0.19	0.22	0.20
Loss	1.60	2.80	0.60	2.00	1.80	0.60	2.40	0.00	1.80	1.60	0.60
TOTAL	99.19	99.91	99.80	100.30	99.52	100.10	100.03	100.58	100.64	100.41	100.82
Nb	7	16	12	17	14	6	7	16	17	14	17
Zr	143	235	112	140	117	140	139	284	312	269	291
Y	23	31	28	40	24	18	17	26	26	24	26
Sr	531	881	603	541	698	636	360	359	376	460	371
Rb	38	34	49	66	46	41	44	114	106	105	107
Th	15	6	4	7	3	2	9	12	15	13	14
Pb	14	6	14	22	10	0	13	20	20	13	21
Zn	3	11	0	3	33	26	36	6	13	14	7
Cu	92	66	87	94	95	71	87	61	48	49	61
Ni	6	18	7	4	43	13	105	16	13	18	13
Cr	37	25	38	19	75	46	393	13	4	23	10
V	424	223	306	170	113	171	108	58	64	81	58
Ba	290	752	511	606	420	274	412	778	852	796	808
Hf	2	6	2	2	3	3	4	8	9	7	8
Ce	58	135	122	179	73	49	29	86	91	98	101
La	12	41	29	39	23	15	13	43	42	49	48

Table B4: Whole rock analyses in wt % and trace elements in ppm for the Glen Tilt pluton.

Sample	GT44	GT28	GT29	GT42	GT45	GT47	GT54	GT55
SiO2	49.11	54.91	55.13	52.70	55.64	58.65	60.06	53.80
TiO2	2.61	1.21	3.31	1.30	1.22	1.21	0.63	1.32
Al2O3	17.61	13.64	17.43	20.46	20.99	18.65	17.42	14.01
Fe2O3	6.59	1.43	1.22	0.71	0.80	1.09	1.20	2.18
FeO	4.65	5.86	5.88	5.83	5.19	5.11	3.65	5.87
MnO	0.09	0.13	0.09	0.09	0.06	0.10	0.10	0.13
MgO	4.29	8.41	4.18	2.89	2.02	2.32	4.00	7.52
CaO	8.36	8.92	7.36	3.82	5.09	5.21	6.29	9.31
Na2O	2.48	2.20	3.25	5.74	4.86	4.89	3.30	2.71
K2O	1.44	1.31	1.65	2.98	2.34	2.23	1.64	1.16
P2O5	0.92	0.33	0.14	0.47	0.41	0.44	0.21	0.44
Loss	1.60	1.00	0.40	2.80	1.00	0.40	1.60	0.80
TOTAL	99.97	99.52	100.23	100.16	100.06	100.51	100.27	99.43
Nb	8	9	10	13	10	16	13	15
Zr	98	93	130	1219	1619	282	111	199
Y	23	21	10	28	32	29	13	40
Sr	909	667	984	965	1228	784	915	707
Rb	35	47	56	134	72	72	49	27
Th	13	8	6	8	7	9	13	4
Pb	12	9	25	11	16	8	16	10
Zn	21	27	46	0	0	2	7	21
Cu	97	76	51	134	97	92	76	90
Ni	8	109	42	7	8	9	43	78
Cr	25	256	33	0	0	14	25	158
V	387	133	242	33	35	157	77	173
Ba	456	196	253	964	1056	489	272	206
Hf	5	3	4	23	30	7	4	4
Ce	67	57	14	113	138	75	66	89
La	15	4	2	33	32	31	19	24

Sample	GT30	GT35	GT37	GT39	GT52	GT53	GT26	GT27
SiO2	53.64	54.67	51.22	57.37	53.28	52.47	55.48	51.64
TiO2	1.88	1.73	1.68	0.94	0.68	0.82	1.25	1.99
Al2O3	17.18	17.36	17.78	10.28	18.13	18.41	16.50	17.70
Fe2O3	2.68	1.19	1.90	0.24	0.04	2.31	1.71	1.55
FeO	5.23	6.24	5.61	7.87	5.54	3.89	5.30	6.82
MnO	0.09	0.11	0.10	0.15	0.09	0.10	0.12	0.12
MgO	4.97	4.96	5.91	9.33	6.43	6.60	5.05	5.24
CaO	7.35	5.32	8.15	7.66	8.36	9.32	7.16	8.80
Na2O	3.09	3.30	2.83	1.53	3.37	2.69	3.21	3.06
K2O	2.01	2.70	2.44	2.06	1.41	1.09	2.12	1.09
P2O5	0.52	0.30	0.33	0.08	0.18	0.21	0.32	0.47
Loss	1.40	2.40	1.40	1.60	1.60	2.00	2.00	1.40
TOTAL	100.23	100.49	99.56	99.29	99.29	100.09	100.42	100.07
Nb	11	8	10	8	4	4	14	13
Zr	155	198	117	80	88	107	198	138
Y	18	13	16	17	14	16	23	30
Sr	840	781	1076	275	969	958	680	839
Rb	61	96	75	48	39	23	47	15
Th	11	8	0	17	7	5	4	2
Pb	12	16	8	13	7	10	12	6
Zn	24	42	39	17	36	37	22	14
Cu	72	76	72	97	61	58	76	81
Ni	30	31	60	173	78	63	62	38
Cr	43	23	64	476	90	71	121	129
V	214	198	185	158	133	126	148	210
Ba	300	520	340	366	292	263	531	315
Hf	2	4	4	1	3	4	5	4
Ce	58	49	64	37	23	43	38	87
La	12	8	1	9	2	5	20	12

Table B4: Continued

Sample	GT36	GT40	GT46	GT31	GT41	GT34	GT32	GT33
SiO2	55.85	52.70	56.84	53.02	65.84	64.25	68.38	70.53
TiO2	1.73	2.88	0.95	1.22	0.65	0.66	0.54	0.52
Al2O3	16.86	17.40	11.63	12.86	16.97	17.80	16.16	15.66
Fe2O3	1.18	0.89	0.67	1.06	0.29	0.09	0.03	2.06
FeO	6.47	7.13	6.47	6.92	3.24	3.59	2.99	1.24
MnO	0.10	0.10	0.14	0.15	0.06	0.07	0.06	0.06
MgO	4.04	4.74	9.34	9.38	1.56	1.96	1.37	1.33
CaO	6.41	7.18	7.89	10.00	2.82	2.98	1.96	2.06
Na2O	3.35	2.86	1.76	2.40	4.87	4.50	3.63	4.00
K2O	1.57	2.38	2.37	1.27	2.59	1.96	3.41	2.57
P2O5	0.15	0.20	0.24	0.33	0.24	0.24	0.24	0.17
Loss	1.40	1.40	2.00	0.60	1.20	1.40	1.40	0.40
TOTAL	99.28	100.08	100.52	99.41	100.54	99.69	100.36	100.77
Nb	7	8	8	10	7	10	14	13
Zr	136	127	108	102	250	215	233	266
Y	16	9	37	24	17	10	15	12
Sr	752	1073	399	510	624	727	474	556
Rb	40	97	91	23	66	61	89	63
Th	8	6	0	5	11	10	13	14
Pb	13	12	16	8	14	15	29	17
Zn	15	40	45	63	7	15	2	24
Cu	69	59	81	86	72	59	64	48
Ni	17	56	167	178	21	19	16	17
Cr	26	21	507	494	15	22	15	13
V	238	304	159	179	54	75	58	45
Ba	277	365	516	246	742	577	700	446
Hf	4	4	3	2	7	7	7	9
Ce	66	11	71	54	122	93	125	111
La	8	0	13	22	66	33	66	36

Sample	GT57	GT59	GT60	GT48	GT49	GT50
SiO2	70.81	70.41	69.04	75.75	75.07	75.94
TiO2	0.35	0.31	0.42	0.14	0.14	0.11
Al2O3	15.56	15.44	16.23	13.73	13.55	13.47
Fe2O3	0.27	1.18	0.52	0.00	0.04	0.02
FeO	1.84	1.10	1.87	0.92	0.79	0.77
MnO	0.05	0.05	0.05	0.03	0.05	0.03
MgO	0.63	1.05	0.98	0.19	0.35	0.07
CaO	1.31	1.40	1.86	0.48	0.51	0.57
Na2O	3.93	5.02	4.09	3.34	3.80	3.11
K2O	4.43	3.81	3.93	4.94	5.02	5.32
P2O5	0.12	0.14	0.17	0.01	0.03	0.01
Loss	0.20	0.60	0.60	0.20	0.60	0.20
TOTAL	99.66	100.69	99.95	99.82	100.03	99.72
Nb	8	19	8	21	21	13
Zr	200	226	231	84	91	88
Y	7	16	10	19	31	14
Sr	429	467	544	86	76	106
Rb	95	65	57	219	209	181
Th	12	16	7	23	20	16
Pb	23	19	20	31	34	30
Zn	11	4	9	9	8	4
Cu	49	46	49	33	27	19
Ni	13	13	14	10	7	11
Cr	3	0	8	0	0	0
V	32	32	47	9	15	13
Ba	636	764	811	289	219	386
Hf	7	7	6	4	4	5
Ce	76	81	64	53	41	54
La	25	46	39	17	23	23

Table B5: Whole rock analyses in wt % and trace elements in ppm of the Carsphairn pluton.

Sample	AS33	77030	AS38	77026	77031	77032	AS40	AS17
SiO2	56.64	57.43	57.09	60.81	61.53	62.09	61.11	61.80
TiO2	1.05	1.01	1.22	1.01	0.92	0.95	1.08	0.94
Al2O3	16.87	17.27	17.38	16.97	16.88	17.49	17.49	17.39
Fe2O3	0.65	0.43	1.24	0.65	0.88	1.01	0.72	0.84
FeO	6.22	6.23	5.21	4.84	4.36	4.03	4.95	4.46
MnO	0.17	0.15	0.13	0.10	0.13	0.13	0.17	0.13
MgO	6.31	5.94	4.20	2.85	2.77	2.01	2.83	2.88
CaO	6.39	6.18	5.13	5.47	5.06	4.65	5.14	5.37
Na2O	3.55	3.35	3.91	4.33	3.80	4.10	3.54	3.87
K2O	1.57	1.46	2.52	2.49	2.74	2.79	2.64	2.56
P2O5	0.27	0.27	0.32	0.29	0.23	0.25	0.23	0.24
Loss	0.20	0.20	1.40	0.20	0.40	0.40	0.60	0.20
TOTAL	100.07	100.09	99.92	100.17	99.86	100.06	100.65	100.83
Nb	3	5	8	7	8	9	8	6
Zr	89	77	126	152	149	138	144	143
Y	22	24	29	28	26	26	25	25
Sr	503	517	489	443	390	439	429	403
Rb	42	40	89	71	88	79	85	72
Th	6	0	17	15	4	13	8	11
Pb	20	18	25	23	21	23	21	22
Zn	152	72	54	65	68	70	74	68
Cu	11	13	11	8	8	7	7	11
Ni	99	87	15	7	9	5	5	8
Cr	216	202	58	21	33	14	21	32
V	168	160	133	117	102	92	115	100
Ba	398	404	515	532	552	580	466	512
Hf	3	2	2	3	4	3	4	3
Ce	54	57	88	72	76	79	70	79
La	18	18	25	27	31	30	26	27

Sample	AS18	AS48	AS19	AS46	AS49
SiO2	61.21	63.66	65.73	71.06	70.95
TiO2	0.89	0.87	0.66	0.47	0.47
Al2O3	17.52	16.72	16.49	14.89	14.46
Fe2O3	0.53	0.60	0.60	0.54	0.45
FeO	4.51	4.21	3.69	2.13	2.18
MnO	0.13	0.08	0.08	0.04	0.05
MgO	2.80	2.24	1.90	0.73	0.85
CaO	5.39	4.11	2.77	1.85	1.78
Na2O	4.15	3.80	3.97	3.13	3.54
K2O	2.26	2.91	2.97	4.90	4.94
P2O5	0.25	0.20	0.18	0.08	0.06
Loss	0.20	1.00	0.80	0.00	0.60
TOTAL	99.99	100.56	99.99	99.99	100.48
Nb	6	8	9	15	14
Zr	144	192	158	248	270
Y	23	30	22	41	36
Sr	421	334	374	182	158
Rb	73	91	87	240	235
Th	6	16	7	43	61
Pb	20	23	19	28	34
Zn	68	64	50	25	32
Cu	11	13	5	4	5
Ni	10	13	15	12	10
Cr	33	33	40	14	7
V	112	98	80	47	44
Ba	504	543	502	510	456
Hf	3	5	4	5	5
Ce	65	69	66	197	115
La	26	30	29	123	61

Table B6: Whole rock analyses in wt % and trace element in ppm of the Loch Doon pluton.

Sample	WL1	WL2	77015	WL3	WL4	78002	78004	78001
SiO2	59.26	64.52	60.28	60.33	59.60	59.88	59.89	57.81
TiO2	0.95	0.81	0.82	0.69	0.85	0.82	0.87	0.80
Al2O3	19.24	12.83	15.44	15.35	15.56	15.52	15.51	15.54
Fe2O3	0.63	0.39	0.48	0.12	1.75	0.75	0.83	0.74
FeO	7.16	4.97	5.15	4.85	3.48	5.03	4.54	5.46
MnO	0.07	0.19	0.12	0.09	0.05	0.10	0.10	0.10
MgO	5.53	4.26	6.15	5.73	6.02	5.66	5.01	6.67
CaO	0.78	8.14	5.53	5.08	3.10	5.30	4.68	6.28
Na2O	1.51	0.78	3.32	4.05	3.28	3.52	3.57	3.48
K2O	2.98	2.09	2.18	2.22	3.33	2.66	2.97	2.08
P2O5	0.16	0.20	0.28	0.23	0.24	0.27	0.29	0.25
Loss	1.20	0.40	0.60	0.80	2.20	0.20	1.60	0.40
TOTAL	99.67	99.73	100.57	99.76	99.69	100.01	100.12	99.88
Nb	16	15	7	8	10	12	12	7
Zr	198	246	106	138	173	115	132	63
Y	29	26	21	16	19	21	21	21
Sr	110	205	519	564	446	648	588	788
Rb	111	76	61	65	85	79	88	57
Th	12	12	8	3	8	11	12	12
Pb	19	10	20	9	20	22	22	22
Zn	111	68	68	60	50	68	68	70
Cu	44	25	15	25	24	26	25	41
Ni	174	110	53	153	147	134	110	177
Cr	251	194	268	276	287	254	241	337
V	152	103	137	106	134	130	122	131
Ba	626	270	827	702	789	1327	1004	929
Hf	5	6	3	6	4	3	2	3
Ce	73	72	56	31	65	81	76	59
La	32	34	23	26	25	29	29	29

Sample	77017	77018	77016	77021	WL5	WL6	WL7	WL8
SiO2	60.73	60.36	59.58	61.03	61.33	59.07	60.12	61.55
TiO2	0.83	0.82	0.89	0.83	0.87	0.80	0.82	0.84
Al2O3	15.08	15.39	15.37	15.30	15.06	15.61	15.53	15.44
Fe2O3	0.69	1.11	0.67	1.09	0.95	1.55	1.23	1.26
FeO	4.40	4.14	4.62	4.10	4.35	4.31	4.26	3.76
MnO	0.10	0.09	0.12	0.11	0.09	0.10	0.09	0.09
MgO	5.62	5.66	5.41	4.82	5.25	5.87	5.54	4.38
CaO	5.06	5.28	4.25	4.41	5.00	5.78	5.47	4.58
Na2O	3.78	3.42	3.65	3.75	3.91	3.77	3.64	3.84
K2O	2.42	2.71	2.72	3.18	2.68	2.59	2.63	2.93
P2O5	0.29	0.30	0.27	0.27	0.30	0.25	0.29	0.30
Loss	0.80	0.60	2.20	1.40	0.40	0.20	0.60	0.80
TOTAL	100.04	100.15	99.98	100.56	100.44	100.19	100.48	100.02
Nb	8	8	10	9	10	4	11	14
Zr	132	117	157	137	131	75	117	181
Y	22	22	21	20	19	21	19	20
Sr	540	649	516	636	611	711	656	568
Rb	69	79	75	97	81	73	80	90
Th	12	6	11	8	3	1	11	18
Pb	21	19	21	21	19	19	22	23
Zn	68	63	66	66	60	67	59	64
Cu	24	36	25	33	28	38	20	27
Ni	156	143	112	112	131	140	140	92
Cr	265	271	250	223	237	281	264	199
V	116	122	133	126	126	126	130	122
Ba	826	1031	815	1067	951	1225	982	958
Hf	5	3	4	4	5	4	5	5
Ce	68	75	75	73	59	72	70	69
La	29	34	31	32	23	28	28	31

Table B6: Continued

Sample	DBL4	DBL5	DBL1	DBL2	DBL3	77022	77023	77024
SiO2	59.86	59.75	62.96	63.17	63.13	64.48	65.97	65.80
TiO2	0.94	0.82	0.80	0.78	0.80	0.69	0.63	0.66
Al2O3	14.87	15.15	15.62	15.62	15.10	14.53	15.11	15.06
Fe2O3	0.30	0.54	0.21	0.64	0.94	0.76	0.56	0.67
FeO	5.37	4.56	4.15	3.66	3.54	3.25	2.98	3.14
MnO	0.11	0.10	0.07	0.08	0.09	0.07	0.08	0.08
MgO	5.58	5.03	3.87	3.89	3.75	3.18	2.92	3.12
CaO	5.27	4.93	4.12	3.90	3.98	3.24	3.26	3.37
Na2O	3.43	3.46	3.43	3.68	3.69	3.60	3.90	3.68
K2O	2.45	2.87	3.46	3.63	3.46	4.09	3.81	3.85
P2O5	0.32	0.29	0.24	0.23	0.23	0.22	0.17	0.20
Loss	1.40	2.40	0.60	0.40	1.00	1.60	0.20	0.20
TOTAL	100.16	100.16	99.76	99.91	99.94	99.92	99.80	100.04
Nb	9	10	10	9	19	9	9	11
Zr	68	154	184	172	177	185	175	183
Y	26	21	20	20	21	23	21	18
Sr	600	580	521	519	493	455	405	440
Rb	75	74	101	103	110	133	128	130
Th	11	9	3	15	4	18	14	21
Pb	21	20	19	25	19	22	22	23
Zn	65	65	61	62	59	49	52	49
Cu	20	7	24	26	22	12	18	19
Ni	126	108	86	86	82	57	66	63
Cr	286	243	174	179	178	116	144	133
V	146	128	104	105	112	85	91	87
Ba	1005	1062	913	879	898	792	822	769
Hf	2	5	7	7	5	5	4	5
Ce	93	69	57	58	80	74	78	80
La	35	30	27	28	31	32	34	35

Sample	77025	77002	WL9	WL10	HH1	HH2	HH4	HH5	HH6
SiO2	63.02	63.84	67.23	68.64	71.34	71.23	71.57	70.25	70.41
TiO2	0.75	0.73	0.59	0.49	0.34	0.28	0.35	0.30	0.41
Al2O3	15.52	15.22	14.83	14.78	14.90	15.15	14.81	15.15	15.15
Fe2O3	0.56	0.59	0.18	0.72	0.11	0.00	0.01	0.00	0.67
FeO	3.97	3.76	3.08	1.86	1.83	1.99	1.85	2.06	1.66
MnO	0.09	0.09	0.07	0.06	0.05	0.05	0.04	0.05	0.05
MgO	3.83	3.97	2.45	1.79	1.33	1.23	1.03	1.34	1.48
CaO	4.29	3.58	2.94	2.16	1.40	1.73	1.72	1.81	1.86
Na2O	4.01	3.43	3.52	3.64	3.25	3.46	3.12	3.21	4.01
K2O	3.00	3.78	3.96	4.46	4.91	4.60	4.75	4.59	4.51
P2O5	0.26	0.23	0.18	0.15	0.10	0.10	0.07	0.09	0.12
Loss	0.20	0.40	0.60	0.80	0.20	0.60	0.80	1.20	0.20
TOTAL	99.73	99.84	99.82	99.73	99.92	100.58	100.27	100.21	100.70
Nb	9	11	16	17	14	13	12	12	11
Zr	173	170	188	172	136	149	140	144	162
Y	18	23	22	23	17	14	16	14	15
Sr	508	494	360	313	249	254	250	277	296
Rb	88	117	150	170	210	196	214	202	197
Th	8	19	27	17	22	21	29	24	19
Pb	20	23	25	23	17	27	37	30	25
Zn	60	57	45	36	36	39	33	37	39
Cu	23	19	14	8	5	4	5	7	7
Ni	82	79	50	33	23	25	23	26	30
Cr	177	165	98	61	33	36	34	47	54
V	103	102	78	61	42	39	40	47	54
Ba	884	799	717	717	630	625	555	626	680
Hf	5	5	5	4	4	4	4	5	5
Ce	83	79	82	66	80	71	81	73	78
La	32	31	46	32	35	34	41	36	38

Appendix C

Electron microprobe mineral analysis:

The microscan V microprobe at Edinburgh University with an energy dispersive analysis system (EDS) was used for most of the analyses presented in this study. The Cambridge Microscan V spectrometer was used, an acceleration potential of 20 KV and a specimen beam current of 6 NA. The analyses were corrected with the aid of a Data General Nova Computer. The correction procedures used are those described by Sweatman and Long (1969). The overall precision using EDS is between 1.0 and 1.5% at the 2 σ level (Dr P Hill personal communication).

The polished thin sections were carbon-coated to prevent charge build up.

Periclase, cobalt and jadeite were used as standards. Periclase used for adjusting the electron beam, cobalt for calibrating the instrument before and during the operation and jadeite for checking calibration. Elements routinely analysed include Si, Ti, Al, Fe, Mn, Mg, Ca, Na, K and P; whereas elements analysed in particular minerals like olivine, orthopyroxene, clinopyroxene and amphibole include Ni and Cr.

Some samples were analysed for mineral chemistry at the University of St Andrews on a Jeol 733 Superprobe under the direction of Dr W.E. Stephens and Donald Herd.

In the key to tables of mineral analyses, the following abbreviations are used.

OL = Olivine

OP = Orthopyroxene

CP = Clinopyroxene

AM = Amphibole

BI = Biotite

PL = Plagioclase

followed by sample numbers

Tables of electron microprobe analyses:

In each table Fe was determined as total FeO and thereafter Fe^{+3} values in structural formula should be ignored.

In the EDA spectrometer values for Cr, and Ni were obtained and values for Sr and Ba should be regarded as not determined. Cr and Ni tabulated as ppm.

Table C1a: Electron microprobe analyses of olivine with structural formulae based on four oxygens for the Garabal Hill gabbros and diorites.

Sample	OLGH33A	OLGH33B	OLGH35A	OLGH35B	OLGH36A	OLGH36B	OLGH36AA	OLGH36AB	OLGH36AC	OLGH10A	OLGH10B	OLGH1A	OLGH1B	OLGH3A	OLGH3B	OLGH5A	OLGH5B
SiO2	39.15	39.48	39.51	40.03	39.15	39.36	39.88	39.50	39.58	39.44	39.15	39.84	40.38	39.18	39.63	38.56	39.26
TiO2	0.00	0.16	0.00	0.00	0.00	0.00	0.00	0.00	0.00	0.00	0.11	0.00	0.00	0.00	0.00	0.00	0.00
Al2O3	0.00	0.00	0.00	0.00	0.00	0.00	0.00	0.00	0.00	0.00	0.00	0.00	0.00	0.00	0.00	0.00	0.00
FeO	18.97	19.06	19.34	18.09	19.76	19.86	18.76	19.27	19.14	19.07	18.61	18.16	19.43	20.03	19.53	21.41	21.49
MnO	0.38	0.22	0.28	0.27	0.34	0.34	0.17	0.32	0.37	0.29	0.21	0.30	0.33	0.39	0.38	0.35	0.37
MgO	41.44	41.22	41.08	41.60	41.20	40.92	41.18	41.40	41.05	41.20	41.53	41.22	39.52	40.69	40.41	39.92	39.59
CaO	0.00	0.00	0.00	0.00	0.00	0.00	0.12	0.00	0.00	0.00	0.10	0.21	0.19	0.00	0.00	0.00	0.00
Na2O	0.00	0.00	0.00	0.00	0.00	0.00	0.00	0.00	0.00	0.00	0.00	0.00	0.00	0.00	0.00	0.00	0.00
K2O	0.00	0.00	0.00	0.00	0.00	0.00	0.00	0.00	0.00	0.00	0.00	0.00	0.00	0.00	0.00	0.00	0.00
P2O5	0.00	0.00	0.00	0.00	0.00	0.00	0.00	0.00	0.00	0.00	0.00	0.00	0.00	0.00	0.00	0.00	0.00
TOTAL	100.15	100.14	100.44	100.15	100.45	100.48	100.11	100.49	100.35	100.23	99.98	100.28	100.08	100.52	100.11	100.41	100.71
Cr	0	0	0	0	0	0	0	0	0	0	0	0	0	0	0	0	0
Ni	2100	0	2300	1600	0	0	0	0	2100	2300	2700	5500	2300	2300	1600	1700	0
Sr	0	0	0	0	0	0	0	0	0	0	0	0	0	0	0	0	0
Ba	0	0	0	0	0	0	0	0	0	0	0	0	0	0	0	0	0
Si	1.0009	1.0074	1.0073	1.0161	1.0005	1.0054	1.0154	1.0058	1.0092	1.0067	1.0007	1.0128	1.0312	1.0026	1.0142	0.9952	1.0079
Ti	0.0000	0.0031	0.0000	0.0000	0.0000	0.0000	0.0000	0.0000	0.0000	0.0000	0.0021	0.0000	0.0000	0.0000	0.0000	0.0000	0.0000
Al	0.0000	0.0000	0.0000	0.0000	0.0000	0.0000	0.0000	0.0000	0.0000	0.0000	0.0000	0.0000	0.0000	0.0000	0.0000	0.0000	0.0000
Fe3	0.0000	0.0000	0.0000	0.0000	0.0000	0.0000	0.0000	0.0000	0.0000	0.0000	0.0000	0.0000	0.0000	0.0000	0.0000	0.0000	0.0000
Fe2	0.4056	0.4067	0.4124	0.3840	0.4223	0.4242	0.3995	0.4104	0.4082	0.4071	0.3978	0.3861	0.4150	0.4287	0.4180	0.4621	0.4614
Mn2	0.0082	0.0048	0.0060	0.0058	0.0074	0.0074	0.0037	0.0069	0.0080	0.0063	0.0045	0.0065	0.0071	0.0085	0.0082	0.0077	0.0080
Mg	1.5789	1.5675	1.5609	1.5738	1.5692	1.5577	1.5627	1.5711	1.5599	1.5673	1.5821	1.5617	1.5042	1.5517	1.5412	1.5354	1.5147
Ca	0.0000	0.0000	0.0000	0.0000	0.0000	0.0000	0.0033	0.0000	0.0000	0.0000	0.0027	0.0057	0.0052	0.0000	0.0000	0.0000	0.0000
Na	0.0000	0.0000	0.0000	0.0000	0.0000	0.0000	0.0000	0.0000	0.0000	0.0000	0.0000	0.0000	0.0000	0.0000	0.0000	0.0000	0.0000
K	0.0000	0.0000	0.0000	0.0000	0.0000	0.0000	0.0000	0.0000	0.0000	0.0000	0.0000	0.0000	0.0000	0.0000	0.0000	0.0000	0.0000
Sr	0.0000	0.0000	0.0000	0.0000	0.0000	0.0000	0.0000	0.0000	0.0000	0.0000	0.0000	0.0000	0.0000	0.0000	0.0000	0.0000	0.0000
Ba	0.0000	0.0000	0.0000	0.0000	0.0000	0.0000	0.0000	0.0000	0.0000	0.0000	0.0000	0.0000	0.0000	0.0000	0.0000	0.0000	0.0000
Cr	0.0000	0.0000	0.0000	0.0000	0.0000	0.0000	0.0000	0.0000	0.0000	0.0000	0.0000	0.0000	0.0000	0.0000	0.0000	0.0000	0.0000
Ni	0.0055	0.0000	0.0060	0.0041	0.0000	0.0000	0.0000	0.0000	0.0055	0.0060	0.0070	0.0143	0.0060	0.0060	0.0042	0.0045	0.0000
Total	2.9991	2.9895	2.9927	2.9839	2.9995	2.9946	2.9846	2.9942	2.9908	2.9933	2.9971	2.9872	2.9688	2.9974	2.9858	3.0048	2.9921

Table C1b: Electron microprobe analyses with structural formulae based on 6 oxygens for orthopyroxenes from the Garabal Hill pluton.

Sample	OPGH21A	OPGH21B	OPGH21C	OPGH10A	OPGH10B	OPGH3A	OPGH3B
SiO2	53.23	52.92	53.45	54.62	54.73	54.55	54.25
TiO2	0.00	0.00	0.26	0.11	0.00	0.00	0.12
Al2O3	1.18	0.98	1.64	1.19	1.39	0.00	0.21
FeO	20.55	20.12	18.05	16.15	16.04	17.84	17.89
MnO	0.42	0.41	0.42	1.07	0.35	0.58	0.67
MgO	23.83	24.51	24.98	25.37	26.11	26.51	26.34
CaO	0.87	0.94	1.07	1.50	1.36	0.34	0.45
Na2O	0.00	0.00	0.00	0.00	0.00	0.00	0.00
K2O	0.00	0.00	0.00	0.00	0.00	0.00	0.00
P2O5	0.00	0.00	0.00	0.00	0.00	0.00	0.00
TOTAL	100.08	99.88	99.87	100.01	100.15	99.82	99.93
Cr	0	0	0	0	0	0	0
Ni	0	0	0	0	1700	0	0
Sr	0	0	0	0	0	0	0
Ba	0	0	0	0	0	0	0
Si	1.9650	1.9566	1.9553	1.9821	1.9761	1.9911	1.9809
Ti	0.0000	0.0000	0.0072	0.0030	0.0000	0.0000	0.0033
Al	0.0514	0.0427	0.0707	0.0509	0.0592	0.0000	0.0090
Fe3	0.0000	0.0000	0.0000	0.0000	0.0000	0.0000	0.0000
Fe2	0.6344	0.6221	0.5522	0.4901	0.4844	0.5446	0.5463
Mn2	0.0131	0.0128	0.0130	0.0329	0.0107	0.0179	0.0207
Mg	1.3110	1.3505	1.3619	1.3721	1.4050	1.4421	1.4334
Ca	0.0344	0.0372	0.0419	0.0583	0.0526	0.0133	0.0176
Na	0.0000	0.0000	0.0000	0.0000	0.0000	0.0000	0.0000
K	0.0000	0.0000	0.0000	0.0000	0.0000	0.0000	0.0000
P	0.0000	0.0000	0.0000	0.0000	0.0000	0.0000	0.0000
Sr	0.0000	0.0000	0.0000	0.0000	0.0000	0.0000	0.0000
Ba	0.0000	0.0000	0.0000	0.0000	0.0000	0.0000	0.0000
Cr	0.0000	0.0000	0.0000	0.0000	0.0000	0.0000	0.0000
Ni	0.0000	0.0000	0.0000	0.0000	0.0063	0.0000	0.0000
Total	4.0093	4.0221	4.0022	3.9894	3.9943	4.0089	4.0113

Table C1c: Electron microprobe analyses with structural formulae based on 6 oxygens for clinopyroxenes from the Garabal Hill pluton.

Sample	CPGH33A	CPGH33B	CPGH33C	CPGH33D	CPGH35A	CPGH35B	CPGH35C	CPGH35D	CPGH36AA	CPGH36AB	CPGH36AC	CPGH36A	CPGH36B	CPGH36C	CPGH36D	CPGH36E
SiO2	52.39	52.48	52.99	52.62	52.05	50.46	51.81	51.92	51.57	51.81	51.30	51.74	51.76	51.87	52.22	52.12
TiO2	0.70	0.76	0.37	0.62	0.75	0.83	0.83	0.75	0.67	0.75	0.61	0.84	0.73	0.78	0.60	0.75
Al2O3	2.70	3.09	1.36	2.72	2.98	3.67	2.90	2.95	3.31	3.21	3.10	3.05	2.85	3.11	2.81	3.08
FeO	6.54	5.86	5.00	5.74	6.26	6.85	6.79	6.26	5.95	5.97	6.17	6.07	6.49	6.12	6.14	5.64
MnO	0.24	0.00	0.21	0.21	0.23	0.15	0.16	0.15	0.18	0.21	0.31	0.14	0.00	0.00	0.15	0.00
MgO	16.03	15.58	14.99	16.05	15.19	16.02	15.65	15.57	15.62	15.58	15.55	15.56	15.62	15.63	16.08	15.78
CaO	21.36	21.74	24.54	21.59	21.70	21.44	21.72	21.81	21.90	21.87	21.92	21.73	21.86	21.71	21.15	22.19
Na2O	0.28	0.00	0.00	0.00	0.00	0.00	0.00	0.00	0.00	0.23	0.00	0.00	0.00	0.00	0.00	0.22
K2O	0.00	0.00	0.00	0.00	0.00	0.00	0.00	0.00	0.00	0.00	0.00	0.00	0.00	0.00	0.00	0.00
P2O5	0.00	0.00	0.00	0.00	0.00	0.00	0.00	0.00	0.00	0.00	0.00	0.00	0.00	0.00	0.00	0.00
TOTAL	100.59	99.91	99.80	100.15	99.57	99.90	100.35	99.85	100.02	100.25	99.65	99.69	99.99	99.75	99.81	100.43
Cr	3500	4000	3400	6000	4100	4800	4900	4400	8200	6200	6900	5600	6800	5300	6600	6500
Ni	0	0	0	0	0	0	0	0	0	0	0	0	0	0	0	0
Sr	0	0	0	0	0	0	0	0	0	0	0	0	0	0	0	0
Ba	0	0	0	0	0	0	0	0	0	0	0	0	0	0	0	0
Si	1.9182	1.9247	1.9570	1.9258	1.9224	1.8677	1.9052	1.9135	1.8967	1.9021	1.8983	1.9084	1.9072	1.9104	1.9196	1.9064
Ti	0.0193	0.0210	0.0103	0.0171	0.0208	0.0231	0.0230	0.0208	0.0185	0.0207	0.0170	0.0233	0.0202	0.0216	0.0156	0.0206
Al	0.1165	0.1336	0.0592	0.1174	0.1298	0.1601	0.1257	0.1282	0.1435	0.1389	0.1352	0.1326	0.1238	0.1350	0.1218	0.1328
Fe3	0.0000	0.0000	0.0000	0.0000	0.0000	0.0000	0.0000	0.0000	0.0000	0.0000	0.0000	0.0000	0.0000	0.0000	0.0000	0.0000
Fe2	0.2003	0.1797	0.1544	0.1757	0.1934	0.2120	0.2088	0.1930	0.1830	0.1833	0.1909	0.1872	0.2000	0.1885	0.1888	0.1725
Mn2	0.0074	0.0000	0.0066	0.0065	0.0072	0.0047	0.0050	0.0047	0.0056	0.0065	0.0097	0.0044	0.0000	0.0000	0.0047	0.0000
Mg	0.8747	0.8516	0.8251	0.8754	0.8361	0.8837	0.8577	0.8552	0.8562	0.8525	0.8575	0.8553	0.8578	0.8579	0.8809	0.8602
Ca	0.8380	0.8543	0.9711	0.8467	0.8588	0.8503	0.8558	0.8613	0.8630	0.8603	0.8691	0.8588	0.8631	0.8568	0.8331	0.8697
Na	0.0199	0.0000	0.0000	0.0000	0.0000	0.0000	0.0000	0.0000	0.0000	0.0164	0.0000	0.0000	0.0000	0.0000	0.0000	0.0156
K	0.0000	0.0000	0.0000	0.0000	0.0000	0.0000	0.0000	0.0000	0.0000	0.0000	0.0000	0.0000	0.0000	0.0000	0.0000	0.0000
P	0.0000	0.0000	0.0000	0.0000	0.0000	0.0000	0.0000	0.0000	0.0000	0.0000	0.0000	0.0000	0.0000	0.0000	0.0000	0.0000
Sr	0.0000	0.0000	0.0000	0.0000	0.0000	0.0000	0.0000	0.0000	0.0000	0.0000	0.0000	0.0000	0.0000	0.0000	0.0000	0.0000
Ba	0.0000	0.0000	0.0000	0.0000	0.0000	0.0000	0.0000	0.0000	0.0000	0.0000	0.0000	0.0000	0.0000	0.0000	0.0000	0.0000
Cr	0.0132	0.0151	0.0129	0.0226	0.0156	0.0183	0.0185	0.0167	0.0310	0.0234	0.0262	0.0212	0.0258	0.0201	0.0249	0.0244
Ni	0.0000	0.0000	0.0000	0.0000	0.0000	0.0000	0.0000	0.0000	0.0000	0.0000	0.0000	0.0000	0.0000	0.0000	0.0000	0.0000
Total	4.0076	3.9800	3.9966	3.9871	3.9841	4.0200	3.9997	3.9933	3.9975	4.0042	4.0040	3.9914	3.9978	3.9904	3.9904	4.0022

Table C1c: Continued

Sample	CPGH36F	CPGH36G	CPGH36H	CPGH36I	CPGH36J	CPGH10A	CPGH10B	CPGH10C	CPGH10D	CPGH1A	CPGH1B	CPGH1C	CPGH3B	CPGH3C	CPGH3D	CPGH5A	CPGH5B	CPGH5C	CPGH5D	CPGH7A	CPGH7B	CPGH7C
SiO2	51.69	51.99	51.96	51.92	52.07	52.09	52.83	52.76	52.20	51.59	51.49	51.62	52.40	51.53	53.40	52.81	52.74	53.28	53.11	53.45	53.03	53.45
TiO2	0.76	0.56	0.66	0.71	0.61	0.85	0.68	0.65	0.63	0.79	0.84	0.69	0.74	0.95	0.44	0.64	0.74	0.46	0.38	0.53	0.50	0.43
Al2O3	2.66	2.97	2.83	2.75	2.75	3.17	2.83	1.94	3.41	3.06	2.95	3.36	2.36	3.57	2.42	3.24	2.13	1.52	2.14	2.27	2.13	2.25
FeO	6.70	5.66	5.99	6.20	6.11	7.12	5.85	7.00	6.73	7.18	6.98	6.99	7.79	8.49	5.89	6.53	8.32	5.01	5.56	6.74	6.45	6.31
MnO	0.25	0.13	0.27	0.19	0.00	0.20	0.00	0.23	0.11	0.17	0.23	0.00	0.30	0.23	0.16	0.15	0.21	0.25	0.00	0.13	0.17	0.19
MgO	16.46	15.76	16.00	16.23	15.88	16.36	16.22	16.77	14.76	15.98	15.98	15.71	16.56	14.79	16.91	15.28	15.50	17.63	17.50	15.94	16.01	15.83
CaO	20.64	22.23	22.00	21.35	21.82	19.70	20.37	20.09	21.04	20.90	21.02	21.07	19.73	20.35	20.10	20.95	20.40	21.29	20.62	20.67	21.72	21.05
Na2O	0.00	0.00	0.00	0.00	0.00	0.23	0.35	0.00	0.43	0.00	0.00	0.00	0.00	0.00	0.00	0.00	0.00	0.00	0.00	0.00	0.00	0.00
K2O	0.00	0.00	0.00	0.00	0.00	0.00	0.00	0.00	0.00	0.00	0.00	0.00	0.00	0.00	0.00	0.00	0.00	0.00	0.00	0.00	0.00	0.00
P2O5	0.00	0.00	0.00	0.00	0.00	0.00	0.00	0.00	0.00	0.00	0.00	0.00	0.00	0.00	0.00	0.00	0.00	0.00	0.00	0.00	0.00	0.00
TOTAL	99.72	99.84	100.38	99.96	99.87	100.37	99.77	99.87	99.95	99.91	99.79	100.03	100.15	100.25	99.99	100.25	100.44	99.97	99.78	100.15	100.33	99.91
Cr	5600	5400	6700	6100	6300	6500	6400	4300	6400	2400	3000	5900	2700	3400	6700	6500	4000	5300	4700	4200	3200	4000
Ni	0	0	0	0	0	0	0	0	0	0	0	0	0	0	0	0	0	0	0	0	0	0
Sr	0	0	0	0	0	0	0	0	0	0	0	0	0	0	0	0	0	0	0	0	0	0
Ba	0	0	0	0	0	0	0	0	0	0	0	0	0	0	0	0	0	0	0	0	0	0
Si	1.9587	1.9432	1.9554	1.9416	1.9464	1.9405	1.9306	1.9468	1.9030	1.9277	1.9005	1.9036	1.9048	1.9209	1.9402	1.9339	1.9069	1.9161	1.9097	1.9055	1.9131	1.9079
Ti	0.0119	0.0138	0.0146	0.0104	0.0126	0.0205	0.0176	0.0121	0.0264	0.0205	0.0191	0.0234	0.0219	0.0174	0.0180	0.0187	0.0234	0.0169	0.0196	0.0182	0.0155	0.0211
Al	0.0972	0.0920	0.0979	0.0922	0.0655	0.0924	0.1396	0.1040	0.1554	0.1024	0.1458	0.1286	0.1332	0.1479	0.0841	0.1221	0.1368	0.1193	0.1193	0.1224	0.1288	0.1158
Fe3	0.0000	0.0000	0.0000	0.0000	0.0000	0.0000	0.0000	0.0000	0.0000	0.0000	0.0000	0.0000	0.0000	0.0000	0.0000	0.0000	0.0000	0.0000	0.0000	0.0000	0.0000	0.0000
Fe2	0.1934	0.1977	0.2062	0.1700	0.1531	0.2560	0.1997	0.1796	0.2622	0.2397	0.2152	0.2158	0.2217	0.2071	0.2153	0.1791	0.2180	0.1880	0.1907	0.1837	0.1742	0.2068
Mn2	0.0059	0.0053	0.0040	0.0000	0.0077	0.0065	0.0046	0.0049	0.0072	0.0093	0.0000	0.0072	0.0053	0.0034	0.0072	0.0000	0.0062	0.0000	0.0059	0.0084	0.0041	0.0078
Mg	0.8646	0.8743	0.8691	0.9534	0.9598	0.8499	0.8325	0.9188	0.8140	0.9079	0.8620	0.8805	0.8793	0.8095	0.9191	0.8849	0.8925	0.8709	0.8897	0.8745	0.8643	0.9055
Ca	0.8266	0.8528	0.8102	0.8077	0.8334	0.8043	0.8207	0.7852	0.8053	0.7777	0.8312	0.8327	0.8268	0.8296	0.7916	0.7990	0.7727	0.8604	0.8415	0.8645	0.8765	0.8163
Na	0.0000	0.0000	0.0000	0.0000	0.0000	0.0000	0.0000	0.0000	0.0000	0.0000	0.0000	0.0000	0.0000	0.0307	0.0000	0.0248	0.0163	0.0000	0.0000	0.0000	0.0000	0.0000
K	0.0000	0.0000	0.0000	0.0000	0.0000	0.0000	0.0000	0.0000	0.0000	0.0000	0.0000	0.0000	0.0000	0.0000	0.0000	0.0000	0.0000	0.0000	0.0000	0.0000	0.0000	0.0000
P	0.0000	0.0000	0.0000	0.0000	0.0000	0.0000	0.0000	0.0000	0.0000	0.0000	0.0000	0.0000	0.0000	0.0000	0.0000	0.0000	0.0000	0.0000	0.0000	0.0000	0.0000	0.0000
Sr	0.0000	0.0000	0.0000	0.0000	0.0000	0.0000	0.0000	0.0000	0.0000	0.0000	0.0000	0.0000	0.0000	0.0000	0.0000	0.0000	0.0000	0.0000	0.0000	0.0000	0.0000	0.0000
Ba	0.0000	0.0000	0.0000	0.0000	0.0000	0.0000	0.0000	0.0000	0.0000	0.0000	0.0000	0.0000	0.0000	0.0000	0.0000	0.0000	0.0000	0.0000	0.0000	0.0000	0.0000	0.0000
Cr	0.0151	0.0121	0.0158	0.0177	0.0199	0.0151	0.0244	0.0251	0.0129	0.0102	0.0223	0.0114	0.0091	0.0242	0.0163	0.0241	0.0245	0.0238	0.0231	0.0253	0.0204	0.0212
Ni	0.0000	0.0000	0.0000	0.0000	0.0000	0.0000	0.0000	0.0000	0.0000	0.0000	0.0000	0.0000	0.0000	0.0000	0.0000	0.0000	0.0000	0.0000	0.0000	0.0000	0.0000	0.0000
Total	3.9733	3.9910	3.9732	3.9930	3.9983	3.9853	3.9697	3.9765	3.9864	3.9955	3.9963	4.0031	4.0021	3.9909	3.9917	3.9867	3.9973	3.9954	3.9995	4.0024	3.9968	4.0025

Table C1d: Electron microprobe analyses with structural formulae based on 23 oxygens for amphibole of the Garabal Hill pluton.

Sample	AMGH15A	AMGH15B	AMGH15C	AMGH21A	AMGH21B	AMGH21C	AMGH21D	AMGH21E	AMGH21F	AMGH21G	AMGH7A	AMGH7B	AMGH6A	AMGH6B	AMGH25A	AMGH25B
SiO2	44.13	43.56	43.60	41.50	41.83	41.63	41.43	41.28	41.88	41.59	49.69	48.66	47.90	49.74	47.20	48.54
TiO2	2.32	2.31	2.38	3.63	3.41	3.42	3.74	3.87	3.22	3.21	0.54	1.10	0.97	0.84	1.16	0.91
Al2O3	10.77	11.02	10.83	12.67	12.54	12.53	12.14	12.39	12.30	12.74	6.41	6.21	7.31	5.67	7.21	6.80
FeO	9.99	9.98	10.37	11.01	10.97	10.97	11.00	11.10	11.00	9.95	13.11	14.18	14.22	12.75	15.07	14.78
MnO	0.23	0.18	0.21	0.14	0.20	0.22	0.21	0.18	0.13	0.17	0.44	0.41	0.27	0.30	0.34	0.19
MgO	15.26	14.97	14.73	13.93	13.40	13.64	13.68	13.32	13.64	14.31	14.53	13.70	13.41	14.37	12.85	13.61
CaO	11.74	11.63	11.62	11.46	11.79	11.52	11.56	11.37	11.74	11.75	11.50	11.94	12.00	12.20	11.55	11.63
Na2O	1.99	1.90	2.23	2.41	2.14	2.16	2.24	2.52	2.13	2.33	0.54	0.73	0.68	0.40	0.91	0.74
K2O	0.52	0.51	0.59	0.00	0.00	0.78	0.61	0.54	0.77	0.51	0.00	0.47	0.39	0.30	0.62	0.57
P2O5	0.00	0.00	0.00	0.00	0.00	0.00	0.00	0.00	0.00	0.00	0.00	0.00	0.00	0.00	0.00	0.00
TOTAL	97.32	96.39	96.91	96.92	96.40	96.87	96.61	96.57	96.96	96.56	97.03	97.40	97.38	96.76	96.91	97.77
Cr	3700	3300	3500	1700	1200	0	0	0	1500	0	2700	0	2300	1900	0	0
Ni	0	0	0	0	0	0	0	0	0	0	0	0	0	0	0	0
Sr	0	0	0	0	0	0	0	0	0	0	0	0	0	0	0	0
Ba	0	0	0	0	0	0	0	0	0	0	0	0	0	0	0	0
Si	6.4575	6.4328	6.4297	6.1310	6.2043	6.1699	6.1609	6.1433	6.2052	6.1514	7.2540	7.1567	7.0524	7.2921	7.0224	7.1190
Ti	0.2553	0.2566	0.2640	0.4033	0.3804	0.3812	0.4183	0.4331	0.3588	0.3571	0.0593	0.1217	0.1074	0.0926	0.1298	0.1004
Al	1.8579	1.9186	1.8829	2.2067	2.1927	2.1893	2.1283	2.1738	2.1485	2.2215	1.1032	1.0768	1.2688	0.9800	1.2646	1.1758
Fe3	0.0000	0.0000	0.0000	0.0000	0.0000	0.0000	0.0000	0.0000	0.0000	0.0000	0.0000	0.0000	0.0000	0.0000	0.0000	0.0000
Fe2	1.2226	1.2326	1.2790	1.3603	1.3608	1.3597	1.3680	1.3815	1.3631	1.2308	1.6006	1.7442	1.7510	1.5633	1.8751	1.8129
Mn2	0.0285	0.0225	0.0262	0.0175	0.0251	0.0276	0.0265	0.0227	0.0163	0.0213	0.0544	0.0511	0.0337	0.0373	0.0428	0.0236
Mg	3.3279	3.2947	3.2374	3.0670	2.9620	3.0128	3.0318	2.9543	3.0119	3.1543	3.1612	3.0029	2.9425	3.1397	2.8492	2.9748
Ca	1.8407	1.8403	1.8361	1.8141	1.8737	1.8295	1.8420	1.8131	1.8639	1.8622	1.7989	1.8817	1.8931	1.9165	1.8413	1.8277
Na	0.5646	0.5440	0.6376	0.6903	0.6154	0.6207	0.6459	0.7272	0.6119	0.6682	0.1529	0.2082	0.1941	0.1137	0.2625	0.2104
K	0.0971	0.0961	0.1110	0.0000	0.0000	0.1475	0.1157	0.1025	0.1456	0.0962	0.0000	0.0882	0.0733	0.0561	0.1177	0.1067
P	0.0000	0.0000	0.0000	0.0000	0.0000	0.0000	0.0000	0.0000	0.0000	0.0000	0.0000	0.0000	0.0000	0.0000	0.0000	0.0000
Sr	0.0000	0.0000	0.0000	0.0000	0.0000	0.0000	0.0000	0.0000	0.0000	0.0000	0.0000	0.0000	0.0000	0.0000	0.0000	0.0000
Ba	0.0370	0.0333	0.0353	0.0172	0.0122	0.0000	0.0000	0.0000	0.0152	0.0000	0.0270	0.0000	0.0232	0.0191	0.0000	0.0000
Cr	0.0000	0.0000	0.0000	0.0000	0.0000	0.0000	0.0000	0.0000	0.0000	0.0000	0.0000	0.0000	0.0000	0.0000	0.0000	0.0000
Ni	15.6891	15.6714	15.7392	15.7075	15.6267	15.7383	15.7374	15.7515	15.7404	15.7630	15.2115	15.3314	15.3394	15.2102	15.4056	15.3512
Total																

Table C1d: Continued

Sample	AMGH25C	AMGH26A	AMGH26B	AMGH26C	AMGH26D	AMGH26E	AMGH11A	AMGH11B	AMGH11C	AMGH28A	AMGH28B	AMGH28C	AMGH28D	AMGH31A	AMGH31B	AMGH39A	AMGH39B	AMGH39C	AMGH39D	AMGH39E	AMGH29A	AMGH29B	AMGH29C
SiO2	48.29	49.80	48.87	51.03	49.08	49.62	52.38	49.29	50.17	47.99	47.59	48.07	47.82	49.25	50.53	50.23	49.74	50.03	51.57	48.32	51.60	46.45	50.77
TiO2	1.06	0.61	0.86	0.14	0.70	0.95	0.64	1.16	0.92	1.08	1.36	0.90	0.96	0.63	0.55	0.83	0.78	0.83	0.72	1.16	0.42	1.39	0.55
Al2O3	6.59	5.44	5.79	4.79	5.61	5.39	4.70	6.34	6.12	5.77	6.75	6.40	6.42	5.26	4.84	4.74	5.58	4.72	3.95	6.63	3.74	7.40	3.99
FeO	14.60	12.95	12.65	12.74	13.06	12.59	9.36	10.50	10.67	13.88	14.32	14.07	14.07	13.59	13.38	13.03	13.44	13.13	12.50	14.79	12.54	15.20	12.72
MnO	0.37	0.34	0.30	0.29	0.25	0.33	0.12	0.22	0.25	0.35	0.41	0.45	0.45	0.51	0.50	0.62	0.53	0.55	0.64	0.52	0.64	0.63	0.64
MgO	13.83	14.47	14.24	15.17	15.38	14.91	17.47	15.65	15.98	13.70	13.62	14.12	13.61	14.33	14.62	14.97	14.50	14.71	15.64	13.23	15.87	12.66	15.34
CaO	11.97	11.89	11.59	12.24	10.57	11.42	12.43	11.70	12.38	11.76	11.93	11.45	11.98	11.83	11.77	11.97	11.95	11.76	11.95	12.06	12.13	11.53	11.49
Na2O	0.67	0.69	0.61	0.40	0.74	0.59	0.53	1.05	0.86	0.88	1.20	0.78	0.89	0.72	0.67	0.73	1.12	0.78	0.56	0.84	0.68	1.13	0.84
K2O	0.41	0.39	0.47	0.23	0.34	0.47	0.00	0.34	0.33	0.51	0.64	0.51	0.59	0.45	0.39	0.43	0.47	0.40	0.36	0.62	0.32	0.84	0.34
P2O5	0.00	0.00	0.00	0.00	0.00	0.00	0.00	0.00	0.00	0.00	0.00	0.00	0.00	0.00	0.00	0.00	0.00	0.00	0.00	0.00	0.00	0.00	0.00
TOTAL	97.79	96.58	95.55	97.03	95.73	96.27	97.75	96.41	97.68	96.04	97.82	96.87	96.79	96.57	97.25	97.55	98.11	96.91	97.89	98.17	97.94	97.36	96.68
Cr	0	0	1700	0	0	0	1200	1600	0	1200	0	1200	0	0	0	0	0	0	0	0	0	1300	0
Ni	0	0	0	0	0	0	0	0	0	0	0	0	0	0	0	0	0	0	0	0	0	0	0
Sr	0	0	0	0	0	0	0	0	0	0	0	0	0	0	0	0	0	0	0	0	0	0	0
Ba	0	0	0	0	0	0	0	0	0	0	0	0	0	0	0	0	0	0	0	0	0	0	0
Si	7.0879	7.3198	7.2632	7.4331	7.2618	7.2999	7.4406	7.1884	7.2207	7.1677	7.0102	7.1130	7.0984	7.2816	7.3856	7.3291	7.2402	7.3462	7.4556	7.0892	7.4647	6.9254	7.4468
Ti	0.1170	0.0674	0.0961	0.0153	0.0779	0.1051	0.0684	0.1272	0.0996	0.1213	0.1507	0.1002	0.1072	0.0701	0.0605	0.0911	0.0854	0.0917	0.0783	0.1280	0.0457	0.1559	0.0607
Al	1.1403	0.9427	1.0145	0.8226	0.9786	0.9348	0.7871	1.0901	1.0384	1.0160	1.1722	1.1165	1.1235	0.9168	0.8340	0.8154	0.9576	0.8171	0.6732	1.1468	0.6379	1.3007	0.6900
Fe3	0.0000	0.0000	0.0000	0.0000	0.0000	0.0000	0.0000	0.0000	0.0000	0.0000	0.0000	0.0000	0.0000	0.0000	0.0000	0.0000	0.0000	0.0000	0.0000	0.0000	0.0000	0.0000	0.0000
Fe2	1.7922	1.5919	1.5724	1.5520	1.6161	1.5490	1.1120	1.2807	1.2843	1.7338	1.7642	1.7412	1.7467	1.6804	1.6356	1.5900	1.6361	1.6124	1.5114	1.8147	1.5172	1.8953	1.5604
Mn2	0.0460	0.0423	0.0378	0.0358	0.0313	0.0411	0.0144	0.0272	0.0305	0.0443	0.0512	0.0564	0.0566	0.0639	0.0619	0.0766	0.0653	0.0684	0.0784	0.0646	0.0784	0.0796	0.0795
Mg	3.0253	3.1697	3.1541	3.2932	3.3914	3.2690	3.6984	3.4015	3.4276	3.0495	2.9900	3.1138	3.0109	3.1575	3.1847	3.2553	3.1455	3.2190	3.3698	2.8928	3.4216	2.8130	3.3533
Ca	1.8826	1.8726	1.8457	1.9104	1.6757	1.8002	1.8919	1.8283	1.9092	1.8821	1.8830	1.8154	1.9055	1.8741	1.8434	1.8714	1.8638	1.8503	1.8512	1.8959	1.8803	1.8420	1.8058
Na	0.1907	0.1966	0.1758	0.1130	0.2123	0.1683	0.1460	0.2969	0.2400	0.2548	0.3427	0.2238	0.2562	0.2064	0.1899	0.2065	0.3161	0.2221	0.1570	0.2390	0.1907	0.3267	0.2389
K	0.0768	0.0731	0.0891	0.0427	0.0642	0.0882	0.0000	0.0633	0.0606	0.0972	0.1203	0.0963	0.1117	0.0849	0.0727	0.0800	0.0873	0.0749	0.0664	0.1160	0.0591	0.1598	0.0636
P	0.0000	0.0000	0.0000	0.0000	0.0000	0.0000	0.0000	0.0000	0.0000	0.0000	0.0000	0.0000	0.0000	0.0000	0.0000	0.0000	0.0000	0.0000	0.0000	0.0000	0.0000	0.0000	0.0000
Sr	0.0000	0.0000	0.0000	0.0000	0.0000	0.0000	0.0000	0.0000	0.0000	0.0000	0.0000	0.0000	0.0000	0.0000	0.0000	0.0000	0.0000	0.0000	0.0000	0.0000	0.0000	0.0000	0.0000
Ba	0.0000	0.0000	0.0173	0.0000	0.0000	0.0000	0.0117	0.0160	0.0000	0.0123	0.0000	0.0121	0.0000	0.0000	0.0000	0.0000	0.0000	0.0000	0.0000	0.0000	0.0000	0.0133	0.0000
Cr	0.0000	0.0000	0.0000	0.0000	0.0000	0.0000	0.0000	0.0000	0.0000	0.0000	0.0000	0.0000	0.0000	0.0000	0.0000	0.0000	0.0000	0.0000	0.0000	0.0000	0.0000	0.0000	0.0000
Ni	15.3587	15.2763	15.2659	15.2181	15.3393	15.2558	15.1705	15.3195	15.3108	15.3790	15.4845	15.3887	15.4166	15.3356	15.2682	15.3155	15.3973	15.3021	15.2412	15.3869	15.2955	15.5116	15.2989
Total																							

Table C1e: Electron microprobe analyses with structural formulae based on 23 oxygens for biotites of the Garabal Hill pluton.

Sample	BIGH10A	BIGH10B	BIGH1A	BIGH1B	BIGH1C	BIGH1D	BIGH3A	BIGH3B	BIGH3C	BIGH5A	BIGH5B	BIGH5C	BIGH5D	BIGH7A	BIGH25A	BIGH25B
SiO2	37.36	37.72	37.15	37.51	37.32	38.65	37.88	37.41	38.43	37.58	37.81	37.71	36.89	36.72	37.37	37.82
TiO2	5.07	4.97	3.47	3.80	4.03	3.65	4.66	4.91	4.75	4.61	4.51	4.79	4.40	4.67	3.35	3.95
Al2O3	14.37	14.30	14.18	13.95	14.08	14.01	13.48	13.64	13.72	13.68	13.61	13.65	14.06	14.20	14.66	14.52
FeO	14.82	14.64	16.59	17.56	16.83	14.84	16.16	16.45	16.05	16.86	16.92	17.04	18.37	18.54	17.71	17.35
MnO	0.00	0.12	0.00	0.00	0.16	0.00	0.00	0.15	0.00	0.00	0.00	0.00	0.00	0.12	0.17	0.18
MgO	14.03	14.19	14.26	13.44	13.51	15.06	14.09	13.51	14.33	13.07	13.67	13.63	12.42	12.19	13.02	13.00
CaO	0.00	0.10	0.00	0.00	0.00	0.00	0.00	0.09	0.00	0.00	0.00	0.00	0.00	0.10	0.12	0.00
Na2O	0.00	0.00	0.00	0.00	0.00	0.00	0.00	0.00	0.00	0.00	0.00	0.00	0.00	0.00	0.00	0.00
K2O	9.41	9.47	9.05	9.15	9.22	8.94	9.48	9.40	9.55	9.30	9.58	9.50	9.35	9.47	9.22	9.09
P2O5	0.00	0.00	0.00	0.00	0.00	0.00	0.00	0.00	0.00	0.00	0.00	0.00	0.00	0.00	0.00	0.00
TOTAL	95.06	95.51	94.70	95.41	95.15	95.15	95.75	95.56	96.83	95.10	96.10	96.32	95.49	96.01	95.62	95.91
Sr	0	0	0	0	0	0	0	0	0	0	0	0	0	0	0	0
Ba	0	0	0	0	0	0	0	0	0	0	0	0	0	0	0	0
Cr	0	0	0	0	0	0	0	0	0	0	0	0	0	0	0	0
Ni	0	0	0	0	0	0	0	0	0	0	0	0	0	0	0	0
Si	5.8429	5.8680	5.8727	5.9108	5.8861	6.0014	5.9200	5.8757	5.9266	5.9284	5.9116	5.8847	5.8475	5.8046	5.8841	5.9136
Ti	0.5963	0.5815	0.4125	0.4503	0.4780	0.4262	0.5477	0.5800	0.5509	0.5459	0.5303	0.5622	0.5245	0.5552	0.3967	0.4645
Al	2.6495	2.6227	2.6427	2.5916	2.6181	2.5647	2.4837	2.5257	2.4945	2.5442	2.5087	2.5112	2.6275	2.6464	2.7213	2.6766
Fe3	0.0000	0.0000	0.0000	0.0000	0.0000	0.0000	0.0000	0.0000	0.0000	0.0000	0.0000	0.0000	0.0000	0.0000	0.0000	0.0000
Fe2	1.9384	1.9048	2.1933	2.3142	2.2200	1.9271	2.1122	2.1608	2.0701	2.2244	2.2124	2.2239	2.4353	2.4511	2.3321	2.2689
Mn2	0.0000	0.0158	0.0000	0.0000	0.0214	0.0000	0.0000	0.0200	0.0000	0.0000	0.0000	0.0000	0.0000	0.0161	0.0227	0.0238
Mg	3.2701	3.2899	3.3596	3.1563	3.1756	3.4851	3.2818	3.1624	3.2936	3.0728	3.1853	3.1699	2.9340	2.8718	3.0553	3.0294
Ca	0.0000	0.0167	0.0000	0.0000	0.0000	0.0000	0.0000	0.0151	0.0000	0.0000	0.0000	0.0000	0.0000	0.0169	0.0202	0.0000
Na	0.0000	0.0000	0.0000	0.0000	0.0000	0.0000	0.0000	0.0000	0.0000	0.0000	0.0000	0.0000	0.0000	0.0000	0.0000	0.0000
K	1.8776	1.8795	1.8252	1.8395	1.8552	1.7710	1.8902	1.8836	1.8790	1.8717	1.9109	1.8914	1.8908	1.9099	1.8521	1.8133
Cr	0.0000	0.0000	0.0000	0.0000	0.0000	0.0000	0.0000	0.0000	0.0000	0.0000	0.0000	0.0000	0.0000	0.0000	0.0000	0.0000
Ni	0.0000	0.0000	0.0000	0.0000	0.0000	0.0000	0.0000	0.0000	0.0000	0.0000	0.0000	0.0000	0.0000	0.0000	0.0000	0.0000
Sr	0.0000	0.0000	0.0000	0.0000	0.0000	0.0000	0.0000	0.0000	0.0000	0.0000	0.0000	0.0000	0.0000	0.0000	0.0000	0.0000
Ba	0.0000	0.0000	0.0000	0.0000	0.0000	0.0000	0.0000	0.0000	0.0000	0.0000	0.0000	0.0000	0.0000	0.0000	0.0000	0.0000
Total	16.1748	16.1789	16.3060	16.2628	16.2544	16.1755	16.2355	16.2232	16.2147	16.1885	16.2592	16.2432	16.2596	16.2719	16.2846	16.1902

Table C1e: Continued

Sample	BIGH25C	BIGH11A	BIGH11B	BIGH11C	BIGH28A	BIGH28B	BIGH28C	BIGH31A	BIGH31B	BIGH31C	BIGH31D	BIGH39A	BIGH39B	BIGH39C	BIGH39D	BIGH29A	BIGH29B
SiO2	36.77	38.73	37.99	38.12	37.87	37.88	37.29	37.69	37.84	38.12	37.86	38.00	37.98	37.74	37.34	37.78	37.09
TiO2	3.44	4.50	3.23	3.36	3.67	3.24	3.65	3.44	3.45	3.76	3.56	3.71	3.64	2.98	3.70	3.08	3.06
Al2O3	14.56	13.05	14.45	14.55	13.95	13.99	14.09	13.68	13.58	13.62	13.85	13.45	13.66	13.79	13.74	13.45	13.72
FeO	18.26	13.68	13.85	13.03	17.27	17.17	17.25	17.34	17.34	17.27	17.37	17.76	17.34	17.64	17.46	17.34	17.03
MnO	0.13	0.00	0.00	0.00	0.21	0.30	0.28	0.28	0.45	0.37	0.30	0.36	0.34	0.32	0.23	0.35	0.47
MgO	12.70	14.94	15.55	15.80	13.45	13.60	12.95	13.27	13.40	13.26	13.25	12.94	13.12	13.44	13.32	13.86	13.36
CaO	0.00	0.18	0.15	0.00	0.00	0.00	0.00	0.00	0.11	0.00	0.00	0.00	0.17	0.00	0.00	0.00	0.00
Na2O	0.00	0.00	0.00	0.00	0.00	0.00	0.00	0.00	0.00	0.00	0.00	0.00	0.00	0.00	0.00	0.00	0.00
K2O	9.22	8.97	9.16	9.19	9.51	9.54	9.80	9.31	9.49	9.47	9.57	9.70	9.60	9.66	9.84	9.31	9.32
P2O5	0.00	0.00	0.00	0.00	0.00	0.00	0.00	0.00	0.00	0.00	0.00	0.00	0.00	0.00	0.00	0.00	0.00
TOTAL	95.08	94.05	94.38	94.05	95.93	95.72	95.31	95.01	95.66	95.87	95.76	95.92	95.85	95.57	95.63	95.17	94.05
Sr	0	0	0	0	0	0	0	0	0	0	0	0	0	0	0	0	0
Ba	0	0	0	0	0	0	0	0	0	0	0	0	0	0	0	0	0
Cr	0	0	0	0	0	0	0	0	0	0	0	0	0	0	0	0	0
Ni	0	0	0	0	0	0	0	0	0	0	0	0	0	0	0	0	0
Si	5.8465	6.0628	5.9378	5.9510	5.9389	5.9535	5.9068	5.9648	5.9702	5.9831	5.9561	5.9865	5.9733	5.9631	5.9038	5.9774	5.9430
Ti	0.4114	0.5298	0.3797	0.3945	0.4328	0.3830	0.4348	0.4090	0.4098	0.4438	0.4212	0.4396	0.4305	0.3541	0.4400	0.3665	0.3687
Al	2.7293	2.4084	2.6626	2.6778	2.5791	2.5922	2.6312	2.5237	2.5547	2.5202	2.5687	2.4980	2.5328	2.5688	2.5611	2.5088	2.5917
Fe3	0.0000	0.0000	0.0000	0.0000	0.0000	0.0000	0.0000	0.0000	0.0000	0.0000	0.0000	0.0000	0.0000	0.0000	0.0000	0.0000	0.0000
Fe2	2.4282	1.7910	1.8104	1.7012	2.2651	2.2569	2.2852	2.2860	2.2971	2.2669	2.2854	2.3399	2.2808	2.3310	2.3088	2.2944	2.2821
Mn2	0.0175	0.0000	0.0000	0.0000	0.0279	0.0399	0.0376	0.0601	0.0376	0.0492	0.0400	0.0480	0.0453	0.0428	0.0308	0.0469	0.0638
Mg	3.0095	3.4854	3.6222	3.6760	3.1435	3.1855	3.0571	3.1480	3.1327	3.1017	3.1066	3.0381	3.0752	3.1649	3.1387	3.2681	3.1903
Ca	0.0000	0.0302	0.0251	0.0000	0.0000	0.0000	0.0000	0.0186	0.0000	0.0000	0.0000	0.0000	0.0286	0.0000	0.0000	0.0000	0.0000
Na	0.0000	0.0000	0.0000	0.0000	0.0000	0.0000	0.0000	0.0000	0.0000	0.0000	0.0000	0.0000	0.0000	0.0000	0.0000	0.0000	0.0000
K	1.8703	1.7914	1.8266	1.8303	1.9027	1.9129	1.9804	1.9085	1.8814	1.8963	1.9208	1.9496	1.9263	1.9473	1.9849	1.8792	1.9052
Cr	0.0000	0.0000	0.0000	0.0000	0.0000	0.0000	0.0000	0.0000	0.0000	0.0000	0.0000	0.0000	0.0000	0.0000	0.0000	0.0000	0.0000
Ni	0.0000	0.0000	0.0000	0.0000	0.0000	0.0000	0.0000	0.0000	0.0000	0.0000	0.0000	0.0000	0.0000	0.0000	0.0000	0.0000	0.0000
Sr	0.0000	0.0000	0.0000	0.0000	0.0000	0.0000	0.0000	0.0000	0.0000	0.0000	0.0000	0.0000	0.0000	0.0000	0.0000	0.0000	0.0000
Ba	0.0000	0.0000	0.0000	0.0000	0.0000	0.0000	0.0000	0.0000	0.0000	0.0000	0.0000	0.0000	0.0000	0.0000	0.0000	0.0000	0.0000
Total	16.3126	16.0990	16.2645	16.2308	16.2900	16.3239	16.3331	16.3186	16.2834	16.2612	16.2987	16.2997	16.2929	16.3720	16.3681	16.3413	16.3450

Table C1f: Electron microprobe analyses with structural formulae based on 8 oxygens for plagioclase from the Garabal Hill pluton.

Sample	PLGH10A	PLGH10B	PLGH10C	PLGH1A	PLGH1B	PLGH1C	PLGH3A	PLGH3B	PLGH5A	PLGH5B	PLGH5C	PLGH5D	PLGH7A	PLGH7B	PLGH7C	PLGH25A	PLGH25B	PLGH25C	PLGH26A	PLGH26B	PLGH26C	PLGH28A	PLGH28B
SiO2	57.03	55.64	54.99	60.58	57.06	60.45	57.69	58.31	59.33	59.11	59.35	57.46	55.68	55.18	59.64	57.87	58.35	60.30	61.21	58.18	58.78	62.79	62.23
TiO2	0.00	0.00	0.00	0.11	0.00	0.00	0.00	0.00	0.00	0.00	0.00	0.00	0.00	0.19	0.00	0.00	0.00	0.00	0.00	0.00	0.11	0.00	0.00
Al2O3	26.91	27.65	28.77	24.63	26.87	24.30	25.95	26.44	25.33	25.25	25.17	26.79	27.65	27.89	24.97	26.20	26.07	24.85	23.93	25.88	25.84	23.07	23.52
FeO	0.26	0.25	0.19	0.40	0.42	0.36	0.68	0.31	0.00	0.16	0.41	0.00	0.25	0.74	0.16	0.12	0.15	0.00	0.00	0.32	0.15	0.00	0.11
MnO	0.00	0.00	0.00	0.00	0.00	0.00	0.00	0.00	0.00	0.00	0.00	0.00	0.00	0.00	0.00	0.00	0.00	0.00	0.00	0.00	0.00	0.00	0.00
MgO	0.00	0.00	0.00	0.00	0.00	0.00	0.00	0.00	0.00	0.00	0.00	0.00	0.00	0.00	0.00	0.00	0.00	0.00	0.00	0.00	0.00	0.00	0.00
CaO	9.32	10.28	11.21	6.80	9.26	6.32	8.58	8.41	7.23	8.13	7.79	9.31	9.88	10.12	7.99	8.47	8.18	6.74	5.96	8.09	8.18	4.73	5.18
Na2O	6.25	5.53	5.22	7.53	6.58	8.04	6.65	6.55	7.63	6.88	7.08	6.25	6.13	5.61	6.92	6.75	6.90	7.84	8.45	6.84	6.89	8.71	8.62
K2O	0.27	0.15	0.13	0.16	0.09	0.11	0.26	0.26	0.28	0.27	0.25	0.23	0.16	0.16	0.24	0.09	0.07	0.00	0.09	0.21	0.14	0.38	0.34
P2O5	0.00	0.00	0.00	0.00	0.00	0.00	0.00	0.00	0.00	0.00	0.00	0.00	0.00	0.00	0.00	0.00	0.00	0.00	0.00	0.00	0.00	0.00	0.00
TOTAL	100.04	99.50	100.51	100.21	100.28	99.58	99.81	100.28	99.80	99.80	100.05	100.04	99.75	99.89	99.92	99.50	99.72	99.73	99.64	99.52	100.09	99.68	100.00
Cr	0	0	0	0	0	0	0	0	0	0	0	0	0	0	0	0	0	0	0	0	0	0	0
Ni	0	0	0	0	0	0	0	0	0	0	0	0	0	0	0	0	0	0	0	0	0	0	0
Sr	0	0	0	0	0	0	0	0	0	0	0	0	0	0	0	0	0	0	0	0	0	0	0
Ba	0	0	0	0	0	0	0	0	0	0	0	0	0	0	0	0	0	0	0	0	0	0	0
Si	10.2478	10.0673	9.8764	10.7755	10.2380	10.8182	10.3920	10.4147	10.6198	10.5932	10.6146	10.3023	10.0610	9.9778	10.6623	10.4124	10.4648	10.7578	10.9198	10.4695	10.5035	11.1545	11.0446
Ti	0.0000	0.0000	0.0000	0.0147	0.0000	0.0000	0.0000	0.0000	0.0000	0.0000	0.0000	0.0000	0.0000	0.0258	0.0000	0.0000	0.0000	0.0000	0.0000	0.0000	0.0148	0.0000	0.0000
Al	5.7007	5.8981	6.0917	5.1649	5.6838	5.1269	5.5109	5.5674	5.3452	5.3348	5.3070	5.6628	5.8901	5.9455	5.2628	5.5576	5.5121	5.2266	5.0329	5.4904	5.4436	4.8316	4.9221
Fe3	0.0000	0.0000	0.0000	0.0000	0.0000	0.0000	0.0000	0.0000	0.0000	0.0000	0.0000	0.0000	0.0000	0.0000	0.0000	0.0000	0.0000	0.0000	0.0000	0.0000	0.0000	0.0000	0.0000
Fe2	0.0391	0.0378	0.0285	0.0595	0.0630	0.0539	0.1024	0.0463	0.0000	0.0240	0.0613	0.0000	0.0378	0.1119	0.0239	0.0181	0.0225	0.0000	0.0000	0.0482	0.0224	0.0000	0.0163
Mn2	0.0000	0.0000	0.0000	0.0000	0.0000	0.0000	0.0000	0.0000	0.0000	0.0000	0.0000	0.0000	0.0000	0.0000	0.0000	0.0000	0.0000	0.0000	0.0000	0.0000	0.0000	0.0000	0.0000
Mg	0.0000	0.0000	0.0000	0.0000	0.0000	0.0000	0.0000	0.0000	0.0000	0.0000	0.0000	0.0000	0.0000	0.0000	0.0000	0.0000	0.0000	0.0000	0.0000	0.0000	0.0000	0.0000	0.0000
Ca	1.7945	1.9930	2.1573	1.2960	1.7803	1.2119	1.6561	1.6095	1.3867	1.5612	1.4928	1.7886	1.9129	1.9608	1.5306	1.6330	1.5719	1.2884	1.1393	1.5599	1.5662	0.9004	0.9853
Na	2.1776	1.9401	1.8178	2.5970	2.2892	2.7899	2.3227	2.2683	2.6481	2.3907	2.4552	2.1728	2.1477	1.9669	2.3987	2.3549	2.3994	2.7120	2.9229	2.3866	2.3872	3.0002	2.9669
K	0.0619	0.0346	0.0298	0.0363	0.0206	0.0251	0.0598	0.0592	0.0639	0.0617	0.0570	0.0526	0.0369	0.0369	0.0547	0.0207	0.0160	0.0000	0.0205	0.0482	0.0319	0.0861	0.0770
Cr	0.0000	0.0000	0.0000	0.0000	0.0000	0.0000	0.0000	0.0000	0.0000	0.0000	0.0000	0.0000	0.0000	0.0000	0.0000	0.0000	0.0000	0.0000	0.0000	0.0000	0.0000	0.0000	0.0000
Ni	0.0000	0.0000	0.0000	0.0000	0.0000	0.0000	0.0000	0.0000	0.0000	0.0000	0.0000	0.0000	0.0000	0.0000	0.0000	0.0000	0.0000	0.0000	0.0000	0.0000	0.0000	0.0000	0.0000
Sr	0.0000	0.0000	0.0000	0.0000	0.0000	0.0000	0.0000	0.0000	0.0000	0.0000	0.0000	0.0000	0.0000	0.0000	0.0000	0.0000	0.0000	0.0000	0.0000	0.0000	0.0000	0.0000	0.0000
Ba	0.0000	0.0000	0.0000	0.0000	0.0000	0.0000	0.0000	0.0000	0.0000	0.0000	0.0000	0.0000	0.0000	0.0000	0.0000	0.0000	0.0000	0.0000	0.0000	0.0000	0.0000	0.0000	0.0000
Total	20.0216	19.9710	20.0016	19.9440	20.0749	20.0258	20.0438	19.9654	20.0637	19.9656	19.9880	19.9790	20.0863	20.0256	19.9331	19.9966	19.9868	19.9849	20.0354	20.0027	19.9695	19.9728	20.0143

Table C2a: Electron microprobe analyses with structural formulae based on 6 oxygens for orthopyroxenes of the Comrie pluton.

Sample	OPCM7A	OPCM10A	OPCM10B	OPCM10C	OPCM22A	OPCM22B	OPCM22C	OPCM22D	OPCM20A	OPCM20B	OPCM20C	OPCM20D	OPCM25A	OPCM25B	OPCM25C
SiO2	52.76	53.75	53.33	53.61	52.92	53.02	53.79	52.98	53.86	54.19	53.41	53.71	51.96	51.71	51.60
TiO2	0.23	0.18	0.00	0.49	0.40	0.30	0.38	0.37	0.00	0.18	0.00	0.15	0.55	0.51	0.33
Al2O3	0.77	0.40	0.25	1.31	1.34	0.63	1.30	1.31	0.50	0.57	0.49	0.37	1.13	1.22	0.61
FeO	21.64	20.33	21.10	19.65	20.20	20.99	19.24	20.44	20.42	19.88	20.40	20.29	24.54	23.89	27.24
MnO	0.63	0.46	0.66	0.33	0.48	0.52	0.46	0.41	0.63	0.54	0.67	0.52	0.61	0.68	0.71
MgO	22.89	23.89	23.67	23.59	23.34	23.68	23.53	23.33	23.43	23.67	23.54	23.56	19.53	19.52	17.99
CaO	1.12	0.90	0.81	1.07	1.42	1.13	1.12	1.35	1.07	1.16	1.36	1.34	1.86	2.17	1.62
Na2O	0.00	0.00	0.00	0.00	0.00	0.00	0.00	0.00	0.00	0.00	0.00	0.00	0.00	0.00	0.00
K2O	0.00	0.00	0.00	0.00	0.00	0.00	0.00	0.00	0.00	0.00	0.00	0.00	0.00	0.00	0.00
P2O5	0.00	0.00	0.00	0.00	0.00	0.00	0.00	0.00	0.00	0.00	0.00	0.00	0.00	0.00	0.00
TOTAL	100.04	99.91	99.82	100.05	100.10	100.27	99.82	100.19	99.91	100.19	99.87	99.94	100.18	99.70	100.10
Cr	0	0	0	0	0	0	0	0	0	0	0	0	0	0	0
Ni	0	0	0	0	0	0	0	0	0	0	0	0	0	0	0
Sr	0	0	0	0	0	0	0	0	0	0	0	0	0	0	0
Ba	0	0	0	0	0	0	0	0	0	0	0	0	0	0	0
Si	1.9641	1.9854	1.9819	1.9699	1.9550	1.9625	1.9776	1.9563	1.9914	1.9915	1.9799	1.9861	1.9622	1.9597	1.9757
Ti	0.0064	0.0050	0.0000	0.0135	0.0111	0.0084	0.0105	0.0103	0.0000	0.0050	0.0000	0.0042	0.0156	0.0145	0.0095
Al	0.0338	0.0174	0.0110	0.0567	0.0584	0.0275	0.0563	0.0570	0.0218	0.0247	0.0214	0.0161	0.0503	0.0545	0.0275
Fe3	0.0000	0.0000	0.0000	0.0000	0.0000	0.0000	0.0000	0.0000	0.0000	0.0000	0.0000	0.0000	0.0000	0.0000	0.0000
Fe2	0.6737	0.6280	0.6558	0.6038	0.6241	0.6498	0.5916	0.6312	0.6314	0.6110	0.6325	0.6275	0.7750	0.7572	0.8723
Mn2	0.0199	0.0144	0.0208	0.0103	0.0150	0.0163	0.0143	0.0128	0.0197	0.0168	0.0210	0.0163	0.0195	0.0218	0.0230
Mg	1.2699	1.3151	1.3110	1.2918	1.2850	1.3062	1.2893	1.2839	1.2910	1.2964	1.3005	1.2984	1.0991	1.1025	1.0266
Ca	0.0447	0.0356	0.0323	0.0421	0.0562	0.0448	0.0441	0.0534	0.0424	0.0457	0.0540	0.0531	0.0753	0.0881	0.0665
Na	0.0000	0.0000	0.0000	0.0000	0.0000	0.0000	0.0000	0.0000	0.0000	0.0000	0.0000	0.0000	0.0000	0.0000	0.0000
K	0.0000	0.0000	0.0000	0.0000	0.0000	0.0000	0.0000	0.0000	0.0000	0.0000	0.0000	0.0000	0.0000	0.0000	0.0000
P	0.0000	0.0000	0.0000	0.0000	0.0000	0.0000	0.0000	0.0000	0.0000	0.0000	0.0000	0.0000	0.0000	0.0000	0.0000
Sr	0.0000	0.0000	0.0000	0.0000	0.0000	0.0000	0.0000	0.0000	0.0000	0.0000	0.0000	0.0000	0.0000	0.0000	0.0000
Ba	0.0000	0.0000	0.0000	0.0000	0.0000	0.0000	0.0000	0.0000	0.0000	0.0000	0.0000	0.0000	0.0000	0.0000	0.0000
Cr	0.0000	0.0000	0.0000	0.0000	0.0000	0.0000	0.0000	0.0000	0.0000	0.0000	0.0000	0.0000	0.0000	0.0000	0.0000
Ni	0.0000	0.0000	0.0000	0.0000	0.0000	0.0000	0.0000	0.0000	0.0000	0.0000	0.0000	0.0000	0.0000	0.0000	0.0000
Total	4.0126	4.0009	4.0126	3.9882	4.0047	4.0154	3.9837	4.0049	3.9977	3.9911	4.0094	4.0017	3.9970	3.9985	4.0010

Table C2b: Electron microprobe analyses with structural formulae based on 6 oxygens for clinopyroxene of the Comrie pluton.

Sample	CPCM10A	CPCM10B	CPCM20A	CPCM21A	CPCM21B	CPCM25A	CPCM25B
SiO2	50.16	53.31	52.58	53.62	53.28	52.85	52.33
TiO2	2.79	0.00	0.37	0.19	0.31	0.00	0.70
Al2O3	1.57	0.51	1.18	0.56	0.68	0.61	1.54
FeO	10.46	7.70	10.09	10.55	9.95	11.48	11.58
MnO	0.33	0.29	0.27	0.41	0.47	0.50	0.32
MgO	14.00	15.09	15.38	13.71	13.89	13.19	13.81
CaO	20.42	22.66	19.98	21.06	21.44	20.91	19.84
Na2O	0.00	0.00	0.00	0.00	0.00	0.45	0.00
K2O	0.00	0.00	0.00	0.00	0.00	0.00	0.00
P2O5	0.00	0.00	0.00	0.00	0.00	0.00	0.00
TOTAL	100.05	99.86	99.85	100.10	100.02	100.12	100.24
Cr	3200	3000	0	0	0	1300	1200
Ni	0	0	0	0	0	0	0
Sr	0	0	0	0	0	0	0
Ba	0	0	0	0	0	0	0
Si	1.8862	1.9813	1.9619	2.0022	1.9903	1.9881	1.9573
Ti	0.0789	0.0000	0.0104	0.0053	0.0087	0.0000	0.0197
Al	0.0696	0.0223	0.0519	0.0247	0.0299	0.0271	0.0679
Fe3	0.0000	0.0000	0.0000	0.0000	0.0000	0.0000	0.0000
Fe2	0.3290	0.2393	0.3149	0.3295	0.3108	0.3612	0.3622
Mn2	0.0105	0.0091	0.0085	0.0130	0.0149	0.0159	0.0101
Mg	0.7846	0.8358	0.8553	0.7629	0.7733	0.7395	0.7698
Ca	0.8228	0.9024	0.7988	0.8426	0.8582	0.8428	0.7951
Na	0.0000	0.0000	0.0000	0.0000	0.0000	0.0328	0.0000
K	0.0000	0.0000	0.0000	0.0000	0.0000	0.0000	0.0000
P	0.0000	0.0000	0.0000	0.0000	0.0000	0.0000	0.0000
Sr	0.0000	0.0000	0.0000	0.0000	0.0000	0.0000	0.0000
Ba	0.0000	0.0000	0.0000	0.0000	0.0000	0.0000	0.0000
Cr	0.0124	0.0115	0.0000	0.0000	0.0000	0.0050	0.0046
Ni	0.0000	0.0000	0.0000	0.0000	0.0000	0.0000	0.0000
Total	3.9939	4.0018	4.0017	3.9802	3.9861	4.0123	3.9868

Table C2c: Electron microprobe analyses with structural formulae based on 23 oxygens for amphibole from the Comrie pluton.

Sample	AMCM7A	AMCM9A	AMCM9B	AMCM25A	AMCM25B	AMCM25C	AMCM25D	AMCM25E	AMCM28A	AMCM28B	AMCM28C
SiO2	51.57	50.11	50.22	47.59	47.44	47.80	48.59	47.63	49.52	53.24	54.38
TiO2	0.69	1.16	0.76	1.31	1.35	1.26	1.11	1.41	0.93	0.26	0.25
Al2O3	4.10	4.91	4.62	5.30	5.79	5.64	5.25	5.67	4.52	2.47	1.81
FeO	11.17	13.18	13.24	15.81	15.91	16.10	15.15	15.79	13.82	10.88	11.06
MnO	0.33	0.36	0.43	0.40	0.38	0.54	0.44	0.33	0.52	0.59	0.57
MgO	16.68	15.35	15.86	12.98	12.75	13.08	13.64	13.00	14.40	16.72	17.04
CaO	11.14	11.18	11.26	11.09	11.32	11.16	11.22	11.35	11.53	12.34	12.45
Na2O	0.28	0.78	0.75	1.10	1.34	1.04	1.17	1.18	1.10	0.00	0.00
K2O	0.00	0.43	0.41	0.46	0.66	0.66	0.55	0.62	0.44	0.10	0.13
P2O5	0.00	0.00	0.00	0.00	0.00	0.00	0.00	0.00	0.00	0.00	0.00
TOTAL	96.23	97.46	97.55	96.04	96.94	97.28	97.12	96.98	96.78	96.60	97.69
Cr	1200	0	0	0	0	0	0	0	0	0	0
Ni	1500	0	0	0	0	0	0	0	0	0	0
Sr	0	0	0	0	0	0	0	0	0	0	0
Ba	0	0	0	0	0	0	0	0	0	0	0
Si	7.4855	7.3009	7.3160	7.1695	7.1023	7.1264	7.2096	7.1150	7.3201	7.6993	7.7740
Ti	0.0753	0.1271	0.0833	0.1484	0.1520	0.1413	0.1239	0.1584	0.1034	0.0283	0.0269
Al	0.7016	0.8434	0.7935	0.9413	1.0219	0.9913	0.9184	0.9985	0.7877	0.4211	0.3050
Fe3	0.0000	0.0000	0.0000	0.0000	0.0000	0.0000	0.0000	0.0000	0.0000	0.0000	0.0000
Fe2	1.3560	1.6060	1.6131	1.9919	1.9921	2.0074	1.8800	1.9727	1.7085	1.3159	1.3223
Mn2	0.0406	0.0444	0.0531	0.0510	0.0482	0.0682	0.0553	0.0418	0.0651	0.0723	0.0690
Mg	3.6083	3.3330	3.4434	2.9142	2.8448	2.9062	3.0162	2.8942	3.1724	3.6036	3.6304
Ca	1.7326	1.7454	1.7576	1.7902	1.8159	1.7828	1.7838	1.8167	1.8263	1.9122	1.9071
Na	0.0788	0.2203	0.2118	0.3213	0.3890	0.3006	0.3366	0.3418	0.3153	0.0000	0.0000
K	0.0000	0.0799	0.0762	0.0884	0.1261	0.1255	0.1041	0.1182	0.0830	0.0184	0.0237
P	0.0000	0.0000	0.0000	0.0000	0.0000	0.0000	0.0000	0.0000	0.0000	0.0000	0.0000
Sr	0.0000	0.0000	0.0000	0.0000	0.0000	0.0000	0.0000	0.0000	0.0000	0.0000	0.0000
Ba	0.0000	0.0000	0.0000	0.0000	0.0000	0.0000	0.0000	0.0000	0.0000	0.0000	0.0000
Cr	0.0179	0.0000	0.0000	0.0000	0.0000	0.0000	0.0000	0.0000	0.0000	0.0000	0.0000
Ni	0.0222	0.0000	0.0000	0.0000	0.0000	0.0000	0.0000	0.0000	0.0000	0.0000	0.0000
Total	15.1188	15.3005	15.3480	15.4163	15.4922	15.4498	15.4278	15.4572	15.3818	15.0711	15.0585

Table C2d: Electron microprobe analyses with structural formulae based on 23 oxygens for biotites of the Comrie pluton.

Sample	BICM7A	BICM7B	BICM9A	BICM9B	BICM9C	BICM10A	BICM10B	BICM10C	BICM20A	BICM20B	BICM20C	BICM21A	BICM21B	BICM21C	BICM22A	BICM22B
SiO2	36.85	37.33	37.90	38.01	37.08	37.89	37.71	37.70	37.30	37.81	37.87	37.54	37.34	38.31	38.01	37.32
TiO2	5.44	5.47	4.58	4.62	4.43	5.04	4.42	5.08	5.45	4.05	5.43	4.98	4.59	5.28	5.95	6.04
Al2O3	13.74	13.49	13.90	13.33	13.33	12.97	13.14	13.08	13.47	14.13	13.42	13.08	13.23	13.19	13.74	13.67
FeO	15.97	16.15	17.19	17.05	17.14	14.58	14.88	14.59	15.04	15.10	15.44	17.44	16.49	17.46	15.22	14.70
MnO	0.00	0.16	0.00	0.18	0.18	0.17	0.00	0.00	0.24	0.14	0.25	0.18	0.19	0.00	0.00	0.00
MgO	13.89	13.50	13.09	13.05	13.23	15.31	15.40	15.27	14.36	14.86	14.30	13.11	13.69	13.11	14.45	14.12
CaO	0.00	0.00	0.00	0.00	0.00	0.00	0.15	0.00	0.00	0.00	0.00	0.00	0.00	0.00	0.00	0.00
Na2O	0.00	0.00	0.00	0.00	0.00	0.00	0.00	0.00	0.00	0.00	0.00	0.00	0.00	0.00	0.00	0.00
K2O	9.07	9.05	9.34	9.43	9.28	9.17	9.21	9.11	9.02	8.72	9.12	9.47	9.31	9.48	9.28	8.93
P2O5	0.00	0.00	0.00	0.00	0.00	0.00	0.00	0.00	0.00	0.00	0.00	0.00	0.00	0.00	0.00	0.00
TOTAL	94.96	95.15	96.00	95.67	94.67	95.13	94.91	94.83	94.88	94.81	95.83	95.80	94.84	96.83	96.65	94.78
Cr	0	0	0	0	0	0	0	0	0	0	0	0	0	0	0	0
Ni	0	0	0	0	0	0	0	0	0	0	0	0	0	0	0	0
Sr	0	0	0	0	0	0	0	0	0	0	0	0	0	0	0	0
Ba	0	0	0	0	0	0	0	0	0	0	0	0	0	0	0	0
Si	5.8042	5.8696	5.9254	5.9708	5.9012	5.9163	5.9108	5.9010	5.8538	5.9096	5.8895	5.9131	5.9118	5.9506	5.8496	5.8419
Ti	0.6444	0.6468	0.5385	0.5458	0.5302	0.5918	0.5210	0.5980	0.6433	0.4761	0.6351	0.5899	0.5465	0.6168	0.6887	0.7111
Al	2.5514	2.5006	2.5620	2.4686	2.5010	2.3875	2.4281	2.4137	2.4922	2.6037	2.4605	2.4289	2.4694	2.4153	2.4929	2.5227
Fe3	0.0000	0.0000	0.0000	0.0000	0.0000	0.0000	0.0000	0.0000	0.0000	0.0000	0.0000	0.0000	0.0000	0.0000	0.0000	0.0000
Fe2	2.1037	2.1237	2.2477	2.2399	2.2813	1.9039	1.9506	1.9099	1.9740	1.9738	2.0082	2.2974	2.1834	2.2681	1.9589	1.9244
Mn2	0.0000	0.0213	0.0000	0.0240	0.0243	0.0225	0.0000	0.0000	0.0319	0.0185	0.0329	0.0240	0.0255	0.0000	0.0000	0.0000
Mg	3.2606	3.1635	3.0500	3.0551	3.1379	3.5627	3.5974	3.5621	3.3587	3.4614	3.3143	3.0775	3.2302	3.0348	3.3142	3.2940
Ca	0.0000	0.0000	0.0000	0.0000	0.0000	0.0000	0.0252	0.0000	0.0000	0.0000	0.0000	0.0000	0.0000	0.0000	0.0000	0.0000
Na	0.0000	0.0000	0.0000	0.0000	0.0000	0.0000	0.0000	0.0000	0.0000	0.0000	0.0000	0.0000	0.0000	0.0000	0.0000	0.0000
K	1.8226	1.8154	1.8630	1.8898	1.8842	1.8267	1.8418	1.8192	1.8060	1.7388	1.8095	1.9031	1.8805	1.8786	1.8220	1.7834
P	0.0000	0.0000	0.0000	0.0000	0.0000	0.0000	0.0000	0.0000	0.0000	0.0000	0.0000	0.0000	0.0000	0.0000	0.0000	0.0000
Sr	0.0000	0.0000	0.0000	0.0000	0.0000	0.0000	0.0000	0.0000	0.0000	0.0000	0.0000	0.0000	0.0000	0.0000	0.0000	0.0000
Ba	0.0000	0.0000	0.0000	0.0000	0.0000	0.0000	0.0000	0.0000	0.0000	0.0000	0.0000	0.0000	0.0000	0.0000	0.0000	0.0000
Cr	0.0000	0.0000	0.0000	0.0000	0.0000	0.0000	0.0000	0.0000	0.0000	0.0000	0.0000	0.0000	0.0000	0.0000	0.0000	0.0000
Ni	0.0000	0.0000	0.0000	0.0000	0.0000	0.0000	0.0000	0.0000	0.0000	0.0000	0.0000	0.0000	0.0000	0.0000	0.0000	0.0000
Total	16.1870	16.1410	16.1866	16.1940	16.2602	16.2115	16.2750	16.2038	16.1598	16.1819	16.1500	16.2340	16.2473	16.1643	16.1263	16.0774

Table C2d: Continued

Sample	BICM22C	BICM25A	BICM25B	BICM25C	BICM25D	BICM25E	BICM25F	BICM25G	BICM27A	BICM27B	BICM27C	BICM28A	BICM28B	BICM28C	BICM28D	BICM28E	BICM28F	BICM8A	BICM8B	BICM8C
SiO2	38.17	37.90	37.26	37.60	37.61	37.18	37.79	37.43	36.90	36.73	36.76	37.16	37.15	37.01	37.16	37.37	37.35	37.87	37.59	37.85
TiO2	5.90	5.10	4.95	4.74	4.80	5.08	5.02	5.18	5.05	5.31	5.26	5.12	5.04	4.82	5.31	4.41	4.99	4.63	4.34	4.18
Al2O3	13.43	12.41	12.21	12.59	12.53	13.04	13.08	13.13	13.20	13.14	13.38	13.08	13.10	13.03	12.90	13.15	12.65	12.61	13.60	13.00
FeO	15.58	17.81	17.28	17.65	17.57	17.48	17.33	17.95	17.08	16.83	17.44	17.74	17.39	16.84	17.50	17.06	17.66	17.48	16.94	17.46
MnO	0.00	0.13	0.21	0.29	0.00	0.00	0.00	0.00	0.00	0.00	0.22	0.24	0.00	0.29	0.24	0.31	0.18	0.29	0.18	0.27
MgO	14.46	12.75	12.95	13.00	13.03	13.17	13.11	13.20	12.82	12.99	12.68	12.74	12.89	13.03	12.85	13.31	12.88	12.98	13.75	13.03
CaO	0.00	0.11	0.00	0.00	0.00	0.00	0.00	0.00	0.00	0.00	0.00	0.10	0.00	0.00	0.00	0.00	0.00	0.16	0.00	0.00
Na2O	0.00	0.00	0.00	0.00	0.00	0.00	0.00	0.00	0.00	0.00	0.00	0.00	0.00	0.00	0.00	0.00	0.00	0.00	0.00	0.00
K2O	8.94	9.41	9.44	9.49	9.26	9.34	9.63	9.42	9.56	9.53	9.63	9.68	9.41	9.60	9.30	9.76	9.50	9.00	9.38	9.28
P2O5	0.00	0.00	0.00	0.00	0.00	0.00	0.00	0.00	0.00	0.00	0.00	0.00	0.00	0.00	0.00	0.00	0.00	0.00	0.00	0.00
TOTAL	96.48	95.62	94.30	95.36	94.80	95.29	95.96	96.31	94.61	94.53	95.37	95.86	94.98	94.62	95.26	95.37	95.21	95.02	95.18	95.07
Cr	0	0	0	0	0	0	0	0	0	0	0	0	0	0	0	0	0	0	0	0
Ni	0	0	0	0	0	0	0	0	0	0	0	0	0	0	0	0	0	0	0	0
Sr	0	0	0	0	0	0	0	0	0	0	0	0	0	0	0	0	0	0	0	0
Ba	0	0	0	0	0	0	0	0	0	0	0	0	0	0	0	0	0	0	0	0
Si	5.8823	5.9893	5.9716	5.9630	5.9815	5.8867	5.9355	5.8738	5.8845	5.8586	5.8347	5.8757	5.9008	5.9038	5.8927	5.9187	5.9346	6.0018	5.9424	5.9978
Ti	0.6838	0.6061	0.5966	0.5653	0.5741	0.6049	0.5930	0.6113	0.6057	0.6370	0.6279	0.6088	0.6021	0.5782	0.6333	0.5253	0.5963	0.5519	0.5160	0.4981
Al	2.4400	2.3120	2.3070	2.3539	2.3493	2.4341	2.4220	2.4291	2.4817	2.4709	2.5037	2.4383	2.4531	2.4504	2.4116	2.4554	2.3696	2.3561	2.4228	2.4286
Fe3	0.0000	0.0000	0.0000	0.0000	0.0000	0.0000	0.0000	0.0000	0.0000	0.0000	0.0000	0.0000	0.0000	0.0000	0.0000	0.0000	0.0000	0.0000	0.0000	0.0000
Fe2	2.0080	2.3538	2.3162	2.3410	2.3370	2.3146	2.2764	2.3558	2.2779	2.2451	2.3151	2.3459	2.3101	2.2466	2.3209	2.2597	2.3467	2.3169	2.2396	2.3139
Mn2	0.0000	0.0174	0.0285	0.0390	0.0000	0.0000	0.0000	0.0000	0.0000	0.0000	0.0296	0.0321	0.0000	0.0392	0.0322	0.0416	0.0242	0.0389	0.0241	0.0362
Mg	3.3210	3.0028	3.0932	3.0726	3.0884	3.1077	3.0688	3.0871	3.0468	3.0879	2.9995	3.0022	3.0513	3.0977	3.0368	3.1417	3.0500	3.0658	3.2395	3.0772
Ca	0.0000	0.0186	0.0000	0.0000	0.0000	0.0000	0.0000	0.0000	0.0000	0.0000	0.0000	0.0169	0.0000	0.0000	0.0000	0.0000	0.0000	0.0272	0.0000	0.0000
Na	0.0000	0.0000	0.0000	0.0000	0.0000	0.0000	0.0000	0.0000	0.0000	0.0000	0.0000	0.0000	0.0000	0.0000	0.0000	0.0000	0.0000	0.0000	0.0000	0.0000
K	1.7577	1.8972	1.9302	1.9201	1.8789	1.8867	1.9297	1.8860	1.9450	1.9393	1.9501	1.9527	1.9069	1.9537	1.8815	1.9721	1.9258	1.8197	1.8918	1.8761
P	0.0000	0.0000	0.0000	0.0000	0.0000	0.0000	0.0000	0.0000	0.0000	0.0000	0.0000	0.0000	0.0000	0.0000	0.0000	0.0000	0.0000	0.0000	0.0000	0.0000
Sr	0.0000	0.0000	0.0000	0.0000	0.0000	0.0000	0.0000	0.0000	0.0000	0.0000	0.0000	0.0000	0.0000	0.0000	0.0000	0.0000	0.0000	0.0000	0.0000	0.0000
Ba	0.0000	0.0000	0.0000	0.0000	0.0000	0.0000	0.0000	0.0000	0.0000	0.0000	0.0000	0.0000	0.0000	0.0000	0.0000	0.0000	0.0000	0.0000	0.0000	0.0000
Cr	0.0000	0.0000	0.0000	0.0000	0.0000	0.0000	0.0000	0.0000	0.0000	0.0000	0.0000	0.0000	0.0000	0.0000	0.0000	0.0000	0.0000	0.0000	0.0000	0.0000
Ni	0.0000	0.0000	0.0000	0.0000	0.0000	0.0000	0.0000	0.0000	0.0000	0.0000	0.0000	0.0000	0.0000	0.0000	0.0000	0.0000	0.0000	0.0000	0.0000	0.0000
Total	16.0928	16.1972	16.2433	16.2548	16.2092	16.2347	16.2254	16.2432	16.2416	16.2387	16.2606	16.2727	16.2241	16.2696	16.2090	16.3144	16.2472	16.1782	16.2761	16.2279

Table C2e: Electron microprobe analyses with structural formulae based on 8 oxygens for plagioclase of the Comrie pluton.

Sample	PLCM20A	PLCM20B	PLCM20C	PLCM7A	PLCM7B	PLCM9A	PLCM9B	PLCM9C	PLCM10A	PLCM10B	PLCM10C	PLCM21A	PLCM21B	PLCM21C	PLCM25A	PLCM25B	PLCM25C	PLCM28A	PLCM28B	PLCM8A	PLCM8B
SiO2	55.99	54.23	54.10	59.46	58.82	60.50	60.36	58.18	59.74	59.50	56.21	57.73	60.02	56.60	62.03	61.05	61.28	62.06	62.13	59.51	60.72
TiO2	0.00	0.00	0.00	0.00	0.00	0.00	0.00	0.00	0.00	0.00	0.14	0.00	0.00	0.12	0.00	0.00	0.00	0.00	0.00	0.14	0.00
Al2O3	27.09	28.83	28.79	25.59	26.08	24.76	24.99	26.32	25.58	25.45	27.30	26.30	25.05	27.64	23.28	24.31	23.97	23.30	23.19	25.26	24.76
FeO	0.24	0.27	0.41	0.23	0.11	0.29	0.18	0.20	0.33	0.24	0.49	0.28	0.12	0.12	0.50	0.38	0.21	0.49	0.51	0.19	0.13
MnO	0.00	0.00	0.00	0.00	0.00	0.00	0.00	0.00	0.00	0.00	0.00	0.00	0.00	0.00	0.00	0.00	0.00	0.00	0.00	0.00	0.00
MgO	0.00	0.00	0.00	0.00	0.00	0.00	0.00	0.00	0.00	0.00	0.00	0.00	0.00	0.00	0.23	0.00	0.00	0.00	0.00	0.00	0.00
CaO	10.10	11.89	11.33	7.60	8.16	6.74	6.69	8.27	7.63	7.12	7.62	8.78	7.21	7.71	5.72	5.95	5.93	4.96	4.70	5.15	5.60
Na2O	5.82	4.58	4.94	7.05	7.01	7.28	7.28	6.76	6.66	7.02	7.75	6.65	7.43	7.84	8.49	8.47	8.19	9.48	8.99	8.94	8.36
K2O	0.26	0.17	0.23	0.40	0.33	0.46	0.45	0.34	0.31	0.41	0.29	0.34	0.26	0.21	0.08	0.23	0.30	0.11	0.09	0.37	0.41
P2O5	0.00	0.00	0.00	0.00	0.00	0.00	0.00	0.00	0.00	0.00	0.00	0.00	0.00	0.00	0.00	0.00	0.00	0.00	0.00	0.00	0.00
TOTAL	99.50	99.97	99.80	100.33	100.51	100.03	99.95	100.07	100.25	99.74	99.80	100.08	100.09	100.24	100.33	100.39	99.88	100.40	99.61	99.56	99.98
Cl	0	0	0	0	0	0	0	0	0	0	0	0	0	0	0	0	0	0	0	0	0
Ni	0	0	0	0	0	0	0	0	0	0	0	0	0	0	0	0	0	0	0	0	0
Sr	0	0	0	0	0	0	0	0	0	0	0	0	0	0	0	0	0	0	0	0	0
Ba	0	0	0	0	0	0	0	0	0	0	0	0	0	0	0	0	0	0	0	0	0
Si	10.1387	9.8067	9.8068	10.5943	10.4801	10.7794	10.7560	10.4182	10.6310	10.6427	10.1519	10.3624	10.6980	10.1550	11.0031	10.8448	10.9179	11.0140	11.0758	10.6696	10.8126
Ti	0.0000	0.0000	0.0000	0.0000	0.0000	0.0000	0.0000	0.0000	0.0000	0.0000	0.0190	0.0000	0.0000	0.0162	0.0000	0.0000	0.0000	0.0000	0.0000	0.0189	0.0000
Al	5.7832	6.1463	6.1526	5.3753	5.4782	5.2009	5.2500	5.5564	5.3666	5.3667	5.8128	5.5655	5.2638	5.8464	4.8684	5.0911	5.0347	4.8750	4.8737	5.3392	5.1980
Fe3	0.0000	0.0000	0.0000	0.0000	0.0000	0.0000	0.0000	0.0000	0.0000	0.0000	0.0000	0.0000	0.0000	0.0000	0.0000	0.0000	0.0000	0.0000	0.0000	0.0000	0.0000
Fe2	0.0363	0.0408	0.0622	0.0343	0.0164	0.0432	0.0268	0.0300	0.0491	0.0359	0.0740	0.0420	0.0179	0.0180	0.0742	0.0565	0.0313	0.0727	0.0760	0.0285	0.0194
Mn2	0.0000	0.0000	0.0000	0.0000	0.0000	0.0000	0.0000	0.0000	0.0000	0.0000	0.0000	0.0000	0.0000	0.0000	0.0000	0.0000	0.0000	0.0000	0.0000	0.0000	0.0000
Mg	0.0000	0.0000	0.0000	0.0000	0.0000	0.0000	0.0000	0.0000	0.0000	0.0000	0.0000	0.0000	0.0000	0.0000	0.0608	0.0000	0.0000	0.0000	0.0000	0.0000	0.0000
Ca	1.9597	2.3039	2.2007	1.4510	1.5578	1.2868	1.2774	1.5868	1.4549	1.3646	1.4746	1.6887	1.3770	1.4822	1.0872	1.1325	1.1321	0.9432	0.8978	0.9894	1.0685
Na	2.0434	1.6059	1.7363	2.4356	2.4217	2.5150	2.5154	2.3471	2.2980	2.4347	2.7139	2.3145	2.5678	2.7274	2.9200	2.9173	2.8293	3.2622	3.1074	3.1079	2.8865
K	0.0601	0.0392	0.0532	0.0909	0.0750	0.1046	0.1023	0.0777	0.0704	0.0936	0.0668	0.0779	0.0591	0.0481	0.0181	0.0521	0.0682	0.0249	0.0205	0.0846	0.0931
P	0.0000	0.0000	0.0000	0.0000	0.0000	0.0000	0.0000	0.0000	0.0000	0.0000	0.0000	0.0000	0.0000	0.0000	0.0000	0.0000	0.0000	0.0000	0.0000	0.0000	0.0000
Sr	0.0000	0.0000	0.0000	0.0000	0.0000	0.0000	0.0000	0.0000	0.0000	0.0000	0.0000	0.0000	0.0000	0.0000	0.0000	0.0000	0.0000	0.0000	0.0000	0.0000	0.0000
Ba	0.0000	0.0000	0.0000	0.0000	0.0000	0.0000	0.0000	0.0000	0.0000	0.0000	0.0000	0.0000	0.0000	0.0000	0.0000	0.0000	0.0000	0.0000	0.0000	0.0000	0.0000
Cr	0.0000	0.0000	0.0000	0.0000	0.0000	0.0000	0.0000	0.0000	0.0000	0.0000	0.0000	0.0000	0.0000	0.0000	0.0000	0.0000	0.0000	0.0000	0.0000	0.0000	0.0000
Ni	0.0000	0.0000	0.0000	0.0000	0.0000	0.0000	0.0000	0.0000	0.0000	0.0000	0.0000	0.0000	0.0000	0.0000	0.0000	0.0000	0.0000	0.0000	0.0000	0.0000	0.0000
Total	20.0214	19.9427	20.0117	19.9813	20.0292	19.9299	19.9278	20.0160	19.8699	19.9381	20.3131	20.0510	19.9836	20.2933	20.0318	20.0944	20.0134	20.1920	20.0513	20.2381	20.0782

Table C3a: Electron microprobe analyses with structural formulae based on 4 oxygens for olivines of the Glen Doll pluton.

Sample	OLGD26A	OLGD26B	OLGD26C	OLGD49A	OLGD49B	OLGD49C
SiO2	39.74	39.80	39.57	39.84	39.33	40.03
TiO2	0.00	0.00	0.00	0.00	0.00	0.00
Al2O3	0.00	0.00	0.00	0.00	0.00	0.00
FeO	20.00	20.36	20.62	20.32	20.47	20.13
MnO	0.35	0.18	0.26	0.21	0.25	0.19
MgO	39.76	39.30	39.84	39.61	39.90	39.88
CaO	0.00	0.00	0.00	0.08	0.00	0.00
Na2O	0.00	0.00	0.00	0.00	0.00	0.00
K2O	0.00	0.00	0.00	0.00	0.00	0.00
P2O5	0.00	0.00	0.00	0.00	0.00	0.00
TOTAL	99.85	99.83	100.29	100.06	99.95	100.23
Cr	0	0	0	0	0	0
Ni	0	1900	0	0	0	0
Sr	0	0	0	0	0	0
Ba	0	0	0	0	0	0
Si	1.0206	1.0235	1.0147	1.0217	1.0120	1.0232
Ti	0.0000	0.0000	0.0000	0.0000	0.0000	0.0000
Al	0.0000	0.0000	0.0000	0.0000	0.0000	0.0000
Fe3	0.0000	0.0000	0.0000	0.0000	0.0000	0.0000
Fe2	0.4296	0.4379	0.4422	0.4358	0.4405	0.4303
Mn2	0.0076	0.0039	0.0056	0.0046	0.0054	0.0041
Mg	1.5217	1.5062	1.5226	1.5139	1.5301	1.5192
Ca	0.0000	0.0000	0.0000	0.0022	0.0000	0.0000
Na	0.0000	0.0000	0.0000	0.0000	0.0000	0.0000
K	0.0000	0.0000	0.0000	0.0000	0.0000	0.0000
Sr	0.0000	0.0000	0.0000	0.0000	0.0000	0.0000
Ba	0.0000	0.0000	0.0000	0.0000	0.0000	0.0000
Cr	0.0000	0.0000	0.0000	0.0000	0.0000	0.0000
Ni	0.0000	0.0050	0.0000	0.0000	0.0000	0.0000
Total	2.9794	2.9765	2.9853	2.9783	2.9880	2.9768

Table C3b: Electron microprobe analyses with structural formulae Glen Doll pluton.

Sample	OPGD26A	OPGD26B	OPGD26C	OPGD49A	OPGD49B	OPGD49C	OPGD41A	OPGD41B
SiO2	55.45	55.32	55.42	56.43	56.32	56.08	54.40	54.54
TiO2	0.22	0.45	0.46	0.00	0.00	0.13	0.56	0.58
Al2O3	1.12	1.45	1.12	0.84	0.66	1.18	1.23	1.39
FeO	11.94	11.58	11.73	11.87	11.67	11.38	14.76	14.82
MnO	0.39	0.34	0.32	0.32	0.26	0.24	0.35	0.37
MgO	29.85	29.84	29.82	29.84	30.14	29.92	26.71	26.49
CaO	1.24	1.28	1.28	0.87	0.99	1.09	2.11	2.04
Na2O	0.00	0.00	0.00	0.00	0.00	0.00	0.00	0.00
K2O	0.00	0.00	0.00	0.00	0.00	0.00	0.00	0.00
P2O5	0.00	0.00	0.00	0.00	0.00	0.00	0.00	0.00
TOTAL	100.32	100.49	100.41	100.17	100.04	100.02	100.12	100.23
Cr	1100	2300	2600	0	0	0	0	0
Ni	0	0	0	0	0	0	0	0
Sr	0	0	0	0	0	0	0	0
Ba	0	0	0	0	0	0	0	0
Si	1.9627	1.9519	1.9582	1.9923	1.9905	1.9802	1.9601	1.9621
Ti	0.0059	0.0119	0.0122	0.0000	0.0000	0.0035	0.0152	0.0157
Al	0.0467	0.0603	0.0467	0.0350	0.0275	0.0491	0.0522	0.0590
Fe3	0.0000	0.0000	0.0000	0.0000	0.0000	0.0000	0.0000	0.0000
Fe2	0.3535	0.3417	0.3466	0.3505	0.3449	0.3361	0.4448	0.4459
Mn2	0.0117	0.0102	0.0096	0.0096	0.0078	0.0072	0.0107	0.0113
Mg	1.5746	1.5691	1.5703	1.5701	1.5875	1.5745	1.4343	1.4202
Ca	0.0470	0.0484	0.0485	0.0329	0.0375	0.0412	0.0815	0.0786
Na	0.0000	0.0000	0.0000	0.0000	0.0000	0.0000	0.0000	0.0000
K	0.0000	0.0000	0.0000	0.0000	0.0000	0.0000	0.0000	0.0000
P	0.0000	0.0000	0.0000	0.0000	0.0000	0.0000	0.0000	0.0000
Sr	0.0000	0.0000	0.0000	0.0000	0.0000	0.0000	0.0000	0.0000
Ba	0.0000	0.0000	0.0000	0.0000	0.0000	0.0000	0.0000	0.0000
Cr	0.0040	0.0083	0.0094	0.0000	0.0000	0.0000	0.0000	0.0000
Ni	0.0000	0.0000	0.0000	0.0000	0.0000	0.0000	0.0000	0.0000
Total	4.0061	4.0018	4.0015	3.9903	3.9958	3.9918	3.9986	3.9928

based on 6 oxygens for orthopyroxenes of the

OPGD41C	OPGD42A	OPGD42B	OPGD42C	OPGD2A	OPGD3A	OPGD3B
54.62	54.00	54.00	54.00	52.70	53.05	53.38
0.59	0.47	0.48	0.51	0.40	0.32	0.38
1.27	1.42	1.45	1.39	1.14	1.69	1.61
14.74	15.35	14.91	15.27	21.60	17.16	16.90
0.36	0.37	0.35	0.36	0.37	0.39	0.30
26.74	27.06	27.15	26.98	22.04	25.56	25.91
2.07	1.49	1.76	1.72	1.94	1.95	1.62
0.00	0.00	0.00	0.00	0.00	0.00	0.00
0.00	0.00	0.00	0.00	0.00	0.00	0.00
0.00	0.00	0.00	0.00	0.00	0.00	0.00
100.39	100.16	100.10	100.23	100.19	100.12	100.22
0	0	0	0	0	0	1200
0	0	0	0	0	0	0
0	0	0	0	0	0	0
0	0	0	0	0	0	0
1.9615	1.9484	1.9471	1.9477	1.9601	1.9357	1.9399
0.0159	0.0128	0.0130	0.0138	0.0112	0.0088	0.0104
0.0538	0.0604	0.0616	0.0591	0.0500	0.0727	0.0690
0.0000	0.0000	0.0000	0.0000	0.0000	0.0000	0.0000
0.4427	0.4632	0.4496	0.4606	0.6719	0.5237	0.5136
0.0110	0.0113	0.0107	0.0110	0.0117	0.0121	0.0092
1.4311	1.4551	1.4590	1.4503	1.2217	1.3900	1.4033
0.0797	0.0576	0.0680	0.0665	0.0773	0.0762	0.0631
0.0000	0.0000	0.0000	0.0000	0.0000	0.0000	0.0000
0.0000	0.0000	0.0000	0.0000	0.0000	0.0000	0.0000
0.0000	0.0000	0.0000	0.0000	0.0000	0.0000	0.0000
0.0000	0.0000	0.0000	0.0000	0.0000	0.0000	0.0000
0.0000	0.0000	0.0000	0.0000	0.0000	0.0000	0.0045
0.0000	0.0000	0.0000	0.0000	0.0000	0.0000	0.0000
3.9957	4.0087	4.0091	4.0089	4.0038	4.0191	4.0130

Table C3c: Electron microprobe analyses with structural formulae based on 6 oxygens for clinopyroxene of the Glen Doll pluton.

Sample	CPGD26A	CPGD26B	CPGD26C	CPGD49A	CPGD49B	CPGD49C	CPGD41A	CPGD41B	CPGD41C	CPGD42A	CPGD42B	CPGD42C	CPGD4A	CPGD4B	CPGD4C	CPGD3A	CPGD3B	CPGD5A	CPGD5B	CPGD10A	CPGD10B	CPGD33A	CPGD33B	CPGD33C
SiO2	52.06	52.17	52.10	52.83	52.29	52.45	51.71	51.69	51.72	52.00	52.00	52.10	53.02	53.36	52.79	51.73	52.69	52.50	53.56	52.58	50.89	52.36	52.29	52.30
TiO2	0.83	0.72	0.82	0.52	0.69	0.71	0.88	0.87	0.87	0.77	0.74	0.79	0.49	0.11	0.28	0.73	0.46	0.54	0.00	0.46	1.06	0.23	0.27	0.25
Al2O3	2.67	2.57	2.64	2.57	2.67	2.66	2.81	2.85	2.79	2.73	2.45	2.64	1.54	0.67	1.02	2.68	1.68	1.60	0.51	1.81	3.55	0.75	0.81	0.83
FeO	5.52	5.43	5.49	5.35	5.43	5.51	7.15	7.19	7.21	6.78	8.04	7.79	9.20	8.97	9.57	7.56	8.84	9.75	7.99	8.59	8.00	10.44	10.12	9.98
MnO	0.00	0.00	0.00	0.00	0.00	0.00	0.18	0.21	0.22	0.20	0.31	0.29	0.23	0.27	0.34	0.15	0.27	0.30	0.46	0.40	0.24	0.32	0.34	0.35
MgO	15.63	15.74	15.67	15.99	15.87	15.73	14.87	14.79	14.85	14.69	15.39	14.89	14.18	13.72	14.11	15.13	14.45	14.60	14.23	14.52	14.63	12.72	12.67	12.71
CaO	22.21	22.27	22.28	21.58	22.01	22.21	21.82	21.84	21.85	22.50	20.91	21.78	21.08	22.51	21.71	21.29	21.37	20.95	23.13	21.41	21.06	23.34	23.40	23.17
Na2O	0.00	0.00	0.00	0.00	0.00	0.00	0.00	0.00	0.00	0.00	0.00	0.00	0.00	0.40	0.00	0.00	0.23	0.00	0.00	0.00	0.00	0.00	0.00	0.00
K2O	0.00	0.00	0.00	0.00	0.00	0.00	0.00	0.00	0.00	0.00	0.00	0.00	0.00	0.00	0.00	0.00	0.00	0.00	0.00	0.00	0.00	0.00	0.00	0.00
P2O5	0.00	0.00	0.00	0.00	0.00	0.00	0.00	0.00	0.00	0.00	0.00	0.00	0.00	0.00	0.00	0.00	0.00	0.00	0.00	0.00	0.00	0.00	0.00	0.00
TOTAL	99.52	99.69	99.76	99.64	99.85	99.89	99.69	99.75	99.85	100.04	100.10	100.56	99.87	100.13	99.82	99.62	99.99	100.44	99.88	99.77	99.57	100.29	100.05	99.76
Cr	6000	7900	7600	8000	8900	6200	2700	3100	3400	3700	2600	2800	1300	1200	0	3500	0	2000	0	0	1400	1300	1500	1700
Ni	0	0	0	0	0	0	0	0	0	0	0	0	0	0	0	0	0	0	0	0	0	0	0	0
Sr	0	0	0	0	0	0	0	0	0	0	0	0	0	0	0	0	0	0	0	0	0	0	0	0
Ba	0	0	0	0	0	0	0	0	0	0	0	0	0	0	0	0	0	0	0	0	0	0	0	0
Si	1.9196	1.9198	1.9167	1.9370	1.9190	1.9250	1.9175	1.9163	1.9160	1.9212	1.9239	1.9204	1.9721	1.9893	1.9748	1.9201	1.9597	1.9497	1.9950	1.9576	1.8950	1.9689	1.9688	1.9721
Ti	0.0230	0.0199	0.0227	0.0143	0.0190	0.0196	0.0245	0.0243	0.0242	0.0214	0.0206	0.0219	0.0137	0.0031	0.0079	0.0204	0.0129	0.0151	0.0000	0.0129	0.0297	0.0065	0.0076	0.0071
Al	0.1161	0.1115	0.1145	0.1111	0.1155	0.1151	0.1228	0.1246	0.1218	0.1189	0.1069	0.1147	0.0675	0.0294	0.0450	0.1173	0.0737	0.0701	0.0224	0.0794	0.1558	0.0332	0.0360	0.0369
Fe3	0.0000	0.0000	0.0000	0.0000	0.0000	0.0000	0.0000	0.0000	0.0000	0.0000	0.0000	0.0000	0.0000	0.0000	0.0000	0.0000	0.0000	0.0000	0.0000	0.0000	0.0000	0.0000	0.0000	0.0030
Fe2	0.1702	0.1671	0.1689	0.1640	0.1667	0.1691	0.2217	0.2229	0.2234	0.2095	0.2488	0.2401	0.2862	0.2797	0.2994	0.2347	0.2750	0.3028	0.2489	0.2675	0.2491	0.3283	0.3187	0.3147
Mn2	0.0000	0.0000	0.0000	0.0000	0.0000	0.0000	0.0057	0.0066	0.0069	0.0063	0.0097	0.0091	0.0072	0.0085	0.0108	0.0047	0.0085	0.0094	0.0145	0.0126	0.0076	0.0102	0.0108	0.0112
Mg	0.8589	0.8632	0.8592	0.8737	0.8680	0.8604	0.8218	0.8172	0.8198	0.8089	0.8486	0.8180	0.7860	0.7623	0.7867	0.8370	0.8010	0.8081	0.7899	0.8057	0.8119	0.7128	0.7109	0.7143
Ca	0.8775	0.8781	0.8783	0.8478	0.8655	0.8734	0.8670	0.8676	0.8673	0.8907	0.8289	0.8602	0.8401	0.8992	0.8702	0.8467	0.8516	0.8336	0.9231	0.8541	0.8403	0.9404	0.9440	0.9362
Na	0.0000	0.0000	0.0000	0.0000	0.0000	0.0000	0.0000	0.0000	0.0000	0.0000	0.0000	0.0000	0.0000	0.0289	0.0000	0.0000	0.0166	0.0000	0.0000	0.0000	0.0000	0.0000	0.0000	0.0000
K	0.0000	0.0000	0.0000	0.0000	0.0000	0.0000	0.0000	0.0000	0.0000	0.0000	0.0000	0.0000	0.0000	0.0000	0.0000	0.0000	0.0000	0.0000	0.0000	0.0000	0.0000	0.0000	0.0000	0.0000
P	0.0000	0.0000	0.0000	0.0000	0.0000	0.0000	0.0000	0.0000	0.0000	0.0000	0.0000	0.0000	0.0000	0.0000	0.0000	0.0000	0.0000	0.0000	0.0000	0.0000	0.0000	0.0000	0.0000	0.0000
Sr	0.0000	0.0000	0.0000	0.0000	0.0000	0.0000	0.0000	0.0000	0.0000	0.0000	0.0000	0.0000	0.0000	0.0000	0.0000	0.0000	0.0000	0.0000	0.0000	0.0000	0.0000	0.0000	0.0000	0.0000
Ba	0.0000	0.0000	0.0000	0.0000	0.0000	0.0000	0.0000	0.0000	0.0000	0.0000	0.0000	0.0000	0.0000	0.0000	0.0000	0.0000	0.0000	0.0000	0.0000	0.0000	0.0000	0.0000	0.0000	0.0000
Cr	0.0227	0.0299	0.0287	0.0301	0.0336	0.0234	0.0103	0.0118	0.0129	0.0140	0.0099	0.0106	0.0050	0.0046	0.0000	0.0134	0.0000	0.0076	0.0000	0.0000	0.0054	0.0050	0.0058	0.0066
Ni	0.0000	0.0000	0.0000	0.0000	0.0000	0.0000	0.0000	0.0000	0.0000	0.0000	0.0000	0.0000	0.0000	0.0000	0.0000	0.0000	0.0000	0.0000	0.0000	0.0000	0.0000	0.0000	0.0000	0.0000
Total	3.9883	3.9896	3.9890	3.9781	3.9874	3.9861	3.9914	3.9912	3.9924	3.9909	3.9972	3.9950	3.9779	4.0050	3.9948	3.9942	3.9989	3.9964	3.9938	3.9898	3.9947	4.0055	4.0027	3.9990

Table C3d: Electron microprobe analyses with structural formul

Sample	AMGD26A	AMGD26B	AMGD26C	AMGD26D	AMGD26E	AMGD26F	AMGD26G	AMGD26H
SiO2	43.62	43.40	43.11	42.49	42.34	43.21	45.38	52.19
TiO2	2.81	2.27	3.24	2.96	4.33	3.47	0.28	0.13
Al2O3	11.46	11.36	11.57	11.34	11.02	11.28	10.61	4.79
FeO	8.27	8.24	8.34	8.85	8.20	8.70	8.61	6.16
MnO	0.00	0.00	0.00	0.00	0.00	0.16	0.18	0.00
MgO	15.52	16.04	15.25	15.13	14.86	15.25	17.01	19.88
CaO	11.80	11.59	11.80	11.47	11.72	11.83	11.74	12.43
Na2O	2.69	2.55	2.41	2.61	2.70	2.53	2.37	0.91
K2O	0.73	0.77	0.76	0.79	0.62	0.80	0.56	0.00
P2O5	0.00	0.00	0.00	0.00	0.00	0.00	0.00	0.00
TOTAL	97.85	96.85	97.21	96.32	96.38	97.95	96.74	96.49
Cr	9500	6300	7300	6800	5900	7200	0	0
Ni	0	0	0	0	0	0	0	0
Sr	0	0	0	0	0	0	0	0
Ba	0	0	0	0	0	0	0	0
Si	6.3114	6.3397	6.2816	6.2722	6.2358	6.2712	6.6109	7.4085
Ti	0.3058	0.2494	0.3551	0.3286	0.4796	0.3787	0.0307	0.0139
Al	1.9548	1.9563	1.9875	1.9735	1.9134	1.9300	1.8222	0.8016
Fe3	0.0000	0.0000	0.0000	0.0000	0.0000	0.0000	0.0000	0.0000
Fe2	1.0007	1.0067	1.0163	1.0926	1.0100	1.0560	1.0490	0.7313
Mn2	0.0000	0.0000	0.0000	0.0000	0.0000	0.0197	0.0222	0.0000
Mg	3.3467	3.4919	3.3117	3.3286	3.2617	3.2985	3.6930	4.2057
Ca	1.8294	1.8141	1.8423	1.8142	1.8495	1.8397	1.8326	1.8906
Na	0.7547	0.7222	0.6809	0.7470	0.7710	0.7120	0.6694	0.2505
K	0.1348	0.1435	0.1413	0.1488	0.1165	0.1481	0.1041	0.0000
P	0.0000	0.0000	0.0000	0.0000	0.0000	0.0000	0.0000	0.0000
Sr	0.0000	0.0000	0.0000	0.0000	0.0000	0.0000	0.0000	0.0000
Ba	0.0000	0.0000	0.0000	0.0000	0.0000	0.0000	0.0000	0.0000
Cr	0.1413	0.0946	0.1093	0.1032	0.0893	0.1074	0.0000	0.0000
Ni	0.0000	0.0000	0.0000	0.0000	0.0000	0.0000	0.0000	0.0000
Total	15.7795	15.8184	15.7260	15.8087	15.7270	15.7614	15.8341	15.3021

lae on 23 oxygens for amphibole of the Glen Doll pluton.

AMGD26I	AMGD26J	AMGD49A	AMGD49B	AMGD49C	AMGD49D	AMGD49E	AMGD49F
52.19	52.12	43.22	43.79	43.20	52.12	52.20	52.21
0.13	0.15	3.27	2.63	2.89	0.14	0.15	0.15
4.81	4.76	11.48	11.28	11.37	4.79	4.74	4.82
6.21	6.18	8.31	8.03	8.21	6.10	6.18	6.24
0.00	0.00	0.00	0.00	0.00	0.00	0.00	0.00
19.85	19.91	15.21	15.84	15.87	19.87	19.86	19.89
12.49	12.46	11.79	11.81	11.85	12.44	12.46	12.44
0.94	0.93	2.39	2.79	2.64	0.92	0.93	0.95
0.00	0.00	0.75	0.77	0.76	0.00	0.00	0.00
0.00	0.00	0.00	0.00	0.00	0.00	0.00	0.00
96.62	96.51	97.10	97.74	97.52	96.38	96.52	96.70
0	0	6800	8000	7300	0	0	0
0	0	0	0	0	0	0	0
0	0	0	0	0	0	0	0
0	0	0	0	0	0	0	0
7.4027	7.4008	6.3013	6.3388	6.2791	7.4063	7.4099	7.3997
0.0139	0.0160	0.3586	0.2863	0.3159	0.0150	0.0160	0.0160
0.8043	0.7968	1.9732	1.9250	1.9483	0.8025	0.7932	0.8054
0.0000	0.0000	0.0000	0.0000	0.0000	0.0000	0.0000	0.0000
0.7367	0.7339	1.0133	0.9721	0.9980	0.7249	0.7337	0.7396
0.0000	0.0000	0.0000	0.0000	0.0000	0.0000	0.0000	0.0000
4.1961	4.2134	3.3049	3.4172	3.4378	4.2080	4.2015	4.2012
1.8983	1.8958	1.8419	1.8318	1.8456	1.8941	1.8952	1.8892
0.2585	0.2561	0.6756	0.7831	0.7440	0.2535	0.2560	0.2611
0.0000	0.0000	0.1395	0.1422	0.1409	0.0000	0.0000	0.0000
0.0000	0.0000	0.0000	0.0000	0.0000	0.0000	0.0000	0.0000
0.0000	0.0000	0.0000	0.0000	0.0000	0.0000	0.0000	0.0000
0.0000	0.0000	0.0000	0.0000	0.0000	0.0000	0.0000	0.0000
0.0000	0.0000	0.1019	0.1190	0.1090	0.0000	0.0000	0.0000
0.0000	0.0000	0.0000	0.0000	0.0000	0.0000	0.0000	0.0000
15.3105	15.3128	15.7101	15.8155	15.8187	15.3043	15.3055	15.3122

Table C3d: Continued

Sample	AMGD41A	AMGD41B	AMGD41C	AMGD41D	AMGD41E	AMGD42A	AMGD42B	AMGD42C
SiO2	42.88	43.45	42.99	50.74	50.46	49.13	50.01	49.78
TiO2	4.29	3.55	4.41	1.41	1.51	1.30	1.29	1.32
Al2O3	10.97	10.20	10.87	5.69	5.53	6.45	6.32	6.41
FeO	10.61	11.06	10.84	9.09	9.35	11.60	11.47	11.52
MnO	0.15	0.16	0.17	0.15	0.11	0.15	0.14	0.15
MgO	13.71	13.96	13.72	17.05	16.95	15.31	15.07	15.19
CaO	11.87	11.84	11.83	12.01	12.13	12.55	12.34	12.43
Na2O	1.30	1.38	1.75	0.52	0.39	0.47	0.45	0.45
K2O	0.92	1.02	0.84	0.52	0.48	0.66	0.59	0.61
P2O5	0.00	0.00	0.00	0.00	0.00	0.00	0.00	0.00
TOTAL	96.85	97.01	97.71	97.30	97.04	97.76	97.80	97.98
Cr	1500	3900	2900	1200	1300	1400	1200	1200
Ni	0	0	0	0	0	0	0	0
Sr	0	0	0	0	0	0	0	0
Ba	0	0	0	0	0	0	0	0
Si	6.3285	6.4166	6.3040	7.2625	7.2524	7.1155	7.2103	7.1734
Ti	0.4762	0.3943	0.4863	0.1518	0.1632	0.1416	0.1399	0.1431
Al	1.9087	1.7758	1.8792	0.9601	0.9370	1.1013	1.0742	1.0890
Fe3	0.0000	0.0000	0.0000	0.0000	0.0000	0.0000	0.0000	0.0000
Fe2	1.3096	1.3660	1.3294	1.0881	1.1239	1.4051	1.3830	1.3883
Mn2	0.0188	0.0200	0.0211	0.0182	0.0134	0.0184	0.0171	0.0183
Mg	3.0155	3.0724	2.9984	3.6370	3.6307	3.3046	3.2381	3.2622
Ca	1.8771	1.8735	1.8588	1.8419	1.8681	1.9476	1.9064	1.9193
Na	0.3720	0.3952	0.4976	0.1443	0.1087	0.1320	0.1258	0.1257
K	0.1732	0.1922	0.1571	0.0950	0.0880	0.1220	0.1085	0.1121
P	0.0000	0.0000	0.0000	0.0000	0.0000	0.0000	0.0000	0.0000
Sr	0.0000	0.0000	0.0000	0.0000	0.0000	0.0000	0.0000	0.0000
Ba	0.0000	0.0000	0.0000	0.0000	0.0000	0.0000	0.0000	0.0000
Cr	0.0228	0.0592	0.0437	0.0177	0.0192	0.0208	0.0178	0.0178
Ni	0.0000	0.0000	0.0000	0.0000	0.0000	0.0000	0.0000	0.0000
Total	15.5023	15.5652	15.5756	15.2165	15.2046	15.3088	15.2210	15.2491

AMGD42D	AMGD42E	AMGD42F	AMGD2A	AMGD2B	AMGD3A	AMGD3B	AMGD3C
42.26	42.34	42.45	49.19	45.78	44.67	46.00	48.16
4.16	4.11	4.23	1.57	2.20	2.51	1.94	1.46
11.59	11.52	11.54	5.75	8.18	9.14	7.74	6.20
11.43	11.39	11.46	13.00	14.22	15.02	15.81	16.18
0.00	0.00	0.00	0.16	0.22	0.24	0.26	0.38
13.54	13.51	13.49	14.67	13.32	12.78	12.66	13.07
11.76	11.69	11.72	11.44	11.26	11.21	11.20	11.19
1.74	1.81	1.84	0.52	1.47	1.60	1.16	0.78
0.93	0.89	0.92	0.42	0.68	0.78	0.66	0.53
0.00	0.00	0.00	0.00	0.00	0.00	0.00	0.00
97.41	97.46	97.84	96.84	97.33	97.95	97.57	97.95
0	2000	1900	1200	0	0	1400	0
0	0	0	0	0	0	0	0
0	0	0	0	0	0	0	0
0	0	0	0	0	0	0	0
6.2350	6.2404	6.2355	7.2064	6.7849	6.6220	6.8400	7.1052
0.4616	0.4556	0.4673	0.1730	0.2452	0.2798	0.2169	0.1620
2.0159	2.0017	1.9984	0.9931	1.4293	1.5974	1.3568	1.0784
0.0000	0.0000	0.0000	0.0000	0.0000	0.0000	0.0000	0.0000
1.4103	1.4040	1.4078	1.5928	1.7626	1.8622	1.9661	1.9964
0.0000	0.0000	0.0000	0.0199	0.0276	0.0301	0.0327	0.0475
2.9772	2.9676	2.9531	3.2030	2.9421	2.8235	2.8055	2.8737
1.8591	1.8462	1.8446	1.7958	1.7881	1.7806	1.7845	1.7689
0.4978	0.5173	0.5241	0.1477	0.4224	0.4599	0.3344	0.2231
0.1751	0.1674	0.1724	0.0785	0.1286	0.1475	0.1252	0.0998
0.0000	0.0000	0.0000	0.0000	0.0000	0.0000	0.0000	0.0000
0.0000	0.0000	0.0000	0.0000	0.0000	0.0000	0.0000	0.0000
0.0000	0.0000	0.0000	0.0000	0.0000	0.0000	0.0000	0.0000
0.0000	0.0303	0.0287	0.0181	0.0000	0.0000	0.0214	0.0000
0.0000	0.0000	0.0000	0.0000	0.0000	0.0000	0.0000	0.0000
15.6319	15.6303	15.6319	15.2282	15.5308	15.6031	15.4837	15.3550

Table C3d: Continued

Sample	AMGD3D	AMGD4A	AMGD4B	AMGD4C	AMGD10A	AMGD10B	AMGD10C	AMGD10D	AMGD12A	AMGD34A	AMGD34B	AMGD34C	AMGD27A	AMGD27B	AMGD27C	AMGD33A	AMGD33B	AMGD33C	AMGD33D	AMGD40AA	AMGD40AB	AMGD40AC
SiO2	46.56	48.38	47.07	48.02	47.85	44.64	48.58	49.61	49.92	48.36	48.79	49.01	49.08	48.97	48.79	48.05	45.93	47.93	46.30	47.59	48.07	47.82
TiO2	2.04	1.41	1.75	1.48	1.57	2.62	1.59	1.06	1.34	1.47	1.47	1.45	1.45	1.47	1.52	1.63	2.20	1.30	2.12	1.36	0.90	0.96
Al2O3	7.49	5.91	6.78	6.26	6.72	8.88	6.74	5.51	6.12	6.17	6.21	6.07	6.01	6.11	6.21	6.29	7.62	6.51	7.50	6.75	6.40	6.42
FeO	14.85	16.52	15.40	16.38	13.79	12.98	13.33	12.57	12.21	15.17	13.93	14.57	14.76	15.01	14.69	14.54	14.60	16.32	14.02	14.32	14.07	14.07
MnO	0.20	0.28	0.25	0.28	0.19	0.27	0.19	0.18	0.16	0.37	0.33	0.34	0.25	0.29	0.33	0.33	0.26	0.28	0.29	0.41	0.45	0.45
MgO	13.14	12.81	12.93	12.65	14.07	13.79	14.84	15.41	15.81	13.25	13.91	13.58	13.90	13.55	13.59	13.21	12.83	12.44	13.10	13.62	14.12	13.61
CaO	11.09	11.17	11.17	11.37	11.45	11.24	11.50	11.42	11.66	11.61	11.77	11.64	11.42	11.46	11.65	12.24	11.51	12.26	11.45	11.93	11.45	11.98
Na2O	1.66	0.91	1.11	0.69	0.88	1.54	1.10	0.69	0.93	0.69	0.44	0.49	0.96	0.97	0.69	0.78	1.16	0.80	1.17	1.20	0.78	0.89
K2O	0.73	0.51	0.59	0.56	0.53	0.72	0.62	0.46	0.50	0.47	0.64	0.61	0.50	0.62	0.57	0.57	0.68	0.64	0.73	0.64	0.51	0.59
P2O5	0.00	0.00	0.00	0.00	0.00	0.00	0.00	0.00	0.00	0.00	0.00	0.00	0.00	0.00	0.00	0.00	0.00	0.00	0.00	0.00	0.00	0.00
TOTAL	97.76	98.10	97.05	97.69	97.05	96.68	98.49	96.91	98.81	97.56	97.49	97.76	98.33	98.45	98.04	97.83	96.79	98.67	96.68	97.82	96.75	96.79
Cr	0	2000	0	0	0	0	0	0	1600	0	0	0	0	0	0	1900	0	1900	0	0	0	0
Ni	0	0	0	0	0	0	0	0	0	0	0	0	0	0	0	0	0	0	0	0	0	0
Sr	0	0	0	0	0	0	0	0	0	0	0	0	0	0	0	0	0	0	0	0	0	0
Ba	0	0	0	0	0	0	0	0	0	0	0	0	0	0	0	0	0	0	0	0	0	0
Si	6.8839	7.1347	7.0052	7.1102	7.0517	6.6430	7.0415	7.2498	7.1515	7.1301	7.1531	7.1806	7.1569	7.1483	7.1393	7.0694	6.8558	7.0500	6.8964	7.0102	7.1167	7.0984
Ti	0.2266	0.1564	0.1959	0.1648	0.1740	0.2932	0.1733	0.1165	0.1444	0.1630	0.1621	0.1598	0.1590	0.1614	0.1673	0.1804	0.2470	0.1438	0.2375	0.1507	0.1002	0.1072
Al	1.3055	1.0275	1.1896	1.0928	1.1675	1.5579	1.1517	0.9493	1.0336	1.0725	1.0734	1.0485	1.0332	1.0515	1.0713	1.0910	1.3409	1.1289	1.3170	1.1722	1.1171	1.1235
Fe3	0.0000	0.0000	0.0000	0.0000	0.0000	0.0000	0.0000	0.0000	0.0000	0.0000	0.0000	0.0000	0.0000	0.0000	0.0000	0.0000	0.0000	0.0000	0.0000	0.0000	0.0000	0.0000
Fe2	1.8362	2.0375	1.9168	2.0284	1.6996	1.6154	1.6159	1.5363	1.4629	1.8705	1.7080	1.7853	1.8000	1.8324	1.7977	1.7891	1.8226	2.0076	1.7465	1.7642	1.7421	1.7467
Mn2	0.0250	0.0350	0.0315	0.0351	0.0237	0.0340	0.0233	0.0223	0.0194	0.0462	0.0410	0.0422	0.0309	0.0359	0.0409	0.0411	0.0329	0.0349	0.0366	0.0512	0.0564	0.0566
Mg	2.8953	2.8154	2.8678	2.7915	3.0902	3.0584	3.2057	3.3561	3.3755	2.9114	3.0393	2.9652	3.0208	2.9478	2.9636	2.8965	2.8541	2.7270	2.9080	2.9900	3.1155	3.0109
Ca	1.7569	1.7651	1.7812	1.8039	1.8081	1.7923	1.7861	1.7882	1.7898	1.8341	1.8490	1.8273	1.7844	1.7925	1.8266	1.9296	1.8409	1.9323	1.8274	1.8830	1.8164	1.9055
Na	0.4759	0.2602	0.3203	0.1981	0.2515	0.4444	0.3091	0.1955	0.2583	0.1973	0.1251	0.1392	0.2714	0.2745	0.1958	0.2225	0.3357	0.2282	0.3379	0.3427	0.2239	0.2562
K	0.1377	0.0960	0.1120	0.1058	0.0996	0.1367	0.1147	0.0858	0.0914	0.0884	0.1197	0.1140	0.0930	0.1155	0.1064	0.1070	0.1295	0.1201	0.1387	0.1203	0.0963	0.1117
P	0.0000	0.0000	0.0000	0.0000	0.0000	0.0000	0.0000	0.0000	0.0000	0.0000	0.0000	0.0000	0.0000	0.0000	0.0000	0.0000	0.0000	0.0000	0.0000	0.0000	0.0000	0.0000
Sr	0.0000	0.0000	0.0000	0.0000	0.0000	0.0000	0.0000	0.0000	0.0000	0.0000	0.0000	0.0000	0.0000	0.0000	0.0000	0.0000	0.0000	0.0000	0.0000	0.0000	0.0000	0.0000
Ba	0.0000	0.0000	0.0000	0.0000	0.0000	0.0000	0.0000	0.0000	0.0000	0.0000	0.0000	0.0000	0.0000	0.0000	0.0000	0.0000	0.0000	0.0000	0.0000	0.0000	0.0000	0.0000
Cr	0.0000	0.0303	0.0000	0.0000	0.0000	0.0000	0.0000	0.0000	0.0236	0.0000	0.0000	0.0000	0.0000	0.0000	0.0000	0.0287	0.0000	0.0287	0.0000	0.0000	0.0000	0.0000
Ni	0.0000	0.0000	0.0000	0.0000	0.0000	0.0000	0.0000	0.0000	0.0000	0.0000	0.0000	0.0000	0.0000	0.0000	0.0000	0.0000	0.0000	0.0000	0.0000	0.0000	0.0000	0.0000
Total	15.5433	15.3581	15.4203	15.3305	15.3660	15.5753	15.4213	15.2997	15.3504	15.3135	15.2706	15.2620	15.3497	15.3596	15.3089	15.3552	15.4594	15.4015	15.4460	15.4845	15.3846	15.4166

Table C3e: Electron microprobe analyses with structural formulae based on 23 oxygens for biotite of the Glen Doll pluton.

Sample	BIGD26A	BIGD26B	BIGD26C	BIGD49A	BIGD49B	BIGD49C	BIGD41A	BIGD41B	BIGD41C	BIGD42A	BIGD42B	BIGD42C	BIGD2A	BIGD2B	BIGD3A	BIGD4A	BIGD4B	BIGD4C	BIGD5A	BIGD5B	BIGD6A	BIGD6B	BIGD10A	BIGD10B
SiO2	38.71	38.41	38.56	38.90	38.61	38.67	38.37	36.97	37.73	36.93	36.87	36.91	36.19	37.02	36.58	37.01	36.51	36.14	37.55	37.98	38.79	39.30	38.54	38.14
TiO2	1.80	1.83	2.13	1.51	1.87	1.74	4.77	5.23	4.89	5.00	4.91	5.03	3.93	3.68	5.12	4.97	4.02	5.44	4.87	5.00	4.27	4.17	4.36	4.36
Al2O3	14.97	15.22	15.13	15.40	15.57	15.52	13.75	14.03	14.01	14.35	14.09	14.05	14.24	14.34	14.01	13.95	13.94	13.80	14.19	13.90	14.06	14.30	14.57	14.15
FeO	7.85	8.47	7.57	7.23	7.49	7.37	10.99	15.32	13.21	15.17	15.03	15.09	19.73	18.50	19.76	20.64	21.18	20.90	14.78	16.51	15.18	15.14	16.54	17.61
MnO	0.00	0.00	0.00	0.00	0.00	0.00	0.00	0.11	0.06	0.00	0.00	0.00	0.00	0.00	0.00	0.00	0.15	0.00	0.00	0.00	0.00	0.19	0.19	0.15
MgO	20.47	20.23	20.73	21.43	21.34	21.39	16.38	13.98	14.35	13.79	13.68	13.84	12.03	12.81	11.01	10.85	10.65	10.00	14.66	13.68	14.86	15.38	13.34	13.23
CaO	0.00	0.00	0.09	0.00	0.00	0.00	0.00	0.00	0.00	0.00	0.00	0.00	0.00	0.00	0.00	0.00	0.18	0.00	0.00	0.00	0.00	0.00	0.00	0.00
Na2O	0.58	0.99	0.70	0.95	0.75	0.81	0.00	0.00	0.00	0.00	0.00	0.00	0.00	0.00	0.00	0.00	0.00	0.00	0.00	0.00	0.00	0.00	0.00	0.00
K2O	8.61	8.16	8.55	8.32	8.66	8.45	9.54	9.78	9.62	9.64	9.62	9.71	8.22	8.90	8.78	9.19	8.98	8.76	8.69	8.66	8.44	8.44	8.88	8.92
P2O5	0.00	0.00	0.00	0.00	0.00	0.00	0.00	0.00	0.00	0.00	0.00	0.00	0.00	0.00	0.00	0.00	0.00	0.00	0.00	0.00	0.00	0.00	0.00	0.00
TOTAL	93.38	93.31	93.46	93.74	94.29	93.95	93.80	95.42	93.87	94.88	94.20	94.63	94.34	95.25	95.26	96.61	95.61	95.04	94.74	95.73	95.60	96.92	96.42	96.56
Zr	3900	0	0	0	0	0	0	0	0	0	0	0	0	0	0	0	0	0	0	0	0	0	0	0
Ba	0	0	0	0	0	0	0	0	0	0	0	0	0	0	0	0	0	0	0	0	0	0	0	0
Cr	0	0	0	0	0	0	0	0	0	0	0	0	0	0	0	0	0	0	0	0	0	0	0	0
Ni	0	0	0	0	0	0	0	0	0	0	0	0	0	0	0	0	0	0	0	0	0	0	0	0
Si	5.9226	5.8940	5.8916	5.9049	5.8467	5.8660	5.9662	5.8004	5.9352	5.8120	5.8429	5.8277	5.8148	5.8651	5.8357	5.8520	5.8578	5.8194	5.8644	5.9110	5.9840	5.9747	5.9514	5.9223
Ti	0.2071	0.2112	0.2448	0.1724	0.2130	0.1985	0.5578	0.6171	0.5785	0.5918	0.5852	0.5973	0.4749	0.4385	0.6143	0.5910	0.4851	0.6588	0.5720	0.5852	0.4954	0.4768	0.5063	0.5092
Al	2.7002	2.7534	2.7253	2.7560	2.7796	2.7756	2.5206	2.5951	2.5982	2.6625	2.6324	2.6153	2.6974	2.6784	2.6350	2.6005	2.6368	2.6197	2.6126	2.5504	2.5571	2.5630	2.6525	2.5903
Fe3	0.0000	0.0000	0.0000	0.0000	0.0000	0.0000	0.0000	0.0000	0.0000	0.0000	0.0000	0.0000	0.0000	0.0000	0.0000	0.0000	0.0000	0.0000	0.0000	0.0000	0.0000	0.0000	0.0000	0.0000
Fe2	1.0045	1.0870	0.9673	0.9179	0.9486	0.9350	1.4292	2.0102	1.7379	1.9967	1.9920	1.9926	2.6513	2.4512	2.6364	2.7294	2.8420	2.8146	1.9305	2.1490	1.9585	1.9250	2.1361	2.2669
Mn2	0.0000	0.0000	0.0000	0.0000	0.0000	0.0000	0.0000	0.0146	0.0080	0.0000	0.0000	0.0000	0.0000	0.0000	0.0000	0.0000	0.0204	0.0000	0.0000	0.0000	0.0000	0.0245	0.0249	0.0197
Mg	4.6675	4.6264	4.7203	4.8481	4.8160	4.8358	3.7958	3.2688	3.3642	3.2344	3.2309	3.2566	2.8807	3.0246	2.6177	2.5568	2.5466	2.3998	3.4121	3.1731	3.4164	3.4847	3.0701	3.0616
Ca	0.0000	0.0000	0.0147	0.0000	0.0000	0.0000	0.0000	0.0000	0.0000	0.0000	0.0000	0.0000	0.0000	0.0000	0.0000	0.0000	0.0309	0.0000	0.0000	0.0000	0.0000	0.0000	0.0000	0.0000
Na	0.1721	0.2946	0.2074	0.2796	0.2202	0.2382	0.0000	0.0000	0.0000	0.0000	0.0000	0.0000	0.0000	0.0000	0.0000	0.0000	0.0000	0.0000	0.0000	0.0000	0.0000	0.0000	0.0000	0.0000
K	1.6806	1.5975	1.6666	1.6113	1.6731	1.6353	1.8925	1.9576	1.9306	1.9355	1.9450	1.9559	1.6850	1.7989	1.7870	1.8539	1.8382	1.7996	1.7315	1.7195	1.6611	1.6370	1.7495	1.7677
Cr	0.0000	0.0000	0.0000	0.0000	0.0000	0.0000	0.0000	0.0000	0.0000	0.0000	0.0000	0.0000	0.0000	0.0000	0.0000	0.0000	0.0000	0.0000	0.0000	0.0000	0.0000	0.0000	0.0000	0.0000
Ni	0.0000	0.0000	0.0000	0.0000	0.0000	0.0000	0.0000	0.0000	0.0000	0.0000	0.0000	0.0000	0.0000	0.0000	0.0000	0.0000	0.0000	0.0000	0.0000	0.0000	0.0000	0.0000	0.0000	0.0000
Sr	0.0000	0.0000	0.0000	0.0000	0.0000	0.0000	0.0000	0.0000	0.0000	0.0000	0.0000	0.0000	0.0000	0.0000	0.0000	0.0000	0.0000	0.0000	0.0000	0.0000	0.0000	0.0000	0.0000	0.0000
Ba	0.0613	0.0000	0.0000	0.0000	0.0000	0.0000	0.0000	0.0000	0.0000	0.0000	0.0000	0.0000	0.0000	0.0000	0.0000	0.0000	0.0000	0.0000	0.0000	0.0000	0.0000	0.0000	0.0000	0.0000
Total	0.0000	0.0000	0.0000	0.0000	0.0000	0.0000	0.0000	0.0000	0.0000	0.0000	0.0000	0.0000	0.0000	0.0000	0.0000	0.0000	0.0000	0.0000	0.0000	0.0000	0.0000	0.0000	0.0000	0.0000
	16.4159	16.4641	16.4380	16.4901	16.4971	16.4845	16.1620	16.2638	16.1526	16.2328	16.2282	16.2454	16.2041	16.2567	16.1260	16.1837	16.2578	16.1118	16.1230	16.0883	16.0726	16.0855	16.0907	16.157

Table C3e: Continued

Sample	BIGD10C	BIGD34A	BIGD27A	BIGD27B	BIGD37A	BIGD37B	BIGD37C	BIGD33A	BIGD33B	BIGD33C	BIGD33D	BIGD51A	BIGD51B	BIGD51C	BIGD51D	BIGD51E	BIGD40A	BIGD40B	BIGD40C	BIGD40D	BIGD40AA	BIGD40AB
SiO2	38.06	36.90	37.52	37.34	37.55	37.39	37.62	36.61	37.37	36.70	36.50	37.79	37.09	37.93	37.62	37.73	38.58	38.64	37.78	38.01	36.11	37.01
TiO2	5.00	5.25	4.62	4.89	4.49	4.99	5.44	5.25	4.85	4.39	4.98	3.77	4.43	4.68	4.07	4.02	4.52	4.15	4.70	4.21	5.61	4.52
Al2O3	13.94	14.10	14.06	14.01	14.04	13.51	13.47	13.51	13.59	13.41	13.34	15.22	14.65	14.46	14.57	14.74	12.35	12.17	12.66	12.62	13.39	13.61
FeO	16.17	16.21	18.72	16.79	18.81	19.64	18.81	19.70	20.32	18.97	20.23	14.54	14.87	14.69	13.86	14.47	17.01	16.48	16.81	16.29	19.91	19.68
MnO	0.00	0.00	0.00	0.00	0.19	0.27	0.25	0.20	0.23	0.18	0.14	0.16	0.22	0.31	0.27	0.23	0.28	0.33	0.33	0.29	0.16	0.12
MgO	13.94	11.94	12.03	12.01	12.24	11.80	11.91	11.11	11.11	11.26	10.95	14.40	14.01	14.43	14.80	13.89	14.03	14.24	13.80	13.76	10.66	11.42
CaO	0.00	0.00	0.00	0.00	0.12	0.16	0.13	0.00	0.00	0.00	0.13	0.02	0.00	0.01	0.04	0.01	0.00	0.00	0.00	0.00	0.00	0.08
Na2O	0.00	0.00	0.00	0.00	0.00	0.00	0.00	0.00	0.00	0.00	0.00	0.23	0.36	0.38	0.30	0.35	0.00	0.00	0.00	0.00	0.00	0.00
K2O	8.81	9.16	9.25	9.21	9.89	9.77	9.38	9.37	9.56	9.28	9.42	9.19	8.93	9.22	8.84	9.09	9.68	9.37	9.51	9.35	9.39	9.44
P2O5	0.00	0.00	0.00	0.00	0.00	0.00	0.00	0.00	0.00	0.00	0.00	0.00	0.00	0.00	0.00	0.00	0.00	0.00	0.00	0.00	0.00	0.00
TOTAL	95.92	95.56	96.20	96.25	97.33	97.53	97.01	95.75	97.03	94.19	95.69	95.40	94.64	96.11	94.37	94.58	96.45	95.38	95.59	94.53	95.23	95.88
Sr	0	0	0	0	0	0	0	0	0	0	0	800	500	0	0	0	0	0	0	0	0	0
Ba	0	0	0	0	0	0	0	0	0	0	0	0	300	0	0	500	0	0	0	0	0	0
Cr	0	0	0	0	0	0	0	0	0	0	0	0	0	0	0	0	0	0	0	0	0	0
Ni	0	0	0	0	0	0	0	0	0	0	0	0	0	0	0	0	0	0	0	0	0	0
Si	5.9063	5.8331	5.8970	5.8703	5.8651	5.8573	5.8838	5.8398	5.8906	5.9262	5.8467	5.8667	5.8268	5.8634	5.8870	5.9125	6.0222	6.0744	5.9521	6.0287	5.8079	5.8876
Ti	0.5835	0.6241	0.5461	0.5782	0.5274	0.5879	0.6399	0.6298	0.5750	0.5331	0.5999	0.4402	0.5234	0.5441	0.4790	0.4738	0.5306	0.4907	0.5569	0.5022	0.6786	0.5408
Al	2.5503	2.6277	2.6052	2.5966	2.5853	2.4951	2.4837	2.5406	2.5255	2.5529	2.5192	2.7856	2.7133	2.6353	2.6880	2.7232	2.2727	2.2555	2.3514	2.3598	2.5390	2.5526
Fe3	0.0000	0.0000	0.0000	0.0000	0.0000	0.0000	0.0000	0.0000	0.0000	0.0000	0.0000	0.0000	0.0000	0.0000	0.0000	0.0000	0.0000	0.0000	0.0000	0.0000	0.0000	0.0000
Fe2	2.0986	2.4074	2.4607	2.4705	2.4571	2.5731	2.4604	2.6281	2.6788	2.5618	2.7101	1.8878	1.9537	1.8992	1.8139	1.8964	2.2206	2.1667	2.2149	2.1609	2.6782	2.6184
Mn2	0.0000	0.0000	0.0000	0.0000	0.0251	0.0358	0.0331	0.0270	0.0307	0.0246	0.0190	0.0210	0.0293	0.0406	0.0358	0.0305	0.0370	0.0439	0.0440	0.0390	0.0218	0.0162
Mg	3.2240	2.8129	2.8179	2.8139	2.8492	2.7549	2.7751	2.6412	2.6099	2.7098	2.6140	3.3317	3.2801	3.3244	3.4516	3.2440	3.2638	3.3363	3.2402	3.2526	2.5552	2.7076
Ca	0.0000	0.0000	0.0000	0.0000	0.0201	0.0269	0.0218	0.0000	0.0000	0.0000	0.0223	0.0033	0.0000	0.0017	0.0067	0.0017	0.0000	0.0000	0.0000	0.0000	0.0000	0.0136
Na	0.0000	0.0000	0.0000	0.0000	0.0000	0.0000	0.0000	0.0000	0.0000	0.0000	0.0000	0.0692	0.1097	0.1139	0.0910	0.1063	0.0000	0.0000	0.0000	0.0000	0.0000	0.0000
K	1.7442	1.8473	1.8548	1.8473	1.9708	1.9526	1.8716	1.9069	1.9225	1.9118	1.9251	1.8202	1.7698	1.8184	1.7649	1.8173	1.9277	1.8793	1.9115	1.8920	1.9268	1.9160
Cr	0.0000	0.0000	0.0000	0.0000	0.0000	0.0000	0.0000	0.0000	0.0000	0.0000	0.0000	0.0000	0.0000	0.0000	0.0000	0.0000	0.0000	0.0000	0.0000	0.0000	0.0000	0.0000
Ni	0.0000	0.0000	0.0000	0.0000	0.0000	0.0000	0.0000	0.0000	0.0000	0.0000	0.0000	0.0000	0.0000	0.0000	0.0000	0.0000	0.0000	0.0000	0.0000	0.0000	0.0000	0.0000
Sr	0.0000	0.0000	0.0000	0.0000	0.0000	0.0000	0.0000	0.0000	0.0000	0.0000	0.0000	0.0000	0.0000	0.0000	0.0000	0.0000	0.0000	0.0000	0.0000	0.0000	0.0000	0.0000
Ba	0.0000	0.0000	0.0000	0.0000	0.0000	0.0000	0.0000	0.0000	0.0000	0.0000	0.0000	0.0128	0.0081	0.0000	0.0000	0.0000	0.0000	0.0000	0.0000	0.0000	0.0000	0.0000
Total	16.1071	16.1526	16.1817	16.1768	16.3002	16.2836	16.1703	16.2135	16.2330	16.2202	16.2563	16.2386	16.2389	16.2410	16.2179	16.2139	16.2747	16.2468	16.2710	16.2352	16.2074	16.2530

Table C3f: Electron microprobe analyses with structural formulae based on 8 oxygens for plagioclase of the Glen Doll pluton.

Sample	PLGD26A	PLGD26B	PLGD26C	PLGD41A	PLGD41B	PLGD41C	PLGD41D	PLGD42A	PLGD42B	PLGD42C	PLGD2A	PLGD2B	PLGD2C	PLGD3A	PLGD3B	PLGD4A	PLGD4B	PLGD5A	PLGD5B	PLGD5C	PLGD6A	PLGD6B	PLGD10A	PLGD10B
SiO2	49.28	48.89	49.10	51.54	51.96	48.32	49.66	54.13	53.33	54.11	52.65	53.53	52.87	52.83	54.66	54.36	54.87	54.97	54.29	54.04	54.24	54.06	53.82	54.09
TiO2	0.00	0.00	0.00	0.00	0.00	0.00	0.00	0.00	0.00	0.00	0.00	0.00	0.00	0.00	0.14	0.14	0.00	0.00	0.00	0.00	0.00	0.00	0.00	0.00
Al2O3	32.19	32.25	32.15	29.85	29.72	32.52	31.59	28.74	29.58	28.89	29.67	29.14	29.69	30.04	28.55	28.61	28.20	28.17	28.64	28.85	28.93	28.84	29.34	29.09
FeO	0.15	0.17	0.18	0.18	0.17	0.42	0.42	0.32	0.38	0.36	0.35	0.40	0.37	0.29	0.36	0.39	0.33	0.37	0.25	0.52	0.22	0.37	0.35	0.54
MnO	0.00	0.00	0.00	0.00	0.00	0.00	0.00	0.00	0.00	0.00	0.00	0.00	0.00	0.00	0.00	0.00	0.00	0.00	0.00	0.00	0.00	0.00	0.00	0.00
MgO	0.00	0.00	0.00	0.00	0.00	0.00	0.00	0.00	0.00	0.00	0.00	0.00	0.00	0.00	0.00	0.00	0.00	0.00	0.00	0.00	0.00	0.00	0.00	0.00
CaO	15.58	16.21	16.12	13.91	14.21	16.53	15.57	11.81	12.67	12.14	12.41	11.87	12.45	12.86	11.19	11.58	10.68	11.15	11.25	11.83	11.12	11.23	12.64	11.50
Na2O	2.67	2.34	2.32	3.82	3.60	2.25	2.71	4.93	4.38	4.72	4.32	4.57	4.20	4.14	4.80	4.83	5.29	4.94	5.04	4.68	5.32	5.17	4.18	4.77
K2O	0.00	0.00	0.00	0.00	0.00	0.00	0.00	0.11	0.00	0.00	0.28	0.29	0.09	0.12	0.23	0.08	0.18	0.30	0.16	0.19	0.16	0.24	0.18	0.23
P2O5	0.00	0.00	0.00	0.00	0.00	0.00	0.00	0.00	0.00	0.00	0.00	0.00	0.00	0.00	0.00	0.00	0.00	0.00	0.00	0.00	0.00	0.00	0.00	0.00
TOTAL	99.87	99.86	99.87	99.70	99.66	100.04	99.95	100.04	100.34	100.22	99.68	99.80	99.67	100.28	99.93	99.99	99.55	99.90	99.63	100.11	99.99	99.91	100.51	100.22
Sr	0	0	0	0	0	0	0	0	0	0	0	0	0	0	0	0	0	0	0	0	0	0	0	0
Ba	0	0	0	0	0	0	0	0	0	0	0	0	0	0	0	0	0	0	0	0	0	0	0	0
Cr	0	0	0	0	0	0	0	0	0	0	0	0	0	0	0	0	0	0	0	0	0	0	0	0
Ni	0	0	0	0	0	0	0	0	0	0	0	0	0	0	0	0	0	0	0	0	0	0	0	0
Si	9.0167	8.9609	8.9924	9.4746	9.4831	8.8664	9.0887	9.6356	9.7942	9.7719	9.7184	9.5877	9.6115	9.5569	9.8759	9.8282	9.9441	9.9385	9.8441	9.7773	9.8062	9.7941	9.7012	9.7627
Ti	0.0000	0.0000	0.0000	0.0000	0.0000	0.0000	0.0000	0.0000	0.0000	0.0000	0.0000	0.0000	0.0000	0.0000	0.0190	0.0190	0.0000	0.0000	0.0000	0.0000	0.0000	0.0000	0.0000	0.0000
Al	6.9436	6.9686	6.9416	6.4193	6.3947	7.0349	6.8161	6.3008	6.1306	6.1509	6.2370	6.3697	6.3633	6.4065	6.0814	6.0982	6.0251	6.0044	6.1224	6.1537	6.1662	6.1599	6.2349	6.1944
Fe3	0.0000	0.0000	0.0000	0.0000	0.0000	0.0000	0.0000	0.0000	0.0000	0.0000	0.0000	0.0000	0.0000	0.0000	0.0000	0.0000	0.0000	0.0000	0.0000	0.0000	0.0000	0.0000	0.0000	0.0000
Fe2	0.0230	0.0261	0.0276	0.0275	0.0259	0.0645	0.0643	0.0574	0.0484	0.0584	0.0607	0.0533	0.0563	0.0439	0.0544	0.0590	0.0500	0.0559	0.0379	0.0787	0.0333	0.0561	0.0528	0.0816
Mn2	0.0000	0.0000	0.0000	0.0000	0.0000	0.0000	0.0000	0.0000	0.0000	0.0000	0.0000	0.0000	0.0000	0.0000	0.0000	0.0000	0.0000	0.0000	0.0000	0.0000	0.0000	0.0000	0.0000	0.0000
Mg	0.0000	0.0000	0.0000	0.0000	0.0000	0.0000	0.0000	0.0000	0.0000	0.0000	0.0000	0.0000	0.0000	0.0000	0.0000	0.0000	0.0000	0.0000	0.0000	0.0000	0.0000	0.0000	0.0000	0.0000
Ca	3.0545	3.1835	3.1634	2.7188	2.7789	3.2500	3.0534	2.4529	2.2897	2.3492	2.3091	2.4215	2.4252	2.4927	2.1664	2.2434	2.0739	2.1600	2.1858	2.2934	2.1542	2.1800	2.4413	2.2257
Na	0.9472	0.8316	0.8238	1.3511	1.2739	0.8005	0.9617	1.5344	1.7296	1.6528	1.6087	1.5253	1.4805	1.4521	1.6816	1.6932	1.8589	1.7318	1.7720	1.6418	1.8649	1.8161	1.4609	1.6705
K	0.0000	0.0000	0.0000	0.0000	0.0000	0.0000	0.0000	0.0000	0.0258	0.0000	0.0672	0.0651	0.0209	0.0277	0.0530	0.0185	0.0416	0.0692	0.0370	0.0439	0.0369	0.0555	0.0414	0.0530
P	0.0000	0.0000	0.0000	0.0000	0.0000	0.0000	0.0000	0.0000	0.0000	0.0000	0.0000	0.0000	0.0000	0.0000	0.0000	0.0000	0.0000	0.0000	0.0000	0.0000	0.0000	0.0000	0.0000	0.0000
Sr	0.0000	0.0000	0.0000	0.0000	0.0000	0.0000	0.0000	0.0000	0.0000	0.0000	0.0000	0.0000	0.0000	0.0000	0.0000	0.0000	0.0000	0.0000	0.0000	0.0000	0.0000	0.0000	0.0000	0.0000
Ba	0.0000	0.0000	0.0000	0.0000	0.0000	0.0000	0.0000	0.0000	0.0000	0.0000	0.0000	0.0000	0.0000	0.0000	0.0000	0.0000	0.0000	0.0000	0.0000	0.0000	0.0000	0.0000	0.0000	0.0000
Cr	0.0000	0.0000	0.0000	0.0000	0.0000	0.0000	0.0000	0.0000	0.0000	0.0000	0.0000	0.0000	0.0000	0.0000	0.0000	0.0000	0.0000	0.0000	0.0000	0.0000	0.0000	0.0000	0.0000	0.0000
Ni	0.0000	0.0000	0.0000	0.0000	0.0000	0.0000	0.0000	0.0000	0.0000	0.0000	0.0000	0.0000	0.0000	0.0000	0.0000	0.0000	0.0000	0.0000	0.0000	0.0000	0.0000	0.0000	0.0000	0.0000
Total	19.9851	19.9706	19.9488	19.9913	19.9565	20.0164	19.9841	19.9812	20.0180	19.9791	20.0011	20.0226	19.9575	19.9798	19.9317	19.9595	19.9936	19.9598	19.9992	19.9887	20.0616	20.0617	19.9325	19.9948

Table C3f: Continued

Sample	PLGD10C	PLGD11A	PLGD11B	PLGD11C	PLGD12A	PLGD12B	PLGD12C	PLGD34A	PLGD34B	PLGD34C	PLGD37A	PLGD37B	PLGD33A	PLGD33B	PLGD33C	PLGD51A	PLGD51B	PLGD40A	PLGD40B
SiO2	54.60	54.41	53.05	52.86	52.47	53.07	53.78	58.47	56.36	57.51	57.24	58.21	55.65	55.52	54.93	59.24	59.10	61.99	62.10
TiO2	0.00	0.00	0.00	0.00	0.11	0.12	0.11	0.00	0.00	0.00	0.00	0.00	0.00	0.12	0.00	0.00	0.00	0.00	0.00
Al2O3	29.10	28.55	29.79	29.77	29.59	29.68	28.77	25.74	27.15	26.24	26.52	25.89	27.67	27.69	27.92	25.70	25.32	23.42	22.79
FeO	0.34	0.28	0.39	0.43	0.45	0.43	0.33	0.21	0.30	0.24	0.27	0.24	0.28	0.40	0.24	0.11	0.32	0.18	0.22
MnO	0.00	0.00	0.00	0.00	0.00	0.00	0.00	0.00	0.00	0.00	0.00	0.00	0.00	0.00	0.00	0.00	0.00	0.00	0.00
MgO	0.00	0.00	0.00	0.00	0.00	0.00	0.00	0.00	0.00	0.00	0.00	0.00	0.00	0.00	0.00	0.00	0.00	0.00	0.00
CaO	11.53	11.21	12.43	12.67	12.65	12.56	11.62	8.42	9.92	9.49	9.19	8.82	10.59	10.83	10.67	7.80	7.49	5.66	5.52
Na2O	4.64	5.12	4.28	4.00	4.21	4.24	5.16	6.77	5.61	6.11	6.35	6.57	5.49	5.46	5.79	7.25	7.62	8.41	9.14
K2O	0.22	0.26	0.23	0.18	0.22	0.25	0.14	0.09	0.31	0.15	0.20	0.08	0.24	0.23	0.15	0.14	0.21	0.23	0.24
P2O5	0.00	0.00	0.00	0.00	0.00	0.00	0.00	0.00	0.00	0.00	0.00	0.00	0.00	0.00	0.00	0.00	0.00	0.00	0.00
TOTAL	100.43	99.83	100.17	99.91	99.70	100.35	99.91	99.70	99.65	99.74	99.77	99.81	99.92	100.25	99.70	100.24	100.06	99.89	100.01
Sr	0	0	0	0	0	0	0	0	0	0	0	0	0	0	0	0	0	0	0
Ba	0	0	0	0	0	0	0	0	0	0	0	0	0	0	0	0	0	0	0
Cr	0	0	0	0	0	0	0	0	0	0	0	0	0	0	0	0	0	0	0
Ni	0	0	0	0	0	0	0	0	0	0	0	0	0	0	0	0	0	0	0
Si	9.8192	9.8545	9.6061	9.5949	9.5626	9.6003	9.7549	10.4951	10.1751	10.3499	10.3057	10.4485	10.0447	10.0055	9.9547	10.5612	10.5778	11.0259	11.0637
Ti	0.0000	0.0000	0.0000	0.0000	0.0151	0.0163	0.0150	0.0000	0.0000	0.0000	0.0000	0.0000	0.0000	0.0163	0.0000	0.0000	0.0000	0.0000	0.0000
Al	6.1697	6.0961	6.3594	6.3706	6.3576	6.3298	6.1522	5.4469	5.7786	5.5673	5.6291	5.4787	5.8880	5.8830	5.9651	5.4015	5.3427	4.9110	4.7867
Fe3	0.0000	0.0000	0.0000	0.0000	0.0000	0.0000	0.0000	0.0000	0.0000	0.0000	0.0000	0.0000	0.0000	0.0000	0.0000	0.0000	0.0000	0.0000	0.0000
Fe2	0.0511	0.0424	0.0591	0.0653	0.0686	0.0651	0.0501	0.0315	0.0453	0.0361	0.0407	0.0360	0.0423	0.0603	0.0364	0.0164	0.0479	0.0268	0.0328
Mn2	0.0000	0.0000	0.0000	0.0000	0.0000	0.0000	0.0000	0.0000	0.0000	0.0000	0.0000	0.0000	0.0000	0.0000	0.0000	0.0000	0.0000	0.0000	0.0000
Mg	0.0000	0.0000	0.0000	0.0000	0.0000	0.0000	0.0000	0.0000	0.0000	0.0000	0.0000	0.0000	0.0000	0.0000	0.0000	0.0000	0.0000	0.0000	0.0000
Ca	2.2218	2.1755	2.4117	2.4642	2.4703	2.4346	2.2584	1.6194	1.9190	1.8300	1.7729	1.6964	2.0481	2.0913	2.0719	1.4900	1.4364	1.0787	1.0538
Na	1.6180	1.7980	1.5027	1.4078	1.4877	1.4872	1.8147	2.3562	1.9638	2.1321	2.2168	2.2866	1.9214	1.9079	2.0345	2.5061	2.6444	2.9004	3.1573
K	0.0505	0.0601	0.0531	0.0417	0.0512	0.0577	0.0324	0.0206	0.0714	0.0344	0.0459	0.0183	0.0553	0.0529	0.0347	0.0318	0.0480	0.0522	0.0546
P	0.0000	0.0000	0.0000	0.0000	0.0000	0.0000	0.0000	0.0000	0.0000	0.0000	0.0000	0.0000	0.0000	0.0000	0.0000	0.0000	0.0000	0.0000	0.0000
Sr	0.0000	0.0000	0.0000	0.0000	0.0000	0.0000	0.0000	0.0000	0.0000	0.0000	0.0000	0.0000	0.0000	0.0000	0.0000	0.0000	0.0000	0.0000	0.0000
Ba	0.0000	0.0000	0.0000	0.0000	0.0000	0.0000	0.0000	0.0000	0.0000	0.0000	0.0000	0.0000	0.0000	0.0000	0.0000	0.0000	0.0000	0.0000	0.0000
Cr	0.0000	0.0000	0.0000	0.0000	0.0000	0.0000	0.0000	0.0000	0.0000	0.0000	0.0000	0.0000	0.0000	0.0000	0.0000	0.0000	0.0000	0.0000	0.0000
Ni	0.0000	0.0000	0.0000	0.0000	0.0000	0.0000	0.0000	0.0000	0.0000	0.0000	0.0000	0.0000	0.0000	0.0000	0.0000	0.0000	0.0000	0.0000	0.0000
Total	19.9302	20.0265	19.9921	19.9445	20.0130	19.9909	20.0776	19.9698	19.9532	19.9498	20.0111	19.9646	19.9997	20.0171	20.0973	20.0071	20.0971	19.9949	20.1489

Table C4a: Electron microprobe analyses with structural formulae based on 23 oxygens for amphibole from the Glen Tilt pluton.

Sample	AMGT44A	AMGT44B	AMGT44C	AMGT28A	AMGT28B	AMGT28C	AMGT28D	AMGT28E	AMGT28F	AMGT26A	AMGT26B	AMGT26C	AMGT55A	AMGT55B	AMGT55C	AMGT55D
SiO2	48.77	47.21	48.97	48.79	49.64	49.37	45.50	46.80	44.74	46.73	48.03	48.13	46.46	46.50	47.56	47.00
TiO2	0.87	1.62	1.05	1.62	1.01	0.98	1.64	1.49	2.13	1.57	1.15	1.21	1.85	1.96	1.62	1.81
Al2O3	7.34	8.23	6.91	6.71	6.07	6.16	7.89	7.35	8.71	7.77	6.40	6.88	7.97	8.52	8.32	7.82
FeO	13.99	13.87	13.99	11.13	11.47	11.21	15.63	15.27	15.22	15.40	14.45	14.29	13.80	13.19	12.24	12.41
MnO	0.15	0.21	0.22	0.40	0.22	0.11	0.34	0.17	0.27	0.40	0.33	0.34	0.22	0.17	0.21	0.22
MgO	13.31	12.91	13.61	15.18	15.37	15.38	11.54	12.64	11.83	12.44	12.96	12.60	12.82	12.90	13.60	13.63
CaO	11.05	10.95	10.87	12.21	12.08	12.19	12.11	11.90	12.09	11.92	12.17	12.01	11.06	11.38	11.18	11.90
Na2O	1.17	1.36	1.01	0.54	0.61	0.77	0.76	0.84	1.26	1.01	0.66	0.99	1.30	1.30	1.34	1.38
K2O	0.61	0.75	0.58	0.59	0.56	0.55	0.76	0.70	0.83	0.84	0.59	0.67	0.80	0.77	0.62	0.72
P2O5	0.14	0.00	0.14	0.00	0.00	0.00	0.00	0.00	0.00	0.00	0.00	0.00	0.06	0.07	0.00	0.06
TOTAL	97.45	97.11	97.35	97.28	97.03	96.84	96.17	97.16	97.08	98.25	96.74	97.12	96.39	96.89	96.71	97.00
Cr	100	0	0	1100	0	1200	0	0	0	1700	0	0	100	400	0	0
Ni	400	0	0	0	0	0	0	0	0	0	0	0	400	900	200	500
Sr	0	0	0	0	0	0	0	0	0	0	0	0	0	0	0	0
Ba	0	0	0	0	0	0	0	0	0	0	0	0	0	0	0	0
Si	7.1352	6.9623	7.1648	7.0886	7.2210	7.1940	6.8769	6.9623	6.7090	6.8955	7.1343	7.1180	6.9193	6.8706	6.9831	6.9226
Ti	0.0957	0.1797	0.1155	0.1770	0.1105	0.1074	0.1864	0.1667	0.2402	0.1742	0.1285	0.1346	0.2072	0.2178	0.1789	0.2005
Al	1.2660	1.4309	1.1919	1.1493	1.0410	1.0582	1.4059	1.2891	1.5398	1.3517	1.1207	1.1996	1.3994	1.4841	1.4402	1.3579
Fe3	0.0000	0.0000	0.0000	0.0000	0.0000	0.0000	0.0000	0.0000	0.0000	0.0000	0.0000	0.0000	0.0000	0.0000	0.0000	0.0000
Fe2	1.7118	1.7107	1.7118	1.3524	1.3954	1.3661	1.9757	1.8999	1.9087	1.9005	1.7951	1.7675	1.7188	1.6299	1.5030	1.5287
Mn2	0.0186	0.0262	0.0273	0.0492	0.0271	0.0136	0.0435	0.0214	0.0343	0.0500	0.0415	0.0426	0.0278	0.0213	0.0261	0.0274
Mg	2.9021	2.8374	2.9676	3.2869	3.3321	3.3400	2.5994	2.8025	2.6438	2.7357	2.8690	2.7771	2.8455	2.8406	2.9760	2.9919
Ca	1.7322	1.7303	1.7041	1.9008	1.8829	1.9033	1.9612	1.8969	1.9426	1.8847	1.9370	1.9032	1.7649	1.8017	1.7589	1.8781
Na	0.3319	0.3889	0.2865	0.1521	0.1721	0.2176	0.2227	0.2423	0.3663	0.2890	0.1901	0.2839	0.3754	0.3724	0.3815	0.3941
K	0.1139	0.1411	0.1083	0.1094	0.1039	0.1022	0.1465	0.1329	0.1588	0.1581	0.1118	0.1264	0.1520	0.1451	0.1161	0.1353
P	0.0173	0.0000	0.0173	0.0000	0.0000	0.0000	0.0000	0.0000	0.0000	0.0000	0.0000	0.0000	0.0076	0.0088	0.0000	0.0075
Sr	0.0000	0.0000	0.0000	0.0000	0.0000	0.0000	0.0000	0.0000	0.0000	0.0000	0.0000	0.0000	0.0000	0.0000	0.0000	0.0000
Ba	0.0000	0.0000	0.0000	0.0000	0.0000	0.0000	0.0000	0.0000	0.0000	0.0000	0.0000	0.0000	0.0000	0.0000	0.0000	0.0000
Cr	0.0015	0.0000	0.0000	0.0164	0.0000	0.0180	0.0000	0.0000	0.0000	0.0258	0.0000	0.0000	0.0015	0.0061	0.0000	0.0000
Ni	0.0000	0.0000	0.0000	0.0000	0.0000	0.0000	0.0000	0.0000	0.0000	0.0000	0.0000	0.0000	0.0061	0.0136	0.0030	0.0075
Total	15.3322	15.4076	15.2951	15.2822	15.2860	15.3204	15.4183	15.4140	15.5435	15.4651	15.3279	15.3528	15.4254	15.4121	15.3668	15.4515

Table C4a: Continued

Sample	AMGT55E	AMGT35A	AMGT35B	AMGT35C	AMGT35D	AMGT31A	AMGT31B	AMGT31C	AMGT41A	AMGT41B	AMGT41C
SiO2	47.91	45.65	45.75	47.22	47.04	50.71	50.22	50.31	47.59	48.07	47.82
TiO2	1.78	1.26	1.47	1.56	1.82	0.61	0.87	0.84	1.36	0.90	0.96
Al2O3	7.83	7.52	7.85	6.93	7.10	4.89	5.09	5.01	6.75	6.40	6.42
FeO	12.73	15.96	15.91	15.08	14.80	10.61	11.46	11.37	14.32	14.07	14.07
MnO	0.20	0.21	0.24	0.25	0.32	0.23	0.25	0.23	0.41	0.45	0.45
MgO	13.03	11.78	11.96	12.36	12.51	16.16	15.41	15.36	13.62	14.12	13.61
CaO	11.14	12.14	12.07	12.12	11.94	11.81	12.31	12.22	11.93	11.45	11.98
Na2O	1.23	0.38	0.77	0.79	0.95	0.62	0.64	0.64	1.20	0.78	0.89
K2O	0.65	0.78	0.71	0.58	0.54	0.40	0.37	0.38	0.64	0.51	0.59
P2O5	0.13	0.00	0.00	0.00	0.00	0.00	0.00	0.00	0.00	0.00	0.00
TOTAL	96.66	95.68	96.73	97.03	97.02	96.04	96.62	96.36	97.82	96.87	96.79
Cr	300	0	0	1400	0	0	0	0	0	1200	0
Ni	0	0	0	0	0	0	0	0	0	0	0
Sr	0	0	0	0	0	0	0	0	0	0	0
Ba	0	0	0	0	0	0	0	0	0	0	0
Si	7.0436	6.9327	6.8748	7.0239	6.9925	7.3983	7.3310	7.3564	7.0102	7.1083	7.0984
Ti	0.1968	0.1439	0.1661	0.1745	0.2035	0.0669	0.0955	0.0924	0.1507	0.1001	0.1072
Al	1.3571	1.3464	1.3907	1.2153	1.2443	0.8411	0.8760	0.8637	1.1722	1.1157	1.1235
Fe3	0.0000	0.0000	0.0000	0.0000	0.0000	0.0000	0.0000	0.0000	0.0000	0.0000	0.0000
Fe2	1.5652	2.0271	1.9995	1.8760	1.8399	1.2946	1.3991	1.3904	1.7642	1.7400	1.7467
Mn2	0.0249	0.0270	0.0305	0.0315	0.0403	0.0284	0.0309	0.0285	0.0512	0.0564	0.0566
Mg	2.8549	2.6662	2.6784	2.7400	2.7714	3.5137	3.3525	3.3472	2.9900	3.1118	3.0109
Ca	1.7549	1.9755	1.9434	1.9317	1.9018	1.8462	1.9255	1.9146	1.8830	1.8142	1.9055
Na	0.3506	0.1119	0.2244	0.2278	0.2738	0.1754	0.1811	0.1815	0.3427	0.2236	0.2562
K	0.1219	0.1511	0.1361	0.1101	0.1024	0.0745	0.0689	0.0709	0.1203	0.0962	0.1117
P	0.0162	0.0000	0.0000	0.0000	0.0000	0.0000	0.0000	0.0000	0.0000	0.0000	0.0000
Sr	0.0000	0.0000	0.0000	0.0000	0.0000	0.0000	0.0000	0.0000	0.0000	0.0000	0.0000
Ba	0.0000	0.0000	0.0000	0.0000	0.0000	0.0000	0.0000	0.0000	0.0000	0.0000	0.0000
Cr	0.0045	0.0000	0.0000	0.0214	0.0000	0.0000	0.0000	0.0000	0.0000	0.0182	0.0000
Ni	0.0000	0.0000	0.0000	0.0000	0.0000	0.0000	0.0000	0.0000	0.0000	0.0000	0.0000
Total	15.2907	15.3817	15.4440	15.3522	15.3700	15.2391	15.2605	15.2455	15.4845	15.3846	15.4166

Table C4b: Electron microprobe analyses with structural formulae based on 23 oxygens for biotite of the Glen Tilt pluton.

Sample	BIGT44A	BIGT44B	BIGT28A	BIGT28B	BIGT45A	BIGT45B	BIGT45C	BIGT45D	BIGT45E	BIGT55A	BIGT55B	BIGT41A	BIGT41B	BIGT41C	BIGT33A	BIGT33B	BIGT33C	BIGT48A	BIGT48B	BIGT48C
SiO2	37.25	38.43	37.76	37.34	36.55	36.68	36.47	36.36	36.21	37.65	37.75	37.80	38.64	38.50	37.44	37.63	37.82	37.71	38.42	37.33
TiO2	3.57	3.93	3.73	3.87	3.87	3.88	4.49	4.03	3.57	3.71	4.08	2.84	3.36	3.75	4.26	3.86	3.51	1.93	1.93	1.56
Al2O3	14.89	14.70	14.58	14.38	14.38	14.69	14.86	14.70	14.60	16.13	15.28	14.69	15.25	14.96	15.60	15.70	15.82	16.74	16.27	17.17
FeO	17.70	17.06	14.96	14.91	20.33	20.16	19.51	19.35	20.02	17.46	18.97	18.59	17.46	18.05	18.24	17.27	18.77	16.12	16.16	17.66
MnO	0.19	0.05	0.12	0.14	0.21	0.28	0.00	0.19	0.17	0.32	0.39	0.33	0.23	0.27	0.38	0.36	0.30	0.92	0.95	1.09
MgO	13.48	13.03	14.48	14.52	10.48	10.66	10.50	10.88	10.72	11.25	10.23	11.48	11.64	11.42	9.89	10.31	10.53	10.12	10.75	10.04
CaO	0.05	0.03	0.00	0.00	0.00	0.09	0.00	0.11	0.11	0.00	0.19	0.02	0.00	0.00	0.00	0.00	0.01	0.02	0.04	0.08
Na2O	0.20	0.14	0.00	0.00	0.00	0.00	0.00	0.00	0.00	0.15	0.09	0.18	0.19	0.09	0.13	0.06	0.06	0.20	0.29	0.14
K2O	9.03	8.75	9.55	9.55	9.56	9.63	9.56	9.60	9.54	9.28	9.83	9.18	8.96	9.00	9.65	9.60	9.20	9.26	9.28	9.50
P2O5	0.04	0.01	0.00	0.00	0.00	0.00	0.00	0.00	0.00	0.00	0.00	0.00	0.04	0.01	0.03	0.01	0.09	0.06	0.04	0.00
TOTAL	96.41	96.16	95.18	94.71	95.38	96.07	95.39	95.22	94.94	96.02	96.82	95.20	95.86	96.11	95.72	94.87	96.18	93.08	94.13	94.62
Sr	0	0	0	0	0	0	0	0	0	300	0	400	500	300	600	700	200	0	0	200
Ba	100	300	0	0	0	0	0	0	0	400	100	500	400	300	400	0	500	0	0	300
Cr	0	0	0	0	0	0	0	0	0	0	0	0	0	0	0	0	0	0	0	0
Ni	0	0	0	0	0	0	0	0	0	0	0	0	0	0	0	0	0	0	0	0
Si	5.8141	5.9603	5.9001	5.8723	5.8685	5.8425	5.8236	5.8246	5.8372	5.8830	5.9197	5.9979	6.0232	6.0088	5.9115	5.9584	5.9275	6.0433	6.0865	5.9472
Ti	0.4191	0.4584	0.4383	0.4577	0.4673	0.4648	0.5392	0.4855	0.4328	0.4360	0.4812	0.3389	0.3939	0.4402	0.5059	0.4597	0.4137	0.2326	0.2299	0.1869
Al	2.7399	2.6878	2.6858	2.6661	2.7220	2.7585	2.7975	2.7762	2.7747	2.9713	2.8248	2.7480	2.8025	2.7526	2.9038	2.9308	2.9231	3.1627	3.0387	3.2249
Fe3	0.0000	0.0000	0.0000	0.0000	0.0000	0.0000	0.0000	0.0000	0.0000	0.0000	0.0000	0.0000	0.0000	0.0000	0.0000	0.0000	0.0000	0.0000	0.0000	0.0000
Fe2	2.3105	2.2128	1.9549	1.9610	2.7299	2.6856	2.6055	2.5924	2.6991	2.2817	2.4879	2.4670	2.2762	2.3560	2.4086	2.2870	2.4603	2.1605	2.1410	2.3530
Mn2	0.0251	0.0066	0.0159	0.0186	0.0286	0.0378	0.0000	0.0258	0.0232	0.0424	0.0518	0.0444	0.0304	0.0357	0.0508	0.0483	0.0398	0.1249	0.1275	0.1471
Mg	3.1357	3.0118	3.3719	3.4031	2.5077	2.5305	2.4988	2.5975	2.5755	2.6198	2.3908	2.7148	2.7041	2.6563	2.3272	2.4330	2.4596	2.4170	2.5380	2.3838
Ca	0.0084	0.0050	0.0000	0.0000	0.0000	0.0154	0.0000	0.0189	0.0190	0.0000	0.0319	0.0034	0.0000	0.0000	0.0000	0.0000	0.0017	0.0034	0.0068	0.0137
Na	0.0605	0.0421	0.0000	0.0000	0.0000	0.0000	0.0000	0.0000	0.0000	0.0454	0.0274	0.0554	0.0574	0.0272	0.0398	0.0184	0.0182	0.0621	0.0891	0.0432
K	1.7981	1.7314	1.9037	1.9161	1.9583	1.9569	1.9476	1.9620	1.9620	1.8500	1.9666	1.8584	1.7819	1.7921	1.9439	1.9393	1.8396	1.8933	1.8756	1.9309
Cr	0.0053	0.0013	0.0000	0.0000	0.0000	0.0000	0.0000	0.0000	0.0000	0.0000	0.0000	0.0000	0.0053	0.0013	0.0040	0.0013	0.0119	0.0081	0.0054	0.0000
Ni	0.0000	0.0000	0.0000	0.0000	0.0000	0.0000	0.0000	0.0000	0.0000	0.0000	0.0000	0.0000	0.0000	0.0000	0.0000	0.0000	0.0000	0.0000	0.0000	0.0000
Sr	0.0000	0.0000	0.0000	0.0000	0.0000	0.0000	0.0000	0.0000	0.0000	0.0000	0.0000	0.0000	0.0000	0.0000	0.0000	0.0000	0.0000	0.0000	0.0000	0.0000
Ba	0.0000	0.0000	0.0000	0.0000	0.0000	0.0000	0.0000	0.0000	0.0000	0.0048	0.0000	0.0065	0.0080	0.0048	0.0097	0.0114	0.0032	0.0000	0.0000	0.0033
Total	0.0016	0.0048	0.0000	0.0000	0.0000	0.0000	0.0000	0.0000	0.0000	0.0064	0.0016	0.0081	0.0064	0.0048	0.0065	0.0000	0.0080	0.0000	0.0000	0.0049
	16.3183	16.1222	16.2706	16.2950	16.2823	16.2919	16.2122	16.2828	16.3236	16.1407	16.1837	16.2428	16.0893	16.0799	16.1117	16.0877	16.1066	16.1082	16.1385	16.2389

Table C4c: Electron microprobe analyses with structural formulae based on 8 oxygens for plagioclase of the Glen Tilt pluton.

Sample	PLGT44A	PLGT44B	PLGT44C	PLGT28A	PLGT28B	PLGT29A	PLGT29B	PLGT45A	PLGT45B	PLGT45C	PLGT55A	PLGT55B	PLGT26A	PLGT26B	PLGT26C	PLGT41A	PLGT41B	PLGT41C	PLGT33A	PLGT33B	PLGT48A	PLGT48B	PLGT48C	PLGT48D
SiO2	59.12	54.88	58.42	57.99	55.56	60.44	59.87	59.03	59.77	58.87	57.75	58.88	60.50	60.66	61.27	63.29	63.21	62.94	61.65	61.91	65.87	65.89	65.24	65.94
TiO2	0.04	0.02	0.03	0.00	0.14	0.00	0.00	0.00	0.00	0.00	0.02	0.05	0.00	0.00	0.00	0.00	0.05	0.03	0.02	0.02	0.00	0.02	0.01	0.02
Al2O3	25.92	29.51	26.32	25.93	27.85	24.85	24.97	25.42	24.98	25.74	27.80	27.00	24.88	24.96	24.44	22.84	23.23	23.40	24.57	24.00	20.90	20.92	21.32	20.63
FeO	0.12	0.18	0.11	0.11	0.12	0.15	0.14	0.12	0.14	0.20	0.12	0.27	0.00	0.00	0.18	0.16	0.14	0.12	0.12	0.12	0.06	0.08	0.04	0.02
MnO	0.00	0.00	0.00	0.00	0.00	0.00	0.00	0.00	0.00	0.00	0.04	0.00	0.00	0.00	0.00	0.00	0.00	0.00	0.00	0.00	0.03	0.00	0.03	0.03
MgO	0.00	0.02	0.00	0.00	0.00	0.00	0.00	0.00	0.00	0.00	0.01	0.01	0.00	0.00	0.00	0.00	0.03	0.00	0.03	0.00	0.00	0.00	0.00	0.00
CaO	7.10	9.92	7.28	8.94	9.35	6.39	7.52	7.51	7.53	7.12	8.42	7.19	6.49	6.55	5.89	3.73	3.70	3.78	4.57	4.54	1.92	1.65	1.95	1.61
Na2O	7.50	5.01	7.64	6.89	6.77	7.68	7.27	7.46	7.28	7.77	5.47	5.88	7.80	7.87	8.10	9.42	9.39	9.34	8.63	8.81	10.51	11.15	10.66	11.34
K2O	0.19	0.11	0.14	0.11	0.00	0.29	0.21	0.25	0.21	0.09	0.24	0.61	0.21	0.00	0.00	0.47	0.24	0.41	0.44	0.44	1.00	0.23	0.29	0.27
P2O5	0.00	0.17	0.09	0.00	0.00	0.00	0.00	0.00	0.00	0.00	0.10	0.03	0.00	0.00	0.00	0.00	0.00	0.00	0.06	0.03	0.00	0.00	0.00	0.00
TOTAL	99.99	99.82	100.03	99.97	99.79	99.80	99.98	99.79	99.91	99.79	99.97	99.92	99.88	100.04	99.88	99.91	99.99	100.02	100.09	99.87	100.29	99.94	99.54	99.86
Cr	0	0	0	0	0	0	0	0	0	0	0	0	0	0	0	0	0	0	0	0	0	0	0	0
Ni	0	0	0	0	0	0	0	0	0	0	0	0	0	0	0	0	0	0	0	0	0	0	0	0
Sr	0	0	0	0	0	0	0	0	0	0	0	0	0	0	0	0	0	0	0	0	0	0	0	0
Ba	0	0	0	0	0	0	0	0	0	0	0	0	0	0	0	0	0	0	0	0	0	0	0	0
Si	10.5549	9.8621	10.4433	10.4102	10.0299	10.7792	10.6879	10.5793	10.6797	10.5452	10.2935	10.4862	10.7767	10.7776	10.8880	11.2183	11.1779	11.1415	10.9239	10.9976	11.6033	11.6108	11.5427	11.6370
Ti	0.0054	0.0027	0.0040	0.0000	0.0190	0.0000	0.0000	0.0000	0.0000	0.0000	0.0027	0.0067	0.0000	0.0000	0.0000	0.0000	0.0066	0.0040	0.0027	0.0027	0.0000	0.0027	0.0013	0.0027
Al	5.4556	6.2519	5.5469	5.4878	5.9271	5.2249	5.2552	5.3709	5.2620	5.4357	5.8418	5.6689	5.2248	5.2282	5.1202	4.7728	4.6429	4.8834	5.1326	5.0261	4.3404	4.3460	4.4470	4.2922
Fe3	0.0000	0.0000	0.0000	0.0000	0.0000	0.0000	0.0000	0.0000	0.0000	0.0000	0.0000	0.0000	0.0000	0.0000	0.0000	0.0000	0.0000	0.0000	0.0000	0.0000	0.0000	0.0000	0.0000	0.0000
Fe2	0.0179	0.0271	0.0164	0.0165	0.0181	0.0224	0.0209	0.0180	0.0209	0.0300	0.0179	0.0402	0.0000	0.0000	0.0268	0.0237	0.0207	0.0178	0.0178	0.0178	0.0088	0.0118	0.0059	0.0030
Mn2	0.0000	0.0000	0.0000	0.0000	0.0000	0.0000	0.0000	0.0000	0.0000	0.0000	0.0060	0.0000	0.0000	0.0000	0.0000	0.0000	0.0000	0.0000	0.0000	0.0000	0.0045	0.0000	0.0045	0.0045
Mg	0.0000	0.0054	0.0000	0.0000	0.0000	0.0000	0.0000	0.0000	0.0000	0.0000	0.0027	0.0027	0.0000	0.0000	0.0000	0.0000	0.0079	0.0000	0.0079	0.0000	0.0000	0.0000	0.0000	0.0000
Ca	1.3582	1.9101	1.3944	1.7196	1.8086	1.2211	1.4384	1.4422	1.4417	1.3666	1.6081	1.3721	1.2387	1.2470	1.1215	0.7084	0.7011	0.7170	0.8677	0.8641	0.3624	0.3115	0.3697	0.3044
Na	2.5963	1.7457	2.6481	2.3982	2.3697	2.6556	2.5164	2.5923	2.5222	2.6987	1.8905	2.0305	2.6940	2.7112	2.7909	3.2375	3.2196	3.2058	2.9650	3.0344	3.5897	3.8096	3.6570	3.8804
K	0.0433	0.0252	0.0319	0.0252	0.0000	0.0660	0.0478	0.0572	0.0479	0.0206	0.0546	0.1386	0.0477	0.0000	0.0000	0.1063	0.0541	0.0926	0.0995	0.0997	0.2247	0.0517	0.0655	0.0608
P	0.0000	0.0259	0.0136	0.0000	0.0000	0.0000	0.0000	0.0000	0.0000	0.0000	0.0151	0.0045	0.0000	0.0000	0.0000	0.0000	0.0000	0.0000	0.0090	0.0045	0.0000	0.0000	0.0000	0.0000
Sr	0.0000	0.0000	0.0000	0.0000	0.0000	0.0000	0.0000	0.0000	0.0000	0.0000	0.0000	0.0000	0.0000	0.0000	0.0000	0.0000	0.0000	0.0000	0.0000	0.0000	0.0000	0.0000	0.0000	0.0000
Ba	0.0000	0.0000	0.0000	0.0000	0.0000	0.0000	0.0000	0.0000	0.0000	0.0000	0.0000	0.0000	0.0000	0.0000	0.0000	0.0000	0.0000	0.0000	0.0000	0.0000	0.0000	0.0000	0.0000	0.0000
Cr	0.0000	0.0000	0.0000	0.0000	0.0000	0.0000	0.0000	0.0000	0.0000	0.0000	0.0000	0.0000	0.0000	0.0000	0.0000	0.0000	0.0000	0.0000	0.0000	0.0000	0.0000	0.0000	0.0000	0.0000
Ni	0.0000	0.0000	0.0000	0.0000	0.0000	0.0000	0.0000	0.0000	0.0000	0.0000	0.0000	0.0000	0.0000	0.0000	0.0000	0.0000	0.0000	0.0000	0.0000	0.0000	0.0000	0.0000	0.0000	0.0000
Total	20.0316	19.8559	20.0986	20.0576	20.1724	19.9693	19.9667	20.0599	19.9743	20.0966	19.7328	19.7504	19.9818	19.9639	19.9474	20.0671	20.0309	20.0620	20.0259	20.0470	20.1338	20.1442	20.0936	20.1646

Table C5a: Electron microprobe analyses with structural formulae based on 6 oxygens for orthopyroxenes from the Carsphairn pluton.

Sample	OP77026A	OP77026B	OP77026C	OP77031A	OP77031B	OP77031C	OP77032A	OP77032B	OP77032C	OP77032D	OPAS17A	OPAS17B	OPAS18A	OPAS18B	OPAS18C	OPAS18D	OPAS40A	OPAS40B	OPAS40C
SiO2	51.30	51.33	51.04	51.26	51.18	51.57	53.26	53.09	53.51	53.67	51.60	51.58	51.45	51.77	51.32	51.85	50.48	50.28	50.12
TiO2	0.27	0.25	0.36	0.36	0.32	0.16	0.30	0.37	0.26	0.21	0.34	0.41	0.29	0.42	0.30	0.18	0.22	0.27	0.22
Al2O3	0.61	0.62	0.79	0.71	0.60	0.69	0.52	0.44	0.85	0.51	0.73	0.47	1.13	0.62	0.49	0.63	0.46	0.48	0.55
FeO	28.16	27.93	26.92	27.61	27.90	28.25	21.43	21.10	19.78	20.53	27.26	27.48	25.59	25.69	27.54	26.85	30.47	30.58	30.43
MnO	1.02	0.76	0.81	0.96	0.80	0.99	0.43	0.47	0.49	0.51	0.88	0.68	0.93	0.80	0.95	0.97	1.33	1.34	1.36
MgO	17.19	17.95	17.94	18.02	17.13	17.48	23.38	23.35	23.17	23.83	17.72	17.70	19.26	18.23	18.11	18.42	15.71	15.60	15.86
CaO	1.74	1.04	1.90	1.29	2.07	0.94	0.76	1.25	1.69	1.09	1.48	1.48	1.23	2.27	1.13	1.24	1.24	1.22	1.27
Na2O	0.00	0.00	0.00	0.00	0.00	0.00	0.00	0.00	0.00	0.00	0.00	0.00	0.00	0.00	0.00	0.00	0.02	0.03	0.03
K2O	0.00	0.00	0.00	0.00	0.00	0.00	0.00	0.00	0.00	0.00	0.00	0.00	0.00	0.00	0.00	0.00	0.00	0.00	0.00
P2O5	0.00	0.00	0.00	0.00	0.00	0.00	0.00	0.00	0.00	0.00	0.00	0.00	0.00	0.00	0.00	0.00	0.00	0.00	0.00
TOTAL	100.44	99.88	99.76	100.21	100.00	100.08	100.08	100.07	99.87	100.35	100.01	100.00	100.02	99.80	99.84	100.14	99.94	99.83	99.87
Cr	0	0	0	0	0	0	0	0	1200	0	0	2000	0	0	0	0	100	300	300
Ni	1500	0	0	0	0	0	0	0	0	0	0	0	1400	0	0	0	0	0	0
Sr	0	0	0	0	0	0	0	0	0	0	0	0	0	0	0	0	0	0	0
Ba	0	0	0	0	0	0	0	0	0	0	0	0	0	0	0	0	0	0	0
Si	1.9714	1.9742	1.9632	1.9658	1.9728	1.9819	1.9746	1.9700	1.9770	1.9775	1.9778	1.9783	1.9577	1.9781	1.9739	1.9797	1.9733	1.9697	1.9627
Ti	0.0078	0.0072	0.0104	0.0104	0.0093	0.0046	0.0084	0.0103	0.0072	0.0058	0.0098	0.0118	0.0083	0.0121	0.0087	0.0052	0.0065	0.0080	0.0065
Al	0.0276	0.0281	0.0358	0.0321	0.0273	0.0313	0.0227	0.0192	0.0370	0.0222	0.0330	0.0213	0.0507	0.0279	0.0222	0.0284	0.0212	0.0222	0.0254
Fe3	0.0000	0.0000	0.0000	0.0000	0.0000	0.0000	0.0000	0.0000	0.0000	0.0000	0.0000	0.0000	0.0000	0.0000	0.0000	0.0000	0.0000	0.0000	0.0000
Fe2	0.9050	0.8984	0.8660	0.8855	0.8994	0.9080	0.6645	0.6548	0.6112	0.6326	0.8738	0.8815	0.8143	0.8209	0.8859	0.8574	0.9961	1.0019	0.9966
Mn2	0.0332	0.0248	0.0264	0.0312	0.0261	0.0322	0.0135	0.0148	0.0153	0.0159	0.0286	0.0221	0.0300	0.0259	0.0310	0.0314	0.0440	0.0445	0.0451
Mg	0.9845	1.0289	1.0284	1.0299	0.9840	1.0012	1.2918	1.2913	1.2758	1.3086	1.0122	1.0117	1.0922	1.0381	1.0381	1.0482	0.9152	0.9108	0.9256
Ca	0.0716	0.0429	0.0783	0.0530	0.0855	0.0387	0.0302	0.0497	0.0669	0.0430	0.0608	0.0608	0.0501	0.0929	0.0466	0.0507	0.0519	0.0512	0.0533
Na	0.0000	0.0000	0.0000	0.0000	0.0000	0.0000	0.0000	0.0000	0.0000	0.0000	0.0000	0.0000	0.0000	0.0000	0.0000	0.0000	0.0015	0.0023	0.0023
K	0.0000	0.0000	0.0000	0.0000	0.0000	0.0000	0.0000	0.0000	0.0000	0.0000	0.0000	0.0000	0.0000	0.0000	0.0000	0.0000	0.0000	0.0000	0.0000
P	0.0000	0.0000	0.0000	0.0000	0.0000	0.0000	0.0000	0.0000	0.0000	0.0000	0.0000	0.0000	0.0000	0.0000	0.0000	0.0000	0.0000	0.0000	0.0000
Sr	0.0000	0.0000	0.0000	0.0000	0.0000	0.0000	0.0000	0.0000	0.0000	0.0000	0.0000	0.0000	0.0000	0.0000	0.0000	0.0000	0.0000	0.0000	0.0000
Ba	0.0000	0.0000	0.0000	0.0000	0.0000	0.0000	0.0000	0.0000	0.0000	0.0000	0.0000	0.0000	0.0000	0.0000	0.0000	0.0000	0.0000	0.0000	0.0000
Cr	0.0000	0.0000	0.0000	0.0000	0.0000	0.0000	0.0000	0.0000	0.0046	0.0000	0.0000	0.0079	0.0000	0.0000	0.0000	0.0000	0.0004	0.0012	0.0012
Ni	0.0059	0.0000	0.0000	0.0000	0.0000	0.0000	0.0000	0.0000	0.0000	0.0000	0.0000	0.0000	0.0054	0.0000	0.0000	0.0000	0.0000	0.0000	0.0000
Total	4.0070	4.0045	4.0085	4.0078	4.0043	3.9979	4.0057	4.0101	3.9950	4.0056	3.9959	3.9953	4.0087	3.9959	4.0063	4.0009	4.0102	4.0117	4.0187

Table C5b: Electron microprobe analyses with structural formulae based on 6 oxygens for clinopyroxes from the Carsphairn pluton.

Sample	CP77032A	CP77032B	CP77032C	CP77026A	CP77026B	CP77026C
SiO2	51.99	51.61	51.27	52.53	52.46	52.39
TiO2	0.15	0.21	0.29	0.12	0.19	0.22
Al2O3	0.67	0.60	0.50	0.68	0.62	0.65
FeO	14.26	15.42	14.95	12.33	12.41	12.24
MnO	0.59	1.14	0.95	0.41	0.39	0.42
MgO	11.61	10.51	10.86	12.84	12.77	12.86
CaO	20.75	20.30	20.99	21.16	21.09	21.18
Na2O	0.00	0.00	0.00	0.00	0.00	0.00
K2O	0.00	0.00	0.00	0.00	0.00	0.00
P2O5	0.00	0.00	0.00	0.00	0.00	0.00
TOTAL	100.02	99.79	99.81	100.07	99.93	99.96
Sr	0	0	0	0	0	0
Ba	0	0	0	0	0	0
Cr	0	0	0	0	0	0
Ni	0	0	0	0	0	0
Si	1.9824	1.9866	1.9739	1.9834	1.9841	1.9806
Ti	0.0043	0.0061	0.0084	0.0034	0.0054	0.0063
Al	0.0301	0.0272	0.0227	0.0303	0.0276	0.0290
Fe3	0.0000	0.0000	0.0000	0.0000	0.0000	0.0000
Fe2	0.4547	0.4964	0.4814	0.3893	0.3925	0.3870
Mn2	0.0191	0.0372	0.0310	0.0131	0.0125	0.0134
Mg	0.6598	0.6029	0.6231	0.7225	0.7198	0.7245
Ca	0.8478	0.8373	0.8659	0.8561	0.8547	0.8579
Na	0.0000	0.0000	0.0000	0.0000	0.0000	0.0000
K	0.0000	0.0000	0.0000	0.0000	0.0000	0.0000
P	0.0000	0.0000	0.0000	0.0000	0.0000	0.0000
Sr	0.0000	0.0000	0.0000	0.0000	0.0000	0.0000
Ba	0.0000	0.0000	0.0000	0.0000	0.0000	0.0000
Cr	0.0000	0.0000	0.0000	0.0000	0.0000	0.0000
Ni	0.0000	0.0000	0.0000	0.0000	0.0000	0.0000
Total	3.9982	3.9937	4.0064	3.9981	3.9967	3.9987

Table C5c: Electron microprobe analyses with structural formulae based on 23 oxygens for amphibole of the Carsphairn pluton.

Sample	AMAS38A	AMAS38B	AM77026A	AM77026B	AM77026C	AM77032A	AM77032B	AM77032C	AM77031A	AMAS17A	AMAS17B	AMAS48A	AMAS48B	AMAS46A	AMAS46B
SiO2	46.31	49.65	46.66	46.10	45.57	49.54	49.58	51.68	48.53	49.56	49.69	47.95	48.25	46.85	46.30
TiO2	1.04	0.48	1.22	1.48	1.52	0.55	0.80	0.50	1.01	0.64	0.62	1.01	1.00	0.45	1.04
Al2O3	6.70	4.61	6.15	6.84	6.81	5.50	5.33	4.49	5.04	4.83	4.62	5.51	5.26	5.53	5.69
FeO	17.51	15.96	20.11	20.85	20.65	18.54	11.20	10.38	17.42	17.07	16.86	17.16	17.98	18.38	18.51
MnO	0.39	0.57	1.08	1.02	1.01	0.88	0.21	0.16	0.62	0.52	0.53	0.45	0.53	0.44	0.39
MgO	12.13	13.91	9.83	8.85	9.22	11.27	16.19	17.36	11.94	13.59	12.82	13.48	13.60	12.59	12.13
CaO	10.96	10.72	10.35	10.76	10.50	11.10	11.45	11.39	11.41	10.69	10.89	8.08	8.51	7.91	7.96
Na2O	1.48	0.63	1.14	1.05	1.17	0.56	0.53	0.49	0.60	0.84	0.80	1.22	1.27	0.27	0.31
K2O	0.75	0.37	0.52	0.58	0.63	0.39	0.55	0.41	0.38	0.39	0.40	0.50	0.54	2.94	2.90
P2O5	0.00	0.00	0.00	0.00	0.00	0.00	0.00	0.00	0.00	0.00	0.00	0.00	0.00	0.00	0.00
TOTAL	97.27	96.90	97.06	97.53	97.08	98.33	96.16	96.86	96.95	98.29	97.23	95.36	96.94	95.66	95.23
Cr	0	0	0	0	0	0	3200	0	0	1600	0	0	0	2950	0
Ni	0	0	0	0	0	0	0	0	0	0	0	0	0	0	0
Sr	0	0	0	0	0	0	0	0	0	0	0	0	0	0	0
Ba	0	0	0	0	0	0	0	0	0	0	0	0	0	0	0
Si	6.9734	7.3642	7.1099	7.0251	6.9817	7.3338	7.2592	7.4438	7.2749	7.2902	7.3811	7.2487	7.2177	7.1966	7.1569
Ti	0.1178	0.0535	0.1398	0.1696	0.1751	0.0612	0.0881	0.0542	0.1139	0.0708	0.0693	0.1148	0.1125	0.0520	0.1209
Al	1.1894	0.8061	1.1048	1.2288	1.2300	0.9599	0.9200	0.7624	0.8907	0.8376	0.8091	0.9820	0.9276	1.0014	1.0369
Fe3	0.0000	0.0000	0.0000	0.0000	0.0000	0.0000	0.0000	0.0000	0.0000	0.0000	0.0000	0.0000	0.0000	0.0000	0.0000
Fe2	2.2051	1.9798	2.5628	2.6573	2.6459	2.2954	1.3714	1.2504	2.1839	2.1000	2.0945	2.1695	2.2494	2.3612	2.3929
Mn2	0.0497	0.0716	0.1394	0.1317	0.1311	0.1103	0.0260	0.0195	0.0787	0.0648	0.0667	0.0576	0.0672	0.0573	0.0511
Mg	2.7222	3.0748	2.2323	2.0099	2.1052	2.4864	3.5327	3.7265	2.6675	2.9793	2.8381	3.0370	3.0319	2.8822	2.7944
Ca	1.7684	1.7037	1.6899	1.7569	1.7237	1.7607	1.7963	1.7579	1.8327	1.6849	1.7333	1.3088	1.3640	1.3019	1.3184
Na	0.4321	0.1812	0.3368	0.3102	0.3476	0.1607	0.1505	0.1368	0.1744	0.2396	0.2304	0.3576	0.3684	0.0804	0.0929
K	0.1441	0.0700	0.1011	0.1128	0.1231	0.0737	0.1027	0.0753	0.0727	0.0732	0.0758	0.0964	0.1031	0.5762	0.5719
P	0.0000	0.0000	0.0000	0.0000	0.0000	0.0000	0.0000	0.0000	0.0000	0.0000	0.0000	0.0000	0.0000	0.0000	0.0000
Sr	0.0000	0.0000	0.0000	0.0000	0.0000	0.0000	0.0000	0.0000	0.0000	0.0000	0.0000	0.0000	0.0000	0.0000	0.0000
Ba	0.0000	0.0000	0.0000	0.0000	0.0000	0.0000	0.0000	0.0000	0.0000	0.0000	0.0000	0.0000	0.0000	0.0000	0.0000
Cr	0.0000	0.0000	0.0000	0.0000	0.0000	0.0000	0.0482	0.0000	0.0000	0.0242	0.0000	0.0000	0.0000	0.0466	0.0000
Ni	0.0000	0.0000	0.0000	0.0000	0.0000	0.0000	0.0000	0.0000	0.0000	0.0000	0.0000	0.0000	0.0000	0.0000	0.0000
Total	15.6022	15.3048	15.4168	15.4024	15.4635	15.2422	15.2952	15.2269	15.2894	15.3645	15.2982	15.3725	15.4417	15.5557	15.5362

Table C5d: Electron microprobe analyses with structural formulae based on 23 oxygens for biotites of the Carsphairn pluton.

Sample	BIAS38A	BIAS38B	BIAS38C	BIAS38D	BI77026A	BI77026B	BI77026C	BI77026D	BI77026E	BI77031A	BI77031B	BI77031C	BI77031D	BI77031E	BI77031F	BI77032A
SiO2	37.17	36.80	36.74	37.39	35.98	35.49	36.01	35.65	36.76	37.31	37.26	36.99	36.88	36.66	36.10	38.89
TiO2	4.36	3.98	3.92	4.40	4.88	4.73	4.91	4.72	4.22	4.93	4.31	4.64	4.79	4.41	4.82	5.33
Al2O3	13.48	13.61	13.39	13.58	13.72	13.60	13.52	12.90	13.49	13.12	13.40	13.88	13.51	13.24	13.56	13.15
FeO	20.07	19.92	20.10	19.63	22.60	22.88	22.90	25.94	19.63	20.02	18.73	19.78	21.16	20.92	21.65	12.56
MnO	0.26	0.14	0.00	0.14	0.38	0.41	0.37	0.00	0.00	0.11	0.15	0.12	0.18	0.29	0.36	0.00
MgO	11.82	11.55	11.59	11.72	8.92	8.88	9.03	7.02	11.13	11.24	12.93	11.39	10.31	10.61	10.26	16.19
CaO	0.00	0.00	0.00	0.00	0.11	0.11	0.10	0.09	0.00	0.00	0.00	0.00	0.00	0.00	0.00	0.00
Na2O	0.00	0.00	0.00	0.00	0.00	0.00	0.00	0.00	0.00	0.00	0.00	0.32	0.00	0.00	0.00	0.00
K2O	9.23	9.11	9.18	9.36	9.42	9.19	9.34	9.04	9.22	9.25	9.43	8.92	9.03	9.46	9.18	9.51
P2O5	0.00	0.00	0.00	0.00	0.00	0.00	0.00	0.00	0.00	0.00	0.00	0.00	0.00	0.00	0.00	0.00
TOTAL	96.39	95.11	94.92	96.22	96.01	95.29	96.18	95.36	94.45	95.98	96.21	96.04	95.86	95.59	95.93	95.63
Sr	0	0	0	0	0	0	0	0	0	0	0	0	0	0	0	0
Ba	0	0	0	0	0	0	0	0	0	0	0	0	0	0	0	0
Cr	0	0	0	0	0	0	0	0	0	0	0	0	0	0	0	0
Ni	0	0	0	0	0	0	0	0	0	0	0	0	0	0	0	0
Si	5.8860	5.9000	5.9095	5.9151	5.8193	5.7957	5.8202	5.8891	5.9287	5.9294	5.8787	5.8624	5.8975	5.8982	5.8068	5.9731
Ti	0.5192	0.4799	0.4742	0.5235	0.5936	0.5809	0.5968	0.5864	0.5119	0.5892	0.5114	0.5530	0.5761	0.5336	0.5831	0.6157
Al	2.5165	2.5725	2.5391	2.5328	2.6161	2.6183	2.5762	2.5123	2.5650	2.4581	2.4925	2.5934	2.5469	2.5113	2.5714	2.3811
Fe3	0.0000	0.0000	0.0000	0.0000	0.0000	0.0000	0.0000	0.0000	0.0000	0.0000	0.0000	0.0000	0.0000	0.0000	0.0000	0.0000
Fe2	2.6580	2.6710	2.7038	2.5972	3.0570	3.1248	3.0955	3.5837	2.6477	2.6609	2.4715	2.6217	2.8299	2.8149	2.9125	1.6133
Mn2	0.0349	0.0190	0.0000	0.0188	0.0521	0.0567	0.0507	0.0000	0.0000	0.0148	0.0200	0.0161	0.0244	0.0395	0.0491	0.0000
Mg	2.7895	2.7598	2.7783	2.7632	2.1501	2.1612	2.1751	1.7283	2.6752	2.6621	3.0403	2.6903	2.4571	2.5440	2.4596	3.7059
Ca	0.0000	0.0000	0.0000	0.0000	0.0191	0.0192	0.0173	0.0159	0.0000	0.0000	0.0000	0.0000	0.0000	0.0000	0.0000	0.0000
Na	0.0000	0.0000	0.0000	0.0000	0.0000	0.0000	0.0000	0.0000	0.0000	0.0000	0.0000	0.0983	0.0000	0.0000	0.0000	0.0000
K	1.8647	1.8634	1.8838	1.8891	1.9438	1.9147	1.9260	1.9052	1.8971	1.8755	1.8982	1.8036	1.8422	1.9418	1.8839	1.8635
P	0.0000	0.0000	0.0000	0.0000	0.0000	0.0000	0.0000	0.0000	0.0000	0.0000	0.0000	0.0000	0.0000	0.0000	0.0000	0.0000
Sr	0.0000	0.0000	0.0000	0.0000	0.0000	0.0000	0.0000	0.0000	0.0000	0.0000	0.0000	0.0000	0.0000	0.0000	0.0000	0.0000
Ba	0.0000	0.0000	0.0000	0.0000	0.0000	0.0000	0.0000	0.0000	0.0000	0.0000	0.0000	0.0000	0.0000	0.0000	0.0000	0.0000
Cr	0.0000	0.0000	0.0000	0.0000	0.0000	0.0000	0.0000	0.0000	0.0000	0.0000	0.0000	0.0000	0.0000	0.0000	0.0000	0.0000
Ni	0.0000	0.0000	0.0000	0.0000	0.0000	0.0000	0.0000	0.0000	0.0000	0.0000	0.0000	0.0000	0.0000	0.0000	0.0000	0.0000
Total	16.2688	16.2655	16.2887	16.2396	16.2509	16.2716	16.2578	16.2209	16.2256	16.1900	16.3127	16.2388	16.1741	16.2834	16.2663	16.1525

Table C5d: Continued

Sample	BI77032B	BI77032C	BI77032D	BI77032E	BI77032F	BI77032G	BI77032H	BIAS17A	BIAS17B	BIAS17C	BIAS17D	BIAS40A	BIAS40B	BIAS48A	BIAS48B	BIAS48C	BIAS48D	BIAS49A	BIAS49B	BIAS49C
SiO2	38.29	38.13	37.97	38.11	35.94	36.42	36.08	36.74	37.02	37.23	36.83	35.08	35.36	36.65	35.91	36.28	36.20	35.87	34.50	34.71
TiO2	5.52	4.66	5.33	3.40	4.87	4.45	4.81	4.13	5.12	4.83	4.25	4.86	5.16	4.31	4.38	4.35	4.54	4.40	4.11	3.77
Al2O3	13.18	13.35	13.09	13.26	13.45	13.66	13.88	13.64	13.45	13.44	13.63	13.48	13.66	12.70	12.31	13.01	12.97	12.62	12.80	12.85
FeO	12.89	13.59	13.28	13.95	22.89	23.13	23.05	20.78	20.71	20.32	21.37	20.36	20.34	23.51	23.53	22.54	24.36	23.32	25.02	24.76
MnO	0.00	0.00	0.00	0.00	0.47	0.33	0.36	0.36	0.23	0.23	0.19	0.19	0.17	0.26	0.35	0.37	0.29	0.36	0.40	0.39
MgO	15.34	15.56	15.48	15.90	8.82	8.94	8.92	11.24	10.53	11.20	11.14	10.98	10.84	8.81	8.78	9.28	8.44	8.70	8.23	8.72
CaO	0.00	0.00	0.00	0.12	0.00	0.10	0.00	0.13	0.00	0.14	0.00	0.00	0.00	0.13	0.12	0.00	0.00	0.10	0.00	0.00
Na2O	0.00	0.00	0.00	0.00	0.00	0.00	0.00	0.00	0.00	0.00	0.00	0.09	0.11	0.00	0.00	0.00	0.00	0.00	0.06	0.06
K2O	9.51	9.46	9.59	9.54	9.17	9.40	9.25	9.07	9.37	9.38	9.09	9.36	9.45	9.25	9.11	9.38	9.16	9.09	9.32	9.31
P2O5	0.00	0.00	0.00	0.00	0.00	0.00	0.00	0.00	0.00	0.00	0.00	0.00	0.00	0.00	0.00	0.00	0.00	0.00	0.00	0.00
TOTAL	94.73	94.75	94.74	94.28	95.61	96.43	96.35	96.09	96.43	96.77	96.50	94.40	95.09	95.62	94.49	95.21	95.96	94.46	94.44	94.57
Sr	0	0	0	0	0	0	0	0	0	0	0	0	0	0	0	0	0	0	0	0
Ba	0	0	0	0	0	0	0	0	0	0	0	0	0	0	0	0	0	0	0	0
Cr	0	0	0	0	0	0	0	0	0	0	0	0	0	0	0	0	0	0	0	0
Ni	0	0	0	0	0	0	0	0	0	0	0	0	0	0	0	0	0	0	0	0
Si	5.9546	5.9470	5.9248	5.9889	5.8408	5.8684	5.8146	5.8612	5.8838	5.8849	5.8586	5.7256	5.7240	5.9660	5.9344	5.9143	5.8964	5.9202	5.7772	5.7915
Ti	0.6456	0.5466	0.6255	0.4018	0.5952	0.5393	0.5830	0.4955	0.6120	0.5742	0.5084	0.5966	0.6282	0.5276	0.5444	0.5333	0.5561	0.5462	0.5176	0.4731
Al	2.4164	2.4547	2.4080	2.4566	2.5769	2.5949	2.6371	2.5653	2.5202	2.5046	2.5561	2.5938	2.6069	2.4372	2.3983	2.5004	2.4906	2.4556	2.5270	2.5277
Fe3	0.0000	0.0000	0.0000	0.0000	0.0000	0.0000	0.0000	0.0000	0.0000	0.0000	0.0000	0.0000	0.0000	0.0000	0.0000	0.0000	0.0000	0.0000	0.0000	0.0000
Fe2	1.6765	1.7727	1.7330	1.8334	3.1111	3.1170	3.1067	2.7725	2.7528	2.6862	2.8430	2.7792	2.7537	3.2006	3.2521	3.0730	3.3184	3.2189	3.5040	3.4551
Mn2	0.0000	0.0000	0.0000	0.0000	0.0647	0.0450	0.0491	0.0486	0.0310	0.0308	0.0256	0.0263	0.0233	0.0359	0.0490	0.0511	0.0400	0.0503	0.0567	0.0551
Mg	3.5553	3.6168	3.5999	3.7238	2.1362	2.1468	2.1424	2.6723	2.4942	2.6384	2.6409	2.6708	2.6152	2.1373	2.1624	2.2546	2.0488	2.1400	2.0539	2.1684
Ca	0.0000	0.0000	0.0000	0.0202	0.0000	0.0173	0.0000	0.0222	0.0000	0.0237	0.0000	0.0000	0.0000	0.0227	0.0212	0.0000	0.0000	0.0177	0.0000	0.0000
Na	0.0000	0.0000	0.0000	0.0000	0.0000	0.0000	0.0000	0.0000	0.0000	0.0000	0.0000	0.0285	0.0345	0.0000	0.0000	0.0000	0.0000	0.0000	0.0195	0.0194
K	1.8868	1.8824	1.9091	1.9126	1.9013	1.9324	1.9018	1.8460	1.9000	1.8916	1.8447	1.9490	1.9516	1.9210	1.9207	1.9508	1.9035	1.9140	1.9911	1.9818
P	0.0000	0.0000	0.0000	0.0000	0.0000	0.0000	0.0000	0.0000	0.0000	0.0000	0.0000	0.0000	0.0000	0.0000	0.0000	0.0000	0.0000	0.0000	0.0000	0.0000
Sr	0.0000	0.0000	0.0000	0.0000	0.0000	0.0000	0.0000	0.0000	0.0000	0.0000	0.0000	0.0000	0.0000	0.0000	0.0000	0.0000	0.0000	0.0000	0.0000	0.0000
Ba	0.0000	0.0000	0.0000	0.0000	0.0000	0.0000	0.0000	0.0000	0.0000	0.0000	0.0000	0.0000	0.0000	0.0000	0.0000	0.0000	0.0000	0.0000	0.0000	0.0000
Cr	0.0000	0.0000	0.0000	0.0000	0.0000	0.0000	0.0000	0.0000	0.0000	0.0000	0.0000	0.0000	0.0000	0.0000	0.0000	0.0000	0.0000	0.0000	0.0000	0.0000
Ni	0.0000	0.0000	0.0000	0.0000	0.0000	0.0000	0.0000	0.0000	0.0000	0.0000	0.0000	0.0000	0.0000	0.0000	0.0000	0.0000	0.0000	0.0000	0.0000	0.0000
Total	16.1351	16.2202	16.2003	16.3373	16.2262	16.2611	16.2348	16.2837	16.1940	16.2344	16.2773	16.3697	16.3374	16.2483	16.2824	16.2776	16.2539	16.2629	16.4470	16.4722

Table C5e: Electron microprobe analyses with structural formulae based on 8 oxygens for plagioclase from the Carsphairn pluton.

Sample	PLAS38A	PLAS38B	PLAS38C	PLAS38D	PLAS38E	PL77032A	PL77032B	PL77032C	PL77032D	PL77026A	PL77026B	PL77026C	PLAS17A	PLAS18A	PLAS48A	PLAS48B	PLAS49A	PLAS49B
SiO2	55.70	54.76	55.61	55.57	54.99	60.47	60.40	60.49	60.55	57.85	59.22	59.04	60.42	59.20	60.64	60.05	60.64	60.86
TiO2	0.00	0.00	0.00	0.06	0.05	0.00	0.00	0.00	0.10	0.12	0.00	0.00	0.00	0.00	0.00	0.05	0.00	0.00
Al2O3	27.85	28.58	27.65	27.67	28.41	24.82	24.64	24.75	24.94	26.30	25.46	25.58	24.88	25.53	24.42	25.11	24.72	24.50
FeO	0.28	0.32	0.27	0.14	0.15	0.13	0.31	0.00	0.15	0.00	0.34	0.25	0.13	0.17	0.09	0.15	0.00	0.13
MnO	0.00	0.00	0.00	0.00	0.00	0.00	0.00	0.00	0.00	0.00	0.00	0.00	0.00	0.00	0.00	0.00	0.00	0.00
MgO	0.00	0.00	0.00	0.02	0.03	0.00	0.00	0.00	0.00	0.00	0.00	0.00	0.00	0.00	0.00	0.00	0.00	0.00
CaO	10.22	11.31	10.41	10.55	10.69	6.46	6.47	6.47	6.84	8.57	7.30	7.41	6.61	7.49	6.70	6.59	5.95	5.68
Na2O	5.71	4.79	5.79	5.52	5.32	7.73	7.88	7.85	7.12	6.83	7.26	7.19	7.64	7.28	7.70	7.75	8.31	8.31
K2O	0.30	0.27	0.23	0.28	0.26	0.47	0.23	0.33	0.22	0.26	0.24	0.28	0.38	0.29	0.28	0.34	0.23	0.41
P2O5	0.00	0.00	0.00	0.00	0.00	0.00	0.00	0.00	0.00	0.00	0.00	0.00	0.00	0.00	0.00	0.00	0.00	0.00
TOTAL	100.06	100.03	99.96	99.81	99.90	100.08	99.93	99.89	99.92	99.93	99.82	99.75	100.06	99.96	99.83	100.04	99.85	99.89
Sr	0	0	0	0	0	0	0	0	0	0	0	0	0	0	0	0	0	0
Ba	0	0	0	0	0	0	0	0	0	0	0	0	0	0	0	0	0	0
Cr	0	0	0	0	0	0	0	0	0	0	0	0	0	0	0	0	0	0
Ni	0	0	0	0	0	0	0	0	0	0	0	0	0	0	0	0	0	0
Si	10.0382	9.8854	10.0393	10.0384	9.9281	10.7708	10.7766	10.7837	10.7733	10.3790	10.6010	10.5775	10.7606	10.5857	10.8188	10.7055	10.8061	10.8462
Ti	0.0000	0.0000	0.0000	0.0082	0.0068	0.0000	0.0000	0.0000	0.0134	0.0162	0.0000	0.0000	0.0000	0.0000	0.0000	0.0067	0.0000	0.0000
Al	5.9172	6.0825	5.8848	5.8928	6.0470	5.2119	5.1829	5.2017	5.2314	5.5628	5.3731	5.4029	5.2239	5.3819	5.1363	5.2775	5.1933	5.1475
Fe3	0.0000	0.0000	0.0000	0.0000	0.0000	0.0000	0.0000	0.0000	0.0000	0.0000	0.0000	0.0000	0.0000	0.0000	0.0000	0.0000	0.0000	0.0000
Fe2	0.0422	0.0483	0.0408	0.0212	0.0226	0.0194	0.0463	0.0000	0.0223	0.0000	0.0509	0.0375	0.0194	0.0254	0.0134	0.0224	0.0000	0.0194
Mn2	0.0000	0.0000	0.0000	0.0000	0.0000	0.0000	0.0000	0.0000	0.0000	0.0000	0.0000	0.0000	0.0000	0.0000	0.0000	0.0000	0.0000	0.0000
Mg	0.0000	0.0000	0.0000	0.0054	0.0081	0.0000	0.0000	0.0000	0.0000	0.0000	0.0000	0.0000	0.0000	0.0000	0.0000	0.0000	0.0000	0.0000
Ca	1.9735	2.1877	2.0137	2.0421	2.0680	1.2329	1.2369	1.2359	1.3040	1.6475	1.4002	1.4225	1.2614	1.4351	1.2808	1.2588	1.1361	1.0846
Na	1.9953	1.6766	2.0267	1.9334	1.8623	2.6696	2.7261	2.7134	2.4563	2.3760	2.5199	2.4976	2.6382	2.5240	2.6636	2.6789	2.8713	2.8715
K	0.0690	0.0622	0.0530	0.0645	0.0599	0.1068	0.0524	0.0751	0.0499	0.0595	0.0548	0.0640	0.0863	0.0662	0.0637	0.0773	0.0523	0.0932
P	0.0000	0.0000	0.0000	0.0000	0.0000	0.0000	0.0000	0.0000	0.0000	0.0000	0.0000	0.0000	0.0000	0.0000	0.0000	0.0000	0.0000	0.0000
Sr	0.0000	0.0000	0.0000	0.0000	0.0000	0.0000	0.0000	0.0000	0.0000	0.0000	0.0000	0.0000	0.0000	0.0000	0.0000	0.0000	0.0000	0.0000
Ba	0.0000	0.0000	0.0000	0.0000	0.0000	0.0000	0.0000	0.0000	0.0000	0.0000	0.0000	0.0000	0.0000	0.0000	0.0000	0.0000	0.0000	0.0000
Cr	0.0000	0.0000	0.0000	0.0000	0.0000	0.0000	0.0000	0.0000	0.0000	0.0000	0.0000	0.0000	0.0000	0.0000	0.0000	0.0000	0.0000	0.0000
Ni	0.0000	0.0000	0.0000	0.0000	0.0000	0.0000	0.0000	0.0000	0.0000	0.0000	0.0000	0.0000	0.0000	0.0000	0.0000	0.0000	0.0000	0.0000
Total	20.0354	19.9427	20.0582	20.0060	20.0028	20.0115	20.0211	20.0097	19.8507	20.0411	19.9998	20.0019	19.9898	20.0184	19.9767	20.0272	20.0591	20.0624

Table C6a: Electron microprobe analyses with structural formulae based on 6 oxygens for orthopyroxenes from the Loch Doon pluton.

Sample	OP77018A	OP77018B	OP77018C	OP77018D	OP77018E	OP77018F	OP77018G	OP77018H	OP77018I	OP77018J	OP78002A	OP78002B	OP78002C	OP78002D	OP78002E	OP78002F
SiO2	53.32	53.25	53.46	53.65	53.73	53.17	53.31	53.46	53.07	53.75	53.86	53.45	53.17	53.28	53.35	53.63
TiO2	0.28	0.23	0.56	0.34	0.28	0.36	0.17	0.23	0.96	0.35	0.15	0.29	0.34	0.32	0.27	0.34
Al2O3	0.59	0.64	0.47	0.55	0.79	0.56	0.74	0.36	0.74	0.30	0.41	0.84	0.58	0.54	0.63	0.40
FeO	19.95	20.12	20.17	20.04	20.15	20.38	19.94	21.47	19.93	19.42	20.13	18.97	20.95	20.09	20.50	20.60
MnO	0.48	0.34	0.45	0.46	0.46	0.50	0.50	0.53	0.36	0.42	0.38	0.41	0.52	0.33	0.60	0.51
MgO	24.45	24.23	23.67	23.58	23.38	23.75	23.55	23.40	24.39	24.68	23.53	24.63	23.50	23.50	23.72	23.15
CaO	0.85	1.14	1.42	1.42	1.19	0.79	1.81	0.91	0.72	0.80	1.48	0.99	0.93	1.46	0.95	1.25
Na2O	0.00	0.00	0.00	0.00	0.00	0.00	0.00	0.00	0.00	0.00	0.00	0.00	0.00	0.00	0.00	0.00
K2O	0.00	0.00	0.00	0.00	0.00	0.00	0.00	0.00	0.00	0.00	0.00	0.00	0.00	0.00	0.00	0.00
P2O5	0.00	0.00	0.00	0.00	0.00	0.00	0.00	0.00	0.00	0.00	0.00	0.00	0.00	0.00	0.00	0.00
TOTAL	100.23	100.11	100.20	100.04	100.20	99.51	100.02	100.36	100.30	99.90	100.06	99.80	99.99	99.52	100.02	99.88
Cr	3100	1600	0	0	2200	0	0	0	1300	1800	1200	2200	0	0	0	0
Ni	0	0	0	0	0	0	0	0	0	0	0	0	0	0	0	0
Sr	0	0	0	0	0	0	0	0	0	0	0	0	0	0	0	0
Ba	0	0	0	0	0	0	0	0	0	0	0	0	0	0	0	0
Si	1.9624	1.9641	1.9722	1.9797	1.9781	1.9744	1.9705	1.9781	1.9513	1.9777	1.9866	1.9658	1.9710	1.9774	1.9865	1.9649
Ti	0.0078	0.0064	0.0155	0.0094	0.0078	0.0101	0.0047	0.0064	0.0265	0.0097	0.0042	0.0080	0.0095	0.0089	0.0095	0.0061
Al	0.0256	0.0278	0.0204	0.0239	0.0343	0.0245	0.0322	0.0157	0.0321	0.0130	0.0178	0.0364	0.0253	0.0236	0.0175	0.0335
Fe3	0.0000	0.0000	0.0000	0.0000	0.0000	0.0000	0.0000	0.0000	0.0000	0.0000	0.0000	0.0000	0.0000	0.0000	0.0000	0.0000
Fe2	0.6141	0.6206	0.6223	0.6185	0.6204	0.6329	0.6164	0.6644	0.6128	0.5976	0.6210	0.5835	0.6495	0.6236	0.6382	0.5907
Mn2	0.0150	0.0106	0.0141	0.0144	0.0143	0.0157	0.0157	0.0166	0.0112	0.0131	0.0119	0.0128	0.0163	0.0104	0.0160	0.0119
Mg	1.3411	1.3319	1.3014	1.2968	1.2828	1.3143	1.2973	1.2904	1.3365	1.3533	1.2935	1.3500	1.2983	1.2998	1.2780	1.3422
Ca	0.0335	0.0451	0.0561	0.0561	0.0469	0.0314	0.0717	0.0361	0.0284	0.0315	0.0585	0.0390	0.0369	0.0581	0.0496	0.0521
Na	0.0000	0.0000	0.0000	0.0000	0.0000	0.0000	0.0000	0.0000	0.0000	0.0000	0.0000	0.0000	0.0000	0.0000	0.0000	0.0000
K	0.0000	0.0000	0.0000	0.0000	0.0000	0.0000	0.0000	0.0000	0.0000	0.0000	0.0000	0.0000	0.0000	0.0000	0.0000	0.0000
P	0.0000	0.0000	0.0000	0.0000	0.0000	0.0000	0.0000	0.0000	0.0000	0.0000	0.0000	0.0000	0.0000	0.0000	0.0000	0.0000
Sr	0.0000	0.0000	0.0000	0.0000	0.0000	0.0000	0.0000	0.0000	0.0000	0.0000	0.0000	0.0000	0.0000	0.0000	0.0000	0.0000
Ba	0.0000	0.0000	0.0000	0.0000	0.0000	0.0000	0.0000	0.0000	0.0000	0.0000	0.0000	0.0000	0.0000	0.0000	0.0000	0.0000
Cr	0.0117	0.0061	0.0000	0.0000	0.0083	0.0000	0.0000	0.0000	0.0049	0.0068	0.0045	0.0083	0.0000	0.0000	0.0000	0.0072
Ni	0.0000	0.0000	0.0000	0.0000	0.0000	0.0000	0.0000	0.0000	0.0000	0.0000	0.0000	0.0000	0.0000	0.0000	0.0000	0.0000
Total	4.0112	4.0126	4.0020	3.9989	3.9929	4.0033	4.0086	4.0077	4.0037	4.0027	3.9980	4.0038	4.0069	4.0018	3.9952	4.0086

Table C6a: Continued

Sample	OP78002G	OP78002H	OP78002I	OP77017A	OP77017B	OP77017C	OPWL6A	OPWL6B	OPWL6C	OPWL6D	OPDBL1A	OPDBL1B	OPDBL1C
SiO2	53.30	52.93	53.32	53.12	53.76	52.85	53.49	52.99	52.93	53.01	52.97	52.94	53.03
TiO2	0.22	0.22	0.26	0.32	0.31	0.23	0.28	0.28	0.28	0.23	0.25	0.21	0.28
Al2O3	0.77	0.82	0.73	0.71	0.61	0.96	0.60	0.60	0.78	0.54	0.72	0.74	0.69
FeO	19.16	19.89	20.07	20.72	20.29	19.20	20.84	20.46	20.89	20.43	19.97	19.85	20.81
MnO	0.38	0.35	0.54	0.38	0.47	0.38	0.47	0.44	0.44	0.46	0.46	0.42	0.48
MgO	24.43	24.03	23.80	23.80	22.91	23.91	23.13	22.94	23.33	23.42	23.39	23.69	23.52
CaO	1.32	0.84	1.56	1.12	1.62	2.12	0.88	1.78	0.79	1.57	1.68	1.68	1.18
Na2O	0.00	0.00	0.00	0.04	0.05	0.19	0.03	0.06	0.02	0.04	0.04	0.04	0.04
K2O	0.00	0.00	0.00	0.00	0.00	0.00	0.00	0.00	0.00	0.00	0.00	0.00	0.00
P2O5	0.00	0.00	0.00	0.00	0.00	0.00	0.00	0.00	0.00	0.00	0.00	0.00	0.00
TOTAL	99.77	99.63	100.41	100.32	100.12	99.84	99.82	99.63	99.56	99.77	99.55	99.65	100.11
Cr	1900	4200	1300	1100	1000	0	1000	800	1000	700	700	800	800
Ni	0	1300	0	0	0	0	0	0	0	0	0	0	0
Sr	0	0	0	0	0	0	0	0	0	0	0	0	0
Ba	0	0	0	0	0	0	0	0	0	0	0	0	0
Si	1.9730	1.9596	1.9638	1.9613	1.9848	1.9548	1.9825	1.9721	1.9690	1.9691	1.9681	1.9640	1.9642
Ti	0.0075	0.0061	0.0072	0.0089	0.0086	0.0064	0.0078	0.0078	0.0078	0.0064	0.0070	0.0059	0.0078
Al	0.0275	0.0358	0.0317	0.0309	0.0266	0.0419	0.0262	0.0263	0.0342	0.0236	0.0315	0.0324	0.0301
Fe3	0.0000	0.0000	0.0000	0.0000	0.0000	0.0000	0.0000	0.0000	0.0000	0.0000	0.0000	0.0000	0.0000
Fe2	0.6340	0.6158	0.6182	0.6398	0.6265	0.5939	0.6460	0.6368	0.6499	0.6347	0.6205	0.6159	0.6446
Mn2	0.0188	0.0110	0.0168	0.0119	0.0147	0.0119	0.0148	0.0139	0.0139	0.0145	0.0145	0.0132	0.0151
Mg	1.3073	1.3259	1.3064	1.3096	1.2606	1.3180	1.2776	1.2723	1.2934	1.2965	1.2952	1.3098	1.2983
Ca	0.0376	0.0333	0.0616	0.0443	0.0641	0.0840	0.0349	0.0710	0.0315	0.0625	0.0669	0.0668	0.0468
Na	0.0000	0.0000	0.0000	0.0029	0.0036	0.0136	0.0022	0.0043	0.0014	0.0029	0.0029	0.0029	0.0029
K	0.0000	0.0000	0.0000	0.0000	0.0000	0.0000	0.0000	0.0000	0.0000	0.0000	0.0000	0.0000	0.0000
P	0.0000	0.0000	0.0000	0.0000	0.0000	0.0000	0.0000	0.0000	0.0000	0.0000	0.0000	0.0000	0.0000
Sr	0.0000	0.0000	0.0000	0.0000	0.0000	0.0000	0.0000	0.0000	0.0000	0.0000	0.0000	0.0000	0.0000
Ba	0.0000	0.0000	0.0000	0.0000	0.0000	0.0000	0.0000	0.0000	0.0000	0.0000	0.0000	0.0000	0.0000
Cr	0.0000	0.0160	0.0049	0.0042	0.0038	0.0000	0.0038	0.0031	0.0038	0.0027	0.0027	0.0031	0.0030
Ni	0.0000	0.0049	0.0000	0.0000	0.0000	0.0000	0.0000	0.0000	0.0000	0.0000	0.0000	0.0000	0.0000
Total	4.0058	4.0084	4.0107	4.0137	3.9932	4.0246	3.9958	4.0076	4.0049	4.0128	4.0093	4.0139	4.0129

Table C6b: Electron microprobe analyses with structural formulae based on 6 oxygens for clinopyroxenes from the Loch Doon pluton.

Sample	CPWL6A	CPWL6B	CP78002A	CP78002B	CPDBL3A	CPDBL3B	CPDBL3C
SiO2	51.75	52.44	52.88	51.56	52.12	52.43	52.03
TiO2	0.43	0.59	0.53	0.78	0.18	0.00	0.13
Al2O3	1.65	2.04	1.56	1.77	0.51	0.38	0.75
FeO	9.17	8.38	8.24	9.69	14.73	14.93	13.58
MnO	0.23	0.21	0.21	0.26	0.73	1.10	0.49
MgO	14.82	13.99	14.30	15.65	10.99	10.57	11.83
CaO	21.25	21.04	21.71	19.87	20.74	20.21	20.54
Na2O	0.48	0.54	0.48	0.36	0.00	0.25	0.00
K2O	0.00	0.00	0.00	0.00	0.00	0.00	0.00
P2O5	0.00	0.00	0.00	0.00	0.00	0.00	0.00
TOTAL	100.09	99.67	100.07	100.15	100.00	100.12	99.52
Cr	3100	4400	1600	2100	0	2500	1700
Ni	0	0	0	0	0	0	0
Sr	0	0	0	0	0	0	0
Ba	0	0	0	0	0	0	0
Si	1.9318	1.9524	1.9625	1.9211	1.9925	2.0039	1.9852
Ti	0.0121	0.0165	0.0148	0.0219	0.0052	0.0000	0.0037
Al	0.0726	0.0895	0.0683	0.0777	0.0230	0.0171	0.0337
Fe3	0.0000	0.0000	0.0000	0.0000	0.0000	0.0000	0.0000
Fe2	0.2863	0.2609	0.2558	0.3019	0.4709	0.4772	0.4333
Mn2	0.0073	0.0066	0.0066	0.0082	0.0236	0.0356	0.0158
Mg	0.8245	0.7762	0.7909	0.8690	0.6261	0.6021	0.6727
Ca	0.8500	0.8393	0.8633	0.7933	0.8495	0.8277	0.8397
Na	0.0347	0.0390	0.0345	0.0260	0.0000	0.0185	0.0000
K	0.0000	0.0000	0.0000	0.0000	0.0000	0.0000	0.0000
P	0.0000	0.0000	0.0000	0.0000	0.0000	0.0000	0.0000
Sr	0.0000	0.0000	0.0000	0.0000	0.0000	0.0000	0.0000
Ba	0.0000	0.0000	0.0000	0.0000	0.0000	0.0000	0.0000
Cr	0.0119	0.0168	0.0061	0.0080	0.0000	0.0098	0.0067
Ni	0.0000	0.0000	0.0000	0.0000	0.0000	0.0000	0.0000
Total	4.0312	3.9974	4.0028	4.0272	3.9909	3.9919	3.9909

Table C6c: Electron microprobe analyses with structural formulae based on 23 oxygens for amphibole of the Loch Doon pluton.

Sample	AM78004A	AM78004B	AM78004C	AM78004D	AM78004E	AM78004F	AM78004G	AM78004H	AM77016A	AM77016B	AM78001A	AM78001B	AM78001C	AWL8A	AWL8B	AM77021A	AM77021B	AM77021C	AM77021D	AM77021E	AM77021F	AMDBL1A	AMDBL1B	AMDBL3A
SiO2	50.74	49.84	50.77	52.14	49.86	49.81	50.36	51.64	53.69	51.25	49.46	49.78	49.35	52.82	53.30	51.95	50.52	51.07	50.15	52.72	49.87	49.66	49.84	50.03
TiO2	0.79	0.85	0.78	0.49	1.02	1.04	0.74	0.28	0.28	0.83	1.16	0.97	1.16	0.47	0.31	0.49	0.84	0.66	0.85	0.26	0.97	0.94	0.97	0.65
Al2O3	4.72	4.79	4.46	3.65	5.22	4.96	4.56	3.73	1.91	3.82	5.44	5.07	5.06	2.73	2.14	4.04	5.00	4.63	4.76	2.16	4.96	5.10	4.74	4.31
FeO	12.27	12.49	12.39	11.67	12.87	12.41	13.14	12.78	10.94	12.22	12.89	13.20	12.89	11.95	11.64	13.13	12.86	13.09	12.84	13.19	12.36	13.51	13.34	13.56
MnO	0.33	0.31	0.30	0.34	0.31	0.25	0.45	0.48	0.34	0.27	0.33	0.36	0.35	0.37	0.38	0.52	0.44	0.36	0.41	0.58	0.41	0.36	0.35	0.37
MgO	15.15	15.67	15.74	16.18	15.55	15.78	15.16	16.16	16.72	16.12	15.12	15.28	14.67	15.99	16.39	15.71	14.89	15.45	15.32	17.32	15.24	14.82	14.77	14.93
CaO	11.95	11.23	10.97	11.66	11.08	11.45	10.99	11.26	11.67	11.12	11.07	11.15	11.03	12.09	12.10	10.85	11.46	11.26	11.29	9.41	11.46	11.32	11.35	10.85
Na2O	0.54	0.55	0.80	0.42	0.89	0.74	0.50	0.45	0.00	0.36	1.03	0.90	0.93	0.00	0.42	0.71	0.62	1.06	0.67	0.00	0.97	1.09	1.03	0.93
K2O	0.00	0.32	0.33	0.23	0.47	0.47	0.28	0.14	0.11	0.32	0.48	0.34	0.39	0.29	0.29	0.29	0.37	0.37	0.33	0.18	0.43	0.51	0.43	0.37
P2O5	0.00	0.00	0.00	0.00	0.00	0.00	0.00	0.00	0.00	0.00	0.00	0.00	0.00	0.00	0.00	0.00	0.00	0.00	0.00	0.00	0.00	0.00	0.00	0.00
TOTAL	96.72	96.05	96.54	97.08	97.42	97.16	96.33	97.15	95.84	96.31	96.98	97.05	95.83	96.71	96.97	97.69	97.00	97.95	96.91	95.82	96.89	97.31	96.82	96.00
Cr	2300	0	0	3000	1500	2300	1300	2300	1800	0	0	0	0	0	0	0	0	0	2900	0	2200	0	0	0
Ni	0	0	0	0	0	0	0	0	0	0	0	0	0	0	0	0	0	0	0	0	0	0	0	0
Sr	0	0	0	0	0	0	0	0	0	0	0	0	0	0	0	0	0	0	0	0	0	0	0	0
Ba	0	0	0	0	0	0	0	0	0	0	0	0	0	0	0	0	0	0	0	0	0	0	0	0
Si	7.3948	7.3359	7.4180	7.5355	7.2603	7.2628	7.3995	7.4972	7.7966	7.4868	7.2437	7.2862	7.3087	7.6671	7.7153	7.5094	7.3737	7.3909	7.3320	7.7143	7.2965	7.2771	7.3284	7.4382
Ti	0.0866	0.0941	0.0857	0.0533	0.1117	0.1140	0.0818	0.0306	0.0306	0.0912	0.1278	0.1068	0.1292	0.0513	0.0337	0.0533	0.0922	0.0718	0.0935	0.0286	0.1067	0.1036	0.1073	0.0724
Al	0.8110	0.8312	0.7683	0.6219	0.8961	0.8561	0.7934	0.6384	0.3270	0.6579	0.9393	0.8749	0.8835	0.4672	0.3652	0.6885	0.8604	0.7899	0.8204	0.3726	0.8555	0.8811	0.8217	0.7524
Fe3	0.0000	0.0000	0.0000	0.0000	0.0000	0.0000	0.0000	0.0000	0.0000	0.0000	0.0000	0.0000	0.0000	0.0000	0.0000	0.0000	0.0000	0.0000	0.0000	0.0000	0.0000	0.0000	0.0000	0.0000
Fe2	1.4955	1.5375	1.5140	1.4105	1.5673	1.5133	1.6147	1.5517	1.3286	1.4930	1.5788	1.6158	1.5965	1.4507	1.4091	1.5873	1.5698	1.5843	1.5700	1.6141	1.5124	1.6557	1.6405	1.6792
Mn2	0.0407	0.0386	0.0371	0.0416	0.0382	0.0309	0.0560	0.0590	0.0418	0.0334	0.0409	0.0446	0.0439	0.0455	0.0466	0.0637	0.0544	0.0441	0.0508	0.0719	0.0508	0.0447	0.0436	0.0464
Mg	3.2905	3.4374	3.4274	3.4850	3.3745	3.4291	3.3197	3.4965	3.6185	3.5095	3.3002	3.3331	3.2379	3.4591	3.5358	3.3843	3.2389	3.3323	3.3380	3.7770	3.3231	3.2366	3.2366	3.2947
Ca	1.8661	1.7711	1.7174	1.8056	1.7268	1.7889	1.7302	1.7517	1.8158	1.7406	1.7372	1.7487	1.7503	1.8804	1.8768	1.6805	1.7923	1.7461	1.7686	1.4754	1.7966	1.7774	1.7882	1.7215
Na	0.1526	0.1570	0.2266	0.1177	0.2513	0.2092	0.1424	0.1267	0.0000	0.1020	0.2925	0.2554	0.2671	0.0000	0.1179	0.1990	0.1755	0.2974	0.1899	0.0000	0.2752	0.3097	0.2937	0.2670
K	0.0000	0.0601	0.0615	0.0424	0.0873	0.0874	0.0525	0.0259	0.0204	0.0596	0.0897	0.0635	0.0737	0.0537	0.0536	0.0535	0.0689	0.0683	0.0616	0.0336	0.0803	0.0953	0.0807	0.0699
P	0.0000	0.0000	0.0000	0.0000	0.0000	0.0000	0.0000	0.0000	0.0000	0.0000	0.0000	0.0000	0.0000	0.0000	0.0000	0.0000	0.0000	0.0000	0.0000	0.0000	0.0000	0.0000	0.0000	0.0000
Sr	0.0000	0.0000	0.0000	0.0000	0.0000	0.0000	0.0000	0.0000	0.0000	0.0000	0.0000	0.0000	0.0000	0.0000	0.0000	0.0000	0.0000	0.0000	0.0000	0.0000	0.0000	0.0000	0.0000	0.0000
Ba	0.0000	0.0000	0.0000	0.0000	0.0000	0.0000	0.0000	0.0000	0.0000	0.0000	0.0000	0.0000	0.0000	0.0000	0.0000	0.0000	0.0000	0.0000	0.0000	0.0000	0.0000	0.0000	0.0000	0.0000
Cr	0.0344	0.0000	0.0000	0.0446	0.0224	0.0345	0.0196	0.0343	0.0269	0.0000	0.0000	0.0000	0.0000	0.0000	0.0000	0.0000	0.0000	0.0000	0.0436	0.0000	0.0331	0.0000	0.0000	0.0000
Ni	0.0000	0.0000	0.0000	0.0000	0.0000	0.0000	0.0000	0.0000	0.0000	0.0000	0.0000	0.0000	0.0000	0.0000	0.0000	0.0000	0.0000	0.0000	0.0000	0.0000	0.0000	0.0000	0.0000	0.0000
Total	15.1723	15.2629	15.2562	15.1581	15.3380	15.3262	15.2097	15.2121	15.0061	15.1739	15.3500	15.3290	15.2908	15.0749	15.1540	15.2194	15.2261	15.3252	15.2683	15.0876	15.3302	15.3813	15.3406	15.3117

Table C6c: Continued

Sample	AMDBL3B	AMDBL3C	AMDBL3D	AM77022A	AM77022B	AM77022C	AM77022D	AM77022E	AM77022F	AM77022G	AM77022H	AM77022I	AM77022J	AM77024A	AM77024B	AM77024C	AM77024D	AM77024E	AM77024F	AMWL9A	AMWL9B	AMWL9C	AMWL9D	AMWL9E
SiO2	50.45	50.27	48.79	50.11	53.30	52.81	49.30	50.02	49.94	49.72	49.33	49.82	51.08	53.07	49.48	50.73	48.84	49.80	49.68	47.85	48.05	48.23	48.52	48.24
TiO2	0.86	0.63	0.90	0.97	0.26	0.49	1.00	0.86	0.96	0.94	0.96	0.84	0.88	0.38	0.94	0.77	0.89	1.01	0.84	1.01	1.01	0.91	0.98	1.00
Al2O3	4.38	4.29	5.17	5.04	2.12	2.70	5.15	5.04	4.59	4.86	5.08	4.77	4.10	2.41	4.86	4.50	5.22	5.18	5.04	5.51	5.35	5.26	5.19	5.37
FeO	12.63	13.66	13.41	13.14	11.59	11.90	13.68	14.17	13.71	13.48	13.86	13.51	12.89	11.97	13.37	13.19	13.83	13.59	14.09	14.16	13.63	13.93	13.66	14.26
MnO	0.33	0.37	0.37	0.49	0.40	0.39	0.47	0.53	0.43	0.50	0.54	0.58	0.40	0.57	0.42	0.46	0.57	0.39	0.50	0.45	0.45	0.53	0.46	0.50
MgO	15.23	15.08	14.53	14.21	16.48	15.96	13.65	14.15	14.20	14.24	14.31	14.33	15.31	16.19	14.38	14.91	14.47	14.40	14.68	13.48	13.84	13.60	13.65	13.41
CaO	11.42	10.85	11.20	11.54	12.07	12.19	11.55	10.89	11.22	11.68	11.21	11.54	12.06	11.80	11.22	11.80	11.06	11.58	10.86	11.08	10.89	11.26	11.51	11.05
Na2O	0.96	0.95	1.07	0.79	0.35	0.00	0.78	1.07	0.97	0.99	1.09	0.90	0.70	0.25	0.76	0.54	0.78	0.78	1.11	1.22	1.32	1.19	1.10	1.31
K2O	0.35	0.38	0.48	0.47	0.13	0.20	0.49	0.36	0.38	0.38	0.42	0.39	0.33	0.15	0.39	0.36	0.49	0.40	0.38	0.53	0.50	0.48	0.48	0.44
P2O5	0.00	0.00	0.00	0.00	0.00	0.00	0.00	0.00	0.00	0.00	0.00	0.00	0.00	0.00	0.00	0.00	0.00	0.00	0.00	0.00	0.00	0.00	0.00	0.00
TOTAL	96.81	96.48	95.92	96.87	96.70	96.64	96.07	97.23	96.40	96.79	96.96	96.68	97.75	96.79	95.82	97.26	96.28	97.13	97.35	95.29	95.04	95.39	95.55	95.56
Cr	0	0	0	1100	0	0	0	1400	0	0	1600	0	0	0	0	0	1300	0	1700	0	0	0	0	0
Ni	0	0	0	0	0	0	0	0	0	0	0	0	0	0	0	0	0	0	0	0	0	0	0	0
Sr	0	0	0	0	0	0	0	0	0	0	0	0	0	0	0	0	0	0	0	0	0	0	0	0
Ba	0	0	0	0	0	0	0	0	0	0	0	0	0	0	0	0	0	0	0	0	0	0	0	0
Si	7.3900	7.4080	7.2584	7.3515	7.7252	7.6686	7.3231	7.3378	7.3800	7.3265	7.2709	7.3466	7.4131	7.6973	7.3448	7.4028	7.2480	7.3023	7.2854	7.2087	7.2348	7.2492	7.2675	7.2420
Ti	0.0969	0.0698	0.1007	0.1070	0.0283	0.0535	0.1117	0.0949	0.1067	0.1042	0.1064	0.0932	0.0960	0.0415	0.1049	0.0845	0.0993	0.1114	0.0926	0.1144	0.1144	0.1029	0.1104	0.1129
Al	0.7495	0.7453	0.9067	0.8717	0.3622	0.4622	0.9019	0.8716	0.7997	0.8443	0.8827	0.8293	0.7015	0.4121	0.8505	0.7742	0.9133	0.8955	0.8714	0.9786	0.9497	0.9321	0.9165	0.9564
Fe3	0.0000	0.0000	0.0000	0.0000	0.0000	0.0000	0.0000	0.0000	0.0000	0.0000	0.0000	0.0000	0.0000	0.0000	0.0000	0.0000	0.0000	0.0000	0.0000	0.0000	0.0000	0.0000	0.0000	0.0000
Fe2	1.5718	1.6835	1.6684	1.6122	1.4049	1.4452	1.6995	1.7385	1.6944	1.6612	1.7085	1.6661	1.5645	1.4520	1.6598	1.6097	1.7165	1.6666	1.7281	1.7841	1.7164	1.7510	1.7112	1.7904
Mn2	0.0409	0.0462	0.0466	0.0609	0.0491	0.0480	0.0591	0.0659	0.0538	0.0624	0.0674	0.0724	0.0492	0.0700	0.0528	0.0569	0.0717	0.0484	0.0621	0.0574	0.0574	0.0675	0.0584	0.0636
Mg	3.3248	3.3119	3.2215	3.1069	3.5598	3.4540	3.0218	3.0936	3.1274	3.1272	3.1434	3.1493	3.3114	3.4996	3.1813	3.2426	3.2003	3.1468	3.2084	3.0265	3.1057	3.0464	3.0471	3.0003
Ca	1.7924	1.7132	1.7853	1.8141	1.8745	1.8967	1.8383	1.7118	1.7766	1.8442	1.7704	1.8234	1.8754	1.8338	1.7846	1.8450	1.7587	1.8194	1.7065	1.7886	1.7569	1.8134	1.8473	1.7775
Na	0.2763	0.2714	0.3086	0.2247	0.0984	0.0000	0.2247	0.3043	0.2779	0.2829	0.3115	0.2573	0.1970	0.0703	0.2187	0.1528	0.2244	0.2218	0.3156	0.3564	0.3854	0.3468	0.3195	0.3813
K	0.0654	0.0714	0.0911	0.0880	0.0240	0.0371	0.0929	0.0674	0.0716	0.0714	0.0790	0.0734	0.0611	0.0278	0.0739	0.0670	0.0928	0.0748	0.0711	0.1019	0.0960	0.0920	0.0917	0.0843
P	0.0000	0.0000	0.0000	0.0000	0.0000	0.0000	0.0000	0.0000	0.0000	0.0000	0.0000	0.0000	0.0000	0.0000	0.0000	0.0000	0.0000	0.0000	0.0000	0.0000	0.0000	0.0000	0.0000	0.0000
Sr	0.0000	0.0000	0.0000	0.0000	0.0000	0.0000	0.0000	0.0000	0.0000	0.0000	0.0000	0.0000	0.0000	0.0000	0.0000	0.0000	0.0000	0.0000	0.0000	0.0000	0.0000	0.0000	0.0000	0.0000
Ba	0.0000	0.0000	0.0000	0.0000	0.0000	0.0000	0.0000	0.0000	0.0000	0.0000	0.0000	0.0000	0.0000	0.0000	0.0000	0.0000	0.0000	0.0000	0.0000	0.0000	0.0000	0.0000	0.0000	0.0000
Cr	0.0000	0.0000	0.0000	0.0166	0.0000	0.0000	0.0000	0.0000	0.0000	0.0000	0.0000	0.0000	0.0000	0.0000	0.0000	0.0000	0.0198	0.0000	0.0256	0.0000	0.0000	0.0000	0.0000	0.0000
Ni	0.0000	0.0000	0.0000	0.0000	0.0000	0.0000	0.0000	0.0211	0.0000	0.0000	0.0242	0.0000	0.0000	0.0000	0.0000	0.0000	0.0000	0.0000	0.0000	0.0000	0.0000	0.0000	0.0000	0.0000
Total	15.3102	15.3209	15.3874	15.2536	15.1265	15.0653	15.2730	15.3068	15.2882	15.3243	15.3645	15.3110	15.2691	15.1043	15.2713	15.2355	15.3448	15.2869	15.3668	15.4167	15.4167	15.4014	15.3694	15.4027

Table C6d: Electron microprobe analyses with structural formulae based on 23 oxygens for biotite of the Loch Doon pluton.

Sample	BI77018A	BI77018B	BI77018C	BI77018D	BI77018E	BI77018F	BI77018G	BI78002A	BI78002B	BI78002C	BI78002D	BI78002E	BI78002F	BI78004A	BI78004B	BI78004C	BI78004D	BI78004E	BI78004F	BI78001A	BI78001B	BI78001C	BI78001D	BI77016A
SiO2	38.90	38.92	38.96	38.37	38.53	39.11	38.38	37.33	38.31	38.52	38.59	39.09	38.80	37.06	37.90	37.47	37.58	37.58	37.54	36.60	36.70	36.19	36.58	37.79
TiO2	4.42	5.18	5.21	4.06	3.95	4.96	4.16	4.47	4.86	4.99	4.91	5.06	5.11	5.36	4.85	3.75	5.17	4.59	4.04	4.77	4.33	4.68	4.70	4.54
Al2O3	13.06	13.11	12.72	13.33	13.53	12.88	13.46	13.40	13.04	12.99	13.29	12.56	12.92	13.27	13.59	13.67	13.13	13.55	13.83	14.44	14.45	14.55	14.32	13.60
FeO	13.04	12.43	13.52	13.71	13.80	12.61	14.08	16.60	13.71	12.92	13.62	12.98	13.15	15.98	15.86	16.63	16.18	16.48	16.78	16.17	16.05	16.22	15.92	15.83
MnO	0.10	0.00	0.00	0.00	0.00	0.13	0.00	0.22	0.00	0.00	0.00	0.00	0.00	0.18	0.00	0.30	0.23	0.17	0.15	0.12	0.13	0.12	0.11	0.00
MgO	16.32	16.57	15.74	16.44	16.24	16.71	15.91	13.67	15.57	16.18	15.59	16.01	16.13	13.05	13.90	13.90	13.72	13.71	13.63	13.59	13.84	13.62	13.56	13.34
CaO	0.11	0.09	0.00	0.00	0.00	0.00	0.00	0.09	0.00	0.00	0.12	0.00	0.00	0.00	0.00	0.15	0.00	0.00	0.00	0.00	0.01	0.02	0.01	0.13
Na2O	0.00	0.00	0.00	0.00	0.00	0.00	0.00	0.00	0.00	0.00	0.00	0.00	0.00	0.00	0.00	0.00	0.00	0.00	0.00	0.15	0.16	0.15	0.16	0.00
K2O	9.18	9.31	9.15	9.51	9.40	9.05	9.50	9.56	9.31	9.28	9.52	9.30	9.36	9.17	9.24	9.19	8.95	9.38	9.35	9.34	9.30	9.43	9.36	9.43
P2O5	0.00	0.00	0.00	0.00	0.00	0.00	0.00	0.00	0.00	0.00	0.00	0.00	0.00	0.00	0.00	0.00	0.00	0.00	0.00	0.00	0.00	0.00	0.00	0.00
TOTAL	95.13	95.61	95.30	95.42	95.45	95.45	95.49	95.34	94.80	94.88	95.64	95.00	95.47	94.07	95.34	95.06	94.96	95.46	95.32	95.18	94.97	94.98	94.72	94.66
Sr	0	0	0	0	0	0	0	0	0	0	0	0	0	0	0	0	0	0	0	0	0	0	0	0
Ba	0	0	0	0	0	0	0	0	0	0	0	0	0	0	0	0	0	0	0	0	0	0	0	0
Cr	0	0	0	0	0	0	0	0	0	0	0	0	0	0	0	0	0	0	0	0	0	0	0	0
Ni	0	0	0	0	0	0	0	0	0	0	0	0	0	0	0	0	0	0	0	0	0	0	0	0
Si	6.0116	5.9701	6.0199	5.9447	5.9609	6.0053	5.9497	5.8922	5.9697	5.9719	5.9611	6.0482	5.9836	5.9003	5.9299	5.9168	5.9186	5.9052	5.9117	5.7700	5.7925	5.7288	5.7901	5.9641
Ti	0.5137	0.5976	0.6054	0.4731	0.4596	0.5728	0.4850	0.5306	0.5696	0.5818	0.5704	0.5888	0.5927	0.6418	0.5707	0.4453	0.6124	0.5424	0.4785	0.5655	0.5140	0.5572	0.5595	0.5389
Al	2.3794	2.3708	2.3171	2.4348	2.4677	2.3316	2.4599	2.4935	2.3956	2.3742	2.4203	2.2911	2.3490	2.4907	2.5068	2.5448	2.4379	2.5102	2.5676	2.6838	2.6888	2.7153	2.6722	2.5304
Fe3	0.0000	0.0000	0.0000	0.0000	0.0000	0.0000	0.0000	0.0000	0.0000	0.0000	0.0000	0.0000	0.0000	0.0000	0.0000	0.0000	0.0000	0.0000	0.0000	0.0000	0.0000	0.0000	0.0000	0.0000
Fe2	1.6854	1.5946	1.7471	1.7764	1.7855	1.6193	1.8255	2.1913	1.7867	1.6752	1.7596	1.6796	1.6960	2.1277	2.0753	2.1962	2.1312	2.1658	2.2100	2.1320	2.1186	2.1473	2.1075	2.0894
Mn2	0.0131	0.0000	0.0000	0.0000	0.0000	0.0169	0.0000	0.0294	0.0000	0.0000	0.0000	0.0000	0.0000	0.0243	0.0000	0.0401	0.0307	0.0226	0.0200	0.0160	0.0174	0.0161	0.0147	0.0000
Mg	3.7587	3.7880	3.6246	3.7960	3.7444	3.8239	3.6757	3.2156	3.6159	3.7384	3.5891	3.6918	3.7072	3.0964	3.2412	3.2711	3.2203	3.2107	3.1989	3.1930	3.2555	3.2131	3.1988	3.1377
Ca	0.0182	0.0148	0.0000	0.0000	0.0000	0.0000	0.0000	0.0152	0.0000	0.0000	0.0199	0.0000	0.0000	0.0000	0.0000	0.0254	0.0000	0.0000	0.0000	0.0000	0.0017	0.0034	0.0017	0.0220
Na	0.0000	0.0000	0.0000	0.0000	0.0000	0.0000	0.0000	0.0000	0.0000	0.0000	0.0000	0.0000	0.0000	0.0000	0.0000	0.0000	0.0000	0.0000	0.0000	0.0459	0.0490	0.0460	0.0491	0.0000
K	1.8099	1.8220	1.8037	1.8798	1.8553	1.7729	1.8789	1.9251	1.8509	1.8355	1.8762	1.8358	1.8416	1.8626	1.8444	1.8514	1.7983	1.8805	1.8785	1.8786	1.8727	1.9044	1.8902	1.8587
P	0.0000	0.0000	0.0000	0.0000	0.0000	0.0000	0.0000	0.0000	0.0000	0.0000	0.0000	0.0000	0.0000	0.0000	0.0000	0.0000	0.0000	0.0000	0.0000	0.0000	0.0000	0.0000	0.0000	0.0000
Sr	0.0000	0.0000	0.0000	0.0000	0.0000	0.0000	0.0000	0.0000	0.0000	0.0000	0.0000	0.0000	0.0000	0.0000	0.0000	0.0000	0.0000	0.0000	0.0000	0.0000	0.0000	0.0000	0.0000	0.0000
Ba	0.0000	0.0000	0.0000	0.0000	0.0000	0.0000	0.0000	0.0000	0.0000	0.0000	0.0000	0.0000	0.0000	0.0000	0.0000	0.0000	0.0000	0.0000	0.0000	0.0000	0.0000	0.0000	0.0000	0.0000
Cr	0.0000	0.0000	0.0000	0.0000	0.0000	0.0000	0.0000	0.0000	0.0000	0.0000	0.0000	0.0000	0.0000	0.0000	0.0000	0.0000	0.0000	0.0000	0.0000	0.0000	0.0000	0.0000	0.0000	0.0000
Ni	0.0000	0.0000	0.0000	0.0000	0.0000	0.0000	0.0000	0.0000	0.0000	0.0000	0.0000	0.0000	0.0000	0.0000	0.0000	0.0000	0.0000	0.0000	0.0000	0.0000	0.0000	0.0000	0.0000	0.0000
Total	16.1900	16.1579	16.1179	16.3047	16.2734	16.1426	16.2747	16.2930	16.1883	16.1770	16.1964	16.1353	16.1700	16.1439	16.1683	16.2912	16.1493	16.2375	16.2652	16.2847	16.3100	16.3317	16.2839	16.1612

Table C6d: Continued

Sample	BI77016B	BI77016C	BI77016D	BIWL6A	BIWL6B	BIWL6C	BIWL6D	BI77017A	BIDBL5A	BIDBL5B	BIDBL5C	BI77021A	BI77021B	BI77021C	BI77021D	BI77021E	BI77021F	BI77021G	BIDBL1A	BIDBL1B	BIDBL1C	BIDBL3A	BIDBL3B	BIDBL3C
SiO2	37.42	37.61	38.11	37.65	37.50	37.48	37.42	37.14	36.33	36.73	36.67	37.33	37.32	38.06	38.02	37.94	37.73	38.07	36.60	36.44	36.25	36.51	37.02	36.07
TiO2	4.29	4.52	4.61	4.96	5.20	4.78	4.96	4.26	4.43	4.59	4.11	4.10	5.07	3.75	4.85	3.84	4.32	4.27	4.58	4.85	4.74	4.73	4.88	3.89
Al2O3	13.69	13.81	13.42	13.29	12.78	13.23	12.92	13.36	13.82	14.06	13.81	13.68	13.34	13.58	13.57	13.33	13.59	13.74	13.35	13.15	13.07	12.84	13.29	13.30
FeO	16.15	16.52	16.14	12.75	13.14	13.56	13.26	13.44	16.38	16.27	16.49	16.53	16.09	16.33	16.01	16.26	17.31	17.47	16.96	17.44	16.66	16.63	17.02	16.94
MnO	0.18	0.00	0.23	0.03	0.05	0.04	0.06	0.07	0.12	0.12	0.11	0.24	0.16	0.00	0.15	0.18	0.19	0.13	0.12	0.12	0.11	0.12	0.16	0.13
MgO	13.45	13.30	13.63	16.83	16.62	16.35	16.75	16.60	13.50	13.62	13.95	13.60	13.59	13.97	13.84	14.39	13.43	13.41	13.76	13.10	13.51	13.73	13.71	13.83
CaO	0.00	0.13	0.00	0.00	0.00	0.01	0.00	0.00	0.00	0.00	0.00	0.00	0.00	0.00	0.00	0.00	0.13	0.14	0.00	0.00	0.00	0.00	0.00	0.01
Na2O	0.00	0.00	0.00	0.12	0.14	0.12	0.12	0.13	0.16	0.14	0.14	0.00	0.00	0.00	0.00	0.00	0.00	0.00	0.15	0.14	0.20	0.20	0.14	0.13
K2O	9.56	9.24	9.29	9.34	9.11	9.43	9.14	9.58	9.37	9.47	9.48	9.39	9.42	9.15	9.33	9.10	9.43	9.50	9.46	9.56	9.30	9.29	9.61	9.55
P2O5	0.00	0.00	0.00	0.00	0.00	0.00	0.00	0.00	0.00	0.00	0.00	0.00	0.00	0.00	0.00	0.00	0.00	0.00	0.00	0.00	0.00	0.00	0.00	0.00
TOTAL	94.74	95.13	95.43	94.97	94.54	95.00	94.63	94.58	94.11	95.00	94.76	94.87	94.99	94.84	95.77	95.04	96.13	96.73	94.98	94.80	93.84	94.05	95.83	93.85
Sr	0	0	0	0	0	0	0	0	0	0	0	0	0	0	0	0	0	0	0	0	0	0	0	0
Ba	0	0	0	0	0	0	0	0	0	0	0	0	0	0	0	0	0	0	0	0	0	0	0	0
Cr	0	0	0	0	0	0	0	0	0	0	0	0	0	0	0	0	0	0	0	0	0	0	0	0
Ni	0	0	0	0	0	0	0	0	0	0	0	0	0	0	0	0	0	0	0	0	0	0	0	0
Si	5.9232	5.9204	5.9702	5.8468	5.8606	5.8471	5.8469	5.8273	5.8102	5.8097	5.8246	5.9089	5.8908	5.9921	5.9315	5.9674	5.9115	5.9252	5.8188	5.8254	5.8292	5.8545	5.8339	5.8166
Ti	0.5107	0.5351	0.5431	0.5793	0.6112	0.5608	0.5829	0.5027	0.5328	0.5460	0.4910	0.4881	0.6019	0.4440	0.5690	0.4542	0.5090	0.4998	0.5476	0.5831	0.5732	0.5704	0.5784	0.4718
Al	2.5547	2.5629	2.4785	2.4331	2.3547	2.4333	2.3800	2.4713	2.6057	2.6218	2.5861	2.5528	2.4824	2.5206	2.4959	2.4718	2.5102	2.5211	2.5022	2.4783	2.4778	2.4274	2.4691	2.5285
Fe3	0.0000	0.0000	0.0000	0.0000	0.0000	0.0000	0.0000	0.0000	0.0000	0.0000	0.0000	0.0000	0.0000	0.0000	0.0000	0.0000	0.0000	0.0000	0.0000	0.0000	0.0000	0.0000	0.0000	0.0000
Fe2	2.1379	2.1749	2.1146	1.6559	1.7178	1.7692	1.7328	1.7636	2.1909	2.1523	2.1905	2.1882	2.1241	2.1502	2.0689	2.1389	2.2682	2.2740	2.2550	2.3317	2.2405	2.2302	2.2431	2.2846
Mn2	0.0241	0.0000	0.0305	0.0039	0.0066	0.0053	0.0079	0.0093	0.0163	0.0161	0.0148	0.0322	0.0214	0.0000	0.0198	0.0240	0.0252	0.0171	0.0162	0.0162	0.0150	0.0163	0.0214	0.0178
Mg	3.1729	3.1202	3.1822	3.8951	3.8710	3.8014	3.9005	3.8816	3.2177	3.2106	3.3023	3.2083	3.1970	3.2778	3.2179	3.3731	3.1359	3.1105	3.2602	3.1210	3.2377	3.2812	3.2199	3.3237
Ca	0.0000	0.0219	0.0000	0.0000	0.0000	0.0017	0.0000	0.0000	0.0000	0.0000	0.0000	0.0000	0.0000	0.0000	0.0000	0.0000	0.0218	0.0233	0.0000	0.0000	0.0000	0.0000	0.0000	0.0017
Na	0.0000	0.0000	0.0000	0.0361	0.0424	0.0363	0.0364	0.0395	0.0496	0.0429	0.0431	0.0000	0.0000	0.0000	0.0000	0.0000	0.0000	0.0000	0.0462	0.0434	0.0624	0.0622	0.0428	0.0406
K	1.9306	1.8557	1.8567	1.8505	1.8164	1.8769	1.8220	1.9177	1.9118	1.9110	1.9211	1.8962	1.8970	1.8379	1.8570	1.8261	1.8850	1.8864	1.9188	1.9498	1.9079	1.9005	1.9321	1.9648
P	0.0000	0.0000	0.0000	0.0000	0.0000	0.0000	0.0000	0.0000	0.0000	0.0000	0.0000	0.0000	0.0000	0.0000	0.0000	0.0000	0.0000	0.0000	0.0000	0.0000	0.0000	0.0000	0.0000	0.0000
Sr	0.0000	0.0000	0.0000	0.0000	0.0000	0.0000	0.0000	0.0000	0.0000	0.0000	0.0000	0.0000	0.0000	0.0000	0.0000	0.0000	0.0000	0.0000	0.0000	0.0000	0.0000	0.0000	0.0000	0.0000
Ba	0.0000	0.0000	0.0000	0.0000	0.0000	0.0000	0.0000	0.0000	0.0000	0.0000	0.0000	0.0000	0.0000	0.0000	0.0000	0.0000	0.0000	0.0000	0.0000	0.0000	0.0000	0.0000	0.0000	0.0000
Cr	0.0000	0.0000	0.0000	0.0000	0.0000	0.0000	0.0000	0.0000	0.0000	0.0000	0.0000	0.0000	0.0000	0.0000	0.0000	0.0000	0.0000	0.0000	0.0000	0.0000	0.0000	0.0000	0.0000	0.0000
Ni	0.0000	0.0000	0.0000	0.0000	0.0000	0.0000	0.0000	0.0000	0.0000	0.0000	0.0000	0.0000	0.0000	0.0000	0.0000	0.0000	0.0000	0.0000	0.0000	0.0000	0.0000	0.0000	0.0000	0.0000
Total	16.2541	16.1909	16.1756	16.3007	16.2803	16.3320	16.3094	16.4130	16.3349	16.3104	16.3735	16.2747	16.2146	16.2225	16.1800	16.2555	16.2669	16.2576	16.3650	16.3489	16.3438	16.3427	16.3406	16.4501

Table C6d: Continued

Sample	BIDBL3D	BI77022A	BI77022B	BI77022C	BI77022D	BI77022E	BI77022F	BI77022G	BI77022H	BI77022I	BI77023A	BI77023B	BI77023C	BI77024A	BI77024B	BI77024C	BI77024D	BI77024E	BI77024F	BI77024G	BI77024H	BIWL9A	BIWL9B	BIWL10A	BIWL10B
SiO2	36.16	37.40	37.93	38.05	37.92	38.00	36.62	36.22	36.22	36.62	38.07	37.49	37.12	37.48	37.72	37.52	37.54	37.44	37.39	37.42	37.38	35.30	35.18	36.17	36.00
TiO2	4.61	3.83	4.16	3.94	3.51	3.61	4.83	4.88	4.75	4.84	3.82	3.51	3.30	5.24	4.11	4.21	4.42	4.21	4.53	4.18	4.22	4.40	4.56	3.62	4.10
Al2O3	13.17	13.75	13.66	13.96	14.10	13.59	13.65	13.30	13.57	13.61	13.78	13.87	13.94	13.75	13.81	13.60	13.80	13.72	13.61	13.56	13.82	13.36	13.53	13.78	13.58
FeO	16.54	16.97	16.63	17.42	17.45	17.46	23.26	22.94	22.95	23.02	17.76	17.80	17.45	17.24	17.05	17.98	17.03	17.55	17.05	17.57	17.20	17.01	17.83	16.53	16.39
MnO	0.16	0.25	0.36	0.32	0.21	0.27	0.42	0.46	0.44	0.32	0.18	0.27	0.12	0.26	0.11	0.25	0.12	0.25	0.22	0.17	0.12	0.24	0.22	0.38	0.39
MgO	13.62	12.74	12.90	13.10	12.62	12.72	8.83	8.83	8.69	9.05	13.44	12.93	12.97	12.47	13.20	12.88	12.89	13.11	13.19	13.02	13.13	12.27	11.98	12.06	11.94
CaO	0.01	0.00	0.00	0.00	0.00	0.17	0.09	0.00	0.00	0.00	0.00	0.00	0.00	0.00	0.36	0.00	0.00	0.00	0.12	0.00	0.00	0.01	0.00	0.01	0.00
Na2O	0.15	0.00	0.00	0.00	0.00	0.00	0.00	0.00	0.00	0.00	0.00	0.00	0.00	0.00	0.00	0.00	0.00	0.00	0.00	0.00	0.00	0.12	0.16	0.00	0.01
K2O	9.40	9.56	9.51	9.43	9.51	9.47	9.36	9.04	9.39	9.31	9.52	9.38	9.58	9.52	9.54	9.55	9.36	9.49	9.50	9.35	9.41	9.16	9.03	9.53	9.60
P2O5	0.00	0.00	0.00	0.00	0.00	0.00	0.00	0.00	0.00	0.00	0.00	0.00	0.00	0.00	0.00	0.00	0.00	0.00	0.00	0.00	0.00	0.00	0.00	0.00	0.00
TOTAL	93.82	94.50	95.17	96.22	95.32	95.29	97.06	95.67	96.01	96.77	96.57	95.25	94.48	95.96	95.90	95.99	95.29	95.77	95.61	95.27	95.28	91.87	92.49	94.38	94.01
Sr	0	0	0	0	0	0	0	0	0	0	0	0	0	0	0	0	0	0	0	0	0	0	0	0	0
Ba	0	0	0	0	0	0	0	0	0	0	0	0	0	0	0	0	0	0	0	0	0	0	0	0	0
Cr	0	0	0	0	0	0	0	0	0	0	0	0	0	0	0	0	0	0	0	0	0	0	0	0	0
Ni	0	0	0	0	0	0	0	0	0	0	0	0	0	0	0	0	0	0	0	0	0	0	0	0	0
Si	5.9585	5.9831	5.9497	5.8175	5.9860	6.0080	5.8621	5.8749	5.8629	5.8679	5.9419	5.9403	5.9293	5.8861	5.9203	5.9124	5.9196	5.8999	5.8921	5.9228	5.9047	5.8188	5.7790	5.8571	5.8364
Ti	0.4589	0.4959	0.4633	0.5578	0.4167	0.4292	0.5815	0.5953	0.5783	0.5833	0.4484	0.4183	0.3964	0.6189	0.4851	0.4985	0.5242	0.4989	0.5369	0.4976	0.5013	0.5455	0.5634	0.4409	0.5001
Al	2.5826	2.5403	2.5734	2.4979	2.6241	2.5331	2.5761	2.5432	2.5896	2.5710	2.5356	2.5909	2.6251	2.5458	2.5554	2.5265	2.5655	2.5489	2.5285	2.5303	2.5737	2.5963	2.6203	2.6307	2.5964
Fe3	0.0000	0.0000	0.0000	0.0000	0.0000	0.0000	0.0000	0.0000	0.0000	0.0000	0.0000	0.0000	0.0000	0.0000	0.0000	0.0000	0.0000	0.0000	0.0000	0.0000	0.0000	0.0000	0.0000	0.0000	0.0000
Fe2	2.2611	2.1939	2.2781	2.2254	2.3038	2.3087	3.1140	3.1116	3.1069	3.0849	2.3182	2.3588	2.3311	2.2643	2.2381	2.3695	2.2459	2.3129	2.2471	2.3258	2.2723	2.3450	2.4496	2.5095	2.4943
Mn2	0.0337	0.0481	0.0424	0.0218	0.0281	0.0362	0.0570	0.0632	0.0603	0.0434	0.0238	0.0362	0.0162	0.0346	0.0146	0.0334	0.0160	0.0334	0.0294	0.0228	0.0161	0.0335	0.0306	0.0521	0.0536
Mg	3.0249	3.0326	3.0528	3.2656	2.9690	2.9972	2.1066	2.1345	2.0964	2.1612	3.1262	3.0533	3.0875	2.9166	3.0877	3.0248	3.0292	3.0789	3.0977	3.0712	3.0910	3.0143	2.9329	2.9104	2.8854
Ca	0.0000	0.0000	0.0000	0.0017	0.0000	0.0288	0.0154	0.0000	0.0000	0.0000	0.0000	0.0000	0.0000	0.0000	0.0605	0.0000	0.0000	0.0000	0.0203	0.0000	0.0000	0.0384	0.0000	0.0017	0.0000
Na	0.0000	0.0000	0.0000	0.0468	0.0000	0.0000	0.0000	0.0000	0.0000	0.0000	0.0000	0.0000	0.0000	0.0000	0.0000	0.0000	0.0000	0.0000	0.0000	0.0000	0.0000	0.0000	0.0510	0.0000	0.0031
K	1.9431	1.9138	1.8812	1.9294	1.9153	1.9102	1.9116	1.8707	1.9392	1.9032	1.8957	1.8962	1.9523	1.9074	1.9103	1.9199	1.8830	1.9079	1.9099	1.8881	1.8964	1.9264	1.8925	1.9688	1.9863
P	0.0000	0.0000	0.0000	0.0000	0.0000	0.0000	0.0000	0.0000	0.0000	0.0000	0.0000	0.0000	0.0000	0.0000	0.0000	0.0000	0.0000	0.0000	0.0000	0.0000	0.0000	0.0000	0.0000	0.0000	0.0000
Sr	0.0000	0.0000	0.0000	0.0000	0.0000	0.0000	0.0000	0.0000	0.0000	0.0000	0.0000	0.0000	0.0000	0.0000	0.0000	0.0000	0.0000	0.0000	0.0000	0.0000	0.0000	0.0000	0.0000	0.0000	0.0000
Ba	0.0000	0.0000	0.0000	0.0000	0.0000	0.0000	0.0000	0.0000	0.0000	0.0000	0.0000	0.0000	0.0000	0.0000	0.0000	0.0000	0.0211	0.0000	0.0000	0.0000	0.0000	0.0000	0.0000	0.0000	0.0000
Cr	0.0000	0.0000	0.0000	0.0000	0.0000	0.0000	0.0000	0.0000	0.0000	0.0000	0.0000	0.0000	0.0000	0.0000	0.0000	0.0000	0.0000	0.0000	0.0000	0.0000	0.0000	0.0000	0.0000	0.0000	0.0000
Ni	0.0000	0.0000	0.0000	0.0000	0.0000	0.0000	0.0000	0.0000	0.0000	0.0000	0.0000	0.0000	0.0000	0.0000	0.0000	0.0000	0.0000	0.0000	0.0000	0.0000	0.0000	0.0000	0.0000	0.0000	0.0000
Total	16.2629	16.2078	16.2409	16.3639	16.2429	16.2513	16.2242	16.1936	16.2336	16.2150	16.2898	16.2940	16.3379	16.1756	16.2720	16.2854	16.2045	16.2807	16.2618	16.2585	16.2554	16.3199	16.3192	16.3712	16.3561

Table C6e: Electron microprobe analyses with structural formula

Sample	PLWL6A	PLWL6B	PLWL6C	PLWL6D	PL78001A	PL78001B	PL78001C	PL77018A
SiO2	59.08	56.94	60.85	60.16	57.24	59.29	59.18	58.23
TiO2	0.09	0.04	0.07	0.02	0.00	0.03	0.01	0.15
Al2O3	25.53	26.55	24.22	25.24	26.71	25.40	25.31	25.82
FeO	0.16	0.20	0.21	0.18	0.05	0.05	0.16	0.18
MnO	0.00	0.00	0.00	0.00	0.00	0.00	0.00	0.00
MgO	0.02	0.03	0.03	0.03	0.02	0.01	0.04	0.00
CaO	7.23	8.87	6.03	6.75	8.86	7.33	7.46	8.15
Na2O	7.30	6.76	7.46	7.43	6.54	7.32	7.48	7.00
K2O	0.37	0.38	0.75	0.32	0.14	0.25	0.35	0.55
P2O5	0.00	0.00	0.00	0.00	0.00	0.00	0.00	0.00
TOTAL	99.78	99.77	99.62	100.13	99.56	99.68	99.99	100.08
Sr	0	0	0	0	0	0	0	0
Ba	0	0	0	0	0	0	0	0
Cr	0	0	0	0	0	0	0	0
Ni	0	0	0	0	0	0	0	0
Si	10.5815	10.2708	10.8765	10.7058	10.3072	10.6166	10.5918	10.4468
Ti	0.0121	0.0054	0.0094	0.0027	0.0000	0.0040	0.0013	0.0202
Al	5.3907	5.6460	5.1038	5.2953	5.6703	5.3620	5.3404	5.4611
Fe3	0.0000	0.0000	0.0000	0.0000	0.0000	0.0000	0.0000	0.0000
Fe2	0.0240	0.0302	0.0314	0.0268	0.0075	0.0075	0.0239	0.0270
Mn2	0.0000	0.0000	0.0000	0.0000	0.0000	0.0000	0.0000	0.0000
Mg	0.0053	0.0081	0.0080	0.0080	0.0054	0.0027	0.0107	0.0000
Ca	1.3875	1.7144	1.1549	1.2871	1.7095	1.4064	1.4306	1.5667
Na	2.5351	2.3643	2.5854	2.5637	2.2834	2.5414	2.5958	2.4350
K	0.0845	0.0874	0.1710	0.0727	0.0322	0.0571	0.0799	0.1259
P	0.0000	0.0000	0.0000	0.0000	0.0000	0.0000	0.0000	0.0000
Sr	0.0000	0.0000	0.0000	0.0000	0.0000	0.0000	0.0000	0.0000
Ba	0.0000	0.0000	0.0000	0.0000	0.0000	0.0000	0.0000	0.0000
Cr	0.0000	0.0000	0.0000	0.0000	0.0000	0.0000	0.0000	0.0000
Ni	0.0000	0.0000	0.0000	0.0000	0.0000	0.0000	0.0000	0.0000
Total	20.0208	20.1266	19.9404	19.9620	20.0155	19.9977	20.0745	20.0828

e based on 8 oxygens for plagioclase from the Loch Doon pluton.

PL77018B	PL77018C	PL77018D	PL78002A	PL78002B	PL78002C	PL78002D	PL78002E
60.01	60.64	60.09	54.58	59.97	57.94	56.66	60.23
0.00	0.00	0.00	0.00	0.00	0.00	0.00	0.00
24.73	24.53	25.17	29.00	24.85	26.02	26.81	24.45
0.18	0.14	0.24	0.28	0.21	0.24	0.28	0.19
0.00	0.00	0.00	0.00	0.00	0.00	0.00	0.00
0.00	0.00	0.00	0.00	0.00	0.00	0.00	0.00
6.98	6.63	6.90	11.03	6.47	8.36	9.06	6.64
7.42	7.79	7.37	5.15	7.78	6.81	6.92	7.89
0.44	0.31	0.47	0.18	0.22	0.46	0.26	0.47
0.00	0.00	0.00	0.00	0.00	0.00	0.00	0.00
99.76	100.04	100.24	100.22	99.50	99.83	99.99	99.87
0	0	0	0	0	0	0	0
0	0	0	0	0	0	0	0
0	0	0	0	0	0	0	0
0	0	0	0	0	0	0	0
10.7367	10.8027	10.6988	9.8340	10.7404	10.4192	10.2120	10.7722
0.0000	0.0000	0.0000	0.0000	0.0000	0.0000	0.0000	0.0000
5.2162	5.1518	5.2833	6.1600	5.2468	5.5164	5.6967	5.1553
0.0000	0.0000	0.0000	0.0000	0.0000	0.0000	0.0000	0.0000
0.0269	0.0209	0.0357	0.0422	0.0315	0.0361	0.0422	0.0284
0.0000	0.0000	0.0000	0.0000	0.0000	0.0000	0.0000	0.0000
0.0000	0.0000	0.0000	0.0000	0.0000	0.0000	0.0000	0.0000
1.3381	1.2656	1.3164	2.1294	1.2416	1.6109	1.7497	1.2725
2.5740	2.6908	2.5443	1.7992	2.7017	2.3745	2.4183	2.7361
0.1004	0.0705	0.1068	0.0414	0.0503	0.1055	0.0598	0.1072
0.0000	0.0000	0.0000	0.0000	0.0000	0.0000	0.0000	0.0000
0.0000	0.0000	0.0000	0.0000	0.0000	0.0000	0.0000	0.0000
0.0000	0.0000	0.0000	0.0000	0.0000	0.0000	0.0000	0.0000
0.0000	0.0000	0.0000	0.0000	0.0000	0.0000	0.0000	0.0000
0.0000	0.0000	0.0000	0.0000	0.0000	0.0000	0.0000	0.0000
19.9924	20.0021	19.9851	20.0062	20.0122	20.0626	20.1787	20.0718

Table C6e: Continued

Sample	PLDBL1A	PLDBL1B	PLDBL1C	PLDBL3A	PLDBL4A	PLDBL4B	PLDBL5A	PLDBL5B
SiO2	61.15	57.76	58.92	58.46	59.55	59.25	53.84	56.07
TiO2	0.02	0.04	0.05	0.07	0.04	0.03	0.04	0.02
Al2O3	24.20	26.33	25.53	25.93	25.10	25.10	29.28	27.87
FeO	0.09	0.15	0.11	0.15	0.11	0.10	0.07	0.07
MnO	0.00	0.00	0.00	0.00	0.00	0.00	0.00	0.00
MgO	0.01	0.03	0.01	0.02	0.03	0.02	0.03	0.02
CaO	6.09	8.47	7.46	7.29	7.30	7.43	10.57	9.51
Na2O	8.19	6.72	7.32	7.71	7.37	7.34	5.84	6.05
K2O	0.31	0.30	0.27	0.29	0.28	0.34	0.16	0.22
P2O5	0.00	0.00	0.00	0.00	0.00	0.00	0.00	0.00
TOTAL	100.06	99.80	99.67	99.92	99.78	99.61	99.83	99.83
Sr	0	0	0	0	0	0	0	0
Ba	0	0	0	0	0	0	0	0
Cr	0	0	0	0	0	0	0	0
Ni	0	0	0	0	0	0	0	0
Si	10.8784	10.3783	10.5668	10.6560	10.4799	10.6314	9.7497	10.0948
Ti	0.0027	0.0054	0.0067	0.0054	0.0094	0.0040	0.0054	0.0027
Al	5.0754	5.5775	5.3978	5.2951	5.4801	5.3096	6.2509	5.9155
Fe3	0.0000	0.0000	0.0000	0.0000	0.0000	0.0000	0.0000	0.0000
Fe2	0.0134	0.0225	0.0165	0.0165	0.0225	0.0150	0.0106	0.0105
Mn2	0.0000	0.0000	0.0000	0.0000	0.0000	0.0000	0.0000	0.0000
Mg	0.0027	0.0080	0.0027	0.0080	0.0053	0.0053	0.0081	0.0054
Ca	1.1609	1.6307	1.4335	1.3997	1.4003	1.4285	2.0509	1.8346
Na	2.8250	2.3412	2.5454	2.5571	2.6799	2.5537	2.0505	2.1120
K	0.0704	0.0688	0.0618	0.0639	0.0663	0.0778	0.0370	0.0505
P	0.0000	0.0000	0.0000	0.0000	0.0000	0.0000	0.0000	0.0000
Sr	0.0000	0.0000	0.0000	0.0000	0.0000	0.0000	0.0000	0.0000
Ba	0.0000	0.0000	0.0000	0.0000	0.0000	0.0000	0.0000	0.0000
Cr	0.0000	0.0000	0.0000	0.0000	0.0000	0.0000	0.0000	0.0000
Ni	0.0000	0.0000	0.0000	0.0000	0.0000	0.0000	0.0000	0.0000
Total	20.0288	20.0325	20.0312	20.0016	20.1438	20.0255	20.1632	20.0260

PL77022A	PL77022B	PL77022C	PL77022D	PL77023A	PL77023B	PLWL9A	PLWL9B	PLWL10A	PLWL10B
59.38	57.29	60.93	60.32	61.56	60.29	60.46	59.35	60.64	61.51
0.00	0.00	0.00	0.00	0.00	0.00	0.02	0.06	0.00	0.00
25.24	26.70	25.53	24.53	23.53	23.94	24.80	25.31	24.42	24.61
0.19	0.00	0.00	0.16	0.17	0.00	0.12	0.15	0.09	0.11
0.00	0.00	0.00	0.00	0.00	0.00	0.00	0.00	0.00	0.00
0.00	0.00	0.00	0.00	0.00	0.00	0.02	0.01	0.03	0.00
7.11	7.75	6.43	6.37	5.33	6.44	5.58	5.89	5.70	5.28
7.92	7.93	7.04	8.03	8.93	8.97	8.31	8.45	8.60	8.63
0.09	0.15	0.15	0.31	0.34	0.25	0.41	0.34	0.18	0.24
0.00	0.00	0.00	0.00	0.00	0.00	0.00	0.00	0.00	0.00
99.93	99.82	100.08	99.72	99.86	99.89	99.72	99.56	99.66	100.38
0	0	0	0	0	0	0	0	0	0
0	0	0	0	0	0	0	0	0	0
0	0	0	0	0	0	0	0	0	0
0	0	0	0	0	0	0	0	0	0
10.6209	10.3060	10.7830	10.7858	10.9771	10.7979	10.7944	10.6452	10.8320	10.8862
0.0000	0.0000	0.0000	0.0000	0.0000	0.0000	0.0027	0.0081	0.0000	0.0000
5.3223	5.6626	5.3266	5.1710	4.9465	5.0548	5.2200	5.3520	5.1426	5.1349
0.0000	0.0000	0.0000	0.0000	0.0000	0.0000	0.0000	0.0000	0.0000	0.0000
0.0284	0.0000	0.0000	0.0239	0.0254	0.0000	0.0179	0.0225	0.0134	0.0163
0.0000	0.0000	0.0000	0.0000	0.0000	0.0000	0.0000	0.0000	0.0000	0.0000
0.0000	0.0000	0.0000	0.0000	0.0000	0.0000	0.0053	0.0027	0.0080	0.0000
1.3627	1.4939	1.2193	1.2205	1.0184	1.2359	1.0675	1.1320	1.0910	1.0013
2.7467	2.7660	2.4157	2.7840	3.0875	3.1150	2.8767	2.9387	2.9786	2.9615
0.6205	0.0344	0.0339	0.0707	0.0773	0.0571	0.0934	0.0778	0.0410	0.0542
0.0000	0.0000	0.0000	0.0000	0.0000	0.0000	0.0000	0.0000	0.0000	0.0000
0.0000	0.0000	0.0000	0.0000	0.0000	0.0000	0.0000	0.0000	0.0000	0.0000
0.0000	0.0000	0.0000	0.0000	0.0000	0.0000	0.0000	0.0000	0.0000	0.0000
0.0000	0.0000	0.0000	0.0000	0.0000	0.0000	0.0000	0.0000	0.0000	0.0000
0.0000	0.0000	0.0000	0.0000	0.0000	0.0000	0.0000	0.0000	0.0000	0.0000
20.1016	20.2629	19.7785	20.0560	20.1321	20.2607	20.0779	20.1790	20.1066	20.0542

Appendix D: Distribution coefficients for trace elements between minerals and melt. Based on a collation of literature values, used for fractional crystallisation modelling.

Mineral	V	Cr	Ni	Rb	Sr	Y	Zr	Nb	Ba	La	Ce	Hf	Th
Olivine	0.08	34	58	0.01	0.01	0.01	0.01	0.01	0.01	0.01	0.01	0.01	0.01
Clinopyroxene	1.10	30	6	0.02	0.08	2.00	0.25	0.30	0.02	0.07	0.25	0.25	0.01
Orthopyroxene	1.10	13	8	0.02	0.03	0.60	0.10	0.35	0.02	0.02	0.05	0.10	0.05
Amphibole	32	30	10	0.05	0.23	4.0	0.4	1.3	0.09	0.16	0.25	0.40	0.15
Spinel	30	32	10	0.01	0.01	0.00	0.40	1.00	0.01	0.23	0.20	0.40	0.10
Biotite	0.00	7	3.7	3.00	0.10	1.20	1.00	6.00	6.40	0.03	0.03	10	0.70
Plagioclase	0.01	0.01	0.01	0.07	1.80	0.08	0.01	0.025	0.16	0.14	0.20	0.01	0.01
K-feldspar	0.00	0.00	0.00	0.66	3.87	0.00	0.03	0.00	6.1	0.07	0.044	0.03	0.02
Apatite	0.00	0.00	0.00	0.00	0.00	30	0.00	0.1	0.00	0.00	30	0.00	0.00
Sphene	0.00	0.00	0.00	0.00	0.00	0.00	0.00	0.00	0.00	0.00	53.3	0.00	0.00
Zircon	0.00	0.00	0.00	0.00	0.00	0.00	50	0.00	0.00	0.00	2.64	0.00	0.00